CRBRP-3

HYPOTHETICAL CORE DISRUPTIVE ACCIDENT CONSIDERATIONS IN CRBRP

VOLUME 2:

ASSESSMENT OF THERMAL MARGIN BEYOND THE DESIGN BASE

CLINCH RIVER BREEDER REACTOR PLANT

8003310164

CRBRP-3

HYPOTHETICAL CORE DISRUPTIVE ACCIDENT CONSIDERATIONS IN CRBRP

VOLUME 2

ASSESSMENT OF THERMAL MARGIN BEYOND THE DESIGN BASE

Department of Energy
Clinch River Breeder Reactor Plant Project Office
Oak Ridge, Tennessee 37830

Hypothetical Core Disruptive Accident Considerations in CRBRP

Abstract

Hypothetical Core Disruptive Accidents (HCDAs) have been excluded from the design base* since the postulated initiators of HCDAs have been identified and the design features necessary to prevent their initiation have been incorporated into the design.

Although HCDAs are not part of the design base, extensive assessments of HCDA consequences have been made. These assessments indicate that the likely consequence of an HCDA would be a non-energetic partial to whole core meltdown.

To further reduce the risk to the public from HCDAs, prudent margins beyond the design base have been incorporated into the design. These margins are in two categories:

Structural Margin Beyond the Design Base (SMBDB)
Thermal Margin Beyond the Design Base (TMBDB)

Volume 1 of this report addresses the Structural Margin Beyond the Design Base. It is shown that the SMBDB requirements encompass not only the energetics associated with the likely HCDA progression paths but also the energetics associated with a wide spectrum of more pessimistic assumptions of data and phenomenology. Analyses and supporting scale model experiments indicate that the reactor coolant boundary would accommodate the SMBDB dynamic load requirements without loss of integrity and with limited leakage of radioactive materials to the reactor containment building.

Volume 2 of this report addresses the Thermal Margin Beyond the Design Base. It is shown that the thermal loads resulting from an HCDA could result in longer term (>1000 seconds) loss of integrity of the reactor vessel and guard vessel. Consequently the TMBDB requirements are based on the assumption of penetration of the reactor vessel and guard vessel, and features are provided to mitigate the resulting thermal and radiological consequences. The evaluation of the plant capability shows that the reactor containment integrity would be maintained for at least 24 hours following an HCDA and the radiological consequences would be comparable to those for similarly low probability occurrences beyond the design base in light water reactors.

It is concluded that the Structural and Thermal Margins Beyond the Design Base effectively mitigate the consequences of HCDAs so as to assure an acceptably low risk to the public.

---

*i.e. HCDAs are not Design Basis Accidents

CHANGE CONTROL RECORD	TITLE Hypothetical Core Disruptive Accident Considerations in CRBRP Volume 2 Assessment of Thermal Margin Beyond the Design Base	DOCUMENT NO. CRBRP-3 Volume 2	
REV NO./DATE	CHANGE RELEASE DOCUMENT	PAGES AFFECTED	REMARKS
0/March 80		All	First formal issue of document

TABLE OF CONTENTS

TABLE OF CONTENTS (Continued)

TABLE OF CONTENTS (Continued)

TABLE OF CONTENTS (Continued)

TABLE OF CONTENTS (Continued)

TABLE OF CONTENTS (Continued)

TABLE OF CONTENTS (Continued)

LIST OF TABLES

LIST OF TABLES (Continued)

LIST OF TABLES (Continued)

LIST OF TABLES (Continued)

LIST OF FIGURES

LIST OF FIGURES (Continued)

LIST OF FIGURES (Continued)

LIST OF FIGURES (Continued)

LIST OF FIGURES (Continued)

LIST OF FIGURES (Continued)

LIST OF FIGURES (Continued)

LIST OF FIGURES (Continued)

LIST OF FIGURES (Continued)

LIST OF FIGURES (Continued)

LIST OF FIGURES (Continued)

LIST OF FIGURES (Continued)

ABBREVIATIONS

ANL	Argonne National Laboratory
ARD	Advanced Reactors Division (of Westinghouse Electric Corporation)
ASME	American Society of Mechanical Engineers
ATWS	Anticipated Transients Without Scram
BOEC	Beginning of Equilibrium Cycle
BOL	Beginning of Life
CAM	Continuous Air Monitors
CFR	Code of Federal Regulation
CRBR	Clinch River Breeder Reactor
CRBRP	Clinch River Breeder Reactor Plant
CRDM	Control Rod Drive Mechanism
CSS	Core Support Structure
DHRS	Direct Heat Removal Service
DOE	U. S. Department of Energy
EOEC	End of Equilibrium Cycle
ERDA	U.S. Energy Research and Development Administration
ESF	Engineered Safety Features
FMEA	Failure Mode and Effects Analysis
FFTF	Fast Flux Test Facility
FWP	Feedwater Pump
GE	General Electric Company
HAA	Head Access Area
HCDA	Hypothetical Core Disruptive Accident
HEDL	Hanford Engineering Development Laboratory
HEPA	High Efficiency Particulate Air
HTS	Heat Transport System
HVAC	Heating, Ventilating and Air Conditioning
IEEE	Institute of Electrical and Electronic Engineers
IHTS	Intermediate Heat Transport System
IHX	Intermediate Heat Exchanger
IMAS	Impurity Monitoring and Analysis System
IRP	Intermediate Rotating Plug
IVTM	In-Vessel Transfer Machine

LMEC	Liquid Metal Engineering Center
LOF	Loss-of-Flow
LOF-d-TOP	LOF-driven-TOP
LPZ	Low Population Zone
LRP	Large Rotating Plug
LSFF	Large Sodium Fire Facility
LWR	Light-Water Reactor
MPC	Maximum Permissible Concentrations
NRC	Nuclear Regulatory Commission
PAPM	Plutonium Air Particulate Monitor
PHTS	Primary Heat Transport System
PPS	Plant Protection System
PRSS	Primary Reactor Shutdown System
PSAR	Preliminary Safety Analysis Report
RC	Reactor Cavity
RCB	Reactor Containment Building
RSB-VEB	Reactor Service Building - Ventilation Equipment Bay
RSS	Reactor Shutdown System
RV	Reactor Vessel
SB	Site Boundary
SCL	Statistical Confidence Limits
SGAHRS	Steam Generator Auxiliary Heat Removal System
SGS	Steam Generator System
SHRS	Shutdown Heat Removal System
SMBDB	Structural Margin Beyond the Design Base
SRI	SRI International
SRP	Small Rotating Plug
SRSS	Secondary Reactor Shutdown System
TBD	To be Determined
TMBDB	Thermal Margin Beyond the Design Base
TOP	Transient Overpower
UIS	Upper Internals Structure
W-LRM	Westinghouse - Lead Reactor Manufacturer
W-RM	Westinghouse - Reactor Manufacturer
ZPPR	Zero Power Plutonium Reactor

1.0 INTRODUCTION

The Clinch River Breeder Reactor Plant Project and the Nuclear Regulatory Commission agreed that the probability of core melt and disruptive accidents can and must be reduced to a sufficiently low level to justify their exclusion from the design basis accident spectrum. Volume 1 of this report discusses potential initiators of an HCDA and the design features that prevent their initiation. Consequently, such accidents are considered to be hypothetical and are beyond the design basis. Nevertheless, prudent margins beyond the design base are being included to provide an extra measure of protection to the public health and safety in recognition of the difference in the state of technology and experience between LMFBRs and LWRs. These structural and thermal margins are discussed in depth in this two-volume report.

Volume 1 of this report assesses the potential for energetics arising from a Hypothetical Core Disruptive Accident (HCDA) scenario, and assesses the Structural Margin Beyond the Design Base (SMBDB). It is concluded that the best estimate of the progression of an HCDA is a non-energetic termination with partial to whole core involvement (i.e., melting). Furthermore, significant deviations in data or phenomenology from current analytical models and experimental data must be invoked to predict an energetic termination of the HCDA progression. Nevertheless, Structural Margin Beyond the Design Base requirements have been specified to require the CRBRP to accommodate substantial energetics that encompass a wide spectrum of more pessimistic assumptions of data and phenomenology. Thus the CRBRP Project has assured that the reactor coolant boundary has margin to accommodate the dynamic load associated with a spectrum of HCDAs.

Volume 2 addresses the thermal margin provided by the design and specifically addresses the consequences of a postulated core melt resulting in penetration of the reactor vessel and guard vessel.

In the remainder of this section (Section 1.0), the design features that provide TMBDB are illustrated and the scenario of the HCDA is outlined. Section 2 of Volume 2 defines the thermal margin requirements, the design features that provide the thermal margin and the sequence of operator actions required to initiate operation of those features. Section 3 assesses the thermal margins within the reactor vessel and external to it and shows that the requirement to maintain containment integrity for 24 hours following a postulated HCDA is met. In fact, analyses in Section 3 predict that containment integrity would be maintained without a need for venting for about 36 hours. Section 4 assesses the radiological consequences and shows that the consequences are comparable to those for accidents beyond the design base for light water reactors.

The appendices provide information on development programs that support the assessments, details on the analytic models and the data base, and alternative scenarios.

The design features that provide the Thermal Margin Beyond the Design Base (TMBDB) described in this report are illustrated in Figure 1-1. Some of these features are provided specifically for TMBDB while other features have been augmented to provide capability for TMBDB. These features are itemized in Table 2-1 and described in Section 2.2.

Considering these features, the analysis of the HCDA results in the following scenario (discussed in more detail in Section 3.2.1).

1. Fuel and other reactor materials would penetrate the reactor and guard vessels at 1000 seconds.

2. Sodium would drain into the reactor cavity.

3. The reactor cavity steel floor liner was assumed to fail, resulting in sodium-concrete and sodium-water reactions within the reactor cavity.

4. Water vapor and carbon dioxide from the concrete would be vented from behind the reactor cavity wall liner to a contiguous air filled cell below the operating floor (cell 105).

5. Sodium would begin boiling in the reactor cavity in approximately 9 hours and would be vented above the operating floor where it would react with air and water vapor.

6. At some time beyond 24 hours, the annulus cooling system would be actuated and containment would be vented down to atmospheric pressure through the containment cleanup system.

7. Subsequently, the containment would be purged to dilute the hydrogen concentration by drawing air through it, resulting in a slightly sub-atmospheric pressure in the containment.

8. The sodium in the reactor cavity would boil dry at some time beyond 100 hours.

9. Fuel penetration into the concrete basemat would begin after the sodium boils dry (defined as "boildry").

10. Maximum penetration into the basemat would occur approximately 2 to 6 months after the HCDA.

11. The molten fuel-concrete pool would freeze with the basemat not totally penetrated.

The scenario summarized here and described in more detail in Section 3.2.1 has been analyzed using state-of-the-art methods and data and the design features described in Section 2.2. This work represents an evolution of work previously reported in References 1-1 and 1-2. These current assessments indicate that containment venting and purging would not need to be initiated until about 36 hours into the scenario. This provides a substantial margin over the NRC requirement to maintain containment integrity for 24 hours following a hypothetical core melt. The radiological analyses in Section 4 indicate that the radiological consequences of an HCDA would be acceptable considering the highly improbable nature of the conditions analyzed.

In addition, this report is based on a homogeneous core design instead of the heterogeneous core design that was adopted in Amendment No. 51 to the PSAR on September 14, 1979. Assessments have been performed and indicate that the conclusions described in this report are appropriate for either core design. As discussed in Section 4, the radiological doses for the homogeneous core bound the doses from the heterogeneous core. Consequently, the core design (i.e., homogeneous vs. heterogeneous) is not a factor in assessing the CRBRP for TMBDB.

1.1 REFERENCES

1-1 Letter S:L:1820, "CRBRP Containment-24-Hour Non-Venting Criteria," from A. R. Buhl to R. S. Boyd (NRC), November 5, 1976.

1-2 J. R. Schornhorst, L. E. Strawbridge and P. Bradbury, "Evaluations of CRBRP Thermal Margin Beyond the Design Base," Proceedings of the Third Post-Accident Heat Removal "Information Exchange", ANL-78-10, November 2-4, 1977, pp. 317-326.

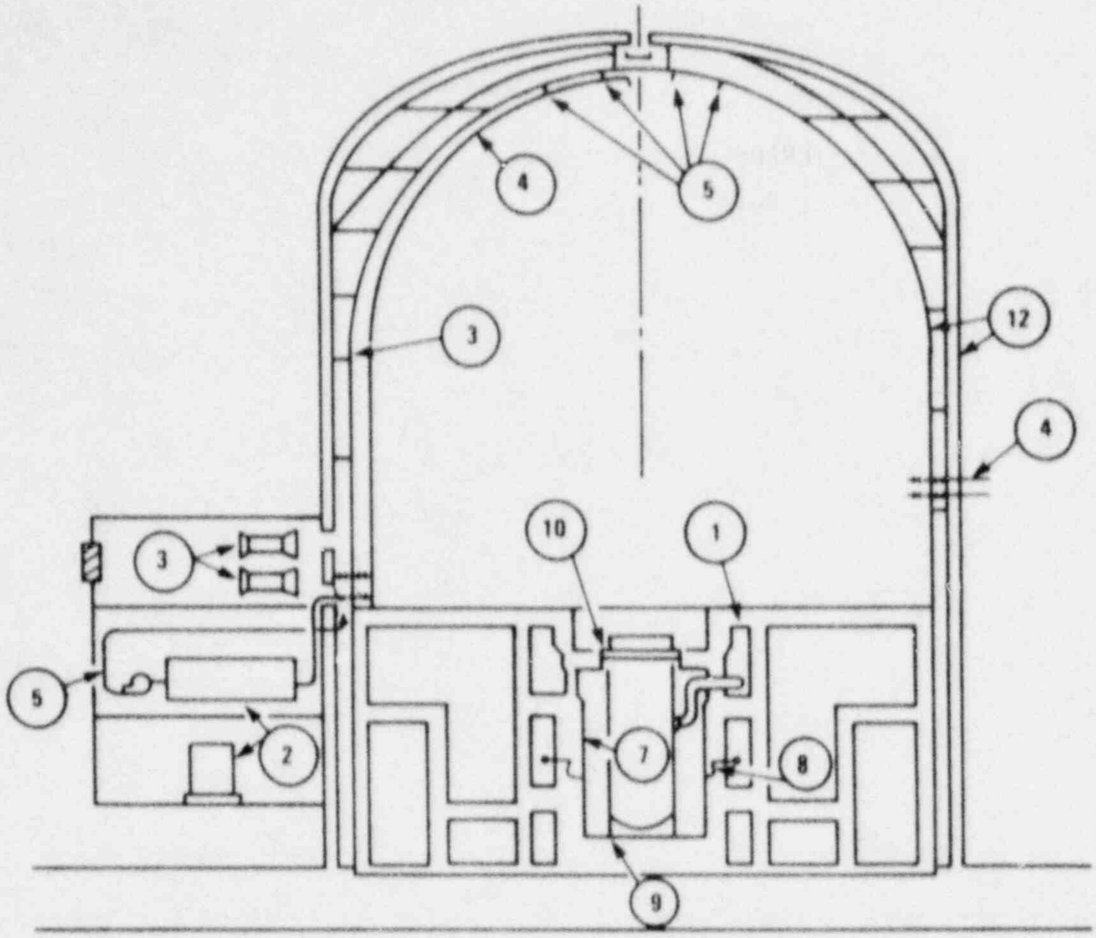

SPECIFIC SYSTEMS OR COMPONENTS FOR TMBDB

1. REACTOR CAVITY VENT SYSTEM
2. CONTAINMENT CLEANUP SYSTEM
3. ANNULUS COOLING SYSTEM
4. CONTAINMENT VENT AND PURGE SYSTEM
5. INSTRUMENTATION

SYSTEMS OR COMPONENTS WITH AUGMENTED CAPABILITIES FOR TMBDB

6. DUAL CONTROL ROOM AIR INTAKES (NOT SHOWN)
7. REACTOR CAVITY AND PIPEWAY CELL LINERS
8. LINER VENT SYSTEM
9. GUARD VESSEL SUPPORT
10. REACTOR CAVITY TO HEAD ACCESS AREA SEALS
11. REACTOR CAVITY RECIRCULATING GAS COOLING SYSTEM (NOT SHOWN)
12. CONTAINMENT-CONFINEMENT SYSTEMS (INCLUDING INSULATION)
13. EMERGENCY ELECTRICAL POWER SYSTEM (NOT SHOWN)
14. RCB STRUCTURES (ADDITION OF REINFORCING STEEL) (NOT SHOWN)

Figure 1-1. Design Features Providing Thermal Margin Beyond the Design Base

1966-1

2.0 DESIGN FEATURES PROVIDING THERMAL MARGIN BEYOND THE DESIGN BASE

This section includes the requirements for and description of features of the CRBRP design which enhance the Thermal Margin Beyond the Design Base (TMBDB). Table 2-1 gives the features specifically required for TMBDB and those whose capabilities were augmented to provide TMBDB. The cross reference to the CRBRP PSAR Section where the features are described is also provided. The design of these features is based on the scenario presented in Section 3.2.1 and on the results of the analyses presented in Sections 3.2.2 and 3.2.3 with appropriate margins to reflect uncertainties in the analysis.

2.1 TMBDB FEATURES REQUIREMENTS

The following requirements are imposed on CRBRP to assure that the CRBRP third level-of-defense capability established to conservatively mitigate design basis events is supplemented by margins to reasonably mitigate a hypothetical core meltdown incident which is beyond the design base.

2.1.1 General

1. General Requirements

    a. The design shall provide margins and features to mitigate the consequences of a hypothetical core meltdown.

    b. These features shall be designed to be consistent with safety, reliability, maintainability and availability of the total plant.

    c. These features are not Engineered Safety Features because they are not required to mitigate any Design Basis Event; however, these features shall be designed to the specifications and requirements associated with Safety Class 3 components and systems.

    d. TMBDB components shall be designed so that appropriate testing and/or inspection can be performed after installation and periodically to provide reasonable confidence that functional capability is maintained throughout the plant life. The containment isolation valves shall be designed to be testable in accordance with OPDD-10, Section 7.8.1.1.3, Criteria 43, 44 and 45.

    e. The TMBDB controls and associated instrumentation shall be physically separated from other controls in the reactor control room. Inadvertant actuation of the TMBDB features shall be prevented by appropriate provisions such as administrative controls.

f. There is not a requirement to meet the allowable site boundary or low population zone doses of 10CFR100 or the control room dose of 10CFR50 under TMBDB conditions.

2. Acceptance Criteria

a. The public risk from accidents beyond the design base shall be comparable to that from light water reactors for events beyond the design base with similar probability of occurrence.

b. Containment integrity shall be maintained without venting following initiation of an accident leading to core meltdown for a period of time sufficient to allow evacuation procedures to be implemented. Per NRC guidance, the period is taken as 24 hours.

2.1.2 Feature Requirements

The following requirements are imposed on the specific TMBDB features as well as other systems or components to provide thermal margin beyond the design base in CRBRP.

2.1.2.1 Reactor Cavity-To-Containment Barrier

To insure that the heat capacity of the pipeway cells is employed from 1000 seconds to 50 hours after a HCDA, the total leakage of sodium vapor through the reactor cavity to head access area seals (not through the reactor head or the planned vent path defined in Section 2.2.6) shall not exceed 10000 pounds (for requirements before 1000 seconds see Section 2.2). These leakages shall be based on the pressure differential for the reactor cavity to head access area seals given on Figure 2-1, on the reactor cavity pressures on Figure 2-2, and on the reactor cavity atmosphere temperatures on Figure 2-3.

2.1.2.2 Reactor Cavity Recirculating Gas Cooling System

To insure that the Cell 105 hydrogen concentration does not exceed 6%, the leakage from the reactor cavity through the recirculating gas cooling system to non-inerted cells shall be less than 4000 pounds of sodium. These leakages shall be based on the reactor cavity pressures and temperatures on Figures 2-2 and 2-3 and on the differential pressure between the reactor cavity and Cell 105 given on Figure 2-4.

2.1.2.3 Guard Vessel Support

To insure that sodium and fuel particulate redistribute in the reactor cavity, a flow area of at least 10 ft^2 shall be provided under the guard vessel skirt bottom flange.

2.1.2.4 Reactor Cavity and Pipeway Cell Liners

To insure that the Reactor Containment Building hydrogen concentration does not exceed 6% (by volume) and to keep from exceeding the containment vent, purge and cleanup system capacities, the reactor cavity wall and pipeway cell liners shall prevent short term (less than 30 hours) sodium-concrete reactions based on the pressure on Figure 2-2 and the temperatures on Figure 2-9 and Figures 2-11 through 2-16. The results of structural analysis will be used to determine the liner failure times assumed in the TMBDB scenario.

To limit the consequences of liner failures, the liner system shall have physical barriers behind the liners between the reactor cavity floor and reactor cavity wall and at 8 feet and 26 feet above the reactor cavity floor. Likewise, the pipeway cells shall have physical barriers behind the liners to separate the vent spaces of the walls, floor, and roof of each cell. Only the spaces of adjacent walls with different liner failure times will be separated.

2.1.2.5 Reactor Cavity and Pipeway Cell Liners Vent System

1. To insure that the pressure buildup, due to the gases released behind the liners, does not impair the ability of the liners to prevent sodium from reacting with concrete, all reactor cavity and pipeway cell liner vent systems shall prevent a pressure buildup behind the liners in excess of 5 psi.

2. To insure that sodium would be prevented from reaching Cell 105 in the event of liner failure, the liner vent system for the reactor cavity floor shall vent the gases released from heated concrete to containment above the operating floor. The floor liner vent system shall have a capacity of 10 $lb/hr\text{-}ft^2$ of water vapor at a density of 0.02 lb/ft^3.

3. The liner vent system for the reactor cavity walls and pipeway cells shall vent the gases released from heated concrete to Cell 105. The liner vent system shall have a capacity of 7 $lb/hr\text{-}ft^2$ of water vapor at a density of 0.02 lb/ft^3.

4. To insure that the Cell 105 hydrogen does not exceed 6%, the sodium leakage from the reactor cavity through the liner vent system to Cell 105 shall be less than 1000 pounds. This leakage shall be based on the reactor cavity pressures and temperatures on Figures 2-2 and 2-3 and on the differential pressure between the reactor cavity and Cell 105 on Figure 2-4.

2.1.2.6 Reactor Cavity Vent System

1. To prevent reactor cavity structural and liner failure by over pressurization, the vent system shall provide redundant flow paths between the reactor cavity and reactor containment building when the pressure differential between the reactor cavity and containment exceeds 11.5 ± 1.5 psi. After passive initiation, the vent path shall remain open.

2. The vent system shall have a pressure drop of less than 0.1 psi with a flow rate of 4000 lb/hr of gases, a density of 0.03 lb/ft^3, and a viscosity of 0.05 lb/ft hr. It shall remain functional if up to 450 pounds of sodium oxide aerosol enter the vent at a maximum rate of 8000 lb/hr.

3. The vent system shall be capable of performing all of its intended functions for 150 hours in the presence of gases and vapors consisting of Ar, N_2, H_2, Na, fission products, and compounds resulting from fission product reactions.

4. To insure that the heat capacity of the pipeway cells is employed, a minimum of 25% of the mass flow into the pipeway cells shall enter each pipeway cell.

5. To allow sodium that condenses in the pipeway cells to drain back into the reactor cavity, two drain pipes shall be provided between each pipeway cell and the reactor cavity, at the elevation of the pipeway cell floor. Each drain pipe shall be capable of a minimum flow rate of 2000 lb/hr of sodium at its boiling point with a pressure head of 0.2 feet of sodium.

6. To assure that the flame at the vent exit does not approach the containment vessel, the pipeway cell to containment vent line diameter shall not exceed 12 inches.

2.1.2.7 Containment Purge System

1. To insure that the Reactor Containment Building hydrogen concentration does not exceed 6% (by volume), the purge system shall be capable of injecting outside air into containment at a maximum rate of 12,000 scfm at pressures not exceeding atmospheric.

2. To insure containment atmosphere mixing before venting, the purge air shall be injected into containment below elevation 840'.

3. The purge system shall prevent backflow from containment to the outside atmosphere.

4. The purge system, in combination with the containment vent and cleanup systems, shall maintain containment at a negative pressure after the containment pressure is reduced by the initial venting after 24 hours.

5. The purge system operations shall be by remote manual actuation from the reactor control room.

2.1.2.8 Containment Vent System

1. To prevent containment failure by excessive pressure, the vent system shall have a capacity between 24,000 and 26,400 acfm with a containment pressure of 30 psia, a containment atmosphere density of 0.07 lb/ft^3 and a viscosity of 0.06 lb/ft hr. It shall remain functional if up to 300,000 pounds of aerosol enter the system at a maximum rate of 5,600 lb/hr.

2. The vent system shall exhaust the containment atmosphere from the top of containment into the containment cleanup system.

3. The containment vent system shall be compatible with the following gases, vapors and aerosols: Ar, N_2, H_2, H_2O, CO, CO_2, O_2, Na_2O, Na_2O_2, NaOH, Na_2CO_3, fission products, and compounds resulting from fission product reactions. The system must remain functional for inlet gas temperatures and pressures given on Figures 2-5 and 2-6.

4. The vent system operations shall be by remote manual actuation from the reactor control room.

2.1.2.9 TMBDB Containment Cleanup System

1. The containment cleanup system efficiency shall be a minimum of 99% for vented materials in the solid or liquid state, 97% for vapors (NaI, SeO_2, and Sb_2O_3) subject to condensation in the cleanup system, and 0% for noble gases. These efficiencies shall apply when subjected to the vent rates on Figure 2-7 and containment atmosphere temperatures on Figure 2-5 with a containment atmosphere density of 0.07 lb/ft^3. It shall be capable of performing all of its intended functions in the presence of Ar, N_2, H_2, H_2O, CO, CO_2, O_2, Na_2O, Na_2O_2, NaOH, Na_2CO_3, fission products, and compounds resulting from fission product reactions.

2. The containment cleanup system shall remain functional at an aerosol mass flow rate of up to 5,600 lb/hr and a total mass of 300,000 pounds of aerosol entering the cleanup system. The principal constitutents of the aerosol are NaOH and Na_2O, the proportions of which can vary from 0 to 100% of the aerosol, and Na_2CO_3 which can vary from 0 to 8% of the aerosol.

The aerosol particle properties are:

Mass Mean Radius (microns):	$5 < r_{50} < 10$
Aerodynamic Equivalent Radius (microns):	$2.3 < AER < 4.7$
Density (g/cc):	$2.1 < \rho < 2.5$
Mass Geometric Standard Deviation:	$3.0 < \sigma < 3.5$

Aerodynamic equivalent radius is based on $AER = r_{50} (\rho\alpha)^{0.5}$

where $\rho = 2.21$ and $\alpha = 0.1$

3. The containment cleanup system shall remain functional at fission products power levels in the accumulated filter aerosol of:

Time (hours)	Fission Product Power (MW)
0	0
24	3.1×10^{-5}
48	0.16*
96	0.16*
240	0.11
720	0.05

4. The containment cleanup system design shall be capable of performing all its intended functions with the following chemical and physical states of the 10 most radiologically significant fission products in the containment atmosphere:

*Maximum value.

MAXIMUM PERCENTAGE OF THE FISSION PRODUCTS BY CHEMICAL AND PHYSICAL FORM

	Elemental		Oxide	
Element	Vapor	Liquid or Solid	Vapor	Liquid or Solid
Se	1%	1%	100%	100%
Rb	1	1	1	100
Sr	1	1	1	100
Zr	1	1	1	100
Sb	1	1	100	100
Te	1	1	1	100
Cs	1	1	1	100
Ba	1	1	1	100
Ce	1	1	1	100
			NaI	
I	1	1	33	100

5. The exhaust from the containment cleanup system shall have a temperature compatible with operation of the TMBDB Exhaust-Plant Effluent Radiation Monitoring System.

6. The containment cleanup system operations shall be by remote manual actuation from the reactor control room.

2.1.2.10 Annulus Cooling System

1. To insure containment and confinement do not fail from excessive temperatures, the annulus cooling system shall remove the heat load into the containment steel shell on Figure 2-8.

2. Steel containment temperatures shall be below those that cause structural failure or excessive containment leakage.

3. Concrete confinement temperatures shall be below those that cause structural failure.

4. The annulus cooling system operations shall be by remote manual actuation from the reactor control room.

2.1.2.11 Containment System Leakage Barrier

At any given time, containment leakage shall not exceed the greater of:

1. The design leakrate (0.1 volume percent per day).

2. The design leakrate adjusted for pressures above the containment design pressure of 10 psig. Leakrate = Design Leakrate x (Actual Pressure (psig))$^{.5}$/3.2.

3. One percent of the mass leaving the containment through the containment vent system.

2.1.2.12 TMBDB Instrumentation System

Operator action to initiate TMBDB systems operation is required only for events beyond the design base. However, mis-operation of TMBDB systems, because of incorrect instrument readings in the reactor control room, could defeat Engineered Safety Features (ESFs) required to mitigate design basis accidents. In accordance with this importance to maintain ESF capability, plant instrumentation has been designated "TMBDB Instrumentation", shall be designed, manufactured and qualified to all standards applied to Class 1E instrumentation. Specifically the following subsystems of the Reactor Containment Instrumentation System (RCIS) and of the Radiation Monitoring System (RMS) shall be considered TMBDB instrumentation:

(1) Containment Pressure (RCIS)
(2) Containment Atmosphere Temperature (RCIS)
(3) Containment Hydrogen Concentration (RCIS)
(4) Containment Vessel Temperature (RCIS)
(5) TMBDB Exhaust-Plant Effluent Radiation Monitoring (RMS)

Note that the last subsystem (5), is not in the category of instrumentation which could be used to defeat ESFs; however, because of its importance in assessing releases from the plant during a TMBDB scenario it is included in the TMBDB instrumentation.

1. The TMBDB instrument ranges shall be:

	Minimum	Maximum
Containment Atmosphere Temperature (degrees F)	60	1100
Containment Steel Dome Temperature (degrees F)	40	500
Containment Atmosphere Pressure (psia)	14.7	37
Containment Hydrogen Concentration (Volume %)	0	8

	Minimum	Maximum
Radioactivity of Released Products (ci/sec)*		
Particulates	0	7
Radioiodines	0	30
Radiogases	0	6000
Fuels and Transuranics	0	0.01

2. Instrument accuracy shall be:

Temperature	(Percent of Maximum Value)	±5
Pressure	(Percent of Maximum Value)	±5
Hydrogen Concentration	(Percent of Maximum Value)	±5
Radioactivity of Released Products at 95% SCL	(Percent of Maximum Value)	+100, -50

3. Instrument response time shall be:

Temperature	Less than 5 minutes
Pressure	Less than 5 minutes
Hydrogen Concentration	Less than 10 minutes
Radioactivity of Released Products	Less than 5 minutes

4. Measurement capability after initiation of the TMBDB condition shall be provided for:

Temperature	500 hours
Pressure	500 hours
Hydrogen Concentration	8,000 hours
Radioactivity of Released Products	8,000 hours

*These are based on total amounts released. Instrument ranges will depend on the sampling rate.

5. The instrument sensor/sampling location inside of containment shall be:

Hydrogen Concentration	Above 970' Elevation
Containment Atmosphere Temperature	Above 955' Elevation
Containment Atmosphere Pressure	Above 823' Elevation
Containment Steel Dome Temperatures	At 817', 823', 833', 854', 875', and 902', 964', and 974' Elevations

6. TMBDB sensors inside containment shall be functional with a maximum containment atmosphere temperature of 1100°F and pressure of 37 psia.

7. TMBDB sensors inside containment shall be functional with containment atmosphere maximum constituent concentrations of:

Oxygen	21% (volume)
Nitrogen	90% (volume)
Water Vapor	10% (volume)
Hydrogen	8%
Carbon Dioxide	6%
NaOH + Na_2O (any proportion of the two from 0 to 100%)	6×10^{-3} lb/ft^3*
Na_2CO_3	5×10^{-4} lb/ft^3*

8. TMBDB sensors inside containment shall be functional with the following masses of settled and plated aerosols (NaOH, Na_2O, and Na_2CO_3) on any unprotected horizontal or vertical surfaces in containment.

Horizontal Surface	80 lb/ft^2
Vertical Surface	0.5 lb/ft^2

*For 0-500 hours.

9. TMBDB sensors inside containment shall be functional with radiation levels of:

Peak radiation level	1×10^6 R/hr
Average radiation level over 30 days	1×10^5 R/hr
Total accumulated dose	1×10^8 R

The above doses are the sum of β and γ releases, which are estimated to be of equal magnitude.

10. The instruments monitoring radioactivity of products leaving the cleanup system shall provide count rates for particulate (including Pu), radioiodine and gaseous release.

11. The radiation monitoring sensors shall be functional with atmosphere maximum constituent concentrations of:

Oxygen	21%
Nitrogen	90%
Water Vapor	Saturated
Hydrogen	8% (volume)
Carbon Dioxide	6% (volume)
$NaOH + Na_2O$ (any proportion of the two from 0-100%)	6×10^{-5} lb/ft^3
Na_2CO_3	5×10^{-6} lb/ft^3

12. The TMBDB instrumentation systems shall be capable of remote manual actuation from the reactor control room. The indicators shall be located in the reactor control room.

2.1.2.13 Electrical Power System

1. Class 1E electrical power shall be provided to all TMBDB systems and components that require electrical power to perform their post accident functions.

2. Electrical loads for TMBDB features shall be remote manually actuated from the reactor control room except for the TMBDB instrumentation which shall be normally connected to Class 1E electrical power.

2.1.2.14 Containment Structures

1. The reactor cavity and pipeway structures shall not collapse prior to sodium boildry. Structural conditions at boildry for the various scenarios are enveloped by the temperatures on Figures 2-9 through 2-18.

2. The reactor containment building and confinement structure shall retain their integrity above the basemat indefinitely based on the limiting temperatures on Figures 2-19 through 2-31.

2.1.2.15 Reactor Control Room Habitability

The exposure to the reactor control room operators following a TMBDB condition shall not exceed the following limits in 30 days:

Organ	Dose (rem)
Whole Body*	25
Thyroid	300
Lung	75
Bone	150
Skin (beta)	150

*The whole body gamma dose consists of contributions from airborne radioactivity inside and outside the reactor control room, as well as direct shine from fission products inside the RCB.

(Because the postulated occurrence of the TMBDB scenario is of such a low probability as to be excluded from the category of a design basis accident, exposure limits intended for design basis accidents should not apply. The 25 rem whole body dose limit for the reactor control room operators corresponds to the once in a lifetime accidental occupation exposure limit recommended in Reference 2-1. The thyroid limit is based on the 10CFR100 equivalent of a 25 rem whole body dose. The corresponding bone and lung limits are the accepted equivalents to the 25 rem whole body dose (Reference 2-2).)

2.2 DESCRIPTION OF DESIGN FEATURES

The design features that are provided to meet the requirements in Section 2.1 are described below. These features are considered in the analysis of thermal and radiological margins discussed in Sections 3 and 4.

Although some of these features may serve a function as Safety Class equipment or as Engineered Safety Features to mitigate a CRBRP design basis event, the features are not considered Engineered Safety Features for the purpose of performing their function of mitigating a core melt event beyond the design basis. However, as noted in Section 2.1.1 these features are designed to the specifications and requirements associated with Safety Class 3 components and systems.

2.2.1 Reactor Cavity to Containment Barrier

The response of the reactor closure head and head-mounted components, and their associated seals to the TMBDB dynamic loadings requires that the head assembly remains intact and integral and the sealing structures remain functional and meet their leakage requirements for 1000 seconds after the dynamic loads. For head mounted components, no special TMBDB seals are required since the sealing systems used for normal operations and to meet SMBDB requirements can meet the TMBDB requirements. These sealing systems are described in Section 5.2.1.3 of the PSAR. For annuli between the head plugs, a special margin seal is provided to the riser annuli sealing system (see Section 5.2.4.4 of the PSAR) to meet the TMBDB leakage requirements. The margin seal design has elastomer-to-metal contact in the area of the bearing races to limit leakage through the bearing.

The reactor cavity to head access area sealing system consists of the reactor cavity seal, which is a low alloy steel circular membrane with an L-shaped cross-section. This reactor cavity seal is bolted to the reactor vessel closure head and to the edge of the reactor cavity support ledge. Sealing is provided between the reactor vessel closure head and the reactor cavity seal by a [illegible] gasket. High temperature packing provides the seal between the reactor cavity support ledge and the reactor cavity seal. Gasket caps provide sealing over the reactor vessel holddown bolts and nuts.

2.2.2 Reactor Cavity Recirculating Gas Cooling System

The Reactor Cavity Gas Cooling System provides cooling of the atmosphere of the reactor cavity.

The special features of this system which are not specifically for TMBDB but which provide additional thermal margin for the plant are the automatic gas isolation valves on the cavity cooling system inlet and outlet lines which are capable of withstanding the thermal and pressure conditions encountered at the valves. The valves are located in Cell 105 just outside the reactor cavity wall and are actuated by the sodium leak detection system or by a high gas temperature signal. The process temperature that the valves are exposed to is expected to be substantially less severe than the conditions in the reactor cavity because the piping configuration acts like a large loop seal. Before sodium or sodium vapors could reach the valves the long run of piping allows cooling of the atmosphere in the piping. In addition, the closure of the valves would occur within seconds after the penetration of the reactor vessel and guard vessel so the flow conditions in the piping would be essentially stagnant. Finally, outside of the isolation valves the system is a closed circuit system so the small amount of sodium leakage through the valves would not enter Cell 105.

2.2.3 Guard Vessel Support

The design requirements for the guard vessel support are accomplished by raising the guard vessel support skirt approximately 5 inches off the floor on steel blocks. This provides 48 openings which are each approximately 5 inches by 6 inches and allows dispersion of the liquid sodium and fuel particulate underneath the guard vessel support and into the reactor cavity. Figure 2-32 depicts the details of this arrangement.

2.2.4 Reactor Cavity and Pipeway Cell Liners

The reactor cavity (RC) and pipeway cell liner are described in Section 3A.8.2 of the PSAR and in Section 3.2.2.5 of this report. Two additional features have been added to reactor cavity cell liner to provide additional thermal margin. The space between the RC liner and concrete is divided into four zones by horizontal baffle plates which a welded to the liner. The reactor cavity liner is fabricated from carbon steel and its purpose is to protect the concrete from the sodium and to direct the steam generated behind the liner to the liner vents.

The baffle plates, shown on Figure 3-34, are provided for zoning of the space behind the RC liner to prevent sodium, steam, or reaction products propagating from one zone to another and to positively separate the venting system into four zones (three along the vertical wall and one including the floor and corner).

The carbon steel solid baffle plates are welded to the liner and extended two feet radially into the wall. The two foot width is selected to ensure that the baffle plates extend into non-degraded concrete until well past the time that liner integrity is important. The baffles are attached to the back of the liner plates near the RC floor, 8 and 26 feet above the floor respectively. Similarly, baffle plates are included behind the pipeway cell liners to separate the walls, floor and roof of each cell.

In addition the anchors for the cell liner are lengthened so that they will remain anchored in non-degraded concrete until integrity is no longer important.

2.2.5 Reactor Cavity and Pipeway Cell Liner Vent System

2.2.5.1 General

The Reactor Cavity and Pipway Cell Liner Vent System is a subsystem of the cell liner steam venting system which functions to remove steam and gases from behind all inerted cell liners in order to prevent failure of the liners due to pressure buildup behind the liner (See PSAR Section 3A.8.2 for a description of the cell liner system including the vents). The system consists of embedded piping connected to the 1/4" gap between the liner and the insulating concrete. The system contains no active features. The piping system is sized so that with ambient pressure in the cell, the liner could collect and vent the peak steaming quantities without exceeding 5 psig differential pressure behind the liner. The pressure drop through the 1/4" air gap was calculated using Darcy's formula for compressible flow in pipes using a hydraulic radius appropriate to the configuration of the gap. Analyses indicated that a 5 psig differential pressure acting behind the liner would result in acceptable plate deflections and an adequate safety margin in the design of the liner vent system.

Deflection of the liner would occur under the TMBDB pressure and temperature conditions; however, the pressure drop behind the liner is a small fraction of the total vent system pressure drop. The reduction in the 1/4" gap will not cause a measurable increase in the steam pressure behind the liner, and cannot cause failure of the liner anchorage system. The close spacing of liner anchors (12" centers) ensures that sufficient flow passages will remain open to pass all the steam and gases that will be produced.

The liner venting system piping will be 100% redundantly installed. In addition, the peak steaming rate occurs immediately after reactor vessel and guard vessel penetration and decreases thereafter; the steaming rate and pressure behind the liner will be greatly reduced from the system's design value before any significant degradation of the concrete occurs. Any reduction of available flow area would be mitigated by the redundancy in the vent pipes. If partial clogging of vent pipes occurs, it would be acceptable at the times when structural degradation of the concrete is expected due to the existing margin available and required vent area. The redundant lines are physically separated to minimize the common potential for line blockage although no mechanism for blockage has been identified.

The steam vent piping integrity will be assured so that the effects of high temperature transients and the weight of degraded concrete resulting from cracking of concrete will not result in unacceptable stresses. If necessary, the design will be modified to preclude restrained thermal growth by providing compressible material between the outer pipe wall and the concrete, thereby allowing for the free thermal expansion of the embedded vent pipe.

Only a thin layer of concrete, generally the lightweight concrete and a portion of the structural concrete not exceeding 5% of the thickness, is expected to be totally degraded before sodium boildry. This degraded concrete is not expected to impose a significant load on the vent pipes due to the presence of the reinforcing steel mesh, the stud anchors, and the tendency of the sections of the degraded concrete to be self supporting by arching action over the piping system.

In the cavity walls, the liner anchors, spaced at 12" on center and properly anchored in non-degraded concrete, will keep the degraded concrete in place and prevent spalling. The R&D program that confirms this assumption is the Sodium Spill Design Qualification Test noted in Appendix A.6.

The redundant liner vent system will prevent water accumulating behind the liners after construction and during operation. The released water will evaporate and be vented into Cell 105 or to containment above the operating floor. Thus, the potential for any explosions between liquid sodium or fuel and water immediately after guard vessel penetration does not exist.

The reactor cavity liner venting subsystem has special features to provide thermal margin in the event of a HCDA. These features are discussed below.

2.2.5.2 Reactor Cavity Floor Liner Vent

The reactor cavity floor liner space is vented directly above the operating floor because failure of this portion of the liner is postulated early in the scenario. Venting directly to containment reduces the potential for sodium and hydrogen to enter Cell 105.

2.2.5.3 Reactor Cavity Wall and Pipeway Cell Liner Vents

The submerged RC wall is vented to Cell 105 through a standpipe. The standpipe is provided because submerged liner failure is postulated at 50 hours and the standpipe will prevent sodium from entering Cell 105. The upper reactor cavity and the pipeway cells liner areas are vented to the atmosphere of Cell 105. It is desirable to vent these areas to Cell 105 to reduce the containment atmosphere pressure that would result from additional volume of gases above the operating floor.

Each liner vent system pipe, upstream of the release point to Cell 105 is provided with a loop seal to prevent sodium vapors from entering Cell 105 after liner failures. The loop seal is sized such that it will permit steam venting without exceeding a liner back pressure of 5 psi. Following liner failure, some sodium vapor could enter the liner venting system; however the driving pressure will not exceed 1 psi for this condition (see Figure 2-4). Sodium condensation in the loop seal and the resulting liquid level will prevent the passage of sodium vapor beyond the loop seal for driving pressure up to 1 psi. Thus the liner vent system can meet its requirement to permit release of steam before liner failure while preventing excessive release of sodium vapor after liner failure.

2.2.6 Reactor Cavity Vent System

The function of the reactor cavity venting system is to prevent overpressurization of the reactor cavity after penetration of the reactor vessel and guard vessel and to promote maximum exchange of heat between the vented cavity gases and the pipeway cell structures before releasing the gases above the operating floor. See Figure 2-33 for the system flow diagram.

The system is actuated by rupture disks. The rupture disks are installed redundantly so that failure of one disk to break would not affect the accident results. The setpoint of the rupture disks is above the predicted pressure for sodium spills in the reactor cavity, so a design basis accident would not open the rupture disks.

The arrangement of the system reflects these functions as follows. The gases and vapors from the Reactor Cavity are vented thru the pipeway cells, which are isolated from the PHTS cells by flexible, low leakage bellows. The venting to the operating floor is accomplished from the North (No. 2) pipeway cell through shielding labyrinths and straight upward pipes, to minimize reactor cavity back pressure due to head losses and to promote local flaring of the vented hydrogen. Up to 50% of the vented gases enters the North (No. 2) PHTS pipeway cell directly and the remaining gases are first vented through the East and West (No. 1 & 3) pipeway cells ($\geq$25% each), then through the North (No. 2) pipeway cell. To assure this flow distribution a gas flow labyrinth is provided in the North pipeway cell, to balance the flow and pressure thru the different vent paths. In this way, maximum heat exchange between the gases and the building structures is facilitated. This will reduce the maximum internal building pressure in the containment before venting. In addition, this arrangement ensures that if only one rupture disk breaks, flow through all pipeway cells occurs, whereas, if a rupture disk were provided for each pipeway, the rupture of one disk could lower the pressure in the cavity below the setpoints of the other two without providing heat exchange between all of the pipeway cells and the vented gases.

Isolation of the rupture disks is provided by remote manually operated gate valves located between the cavity and the rupture disk assembly. These valves are provided to allow periodic replacement of the rupture disks and to provide isolation of the reactor cavity atmosphere should a disk be ruptured under other than TMBDB conditions. To prevent inadvertant operation of these valves, no local operators will be provided, valve position indication will be displayed in the Control Room, and appropriate physical restraints and warning plates will be used for the valve actuation switches. These valves are normally open.

Uncertainties in rupture disk performance were considered in the reactor cavity venting system. The overall scenario analysis results are not sensitive to the exact pressure at which the rupture disk breaks because the rate of pressure increase is large enough so that the rupture disk will break at about the same point in time regardless of the exact reactor cavity pressure. Commercially available rupture disks are usually guaranteed to break within 10% of set pressure. In addition, it was assumed in the TMBDB analysis that only one of the rupture disks breaks.

Analysis has shown that clogging of the piping by sodium reaction products should not be a problem because of the small quantity of aerosol expected and because of the large surface areas available for deposit in reactor and pipeway cells as compared to the small surface areas of the vent system piping. Appendix G.3 shows that margin exists to accommodate a wide range of postulated vent malfunctions.

The system piping material will be suitable for high temperature service. The piping is sloped toward the cavity to provide drainage of condensed sodium. Cell liner penetrations will utilize a combination of bellows sleeves and flued heads in order to reduce pipe stress to a minimum value for the non-embedded portions of the piping. For the embedded piping, anchorage will be provided to prevent piping failure due to thermal expansion and degradation of the supporting concrete.

2.2.7 Containment Purge Capability

The containment purge cabability is provided by the containment cleanup system exhaust blowers which draw a negative pressure in the containment building and by the opening of the redundant containment purge penetrations. The system is shown on Figure 2-34 and has total active redundant capability.

The two purge pipes penetrating the containment are 18 inches in diameter and are designed to the requirements of the ASME Boiler and Pressure Vessel Code, Section III, Division I, Class 2. Each purge line is provided with redundant normally closed isolation valves outside of the steel containment vessel (see Section 2.2.11).

Should a purge of the RCB be required, it would be necessary to vent the RCB first. The venting, along with operation of the containment cleanup system exhaust blowers, decreases the RCB pressure below atmospheric pressure. Operation of the purge requires the opening of the purge line isolation valves from a remote-manual station in the main control room. Flow direction sensing instrumentation is provided to automatically close the purge isolation valves in the event a backflow condition occurs. To prevent inadvertent operation of the purge, the switches for the valve operators are located on a control room panel; no local operators are provided at the valve locations. Valve position indication will be displayed in the Control Room and appropriate physical restraints and warning plates will be used for the valve switches.

2.2.8 Containment Vent Capability

The RCB vent capability is provided by the vent line connected to the Containment Cleanup System. The connected system is shown in Figure 2-34. This vent capability allows the blowdown of the RCB after some time period to reduce the internal pressure and to subsequently reduce the hydrogen concentration through purging. Prior to venting complete isolation of the RCB would be maintained. The vent line is connected to the TMBDB cleanup system through two redundant 24-inch inside diameter pipes which penetrate the RCB with isolation valves located outside the steel containment vessel (see section 2.2.11). The vent line and pipes penetrating the RCB are designed to the requirements of the ASME Boiler and Pressure Vessel Code, Section III, Division I, Class 2. The pipes penetrating the RCB which are used for TMBDB have their valves in the normally closed position.

At the time of venting (estimated to be approximately 36 hours), the isolation valves would be opened to allow the depressurization of the RCB at a maximum rate of 24,000 cfm. The effluent of the depressurization is processed through the Containment Cleanup System.

To prevent inadvertent operation of the valves, no local operators would be provided and the valve actuation system would be equipped with appropriate physical restraints and warning plates.

2.2.9 Containment Cleanup System

The Containment Cleanup System is shown in Figure 2-34 and is provided for filtering of the Reactor Containment Building (RCB) atmosphere prior to release to the environment. The RCB atmosphere exhausted by the Containment Ve it System is treated by a wet scrubber filtration system. The discharge fro the filters is then directed through an exhaust pipe for release at the top f the confinement structure. In addition, the effluent stream is continuously monitored for the levels of particulates, radioiodine, radiogases, and plutonium.

The exhaust filter train is comprised of a jet venturi scrubber in series with a high efficiency wetted fiber bed scrubber unit and redundant blowers. An air washer is located upstream to ensure that virtually all of the sodium oxide is reacted to sodium hydroxide prior to reaching the scrubbers. Additionally, the air washer effectively reduces the air stream temperature from a maximum of 1100^{o}F to approximately 160^{o}F during system operation. The filter train is rated for 24,000 acfm at an air density of 0.06 lbs/ft^3 and will provide a minimum overall filtration system efficiency of 99 percent for all vented solids and liquids and 97% for all vented vapors (excluding noble gases).

The wet scrubber filter system is designed such that the temperature of the aerosol leaving the scrubbers would be maintained below 160^{o}F during the course of the accident. The 150,000 gallon storage capacity of the scrubbing system would accommodate the design level of 300,000 lbs. of containment reaction products.

The wet scrubber filter system requires protected water storage on the order of 150,000 gallons. The recirculation pumps supply approximately 2600 gpm of continuous water flow from the storage tanks to the sodium scrubbers and air washer. Discharge water is then returned to the water supply system. A maximum concentration of sodium hydroxide of 30 percent (by weight) with a corresponding pH of 13 will result from this recirculation in the storage tanks. A heat exchanger, designed for the peak heat load, is provided to ensure cold water supply to the scrubbers during system operation. Cooling water for the heat exchanger and make-up water for the storage tanks are supplied from the Emergency Plant Service Water System.

Hydrogen could only be generated in scrubber units if unreacted sodium were to enter the system. Due to the availability of oxygen and water vapor in the containment and the rapid reaction rate of sodium, no elemental sodium is expected to be present in the scrubber system. Therefore, hydrogen would not be generated in the system.

The water storage tanks, recirculation pumps, heat exchanger, air washer, sodium scrubbers and blowers are located in the Reactor Service Building adjacent to the Reactor Containment Building. The Reactor Service Building is designed as a tornado hardened Seismic Category I structure.

All power requirements of the Containment Cleanup System are supplied from Class 1E redundant power supplies.

Failure of passive components in the Containment Cleanup System is extremely unlikely and the system design has no special provisions for such unlikely failures. However, backup capabilities are provided for all active components, such that failure of any one active component will not preclude 100% operation of the Containment Cleanup System.

2.2.10 Annulus Air Cooling System

The Annulus Air Cooling System is designed to ensure that the structural integrity of the steel containment vessel and concrete confinement building is maintained based on realistic evaluation of TMBDB conditions. These conditions include an increase in the temperature of the steel containment vessel, confinement annulus air, and concrete confinement building. Before actuation of the Annulus Air Cooling System during the postulated TMBDB event, the containment systems function in the same manner as for the design basis accidents occurring inside containment as described in the PSAR.

Radionuclides leaking from the RCB will be confined and treated by the Annulus Filtration System. The control room operator would determine if a reactor vessel penetration had occurred and [illegible]ate the TMBDB features operation at some time beyond 24 hours. It is estimated that the Annulus Air Cooling System would not need to be placed into operation until approximately 36 hours after the reactor vessel penetration. However, it would be permissible to utilize this system any time beyond 24 hours.

When cooling is required, outside air would be introduced into the annulus area through an opening in the confinement structure. Vane axial fans, located in the Reactor Service Building supply air to the annulus space. Redundant fans are provided to ensure adequate redundancy in the system.

The confinement annulus is partitioned to provide a spiral air flow path around the containment vessel from the 816 foot elevation to above the containment spring line. The annulus partition system is designed such that an effective annular flow area of between 180 and 250 square feet is obtained up to elevation 926'-0" and a flow area between 450 to 600 square feet from elevation 926'-0" to the top of the confinement building. These flow areas ensure a velocity range of 2200 to 1500 FPM and 850 to 700 FPM, respectively, are maintained for heat removal. Additionally, the partitions provide a platform system for periodic inspection of the containment vessel penetrations.

Operation of the Annulus Air Cooling System limits the peak containment vessel and confinement structure temperatures to maintain structural integrity following an HCDA.

Leaktight motorized dampers are provided on the entrance of the fan enclosure and on the outlet of the plenum at the top of the confinement structure. Missile hardened enclosures and intake debris screens protect the fans and the exhaust opening.

Should system operation be required, the fans and dampers are operated from a remote-manual station in the main Control Room. To prevent inadvertent operation of these fans and dampers, no local operators or control stations will be provided, damper position indication will be displayed in the Control Room, and restraints and warning switches used for the appropriate actuation switches.

All power requirements of the Annulus Air Cooling System are supplied from Class 1E redundant power distribution systems.

Backup capabilities are provided for all active components, such that failure of any one active component will not preclude 100% operation of the Annulus Cooling System.

2.2.11 Containment System Leakage Barrier

The Containment System is described in PSAR Sections 6.2.1 and 3.8.2. The Containment Isolation System is described in PSAR Sections 6.2.4 and 7.3.1.

The containment inner cell structures are described in PSAR Section 3A.1 and are below the operating floor. The TMBDB equipment is located in the Reactor Service Building and the Reactor Containment Building. The Reactor Containment Building and Reactor Service Building are Seismic Category I buildings located on the common basemat with other Seismic Category I buildings.

The design internal pressure for the containment is 10 psig, and the associated maximum allowable leakage rate is 0.1 (vol.) percent/24 hours. The design methods to assure integrity of the containment from the design basis accident conditions are descr ' in PSAR Section 3.8.2. A negative pressure is maintained in the confinement/containment annulus space and the confinement/containment penetrations are designed to maintain a bypass leakage value of less than 0.001 wt % per day for design basis accidents. PSAR Table 6.2-6 lists each containment penetration and its leakage in lb/day.

The expectation that the containment isolation system will be capable of performing its intended function in the containment environment associated with the TMBDB scenario is based on the fact that the initiation and isolation of the Reactor Containment Building will occur at a time when the environmental conditions are the same or less severe than the containment design basis accident conditions.

Two vent and two purge lines penetrate the reactor containment vessel. These lines communicate with the Reactor Containment Building atmosphere and are each provided with (two) redundant isolation valves. These isolation valves are located outside of the containment. General Design Criterion 47 for the CRBRP specifies one valve inside and one valve outside of the containment "unless it can be demonstrated that the containment isolation provisions for a specific class of lines ... are acceptable on some other defined basis". Since the vent and purge isolation valves are only required to open at least 24 hours into the TMBDB scenario, and the containment atmosphere conditions are very severe, it was elected to locate these valves outside of the containment to assure their operability. To meet the intent of Design criterion 47, that portion of the vent and purge lines outside the RCB up to and including the second valve is designed and will be tested to containment standards. Furthermore, the isolation valves are normally closed, fail-closed types and are locked closed in the control room. No local operators are provided for these valves and an interlock will be provided to prevent opening these valves during plant power operation. Bypass of this interlock will be permitted only when the containment structural integrity would be challenged as indicated by containment pressure, temperature and hydrogen concentration measurements. The testing of these valves will be conducted during refueling shutdowns.

2.2.12 TMBDB Instrumentation System

2.2.12.1 Containment Instrumentation

The reactor containment instrumentation system provides measurements of reactor containment pressure, atmosphere temperature, steel shell temperature and hydrogen levels. Each of these measurements will be redundant, designed to remain functional following a Safe Shutdown Earthquake, and qualified to assure operability under the environmental conditions in Section 2.1.2.12. The locations of the various detectors are shown schematically in Figure 2-35.

2.2.12.1.1 Reactor Containment Pressure

The Reactor Containment Building pressure is measured at two widely separated locations. The instrumentation penetrations are at 108^0 and 285^0 (0^0 is plant north). The design will be such that the pressure element and transmitter are located outside of the Reactor Containment Building and will sense pressure with an impulse or capillary line. This arrangement will allow sensing of containment pressure at temper·.ure up to 1100^{0}F. Each transmitter will send a signal to the main control room. The channels will be completely independent and physically separated in accordance with Regulatory Guide 1.75. Each channel will be powered from the Class 1E power system.

2.2.12.1.2 Reactor Containment Atmosphere Temperature

The Reactor Containment atmosphere temperature is measured near the top of the RCB. The measurement will be redundant so that any single failure will not preclude the operator from receiving temperature data. The channel will be designed to operate 500 hours to a maximum temperature of 1100^{0}F.

The signal conditioning for the temperature sensors will be located in the Steam Generator Building. Each transmitter will send a signal to the main control room. Each channel will be physically separated in accordance with IEEE 384-1974 and will be powered from the Class 1E power system.

2.2.12.1.3 Reactor Containment Vessel Temperature

The Reactor Containment Vessel temperatures will be measured at selected locations on the inside of the steel shell.

2.2.12.1.4 Hydrogen Measurement System

The containment atmosphere hydrogen concentration measurement system consists of redundant, independent and continuous hydrogen analyzers located in the Intermediate Bay of the Steam Generator Building. These are connected to the containment atmosphere through redundant and independent sampling lines. The inlet to the sampling lines is located at the top of containment to prudently protect against hydrogen stratification even though stratification would not occur (Section 3.2.1). Sample transport time and sample plate out will be considered in establishing the exact location of these sampling stations. Each sampling station will include a hydrogen analyzer which will transmit a signal to the main control room. The channels will be physically separated and powered from the Class 1E power system.

The hydrogen measurement system involves severe environmental conditions arising from high temperature and aerosol contamination which may limit instrument lifetime. In view of this, early procurement of this equipment will be initiated. It is anticipated that the procurement process will provide confirmation as to whether this equipment can be obtained from existing sources or whether additional development or design verification requirements are necessary.

2.2.12.2 Radiation Monitoring

Since containment could be vented beyond 24 hours (although such venting is not needed for 36 hours) and therefore most of the radiological release would be through the vent and filter systems, radiation monitors are provided downstream of the filter system where the releases to the atmosphere would occur.

The redundant filter train monitors provide for determination of the radioactivity being released from the filter train. Monitoring will be accomplished using isokinetic sampling nozzles and associated three channel continuous air monitors (CAMs) which provide one channel each for particulates, radioiodines, and radiogases. The detectors and associated electronics are shielded to reduce the accident induced radiation background to levels suitable for system operation.

The three channel CAMs will provide gross count rates for each channel. The predicted radioisotopic inventories within the RCB coupled with gross count rate data will allow estimates of off-site doses to be made and will provide early identification of rapid and/or significant changes in release concentrations.

In addition, a suitably shielded plutonium air particulate monitor (PAPM) specifically designed to measure very low concentration of the long half-life alpha emitters, such as Pu-239, will be provided and will also continuously isokinetically sample the common exhaust. The PAPM provides capability for identifying the plutonium releases at the point where such releases would be the most concentrated and in this way maximizes the sensitivity of the measurement.

Redundancy is provided for the CAMs by the common exhaust monitor and is required due to the inaccessibility of the channels under accident conditions. Redundant PAPMs are not required due to the inherent redundancy of a typical PAPM which is provided as a means of accounting for the natural radon-thoron background (switching collection between dual channels allows the radon-thoron on the "idle" channel to decay (leaving behind the longer lived isotopes)).

The power requirements for the plant radiation monitoring system are supplied by the 1E power distribution system.

Provisions for off-site monitoring are described in the TVA Radiological Emergency Plan, as discussed in Section 13.3.11 of the PSAR.

2.2.13 Electrical Power System

The electrical power requirements for motors, controls, and instruments will be distributed as part of the Class 1E electric power system using the appropriate standards of quality assurance, structural support, and physical separation.

These loads will, however, be remote manually connected to the 1E power source from the control room after removing other loads which are not essential during TMBDB conditions.

2.2.14 Containment Structures

As a result of the structural analysis of the containment building, a few changes in the design have been made to provide increased thermal margins. These include:

1. Modifications of the typical cell liner design have been made in the Reactor Cavity and the pipeway cells. Specifically the modifications are in the wall studs anchor size, spacing, and length, and in the size of the supporting beams in the pipeway floor.

2. Additional reinforcing bars and stirrups are provided in the reactor cavity wall to resist shear, compressive forces, and bending moments at the base, near the top and in the regions restrained by vertical walls.

3. Additional reinforcing bars and stirrups are provided in the pipeway cells to resist the thermal forces and moments.

4. Additional reinforcing bars are provided in the foundation mat, the confinement structure and the containment concrete walls below the operating floor.

The results of analysis of these features and compliance with design requirements are included in the structural analysis in Section 3.

2.2.15 Control Room Habitability

The control room habitability design bases and features are described in PSAR Section 6.3. The control room HVAC System design includes dual control air intakes for control room pressurization. One control room HVAC intake is located at the SW corner of the control building roof and the other one at the NE corner of the steam generator building roof. The HVAC System in conjunction with the radiation monitoring system is provided with the capability to select the air intake for the control room pressurization which is exposed to a lower airborne contamination.

The assumptions used in the control room dose analysis are as follows:

1. Source Term Data: (see case 2 of Section 4.1)

    a. Initial Release to RCB

        100% Noble Gases
        100% Cs and Rb
        1000 lb. of Na with 100 PPB Pu
        0.026% Fuel, Halogens and Solid Fission Products

    b. Release to RCB During Sodium Vaporization

        100% halogens
        100% Te, Se, Sb
        1% Solid Fission Products
        0.015% Fuel
        1.1×10^6 lb of Na

2. RCB Exhaust Filter Efficiencies Assumed:

Class	Efficiency (%)
Noble Gases	0
Halogens	97
Se, Sb	97
Solid Fission Products	99

3. Control room filtered intake rate (500 CFM) and Recirculation (8000 CFM). An unfiltered in-leakage of 3 CFM was assumed throughout the analysis to account for door opening and other unknown leakages.

4. Atmospheric dilution factors (X/Q - values):

   a. Wind speed of 1 m/sec with Pasquill Type D
   b. Building wake effect is included
   c. Long term X/Q adjustment factors are included
   d. Dual intakes placed in major (Class 1) buildings
   e. Guidelines of References 2-3 and 2-4

Atmospheric diffusion factors based on above conditions are:

Time Intervals:	0-8 hrs	8-24 hrs	1D-4D	4D-30D
X/Q-values: (sec/m^3)	6.18×10^{-4}	5.21×10^{-4}	2.54×10^{-4}	9.10×10^{-5}

5. Occupancy Factors

Time Intervals:	0-8 hrs	8-24 hrs	1D-4D	4D-30D
Occupancy Factors:	1.0	1.0	0.6	0.4

6. Breathing Rates

Time Intervals:	0-8 hrs	8-24 hrs	1D-30D
Breathing Rates: (m^3/sec)	3.47×10^{-4}	1.75×10^{-4}	2.32×10^{-4}

The resultant radiation doses for control room operators are:

30-Day Accumulated Dose (Rem)

Organs	Whole Body	Beta Skin	Thyroid	Lung	Bone
Dose (Rem)	4.37	52.9	19.8	0.62	2.01
Guideline	25	150	300	75	150

2.3 OPERATOR ACTION SEQUENCE

The operator action sequence following an HCDA would be as follows:

1. Shortly after the HCDA the various core and primary heat transport system instrumentation would indicate that some unidentified event has occurred, either because of readings outside the normal band or indications of failure of the instrumentation. The event might not be identifiable because the core and PHTS instrumentation is not designed to withstand an HCDA.

2. Immediately after the unidentified event, only actions such as those associated with design basis accidents would be taken in the short term. For instance, containment would isolate and the annulus filtration system would be activated when the radiation monitors sense an abnormal radiological release to containment. The operator would not perform any actions specifically related to TMBDB features.

3. In accordance with PSAR Section 13.3.3, NRC and the Tennessee Department of Public Health would be notified of the accident.

4. If materials are released to the reactor cavity following an HCDA, these releases would be expected to be monitored by radiation, temperature and pressure sensors in the reactor cavity in the short term. However, no operator actions with respect to TMBDB features are required or expected as a result of this information.

5. The operator would only act on information from the containment TMBDB instrumentation that indicates an increase in containment atmosphere pressure and temperature and the presence of hydrogen in the atmosphere that would challenge containment integrity. For design base events (not an HCDA), containment would not be challenged and the operator would not take any action to initiate operation of the TMBDB features.

6. No operator actions that would violate containment integrity (such as venting) or degrade the operation of Engineered Safety Features would be required or expected during the first 24 hours.

7. Beyond 24 hours, the operator would initiate operation of TMBDB features as required to maintain long term structural integrity of the containment. Detailed technical specifications and administrative controls will be included in the information provided for the operating license review. The following are typical of actions that would be taken by the operator:

   A. The annulus cooling system would be activated when the containment steel shell temperature reaches a prescribed value ($\sim$400 to 500^{o}F). At this time the annulus filtration system (design base system) would be deactivated.

   B. The operator would vent containment through the TMBDB venting system when the pressure reaches a prescribed value ($\sim$15 to 20 psig), or the hydrogen concentration reaches a prescribed value (such that the concentration does not exceed 6% either before or after venting). Immediately preceding the containment venting, the cleanup system would be activated. (The TMBDB containment cleanup system is separate from the design base annulus filtration system). Preceding both of these actions the TMBDB features would be manually connected to 1E power supply system.

   C. When it is decided to vent the RCB, the Containment Vent isolation valves would be opened so that the pressure in the RCB can decrease to the atmospheric pressure.

   D. After the RCB has been depressurized, the Containment Cleanup System Exhaust blowers would be turned on and the purge isolation valves opened. The cleanup system exhaust blower would produce a suction to pull purge air through the containment.

E. When the gases released from concrete and the reactions in containment cease, the venting, purging, and cleanup systems operation could be terminated.

F. When the containment steel shell temperature falls below 200°F, the operation of the annulus cooling system could be terminated.

The results of analyses in Section 3 indicate that activation of TMBDB features by operator action would not be required for about 36 hours (although permitted after 24 hours) following an HCDA. Because of the long time available before operator action would be required, the actions are not sensitive to variations in the scenario, such as reactor vessel penetration times ranging from 100 to 10,000 seconds.

2.4 REFERENCES

2-1 Basic Radiation Protection Criteria, NRCP Report No. 39, National Council on Radiation Protection and Measurements, Washington, D. C., 1971.

2-2 "Site Suitability Report by the Office of Nuclear Reactor Regulation U.S. Nuclear Regulatory Commission in the Matter of the Clinch River Breeder Reactor Plant," U.S. Nuclear Regulatory Commission, Docket No. 50-537, March 1977.

2-3 U.S. Nuclear Regulatory Commission Standard Review Plan, "Section 6.4, Habitability Systems," NUREG-75/087, Rev. 1, U.S. NRC, Washington, D.C.

2-4 K. G. Murphy and K. M. Campe, "Nuclear Power Plant Control Room Ventilation System Design for Meeting General Design Criterion 19," in Proceedings of the Thirteenth AEC Air Cleaning Conference, San Francisco, California, 12-15 August 1974, CONF-740807, Vol. 1, March 1975, pp. 401-430.

TABLE 2-1

CRBRP FEATURES PROVIDING THERMAL MARGIN BEYOND THE DESIGN BASE

Specific Systems or Components for TMBDB	PSAR Section
1. Reactor Cavity Vent System	3.8
2. Containment Cleanup System	6.2
3. Annulus Cooling System	6.2
4. Containment Vent and Purge System	9.6
5. Instrumentation and Radiation Monitoring	6.2
Systems or Components with Augmented Capabilities for TMBDB	
6. Dual Control Room Air Intakes	6.3
7. Reactor Cavity and Pipeway Cell Liners	3A.8
8. Liner Vent System	3.8
9. Guard Vessel Support	5.2
10. Reactor Cavity to Head Access Area Seals	3A.1
11. Reactor Cavity Recirculating Gas Cooling System	9.7
12. Containment-Confinement System (including insulation)	6.2
13. Emergency Electrical Power System	8.2 & 8.3
14. Reactor Containment Structures (Addition of Reinforcing Steel)	*

*Details Pertinent to TMBDB not provided in the PSAR.

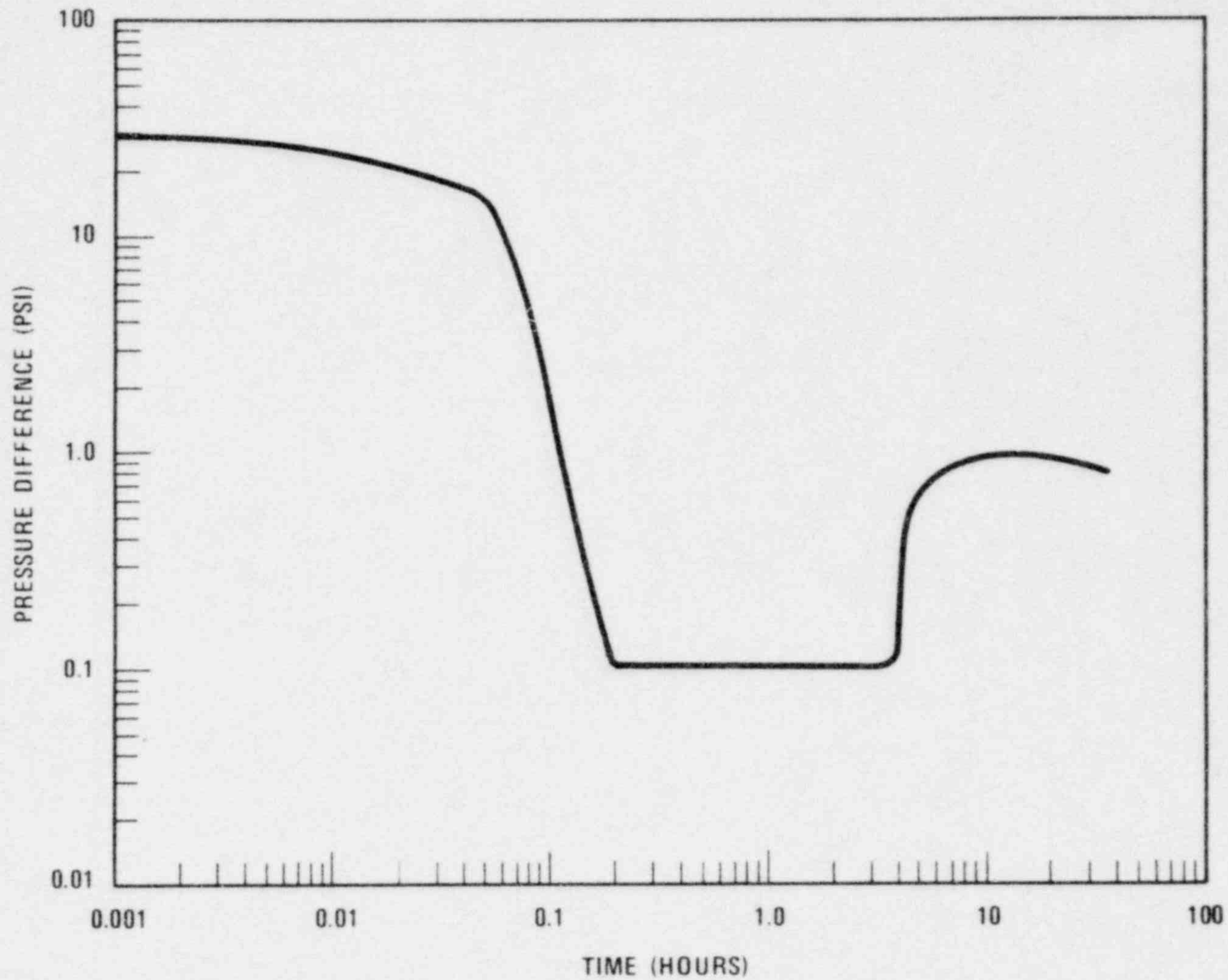

Figure 2-1 Maximum Pressure Differential Between the Reactor Cavity and Head Access Area

1966-2

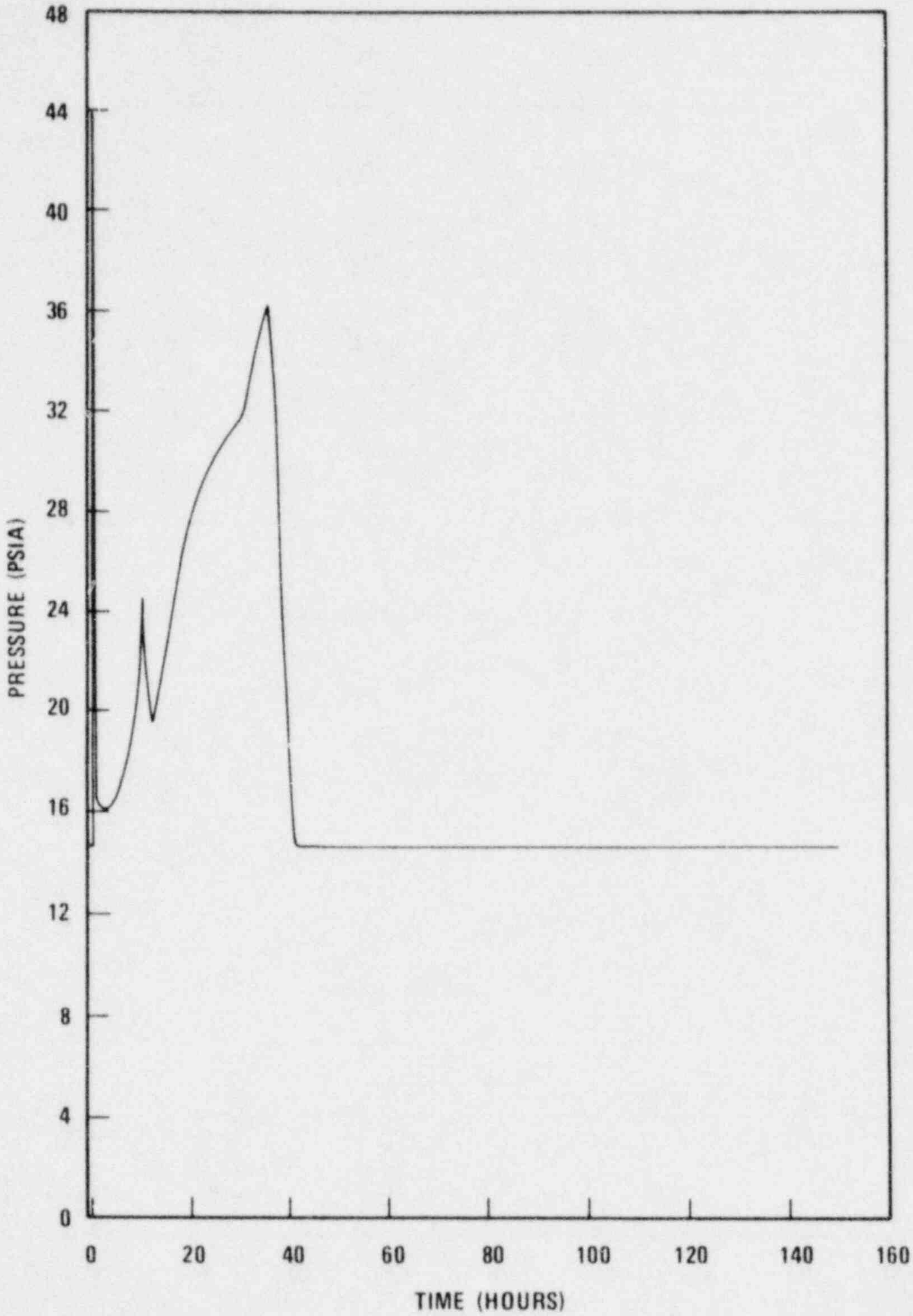

Figure 2-2 Maximum Reactor Cavity Atmosphere Pressure

1966-3

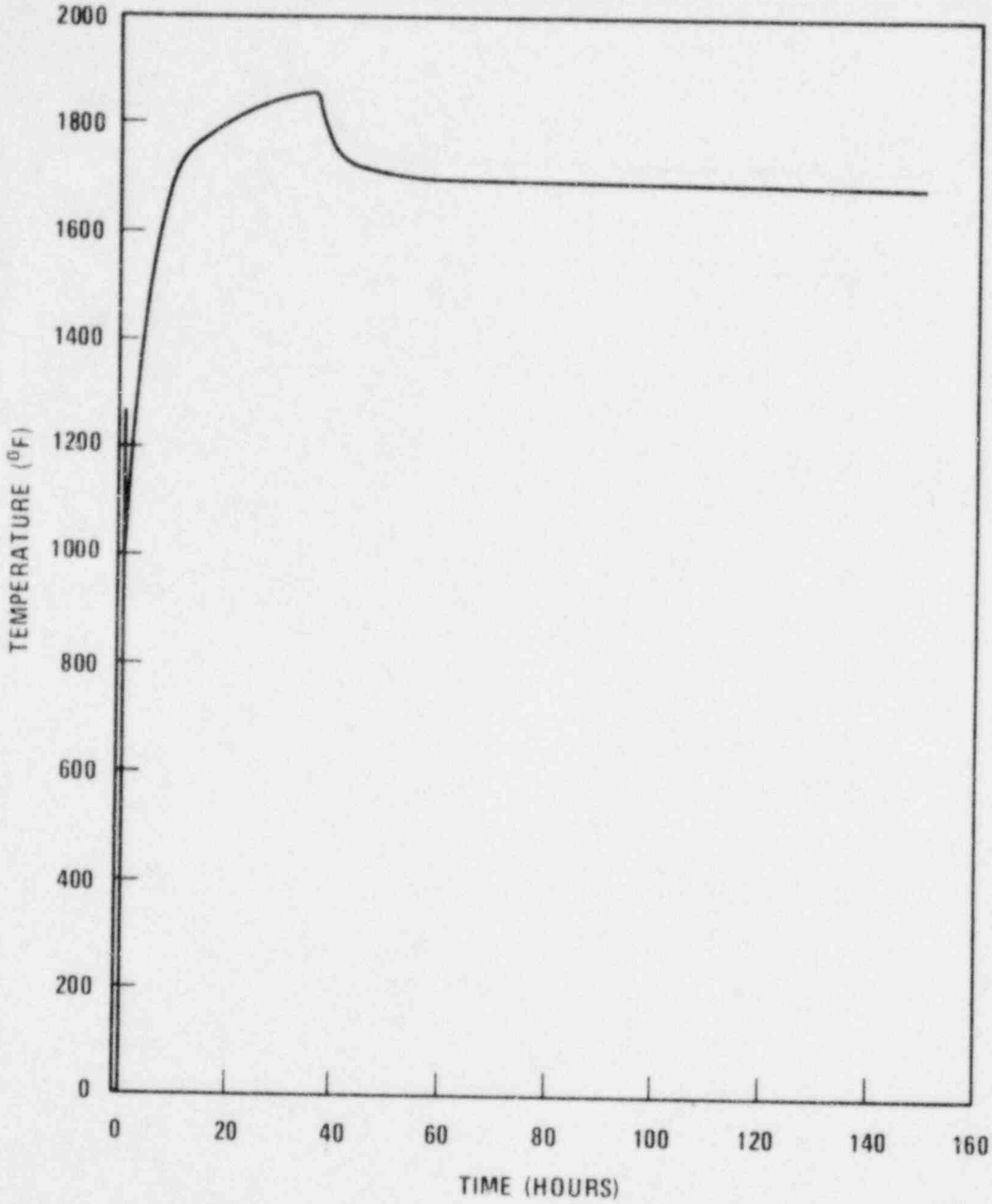

Figure 2-3 Maximum Reactor Cavity Atmosphere and Sodium Pool Temperature

1966-4

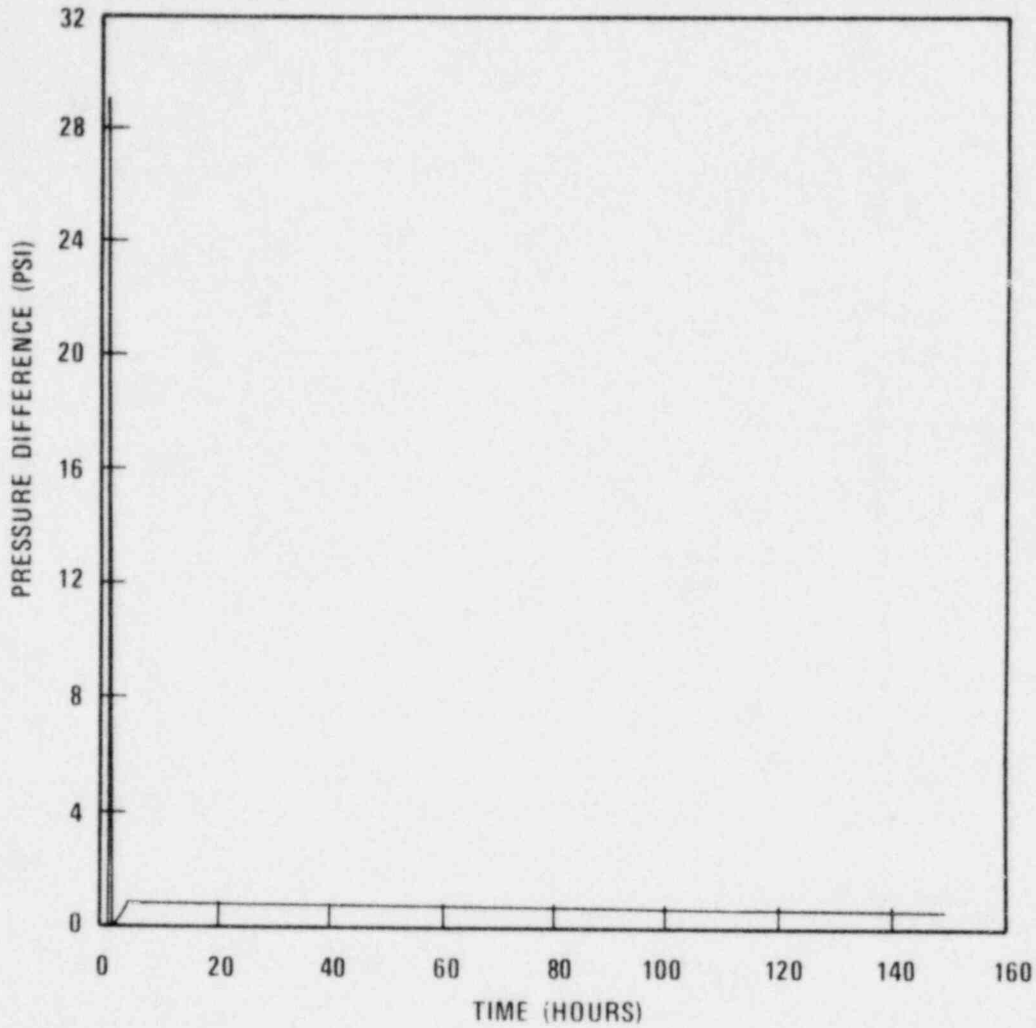

Figure 2-4 Maximum Pressure Differential Between the Reactor Cavity and Cell 105

1966-5

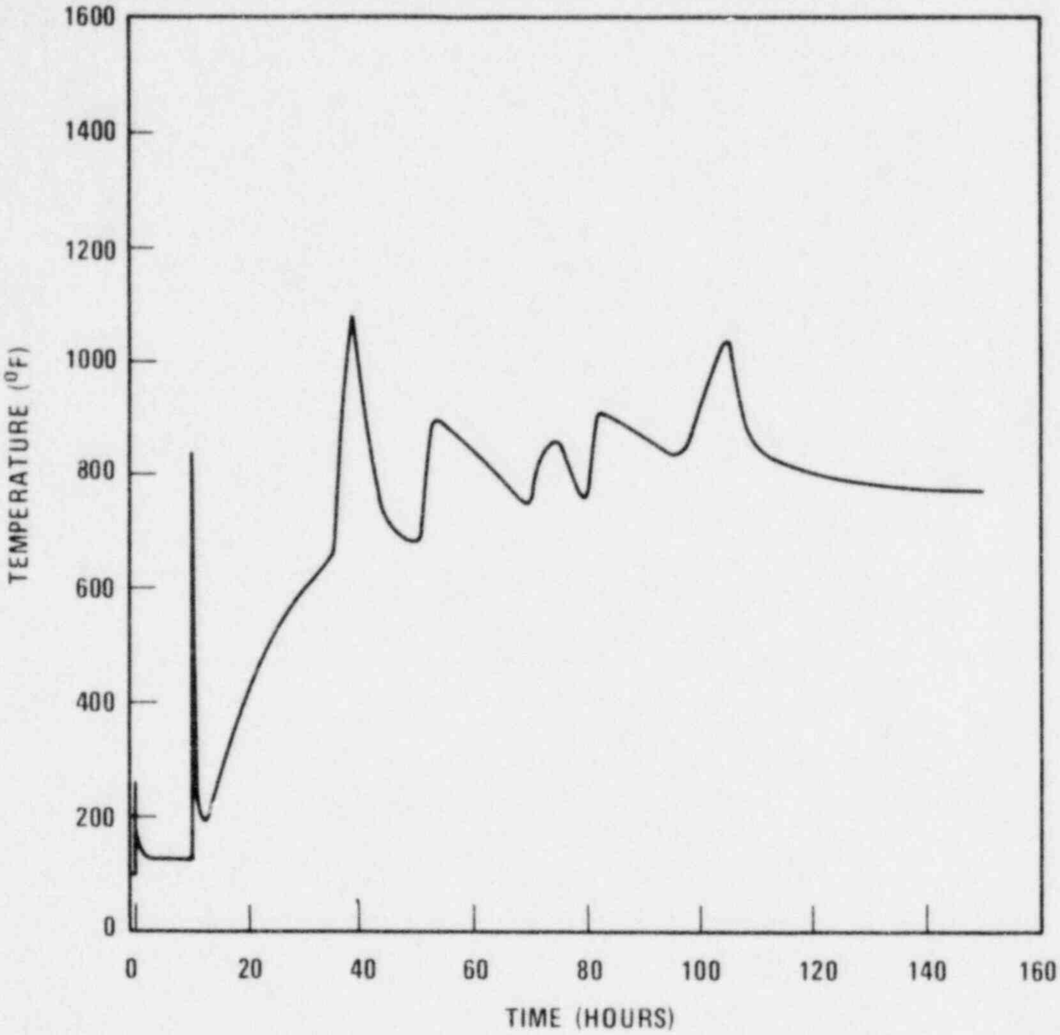

Figure 2-5 Maximum Containment Atmosphere Temperature

1966-6

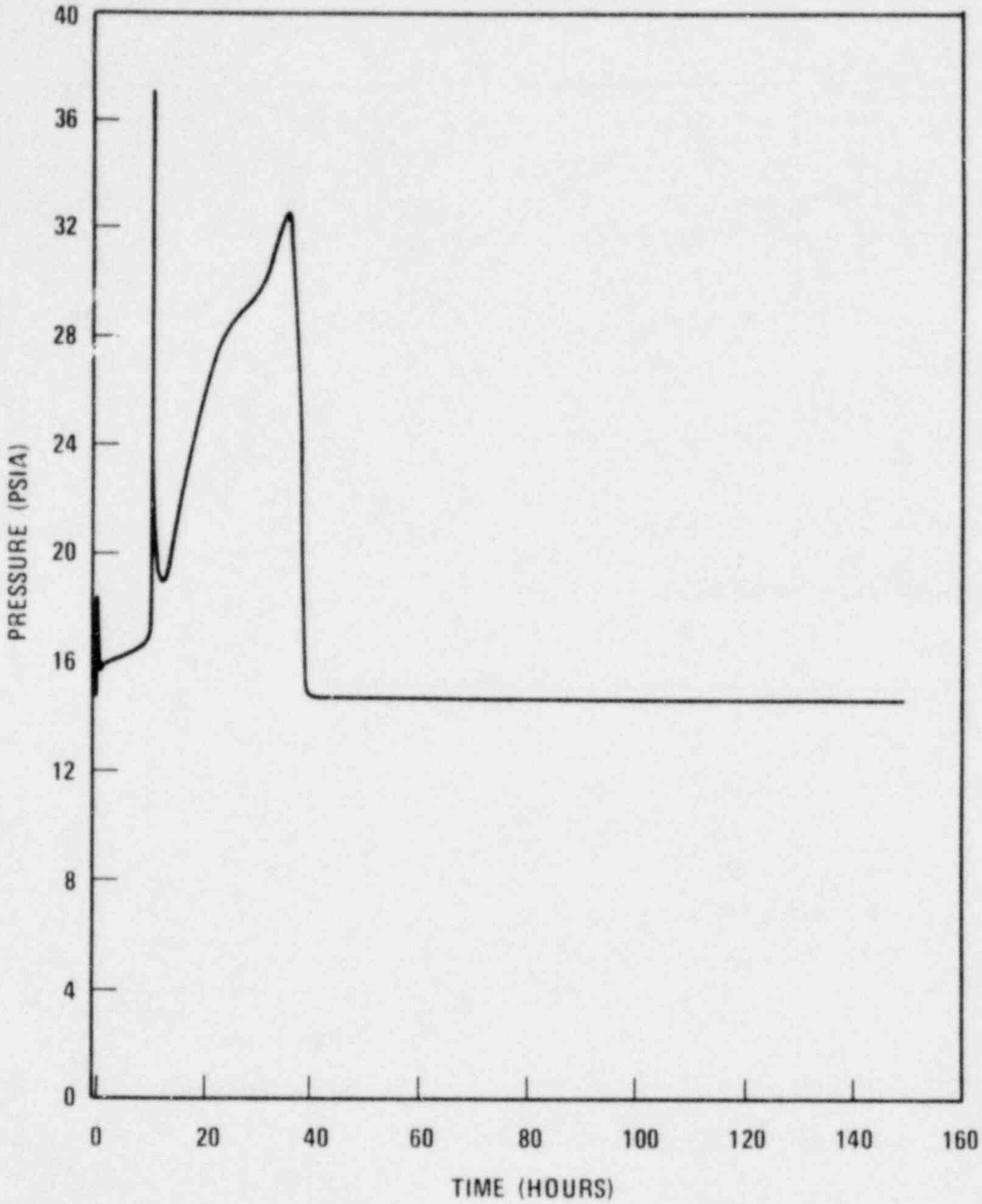

Figure 2-6 Maximum Containment Atmosphere Pressure

1966-7

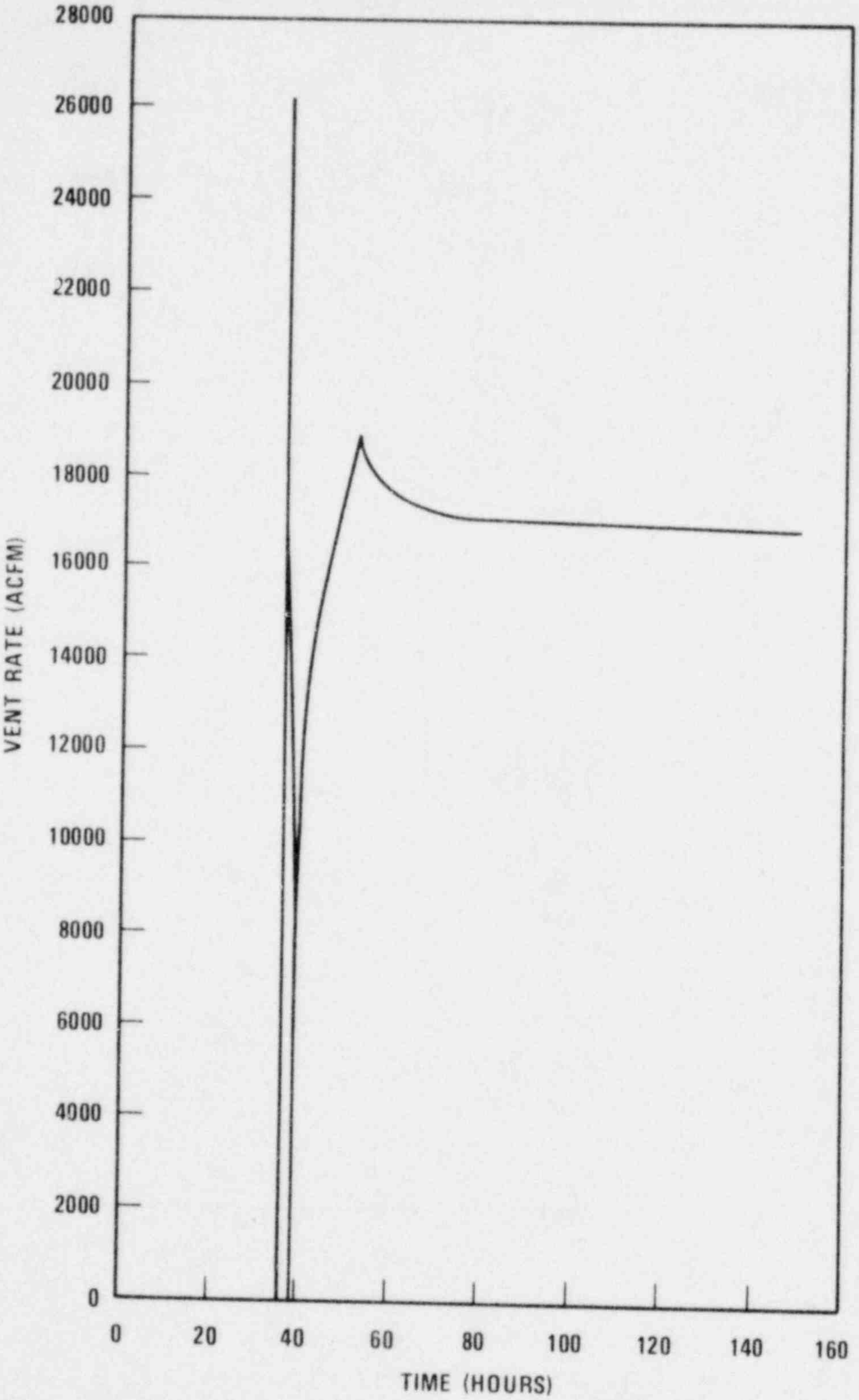

Figure 2-7. Maximum Containment Vent Rates

1966-8

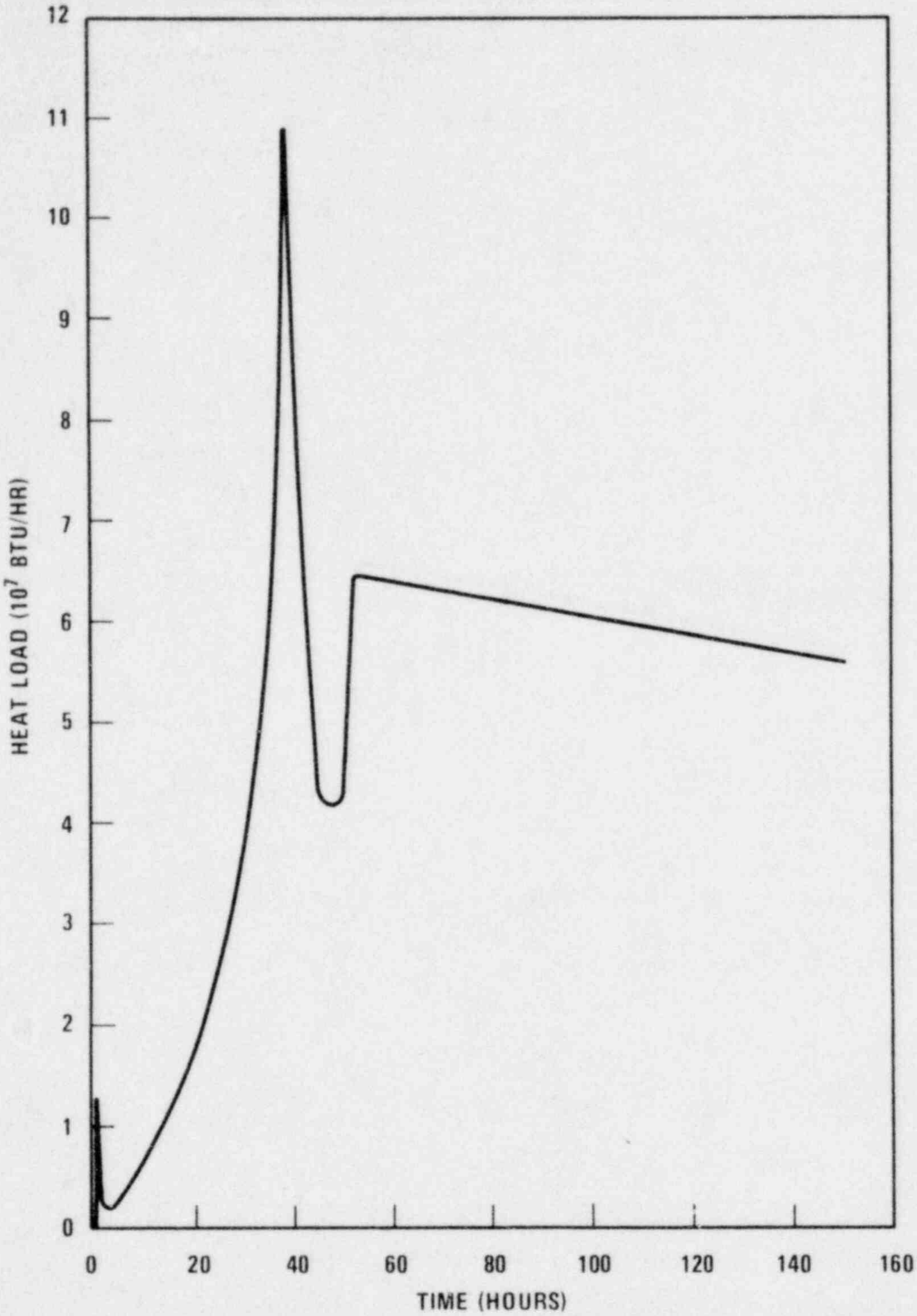

Figure 2-8 Maximum Heat Load Through the Containment Structure Steel Shell

1966-9

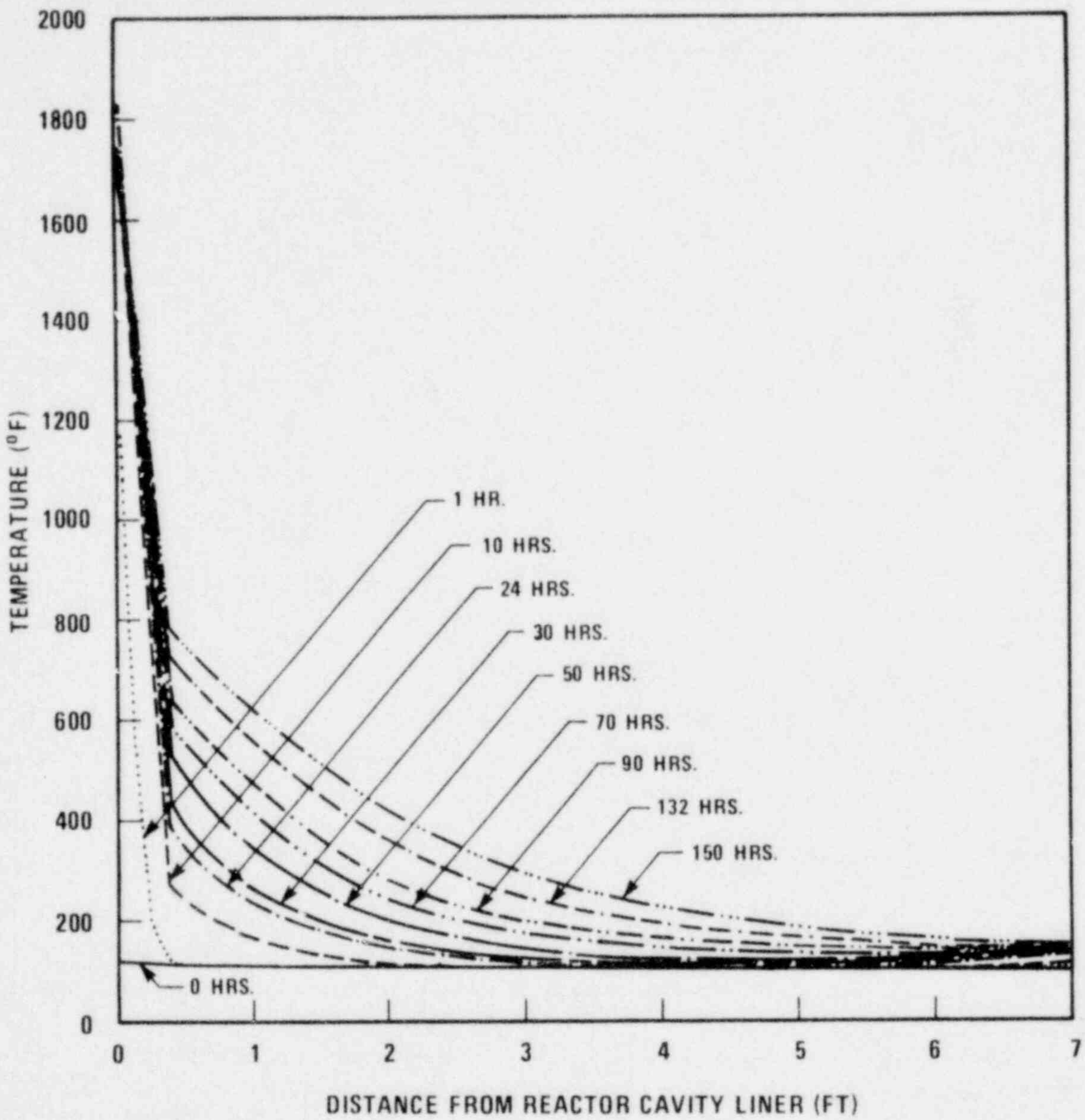

Figure 2-9. Maximum Reactor Cavity Submerged Wall Structural Temperatures

1966-10

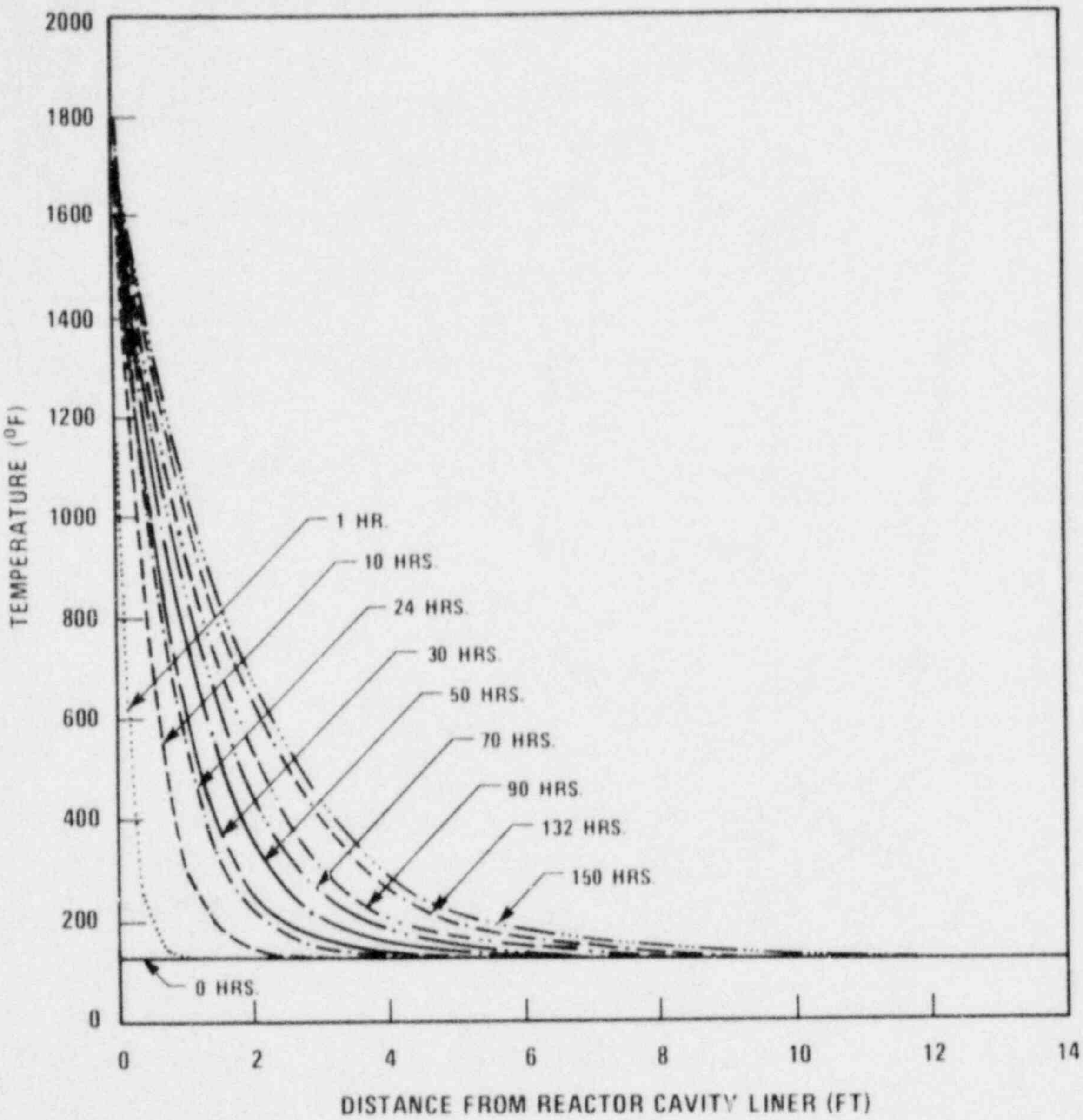

Figure 2-10. Maximum Reactor Cavity Floor Concrete Temperatures

1966-11

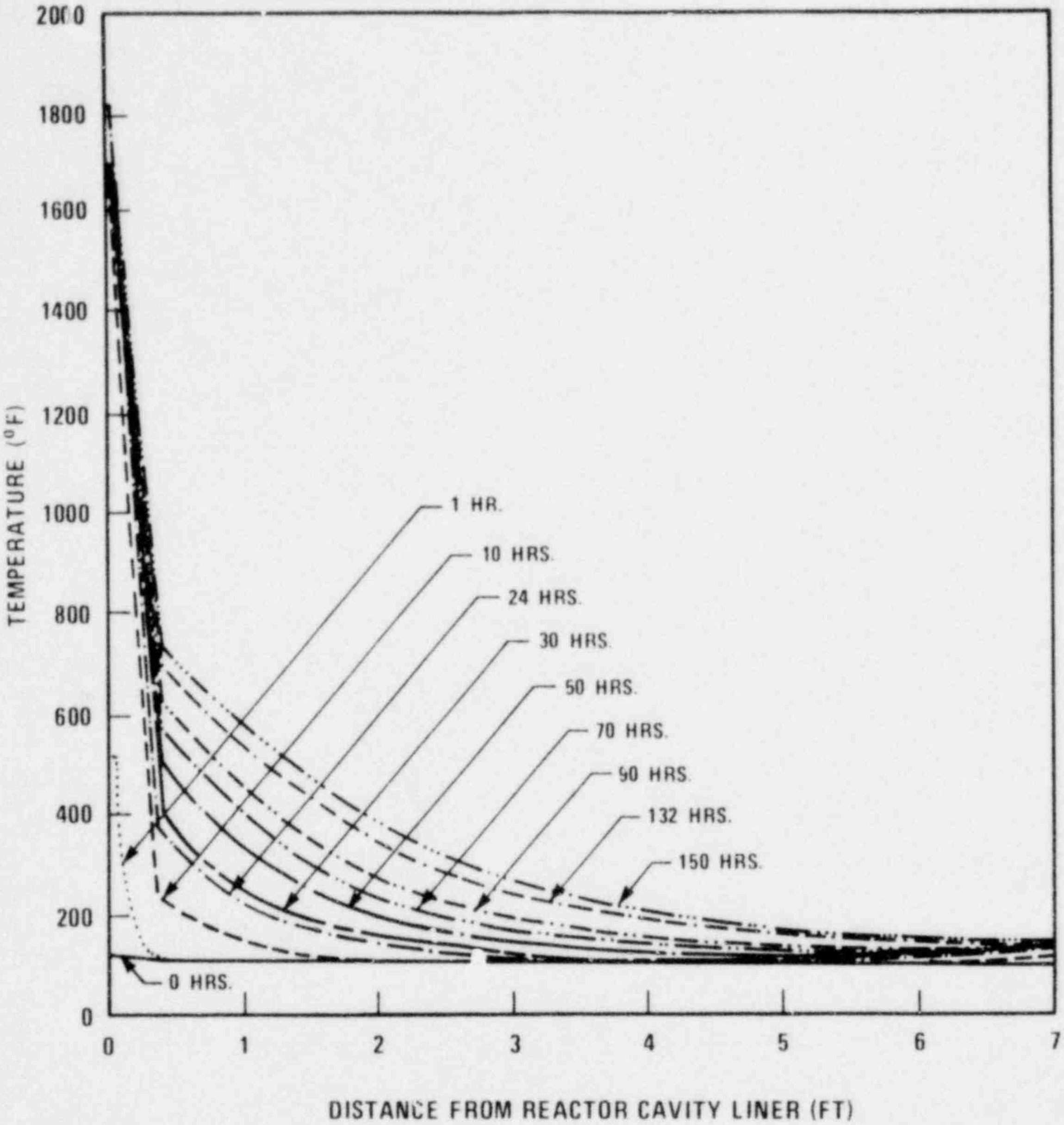

Figure 2-11. Maximum Reactor Cavity Non-Submerged Wall Structural Temperatures

1966-12

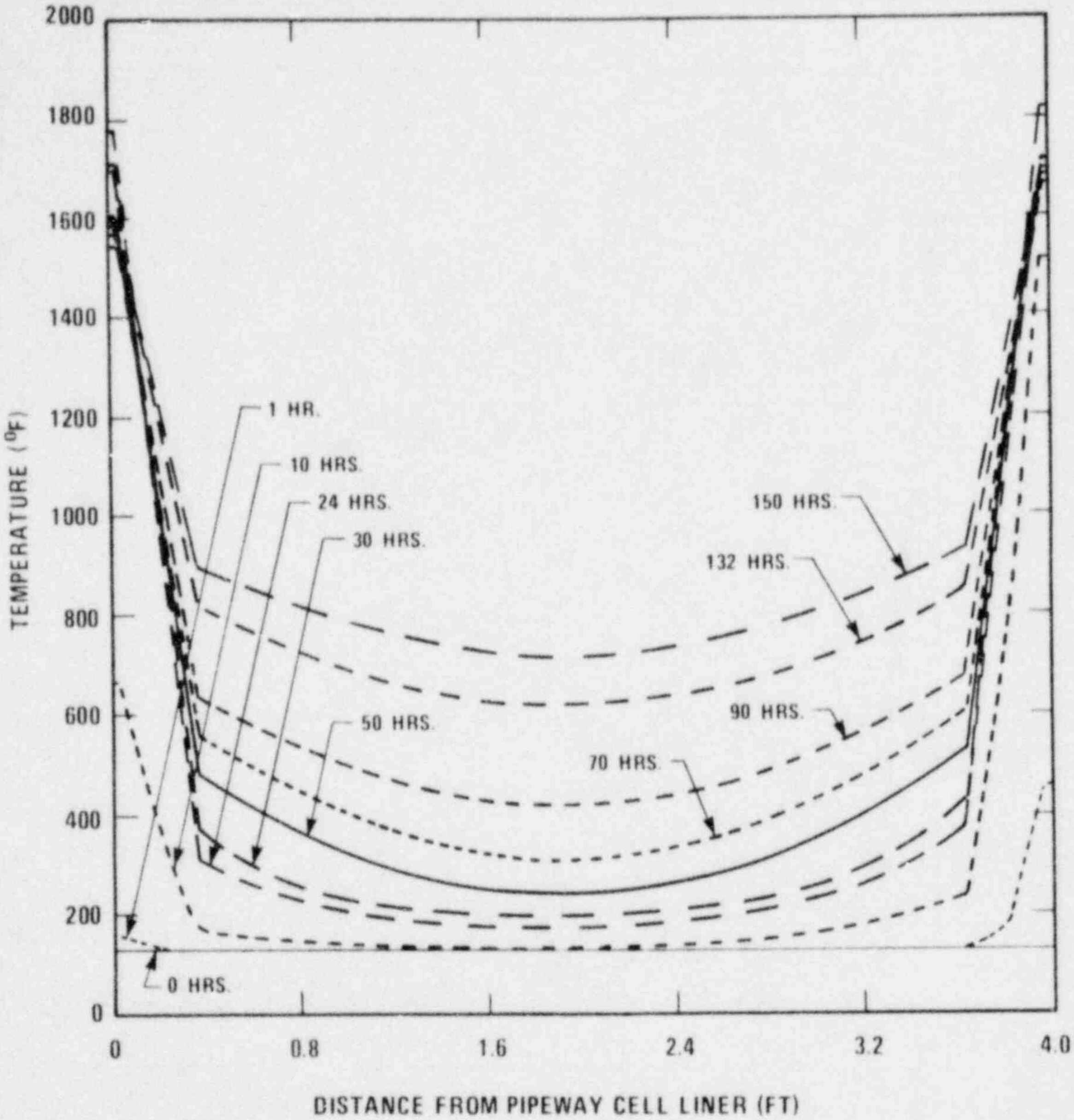

Figure 2-12. Maximum Reactor Cavity-Pipeway Wall Structural Temperatures

1966-13

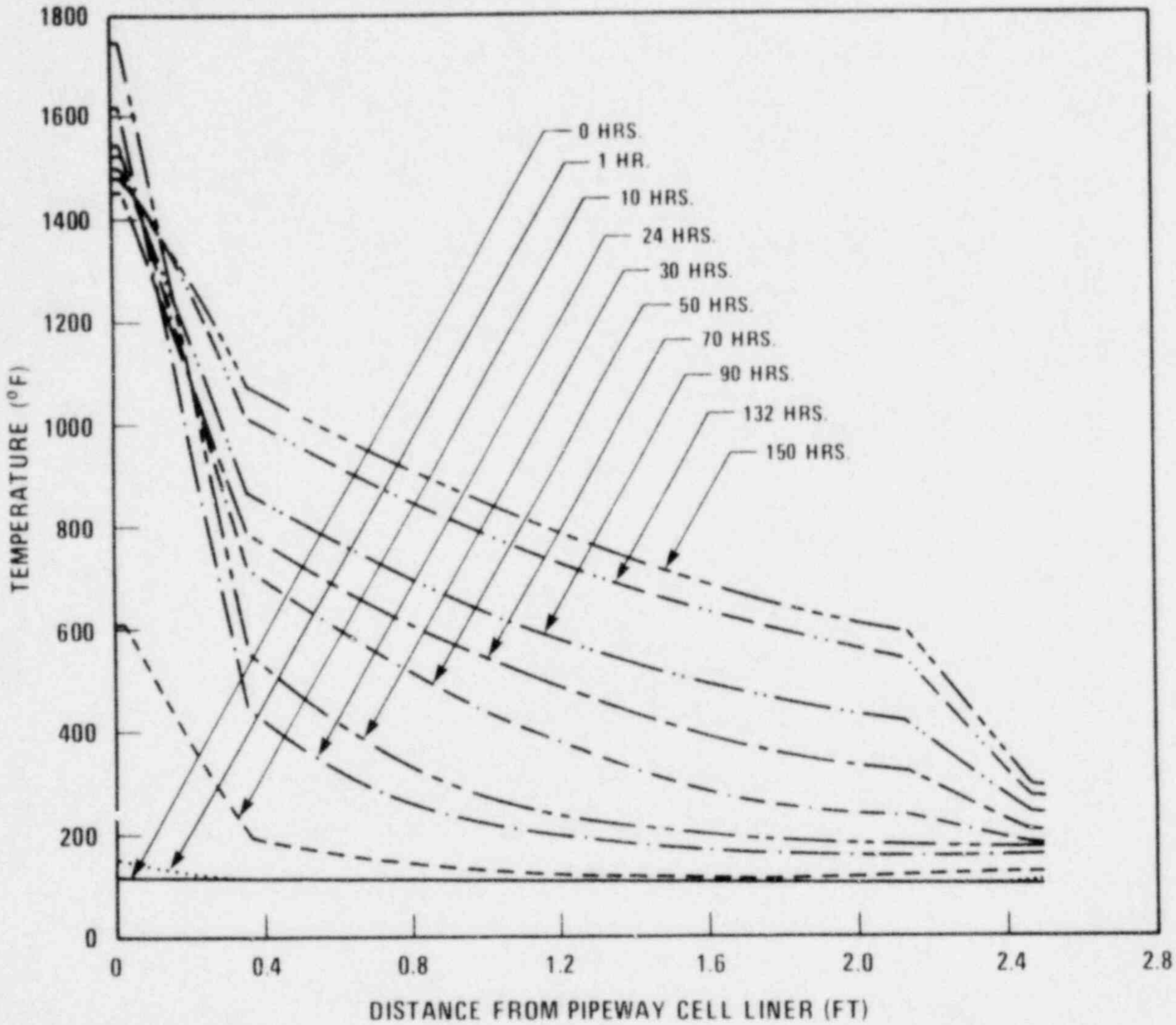

Figure 2-13. Maximum Pipeway Cell Wall Structural Temperatures (2.5 Ft. Thick Wall)

1966-14

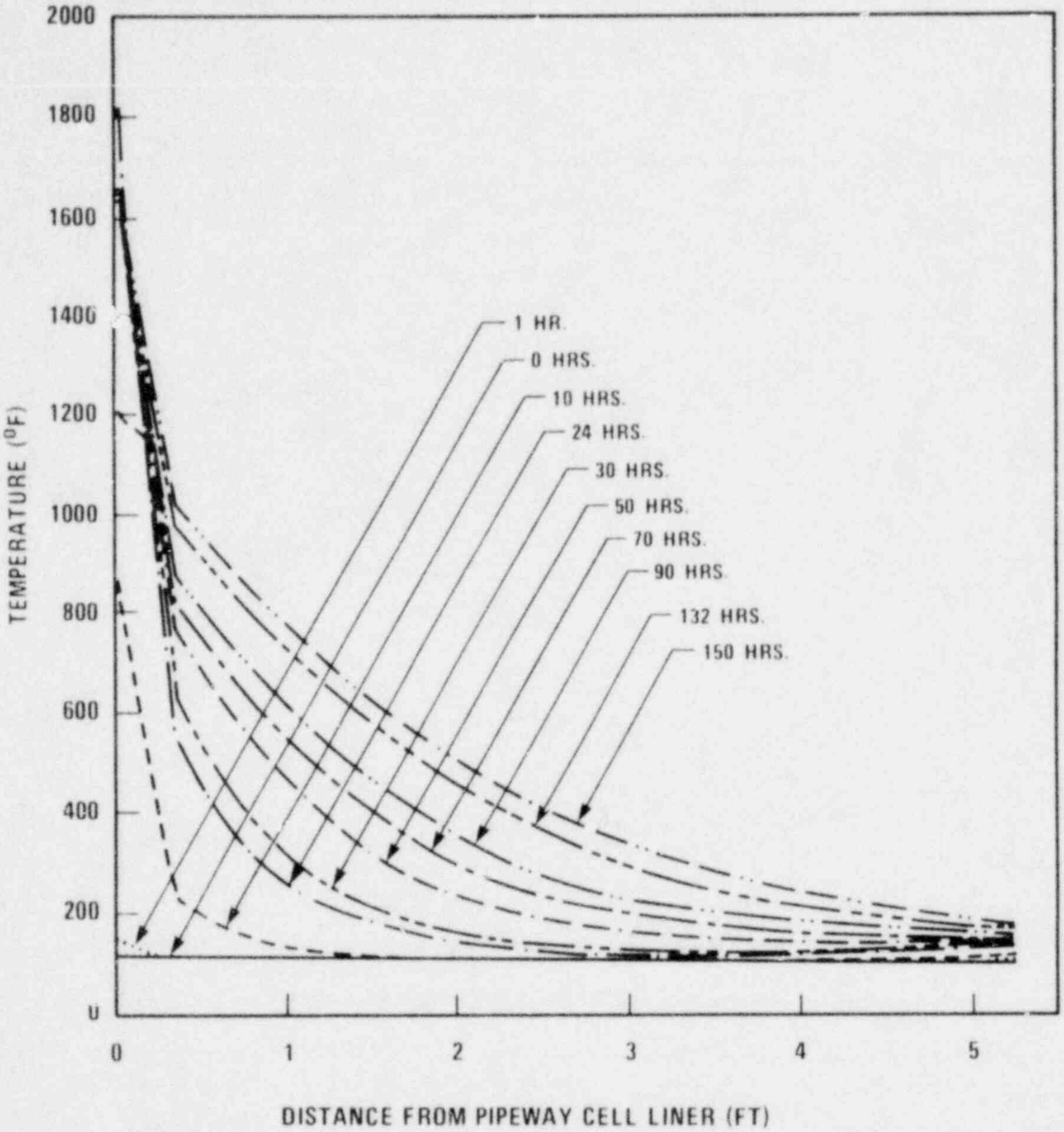

Figure 2-14 Maximum Pipeway Floor Structural Temperatures

1966-15

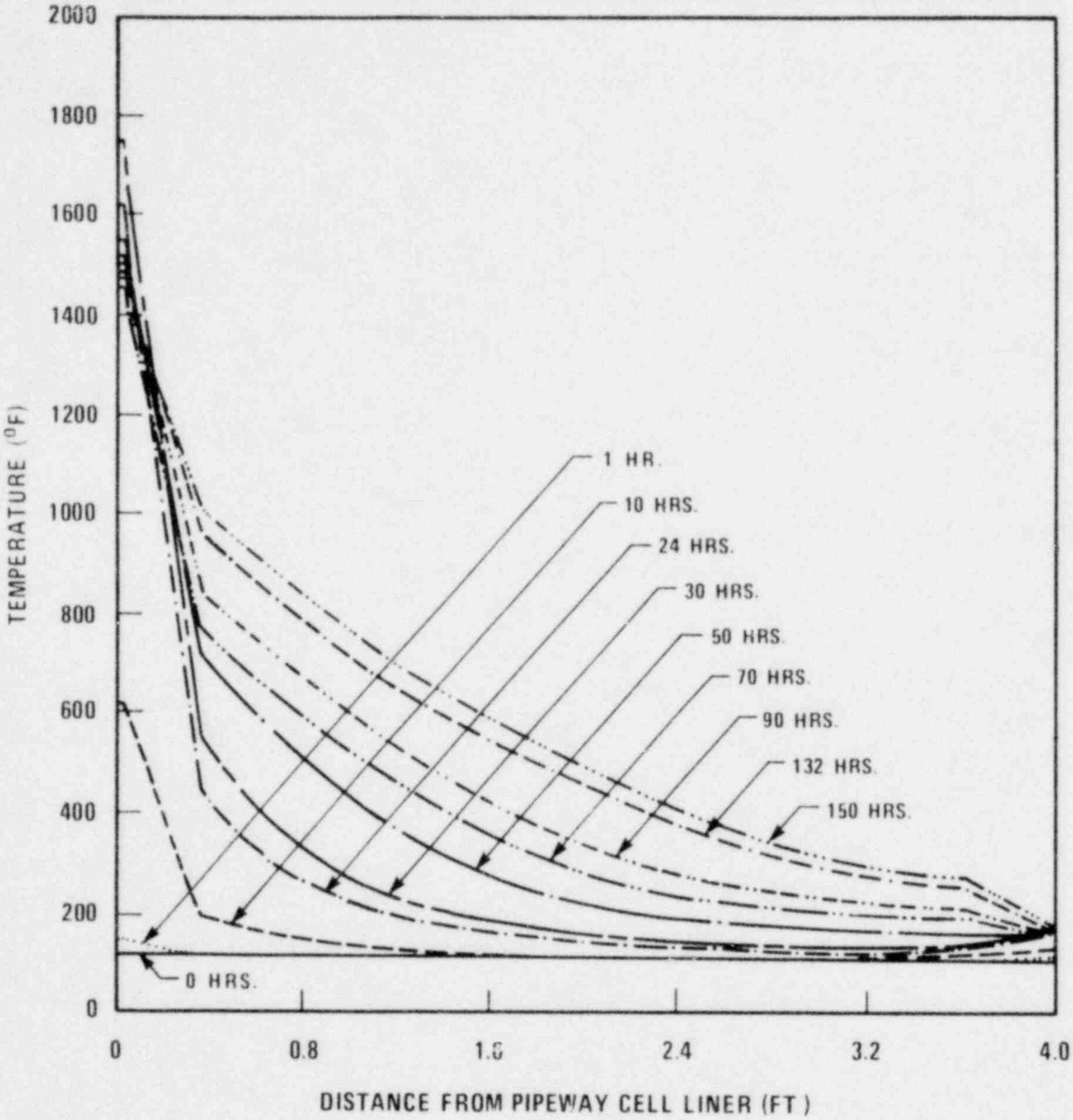

Figure 2-15. Maximum Pipeway Cell Wall Structural Temperatures (4.0 FT. Thick Wall)

1966-16

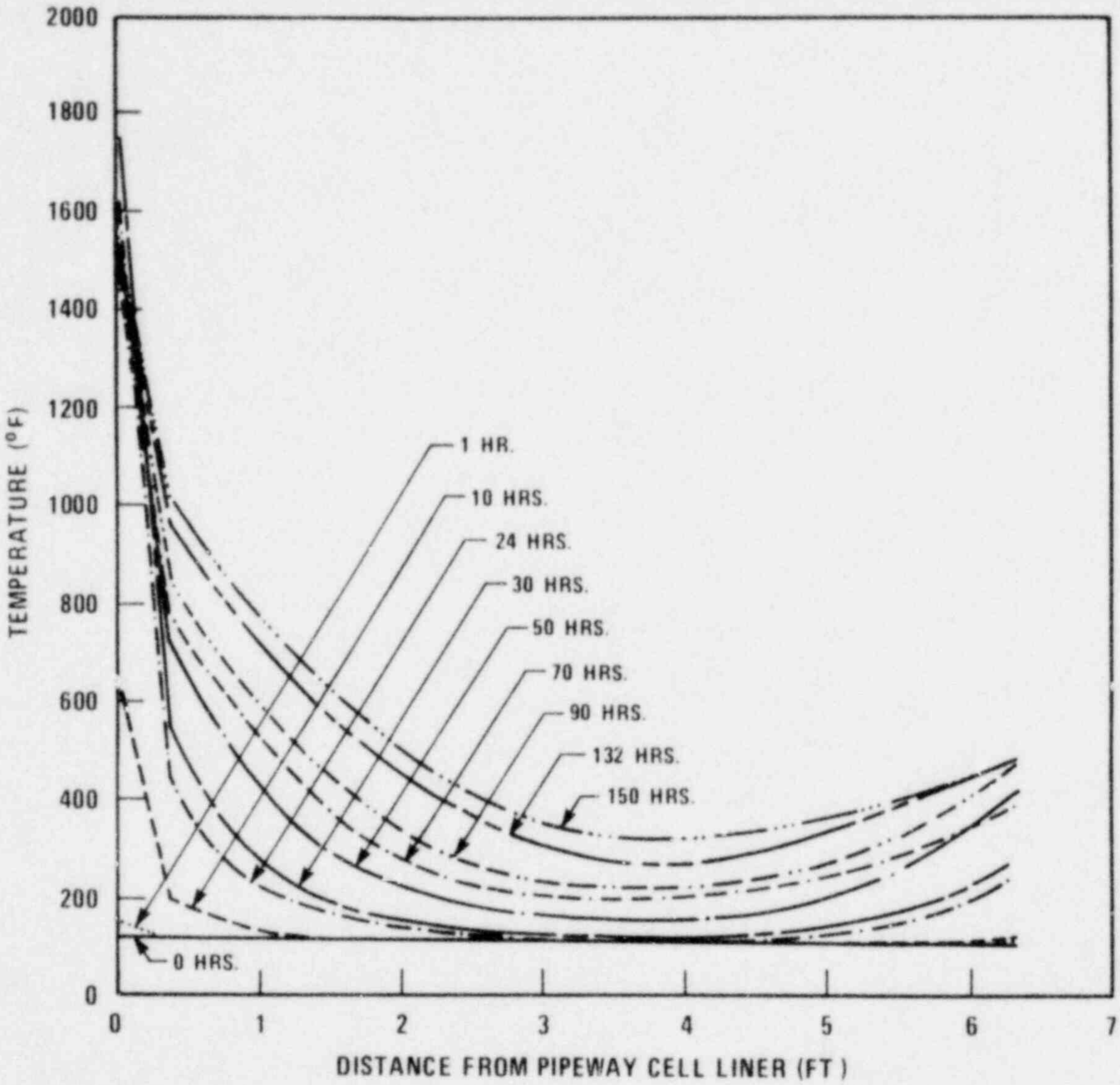

Figure 2-16. Maximum Pipeway Cell Roof and Head Access Area Wall Structural Temperatures

1966-17

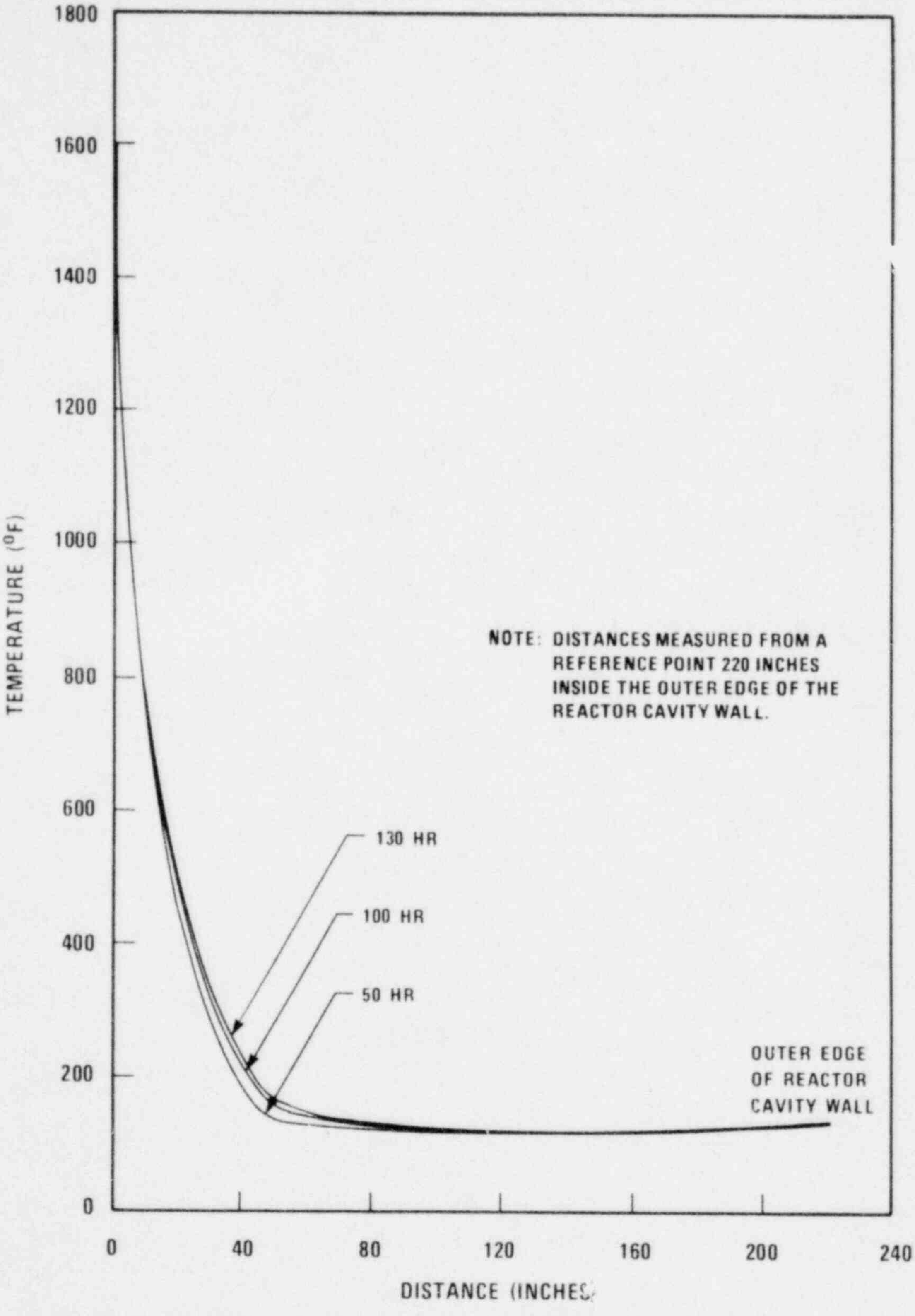

Figure 2-17. Reactor Cavity Ledge Radial Temperature Profile

1966-18

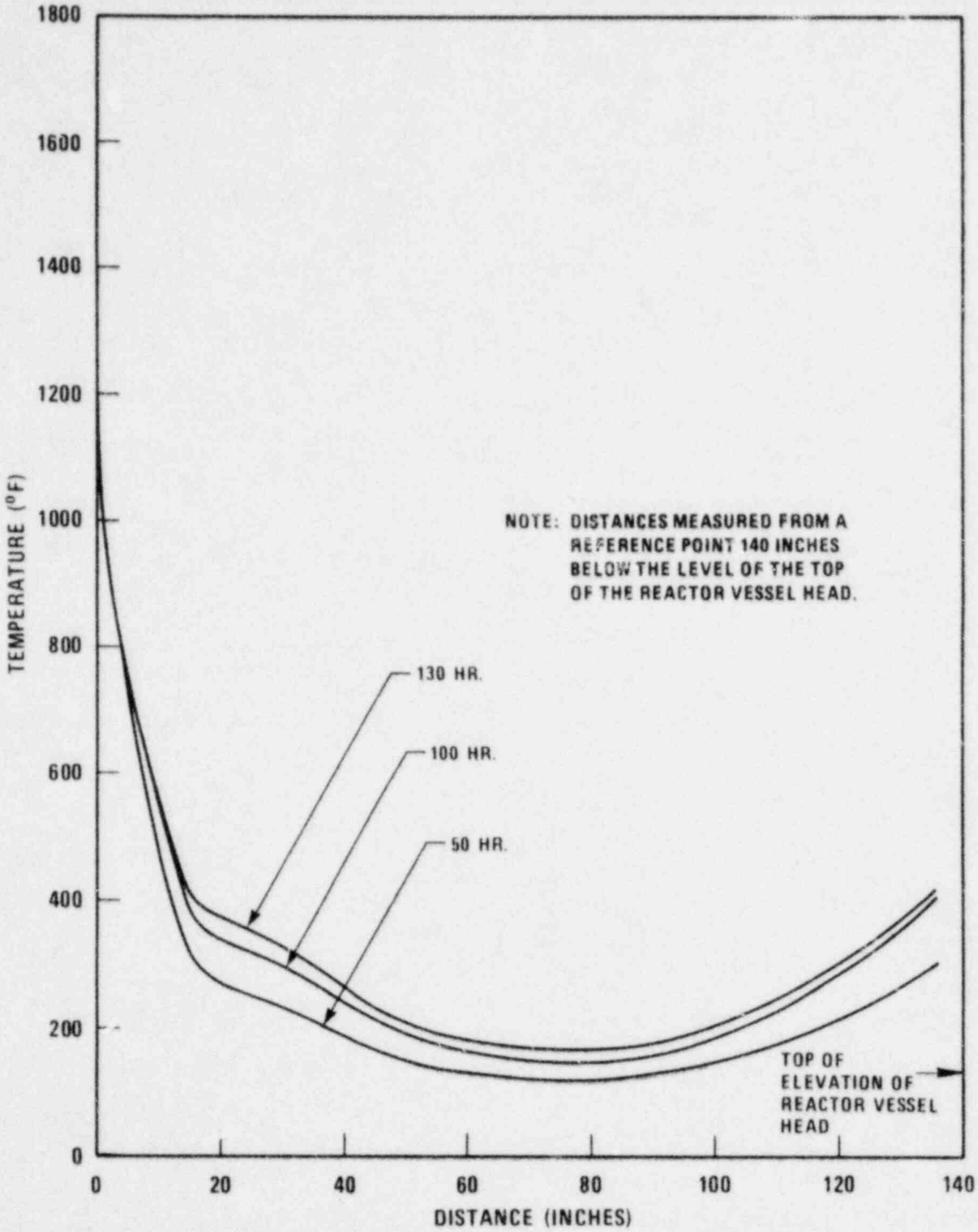

Figure 2-18 Reactor Cavity Ledge Axial Temperature Profile

1966-19

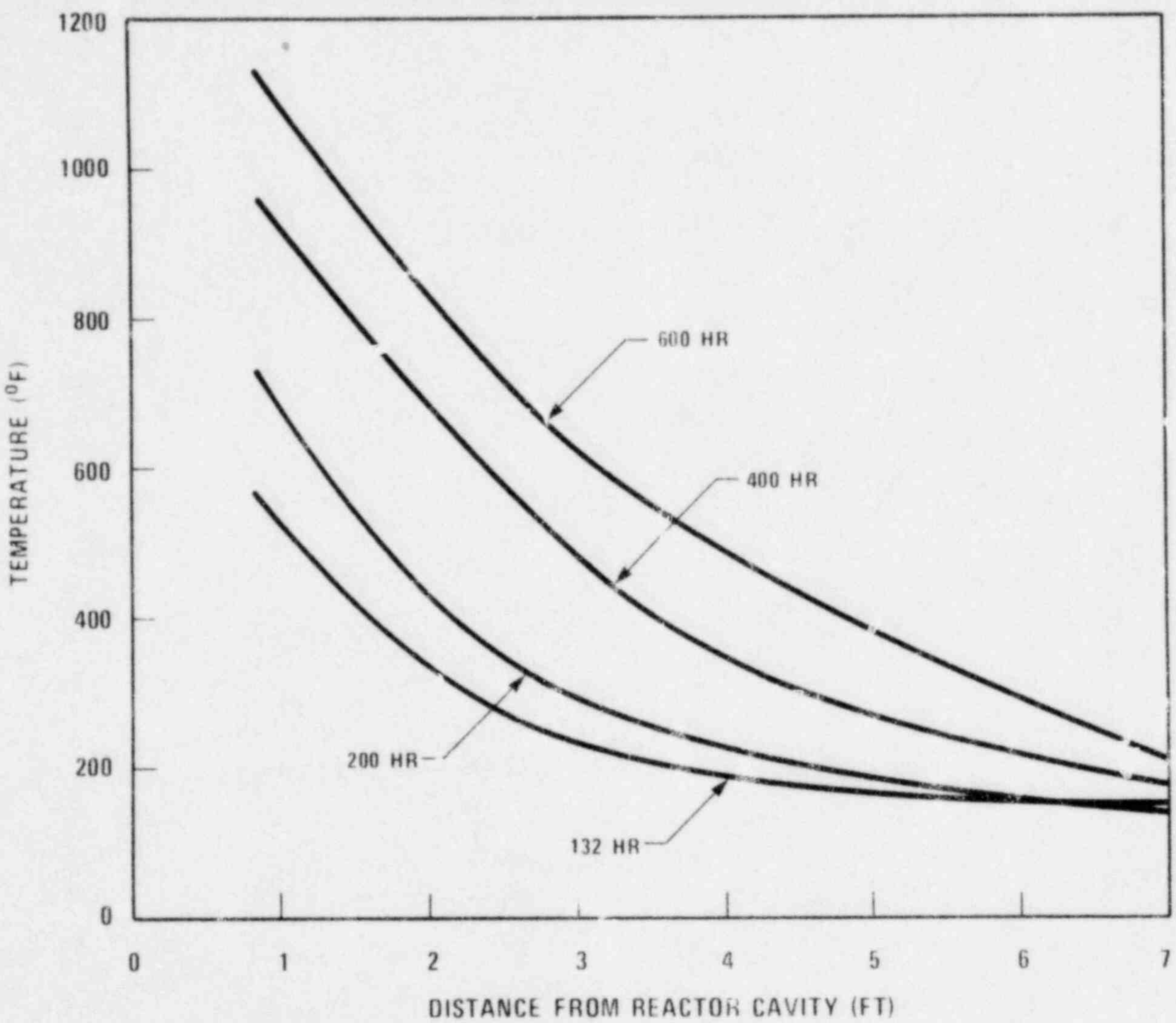

Figure 2-19. Maximum Reactor Cavity Upper Wall Temperatures Prior to Wall Failure

1966-20

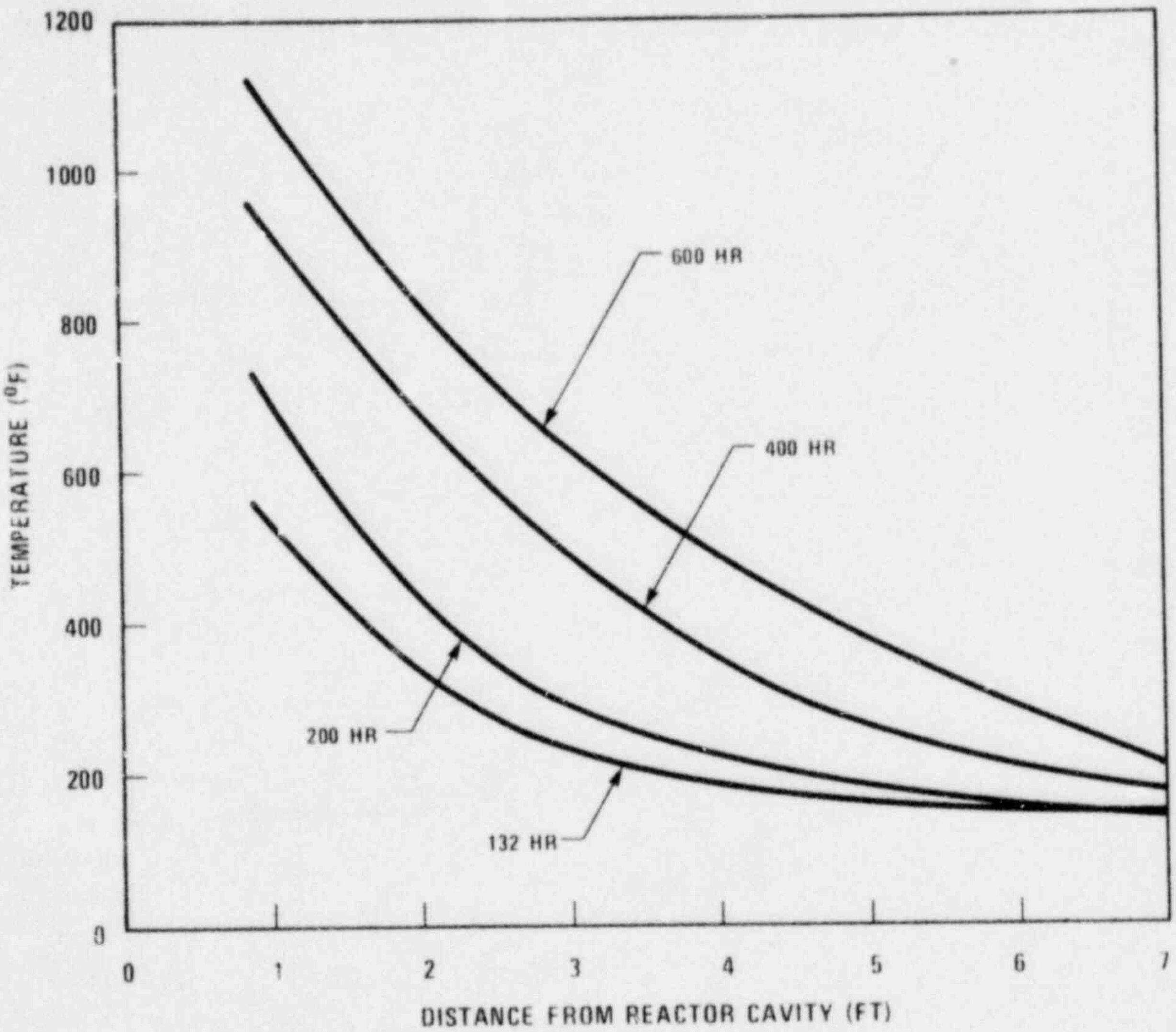

Figure 2-20. Maximum Reactor Cavity Lower Wall Temperatures Prior to Wall Failure

1966-21

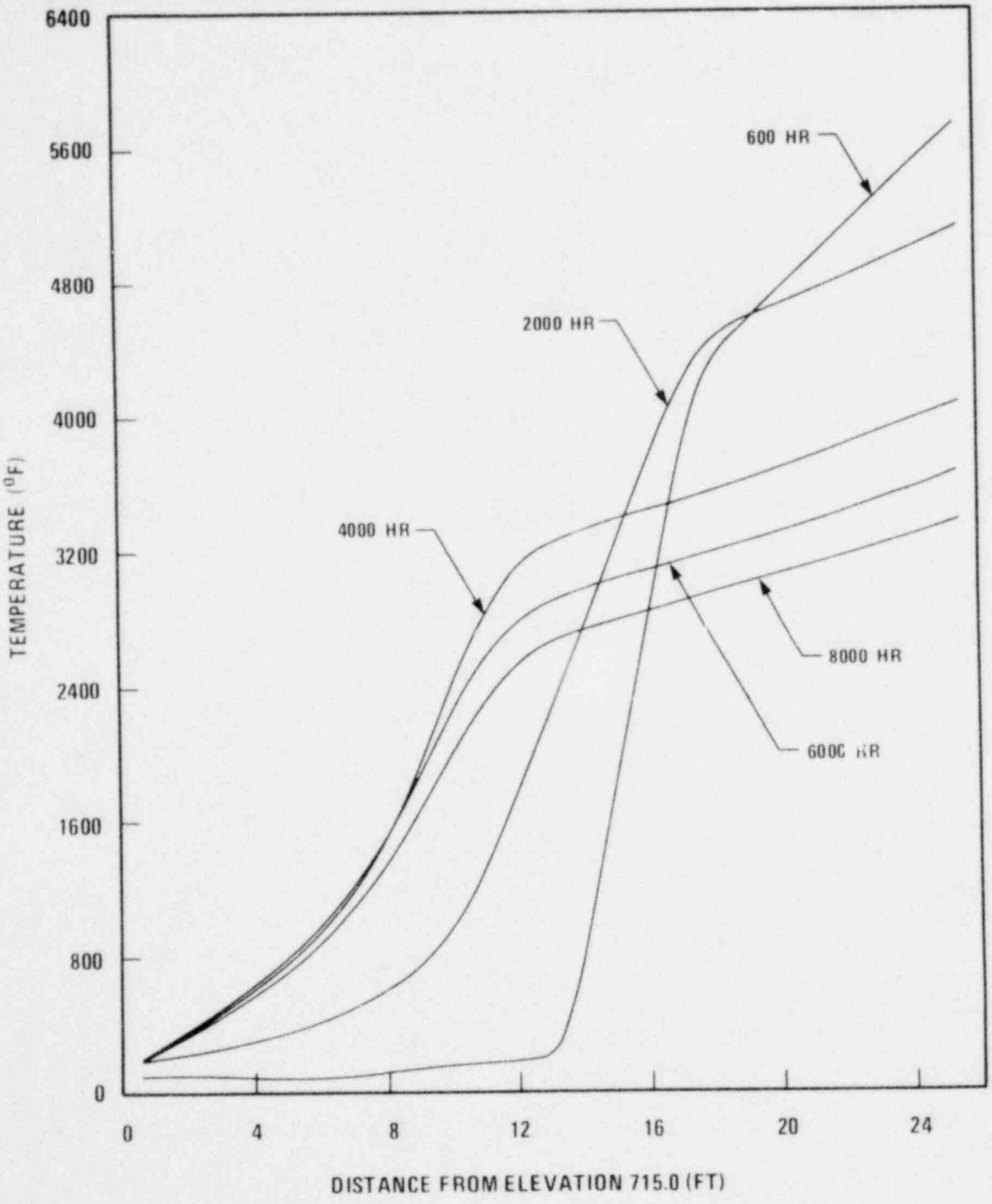

Figure 2-21 Maximum Reactor Cavity Floor and Basemat (Axial Centerline) Temperatures

1966-22

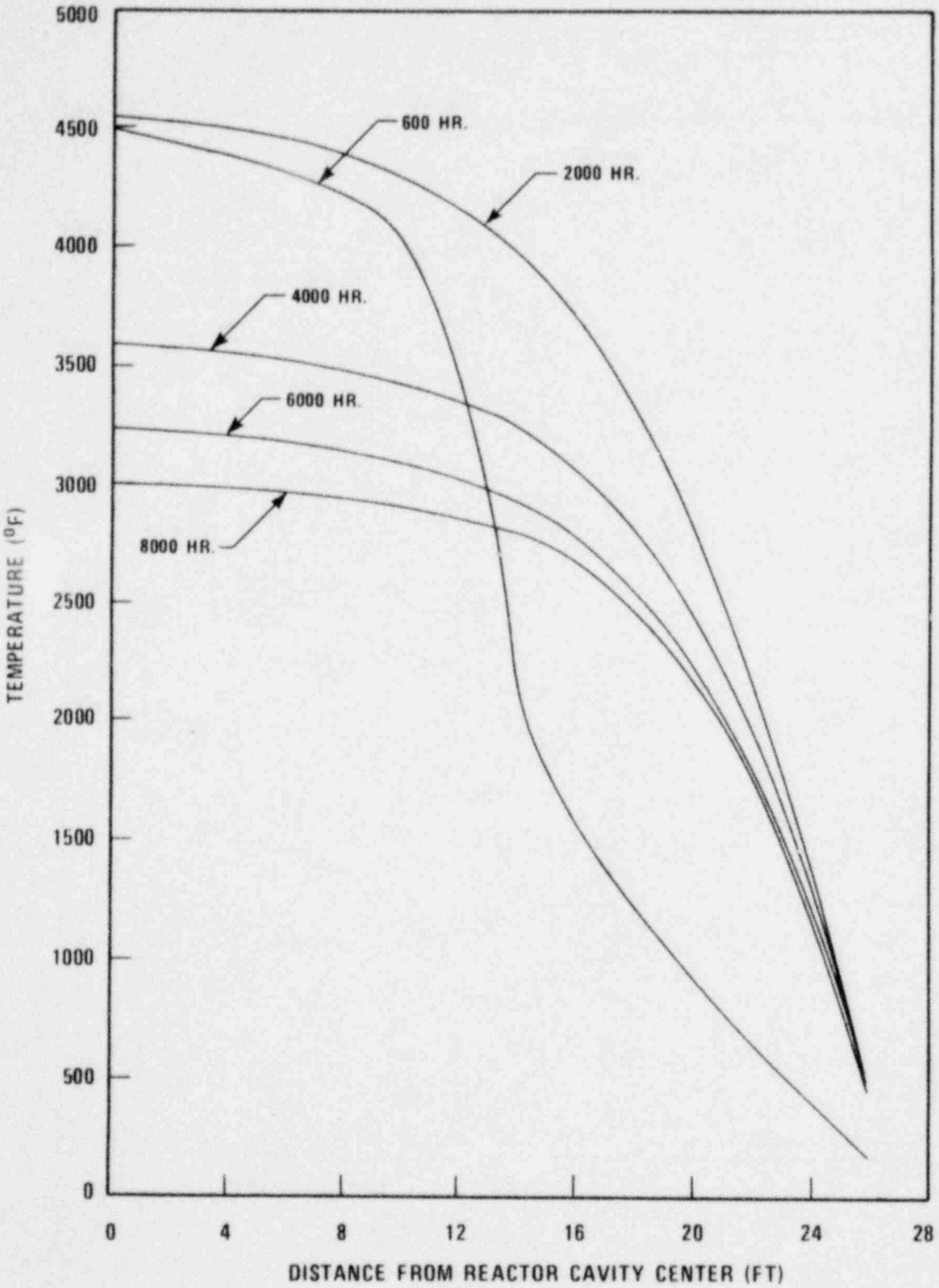

Figure 2-22 Maximum Reactor Cavity Floor (Elevation 733.5) Temperatures

1966-23

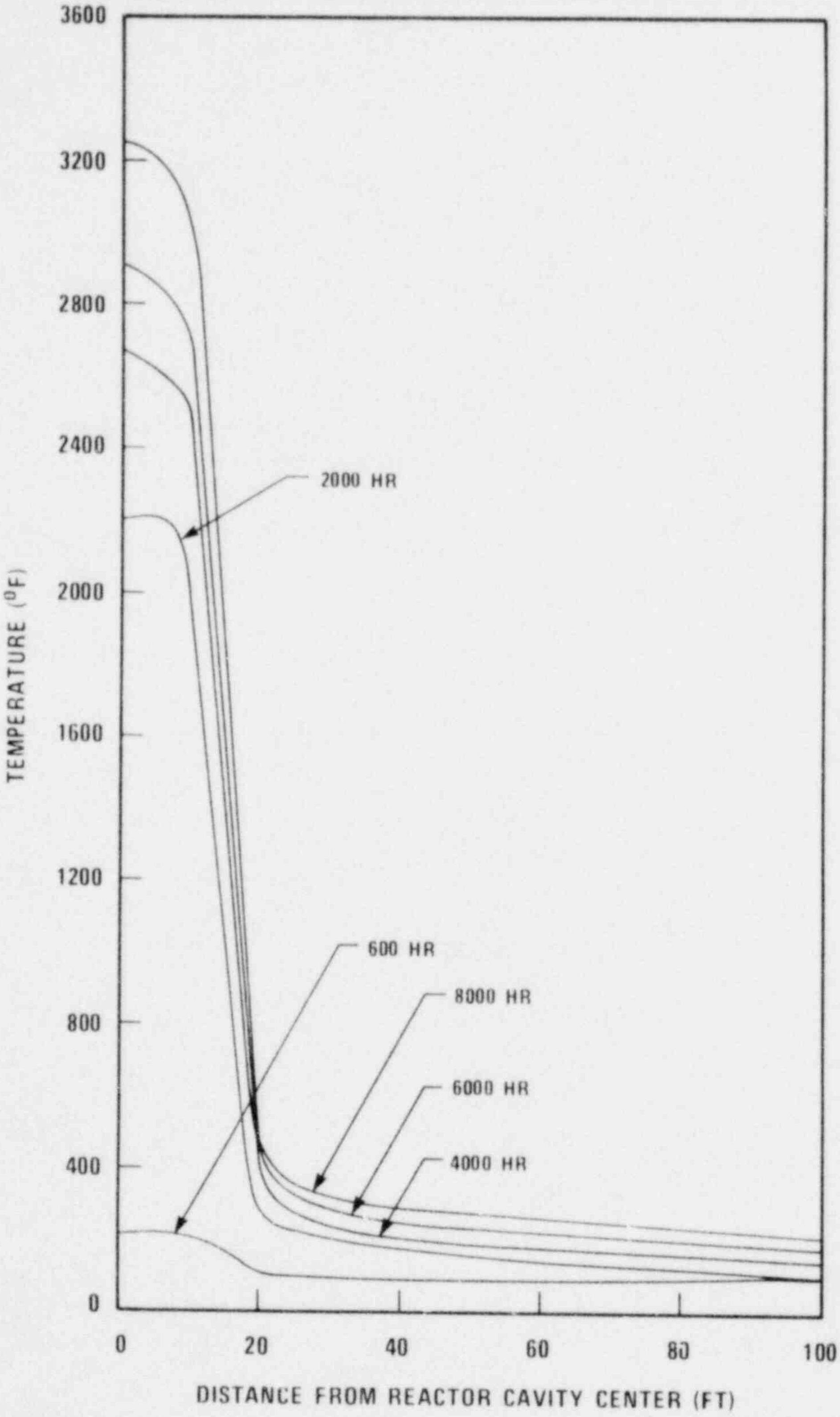

Figure 2-23 Maximum Basemat (Elevation 728.0) Temperatures

1966-24

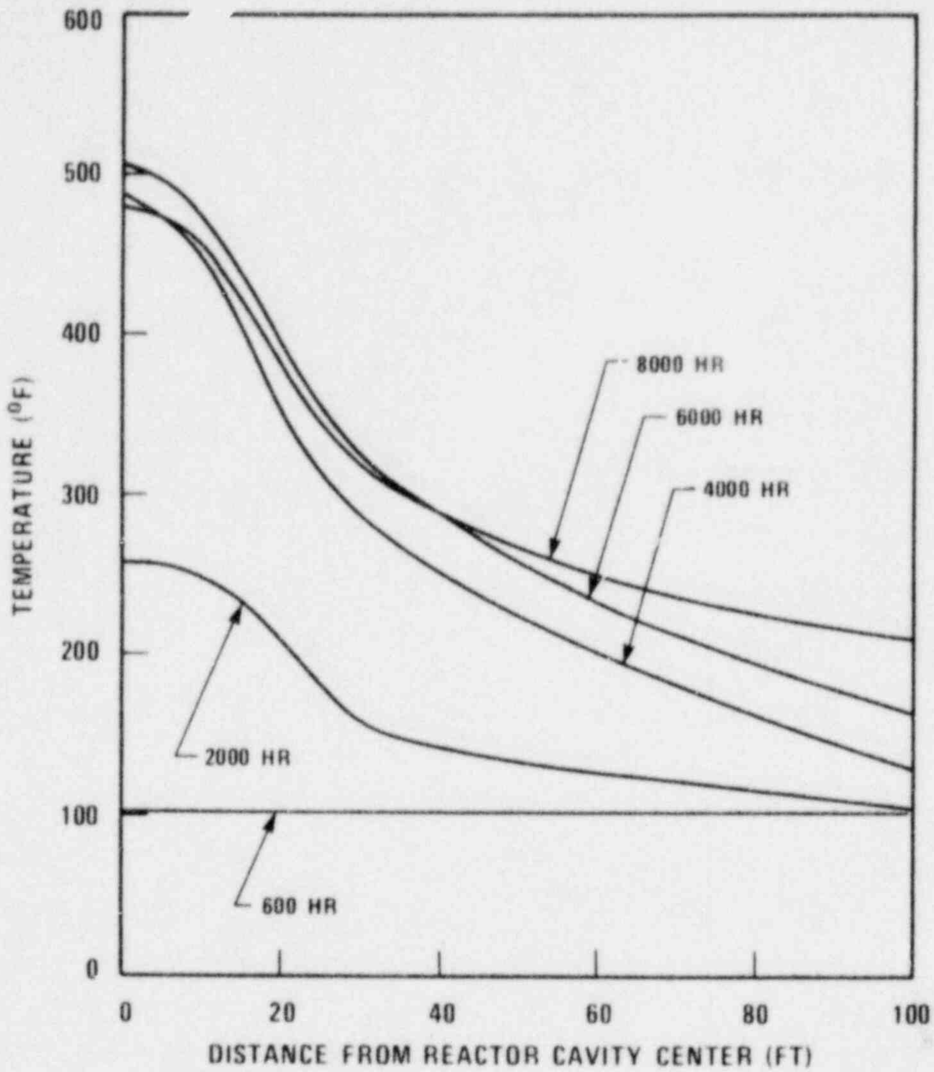

Figure 2-24 Maximum Basemat (Elevation 718.0) Temperatures

1966-25

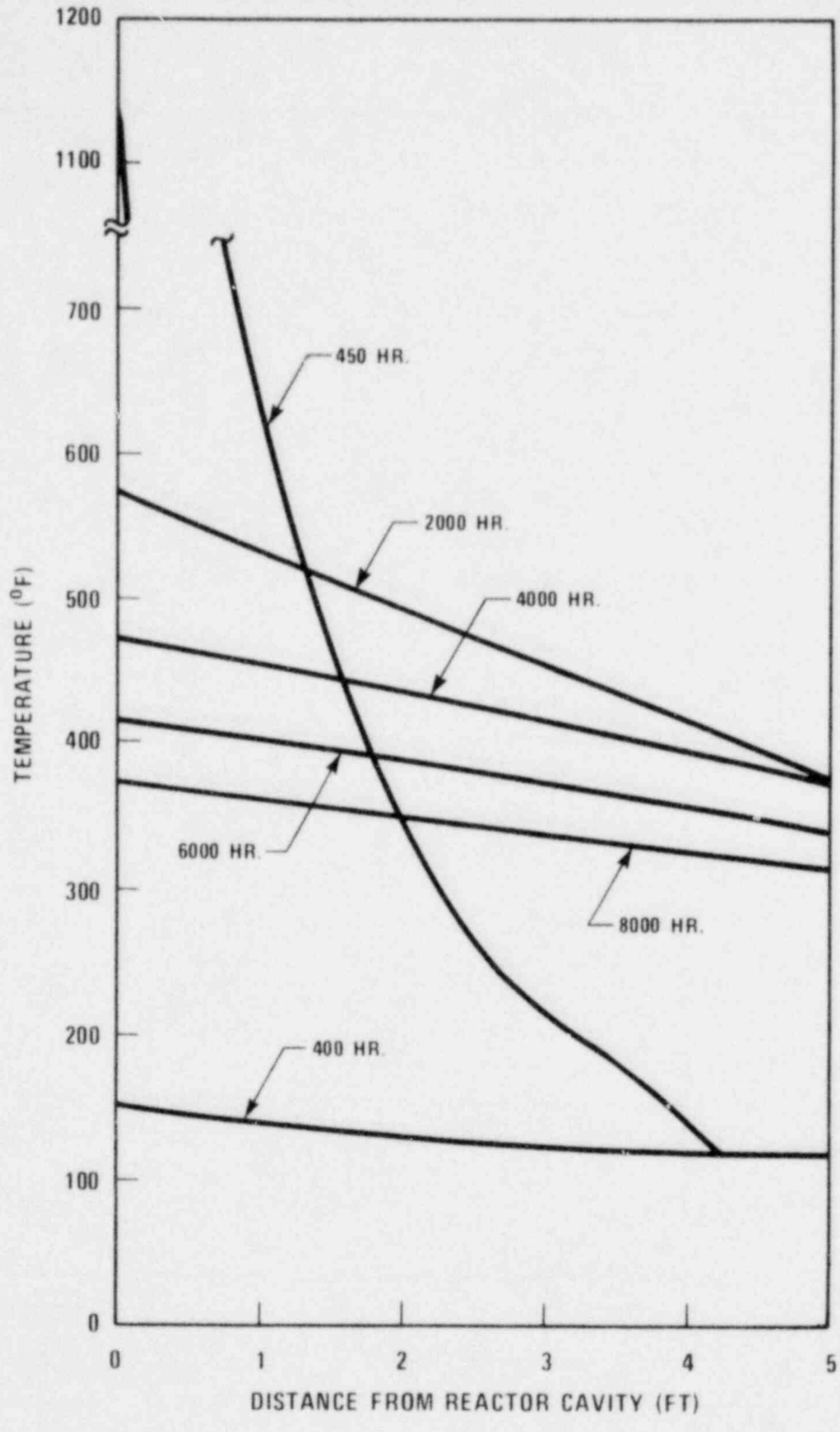

Figure 2-25 Maximum PHTS Wall (Facing RC Wall) Temperatures

1966-26

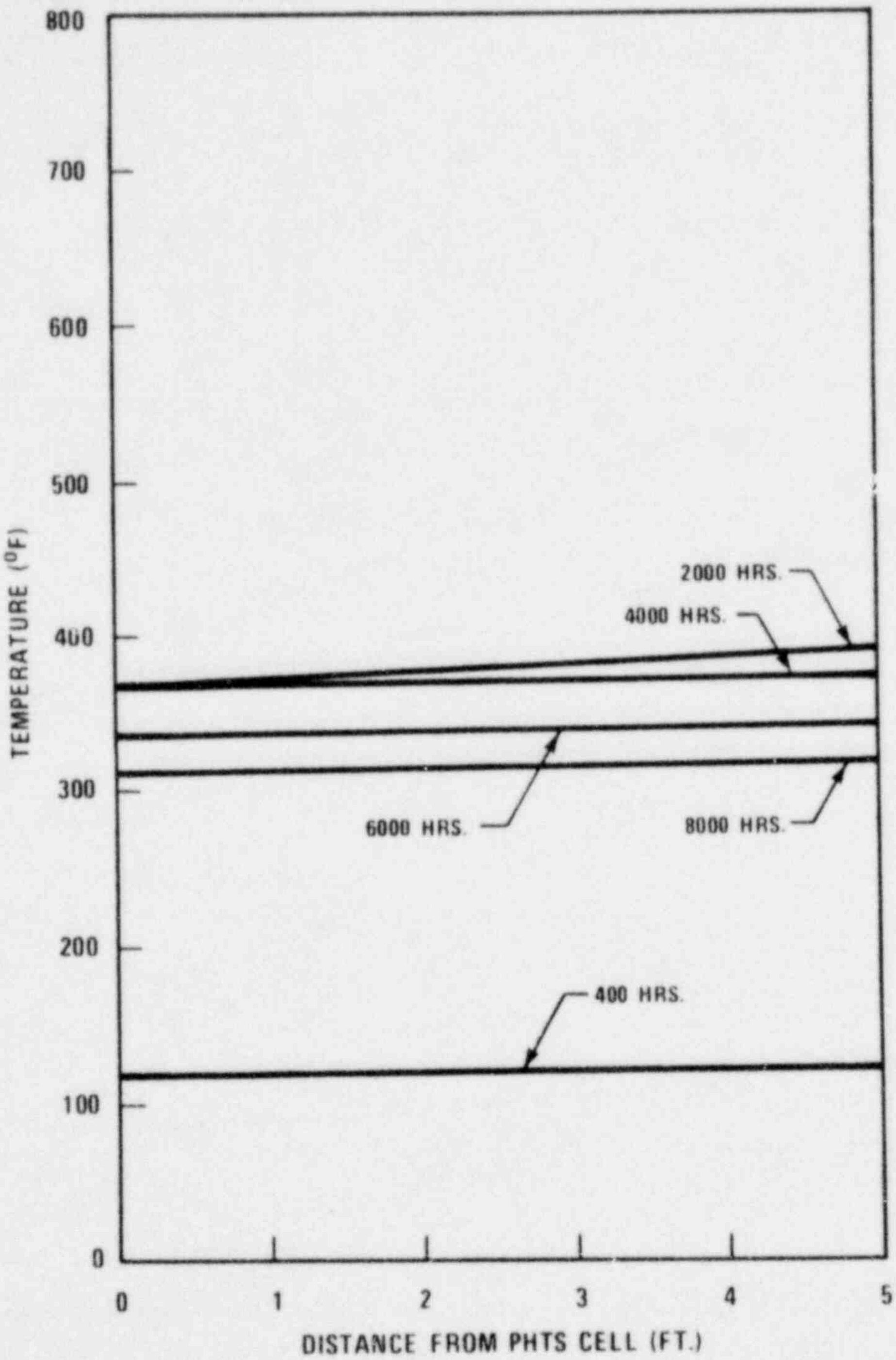

Figure 2-26 Maximum PHTS Wall (Not Facing RC Wall) Temperatures

1966-27

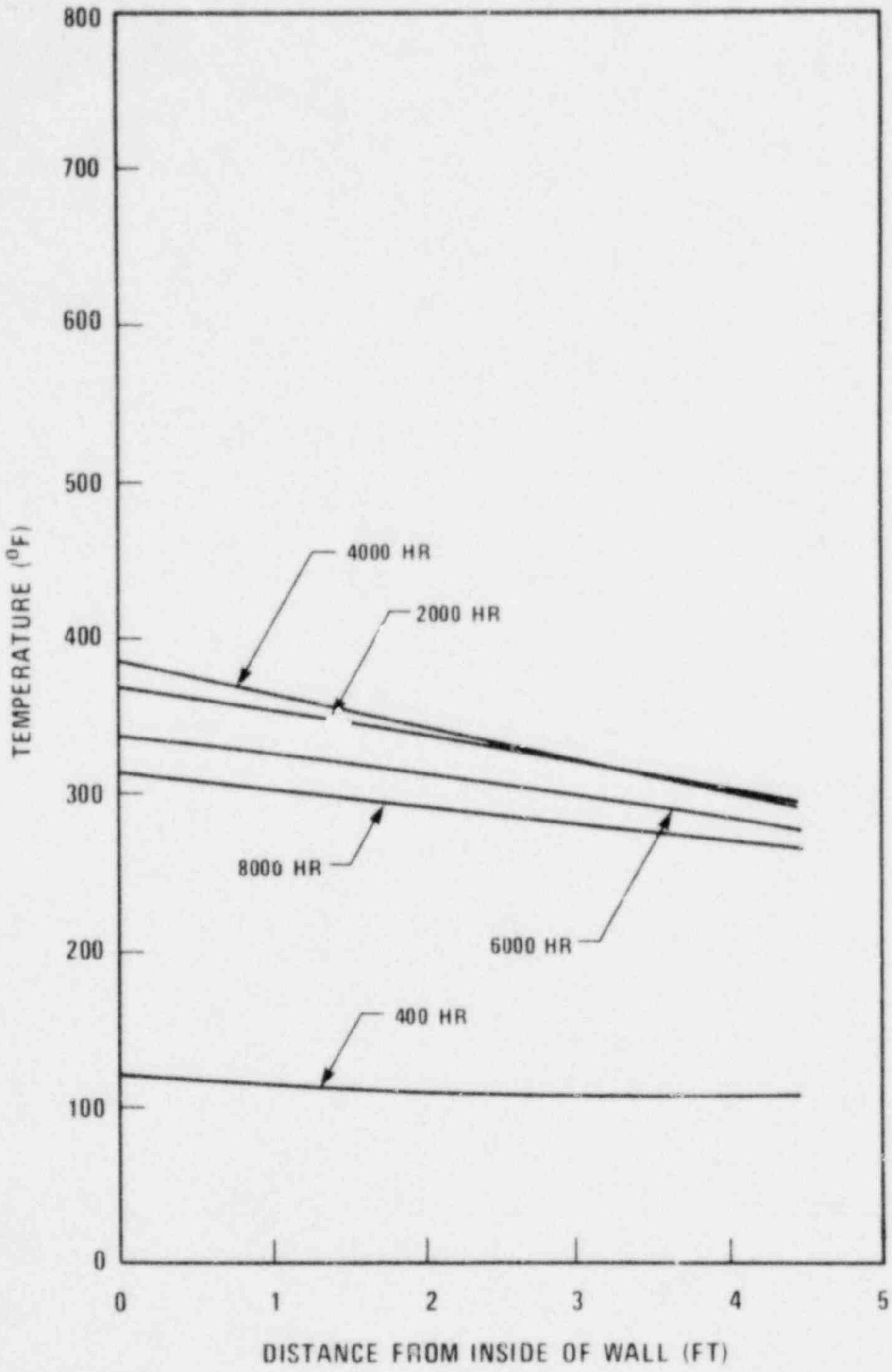

Figure 2-27 Maximum Containment Wall Temperatures (Below Elevation 816.0)

1966-28

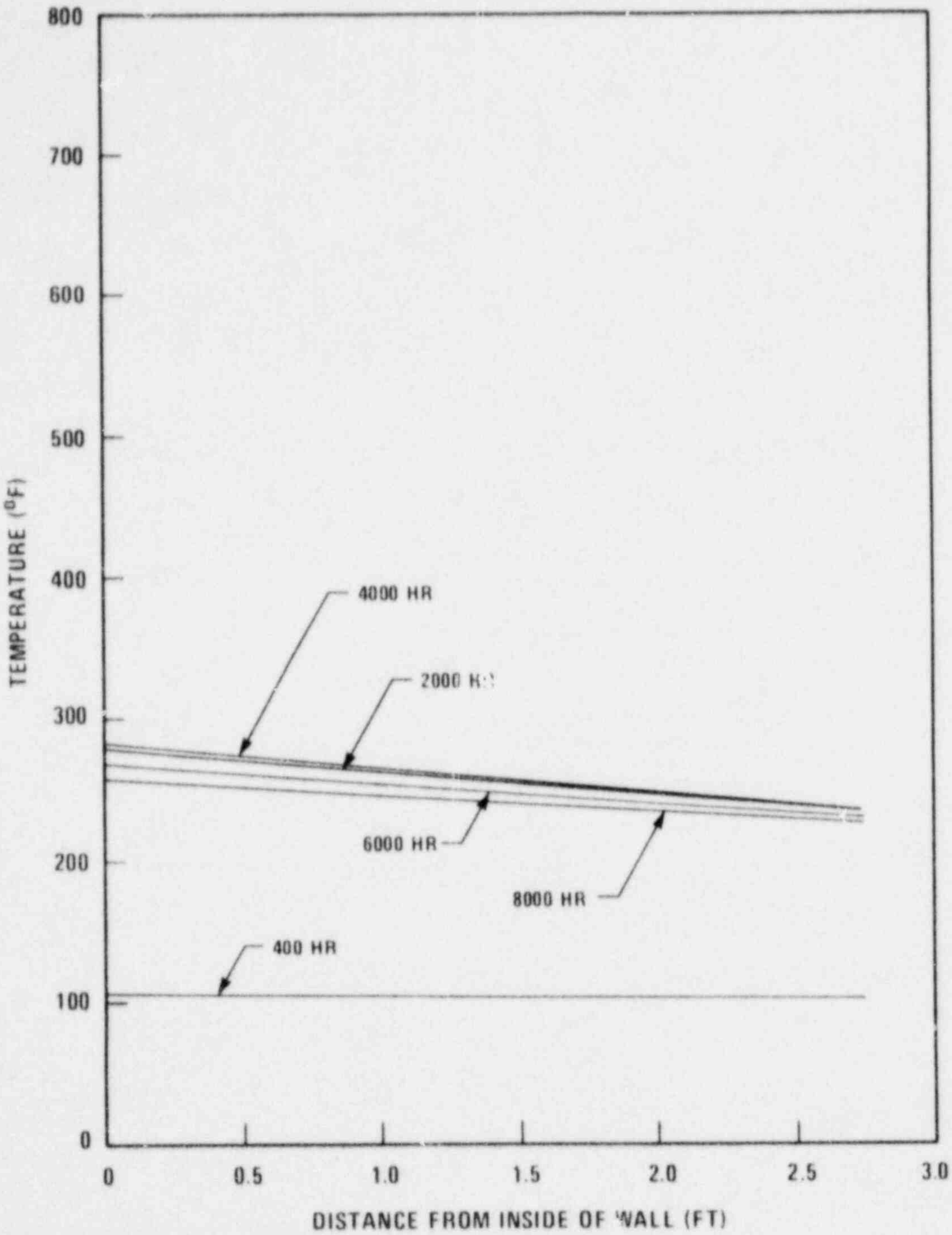

Figure 2-28 Maximum Confinement Wall Temperatures
(Below Elevation 816.0)

1966-29

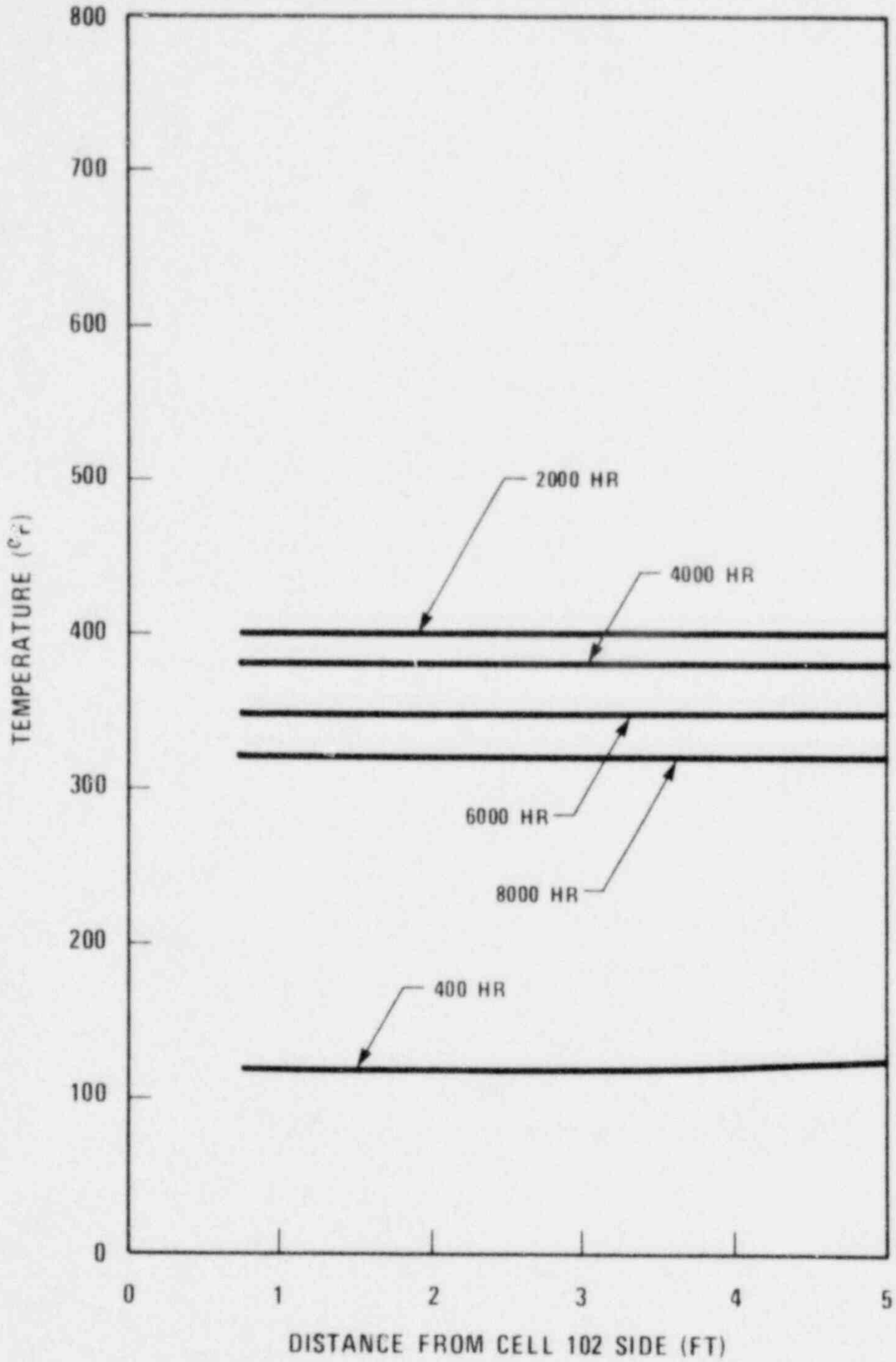

Figure 2-29 Maximum Temperatures of Wall Separating Cells 102 and 105

1966-30

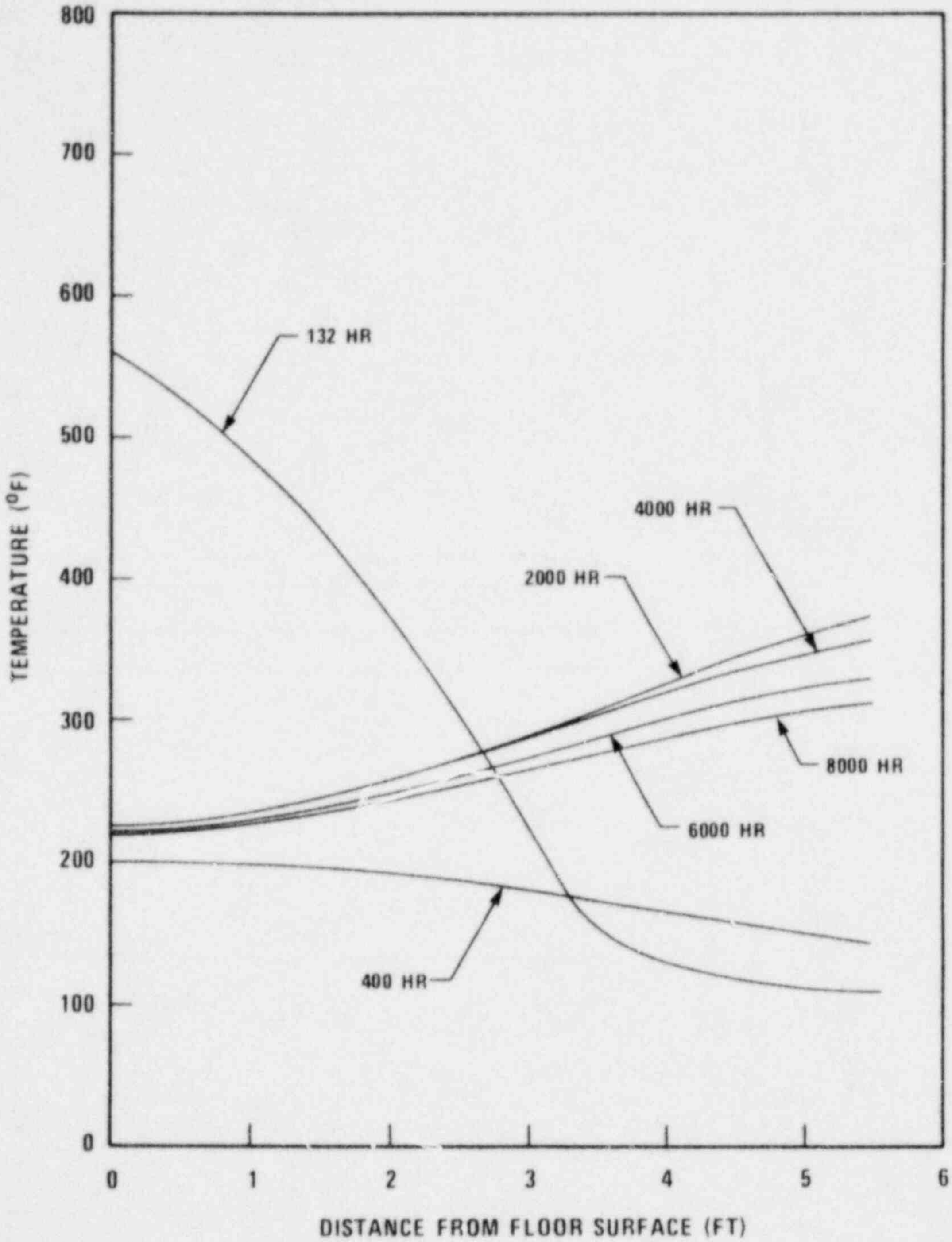

Figure 2-30 Maximum Operating Floor Temperature

1966-31

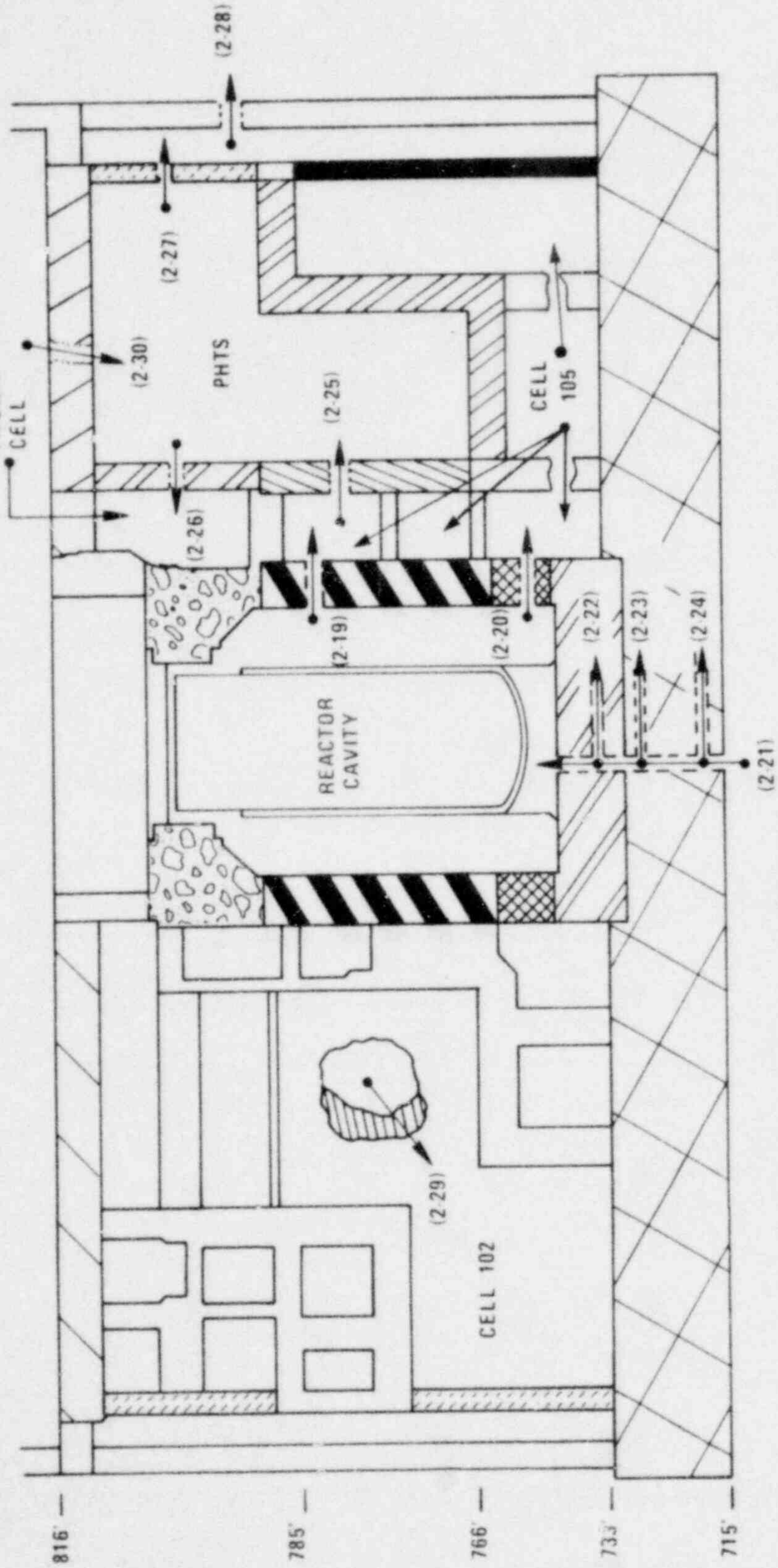

NOTE: ARROW POINTS IN DIRECTION OF THERMAL PROFILE.
FIGURE NUMBERS OF TEMPERATURE PLOTS ARE SHOWN IN PARENTHESIS

Figure 2-31 Location of Post Boildry Temperature Profile Plots

3379-3

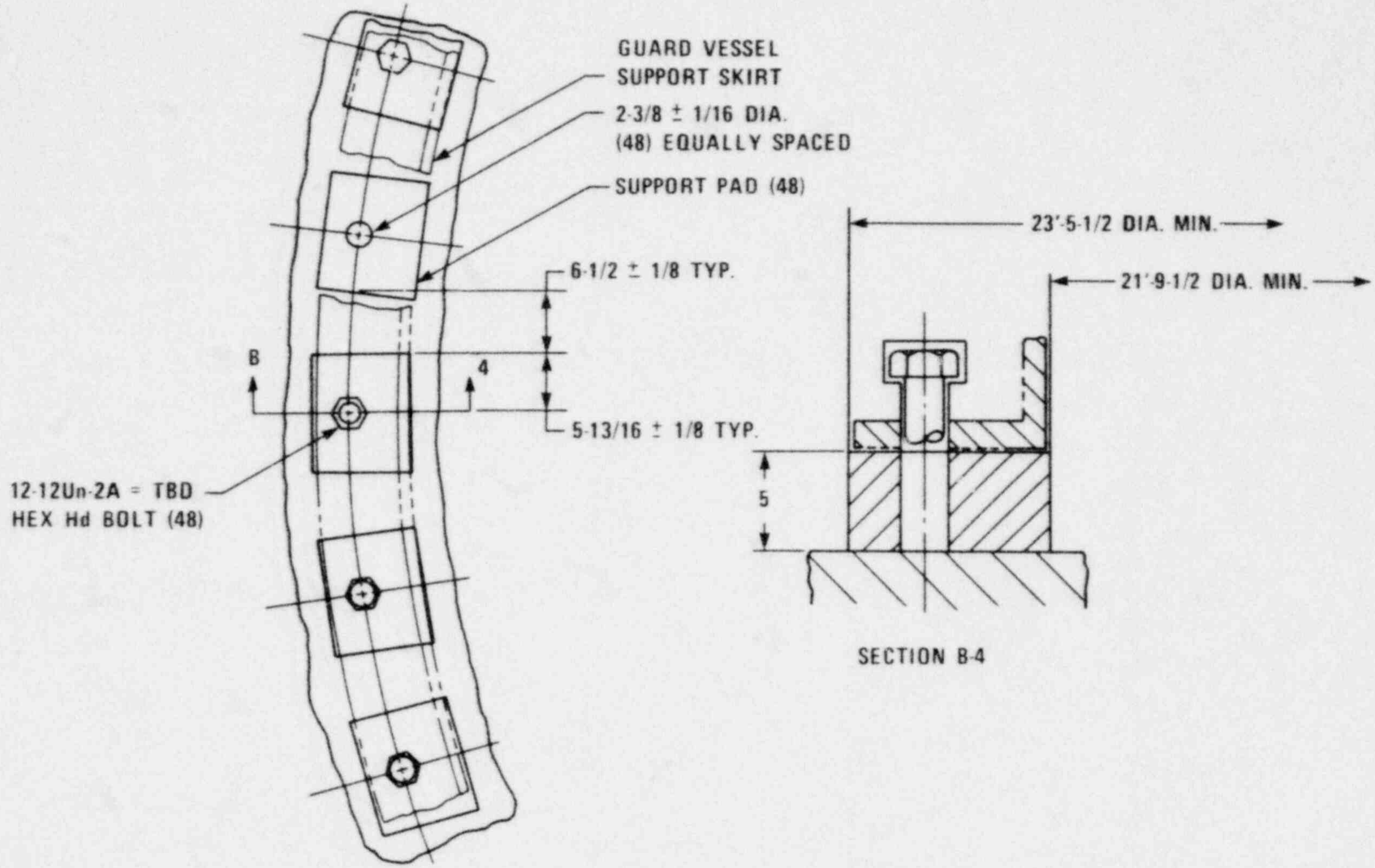

Figure 2-32 Guard Vessel Skirt Support Detail

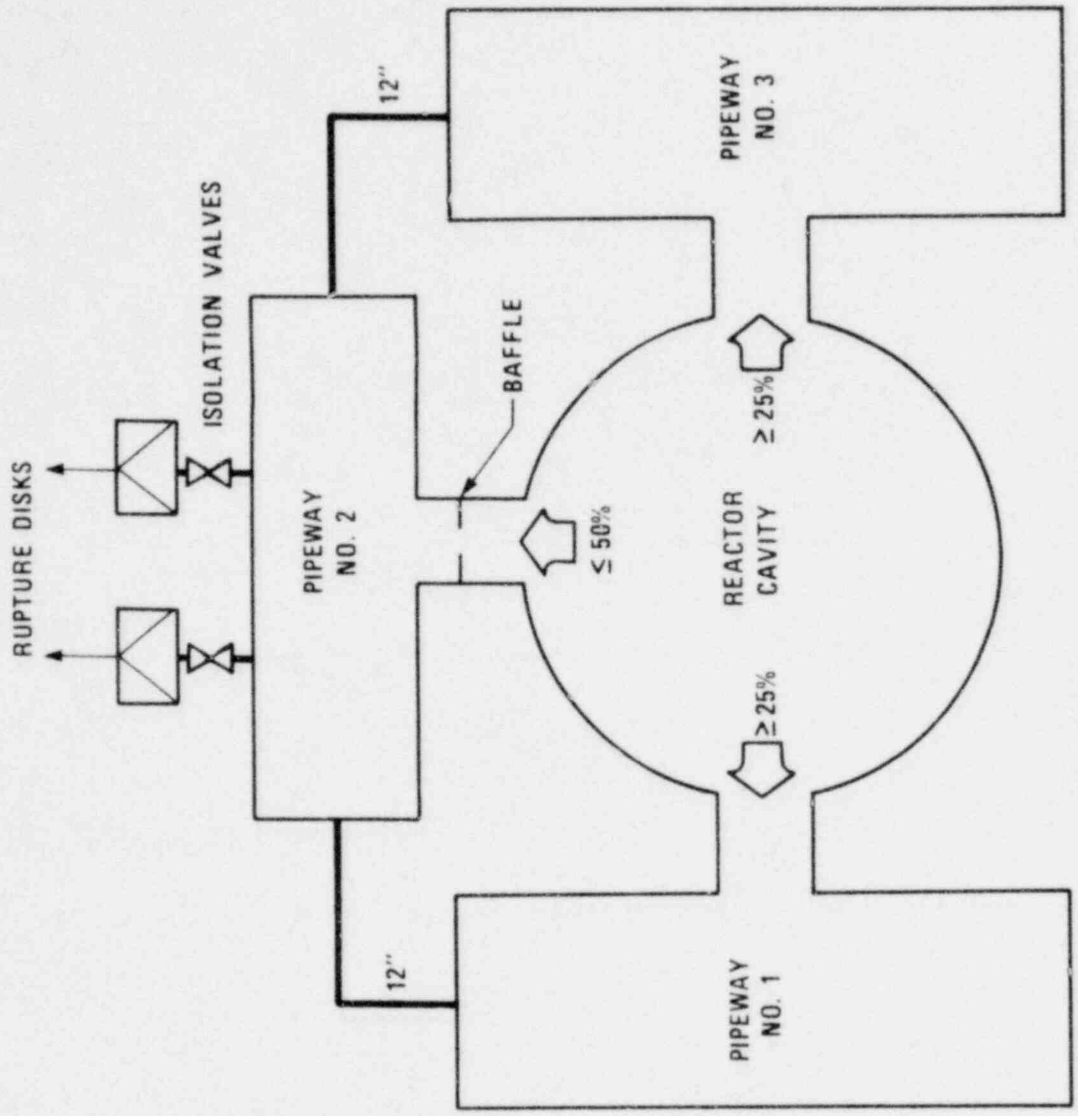

Figure 2-33 Reactor Cavity Vent System

1966-33

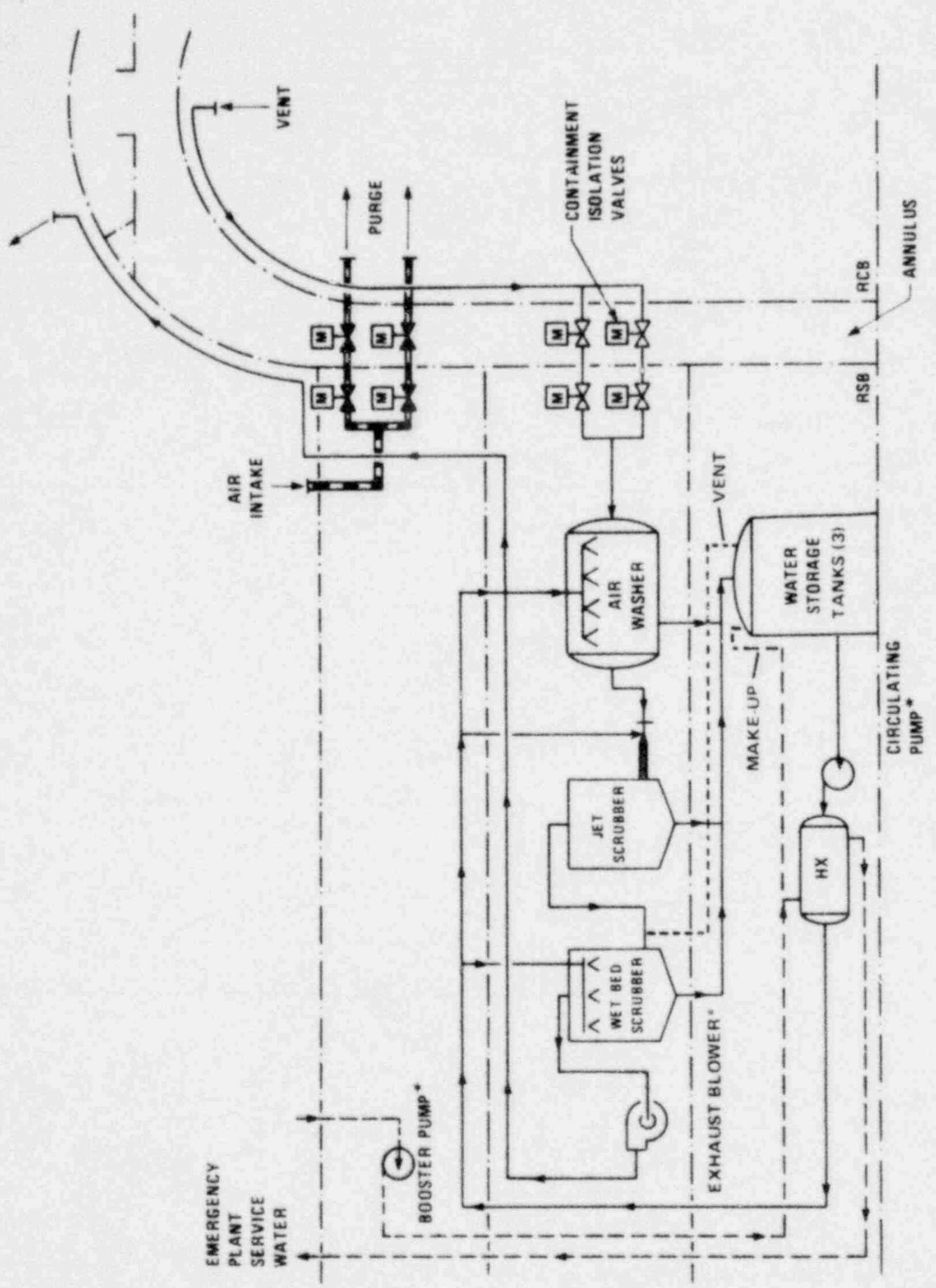

*REDUNDANT COMPONENTS PROVIDED

Figure 2-34 Containment Vent, Purge and Cleanup Systems

1966-34

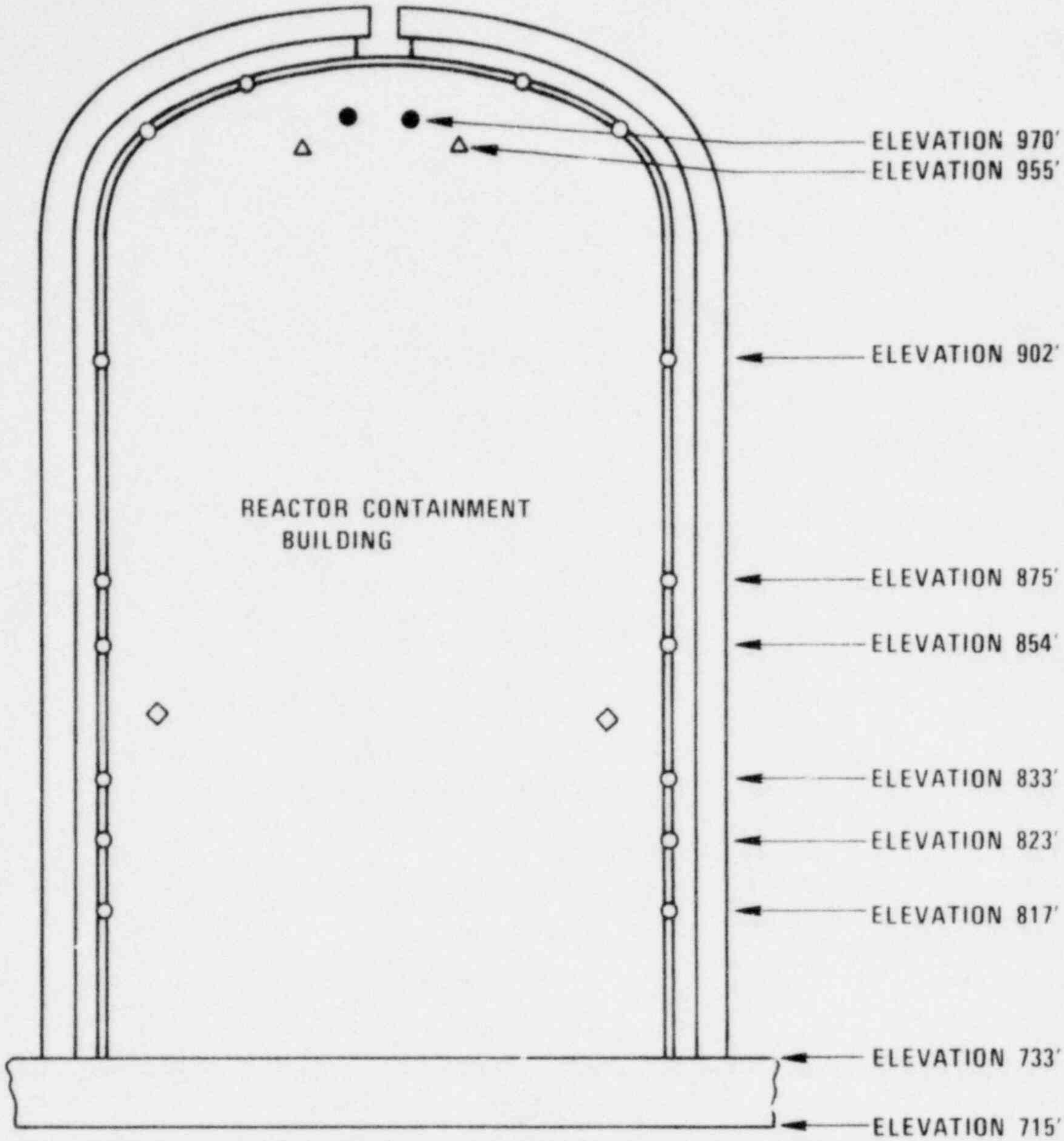

KEY

- ● HYDROGEN MEASUREMENT SYSTEM SAMPLE POINTS
- ○ REACTOR CONTAINMENT VESSEL TEMPERATURE
- △ REACTOR CONTAINMENT ATMOSPHERE TEMPERATURE
- ◇ REACTOR CONTAINMENT PRESSURE

Figure 2-35 CRBRP Containment TMBDB Instrumentation

3379-4

3.0 ASSESSMENT OF THERMAL MARGIN

The core damage associated with a hypothetical core disruptive accident (HCDA) is postulated to result in extensive fuel redistribution. This section considers the redistribution of the core debris, the heat removal characteristics of the primary sodium, and the capability of TMBDB margin features to accommodate the decay heat and the energy associated with sodium burning and its reactions with water vapor, carbon dioxide, and concrete following the hypothetical release of core debris from the reactor and guard vessel to the reactor cavity.

The computer codes applied to the TMBDB analyses are discussed in Appendix A of the PSAR.

3.1 THERMAL MARGIN WITHIN THE REACTOR VESSEL

During a hypothetical core disruptive accident, a large fraction of the fuel and blanket material may be ejected upward from the core region. Upon interacting with sodium, the fuel would particulate, and portions of this material would subsequently settle back into the core, deposit on structural components within the upper and lower reactor vessel plena, deposit on the reactor vessel lower head, or enter the primary heat transport system (PHTS). In this section, an evaluation of the distribution of the core debris within the reactor system is made, the ability of in-vessel and PHTS structures to potentially contain core debris in sodium is considered, secondary criticality is evaluated, and potential penetration times for the reactor and guard vessels are analyzed. The consequences of fuel in the PHTS after reactor vessel and guard vessel penetration and subsequent draining of sodium are given in Appendix I.

3.1.1 Core Debris Distribution

The degree of core damage which may result from an HCDA covers a wide spectrum, i.e. at one extreme is relatively limited damage in which a small fraction of the core leaves the core region and at the other extreme is a whole core meltdown. The redistribution of fuel debris from its original location is dependent on energetics and the timescale for accident progression relative to pump coastdown times. Accident initiators (LOF and TOP) and resulting energetics are discussed in Volume 1 of this document.

In this section, an assessment of the directional distributions of the debris relative to the core is considered for various HCDA sequences. The consequences of the debris distribution are considered in the three subsequent sections (3.1.2, 3.1.3, and 3.1.4).

3.1.1.1 Upward Debris Distribution

In this section, the analysis of upward debris distribution is primarily concerned with estimating the amount of material entering the outlet piping. Thus, assumptions have been made in this part of the analysis to maximize the amount of fuel entering the piping. It should be noted that these assumptions are inconsistent with those analyses presented in Sections 3.2 and 3.3 which consider that 100% of the fuel and non-volatile fission products are spilled onto the reactor cavity floor to bound the thermal loads in the reactor cavity thereby ensuring conservatism.

The quantity of core debris that would be ejected upward during an HCDA depends on the type of initiator. The LOF and TOP initiators are considered in this determination of fuel redistribution.

For the LOF sequence that is predicted to result in a non-energetic core meltdown (transition phase), partial blockages would be expected above and below the core early in the progression. Continued heating and potential pressurization would open other paths from the core to permit additional fuel ejection. This could occur in both the upward and downward direction. Nominally, this transition phase is estimated to result in approximately half the fuel being ejected in each direction because the flow resistance in each direction would be expected to be similar.

If a mechanical disassembly occurs that is sufficiently energetic to relocate or damage structures, the debris distribution would be different. Because of the differences in the structural strength of the above and below core structures, less damage would be sustained by the lower structure. The upper structure would be damaged or displaced to the extent that openings would be provided so that the core materials could be ejected more easily into the upper plenum. For large energetics, where the upward flow resistance would be relatively small, an upward ejection of 90% of the fuel would be possible.

Since the percentage of material ejected upward is estimated to be in the range of 50% to 90%, a nominal LOF case has been defined as having 70% upward fuel ejection.

For the TOP initiator, the SAS-3A code analyses predict termination by fuel sweepout with less than 4% of the core ejected upward.

Analytical Model

The fuel and steel debris ejected into the upper plenum would form particulate as a result of interactions with sodium. The debris settling in the upper plenum and in the piping was assessed by considering the settling of the various particle size groups making up the particle cloud. Because of the low particle concentration (0.7 v/o), settling would occur without hinderance (Reference 3-1), and since agglomeration of particles would enhance in-vessel settling and reduce fuel carried into the piping, it was assumed that no agglomeration occurs.

The trajectory taken by a particle in the upper plenum would be determined by the drag forces exerted on the particle by the surrounding fluid, the buoyancy force generated by the displacement of fluid by the particle, and the gravitational force. The drag forces on a particle are a function of the relative velocity between the particle and its surrounding fluid, acting in both the horizontal and the vertical direction. The buoyancy force acts in an upward direction, and the gravitational force acts in the downward direction. When an imbalance exists between these forces, the particle would be accelerated in the direction of the imbalance until the forces have equalized. As a limit, the particle approaches the velocity of the fluid in the horizontal plane; and in the vertical plane, the particle velocity approaches the vector sum of the fluid velocity and the particle free settling velocity.

The particle free settling velocity is the velocity of a single particle in a stagnant pool of fluid. In this situation, a particle is exposed to an upward force due to both buoyancy effects resulting from forces exerted by the fluid, and to drag effects resulting from the relative motions of the fluid and the particle (assuming a coordinate system relative to the particle velocity, the force is exerted in the direction of the fluid velocity). The single downward force is created by gravitational effects. When upward and downward forces are in balance, the particle is said to have reached its terminal velocity.

For the evaluation of particle transport in the upper plenum of the reactor vessel, these forces, and the subsequent particle motion, have been evaluated using a version of the VARR II computer code (Reference 3-19) which incorporates a subroutine for calculating particle motion. This subroutine, using the fluid velocities calculated by the main program, calculates both the horizontal and vertical drag force acting on the particle using the equation:

$$F_D = \frac{C_D U_0^2 \rho A_p}{2g_c}$$

where

F_D = drag force, lb_f
C_D = drag coefficient obtained from standard curves (Reference 3-1)
U_0 = relative velocity between the particle and fluid, ft/sec
ρ = fluid density, lb_m/ft^3
A_p = cross-sectional area of the particle, ft^2
g_c = gravitational constant, lb_m ft/lb_f sec^2

For the vertical component, the buoyancy and gravitational forces are calculated using the equation:

$$F_T = \frac{mg}{g_c} (1-\rho_f/\rho)$$

where

F_T = combined buoyancy and gravitational force, lb_f
m = particle mass, lb_m
ρ_f = fluid density, lb_m/ft^3
ρ = particle density, lb_m/ft^3
g_c = gravitational constant, lb_m ft/lb_f sec^2
g = acceleration of gravity, ft/sec^2

The resulting particle velocity change is then calculated using the relationship:

$$F = \frac{ma}{g_c} = \frac{m}{g_c} \, dV/dt$$

$$dv = g_c \frac{F}{m} dt$$

where

F = total force, lb_f

m = particle mass, lb_m

g_c = gravitational constant, $lb_m \; ft/lb_f \; sec^2$

dt = problem time step, sec

a = acceleration, ft/sec^2

V = velocity, ft/sec

A schematic of the VARR II computational model used is shown in Figure 3-1. This is the same model that was used to study thermal transients in the upper plenum (Reference 3-15). The VARR II code uses finite element techniques; thus, the upper plenum is represented as a series of connected fluid nodes. The upper internals structure (UIS) is represented as obstacle nodes (non-fluid nodes) and the suppressor plate is represented as a flow resistance between the fluid nodes at the suppressor plate elevation.

Particles are injected into the fluid stream at the entrance to the UIS chimneys (coordinates 2, 3 and 4, 3 on Figure 3-1) 13.4 seconds after the initiation of the flow coastdown. This value was chosen on the basis of studies that show fuel motion initiation 13.4 to 15.9 seconds after the initiation of the flow coastdown (References 3-17 and 3-18).

The flow coastdown data input are given in Table 3-1; the data are consistent with those used in Reference 3-17.

Settling in PHTS Piping

Much of the work on particle settling in horizontal pipe runs has been directed at determining the minimum fluid velocity needed to keep solid particles in suspension so that they can be transported by pipeline. The data from these studies have been used to develop a correlation for the fluid velocity below which the turbulent action of the fluid is not sufficient to keep the particles in suspension, and the particles would settle onto the piping. The correlation developed was

$$V = 3.87\, C_V^{0.5}\, C_D^{-0.25}\, (gD)^{0.5}\, (S-1)^{0.3} \qquad \text{(Reference 3-16)}$$

where

V = fluid velocity, ft/sec

C_V = total volumetric solids concentration

g = acceleration of gravity, ft/sec^2

D = pipe diameter, ft

S = particle density/fluid density

C_D = single particle drag coefficient (see Table 3-4)

When the bulk fluid velocity falls below this value, the particles can no longer be kept in suspension and accumulation of debris on the lower surface of the pipe begins.

Once particle settling begins, the particles are assumed to fall through the fluid at a rate equal to their settling velocity, and, at the same time, the fluid velocity is superimposed on the vertical velocity; thus, the particles will deposit along the length of the piping rather than a single location. The larger particles which have a higher settling velocity will settle quickly, and the smaller particles, which have a lower settling velocity, will be distributed further along the length of the piping. Since there is a wide variance in the size of the particles considered in this evaluation, one would expect a high concentration of particles (composed of all particle sizes) in the upstream portion of the piping (i.e., nearer the reactor vessel outlet) and a low concentration of particles (composed of only the smaller sizes) in the downstream portion of the piping.

The amount of material that settles in a given region can be determined by calculating the amount of settling that occurs when a given fluid increment passes through the region. For the purpose of discussion, a fluid increment is defined as a finite circular fluid plug in which the particles initially are uniformly dispersed. As this plug flows through the piping system, the particles settle and an upper increment of the plug becomes devoid of particles (see Figure 3-2). The net change in the volume of this "void" section multiplied by the initial particle concentration in the element equals the quantity of material which has settled over the given section.

No deposition occurs in the vertical piping sections. However, in vertical sections where the fluid flow is upward, it is possible (due to a flow coastdown) for the net particle velocity (vector sum of the fluid and particle settling velocity) to change from positive to negative. In this instance, these particles, which are initially traveling upward, are calculated to settle in the elbow upstream of the vertical section.

Results

The results of the evaluation are shown in Tables 3-2 and 3-3. Because of the small amount of fuel involved in the TOP event, 4% of the core, the consequences of this event would be bounded by the LOF evaluation. Thus only the LOF, which involves a nominal 70% of the core ejected upward has been evaluated.

The particle size distributions observed during the several molten fuel-sodium interaction tests* can be seen in Figure 3-3 (Reference 3-5). The EDT-1 test contained the highest percentage of "fines", the S3 test has the highest "coarse" content, and the remainder of the distributions tend toward a median in the vicinity of the M-1, M-2 and M-3 distributions. If the S3 distribution, which appears to deviate significantly from the median, is conservatively ignored, the median distribution curve falls in the vicinity of the M-3 distribution. For this reason, the data from the M-3 distribution have been chosen as most representative of the distribution that would result from a loss-of-flow initiated HCDA. However, as a sensitivity study, the EDT-1 distribution has also been analyzed.

*For additional details of these tests, see Appendix G.1.A.

From the data of Table 3-3, it can be seen that more than half of the upward ejected fuel is predicted to remain in-vessel; however, a significant quantity is predicted to leave the reactor vessel and enter the outlet piping. The quantity entering the piping, as expected, is greater for the finer distribution.

The majority of the material entering the piping settles out upstream of the PHTS cell wall; approximately 0 to 2% settles in the piping between the PHTS cell walls and the pumps, and another 0 to 6% reaches the IHX. The consequences of these quantities of fuel in the primary piping prior to reactor vessel and guard vessel penetration and draining of sodium from the piping are addressed in Section 3.1.2. Appendix I addresses the consequences of fuel in the piping following sodium draining.

3.1.1.2 Downward Debris Distribution

For LOF events, downward movement of the fuel is possible. The fuel would either melt the continuously forming steel plug below the molten fuel front or flow through the flow paths in the shield/orifice blocks into the module. Here some particulation may occur; however, the capability of the lower inlet modules to retain fuel either as a debris bed or as molten fuel is limited by the geometry of the module and any fuel in excess of the lower inlet modules capability would enter the lower plenum. Here particulation would occur in the bulk sodium. These progression paths represent the limiting extremes for delivery times to the lower plenum.

As previously described, the percentage of the core estimated to initially move downward ranges from 10 to 50% of the active core for all mechanical disassembly or transition phase scenarios. The resultant debris bed on the lower head of the vessel could exceed the maximum stable bed depth described in Section 3.1.2 and cause penetration of the reactor and guard vessels (Section 3.1.4).

3.1.2 In-Vessel Debris Retention Capability

The in-vessel debris retention capability was determined by comparing the predicted debris distribution in Section 3.1.1 with the maximum debris capacity of the major horizontal surfaces within the reactor system. This section describes debris bed heat removal phenomena followed by an evaluation of the fuel holding capacity of each of the horizontal surfaces in the reactor system.

Debris Bed Heat Removal Phenomena

The fuel debris particulate that settles on horizontal surfaces would be generating heat due to the fission products associated with the fuel. The debris bed can be cooled by internal sodium convection within the bed. The heat rejection capability of such a bed is a function of the bed depth and the heat generation rate. If the heat generation or depth is sufficient to result in bed dryout (sodium film boiling throughout the bed), then particle recoalescence can occur forming a molten pool of fuel and steel which would probably melt through the surface containing the bed.

Using experimental data from References 3-3 and 3-5 for dryout heat flux and the CRBRP decay heat from Table 3-5, the maximum debris bed depth which could be accommodated without debris bed dryout and fuel recoalescence was calculated. The stable debris bed depths are shown in Table 3-6. The decay heat shown in Table 3-5 includes an allowance for all uncertainties; thus, it is more conservative than required for best estimate calculations. Irrespective of the spatial distribution of the debris, the fission products would be distributed within the system according to their type. The fission products can be classified as gaseous, halogens, volatile and non-volatile. The gaseous fission products, the noble gases, would rise to the cover gas space above the upper sodium plenum. Initially these account for about 5% of the total decay heat. The halogens and volatiles, for example, iodine and cesium, are expected to volatilize from the fuel and dissolve in or react with the bulk sodium where they would largely remain. These account for over 25% of the initial heat generation rate. Thus, over 30% of the fission product heat would be initially relocated from the fuel debris. The impact of their removal from the debris was assessed and is shown in Table 3-6. Approximately 70% of the total decay heat comes from the non-volatile fission products (i.e. solids) that remain with the fuel debris.

Since the cooling capability of a bed is a function of the heat generation and the bed constituents, the following assumptions are made:

1. The whole core, axial blankets and first row of radial blanket assemblies are involved in the core meltdown.

2. The steel from the clad, wire wrap and ducts of the affected assemblies over the height of the core and axial blankets is associated with the debris.

3. Any particulate bed formed has a porosity of 0.5 (Reference 3-3).

4. The oxide and steel particulates are mixed uniformly on an equi-volume basis. This reduces the allowable heat flux for a given bed loading of oxide and is conservative. Furthermore, layering in the bed due to the steel settling before the fuel is not considered. This is also conservative. Since the steel particles are larger than the oxide particles, they will tend to settle faster, thus depleting the proportion of steel in the particle cloud. The effect of no steel in the debris beds was assessed as an upper bound indication of the effect of steel depletion in the bed such as may occur in beds in the piping.

5. The times for formation of the particulate beds were considered parametrically in a range considered pertinent to the loss of flow HCDA. However, the results can be adjusted for consideration of transient overpower events. The detailed numerical computations are identified in the appropriate sections.

6. Sufficient heat capacity is available to prevent sodium in the PHTS and vessel from reaching saturation conditions.

The assumptions stated above were applied to four cases having the following characteristics:

(a) The particulates are oxide and steel mixed on a one-to-one basis and all the fission products are retained in the fuel.

(b) The bed has a similar constitution to that described above except that the noble gases and sodium soluble fission products were assumed to have left the oxide particles, thus reducing the heat load.

(c) The bed has a 50% porosity. No steel particles are included. All the fission products are included in the bed heat generation rate.

(d) The bed consists of oxide particles only, and the gaseous and sodium soluble fission products are not included.

The times at which bed formation occurs were taken to be 30, 100, and 200 seconds after subcriticality, and are considered suitable for scoping bed formation calculations for various HCDAs. The stable depths of debris beds are indicated in Table 3-6 for the conditions indicated above. Table 3-6 indicates that the stable bed depth is relatively insensitive to time of formation.

Recent out-of-pile experimental data (Reference 3-6) indicate higher debris bed dryout fluxes than those used to generate Table 3-6. Furthermore, recent in-pile experiments (Reference 3-20) indicate that bed dryout may not be a sufficient condition for fuel melting. The experiments, which were conducted in the Annular Core Pulsed Reactor (ACPR), tended to demonstrate that the threshold power required to produce dryout in both medium-depth and deep beds of 100 to 1000 micron uranium particles does not lead to extremely high temperatures or to melting of the fuel. Thus, the bed depth at which fuel melting would occur would be greater than that predicted by the data of Reference 3-6. Therefore, the maximum coolable debris bed depth is higher than the table indicates and the fuel retention capability of the structures described in the next paragraphs is conservative.

Fuel Retention Capability in the Upper Plenum

The major surface for debris accumulation in the upper plenum is the horizontal baffle. Following the core disruption and neutronic shutdown, the transition and core debris ejection phases are assumed to last 15 seconds and particulate settling occurs over the next 15 seconds. The results are not sensitive to either 15 second assumption. The fractions of the core and blanket assemblies which can be accommodated on the baffle (assuming it remains horizontal) for the cases indicated in the previous section are in the range 28 to 46%. Other surfaces in the upper plenum primarily associated with the upper internals structure represent added capabilities not currently considered but which may provide additional surfaces for particle bed cooling.

Fuel Retention Capability in the Lower Plenum

The capabilities of the lower inlet modules and the vessel lower head have been assessed for various melt-through times of the lower structures of the fuel assemblies and for various PHTS loop transport times. A range of times after attaining subcriticality for fuel and steel to reach the module inlet ports was considered. The range was from 10 to 5000 seconds in order to assess a wide range of melt-through sequences from no holdup to complete shield/orifice block plugging and subsequent melting. The modules could contain in a stable debris bed from 0.9 to 2.5% of the fuel and upper and lower axial blankets of assemblies associated with the module depending upon debris delivery time and fraction of steel in the bed (in the range 0 to 50% of the particulates). The value of 2.5% represents an upper limit for a bed due to the geometry of the module which limits the maximum bed depth before debris overflows through the inlet ports and assumes that the fuel debris is delivered to all the modules. The lower head of the vessel has the capability to retain debris beds with thicknesses in the range 1.6 to 6.4 inches depending on melt-through time (30 to 5000 seconds), fraction of decay heat retained in the bed (70 to 100%) and percentage of steel in the particulates (0 to 50%). These conditions scope those associated with debris transport around the loop. This represents 0.8 to 8.1% of the core, upper and lower axial blankets and radial blanket.

Fuel Retention Capability in the PHTS System

The fuel retention capability of the outlet pipe elbow, the hot leg piping, and the IHX were evaluated using the stable debris bed depths on Table 3-6, the geometry of the system, and the flow and debris settling characteristic from Section 3.1.1. The combined capability of the three outlet elbows is 3-4% of the core, axial blankets and first row of radial blankets; for the outlet piping before the PHTS cells, it is 17-31%; for the piping between the PHTS wall and pump, it is 20-37%; and for the inlet annulus of the IHX, it is 7-14%.

Comparison of Fuel Retention Capability with Predicted Fuel Distribution

The comparison of the fuel retention capability of the various structures of the reactor system is given on Table 3-7. The table also indicates the predicted quantities of fuel debris on the structures.

Fuel retention capability of the lower head is much less than the predicted fuel deposited on it; thus penetration would probably occur. Penetration time predictions are described in Section 3.1.4 and the consequences are described in Section 3.2. Penetration of both the horizontal baffle and the outlet piping in the reactor cavity is also a possibility, although less probable than for the case of the lower head of the vessel. Penetration of the piping within the reactor cavity would not impact the analysis reported in Section 3.2. Penetration of the horizontal baffle would not alter the consequences. Penetration of the other structures does not appear to be probable as the fuel retention capability is much greater than the predicted fuel distribution.

The fuel retention capabilities given in Table 3-7 are based on a sodium cooled debris bed. After guard vessel penetration and draining of sodium from the primary system, melt-through of the piping within the pipeway cells may occur. This is addressed in Appendix I.

3.1.3 Secondary Criticality Considerations

The potential for criticality of the debris bed on the lower head of the vessel was considered. Calculations were performed using the ANISN transport theory program in a one-dimensional slab geometry. The slab was infinite in the transverse direction. Several cases were considered using the beginning of equlibrium cycle core fuel and lower axial blanket, the associated clad and wire wrap steel and a 40% bed porosity. Variations were considered including the duct steel, increased porosity, removal of fission products and bed layering. No case represented a critical configuration; however for a complete core and lower axial blanket, the calculated effective multiplication factor k_{eff} was in the range 0.91 to 0.98. This leaves little margin for uncertainties (calculational, geometric, inventory and temperature). However the inclusion of a larger fraction of blanket fuel or steel would result in a noticeable reduction in k_{eff}; consideration of the curvature of the head would also reduce reactivity. Reduced core fractions also reduce reactivity; a k_{eff} of 0.8 corresponds to 37 to 47% of the active core and lower axial blankets for cases considered.

Combining the above results with the predictions of downward fuel movement from Section 3.1.1 it is concluded that criticality on the lower head would not occur. However, even if criticality is postulated, the increased heat in the bed would cause the bed to boilup and disperse by sodium or steel vaporization to a less reactive configuration. No substantial energetics would be associated with such a criticality. Since the potential debris bed thickness is greater on the curved lower vessel head, than on other surfaces that may be flat (such as the core support plate) criticality on other debris collecting surfaces would be even less likely.

3.1.4 Penetration of the Reactor and Guard Vessels

As indicated in Section 3.1.2 the fuel retention capability of the lower vessel head is less than the predicted amount of fuel settling on it following an HCDA that results in whole core involvement. Therefore, penetration is probable in that case. The holdup time for the core debris and sodium within the reactor and guard vessel before penetration was conservatively taken to be 1000 seconds in the evaluation of plant thermal margins. This penetration time was determined from the computational model described in Appendix B based on the following assumptions:

- o All of the active core fuel is in the debris bed (realistically some of the fuel will be ejected upward which will increase penetration time).
- o No holdup in the reactor internals.
- o A level debris bed is formed on the reactor and guard vessel bottom heads.
- o The lower axial blanket and from 10,000 to 15,000 pounds of steel are included in the debris bed. This amount of blanket and the steel from cladding, wire wrap, duct tubes, etc., are considered to be part of the debris bed since this is the minimum amount of blanket and steel that would be expected to be melted by a complete core meltdown.
- o The entire decay power including uncertainties is generated in the fuel debris (realistically noble gases, halogens and sodium soluble fission products should not be present in the fuel debris).

The dependence of penetration time on the amount of blanket material in the debris bed, the quantity of steel debris present, the holdup time in the core and core support structure, and the depth of the debris bed is also given in Appendix B.

Analyses with penetration times ranging from 100 to 10,000 seconds have indicated that the TMBDB containment transients are not significantly affected by penetration times in this range. Table 3-8 shows the variance from the 1000 second penetration analysis of containment conditions at 24 hours described in Section 3.2.2. From this table, it is evident that penetration time is not a significant factor and no operator actions are required other than those discussed in Section 2.3.

The lack of sensitivity of the containment conditions at 24 hours to the reactor vessel and guard vessel penetration time is the result of competing effects. As penetration time increases, containment conditions would be improved because less energy of reaction enters the sodium pool from gases released from concrete. On the other hand, the reactor coolant boundary is a less effective heat sink than the reactor cavity and pipway structures. The net effect is a minor improvement in containment conditions (and the resulting radiological consequences) as the penetration time increases from 100 to 10,000 seconds.

The sodium temperature at penetration of the reactor and guard vessels ranges from 960°F to 1160°F for the 100 to 10,000 second penetration time range. Since the containment conditions are slightly less severe as penetration times increase, these results can be extrapolated to conclude that containment conditions and radiological consequences would not be significantly different if vessel penetration would be delayed until sodium boiling temperatures are reached in the reactor vessel.

3.2 THERMAL MARGIN EXTERNAL TO THE REACTOR VESSEL

This section evaluates the thermal margin beyond the design base provided to mitigate the effects of reactor and guard vessel penetration following an HCDA.

3.2.1 Scenario

The predicted progression of an HCDA based on current state-of-the-art analyses (Sections 3.2.2 and 3.2.3) is summarized below. This progression is based on the assumption of initiators of an HCDA that are considered incredible, but is nonetheless evaluated for assessment of Thermal Margin Beyond the Design Base, i.e. TMBDB.

1. HCDA is assumed to occur with energetics up to 661 MJ (equivalent work energy if the fuel vapor pressure-volume curve were expanded to one atmosphere). The reactor vessel and head are designed to remain intact following the dynamic loads. The head leak rate would not exceed 1000 scc/sec for the first 1000 seconds. Although leakage paths for release of sodium have not been identified, 1000 pounds are assumed to be ejected during this time. Containment isolation based on radiation levels in the RCB would occur from the initial release through the head or, if those releases are very small, from releases through the planned vent path from the reactor cavity to the RCB (see item 8).

2. Core debris from the HCDA would settle on the reactor structures. The fuel particulate debris bed would dry out (no longer adequately cooled by the sodium within the bed because the thickness of the bed exceeds the stable thickness for the associated decay heat). Following dryout, the fuel would increase in temperature and cause the bottom of the reactor vessel to overheat and fail. The process of fuel particulation, bed formation, dryout and failure would be repeated for the bottom of the guard vessel. The time for penetration of both vessels would be in excess of 1000 seconds. Penetration times ranging from 100 to 10,000 seconds have been evaluated and do not change the basic scenario or consequences (Table 3-8). A penetration time of 1000 seconds has been used in the subsequent analyses.

3. The core debris (the complete fuel and blanket inventory) is assumed to be released into the reactor cavity along with the sodium that would drain and siphon from the reactor vessel and primary heat transport system following reactor vessel and guard vessel penetration (1.1 x 10^6 lbs). The average sodium temperature is estimated to be 990°F, based on no heat loss from the vessel prior to penetration.

4. The core debris would be distributed in the sodium over the 40 ft. diameter reactor cavity floor. The small size of the fuel particulate formed by interaction with the sodium (0.1 - 6000 μm; Figure 3-3) would allow the fuel to be carried by the sodium under the guard vessel skirt into the reactor cavity. Fuel particles would be suspended in the sodium due to either turbulent mixing as they penetrate the guard vessel or during the reparticulation of molten fuel within the reactor cavity. Debris beds also would self-level from the action of boiling sodium in the bed, causing the bed to be approximately level over the reactor cavity floor (Reference 3-5). Also, if penetration of the guard vessel would occur outside the skirt (∽same diameter as guard vessel), self-leveling would be even more rapid because of the large area outside the skirt (∽900 ft^2) compared to the area within the skirt (∽300 ft^2).

   The stable debris bed depths are calculated using data obtained from experiments in which UO_2 particles ranging in size from 0-1000 μm were heated. It has been shown, Reference 3-5, that the addition of finer material to this mixture increases the dryout heat flux because the finer particles are levitated, creating better heat transfer conditions. A second experiment was conducted in which 1 cm cylindrical pellets were added to the mixture, and no noticeable changes in the dryout heat flux was noted.

   Sodium subcooling does not appear to have a large effect on bed dryout heat fluxes. Experiments at ANL (Reference 3-6) indicate a subcooled sodium pool has either no effect or may increase slightly the dryout heat flux of a debris bed. Thus the effect of subcooled sodium may increase the margin between the bed dryout thickness and the depth of a debris bed uniformly distributed over the reactor cavity floor*.

A coolable debris bed geometry would result because of the phenomena previously discussed and because sufficient margin exists between the depth of debris bed that would result in dryout (no longer coolable $\sim$5.3 inches), and the average debris bed depth over the reactor cavity floor ($\sim$1.5 inches) to allow for uneven distribution or incomplete self-levelling.

Appendix G.1 discusses debris bed formation, spreading and levelling in the reactor cavity in greater detail.

5. After the fuel particulate and sodium enter the reactor cavity, the entire floor liner is assumed to fail for analysis purposes. This is a pessimistic assumption since experiments indicate the liner should not fail (Reference 3-6) and, if failure occurs, the failure should be localized. The failed liner assumption implies that flow of gases and liquids between the sodium pool and the concrete would not be impeded but that the physical presence of the liner would impede the movement of solid reaction products from the sodium-concrete reaction. Thus, any removal of the sodium-concrete reaction products would be a localized effect if it were to occur. The treatment of sodium-concrete reactions is described in Section C.1.2.3 and sensitivity studies are provided in Section G.2. Subsequent reactor cavity and pipeway cell liner failures assumed in the analysis are presented in Table 3-12.

---

*Particulate formation due to dropwise condensation of UO_2 vapor would be expected to produce a finer particle size distribution than used in the debris bed cooling analysis. As the droplets would have a large surface area-to-volume ratio, the heat transfer from the particles would be rapid, and the resulting thermal shock would be expected to fragment the particles even more finely than when molten UO_2 is quenched in sodium. This would result in a more coolable bed due to levitation of the finer particles.

6. Hydrogen would be generated by the sodium reacting with water released from the heated reactor cavity floor concrete.

7. Carbon dioxide would be released by the concrete if it is heated to sufficiently high temperatures. The release is small for temperatures less than 1200°F (References 3-7). It would react with the sodium forming solid reaction products.

8. After 1000 seconds and immediately following the penetration of the reactor vessel and guard vessel, the rupture disk in the vent line between the reactor cavity and containment would burst because of the rapid pressure rise in the reactor cavity and pipeway cells. This pressure rise would result from heating of the atmosphere by the sodium entering the cavity and the combustion of the oxygen (2%) in the reactor cavity and pipeway cells atmosphere (sodium vapor leaks from the reactor cavity to the pipeway cells). As soon as the rupture disk bursts, the venting reduces the pressure differential between the reactor cavity and pipeway cells and the reactor containment building to a fraction of 1 psi. The noble gases would be released to the containment atmosphere and would provide a heat source.

   Appendix G.3 indicates that credible mal-operation of the RC-RCB vent system would not result in unacceptable consequences.

9. The decay heat associated with the halogens and volatiles is assumed to be contained in and carried with the sodium. The remainder of the decay heat (associated with the solid fission products and fuel) would provide a heat source in the sodium pool in the reactor cavity. The sodium in the reactor cavity would increase in temperature due to the energies from the fission products, fuel, sodium-24 activity, sodium-concrete reaction, sodium-water reaction, and the sodium-carbon dioxide reaction. The heat sinks due to conduction into the reactor cavity walls are also considered in the energy balance. Sodium boiling is calculated to begin at about 9 hours.

10. The sodium vapor, as well as hydrogen and any remaining nitrogen and argon, would pass through the three pipeway cells into containment through the reactor cavity - containment vent system. Since the flow resistance of head leakage paths is high compared to the vent resistance, the flow would be through the pipeway cells, which serve as heat sinks. The effect of reactor head leakage is shown in Appendix F.6 to be insignificant.

11. The water vapor and carbon dioxide, released from the concrete when it is heated, would be vented from behind the reactor cavity and pipeway wall liners by the liner vent system, to spaces below the operating floor (except the reactor cavity floor which is vented to the RCB atmosphere)*.

12. Upon reaching containment, the sodium vapor would react with the oxygen, carbon dioxide, and water vapor according to their molar concentrations. The reaction with water vapor would take place if the water vapor concentration is greater than the oxygen concentration. If the water vapor concentration is less than the oxygen concentration the sodium vapor would react with oxygen and carbon dioxide according to their molar ratios.

13. Upon reaching containment, the hydrogen generated in the reactor cavity and in the pipeway cells (after 30 hours) and hydrogen generated by the sodium-water reaction in containment would react with oxygen when either criterion (a) or (b) below is met in combination with criterion (c) (Appendix H.1 describes the hydrogen burning criteria in detail).

---

*The accumulation of water prior to a HCDA would be prevented by the liner vent system. The water would evaporate and would be vented to the atmosphere of Cell 105 or the containment building above the operating floor. Steam explosions would be precluded since no liquid water would be present.

Criteria for hydrogen burning:

a. The hydrogen-nitrogen mixture entering containment is above 1450°F.

b. The hydrogen-sodium-nitrogen mixture entering containment contains at least 6 g/m^3 of sodium at temperatures above 500°F.

c. The oxygen concentration is above 8%. With the oxygen concentration above 5% and the hydrogen concentration above 4%, the hydrogen in excess of 4% would burn. Figure 3-4 illustrates this burning criterion.

Criterion (a) is not met for the analyses reported herein. The sodium concentration entering the reactor containment building would satisfy criterion (b) after about ten hours following vessel penetration. At the end of this time the hydrogen concentration in containment would reach approximately 4.5%. This hydrogen would burn while the burning criteria are satisfied as the natural circulation in containment moves the hydrogen through the flame. The oxygen concentration is predicted to remain above 8% (satisfying criterion c) for 36 hours; thus, no hydrogen accumulation would occur during this time (i.e. 10 to 36 hours).

The flame characteristics are shown in Appendix H.2 to be such that excessive local containment steel temperatures would not occur.

When hydrogen burning criteria are no longer satisfied, hydrogen would accumulate in the containment. The hydrogen concentration would be controlled to less than 6% by purging (see item 17). Since the hydrogen concentration is maintained well below explosive levels, the containment integrity would not be challenged by hydrogen reactions.*

14. Water vapor from concrete in the operating floor and head access area would enter the containment atmosphere.

    The sodium oxide created by the sodium-oxygen, sodium-carbon dioxide, and sodium-water reactions in containment would react with the excess water vapor in the containment atmosphere to form sodium-hydroxide.

15. The maximum containment pressure of 22 psig (peak pressure results from assumption that accumulated hydrogen burns instantly) is well below the failure pressure. Scoping calculations indicate that the failure pressure is in excess of 30 psig for these conditions (see Table 3-10).

16. At 36 hours the annulus cooling system is assumed to be activated to maintain the containment temperature at an acceptable level and the containment is vented to avoid excessive long term pressure and to allow a purge of fresh air to be initiated.

---

*Hydrogen stratification would not occur at the top of the containment after hydrogen flame extinguishment. The free convective currents and rapid diffusion of hydrogen in air prevent stratification. The free convective buoyant forces are about twice as large as those due to the density difference between hydrogen and air at the time of hydrogen flame extinguishment in containment. The diffusion coefficient of hydrogen in air is triple that of oxygen in air - thus rapid diffusion of hydrogen throughout a gaseous system will occur.

After 36 hours, when venting and purging begin, hydrogen stratification would not be detrimental, even if it were to occur, as venting would be from the top of containment. Any hydrogen assumed to be stratified would then be preferentially vented.

Even though hydrogen stratification should not occur, the containment hydrogen concentration sensors will prudently be located at the top of containment as described in Section 2. Thus, even if hydrogen stratification were to occur, explosive concentrations would not be reached because the purge rate would maintain the hydrogen concentration (at the most likely stratification point) to less than 6%.

17. At 39 hours a purge of fresh outside air is assumed to be initiated and maintained at a rate sufficient to keep the hydrogen concentration below explosive levels.

18. To reduce radiological consequences, all radioactive materials (except gases) vented from containment would be filtered by the cleanup system. The radiological releases are discussed in Section 4.0.

19. Upon sodium boil-dry, at about 130 hours, the fuel in the reactor cavity would penetrate into the concrete. Shortly after sodium boil-dry, the annulus air cooling system operation could be terminated since sodium reactions are the principal containment heat source.

20. After the sodium boils away and the sodium reactions in containment cease, the vent and purge rates could be reduced. Steam and carbon dioxide from the reactor cavity concrete and possible hydrogen and carbon monoxide from the steam and carbon dioxide reacting with molten steel are the only gases being produced which would necessitate venting and purging.

    At approximately 8000 hours, the quantity of gases generated would be sufficiently small that containment venting and purging could be discontinued.

21. The fuel is calculated to penetrate 10 to 20 feet into the basemat or about 40 to 80% of the total concrete thickness below the reactor cavity before reaching a stable configuration. This maximum penetration would occur approximately 2 to 6 months after the event was initiated.

    The molten fuel-concrete pool would freeze in that location. Therefore, the HCDA progression would be complete. The only residual energy would be a small decay power that would be readily conducted and convected to the environment by natural processes.

22. Long term containment structural capability is maintained above the basemat even though reactor cavity structures and the basemat below the reactor cavity may be degraded.

3.2.2 Containment Transients Prior to Sodium Boildry

3.2.2.1 Containment Pressure, Temperature and Mass Transient Analyses

Analytical Model

Hypothetical containment transients were determined by performing energy and mass balances, including chemical reactions, on four interconnected cells using the CACECO computer code (Figure 3-5). These cells represent the reactor cavity (RC), the three pipeway cells located adjacent to the reactor cavity, the containment volume above the operating floor and reactor head (RCB), and the air atmosphere cell below the operating floor (Cell 105). The analytical model is summarized in this section. Appendix C.1 provides the details of the model and its data base.

The analysis considers the following:

1. The steel liners that cover and protect the concrete roofs, walls and floors of the pipeway cells and the walls and roof of the reactor cavity are vented to Cell 105.

2. Fuel/steel on the reactor cavity liner would be expected to be in the form of particulate cooled by sodium. Consequently, liner failure in the reactor cavity is considered to be unlikely or of limited extent early in the scenario. If liner failure occurred, it is not expected to be by melting but by local rupture due to excessive strains. Fuel is expected to be in particulate form because (1) it should remain in particulate form when penetrating the reactor and guard vessels and (2) even if it is in molten form, the M series of experiments of ANL (Reference 3-6) indicate that it will particulate when contacted by sodium before liner penetration occurs. The M series of experiments

also show that any molten steel will particulate in a manner similar to that of molten fuel (Appendix G.1 discusses these phenomena in greater detail).

The fuel would be expected to remain in particulate form while penetrating the reactor and guard vessels because the physical sequence of events is predicted to be:

a. Immediately after the HCDA, fuel would be quenched in the sodium and settle on the reactor vessel lower head.

b. Due to the probable thickness of the debris bed and the heat generation rate the debris bed would dryout.

c. When this occurs the bed would rise rapidly in temperature to the melting point of steel.

d. When the melting point of steel is reached, the steel in the debris bed would melt and provide a media for transporting heat to the vessel.

e. With molten steel in contact with the vessel, it would fail before the debris bed temperature increases significantly above the melting point of steel.

Therefore the debris bed temperature when it reaches the reactor cavity liner would be near the melting point of steel ($\sim$2500°F) and not at molten fuel temperatures ($\sim$5000°F).

Consequently, liner penetration by melting is not expected because either the fuel should be in particulate form at the time of vessel penetration, or even if molten fuel did contact the liner following penetration of the vessel, experiments show that particulation would occur when sodium contacts the fuel on the liner. Appendix G.1 investigates the sensitivity to bed levelling characteristics in the reactor cavity.

3. Water and carbon dioxide released by heating the concrete floor of the reactor cavity (and other surface areas with failed liners) reacts exothermically with the sodium pool (or sodium atmosphere) producing hydrogen, sodium hydroxide, sodium carbonate, and carbon. Sodium-concrete reactions occur over the areas with failed liners in contact with liquid sodium until an accumulation of reaction products limits the reaction (Appendix C.1).*

4. Water released by heating the concrete floor of the RCB exothermically reacts with sodium forming hydrogen and sodium oxide and reacts with sodium oxide, producing sodium hydroxide.

5. The CACECO modeling, which is appropriate prior to sodium boildry, does not consider any fuel-concrete reactions. The reasons are:

   a. Section 3.2.1 and Appendix G.1 indicate that the fuel would in a coolable debris bed spread over the reactor cavity floor at boiling sodium temperatures. Fuel would not melt through the liner. Liner failures, if they occur, would be localized. Therefore, with a maximum temperature of $\sim 1700^{\circ}F$, fuel melting into concrete would not occur.

   b. Chemical reactions between the oxides in the concrete (MgO and CaO) and fuel would not occur at boiling sodium temperatures (the carbonates in the concrete would decompose into oxides). Experiments at ANL with concrete at molten fuel temperatures

*Other gases released by heating the concrete floor of the RC are given in Table 6b of Reference 3-7. The combustible gases released are (other than hydrogen) a small fraction of the total gases released (a maximum of 6%). When the gases released from the concrete are mixed with the much greater mass of gases in the atmosphere of the containment building, the contribution to the explosive potential is sufficiently small so that it can be neglected. The energy released when the other combustible gases burn is insignificant when compared to the energy released from burning sodium and hydrogen.

(Reference 3-6), and at Westinghouse Advanced Reactors Division with MgO refractory at molten fuel temperatures (Reference 3-14) did not indicate any chemical reactions. If reactions were not observed at molten fuel temperatures, they would not occur at the much lower temperatures associated with boiling sodium.

6. The reactor containment building is vented to atmospheric pressure beginning at 36 hours after the accident. After depressurization, an air purge is provided to maintain the hydrogen concentration below 6 percent.

7. At the assumed time of reactor and guard vessel penetration (1000 seconds), direct interconnection between the reactor cavity, pipeway cells, and RCB was assumed to simulate the burst disk rupture and the reactor cavity-to-containment vent system. Simultaneously a direct interconnection was assumed between Cell 105 and the RCB to simulate leak paths between these spaces.

8. Heat was conducted from the reactor cavity, pipeway cells, containment, and Cell 105 by a series of one-dimensional heat structures. The heat capacity of the steel structures in the reactor cavity and containment were also considered.

Processes Considered

1. The fission product decay heat is based on steady-state operation at 975 MW. The decay heat associated with the noble gases is directed to the containment atmosphere immediately. The heat associated with the halogens and volatiles is conservatively assumed to be contained in and carried with the sodium. The remainder of the decay heat is released to the sodium pool at the bottom of the reactor cavity.

2. Approximately 1.1×10^6 pounds of the primary system sodium inventory would be released into the reactor cavity after penetration of the reactor and guard vessels. The initial sodium mixed mean temperature

would be 990°F which assumes no heat loss from the reactor cavity prior to penetration at 1000 seconds. The sodium pool in the reactor cavity would be approximately 17 feet deep. This is the elevation that would be obtained assuming a uniform level in the reactor cavity. However, to accommodate the possible pressurization of the reactor vessel, relative to the reactor cavity atmosphere, the horizontal baffles behind the reactor cavity liners described in Sections 2.1.2.4 and 2.2.4 are placed at an elevation of 26 feet above the reactor cavity floor. The opening in the bottom of the reactor vessel would limit the effects of vessel pressurization to that associated with displacement of the sodium in the vessel. Complete displacement of the sodium in the reactor vessel would result in an increase in the sodium level in the reactor cavity to less than the 26 foot elevation (see Figure 3-33).

3. The decay energy of the Na-24 is added to the sodium.

4. In the containment atmosphere, sodium vapor reacts with the oxygen, carbon dioxide and water vapor.

5. Hydrogen that is vented from the pipeway cells to containment reacts with oxygen if the hydrogen burning criteria are satisified.

6. At vessel penetration 1000 lb of sodium is assumed to be injected through the head to containment and is assumed to burn instantaneously.

Analysis Results For 36 Hour Vent

The analysis results are based on the scenario in Section 3.2.1 and on the analytical model in the previous section and are described in more detail in Appendix C.1.

The maximum reactor cavity transient pressure peak (29 psig) is calculated to occur immediately after guard vessel penetration. The value is conservative since the CACECO code assumes instantaneous, complete combustion of the 2% oxygen initially in the cavity. In reality, the combustion would require some time: thus the pressure rise would be at a slower rate, which would result in a lower maximum pressure because the reactor cavity would relieve its own pressure through the reactor cavity-to-containment vent system. The maximum pipeway cells transient pressure peak (13 psig) was found to occur in less than one minute after vessel penetration. The corresponding reactor cavity and pipeway cell atmosphere temperatures were found to be 1240°F and 500°F respectively.

The sodium in the reactor cavity would increase in temperature due to the energies from the fission products, fuel, sodium 24 activity, sodium-concrete reaction, sodium-water reaction, and the sodium-carbon dioxide reaction. The reactor cavity atmosphere temperature history is shown in Figure 3-6. Figure 3-7 gives the cavity pressure history. Sodium boiling would begin at about 9 hours as shown by the increase in sodium entering containment in Figure 3-8.

The sodium vapor, as well as hydrogen and any remaining nitrogen and argon, would pass through the three pipeway cells into containment through the reactor cavity-to-containment vent system. The rate of sodium entering the containment from the reactor cavity is shown in Figure 3-8.

The water vapor and carbon dioxide, released from the concrete when it is heated, would be vented from behind the reactor cavity and pipeway wall liners by the liner vent system, to spaces below the operating floor. The water releases per unit area are shown in Figure 3-9. Water and carbon dioxide from the cavity floor would react with the sodium pool.

Upon reaching containment, the hydrogen generated in the reactor cavity and hydrogen generated by the sodium-water reaction in containment would react with oxygen if either criterion (a) or (b) is met in combination with criterion (c) as discussed in Section 3.2.1. The sodium concentration entering the reactor containment building, shown in Figure 3-10 would satisfy criterion (b) after approximately ten hours following vessel penetration. During this time the hydrogen concentration in containment would reach 4.5%. This hydrogen would burn while the burning criteria are satisfied as the natural circulation in containment moves the hydrogen through the flame zone. The oxygen concentration as indicated in Figure 3-12 remains above 8% for 36 hours and above 5% for 38 hours (satisfying criterion c). Hydrogen does not burn between 36 and 38 hours since the containment accumulation is less than 4%.

When the hydrogen burning criteria are no longer satisfied, hydrogen would accumulate in the containment as shown on Figure 3-11. As the figure indicates the hydrogen concentration would remain below 6% well beyond 24 hours. Containment integrity thus would not be challenged by excessive hydrogen concentration.

The maximum containment pressure is 22 psig at 10 hours, from Figure 3-7, well below the calculated failure pressure of containment (greater than 30 psig). The maximum containment pressure results from the assumption that the accumulated hydrogen burns instantly. Section 3.2.2.5 discusses the containment pressure capability.

At 36 hours the annulus cooling system is activated and containment is vented at the rate shown in Figure 3-13 to avoid excessive containment temperatures and long term pressures.

At 39 hours a purge of fresh outside air is initiated and maintained at a rate (8000 scfm) sufficient to keep the hydrogen concentration below explosive levels as indicated on Figure 3-11. The purge rate is shown on Figure 3-14.

The sodium boils away in approximately 130 hours.

The sodium oxide and sodium hydroxide formed in containment (neglecting aerosol leakage) is presented in Figure 3-15 as a function of time.

The concrete structure temperature transients are shown in Figures 3-16 through 3-26. The steel containment vessel temperature history calculated by CACECO is included in Figure 3-6. More detailed thermal analyses of the containment and confinement structures are provided in Section 3.2.2.2 and the structural assessments are provided in Section 3.2.2.5.

The temperatures for structures adjacent to the reactor cavity and pipeway cell atmospheres in Figures 3-16 through 3-26 are based on free convective heat transfer coefficients (see Appendix C.1) during the early part of the scenario when non-condensible vapors (H_2, N_2, Ar) are present in the reactor cavity and pipeway cells. After depletion of the non-condensible vapors the analysis considers condensing sodium heat transfer coefficients.

Analysis Results For 24 Hour Vent

Since the NRC requirement is to maintain containment integrity without venting for 24 hours, additional analyses were performed to determine the impact on containment conditions of initiating RCB venting and the annulus cooling system operation at 24 hours.

With containment pressure less at 24 hours than at 36 hours without venting (11.1 psig versus 13.1 psig) the vent rate would be reduced from 24,000 acfm to 21,000 acfm. Containment would be depressurized at approximately 27.6 hours at which time purging would be initiated. If an 8000 scfm purge rate is used (same as the base case) there would be no hydrogen accumulation in containment since the oxygen concentration would be sufficient (greater than 8%) to burn all of the hydrogen. Alternatively, the purge rate could be reduced to approximately 5,500 scfm, which would maintain sufficient oxygen (greater than 8%) to prevent any hydrogen accumulation in the containment building for the first 80 hours into the scenario. After 80 hours, the hydrogen concentration level would be maintained at approximately 4%, which is comparable to the case with venting at 36 hours.

Based on a peak vent rate of 21,000 acfm initiated at 24 hours and a purge rate of 8000 and 5500 scfm initiated at 27.6 hours, the containment conditions are shown in Figures 3-79 through 3-83.

3.2.2.2 Thermal Analysis of the Containment-Confinement Structures

The containment and confinement thermal transients computed by the CACECO code are one-dimensional. For proper structural analysis of these structures, considering the design of the annulus cooling system, two-dimensional transient analyses are required. Consequently, additional thermal analyses were performed to define the temperatures in the containment and confinement structures.

Model

These analyses used the thermal model shown in Figure 3-27 with the TRUMP computer code. The thermal transients imposed on both the containment and confinement are based on the scenario of Section 3.2.1. The forcing function for the TRUMP model is the heat load to the steel containment, shown in Figure 2-8, and the heat load to the operating floor, both based on CACECO analyses (but increased about 10% to allow for variations in the base case scenario).

Heat is transferred from the RCB atmosphere to the steel containment and the operating floor by convection. Subsequently, heat is transferred from the steel containment to the annulus cooling air (by convection) and to the concrete confinement (by both convection and radiation).

Air flow through the annulus is modelled by nodes 1 through 5. Overall flow is from the 80^{o}F external atmosphere (node 8100) to nodes 1, 2, 3, 4, 5 and finally, back to the external atmosphere. In the annulus, various baffling structures produce different velocities (and hence convective heat transfer coefficients) at different elevations. In the cylindrical region and upwards to 20 feet above the critical structural region, the baffles spiral around the annulus producing high velocity flow and enhance convective heat transfer. In the upper dome region, where the space between the containment vessel and confinement building increases, the cooling air velocity (and hence convective heat transfer coefficients) are relatively low. The annulus flowrate is 400,000 scfm and the coolant flow is assumed to be initiated at 36 hours, consistent with the scenario defined in Section 3.2.1. To reduce steel containment temperatures near the 816 ft. level, insulation on the interior surface is used between elevations 816 ft. and 823 ft. The analysis assumed this was Aluminum Silicate insulation material (7 ft. high and 0.5 ft. thick). The thermal properties of this insulation are included in Table 3-9, along with the thermal properties used for other structures studied.

Results

At 24 hours, the peak containment vessel temperature is $\sim 350^{\circ}$F; the containment vessel temperature at the 816 ft. level (node 1101) is $\sim 140^{\circ}$F; and the peak confinement building temperature is $\sim 180^{\circ}$F. Between 24 and 36 hours temperatures continue to rise, but peak temperatures occur after 36 hours. Figures 3-28 through 3-32 show the containment vessel and confinement building temperatures at selected locations between 36 hours and 200 hours. The peak steel containment vessel temperature is $\sim 640^{\circ}$F. The maximum steel containment vessel temperature at the 816 ft. level is 220°F. The peak concrete confinement building temperature at the operating floor elevation is $\sim 170^{\circ}$F. The peak concrete confinement building temperature is $\sim 380^{\circ}$F, occurring at the 977.5 ft. level (node 315). Also, the concrete confinment building temperature exceeds 350°F for nodes 305 through 314. These nodes represent 6 inches of the confinement building structure in the dome region (i.e., above ~ 925 ft).

The temperature spike observed is caused by the increase in the heat generation rate in the system due to initiation of venting at 36 hours (which decreases the RCB pressure and results in an increased boiloff rate). At that time, the heat generation rate momentarily exceeds the cooling system capability, and there is a rise in temperature which is abated as the generation and removal rates equalize. Later, removal and generation rates are approximately equal and temperatures level out. During this time period, the concrete confinement building temperatures exceed 350°F for nodes 311 through 315. Eventually, the removal rate exceeds the generation rate, and temperatures drop.

3.2.2.3 Thermal Analysis of Reactor Cavity Ledge

The TRUMP finite element model used to analyze the reactor cavity ledge thermal transients prior to sodium boildry is shown in Figure 3-76. The input to the calculation consists of two bounda conditions, one imposed above the vessel support where the reactor containment building atmosphere contacts the concrete; the other is imposed below the reactor vessel support where the reactor cavity atmosphere contacts the walls. The boundary conditions consist of the time dependent temperatures and heat transfer coefficients obtained from the CACECO code output. These are given in Table 3-13. The concrete thermal properties are those listed in Table C.1-6.

Results

Figures 3-77 and 3-78 show the temperature response of the ledge at selected locations. These temperatures were used in the structural assessment of the reactor cavity ledge discussed later.

3.2.2.4 Peak Concrete Water Release Analysis

The CACECO code was used in a simple one-dimensional analysis of the reactor cavity floor and of the reactor cavity submerged wall to determine the peak concrete water release rate behind the liner to define the required liner venting capability.

Model

In the model the cavity liner was represented as a separate heat structure. The insulating concrete (or MgO aggregate-cavity floor) and 12 inches of limestone concrete were represented by 8 heat structures with 25 nodes per structure. The fine nodal representation was developed to provide a realistic water release. The first calculation modelled the reactor cavity floor and employed a sodium pool temperature boundary condition which assumed no floor liner failure in the scenario described in Section 3.2.1. The second calculation modelled the reactor cavity submerged wall liner and used the appropriate boundary condition from the Section 3.2.2 analysis results. Radiation and conduction modes of heat transfer were modelled across the 0.25 inch air gap between the liner and insulating concrete surface (or MgO aggregate surface).

Results

The peak water release rates were found to be 6.3 lb/hr-ft^2 and 8.9 lb/hr-ft^2 for the submerged wall and floor respectively. Figure 3-84 presents the water release as a function of time for the two calculations.

3.2.2.5 Structural Assessments Prior to Boildry

Structural assessments were made to determine whether the internal structures in the RCB as well as the outer containment and confinement structures can withstand the imposed TMBDB temperatures and pressures and meet the scenario requirements. These assessments are preliminary and for this reason the attention in the numerical evaluation was focused on those structures or regions of structures which were considered most critical. Detailed structural evaluations will be carried out in the future and will be incorporated in this report when completed.

The structural assessments include evaluations prior to and after sodium boildry. In the pre-boildry period particular attention is given to the integrity of structures up to 24 hours after the HCDA, and to the times of potential liner or other structural failures. The post boildry assessments examine long term containment integrity and are presented in Section 3.2.3.3.

3.2.2.5.1 Evaluation of Reactor Cavity

The Reactor Cavity is essentially a cylindrical structure that extends approximately 70 feet above the foundation mat (Figure 3-33). The lower portion is 40 feet in diameter with a wall 7 feet thick while the upper 16 foot section provides a ledge for the reactor vessel and varies in diameter and thickness.

A typical section of the Reactor Cavity wall is shown in Figure 3-34. The wall is lined with a 3/8" thick carbon steel plate anchored to the reinforced concrete wall with Nelson studs. Between the liner and the concrete wall there is a 1/4 inch air gap which is provided to allow venting of the gases produced in the concrete by the elevated temperatures. The interior 4 inches of the Reactor Cavity concrete wall consists of a layer of lightweight insulating concrete provided to protect the outer structural concrete from the effects of the elevated temperature during a postulated sodium spill accident.

The floor liner is anchored to the structural concrete of the floor by 1/2 inch web I beams. Between the floor liner and the floor structural concrete there is a 4 inch layer of insulating gravel which, in the case of a sodium spill event, provides protection to the structural concrete and at the same time a venting path for the gases generated by the elevated temperatures.

The vent space behind the liner is separated by baffle plates into four regions, the floor, the lower and upper submerged wall, and the non-submerged wall in order to prevent sodium or sodium vapor from entering one region when liner failure occurs in another region. The floor space is vented in the containment above the operating floor while the spaces between the concrete wall and the liner are vented into Cell 105.

Integrity evaluations were made for the Reactor Cavity concrete wall and the steel liner under the temperature gradients and the pressures specified for the pre-boildry period in Figures 2-1 to 2-18 of this report. The methods of analysis, structural models and criteria are discussed in the following sections. The results of the evaluations may be summarized as follows:

1. The analysis at 24 hours indicates that the steel liners and concrete structures would be intact.

2. Failure of the various steel liners is estimated to occur at the following times:

Reactor Cavity Floor	0 hours (assumed)
Lower Submerged Reactor Cavity Wall (up to 8 ft above the floor)	50 hours
Upper Submerged Reactor Cavity Wall	70 hours
Non-Submerged Reactor Cavity Wall	80 hours

3. The Reactor Cavity concrete wall will be severely cracked with some degradation shortly after the liner failure times. However, this wall is not expected to collapse before sodium boildry time.

The above conclusions are in accordance with the scenario requirements described in Section 3.2.1.

3.2.2.5.1.1 Reactor Cavity Liner

3.2.2.5.1.1.1 Evaluation for First 24 Hours

The Reactor Cavity liner is a 3/8" plate of SA 516 (Grade 55) a low carbon steel. The wall portion is anchored to the concrete with 3/4 inch diameter Nelson studs welded at 12 inches on centers* while the floor liner is supported on 1/2" web I beams (Figure 3-34). The material properties and failure criteria for this type of steel are given in Appendix C.3.

According to the scenario, sodium is released in the Reactor Cavity 1000 seconds after the HCDA at a temperature of about 990^{o}F and fills to a level 26 feet above the floor. The imposed temperatures on the liner range from about 990^{o}F immediately after the sodium release to over 1800^{o}F at the time of sodium boil-dry. The corresponding differential pressures vary as shown in Figures 2-1 and 2-4 with a maximum value of 30 psi shortly after the accident. In addition to the differential pressures the sodium imposes a hydrostatic pressure on the submerged portion of the cavity.

* The typical design of the cell liners utilizes 1/2 inch diameter studs welded to the liner plate on 15 inch centers. The reactor cavity liner anchor stud design has been augmented for TMBDB as described above.

Assumptions and Criteria

The following assumptions were made with regard to the liner, the degraded concrete and floor insulating gravel:

a. The material properties and failure criteria for the liner are those described in Section C.3.4.

b. The floor liner fails completely and the sodium fills the voids of the insulating aggregate above the floor structural concrete. The flow of sodium will be limited by the embedment plate of the vertical wall liner.

   This is a conservative assumption in the calculation of pressures and temperatures in that the liner would likely fail in localized areas, and sodium-concrete reactions would not occur over the entire floor area.

c. As a result of thermal stresses and the self-limiting reaction between sodium and concrete about 12-14 inches of floor structural concrete will be degraded in 24 hours after the HCDA (employing conservative estimates). The portion of concrete degraded by the sodium-concrete reaction is 2 inches, which corresponds to the rate of 0.5 inches per hour for four hours, as discussed in Section C.1.2.3.

d. The degradation of the concrete and of the floor insulating gravel does not affect the given temperature distributions.

e. The wall liner anchors will be given sufficient length such that they will be embedded in sound structural concrete during the time that liner integrity is essential.

f. The wall liner holds the degraded concrete in place preventing the spalled concrete from falling.

9. The degraded concrete allows the liner anchors to bend but support the liner plate against out-of-plane deflection caused by the internal pressure. Also, the degraded concrete provides enough support to prevent the anchors from buckling.

Method of Analysis

The Reactor Cavity wall liner was analyzed by elastic-plastic finite element techniques using the computer program ANSYS. The analyses were carried out applying the temperature and pressure incrementally and using the large deflection theory. The mathematical model of the lower section of the wall liner included the plates that anchor the liner into the wall (Figure 3-35). The portion away from the lower embedment was modeled as a restrained panel supported by the studs (Figure 3-36). The junction of the liner and baffle plate at 26 feet above the floor was represented by the model shown on Figure 3-37.

The lateral displacement of the liner in the outward direction is limited by the Reactor Cavity concrete wall. This was included in the analysis by introducing in the models gap (or friction) elements in the direction of the concrete. In using these elements the computer program iterates internally and when the limiting value of the displacement is reached at a point (that is when the liner comes in contact with the wall) the gap closes and reaction forces are developed at that point.

Results

The results of the investigation using models of restrained panels, which represent the liner away from the floor or other irregularities, show that shortly after the HCDA the liner undergoes significant deformations and comes in contact with the concrete wall in the region at the center of each panel. As the temperature increases, and the potential outward deflection is prevented by the concrete wall, the liner plate near the stud anchors begins to deflect inward imposing forces on the studs in the same direction (Figure 3-38). Thus, the stud anchors go in tension and the internal pressure is transmitted to the concrete wall through the central region of each panel. The liner plate is generally in compression except around the anchor where the bending stresses become significant and the inward face of the plate goes into tension. These effects continue until the temperature reaches 1350^{o}F at about 4 hours after the HCDA at which point the average coefficient of thermal expansion, α_{ave} for steel, begins to decrease (Figure C.3-20) due to changes in the internal structure of the material (Appendix C.3.4.2). From this point on unloading takes place up to T = 1550^{o}F where α_{ave} begins to increase with temperature again. The liner plate is generally in tension and the studs in compression at and near 1550^{o}F and go back to compression and tension respectively at higher temperatures.

The typical design for the cell liners includes 1/2 inch studs anchored in the concrete wall at 15 inches on centers. The results of the analyses for the reactor cavity indicated that with such a system the generalized strains in the stud anchors would exceed the allowable values in tension when the temperature reached 1350^{o}F only a few hours after the HCDA. An analysis with the same model and including the effects of creep indicated that sufficient relief in the mechanical strains would occur because of creep and the allowable limits might not be exceeded at least away from the junction with the floor. The strains, however, were still high and considering the sensitivity of the strains in the studs to certain parameters it was considered essential to introduce changes in the system in order to ensure integrity. Subsequently, the reactor cavity design was augmented by using 3/4 inch studs welded to the liner at 12 inches on centers. The discussion that follows refers to this particular design.

For the submerged portion of the wall liner the calculated values of the von Mises generalized strains at times which are either critical or of particular interest in this study are summarized in Table 3-14. For the portion away from the floor, represented by a restrained panel (Figure 3-36(b)) results are tabulated for T = 1350^{o}F which occurs at approximately 4 hours after the HCDA and for T = 1700^{o}F at 10 to 24 hours. At 1350^{o}F the maximum value of the generalized von Mises strain for the wall plate under biaxial compression, although high, is below the allowable. The strain in the studs, which are in tension, is small. At 1700°F all the values of the generalized strains fall below the allowable. The same is true in the range near 1550°F where the liner plate goes into tension and the anchors in compression. For the portion of the liner near the floor, represented by the model in Figure 3-35, the results indicate large strains but within the allowable values at temperature of 1340°F.

For the liner above the sodium pool the results, which are similar to those for the submerged portion, are summarized in Table 3-15 for T = 1350°F which results in the maximum strain at approximately 9 hours after the HCDA. The generalized von Mises strain for the liner, and the studs are within the allowable values.

Certain analyses were carried out to determine whether the wall liner could sustain pressure build up behind the liner in the inward direction. The results of these analyses, using the model in Figure 3-36(b) and the large deflection theory, indicate that the liner will retain its integrity for differential pressures of at least 5 psi in the inward direction.

The effect of creep on the response of the liner was examined using a model representing a restrained panel of the submerged portion of the liner. Incremental analyses between zero and 24 hours, taking into consideration the effect of creep in the temperature range above 1000°F, showed that creep strains relieve significantly the mechanical strains resulting from temperature. This relieving effect begins early and provides a significant additional margin of safety at the time when the temperature reaches the critical level of 1350°F.

In all the analyses discussed so far the material properties used were those corresponding to testing strain rates of 10^{-4} in/in/sec., which show higher deterioration of the strength at higher temperatures. In the scenario under consideration, however, with the sodium initially at 990°F, it is expected that the liner temperature will reach this level in a short time and then continue to rise at a slower rate. To account for the different rates of temperature rise, and consequently different strain rates, an analysis was carried out using a restrained panel model and material properties corresponding to strain rates of 10^{-1} in/in/sec up to 990°F and rates of 10^{-4} in/in/sec at higher temperatures. The results of this analysis in terms of generalized strains were almost identical to those where material properties corresponding to the slower strain rates were used throughout the analysis.

Conclusions

The results of the investigation show that if the effects of creep are not considered, the wall liner plate and certain studs near the floor are subjected to large but permissible deformations early after the HCDA. When creep is taken into account substantial relief in the mechanical strains begins (at T = 1200°F) and the margins increase significantly.

Based on findings of this study, it is expected that the submerged wall liner and the portion above the sodium pool will retain their integrity for at least 24 hours after the HCDA.

3.2.2.5.1.1.2 Evaluation of RC Liner Beyond 24 Hrs.

Based on results from the 24 hour evaluation and considering material properties and temperatures at later times, it can be concluded that the RC liner will retain its integrity as long as the deformations, degradation and cracking of the supporting concrete are not excessive. This conclusion was used as a basis for the preliminary investigations to determine the time of potential liner failure. The expected degradation of the concrete wall at different times was calculated as explained in Section 3.2.2.5.1.2 and it was found to be generally small. The RC wall deformations were found to be insignificant for the flexible liner plate, and generally in the direction that would be relieving the liner strains, as long as the capacity of the RC wall is not exceeded. When the capacity of the concrete wall is exceeded, indicating plastic hinging or shear slip, it was assumed that the imposed deformations on the liner would be excessive and failure would occur at that time. This method provides a conservative estimate of liner failure time (early) and considerably simplifies a very complicated interaction problem.

The times that the capacity of the reactor cavity is exceeded either in flexure or shear were calculated using the methods and models described in Section 3.2.2.5.1.2 and are as follows:

Lower Submerged Wall (up to 8 ft. above floor)	50 hours
Upper Submerged Wall	70 hours
Non-Submerged Wall	80 hours

3.2.2.5.1.2 Reactor Cavity Concrete Wall

The evaluation of the Reactor Cavity concrete wall was performed by the analysis of the following sections which were considered representative of the structure:

1. The wall as a long cylinder, away from boundaries;

2. The portion near the floor to consider the effects of the restraint that prevents radial deflection and rotation of the cylinder.

3. The portion near the Head Access Area which is radially restrained by the slabs at Elev. 786 ft.

4. A horizontal section of the reactor cavity to consider the effects of radial restraints, representing the massive concrete shield walls.

The temperature gradients and pressures considered are given in Figures 2-1 to 2-11. In addition, the dead load and the hydrostatic pressure due to the liquid sodium were included in the evaluations.

The radial temperature distribution is different in the submerged portion of the wall from the portion above the pool, and it is assumed uniform within each of these regions. A smooth transition exists between the two distributions. However, even if the change in temperature were considered to occur abruptly at the interface the effect of the restraint imposed on the hotter section by the cooler section would be small compared to the similar effect at the base.

The temperature effects on reinforcing steel were accounted for by using temperature dependent properties (Appendix C.3). The concrete cover on the reinforcing steel is such that no contact with liquid sodium is expected before sodium boildry. Even if there is contact of the reinforcing steel with sodium, test results reported in References 3-21 and 3-22 show that there is no significant chemical reaction of carbon steel with sodium.

The dynamic loads associated with the HCDA occur within a few hundred milliseconds as upward and downward impactive type forces. These dynamic loads act several minutes before the thermal loads start acting on the structure. The reactor support ledge is designed to withstand these dynamic loads. The total support ledge load was distributed along the shear section proportional to the stiffness developed by the ledge. The allowable stresses are in accordance with A.C.I. Building Code Requirements 318-77, Section 11.7. The maximum shear stress allowed is 20% of the compressive strength (4000 psi) or a maximum of 800 psi.

Checking the critical section for shear friction in the reactor vessel support ledge, the following maximum shear stresses were calculated:

a - In the plane of anchor bolts: 400 psi.
b - In the critical shear plane: 650 psi.

The results are well below the 800 psi allowed.

The TMBDB loads start seconds after the HCDA dynamic load and therefore the two loads do not act simultaneously. Only the dead weight of the vessel acts on the ledge simultaneously with the TMBDB thermal loads. Based on the current analytical results of the Reactor Cavity wall under the TMBDB loads, it can be concluded that the ledge will be capable of withstanding the vessel weight for at least twenty-four hours after the TMBDB event.

Assumptions and Criteria

The following assumptions were used in the investigation:

a. No concrete strength gain with age is considered.

b. The stress-strain relationship for concrete and steel is temperature dependent and defined by the curves in Figures C.3-9 and C.3-15. Other properties are as described in Appendix C.3.

c. The temperature distribution through the RC wall thickness is constant in the regions above and below the sodium pool.

d. In the flexural analysis of the concrete sections, the liner interaction can be neglected.

The following criteria were used in the investigation:

a. Concrete at temperatures of 1200°F or more is totally degraded and incapable of carrying stress.

b. Concrete with a stress inducing strain exceeding the limits defined in Appendix C.3 is crushed and therefore does not develop any stress.

Reactor Cavity Wall as a Long Cylinder

Elasto-plastic finite element analysis with the computer program ANSYS was performed to determine radial displacements and stresses in a cylinder of infinite length. The simplified analytical model used, consists of a vertical cylinder of the same diameter and wall thickness as the Reactor

Cavity (Figure 3-39). Although the length of the model is three inches, the boundary conditions of the model permit free radial and longitudinal expansion through the wall thickness, thus simulating a cylinder infinitely long. The computer program ANSYS does not have the capability to account for different tensile and compressive material properties, as is the case with concrete, and for this reason cracking was included in the analysis by an iterative process. First, the same properties were assumed in compression and in tension and then the solution was iterated, each time changing the properties of the elements in tension, until the process converged.

Analyses of this type were carried out at different times up to sodium boildry to determine the condition of the cavity wall away from the restraints and to provide information on the potential radial and vertical displacements. Typical results on the distribution of stresses across the wall thickness are shown in Figures 3-40 and 3-41 at 132 hours (boildry time). Bending moments were calculated from these stress distributions and were compared with the ultimate capacity of the section in question.

The results of this analysis indicate that the properties of the Reactor Cavity wall away from restraining elements can sustain the imposed loads at 24 hours after the HCDA with substantial margin and its capacity will not be exceeded before sodium boildry.

Reactor Cavity Wall Section at the Base

The analysis for the infinitely long cylinder provided information on the potential radial displacements of a cylinder free of restraints. The fixity at the base, however, prevents the radial displacement and any rotation of the section. The moment, radial shear, and hoop force required to meet the boundary conditions were calculated and were superimposed on the values calculated for the reactor cavity wall as a long cylinder.

The results of this analysis indicate that the reactor cavity wall near the base, with additional vertical and hoop reinforcing bars and shear reinforcement, can withstand the imposed temperature gradients and other loads for at least 50 hours before its capacity is exceeded. It should be pointed out, however, that a small relative slip between sections is expected to relieve the thermal effects and prevent excessive damage. For this reason, and in view of the results of the long cylinder analysis beyond 50 hours and the naturally stable configuration of the cylindrical shape, collapse of the cavity is not expected to occur before sodium boildry. At 24 hours the cavity near the base can sustain the imposed loads with a substantial margin.

Reactor Cavity Section at Elev. 786 Ft

The non-submerged Reactor Cavity wall near the Head Access Area is restrained radially by the slabs at Elev. 786 ft and the effect is similar to that near the base.

The results of analysis indicate that the portion of the wall in this region, with augmented reinforcing of vertical and hoop bars and stirrups, can withstand the imposed temperature gradients and other loads for at least 80 hours after the HCDA at which time the shear capacity of the wall is exceeded. Due to the self relieving nature of the thermal forces no failure in the form of collapse is expected before sodium boildry. At 24 hours the thermal effects in this region were found to be substantially below the capacity levels.

Effect of Radial Restraints

The presence of thick concrete shield walls around part of the Reactor Cavity wall (about half of the circumference) stiffens that part of the structure providing a restraint to the unstiffened part. To consider this effect in the lower portion of the Reactor Cavity, a horizontal strip of the cavity wall was modeled as an arch (Figure 3-42) for finite element analysis using the computer program ANSYS. The boundary conditions were as follows:

a. At the axis of symmetry the section was assumed restrained against rotation and circumferential displacement.

b. The section at the support of the mathematical model was assumed restrained against rotation and was given an inward radial deflection (the "free" radial displacement of the long cylinder). This represents the effect of the "stiff" section of the reactor cavity which would not allow the "free" radial displacement.

To consider the effect of the two parallel walls on the non-submerged portion of the Reactor Cavity a horizontal strip of the cavity wall was modeled as an arch (Figure 3-43) for finite element analysis using ANSYS. The boundary conditions were as follows:

a. At the two end supports the section was assumed restrained against rotation and circumferential displacement.

b. The support opposite the restraining wall was assumed to be restrained against horizontal movement to simulate the reactions at the base and near the top of the cylinder.

c. At the intersection with the vertical wall the arch was given an inward deflection along the line of the wall equal to the component of the radial displacement of the cylinder in that direction.

The analyses were carried out using iterative procedures in order to account for cracking of the concrete under tension. Thus, the stiffness at first was based on gross section properties, then the stiffness of those elements under tension, exceeding the cracking strength of the concrete, was substituted by values based on cracked sectional properties.

The results of the analysis show that with some additional shear and flexural reinforcing the portion of the cavity wall near the vertical walls can sustain the imposed loads for the following times with some margin:

Submerged Region	70 hours
Non-Submerged Region	80 hours

At later times the capacity of the cavity wall will be exceeded in bending and compression. However, no total failure is expected to occur before boildry since additional cracking and hinging at the critical regions will have a relieving effect.

3.?.?.5.1.3 Pipeway Cells

The Pipeway Cells (Figures 3-44 and 3-45) are adjacent to the upper portion of the Reactor Cavity between Cell 105 and the operating floor. The floor of these cells which is 63 inches thick, for shielding purposes, consists of limestone concrete with 4 inches insulating gravel on top and is lined with SA 516, Grade 55 steel supported on I steel beams. The roof is 6 ft.-3 inches thick and the typical walls are 2 ft.-6 inches, 4 ft.-0 inches, and 4 ft.-3 inches in thickness. Both roof and walls have details similar to the Reactor Cavity wall. The interior is lined with SA 516, Grade 55 steel anchored to the concrete with Nelson studs. The structural concrete, a limestone mix is protected with 4 inches of lightweight concrete insulation. Between the liner and the lightweight concrete there is a 1/4 inch vent space. The walls between the pipeway cells and the Reactor Cavity (double heated walls) vary in thickness (Figure 3-44) and have a steel liner on both sides.

Integrity evaluations or assessments were made for the floor, the 2 ft.-6 inch and 4 ft.-0 inch thick walls and the double heated wall. The methods of analysis, structural models and criteria are discussed in the following sections. The results of the evaluations may be summarized as follows:

1. The concrete walls and the steel liners will retain their structural integrity for at least 24 hours with a margin of safety.

2. The steel liners are not expected to fail for at least the following times:

Pipeway Cell Floor and Roof	30 hours
2 ft. 6 inch Thick Pipeway Wall	35 hours
4 ft. Thick Pipeway Wall	40 hours
Double-Heated Pipeway Wall	70 hours

The vent space between regions when the liner is expected to fail at different times will be separated by baffle plates.

3. The pipeway cell floors must be designed as a two layer system with sacrificial concrete on top (2 feet thick) in order to prevent severe cracking and leakage to Cell 105 before sodium boildry.

4. The 2 ft.-6 inch, and 4 ft.-0 inch pipeway cell walls will have severe cracking with some degradation beyond 60-70 hours, and leakage cannot be prevented beyond this point. These walls separate the pipeway cells from the PHTS cells. However, collapse of these structures is not expected to occur before sodium boildry.

5. Severe cracking of the double heated walls is expected to occur between 70 and 132 hours.

The 70 hour failure time for the double heated wall liner is less than the time assumed in the present scenario (90 hours). Parametric studies (Appendix F.7.2), however, indicated that failure of this liner even as early as 45 hours would be acceptable to the scenario.

3.2.2.5.1.3.1 Pipeway Cell Liners

The wall and roof liners in the pipeway cells are of the same material and have, except for corner details, the same structural system as the Reactor Cavity wall liner. Since these liners experience lower temperatures it may be concluded in this preliminary evaluation that the results of the Reactor Cavity liner for the first 24 hours after the HCDA are applicable to the pipeway liners for the same time period, and the modifications in the stud size, spacing, and length made in the Reactor Cavity are also adequate for the pipeway cell liners.

The pipeway floor liners are supported on I beams which although embedded in sacrificial concrete will be anchored to the structural concrete below (Figure 3-47). A conceptual evaluation based on the results for the RC liner, discussed earlier, indicates that the floor liner will retain its integrity for the first 24 hours with margins of safety similar to those for the wall liner.

The evaluation of the pipeway liners beyond 24 hours has the same basis as for the Reactor Cavity liner, i.e., that the liner will retain its integrity as long as the deformations and the degradation of the supporting concrete are not excessive. Thus, in this preliminary assessment liner failures in the pipeway cells are assumed to occur when the capacity of the supporting concrete is exceeded. Based on the evaluation of the behavior of the various concrete components which will be described later the liners in the pipeway cells will retain structural integrity for at least the times described in Section 3.2.2.5.1.3.

It should be pointed out that the time of failure for the floor liner was based on the response of a concrete slab without sacrificial concrete. With the present design, however, the capacity of the supporting structural concrete is not exceeded before sodium boildry, and for this reason it is expected that the 30 hour failure time represents a conservative estimate.

3.2.2.5.1.3.2 Pipeway Cell Floor and Walls

The pipeway cell floor and walls were investigated under the temperatures and pressures in Figures 2-12, 2-15 and 3-19. The thermal moments were calculated using one way strips which were modeled for finite element analysis with the computer program ANSYS. The analytical model for the calculation of thermal moments (Figure 3-46) is similar to that for the long cylinder except that the boundary conditions represent a strip of wall, restrained against rotation, rather than an axisymmetric structure. The cracking of the concrete was accounted for in the analysis by iterations.

Thermal moments and forces were calculated from the stresses in the elements of the model. The moments were then multiplied by an appropriate factor to account for the two way action.

Analysis was carried out for the following bounding conditions in the evaluations associated with liner integrity.

1. Walls and slabs completely restrained against rotation but free to translate axially.

2. Walls and slabs completely restrained against rotation and translation.

In the evaluations beyond liner failure, calculations indicated that full restraint against translation was too severe a bounding condition and 50 to 75 percent axial fixity is more realistic when the deformations of the restraining structures are considered.

In addition to the dead load, thermal gradients, and pressure, the pipeway floor must sustain the deformations resulting from the relative vertical displacement between the Reactor Cavity wall and the Cell 105 wall. This effect was considered in the evaluations.

A. Assumptions and Criteria

Assumptions a, b and d and criteria and b described under the Reactor Cavity (Section 3.2.2.5.1.2) are applicable to the pipeway cell evaluations.

B. Results for Pipeway Floor

Evaluations were made using a structural concrete thickness of 59 inches consistent with the design of the pipe floor. The results of these evaluations indicated that due primarily to temperature gradients and the deformations imposed by the relative movement of the massive Reactor Cavity wall and the Cell 105 wall, the bending capacity of the pipeway cell floor would be exceeded at 30 hours after the accident. This would cause the development of a plastic hinge at the support, and although no collapse of the floor is expected, the severe deformations at the hinge would cause liner failure at this time.

Evaluations beyond 30 hours, however, showed that due to large rotations, at the region where the capacity was exceeded, there would be severe degradation of the concrete and possibly leakage to Cell 105 in 50 to 60 hours after the HCDA. Since such leakage is unacceptable in the scenario the structural system of the floor has been changed to the two layer system shown in Figure 3-47. This design consists of the same overall thickness but with a structural slab only 35 inches thick and 24 inches of sacrificial concrete above. In this manner the structural concrete is subjected to less severe temperature gradients, and due to its flexibility can sustain better the deformations imposed by the growth of the cavity in the vertical direction.

Numerical evaluations using the double layer system showed that the capacity of the structural slab will not be exceeded before sodium boildry.

C. Results for 2'-6" and 4'-0" Pipeway Walls

The analytical evaluations for the 2'-6" and 4'-0" pipeway walls, using the bounding conditions with respect to axial and rotational restraints (100%), showed that the capacity of the walls will not be exceeded for at least 35 and 40 hours respectively. When the less severe condition of 50 to 75 percent axial fixity was used, the above times increased to 50 and 60 hours. Beyond 60 to 70 hours the walls will have severe structural damage, and leakage is likely. Based on judgement, however, in view of the self relieving nature of thermal forces, collapse of these structures is not expected to occur before sodium boildry.

D. Results for Double Heated Wall

The evaluations for the Double Heated Wall showed that it can sustain the imposed temperatures in Figures 2-12 and 3-19 for at least 70 hours before its capacity is exceeded in compression and bending. Beyond this time the wall will be severely degraded but no collapse is expected before sodium boildry.

3.2.2.5.2 Evaluation of Containment Vessel Structural Integrity Prior to Sodium Boildry

The following structural assessments are based on the temperature distributions in Section 3.2.2.2.

3.2.2.5.2.1 Containment Vessel at 24 Hours

The temperatures of the containment vessel as a function of time are shown on Figure 3-28 for selected nodes shown on Figure 3-27. The maximum temperatures are not reached until well after 24 hours.

The internal pressure capability of the containment vessel was determined from the internal pressure forces and the dead weight of the structures.

The primary stresses resulting from the pressure load were determined and local primary stresses at the discontinuity were added to the membrane stresses. The maximum stress intensity was determined in terms of the pressure. The membrane stress intensity in the upper cylinder was found to be controlling the allowable pressure. Since the allowable stress intensity is a function of temperature (Reference 3-13), a functional relationship betweeen the pressure and the temperature was established. Pressure capability based on two different primary stress intensity allowable criteria given in Reference 3-12 were considered. Allowable pressure at selected temperatures were tabulated and are shown in Table 3-10. Based on a peak containment vessel temperature at 24 hours of 350°F, the first criterion, namely $P_m < S_y$, gave the critical allowable pressure as 41 psig. The second criterion which states that the primary stress intensity should be less than 85% of the allowable specified in ASME Code, Section III, Appendix F, gave the critical allowable pressure as 57 psig.

The maximum pressure in containment during the first 24 hours is 22 psig. Thus, containment vessel structural integrity would not be challenged during the first 24 hours after an HCDA.

The potential for the containment vessel to buckle with the constraint at the operating floor was examined. Calculations indicate the worst instance of interfacing stresses will be less than the critical value if the containment vessel temperature at the operating floor level is less than 240°F. At 24 hours the containment temperature at the 816' level is only 140°F; therefore, the containment vessel would not buckle at 24 hours. Buckling calculations for the hatch cover also indicate that stresses are under the critical values.

It is concluded that containment structural integrity would be maintained at 24 hours.

3.2.2.5.2.2 Containment Vessel between 24 Hours and Boildry

During this time period, the peak pressure in containment is 13 psig. The peak containment vessel temperature is 640°F. At this temperature, the first allowable criterion indicates a pressure capability of 34 psig (see Table 3-10). The second criterion indicates a pressure capability of 52 psig. Thus, the containment vessel can accommodate the pressures between 24 hours and sodium boildry. In addition, the peak containment vessel temperature at the operating floor level during this time period is 220°F (see Figure 3-28) which is less than the 240°F critical temperature for containment vessel buckling, therefore the containment vessel will not buckle. Thus, containment vessel integrity is maintained between 24 hours and sodium boildry.

3.2.2.5.3 Evaluation of Confinement Building Structural Integrity Prior to Sodium Boildry

The confinement building (Figure 3-50) above the operating floor consists of a cylindrical portion, 196 ft. in diameter and 94 ft. high and a dome that rises approximately 84 ft. above the spring line. The wall thickness is 4'-0" in the cylindrical part and tapers to 3'-0" in the dome. The upper portion of the dome near the apex is partitioned as shown in Figure 3-50. The structure is restrained against thermal expansion at the operating floor and by the roof slabs of the Steam Generator Building (El. 857.5), and the Reactor Service Building (El. 882.5).

The following structural assessments are based on the temperature distributions in Section 3.2.2.2.

3.2.2.5.3.1 Confinement Building at 24 Hours

The peak temperature in the confinement structure during the first 24 hours is 180^{0}F. An assessment of the effect of the temperature transient during this period indicates that the integrity of the structure will be maintained.

3.2.2.5.3.2 Confinement Building Between 24 Hours and Sodium Boildry

A preliminary evaluation of the confinement structure was made for the combination of dead load and the temperatures in Section 3.2.2.2 which correspond to an annulus cooling rate of 400,000 scfm with flow entering near grade level and exiting near the top of the building, and the system initiated at 36 hours. Specifically, the evaluation considered the temperature gradients at two times. First, the time at which the temperature at the face of the wall reached their peak values was considered ($\sim$40 hours);second, the time near sodium boildry was considered when the interior concrete temperatures were higher than at 40 hours, although the face temperatures were below their peak values.

The structural analysis was carried out using the computer program ANSYS with axisymmetric finite element models restrained at the base (operating floor) and at the intersections of the shell with the Reactor Service Building and Steam Generator Building roof slabs described earlier. The variation of the temperature along the height of the structure was taken into account. Assumptions (a), (b) and (d) and criteria (a) and (b) of Section 3.2.2.5.1.2 apply to this evaluation as well. Cracking of the concrete was accounted for by an iterative process where the element properties were examined after each iteration and were changed accordingly. Properties based on the cracked section were substituted for those elements with tensile stresses in excess of the limit in C.3.2.4.

The results of this investigation indicate that for the temperature gradients under consideration, the critical regions for structural integrity are at the junction of the confinement wall with the roof slabs. At these locations the restraining effect of the slabs result in high bending moments, compressive forces, and shears. With additional flexural and shear reinforcing steel in these regions, the allowable capacity of the concrete sections taken as 90% ultimate capacity is not exceeded. Elsewhere in the structure, including the upper portion where the temperatures are the highest, the forces and moments are also within the allowable values.

It is concluded that the confinment building will retain its structural integrity between 24 hours and sodium boildry time.

3.2.2.5.4 Evaluation of Foundation Mat Structural Integrity Prior to Sodium Boildry

3.2.2.5.4.1 Foundation Mat at 24 Hours

The foundation mat does not undergo any temperature rise during the first 24 hours after an HCDA. Therefore structural integrity is maintained at 24 hours.

3.2.2.5.4.2 Foundation Mat Between 24 Hours and Sodium Boildry

During the sodium boiling phase of the accident scenario the temperature rise in the reactor cavity floor has not progressed to the point where anv challenge is present to foundation mat integrity. The reactor cavity floor temperature profile is shown on Figure 3-17.

3.2.3 Containment Transients After Sodium Boildry

3.2.3.1 Chemical Reactions and Reaction Products

This section addresses the chemical reactions during the post boildry period. Following sodium boildry, the heat generated in the fuel would be transferred to both the structures in the reactor cavity and the concrete composing the reactor cavity floor and walls. This heating would result in a melting of the steel structures within the reactor cavity, the release of CO_2 and H_2O from the concrete floor, and the melting of the concrete. The most important reactions occur between the molten steel and the gases released by the concrete. The products of these reactions, principally hydrogen and carbon monoxide, would be released to the reactor containment building.

Reactions between other components in the molten steel, molten fuel, molten concrete mixture are unlikely. The highly reactive halogens would be removed from the fuel in the initial phases (prior to boildry) of the incident; thus, they would not be present at sodium boildry. The remaining constituents would be in an oxidized state and not result in substantial further reactions.

Experiments with molten fuel and molten steel on concrete (Reference 3-6) confirm the previous assessments. When concrete was contacted with molten steel, the gases evolving from the concrete reacted with the molten steel. There were no reactions between the oxides in the concrete and the steel. When molten UO_2 contacted concrete, thermal effects were noted. There was no chemical reaction between the UO_2 and the concrete constituents.

The basic chemical reactions occurring during the post boildry period are:

$$3\ Fe + 4\ H_2O \rightleftarrows Fe_3O_4 + 4\ H_2$$

$$2\ Cr + 3\ H_2O \rightleftarrows Cr_2O_3 + 3\ H_2$$

$$4\ CO_2 + 3\ Fe \rightleftarrows Fe_3O_4 + 4\ CO$$

Other reactions which could conceivably occur to produce CO and H_2 would have the same limiting net effect: one mole of water produces one mole of hydrogen, and one mole of carbon monoxide is produced from one mole of carbon dioxide.

These reactions become accelerated at $\sim 2600^oF$, the melting point of steel (Reference 3-6) because of the change from a gas-solid reaction with a limited exposed steel surface area to a gas-liquid reaction with a large exposed steel surface area.

For this evaluation, the following assumptions have been made:

1. The reactions are constrained by the availability of H_2O and CO_2 released from the concrete and these materials react completely.

2. No equilibrium compositions exist.

3. The reaction is instantaneous.

4. The reaction rate is independent of the relative amounts of Fe and Fe_2O_3.

5. Gas evolution from the concrete is controlled by the 95% downward heat transfer case in Section 3.2.3.2.

These assumptions will provide a very conservative estimate of the CO and H_2 quantities that could enter the reactor containment building.

The concentration of CO and CO_2 in containment was calculated by assuming that the reactor containment building behaves as a well mixed vessel having a uniform distribution of all constituents; therefore, venting and purging affects all constituents equally.* For equal feed and vent rates, the equation governing the component concentration for such a vessel is (see Figure 3-85):

$$V \frac{dc}{dt} = q_o c_o - q_o c$$

(accumulation) (input) (output)

V = volume of containment, ft^3

c = concentration of either hydrogen or carbon monoxide, $moles/ft^3$

q_o = feed and vent rate

c_o = concentration of either hydrogen or carbon monoxide in feed stream

The solution to this equation is:

$$c = c_o \left(1 - e^{\frac{-q_o t}{V}}\right)$$

and $\lim\limits_{t \to \infty} c = c_o$

Thus, for equal feed and vent rates, the concentration of either hydrogen or carbon monoxide cannot exceed the concentration of the incoming stream. Because of the system's relatively short time constant, ~8 hours for the normal purge rate, the limiting equation is used for concentration calculations.

*The assumption of uniform mixing is reasonable considering the turbulence due to the release of very hot gases from the reactor cavity and the purging/venting operations.

If the feed and vent rates are different, the analysis is more complicated because of the changing mass inventory of the reactor containment building which must be considered. However, a qualitative assessment of the situation will show that that the concentration of a component can be bounded.

If the vent rate temporarily exceeds the feed rate, the containment building inventory will decrease, resulting in a decreased pressure and a reduced vent rate until it equals the feed rate. At that time, the previously developed equations would apply. If the feed rate temporarily exceeds the vent rate, the net influx of material into the containment would increase the pressure, resulting in a higher vent rate until the vent and feed rates equalize. Again, the earlier developed equation would then apply.

The quantity of CO and H_2 produced as a function of time and the resulting concentrations in the containment atmosphere are summarized in Figures 3-86 through 3-89. The concentrations are based on a purge rate of 8000 scfm, which is well below the design requirement of 12,000 scfm.

The peak concentrations of hydrogen (1.4%) and carbon monoxide (3.1%) are well below the criteria established for hydrogen (6%), and the lower flamability limit for carbon monoxide (12.5%) (Reference 3-23). The combined concentration of hydrogen and carbon monoxide (4.5%) is also well below the lower detonation limit of 19% for such mixtures (Reference 3-23).

Heat evolved from the post boildry reactions is not expected to exceed 500,000 Btu/hr at the peak reaction rates. At any point in time, this reaction energy would be 5% or less of the decay heat during the post boildry period. This small additional heat source would not have a significant impact on the post boildry thermal analyses in Section 3.2.3.2.

It is concluded that the TMBDB features are adquate to limit hydrogen and carbon monoxide concentrations to acceptable levels following sodium boildry, and the heat added to the system as a result of the chemical reactions which produce CO and H_2 is insignificant relative to the decay heat.

3.2.3.2 Containment Thermal Analyses

The post boildry containment thermal analyses consider only the effects of decay heating. As shown in Section 3.2.3.1, the chemical reactions following boildry represents an additional heat release that is small relative to the decay heating.

The post boildry analyses which follow, use as their initial condition the temperature distribution at boildry. The transient temperature response of major containment structures and cell atmospheres was determined after sodium boildry. Fuel penetration into the basemat was also calculated. These temperature histories are employed in Section 3.2.3.3 to assess structural capability.

The penetration of fuel into the basemat was considered to be a melting process. This is because experimental evidence exists (References 3-6 and 3-10) that the oxides in the molten pool of fuel and concrete are well mixed and that concrete spalling and cracking are not significant modes of penetration. Details of the model are given in Appendix C.2.

A parametric approach was adopted in the thermal analyses to bracket the consequences, including the effects of the following uncertainties:

1. Heat transfer from the molten pool, including the effects of vapor and gas release from concrete, potential gas film at the solid-liquid interface, and convection within the pool.

2. Thermophysical properties of concrete at very high temperatures.

3. Size and properties of an overlying crust.

The parametric approach used a very wide range (covering two orders of magnitude) of crust thermal resistances. This resulted in a large variation in the upward heat transfer. For the three parametric cases considered, the upward heat transfer percentages were 80 to 90%, 40 to 55%, and 5 to 15%. The remaining energy is transferred in the radial and downward directions. Structural failure criteria were a midplane temperature of 700°F for concrete structures and the approximate melting point for the reactor head (2500°F). A high (melting point) reactor head failure temperature is conservative because a later failure results in higher containment temperatures below the operating floor. A lower failure temperature would result in higher containment temperatures above the operating floor; however, these would still be less than before sodium boildry. Specifically, the following 3 cases were investigated:

<u>Case 1</u> - The thermal resistance of the crust above the molten pool of concrete and fuel was 0.10 hr-ft^2-°F/Btu. This resulted in an upward heat transfer percentage of 80-90%. The reactor cavity wall and reactor vessel head failed at 400 hours after the HCDA and the annulus cooling system was assumed to be operating.

<u>Case 2</u> - The thermal resistance of the crust above the molten pool of concrete and fuel was 1.0 hr-ft^2-°F/Btu. This resulted in an upward heat transfer percentage of 40-55%. The reactor cavity wall and reactor vessel head failed at 600 hours after the HCDA and the annulus cooling system was assumed to be operating.

<u>Case 3</u> - The thermal resistance of the crust above the molten pool of concrete and fuel was 10.0 hr-ft^2-°F/Btu. This resulted in an upward heat transfer percentage of 5-15%. No structural failure occurred and the annulus cooling system was assumed to be operating.

Figures 3-51 through 3-68 give temperature histories for Case 2 (Intermediate Crust resistance) for the major containment structures described in Appendix C.2 plus the atmosphere temperatures of the PHTS cells, Cell 105, the containment building, and the containment-confinement annulus below the operating deck. The Cell 102 atmosphere temperature was nearly equal to that of Cell 105 and is therefore not provided as a separate curve. Atmosphere temperatures and key structural temperatures are shown for Cases 1 and 3 in Figures 3-69 through 3-72. The temperature response of the structures outside of the reactor cavity was very similar for Cases 1 and 2 (small and intermediate crust resistances). Following wall failure, the Cell 105 atmosphere would become mixed with the reactor cavity atmosphere, reaching thermal equilibrium with the reactor cavity shortly after wall failure. The Cell 105 atmosphere would convect large quantities of heat to the large surface area with which it is in contact, and a maximum temperature of 350-400^{o}F would be reached in the cell after wall failure.

The depth to which the fuel was predicted to penetrate the basemat varied from several feet to about 20 feet for the three crust resistances considered. For the largest crust resistance (10-20% upward heat transfer), the molten pool was predicted to penetrate to a depth of ∼20 feet and to a radius of about 23 feet in the lower mat (below elevation 733). With the intermediate crust (40-55% upward heat transfer), the molten pool would penetrate approximately 10 feet into the RC floor. The radius of the pool was predicted to be about 23 feet at elevation 737. Thus, the fuel should not penetrate the basemat; however, with the unmelted concrete thickness being as small as 6 feet the remaining portion of the basemat could be degraded and cracked and could come into contact with ground water seepage through cracks. The gases released from the concrete basemat or the ground below the basemat could contribute to the containment pressure. The rate at which the containment is pressurized would be determined by the rate at which the temperature wave conducts into the basemat and the ground and the flow resistance of these materials to the gases. This increase in pressure is expected to be gradual relative to the containment pressure buildup prior to boildry. If venting is required after sodium boildry, the vent rate would be much less than the rates required prior to sodium boildry. The radiological consequences of ground water interaction with fuel was investigated in Section 4.3.

The temperatures outside of the reactor cavity and basemat are substantially less for the case with the large crust resistance than for the small and intermediate crust. The containment wall adjacent to Cell 105 reaches a maximum temperature of 300°F for the large crust while it reaches 360 and 370°F for the intermediate and small crust respectively. Figures 3-56, 3-69 and 3-70 show the temperature history for the three cases. Section 3.2.3.3 indicates that these temperatures will not cause containment structural failures.

3.2.3.3 Structural Assessments After Sodium Boildry

3.2.3.3.1 Structural Integrity After Sodium Boildry

Long term integrity is required for the confinement structure, the outer containment wall above the foundation mat, and the containment steel shell. Integrity of the foundation mat is important in the region where it provides support to the containment and confinement walls. Evaluations of these structures are discussed below.

3.2.3.3.1.1 Evaluation of RCB Outer Wall Below Operating Floor

A thermal analysis of the RCB internal structures below the operating floor was performed as described in Section 3.2.3.2. The maximum temperature of the interior surface of the RCB outer wall is 370°F as shown on Figure 3-56. A preliminary assessment of this condition, including the corresponding temperature gradient through the RCB outer wall, indicates that structural integrity of the RCB outer wall will be maintained.

3.2.3.3.1.2 Foundation Mat Analysis

A preliminary evaluation of the foundation mat under the conditions of the Thermal Margin Beyond the Design Base has been conducted. The evaluation is based on an elasto-plastic analysis using the computer program ANSYS. The temperature distribution for one year after the accident shown on Figure 3-48 was used as input in the analysis. The temperature is actually based on a thermal analysis made for a previous scenario; however, a comparison with the temperature distributions shown in Figures 3-65 to 3-66 indicates that for a preliminary assessment the results are applicable to the present condition. The properties for concrete and reinforcing steel were based on preliminary relationships which have been revised to those in Appendix C.3. The actual relationships used were generally on the conservative side compared to those in Appendix C.3. The criteria for material failure are given in Sections C.3.2.2 and C.3.3.1.

Since the part of the overall Nuclear Island mat affected by the accident is below the RCB, the analysis was conducted on an axisymmetrical model, concentric with the RCB and with a 106 ft radius, which is 4 ft beyond the wall of the confinement.

The mathematical model is shown in Figure 3-48. From the center to a radius of 90 ft the mat thickness is 15 ft; beyond this radius, the thickness is 18 ft. An amount of reinforcing steel equal to 7.5 in.^{2}/ft was assumed at the top and bottom in each direction. The liner and fill slab were not included in the model. The bottom of the mat was allowed to slide on the underlying rock. The exterior edge was assumed restrained against radial displacement and rotation.

Results

The results of the analysis are summarized in Figure 3-49. Between the center and a radius of 40 ft, there will be a complete degradation of the mat and this section will have no structural strength. Beyond a 60 ft radius, the mat will remain structurally sound with possible cracking at the step where the thickness is increased (radius 90 ft). If the final evaluation of the mat shows that the cracking in this region is excessive, reinforcing steel will be provided for cracking control.

Between a radius of 40 to 60 ft there will be partial degradation of the concrete. With nominal reinforcing steel in the vertical and horizontal direction this degradation would be contained. Since the outer part of the mat which supports the RCB exterior wall will be structurally sound, and is supported by rock which has a high bearing capacity, no collapse of the RCB exterior walls due to foundation failure is expected.

3.2.3.3.1.3 Evaluation of Containment Vessel Structural Integrity After Sodium Boildry

After boildry the pressure in containment is essentially atmospheric. The peak containment vessel temperature is 490°F. At this temperature, the first allowable criterion (see Table 3-10) indicates a pressure capability of 37 psig. The second criterion indicates a pressure capability of 56 psig. Thus, containment can accommodate post-boildry pressures. In addition, since the containment vessel temperature at the operating floor level after boildry (see Figure 3-28) is less than the 240°F critical containment vessel buckling temperature the containment vessel will not buckle. Thus, long term containment vessel integrity would be maintained.

3.2.3.3.1.4 Evaluation of Confinement Building Structural Integrity After Sodium Boildry

Since confinement temperatures after boildry are very close to those that occur during the time period prior to boildry, the conclusions of Section 3.2.2.5.3.2 apply; i.e., preliminary assessments indicate confinement building integrity would be maintained.

3.2.3.3.2 Summary and Conclusions on Long Term Structural Integrity

As noted earlier, the analyses presented were based on an earlier thermal analysis. Accordingly the conclusion given is also strictly applicable only to that case, and is as follows: Analysis of the capability of the foundation mat to support the RCB outer walls has shown that adequate structural strength is available to support the RCB outer wall. In addition, progressive failure of the RCB internal structures below the operating floor has been assessed and does not represent a severe challenge to the RCB outer walls. Operation of the annulus cooling system coupled with an increase in the spiral arrangement (as discussed above) will assure acceptable containment vessel and confinement building temperatures above the operating floor. Therefore, it can be concluded that integrity of the reactor containment vessel and confinement building above the basemat would be maintained indefinitely. Subsequent more detailed analyses are expected to confirm this conclusion.

3.2.4 Secondary Criticality Considerations (Ex-Vessel)

The potential for criticality in the reactor cavity following reactor vessel and guard vessel penetration was assessed.

The calculations were performed using a one dimensional (slab) geometry in the code ANISN with no transverse (radial) leakage. Since the ENDF/B-III library used in these analyses does not contain calcium, an effective magnesium atom density was used, based on the relative scattering properties of the two elements.

Three basic cases were considered representing:

1. A boiling sodium pool (a particulate debris bed with the steel bed above the fuel in a sodium pool with a 40 foot diameter).

2. A just dry pool (the fuel and blanket are dissolved in approximately 2 inches thick layer mixed with concrete under a layer of steel with a diameter of 40 feet).

3. A "steady state" case representing a potential fuel distribution after a few months. The fuel was assumed to be distributed through a 12.8 feet thick layer of dry concrete and oxidized steel of thirty feet diameter. These geometries are shown in Figures 3-73, 74 and 75. All of these cases considered 100% of the fuel and blankets. A fourth

calculation was performed for sensitivity purposes representing the steady state case but using a reflective boundary condition on the upper surface of the fuel mixture (essentially doubling the fuel mass) and halving the non-fuel atom number densities.

The results of the analyses are provided in Table 3-11. The selected configurations, which are representative of various stages of the accident after vessel failure, are all so far from critical that uncertainties in material composition and neutron cross sections would not result in any approach to criticality. Additional conservatism included is the omission of fission products and omission of any transverse leakage in the one-dimensional slab calculations.

It is concluded that the potential configurations in the reactor cavity would not result in a recriticality.

3.3 CONCLUSIONS ON THERMAL MARGIN BEYOND THE DESIGN BASE

The above analyses and assessments lead to the following conclusions:

1. Thermal loads resulting from an HCDA could cause failure of the reactor and guard vessels.

2. Containment integrity (without venting and purging) would be maintained for more than 24 hours. This provides time to implement evacuation procedures and meets the requirement imposed by NRC. (Analyses indicate capability of about 36 hours.)

3. Uncontrolled failure of containment beyond 24 hours would be prevented by venting and purging.

4. Containment structural capability above the basemat would be maintained indefinitely.

5. The thermal analysis of meltfront progression indicate that basemat penetration would be unlikely.

3.4 REFERENCES

3-1 W. L. Macabe and J. C. Smith, Unit Operations of Chemical Engineering, McGraw-Hill, New York, 1956.

3-2 M. A. Grolmes, G. A. Lambert and T. G. Theofanous, "Hydrodynamic Aspects of Mild LMFBR Core Disassembly," Trans. Amer. Nucl. Soc. 21, pp. 280-281 (1975).

3-3 L. Baker, Jr. et al., "Postaccident Heat Removal Technology," ANL/RAS 74-12, July 1974. (Availability: U. S. DOE Technical Information Center).

3-4 G. W. Govier and K. Aziz, The Flow of Complex Mixtures in Pipes, pp. 617-711, VanNostrand Reinhold, New York, 1972.

3-5 L. Baker, Jr., et al., "Postaccident Heat Removal in Fast Reactors," ANL/RAS-75-44, November 1975. (Availability: U. S. DOE Technical Information Center).

3-6 L. Baker, Jr., et al., "Post Accident Heat Removal Technology," ANL/RAS 77-2, January 1977. (Availability: U. S. DOE Technical Information Center).

3-7 S. A. Meacham, "The Interactions of Tennessee Limestone Aggregate Concrete with Liquid Sodium," WARD-D-0141, December 1976.

3-8 R. H. Norris, F. F. Buckland and N. D. Fitzroy, Heat Transfer Data Book, Section G503.2, p. 3, General Electric Company, Schenectady, New York, 1961.

3-9 R. H. Perry, C. H. Chilton and S. D. Kirkpatrick, Chemical Engineers Handbook, Fourth Edition, pp. 10-11 and 10-35, McGraw Hill, New York, 1963.

3-10 "Light Water Reactor Safety Research Program Quarterly Report, January-March 1976," SAND-76-0369, August 1976.

3-11 L. M. Polentz, "Analysis of FFTF Reactor Cavity Liners Under Ex-Vessel PAHR Conditions," HEDL-TC-572, Rev. 1, June 1976. (Availability: U. S. DOE Technical Information Center).

3-12 U. S. Nuclear Regulatory Commission, "Steel Containment in Standard Review Plan for the Review of Safety Analysis Reports for Nuclear Power Plants," NUREG-75/087, November 1975, Section 3.8.2.

3-13 "Nuclear System Materials Handbook Design Data," TID-26666, Vol. 1, Book 1, Group 3, Section 3. (Availability: Hanford Engineering Development Laboratory).

3-14 S. A. Meacham, "Molten Stainless Steel and Urania Compatibility with Refractory Materials Considered for CRBRP Parallel Design Ex-Vessel Core Retainers - Topical Report," CRBRP-ARD-0098, October 1976. (Availability: U. S. DOE Technical Information Center).

3-15 J. C. Reese, "Reactor Vessel Outlet Plenum Transient Thermal Environment Prediction," CRBRP-ARD-0163, December 1977.

3-16 R. G. Brown, "Assessment of Debris Transport Methods In Horizontal LMFBR Piping for PAHR Conditions," WARD-SR-3045-9, April 1979.

3-17 J. L. McEroy and D. M. Switick, "An Analysis of Hypothetical Core Disruptive Events in the Clinch River Breeder Reactor Plant," CRBRP-GEFR 00103, April 1978. (Availability: U. S. DOE Technical Information Center).

3-18 W. R. Bohl, J. E. Cahalan and D. R. Ferguson, "An Analysis of the Unprotected Loss-of-Flow Accident in the Clinch River Breeder Reactor with an End-of-Equilibrium Cycle Core," ANL/RAS 77-15, May 1977. (Availability: U. S. DOE Technical Information Center).

3-19 P. I. Nakayama and J. L. Cook, "VARR II, A Computer Program for Calculating Turbulent Fluid Flows with Slight Density Variation," CRBRP-ARD-0106, November 1976. (Availability: U.S. DOE Technical Information Center).

3-20 J. B. Rivard, "Postaccident Heat Removal: Debris Bed Experiments D-2 and D-3," SAND 78-1238, (NUREG/CR-0421) November 1978.

3-21 W. D. Boehmer and R. K. Hilliard, "Sodium Fire Protection by Space Isolation, Open Catch Pan and Nitrogen Flooding: FFTF Proof Test F5," HEDL-TME 75-98, October 1975. (Availability: U.S. DOE Technical Information Center).

3-22 R. K. Hilliard, "Sodium Concrete Reactions, Liner Response, and Sodium Fire Extinguishment," HEDL-SA-983, 1975.

3-23 D. Lewis and G. von Elbe, Combustion, Flames and Explosions of Gases, pp. 535,693, Academic Press, New York, 1961.

TABLE 3-1

PUMP COASTDOWN DATA

Time, Seconds	Fraction of Full Flow
0.0	1.0
1.3	0.8
3.2	0.6
6.2	0.4
10.4	0.28
16.2	0.2
300.0	0.1

TABLE 3-2

PARTICLE DISTRIBUTION FOLLOWING
IN-VESSEL SETTLING

Mean Particle	Wt% of Core		Fraction Settling In-Vessel
μ	M-3	EDT-1	
50	14	53	0.53
100	32	18	0.611
200	24	16	0.811
300	8	5	0.907
400	6	2	0.956
500	3	1	0.972
800	13	4	0.989
1000	--	1	1.00

TABLE 3-3

DISTRIBUTION OF UPWARD EJECTED DEBRIS

	Particle Size Distribution	
	M-3	EDT-1
	(% of Core)	(% of Core)
Remaining In-Vessel	52	45
Piping Before HTS Cells	18	17
Piping Between Cell Walls and Pumps	<0.1	2
IHX	0	6
Total Upward Ejection	70	~70

TABLE 3-4

PARTICLE DRAG COEFFICIENTS

Particle Size μ	Settling Velocity ft/sec	Drag Coefficient
50	0.07	16.9
100	0.15	7.4
200	0.28	4.2
300	0.40	3.1
400	0.53	2.4
500	0.61	2.2
800	0.77	2.2

TABLE 3-5

MAXIMUM CRBR FULL EQUILIBRIUM CYCLE DECAY POWER BY REGION*

Time After Shutdown (Seconds)	Inner Core (Fraction of EOEC Region Power)	Outer Core (Fraction of EOEC Region Power)	Radial Blanket (Fraction of EOEC Region Power)	Full Cycle (Fraction of Full Power)
0.0	8.31-2	[illegible]	9.83-2	8.45-2
1.00+0**	7.97-2	7.76-2	9.49-2	8.11-2
3.16+0	7.02-2	6.80-2	8.54-2	7.15-2
1.00+0	5.96-2	5.75-2	7.48-2	6.09-2
3.16+1	4.94-2	4.72-2	6.45-2	5.06-2
1.00+2	4.04-2	3.83-2	5.52-2	4.15-2
3.16+2	3.25-2	3.04-2	4.65-2	3.34-2
1.00+3	2.54-2	2.37-2	3.75-2	2.63-2
3.16+3	1.88-2	1.74-2	2.76-2	1.94-2
1.00+4	1.34-2	1.24-2	2.05-2	1.39-2
3.16+4	9.77-3	8.78-3	1.63-2	1.02-2
1.00+5	6.02-3	6.12-3	1.21-2	7.23-3
3.16+5	4.52-3	4.09-3	6.97-3	4.66-3
1.00+6	2.70-3	2.53-3	2.95-3	2.70-3
3.16+6	1.63-3	1.56-3	1.68-3	1.62-3
1.00+7	8.84-4	8.36-4	1.68-3	8.78-4
3.16+7	4.11-4	3.86-4	9.54-4	4.13-4
1.00+8	1.55-4	1.45-4	2.11-4	1.58-4
3.16+8	4.87-5	4.54-5	7.41-5	5.06-5
1.00+9	1.36-5	1.27-5	2.21-5	1.43-5

*Values include fission products power and Np^{239} and U^{239} decay power with respective uncertainties added.

**$1.00 + 0 = 1.0 \times 10^0$

TABLE 3-6

STABLE DEBRIS BED DEPTHS

Time From Subcriticality, Seconds	Full Decay Heat; Particulate 50% Steel	70% Decay* Heat; Particulate 50% Steel	Full Decay Heat; Particulate 100% Oxide	70% Decay* Heat; Particulate 100% Oxide
30	4.4 inches	4.9 inches	2.8 inches	3.6 inches
100	4.7 inches	5.2 inches	3.4 inches	3.9 inches
200	4.85 inches	5.4 inches	3.5 inches	4.0 inches

*Exclude gaseous fission products, halogens and volatiles.

TABLE 3-7

COMPARISON OF FUEL RETENTION CAPABILITY
WITH PREDICTED FUEL DISTRIBUTION

Structure	Percentage of Fuel* Predicted Fuel Distribution	Fuel Retention Capability
Horizontal Baffle	45-52	28-46
Outlet Pipe Elbow	0	3-4
Outlet Piping Before PHTS Cells	17-18	17-31
Outlet Piping Between PHTS Cell Wall and Pump	0-2	20-37
IHX Inlet Annulus	0-6	7-14
Vessel Lower Head	10-50	1-8

*Core fuel plus axial blankets and the first row of the radial blankets equals 100%.

TABLE 3-8

SENSITIVITY OF CONTAINMENT PARAMETERS AT 24 HOURS AFTER AN HCDA TO VESSEL PENETRATION TIME

	Reference Section 3.2.2	Other Penetration Times	
Penetration Time	10^3 seconds	10^2 seconds	10^4 seconds
RCB Temperature (^oF)	450	450	430
RCB Pressure (psig)	11.1	11.1	10.1
RCB H_2 Concentration (volume %)	0.0	0.0	0.0

TABLE 3-9

ANNULUS COOLING SYSTEM ANALYSIS DATA

		Reference
Annulus Cooling System Flow Rate	400,000 scfm	
Heat Transfer Coefficients		
RCB Air to Containment	1.5 $BTU/hr\text{-}ft^2\text{-}^oF$	3-10
Containment to Cooling Air*	3.5 $BTU/hr\text{-}ft^2\text{-}^oF$	3-9
Cooling Air to Confinement*	3.5 $BTU/hr\text{-}ft^2\text{-}^oF$	3-9
Emissivity		
Concrete	0.93	3-10
Steel	0.73	3-10
Heat Capacity		
Insulation	4.3 $BTU/ft^3\text{-}^oF$	**
Concrete	24 $BTU/ft^3\text{-}^oF$ @70^oF 42 $BTU/ft^3\text{-}^oF$ @750^oF	See Appendix C.1
Steel	59 $BTU/ft^3\text{-}^oF$	See Appendix C.1
Thermal Conductivity		
Insulation	0.042 $BTU/hr\text{-}ft\text{-}^oF$	**
Concrete	1.0 $BTU/hr\text{-}ft\text{-}^oF$ @70^oF 0.65 $BTU/hr\text{-}ft\text{-}^oF$ @950^oF	See Appendix C.1
Steel	25. $BTU/hr\text{-}ft\text{-}^oF$	See Appendix C.1

*Value corresponding to a velocity of 2162 FPM; at other velocities (v), $h_v = 3.5 \left(\frac{v}{2162}\right)^{0.8}$.

**Data obtained from Johns Manville Vendor Information Catalog.

TABLE 3-10

CONTAINMENT STRUCTURAL CAPABILITY

	$P_m \leq S_y$		Primary Stress < 85% (0.7 S_u)	
Temperature (°F)	Sa = Sy (psi)	Pressure (psig)	Su (psi)	Pressure (psig)
100	38,000	46.8	70,000	51.1
150	35,700	43.9	72,900	53.5
200	34,700	42.7	75,300	55.2
250	34,000	41.9	77,000	56.5
300	33,600	41.4	78,200	57.3
350	33,200	41.0	78,800	57.8
400	32,700	40.3	78,900	57.8
450	31,800	39.2	78,400	57.5
500	30,600	37.7	77,400	56.7
550	29,200	36.0	75,800	55.6
600	28,200	34.7	73,800	54.1
650	27,600	34.0	71,200	52.2
700	27,300	33.6	68,100	49.9

Note:

P_m = Primary membrane stress

S_y = Yield stress

S_a = Allowable stress

S_u = Ultimate stress

TABLE 3-11

$k_{effective}$ OF VARIOUS GEOMETRIES

Case Identification	Approximate k_{eff}
a) Boiling pool	0.51
b) Dry debris	0.51
c) "Steady State"	0.25
"Steady State" with reflective upper boundary and half non-fuel atom densities	0.38

TABLE 3-12

REACTOR CAVITY AND PIPEWAY CELL LINER FAILURE TIMES

Area	Liner Failure Time (Hours)
Reactor Cavity Floor	0
Pipeway Cell Floor and Roof	30
2'-6" Thick Pipeway Wall	35
4' Thick Pipeway Wall	40
Lower Submerged Reactor Cavity Wall	50
Head Access Area Pipeway Wall	55
Upper Submerged Reactor Cavity Wall	70
Non-Submerged Reactor Cavity Wall	80
Double-Heated Pipeway Wall	90

TABLE 3-13

HEAT TRANSFER COEFFICIENT USED IN THERMAL ANALYSIS OF THE REACTOR CAVITY LEDGE

Time, Hr.	h_1, Btu/hr-ft^2-^oF	h_2, Btu/hr-ft^2-^oF
0.	1.25	.6
7.	1.25	2.1
19.	1.25	24.2
23.	1.25	14.6
30.	1.25	36.1
35.	1.25	25.9
45.	1.25	50.
55.	1.25	21.8
70.	1.25	26.3
90.	1.25	9.6
125.	1.25	7.4
140.	1.25	.7

TABLE 3-14

SUMMARY OF RESULTS FOR SUBMERGED LINER

(WITHOUT CREEP)

Description	Max. Generalized von Mises Strain ε_e	Strain at Ultimate Tensile Stress ε_u	Actual $\varepsilon_e/\varepsilon_u$	Allowable $\varepsilon_e/\varepsilon_u$
Portion Away From Floor				
~4 Hrs., T = 1350°F				
Wall Plate	0.031 (B.C.)	0.038	0.82	0.90
Stud Anchor	0.0002 (T)	0.038	0.005	0.90
10-24 Hrs., T = 1700°F				
Wall Plant	0.017 (B.C.)	0.061	0.28	0.90
Stud Anchor	0.0002 (T)	0.061	0.003	0.090
Portion Near Floor				
~4 Hrs., T = 1350°F				
Wall Plate	0.033 (B.C.)	0.038	0.87	0.90
Stud Anchor	0.036 (T)*	0.038	0.95	0.95
Stud Anchor	0.033 (C)*	0.038	0.87	0.95

Note: Creep effects reduce the listed 'actual strains'.

B.C. = Biaxial Compression

T = Tension

* = Includes Bending Strains

TABLE 3-15

SUMMARY OF RESULTS FOR LINE ABOVE SODIUM POOL

(WITHOUT CREEP)

Description	Max. Generalized von Mises Strain ε_e	Strain at Ultimate Tensile Stress ε_u	Actual $\varepsilon_e/\varepsilon_u$	Allowable $\varepsilon_e/^r$
~9 Hrs., T = 1350°F				
Wall Plate	0.031 (B.C.)	0.038	0.82	0.90
Stud Anchor	0.0005 (T)	0.038	0.01	0.90

Note: Creep effects reduce the listed 'actual strains'.

B.C. = Biaxial Compression

T = Tension

* = Includes Bending Strains

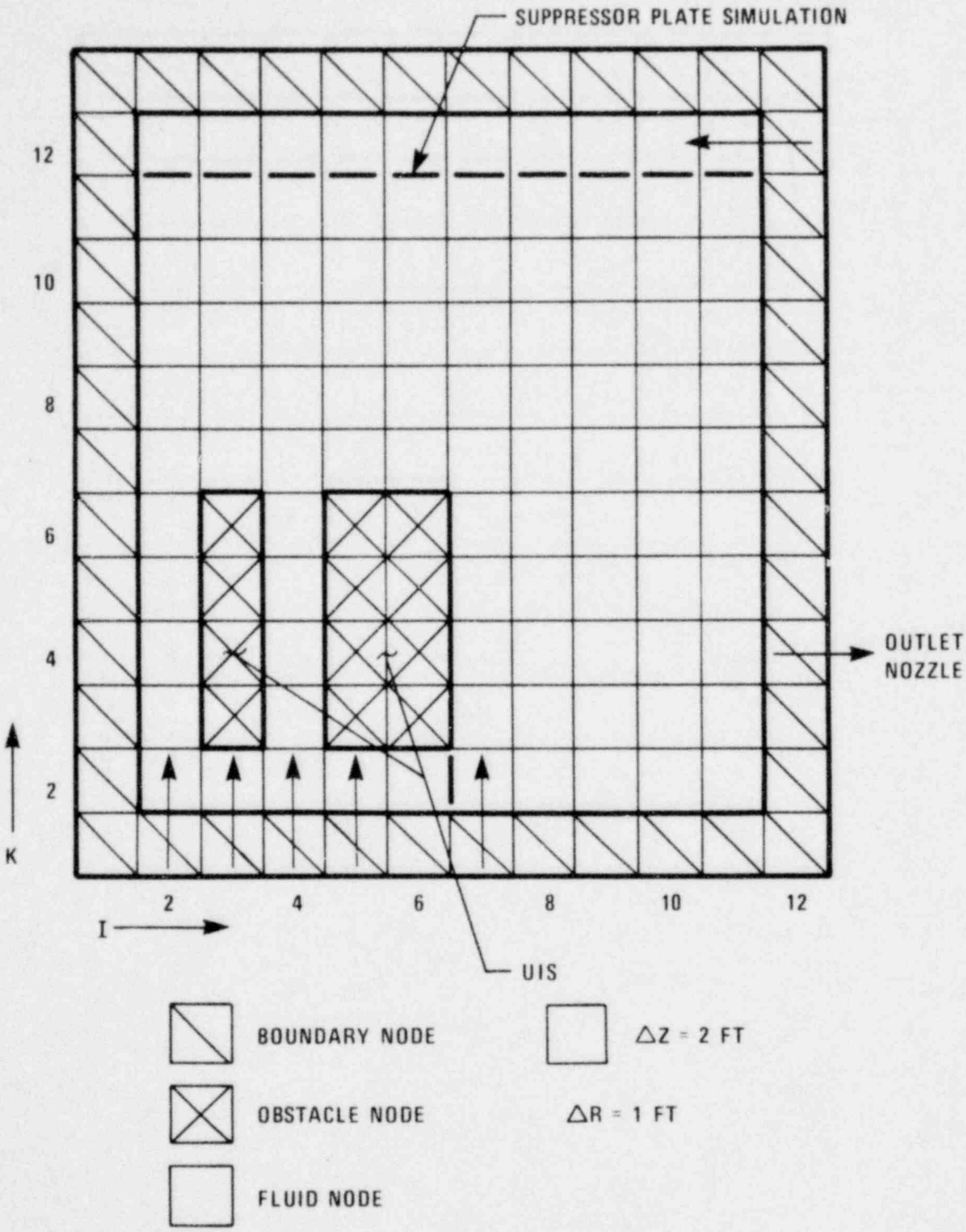

Figure 3-1. 10 X 11 Array VARR-II Outlet Plenum Model with Complex UIS Geometry

1966-35

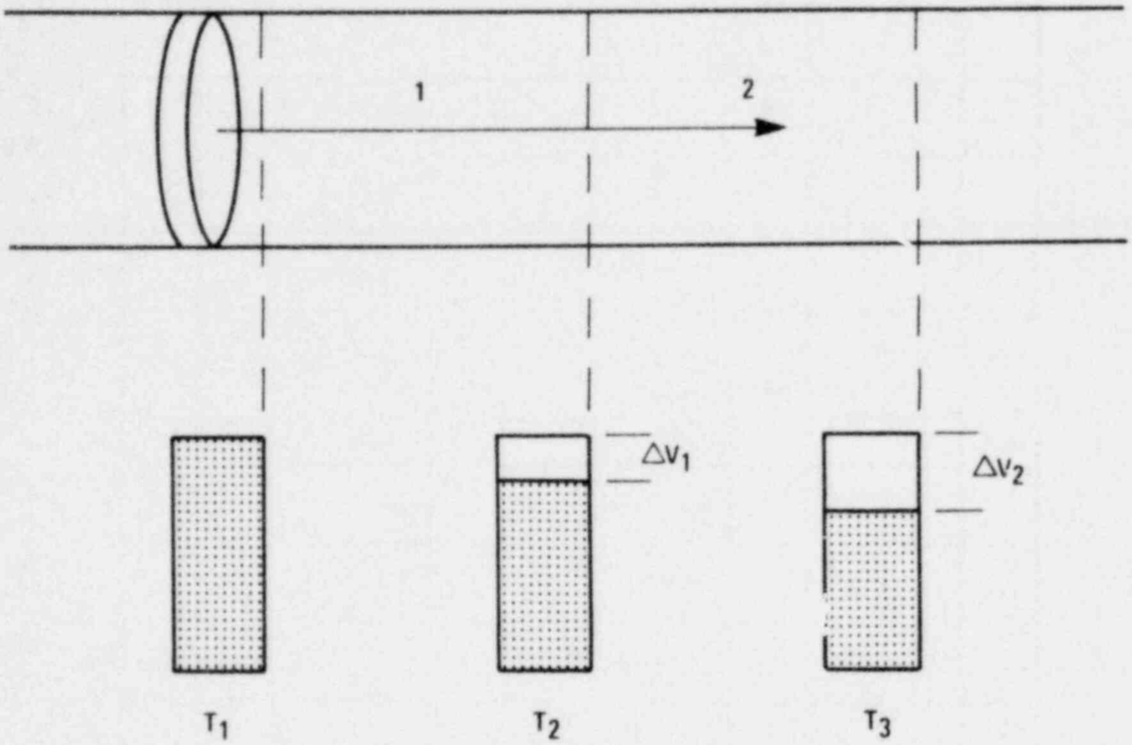

AMOUNT IN SECTION 1 $\Delta V_1 \times \rho_{PARTICLES}$

AMOUNT IN SECTION 2 $(\Delta V_2 - \Delta V_1) \times \rho_{PARTICLES}$

Figure 3-2. Simplified Drawing of Settling in Horizontal Pipes

1966-36

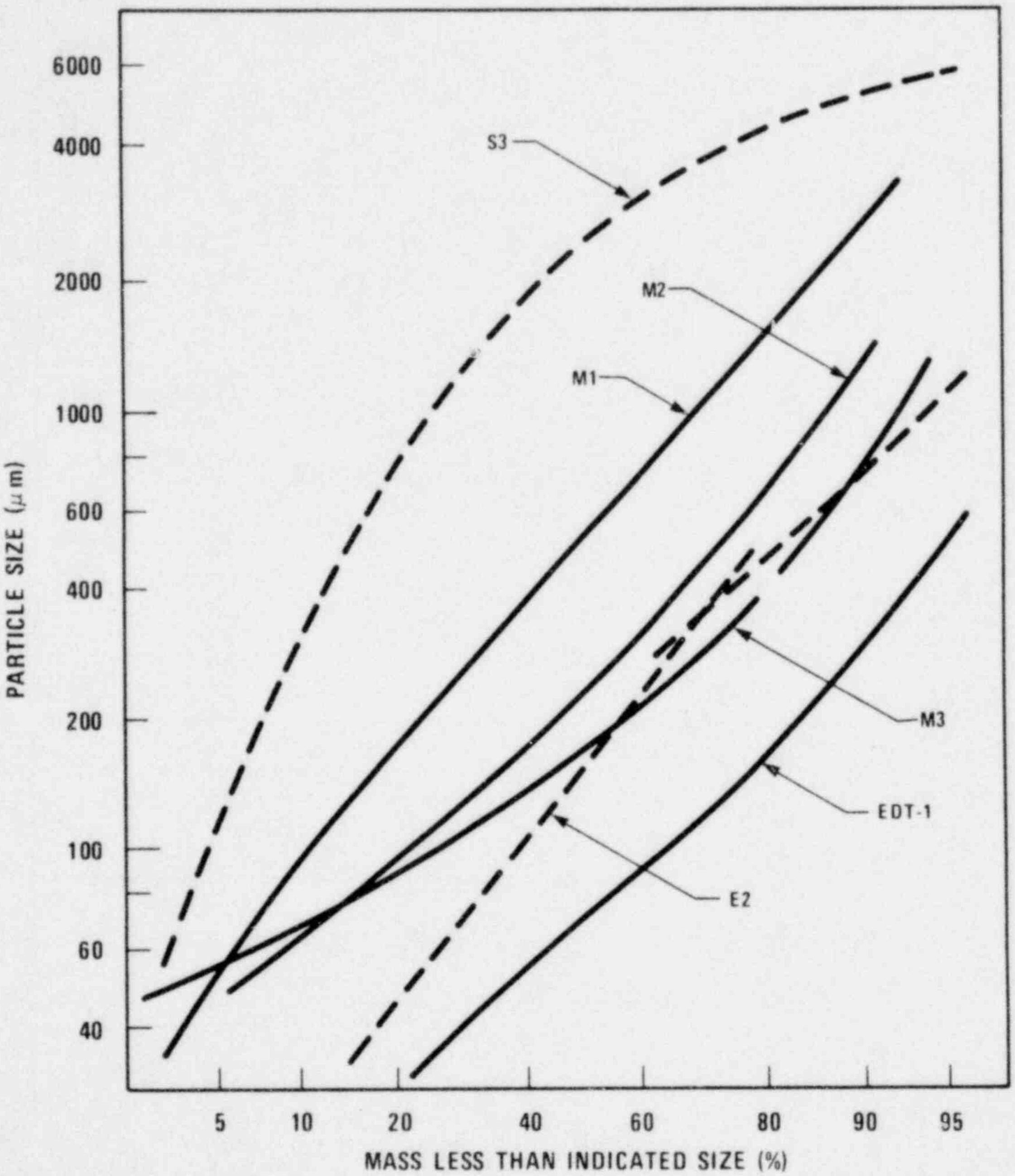

Figure 3-3. Particle Size Distributions from Large-Scale Out-of-Pile Tests

1966-37

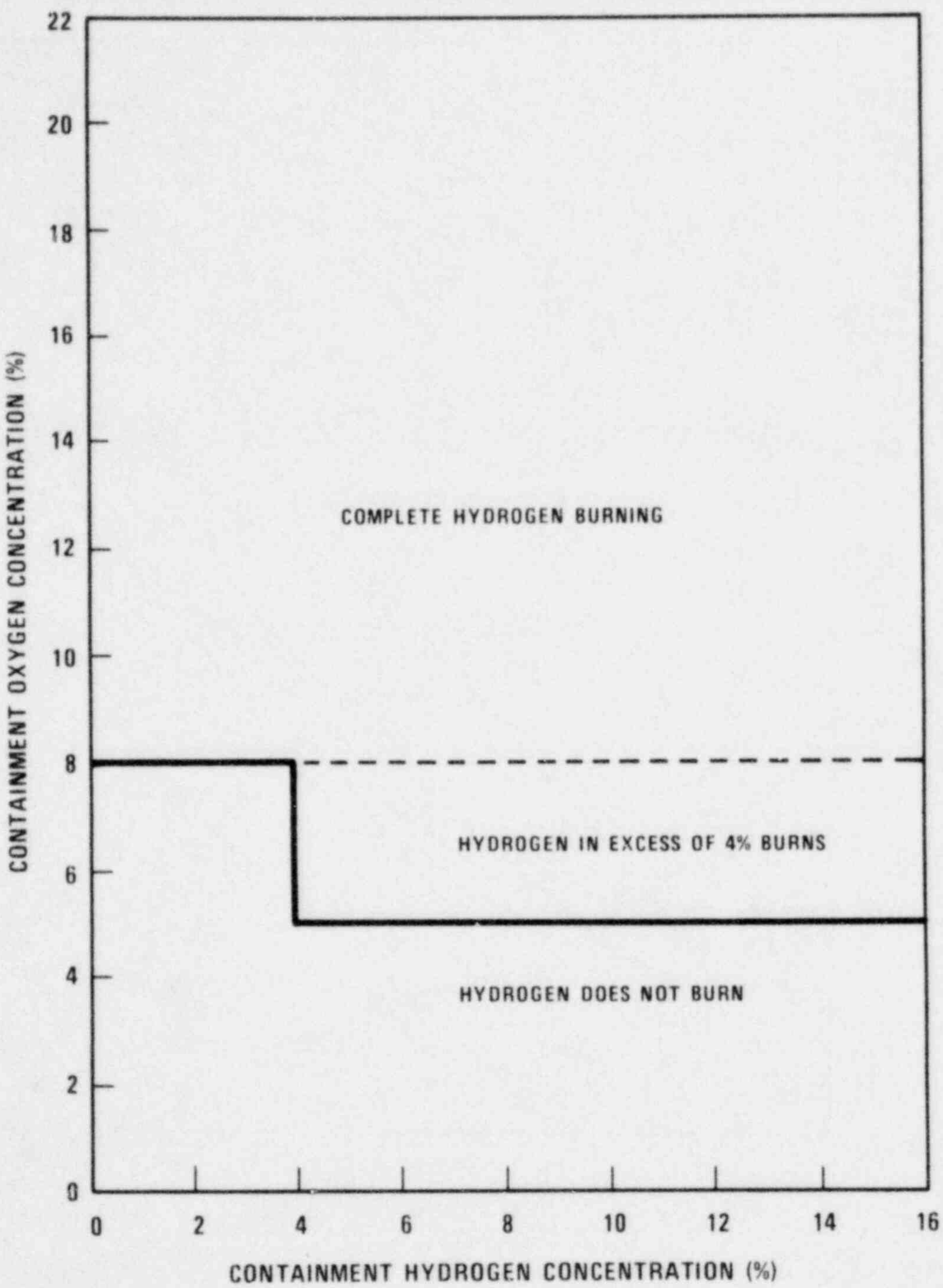

Figure 3-4. Hydrogen Burning Criterion

1966-38

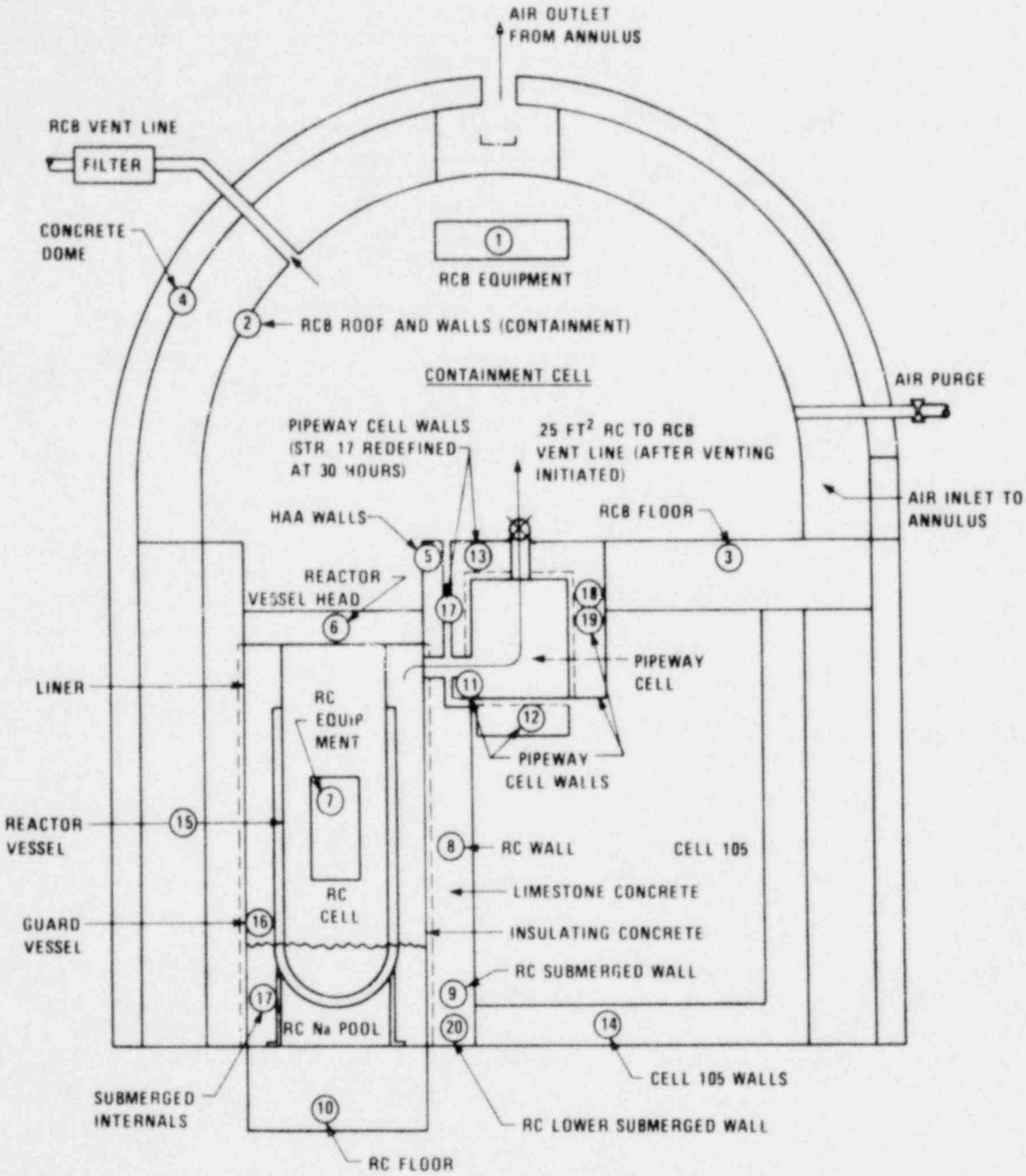

Figure 3-5. CACECO Code Containment Model

1966-39

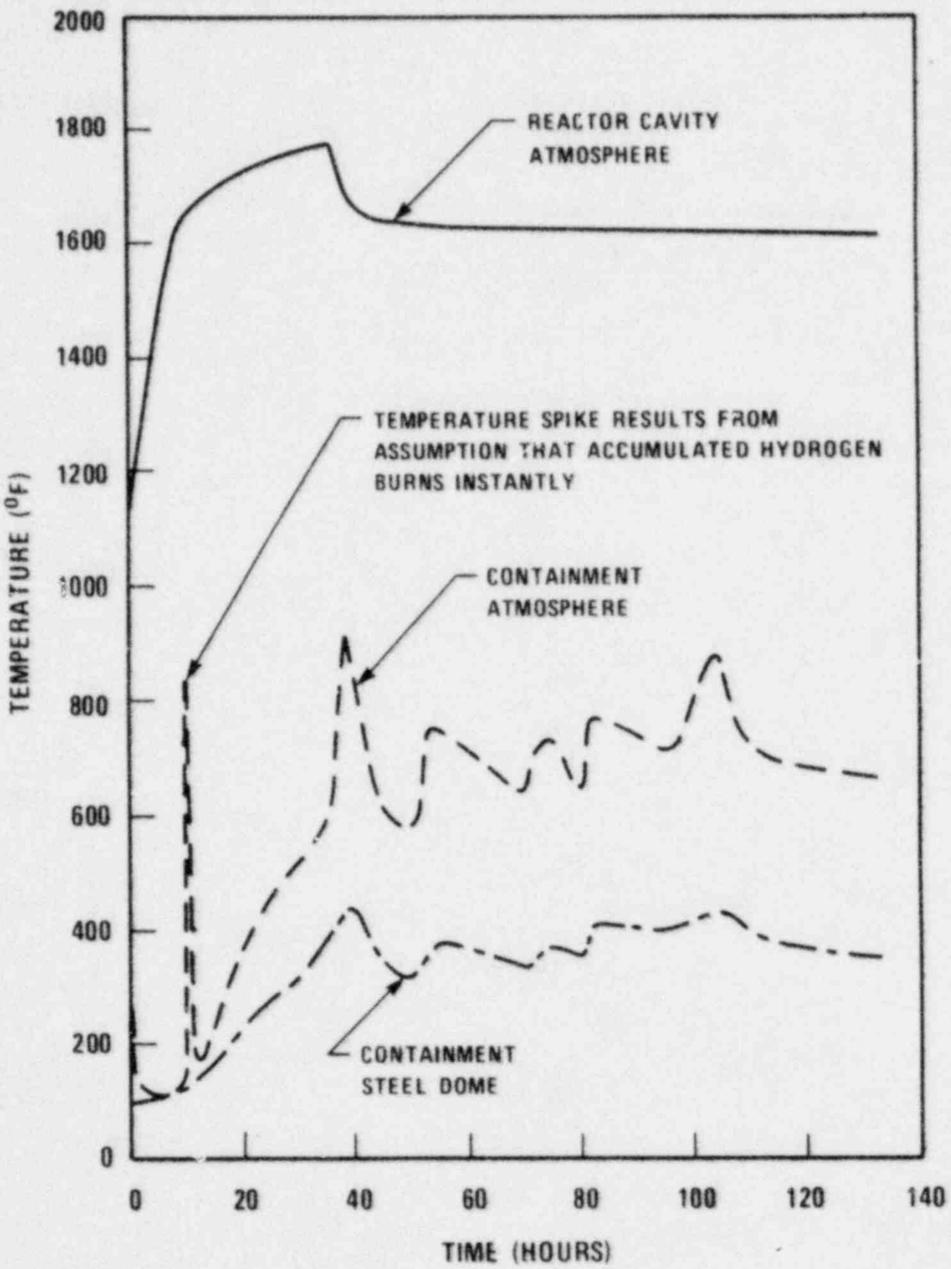

Figure 3-6. Reactor Cavity and Containment Atmosphere and Containment Steel Dome Temperatures

1966-40

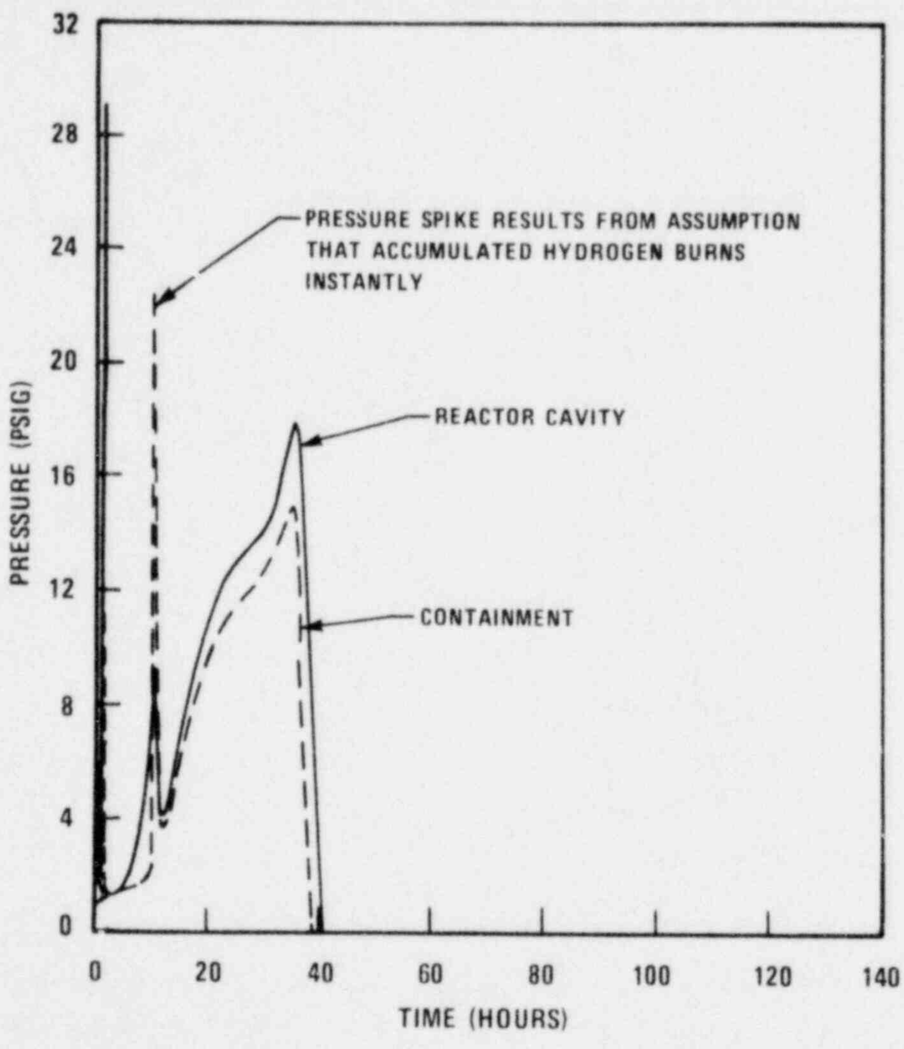

Figure 3-7. Reactor Cavity and Containment Pressures

1966-41

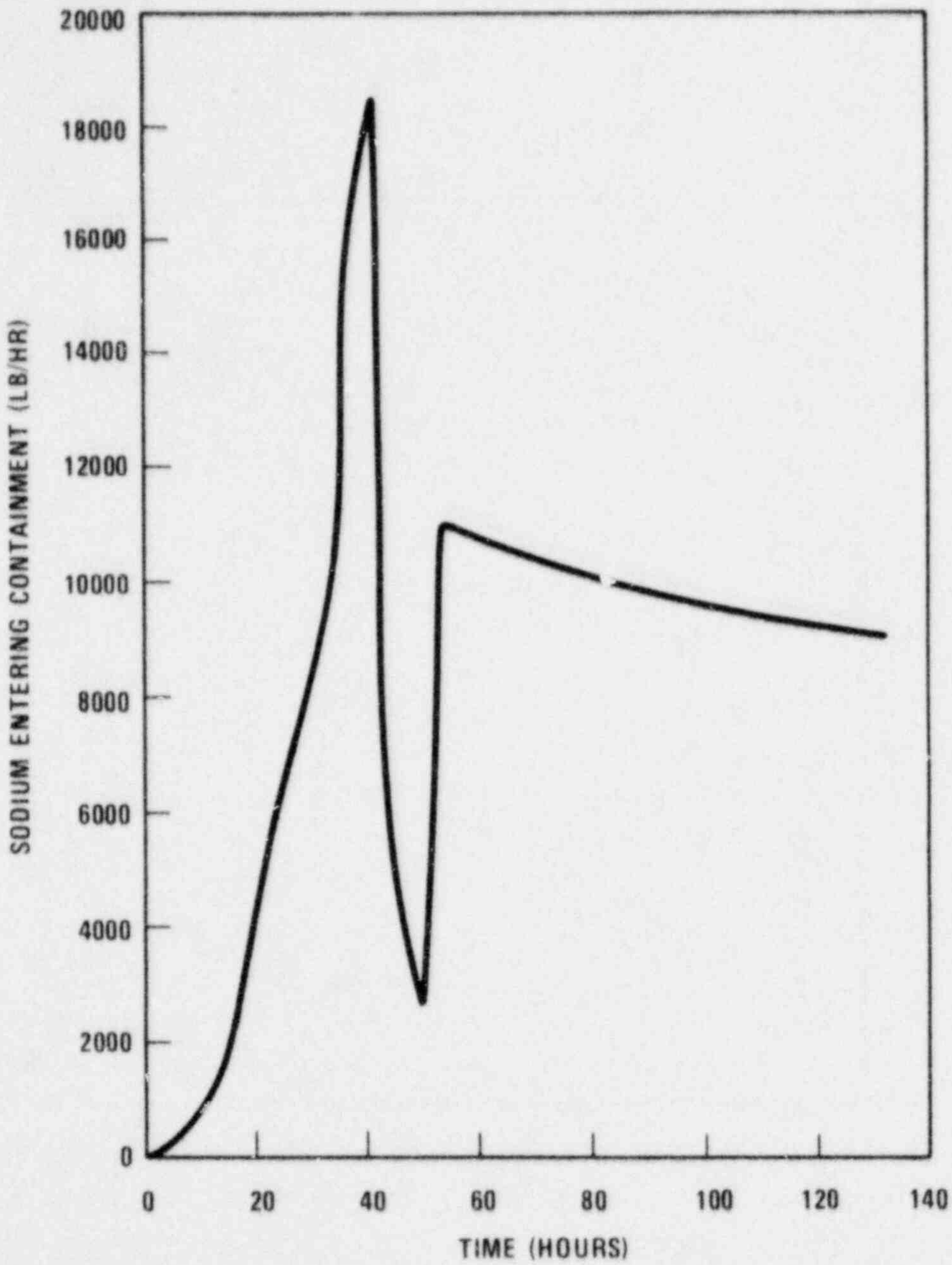

Figure 3-8. Sodium Entering Containment from the Reactor Cavity

1966-42

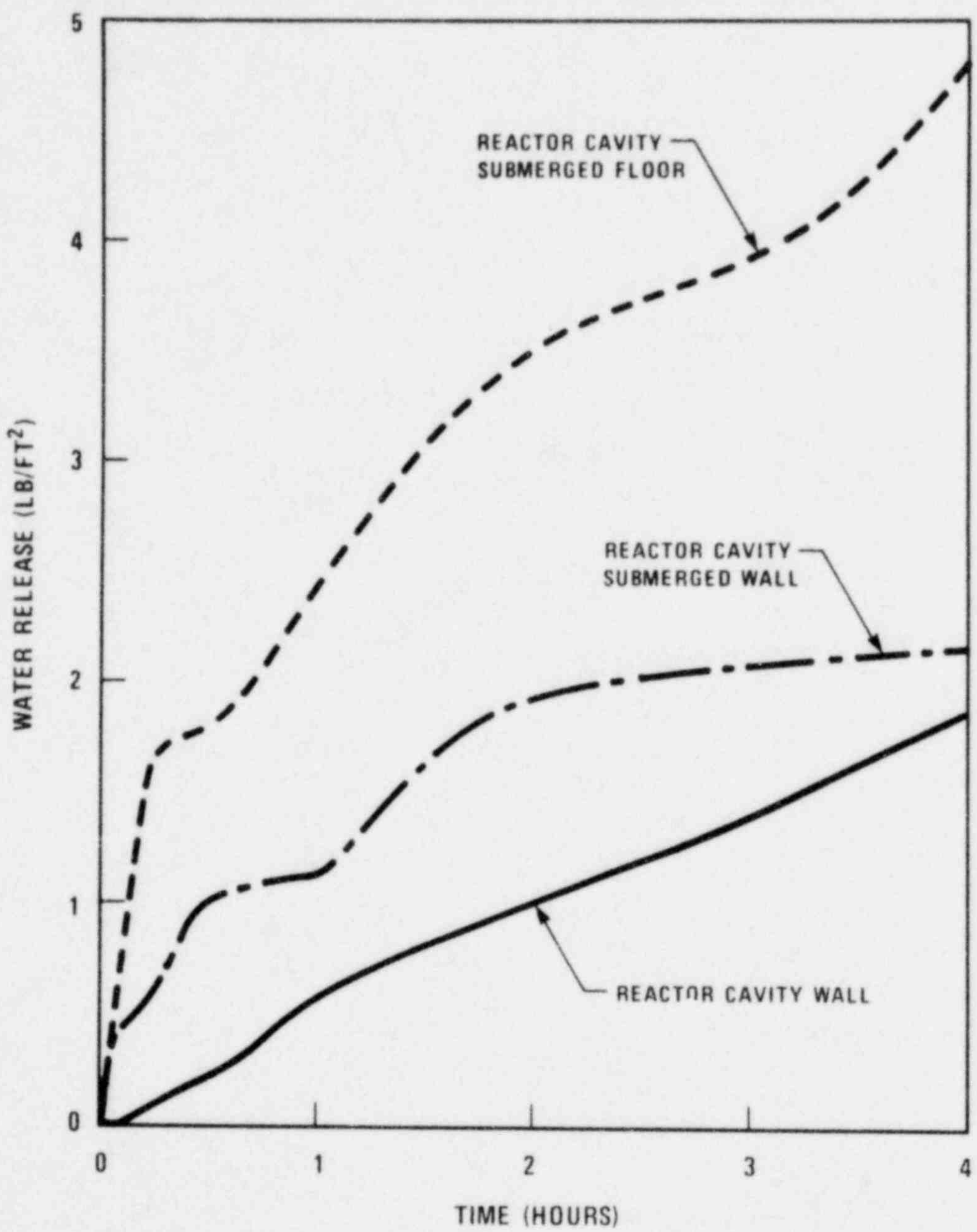

Figure 3-9. Integrated Water Release from Concrete Structures

1966-43

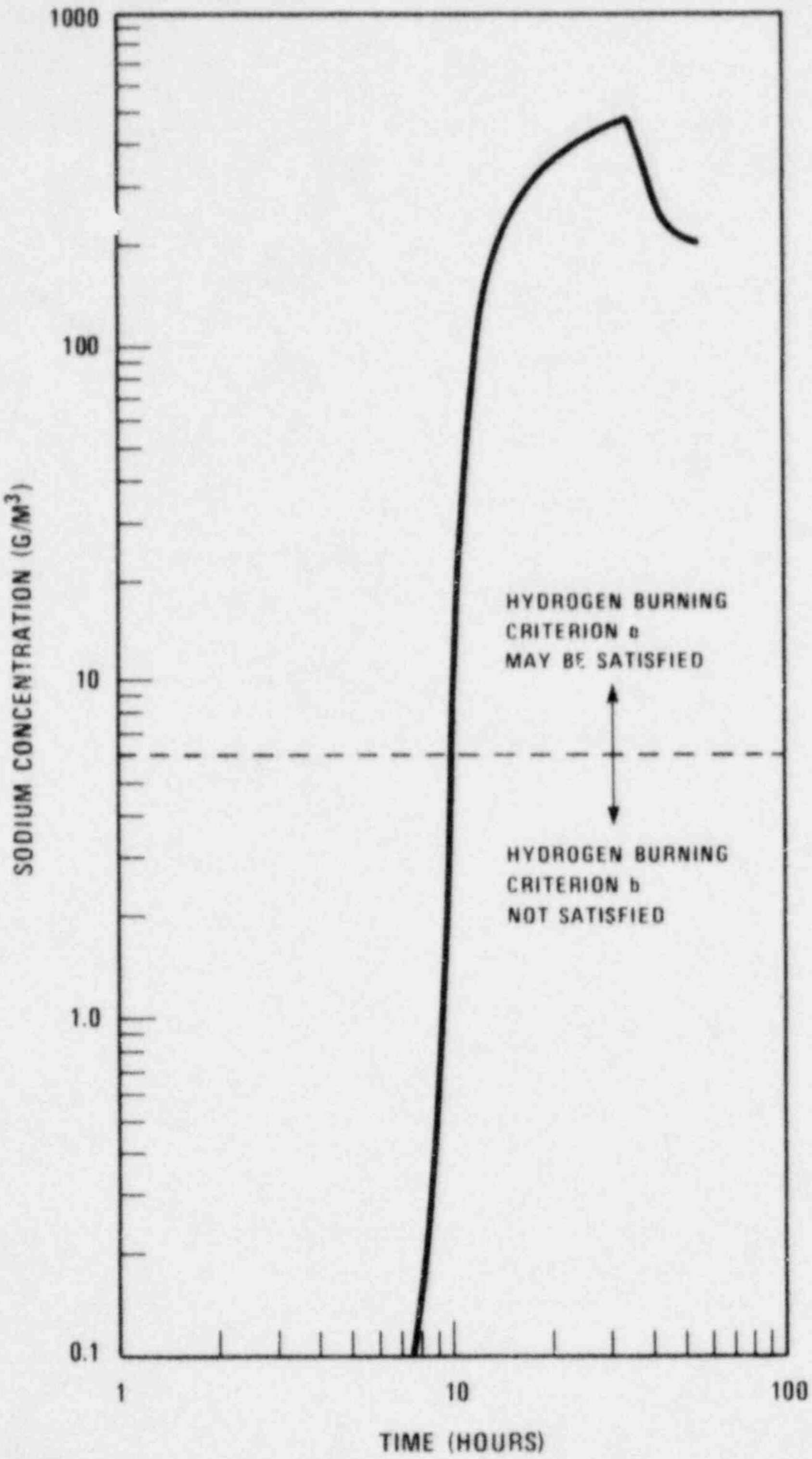

Figure 3-10. Sodium Concentration Entering Containment

1966-44

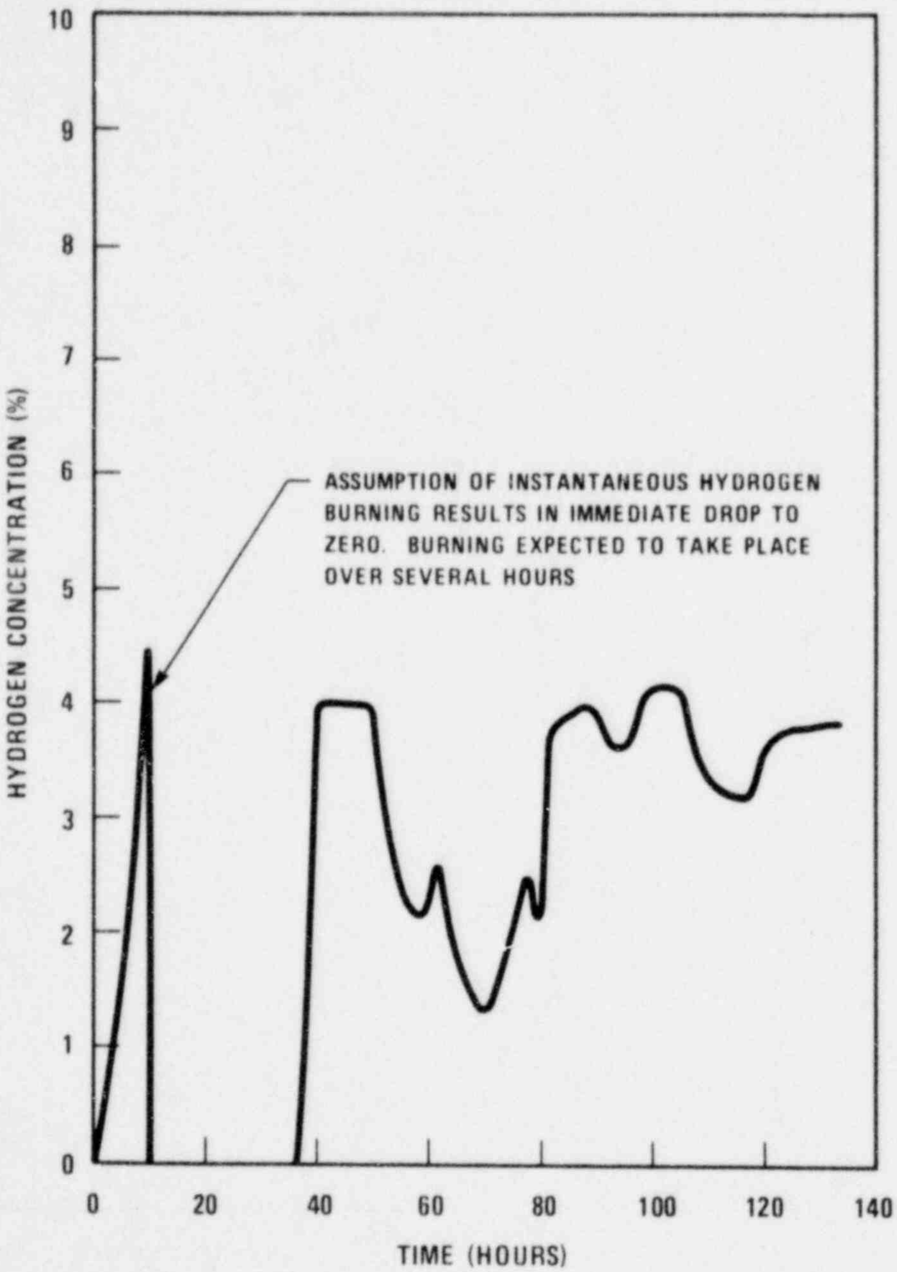

Figure 3-11. Containment Building Hydrogen Concentration

1966-45

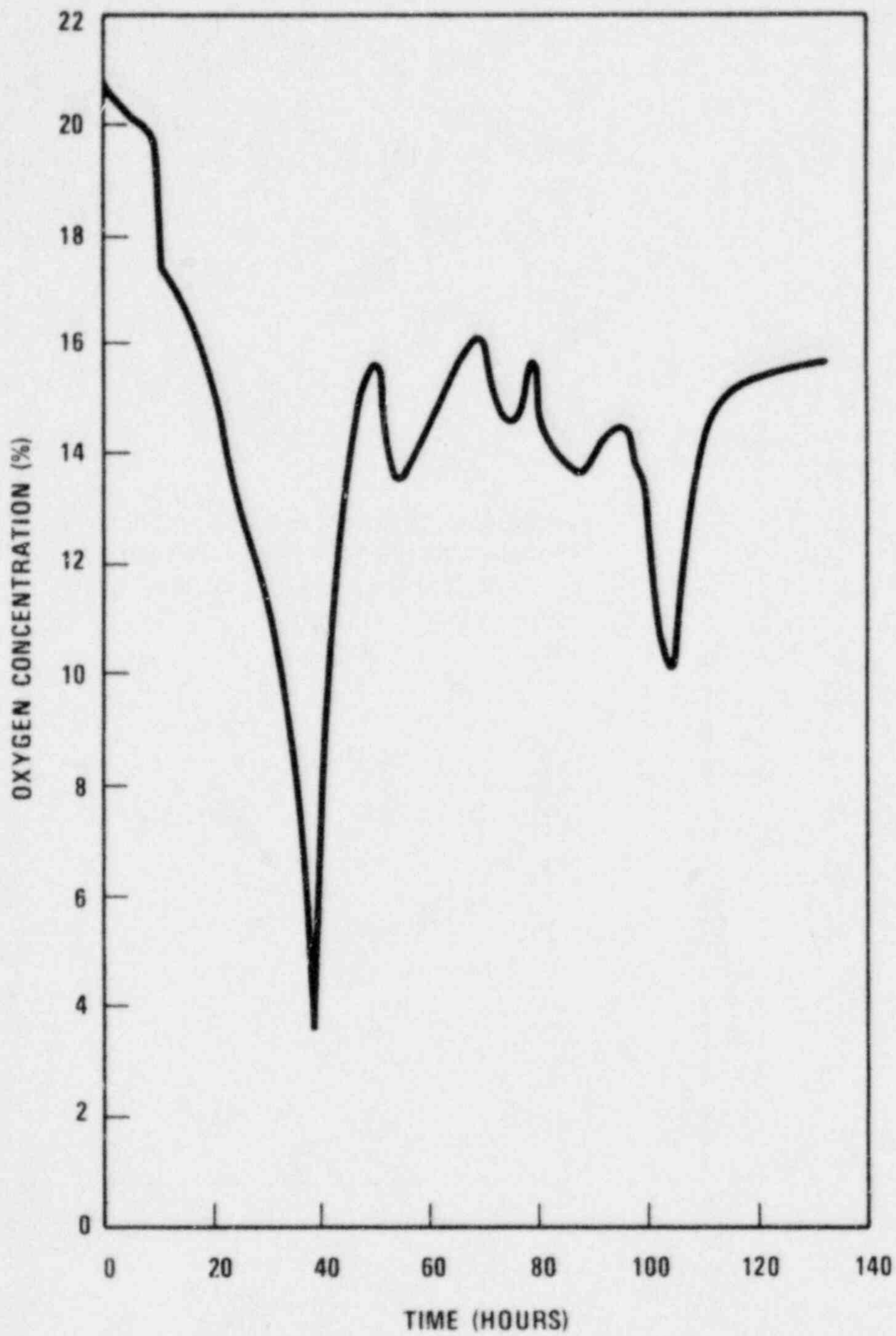

Figure 3-12. Cι tainment Oxygen Concentration

1966-46

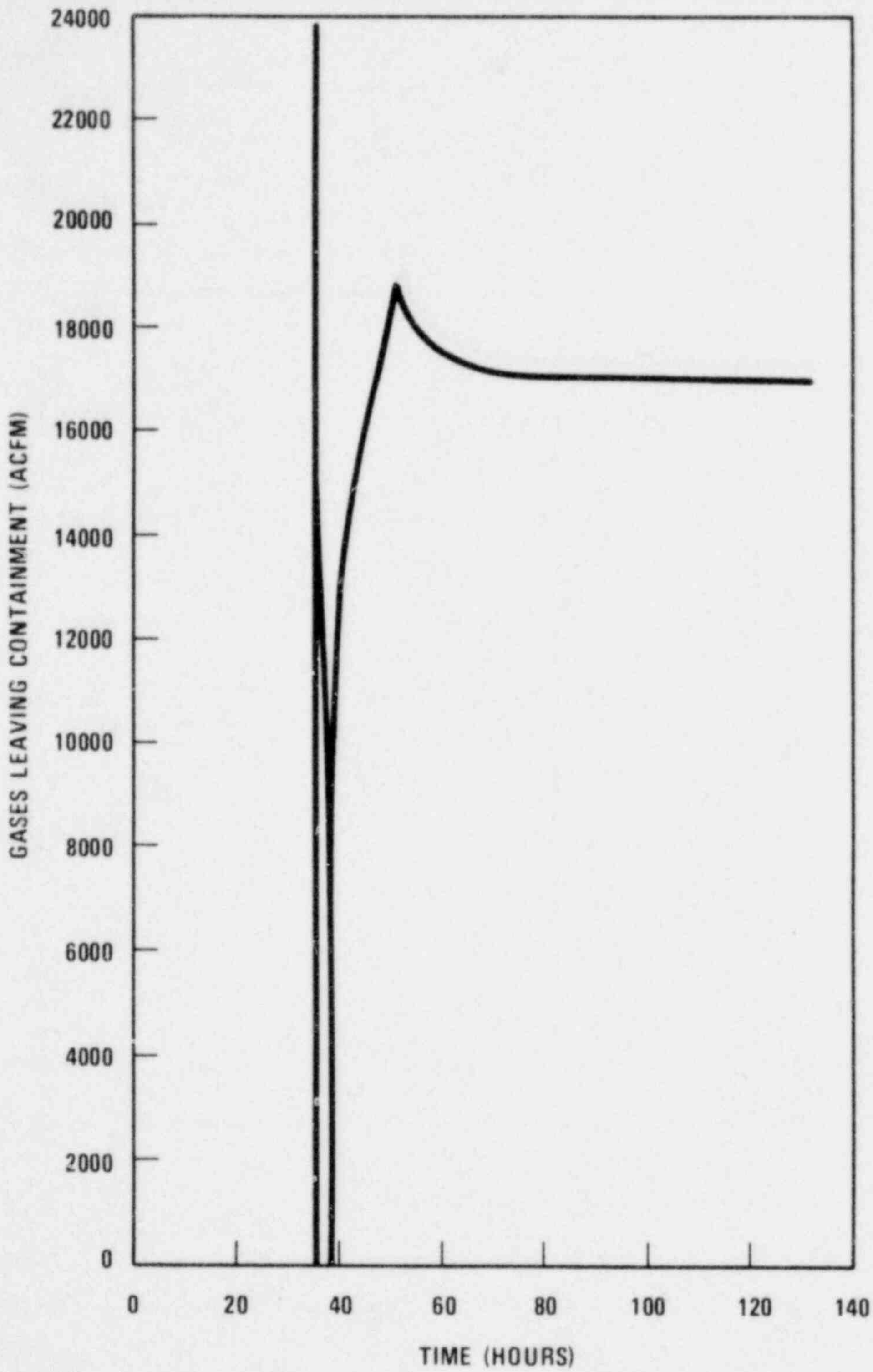

Figure 3-13. Gases Leaving Containment

1966-47

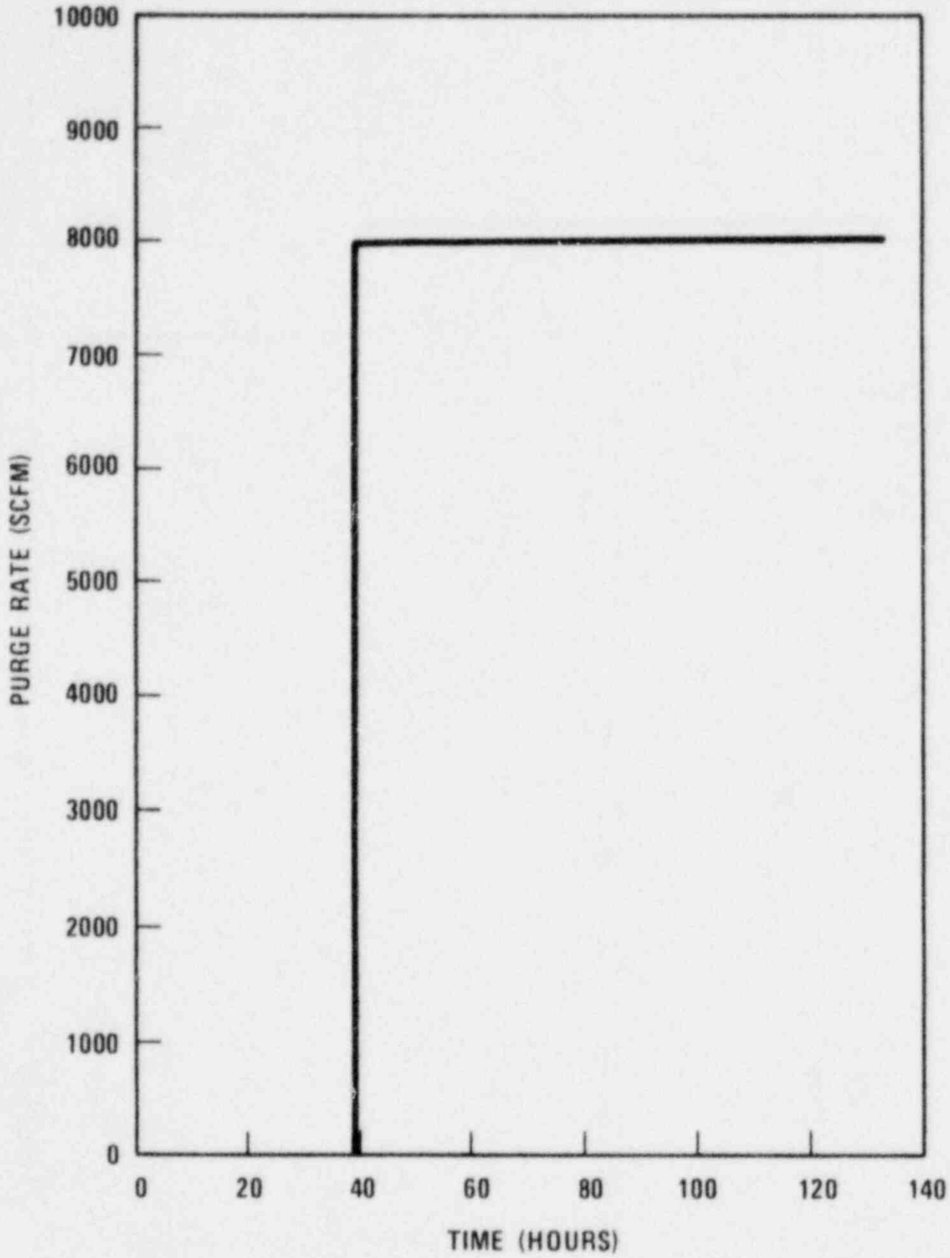

Figure 3-14. Air Purge Rate into Containment

1966-48

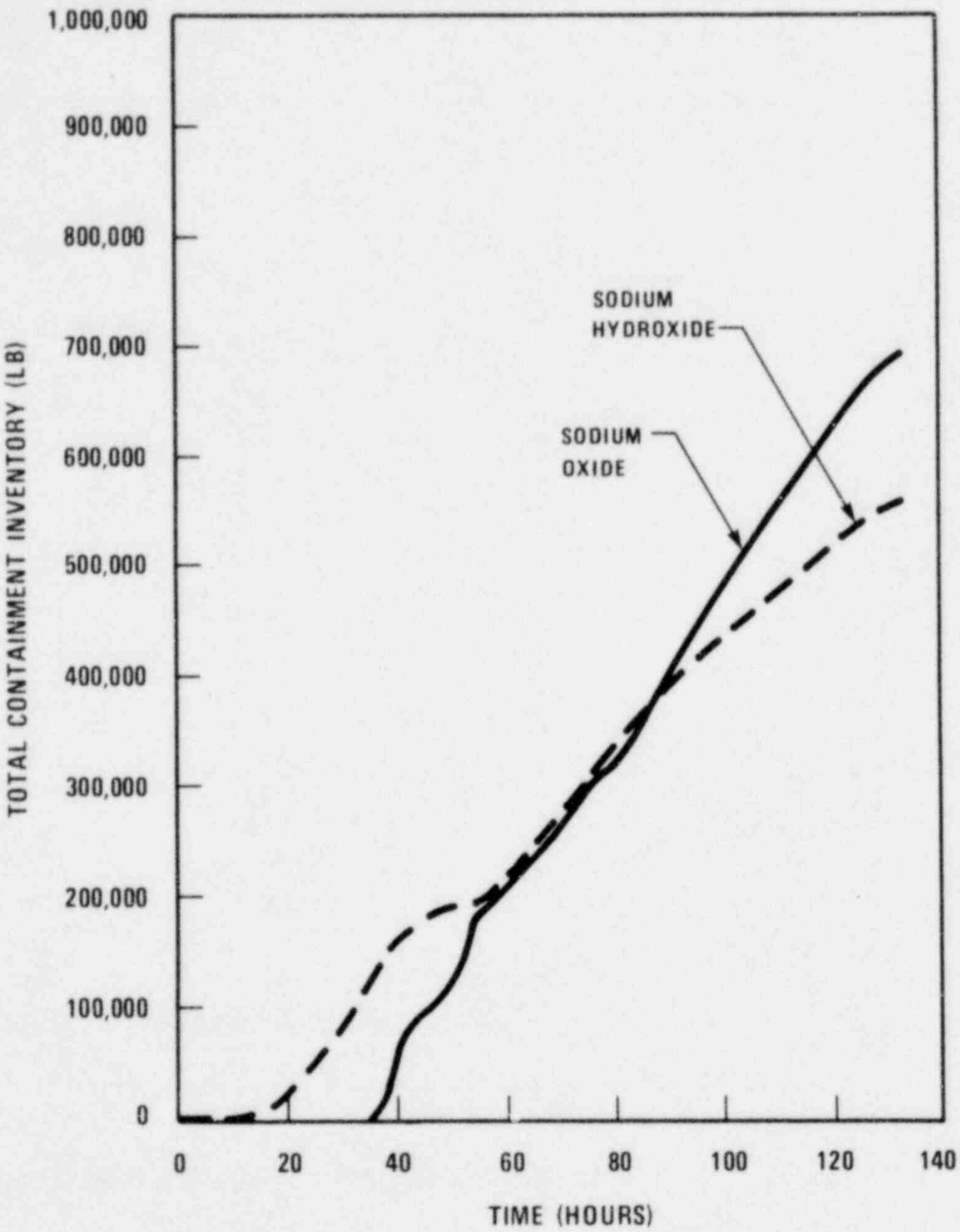

Figure 3-15. Total RCB Sodium Oxide and Sodium Hydroxide Inventory (Neglecting Aerosol Leakage)

1966-194

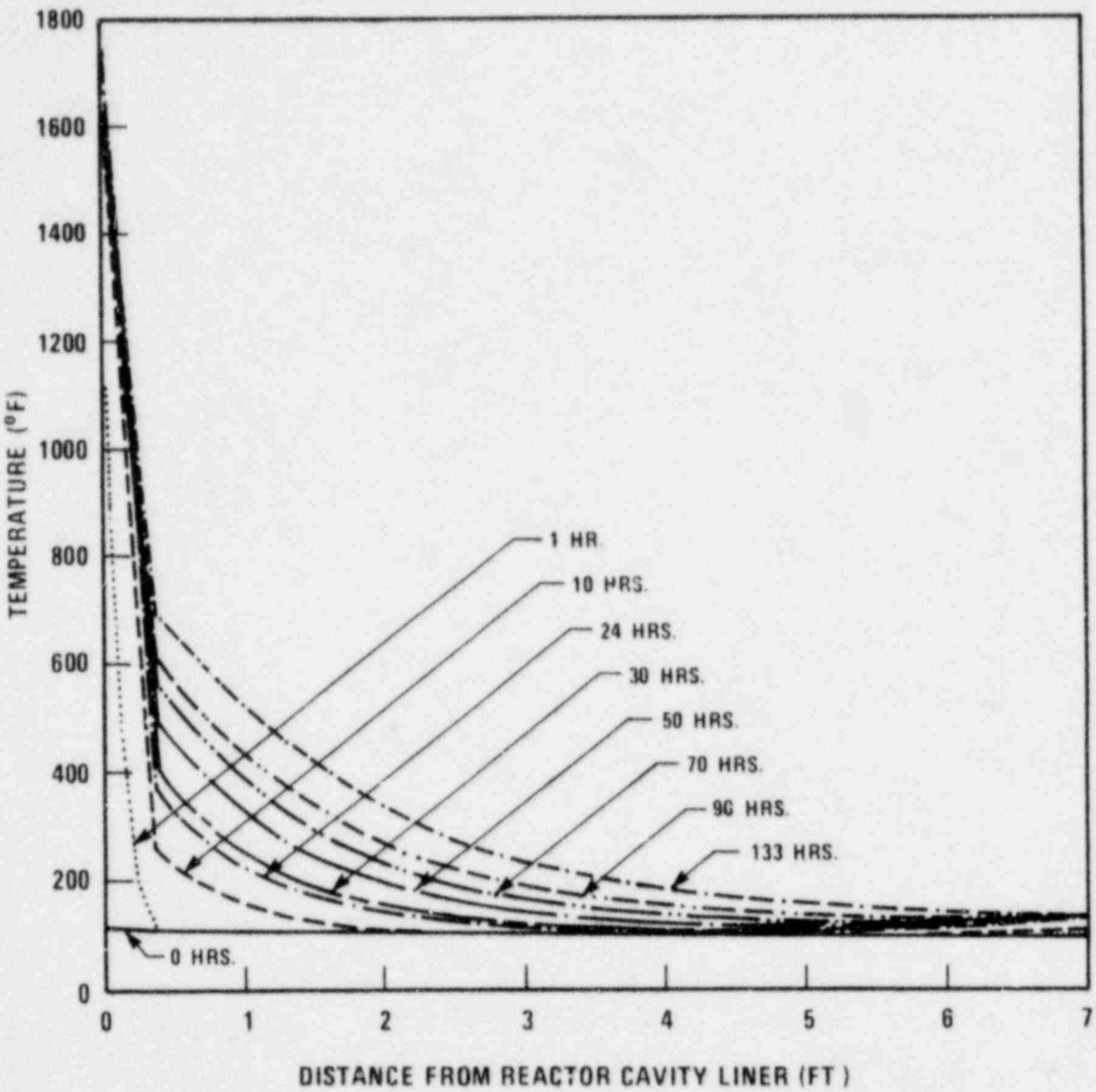

Figure 3-16. Reactor Cavity Submerged Wall Concrete Temperatures

1966-49

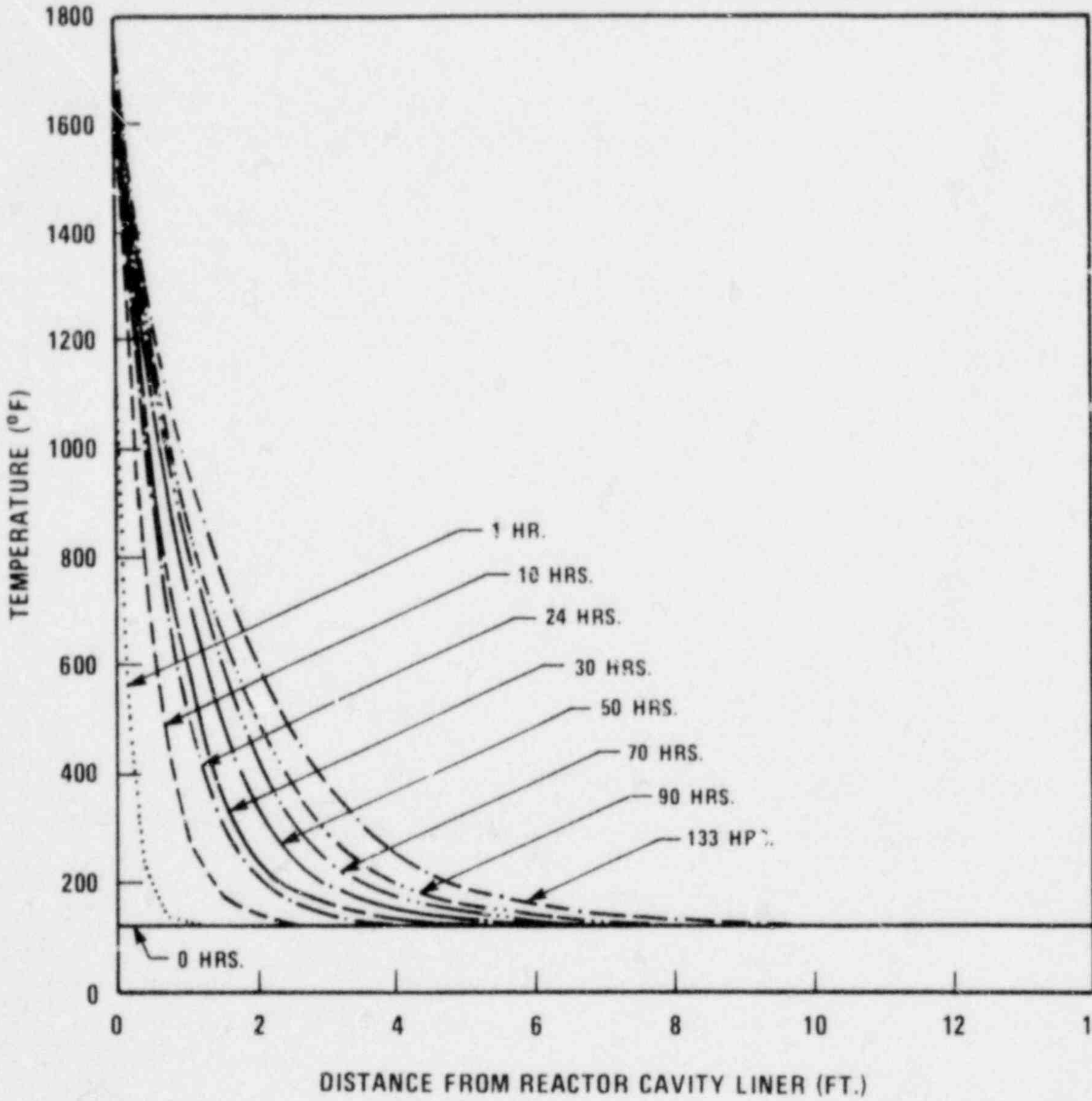

Figure 3-17. Reactor Cavity Floor Concrete Temperatures

1966-50

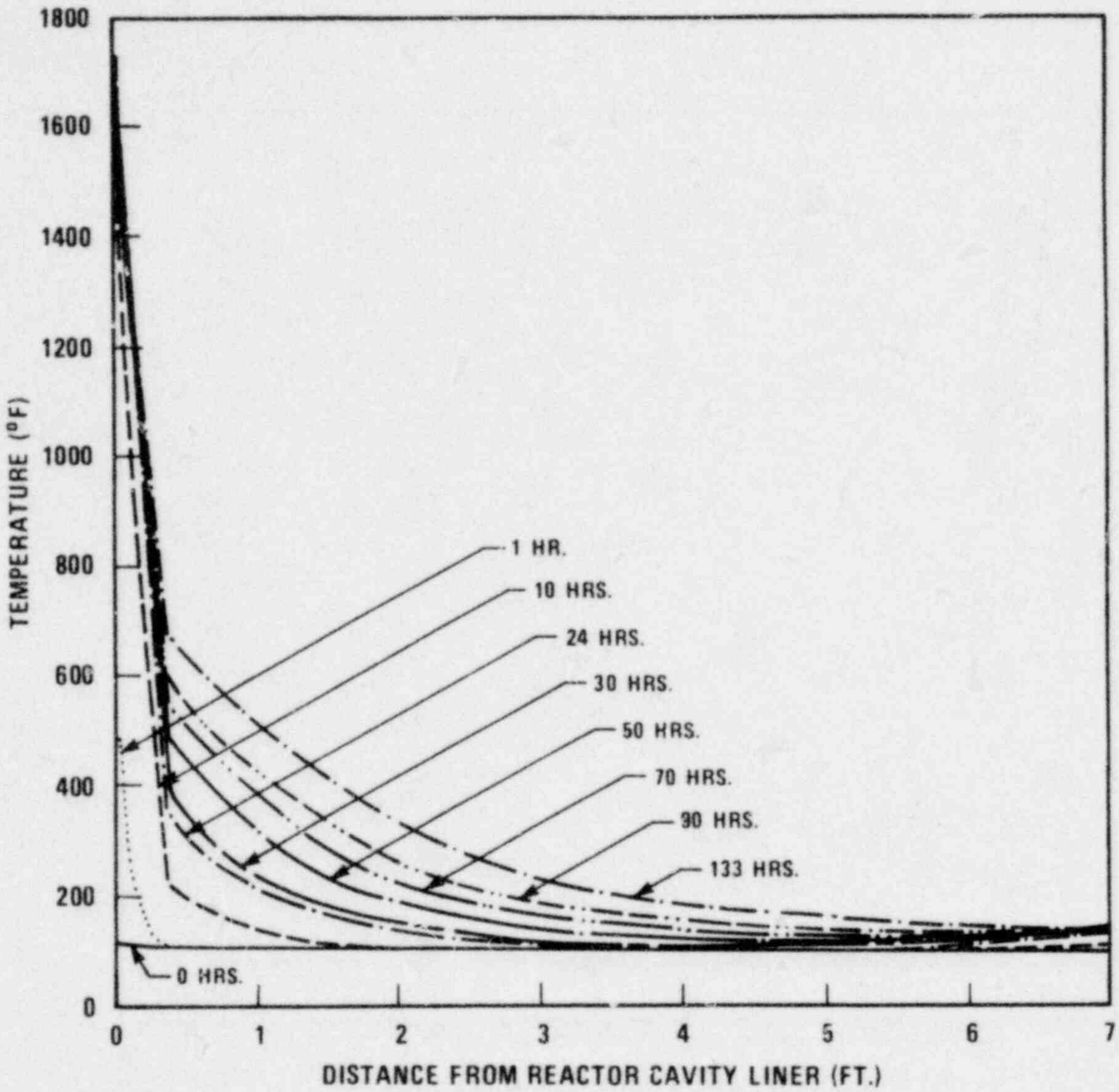

Figure 3-18. Reactor Cavity Non-Submerged Concrete Wall Temperatures

1966-51

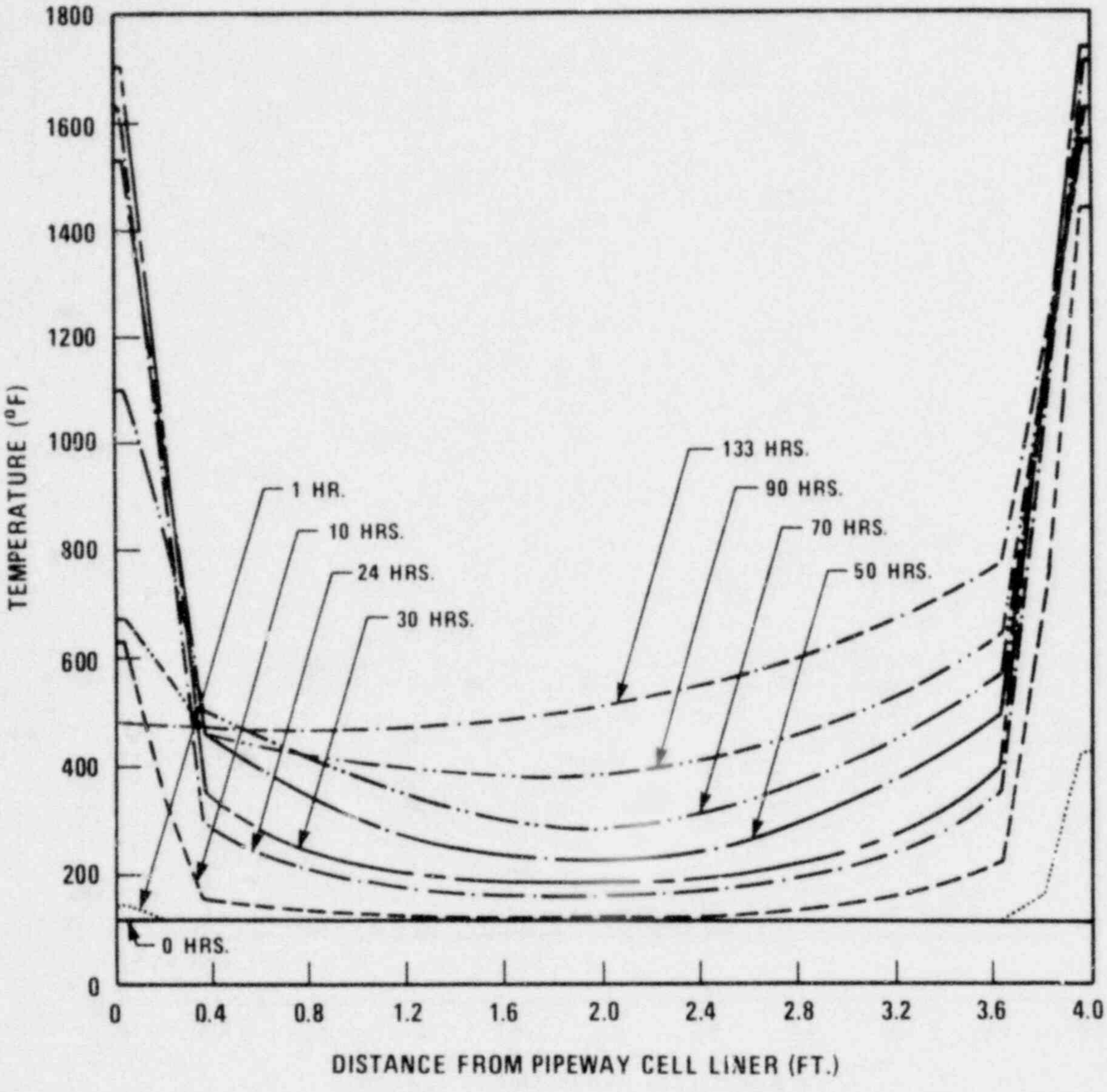

Figure 3-19. Reactor Cavity – Pipeway Wall Concrete Temperatures

1966-52

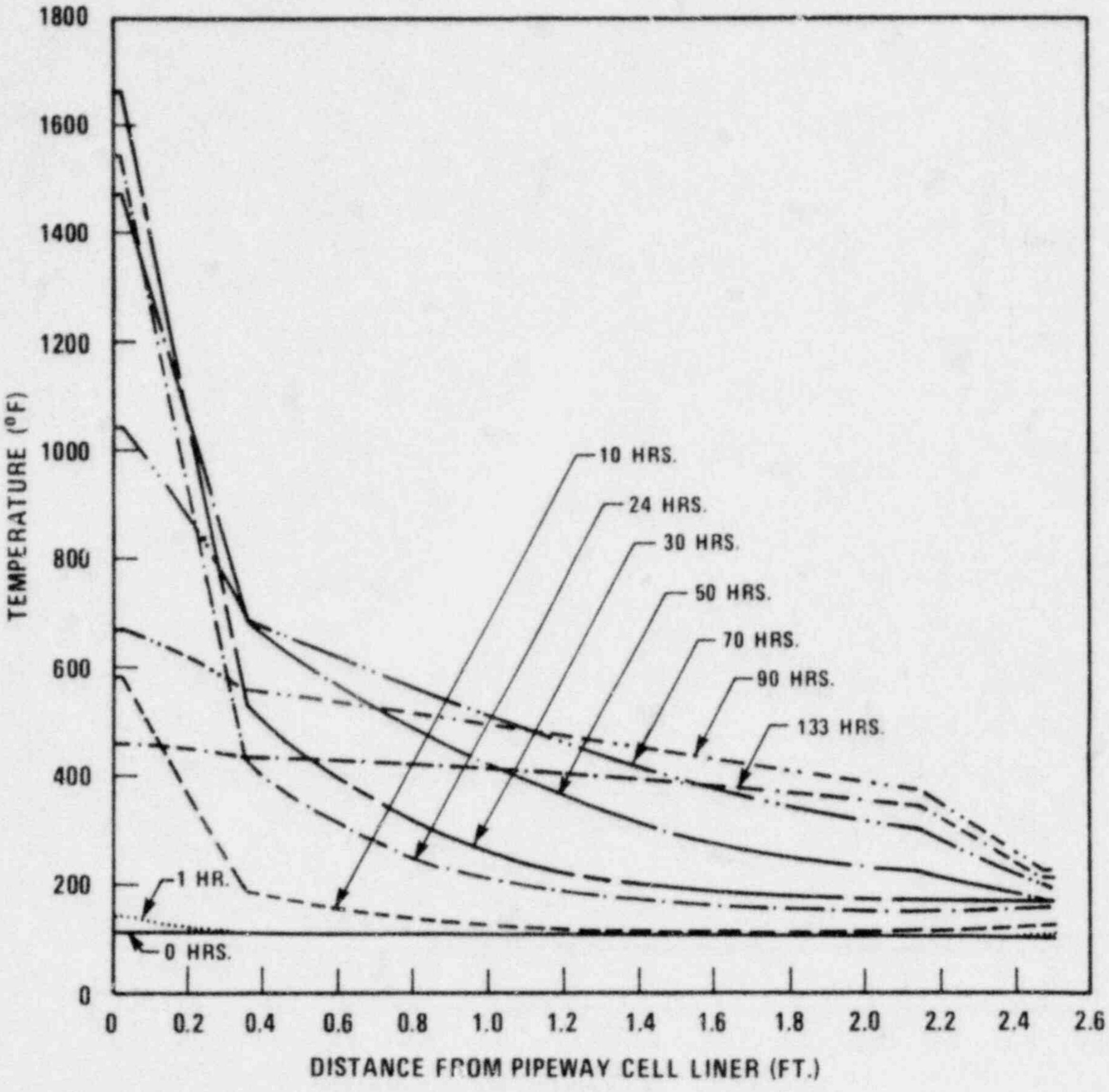

Figure 3-20. Pipeway Cell Wall Structural Temperatures
(2.5 Ft. Thick Wall)

1966-53

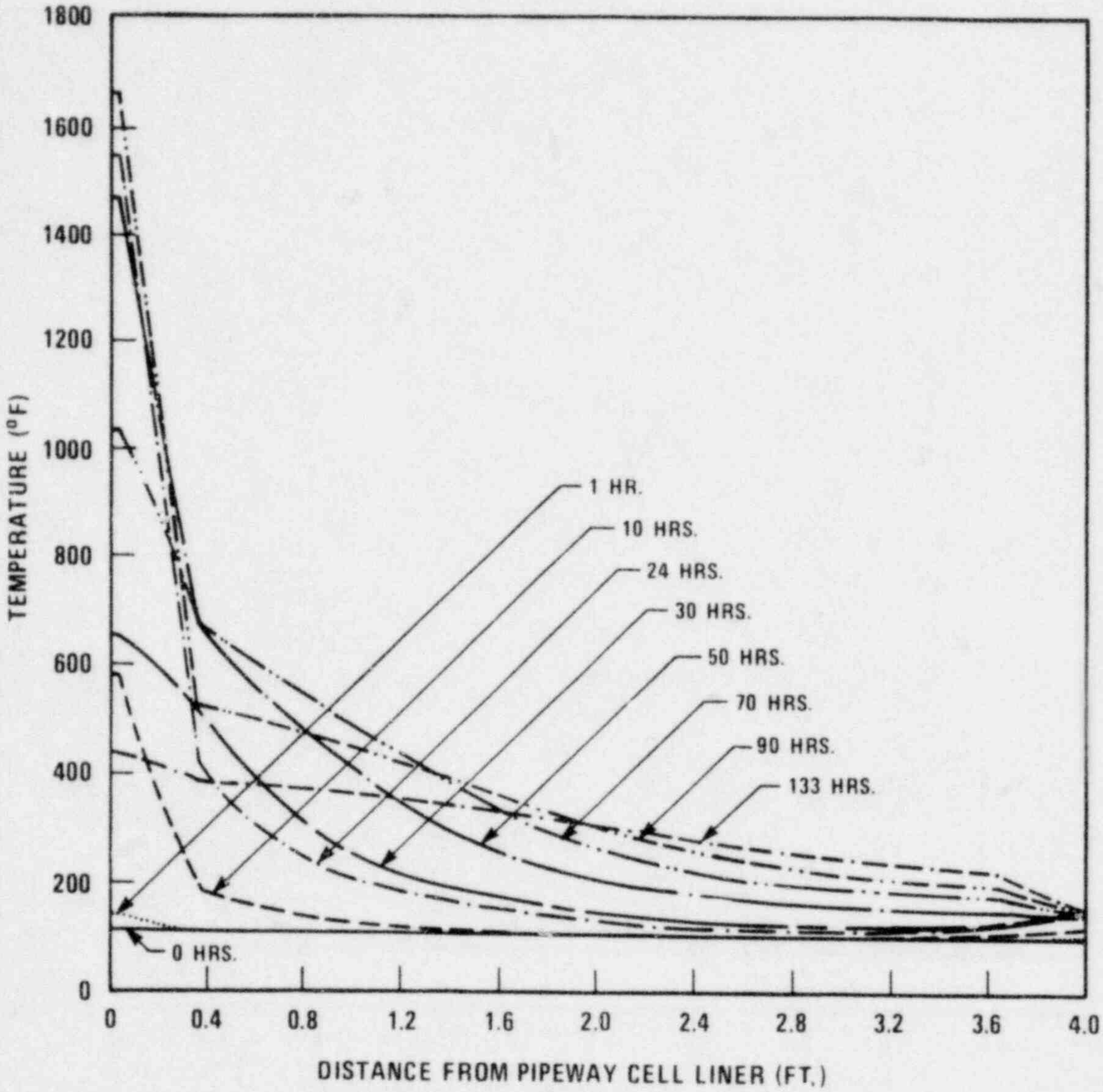

Figure 3-21. Pipeway Cell Wall Structural Temperatures (4.0 Ft. Thick Wall)

1966-54

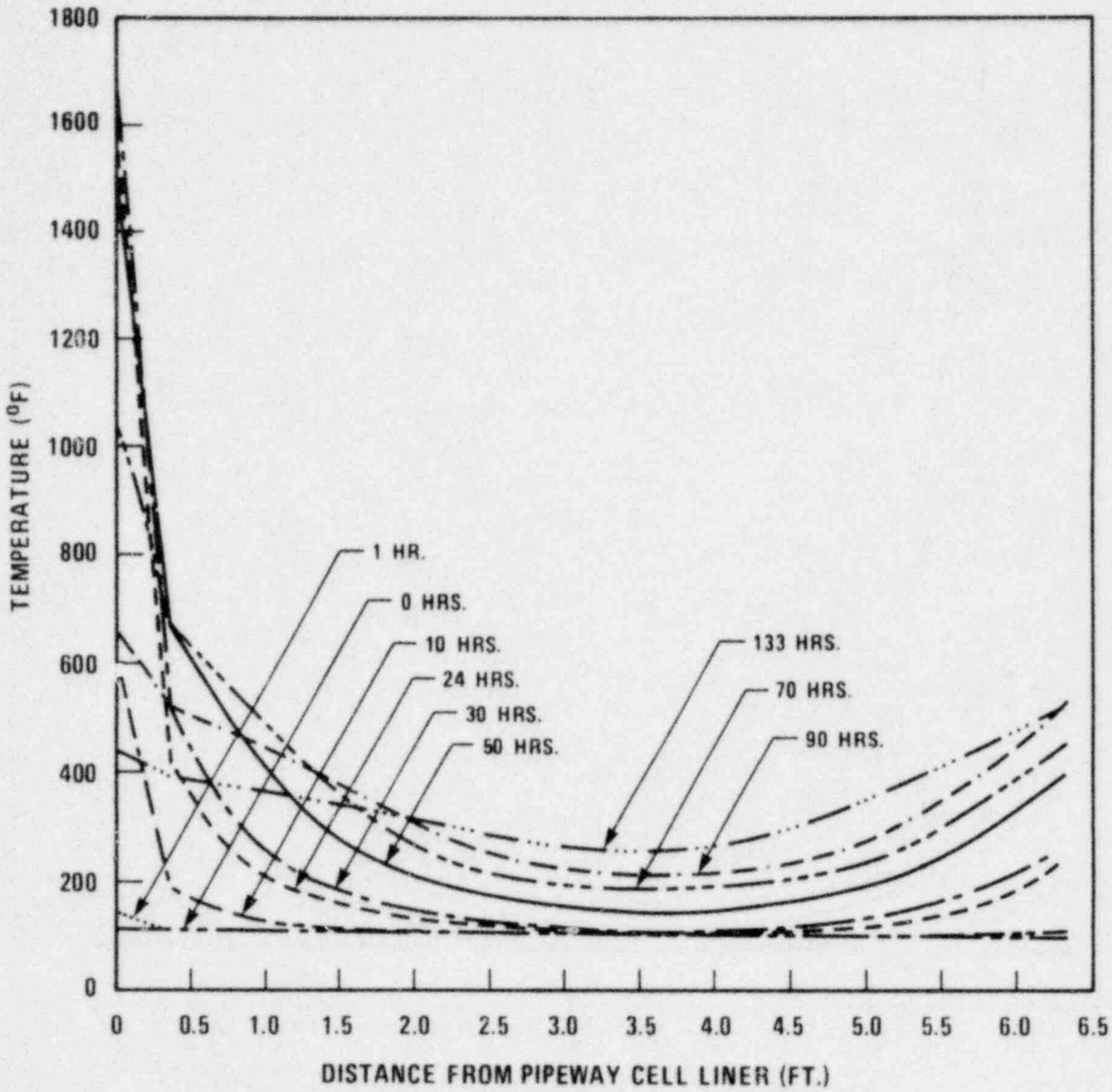

Figure 3-22. Pipeway Cell Roof and Head Access Area Wall Structu. al Temperatures

1966-55

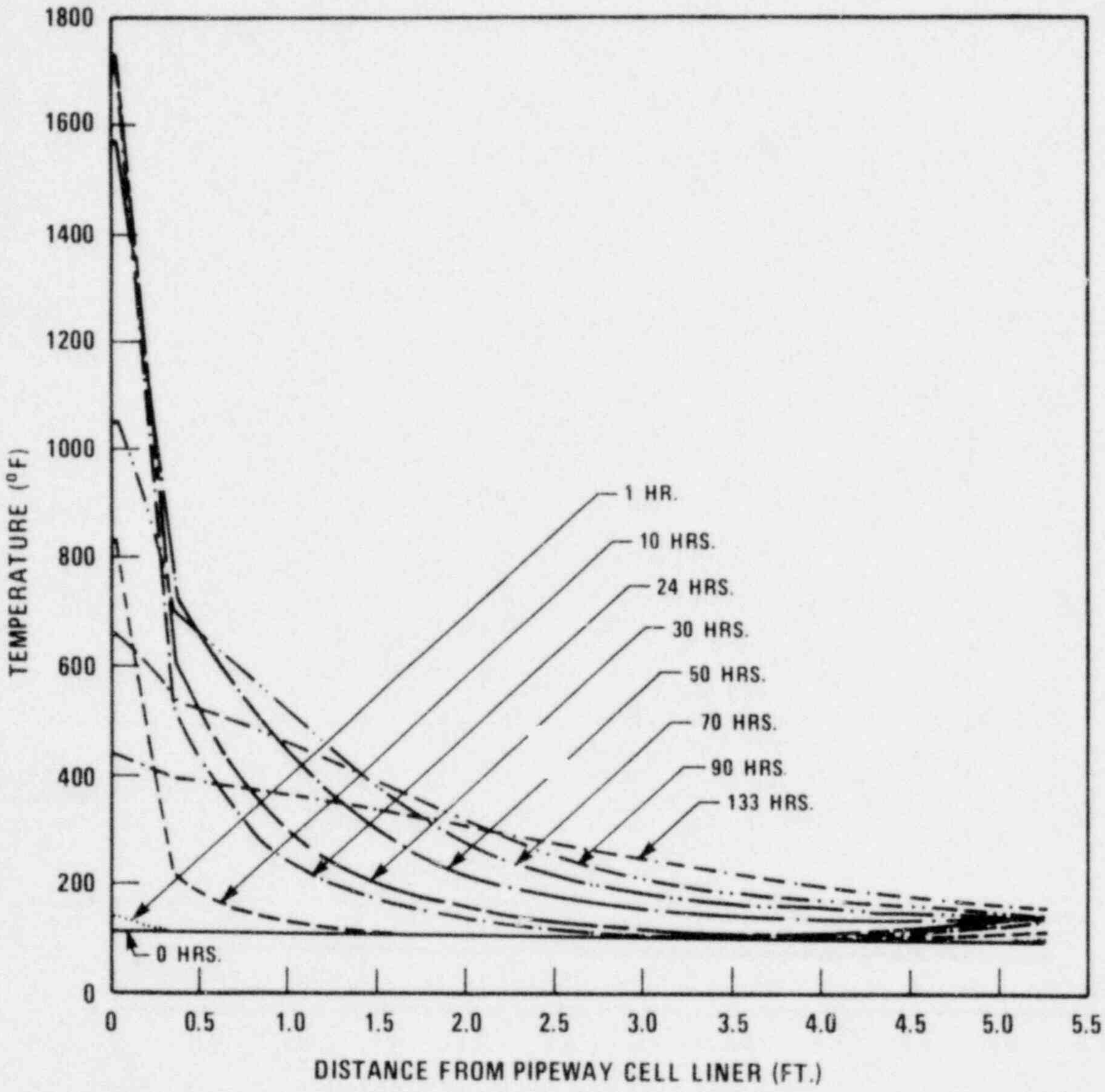

Figure 3-23. Pipeway Floor Concrete Temperatures

1966-56

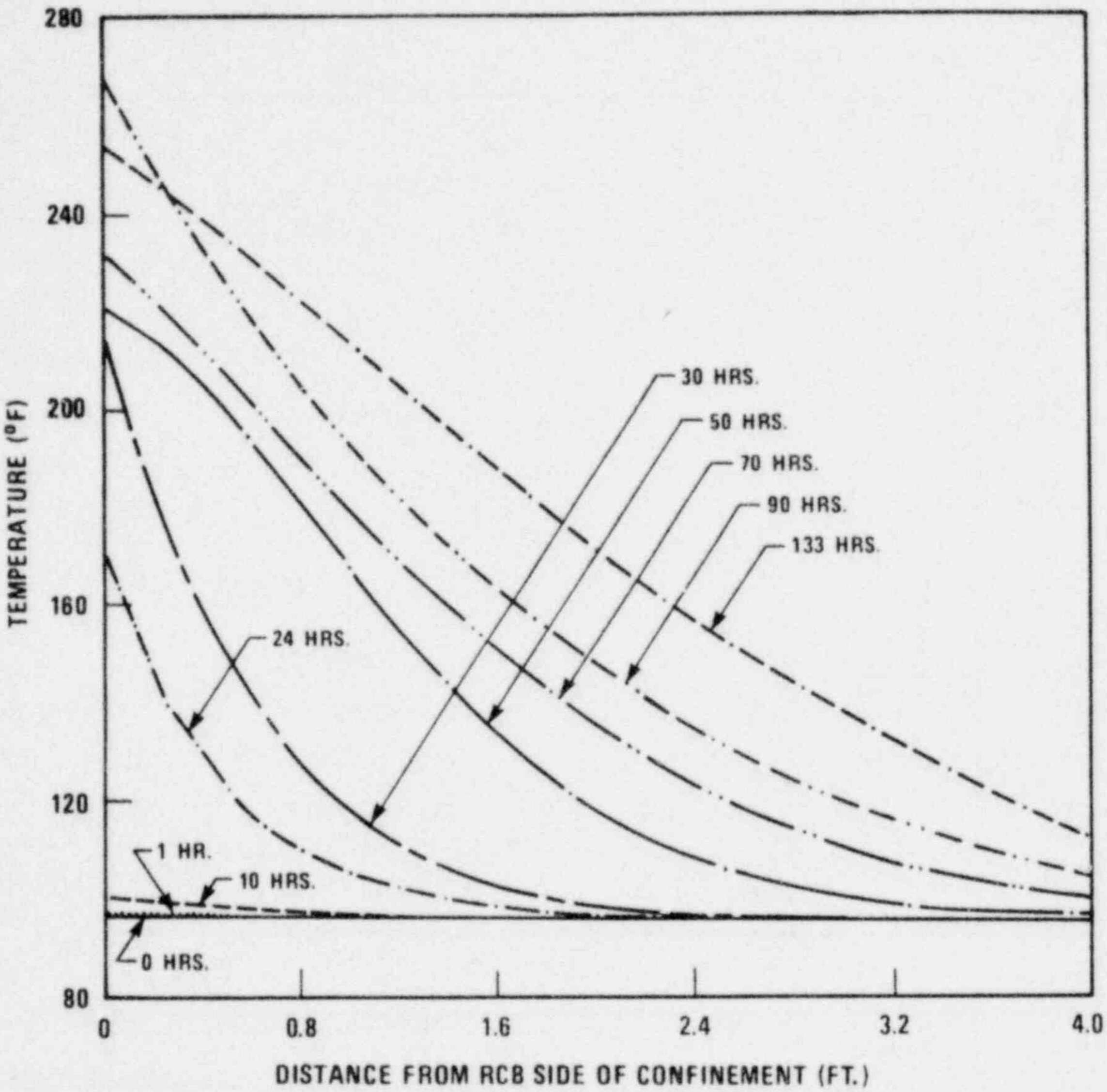

Figure 3-24. Confinement Building Concrete Dome Temperatures

1966-57

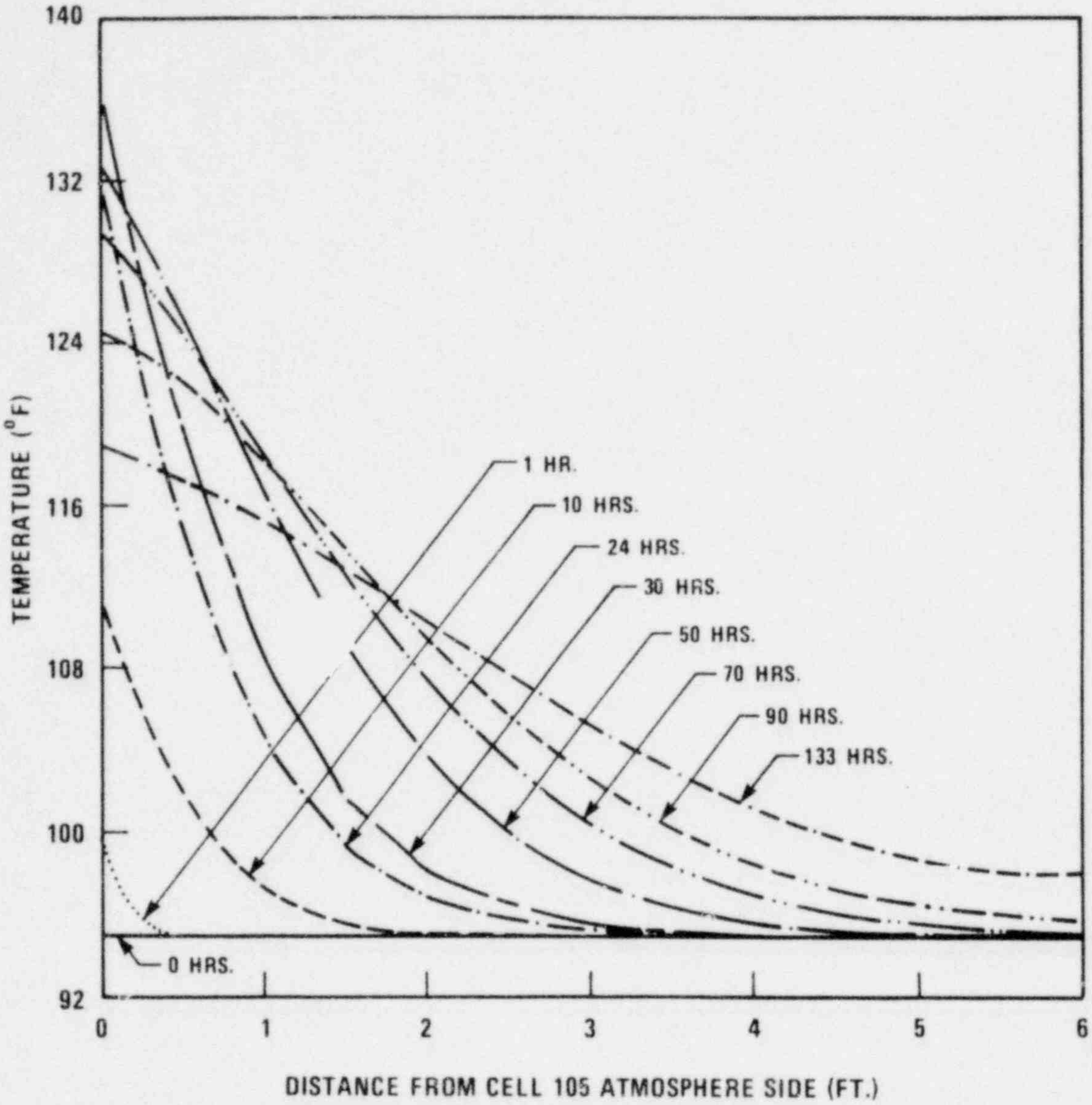

Figure 3-25. Cell 105 Floor and Wall Concrete Temperatures

1966-58

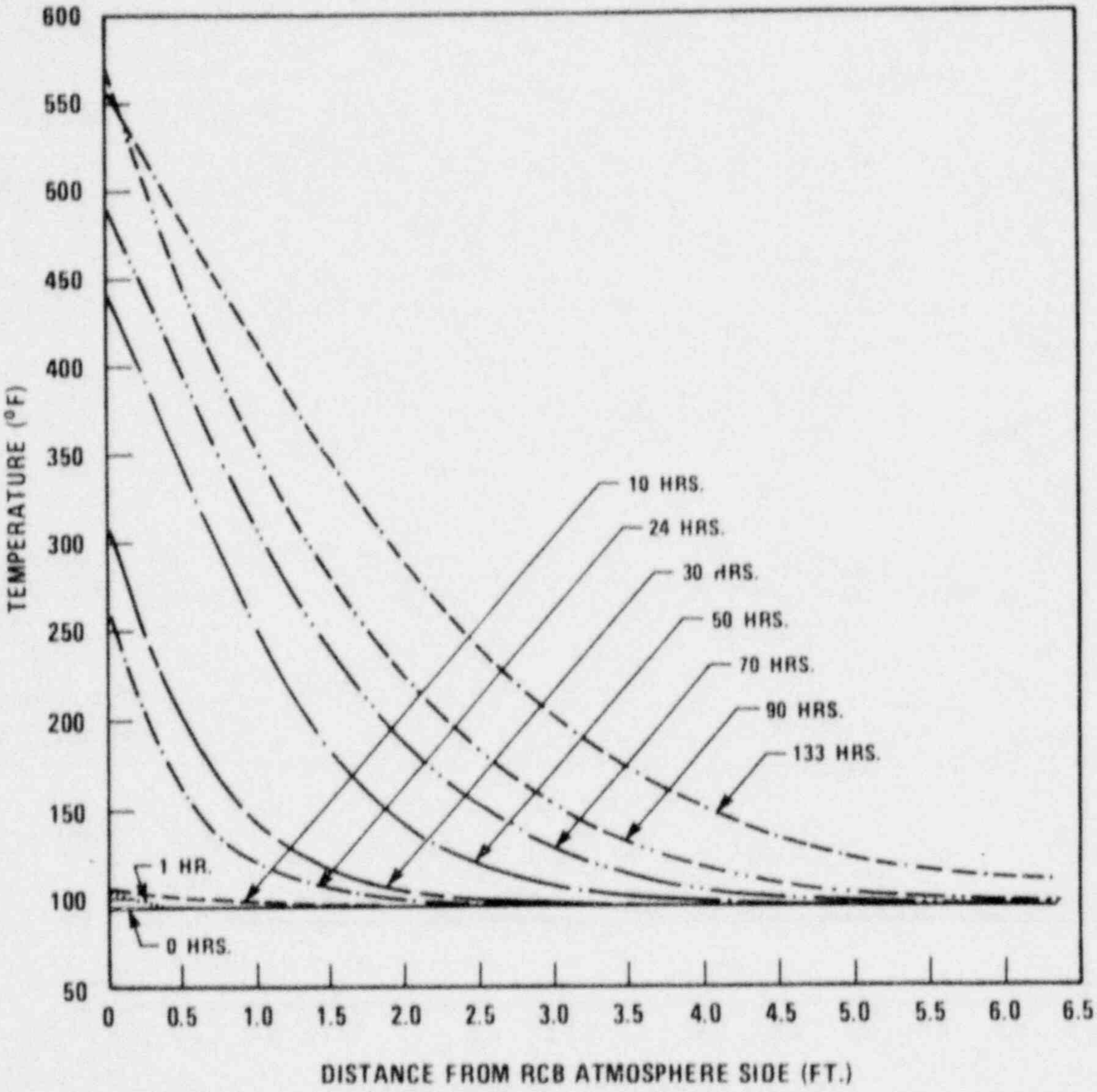

Figure 3-26. Containment Building Floor Concrete Temperatures

1966-59

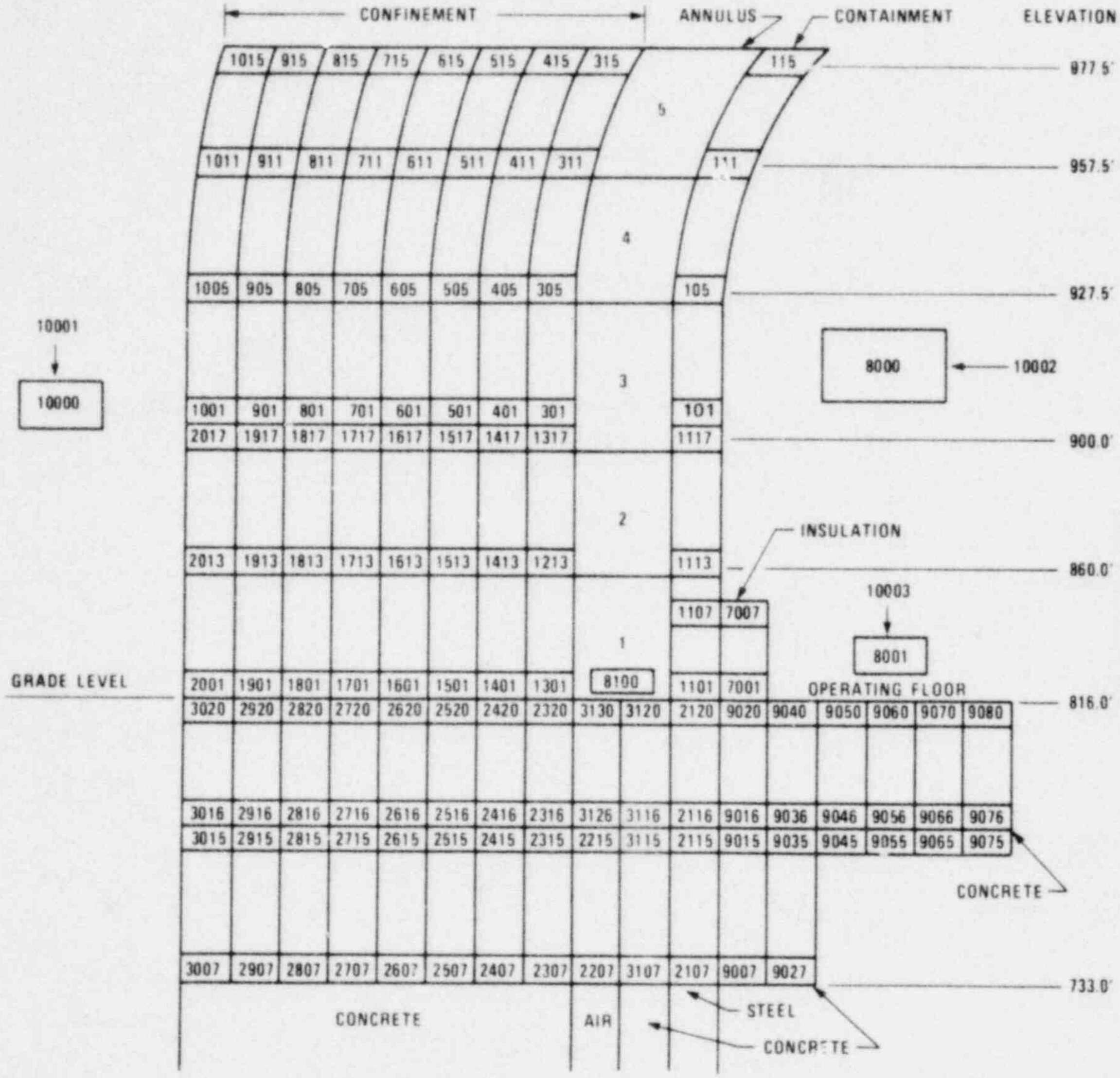

NOTES
(1) NODES 1 THRU 5 REPRESENT AIR FLOW.
(2) NODE 8100 IS SOURCE NODE FOR AIR FLOW.
(3) NODE 8000 IS SOURCE NODE FOR HEAT LOAD TO STEEL CONTAINMENT.
(4) NODE 8001 IS SOURCE NODE FOR HEAT LOAD TO CONCRETE OPERATING FLOOR.
(5) NODE 10000 IS AMBIENT AIR.
(6) NODES 10001, 10002 AND 10003 ARE BOUNDARY NODES.

Figure 3-27. Annulus Cooling System Thermal Model

1966-60

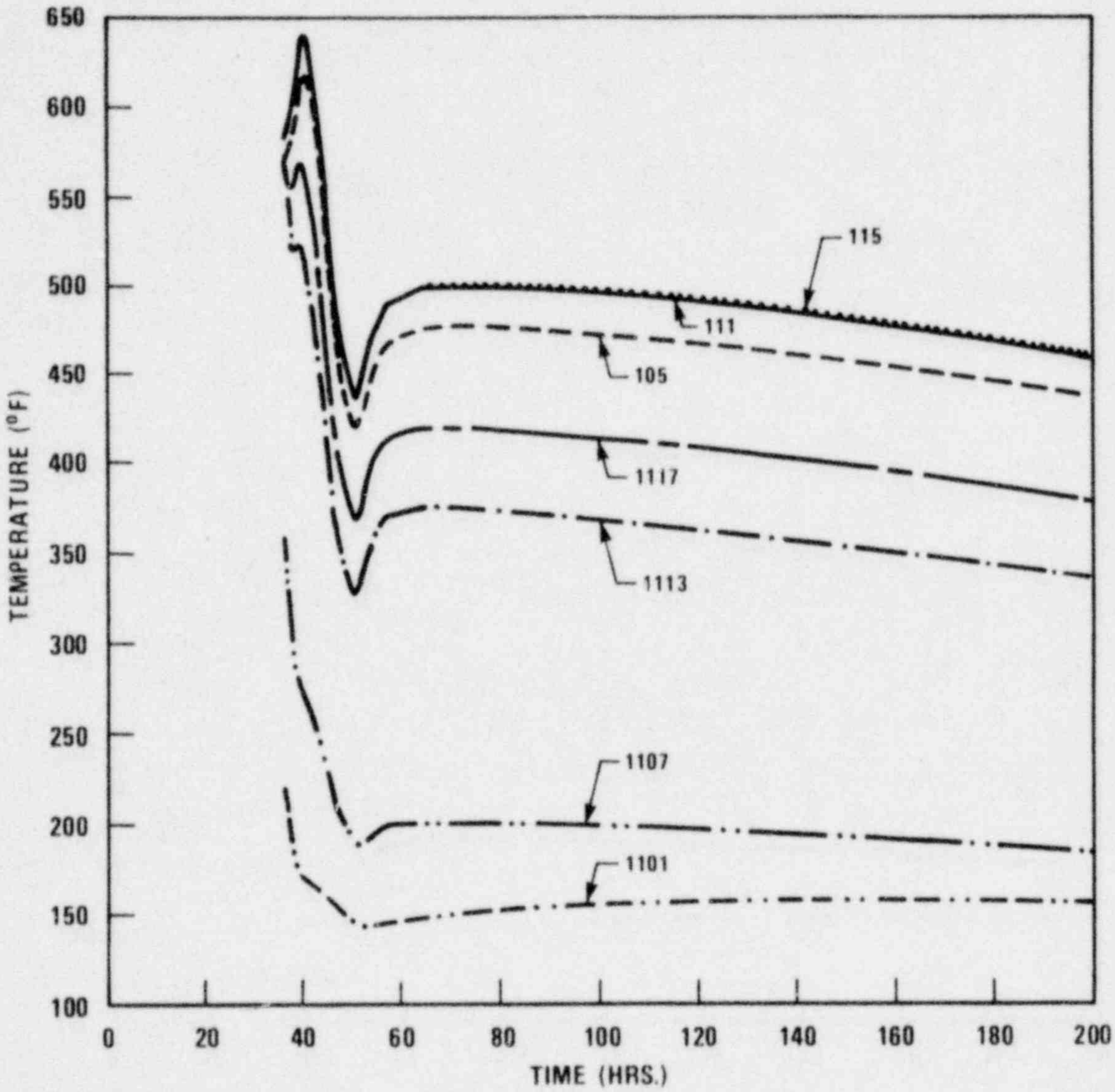

Figure 3-28. Steel Containment Temperatures for Selected Nodes (See Figure 3-27)

1966-61

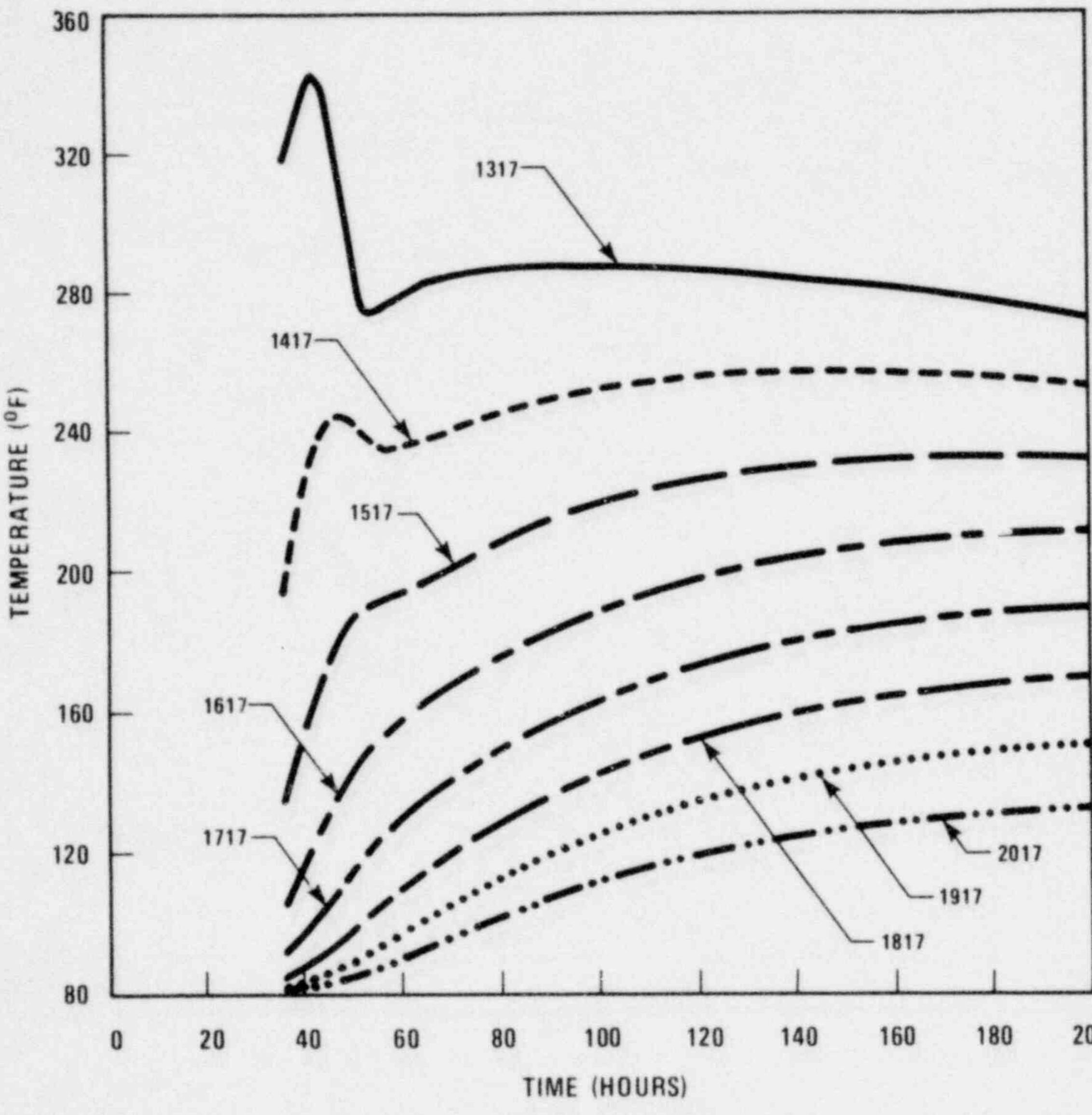

Figure 3-29. Concrete Confinement Temperatures for Nodes 1317-2017 (See Figure 3-27)

1966-62

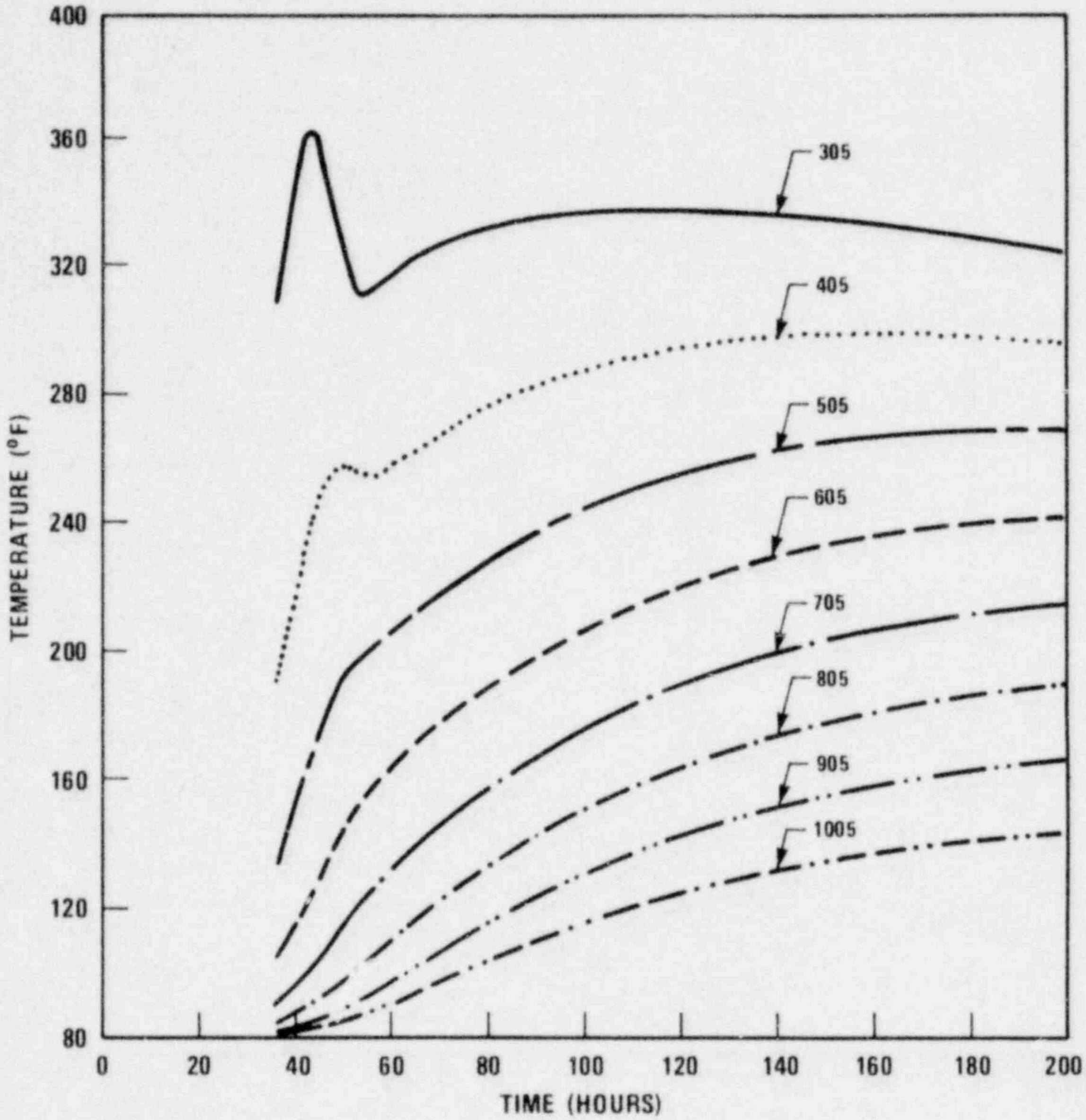

Figure 3-30. Concrete Confinement Temperatures for Nodes 305-1005
(See Figure 3-27)

1966-63

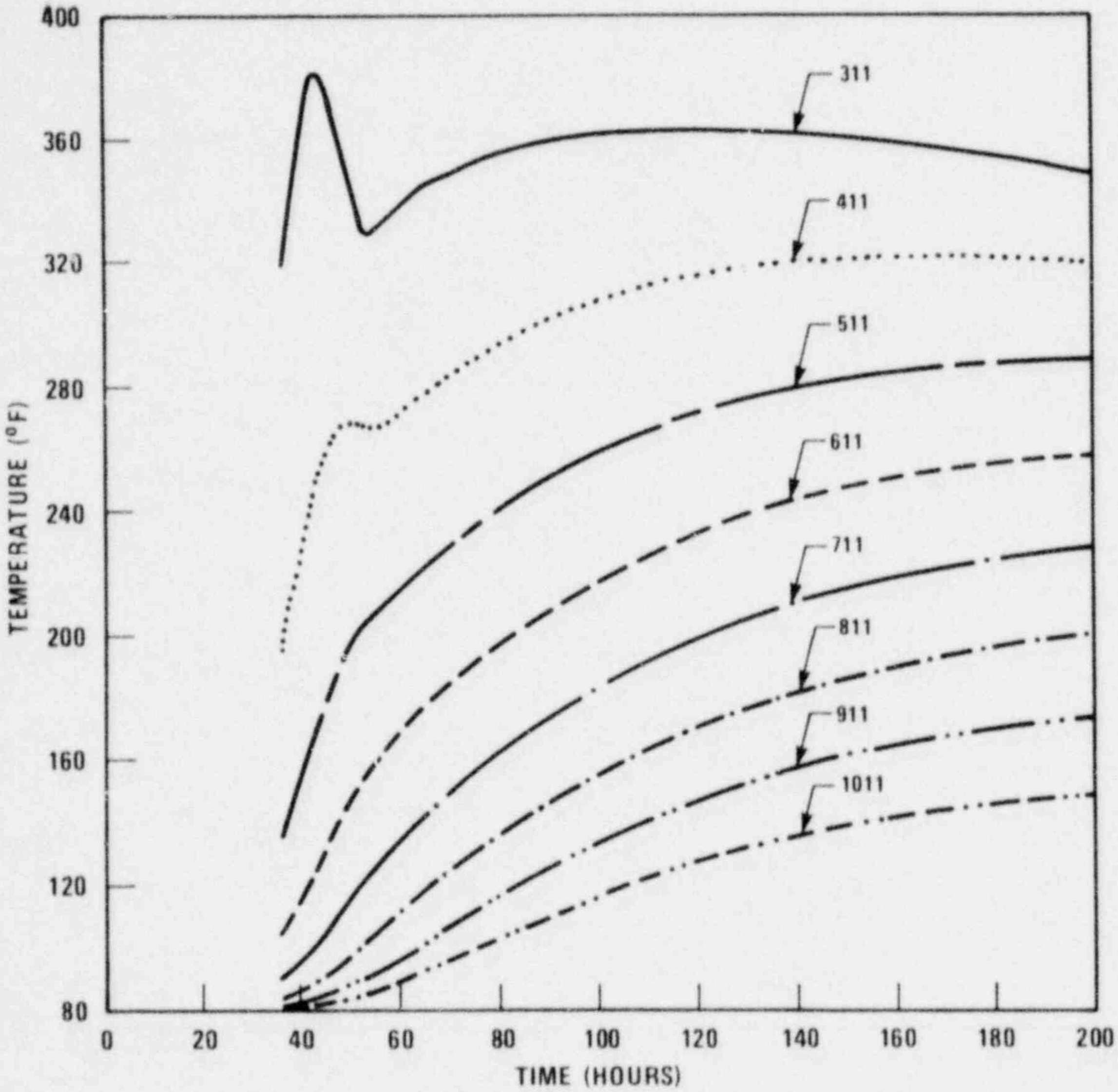

Figure 3-31. Concrete Confinement Temperatures for Nodes 311-1011 (See Figure 3-27)

1966-64

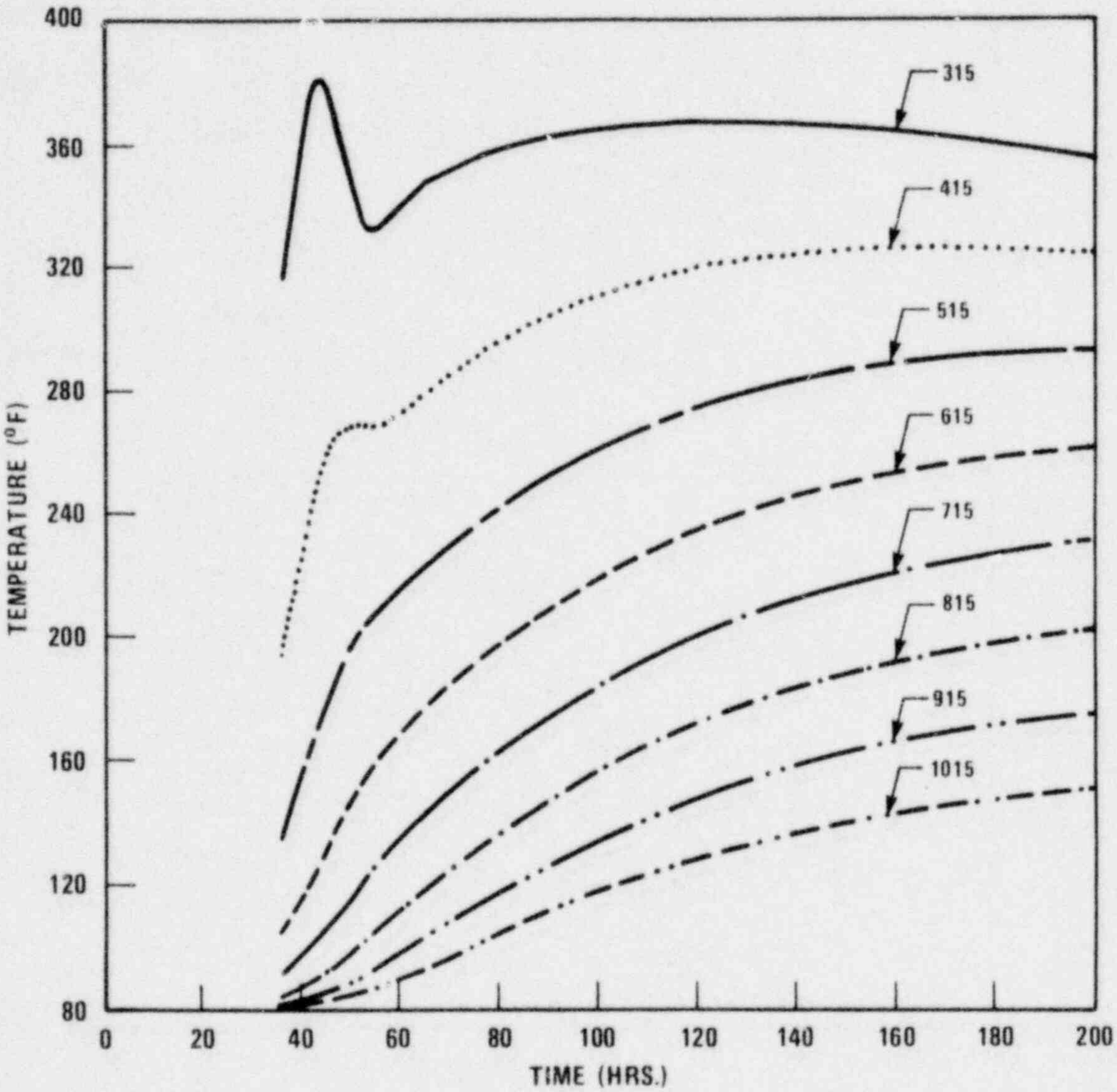

Figure 3-32. Concrete Confinement Temperatures for Nodes 315-1015
(See Figure 3-27)

1966-65

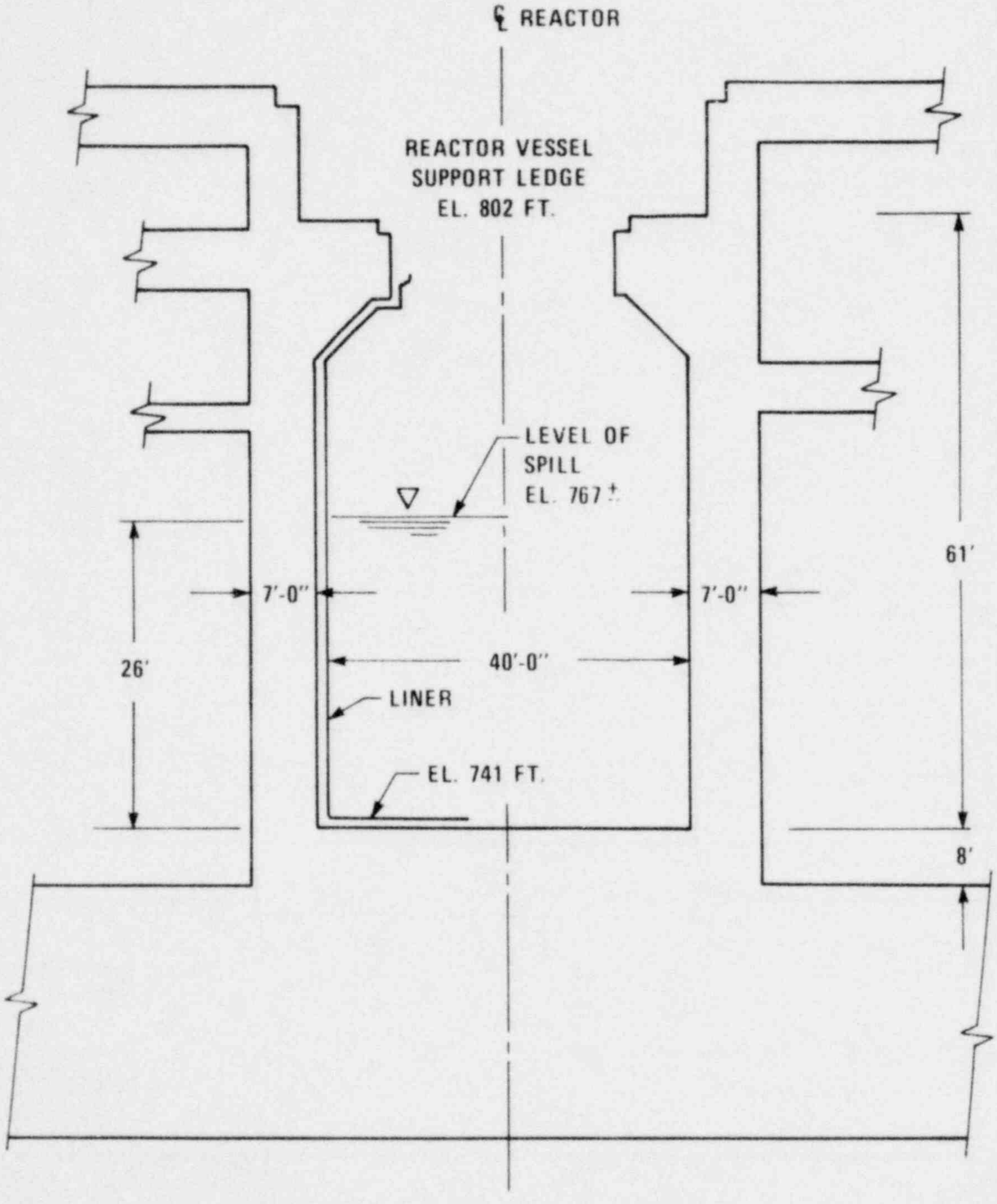

Figure 3-33. Reactor Cavity

1966-66

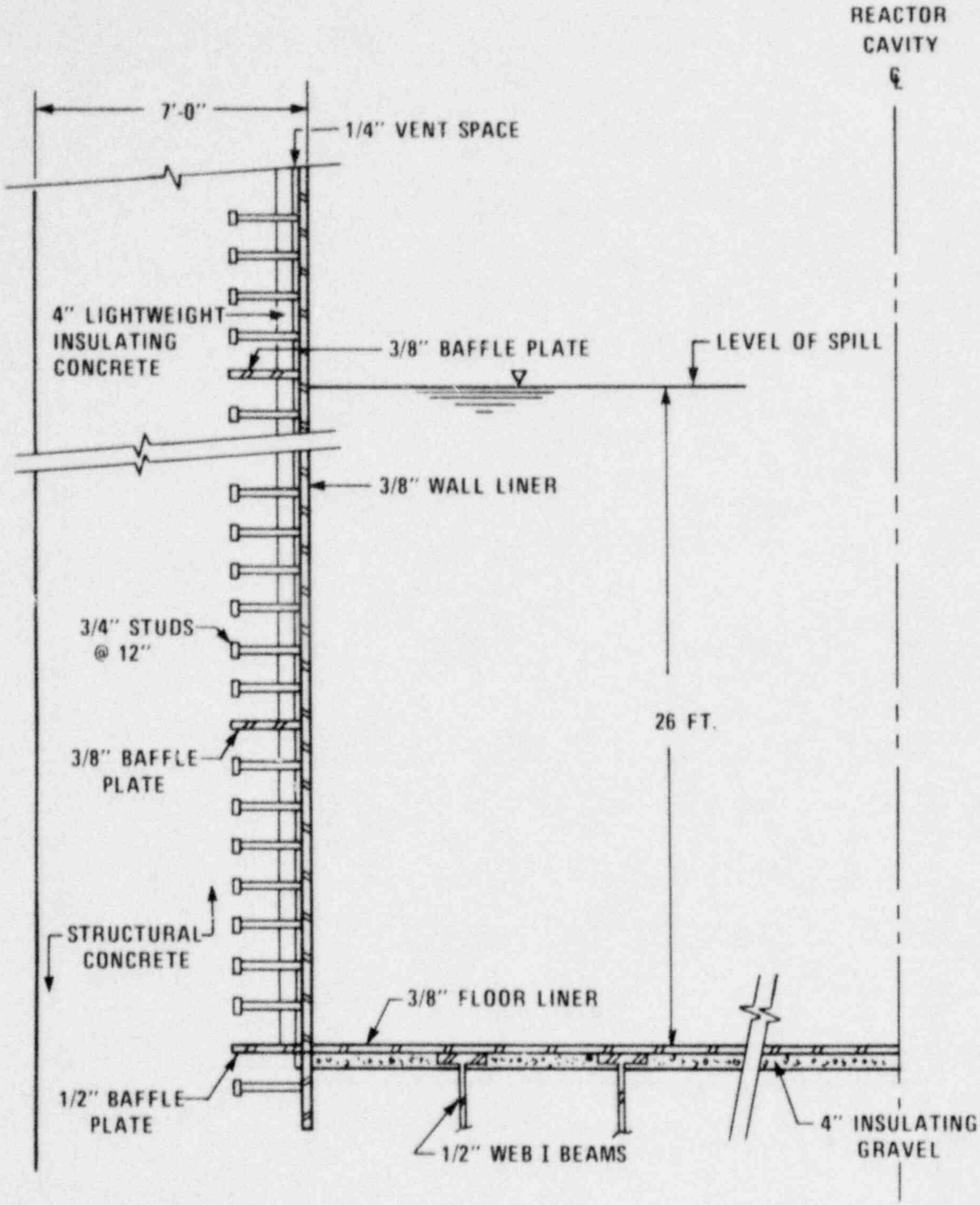

Figure 3-34 Reactor Cavity Details

1966-67

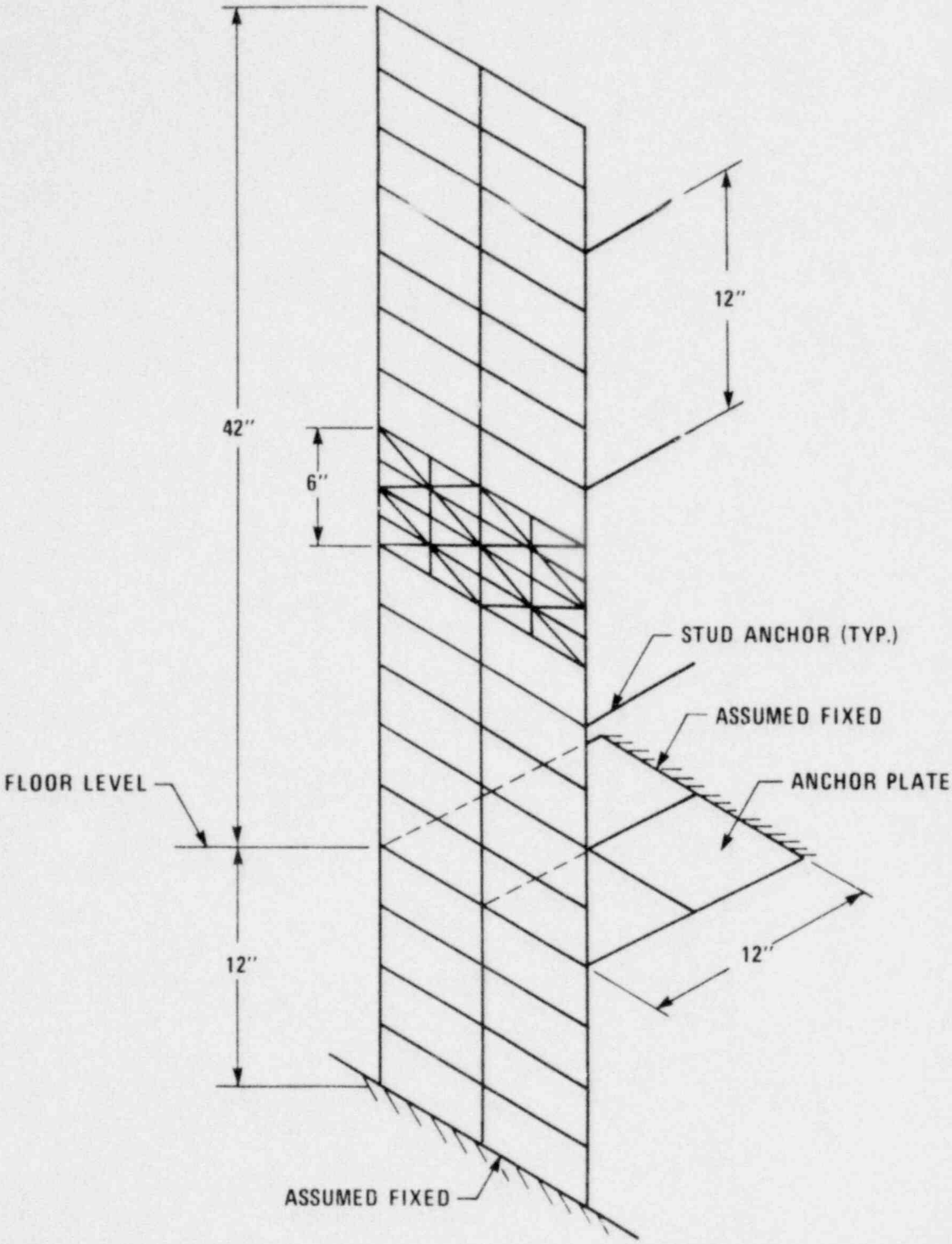

Figure 3-35. Finite Element Model for Lower Portion of Submerged Liner

1966-68

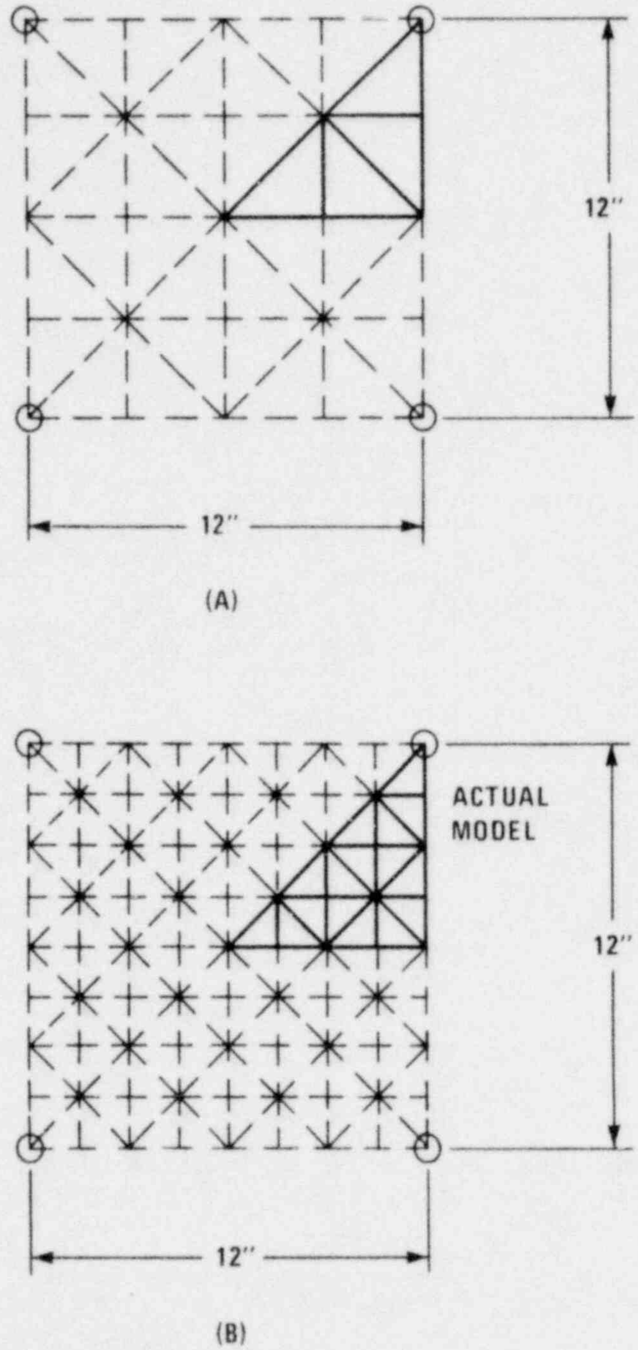

Figure 3-36. Finite Element Models for Upper Portion of Reactor Cavity Liner

1966-69

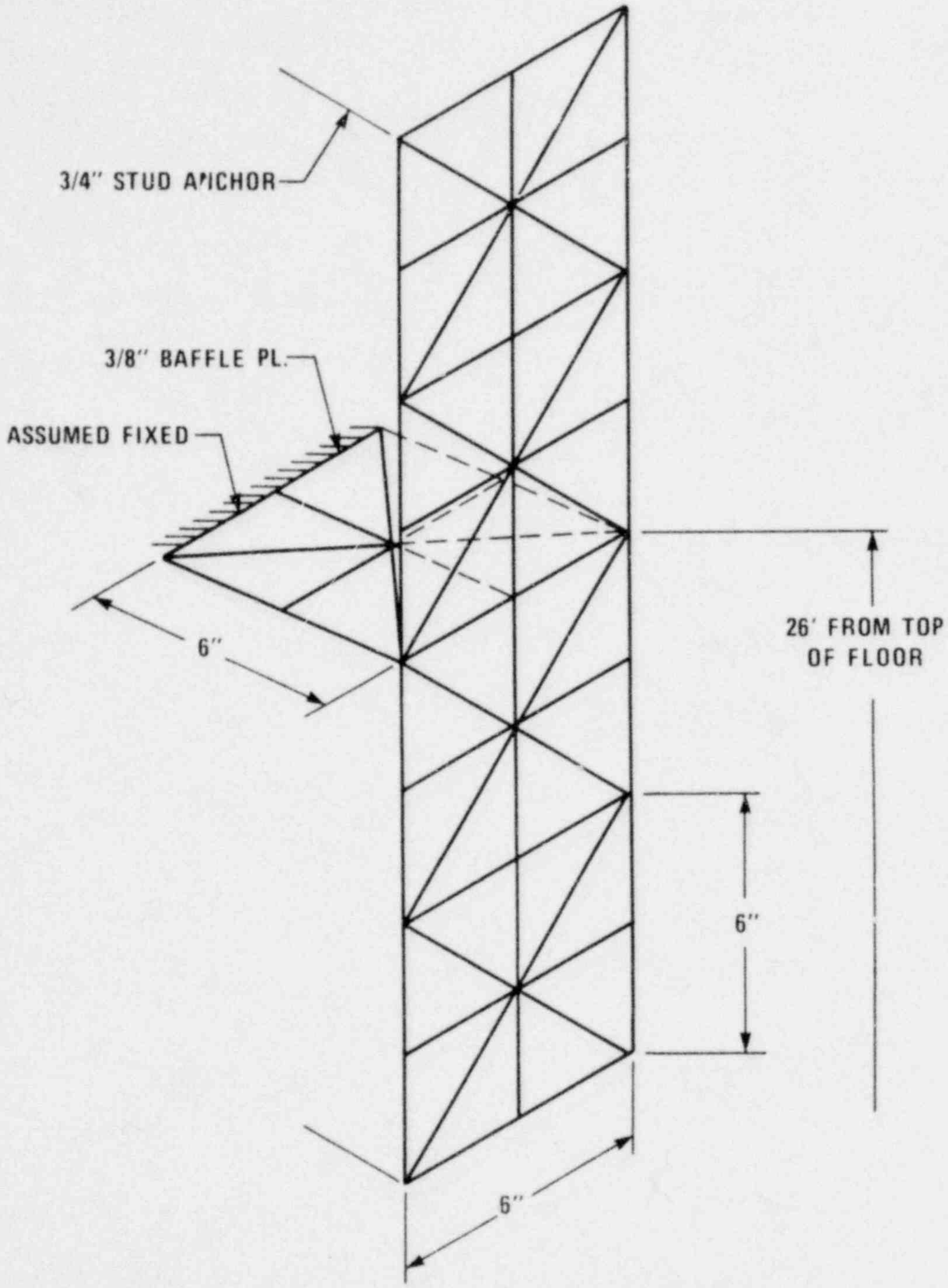

Figure 3-37. Finite Element Model for Liner Above Sodium Pool at Baffle Plate

1966-70

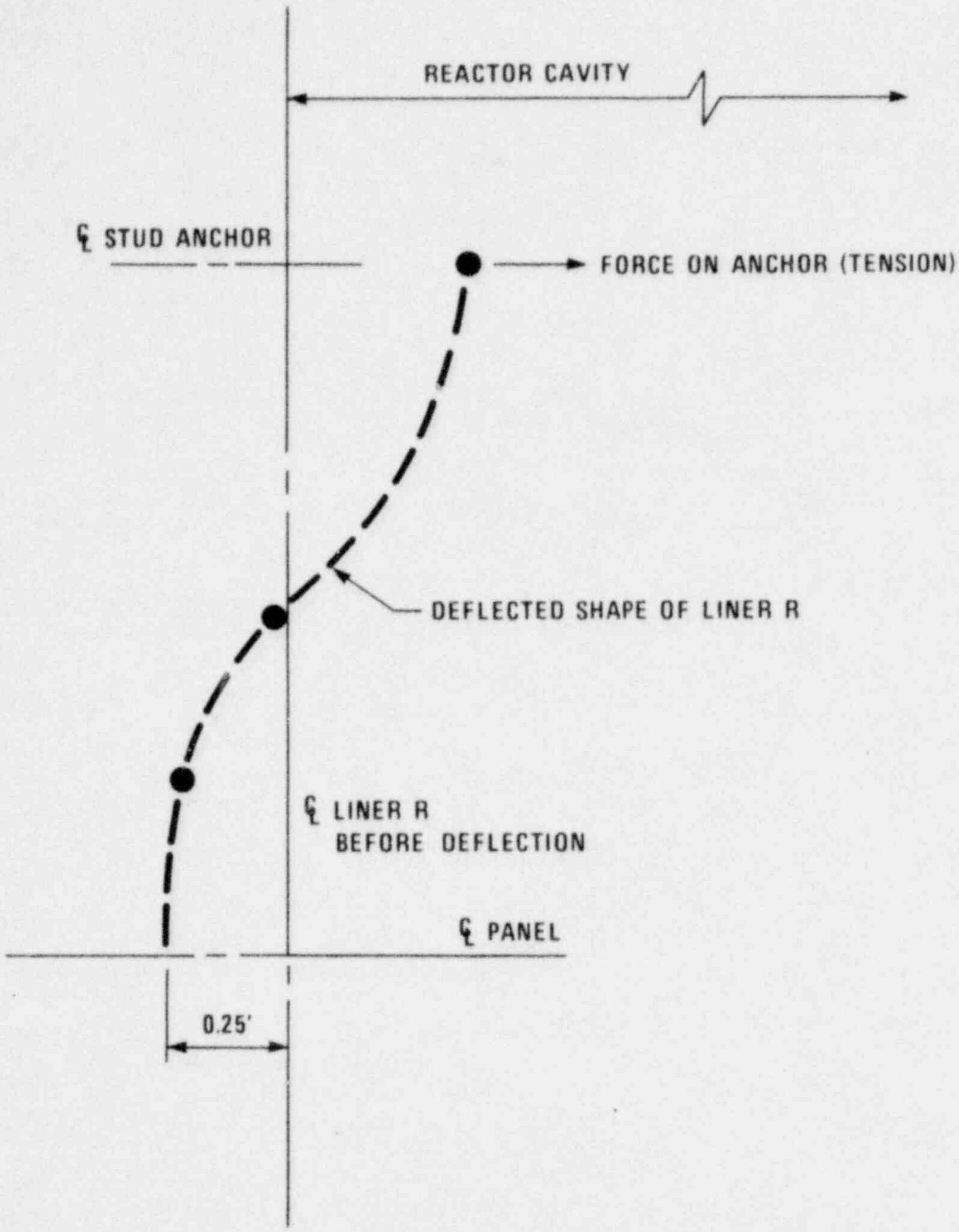

Figure 3-38. Deflection Curve of Liner Plate Along Panel Diagonal at T = 1350°F

1966-71

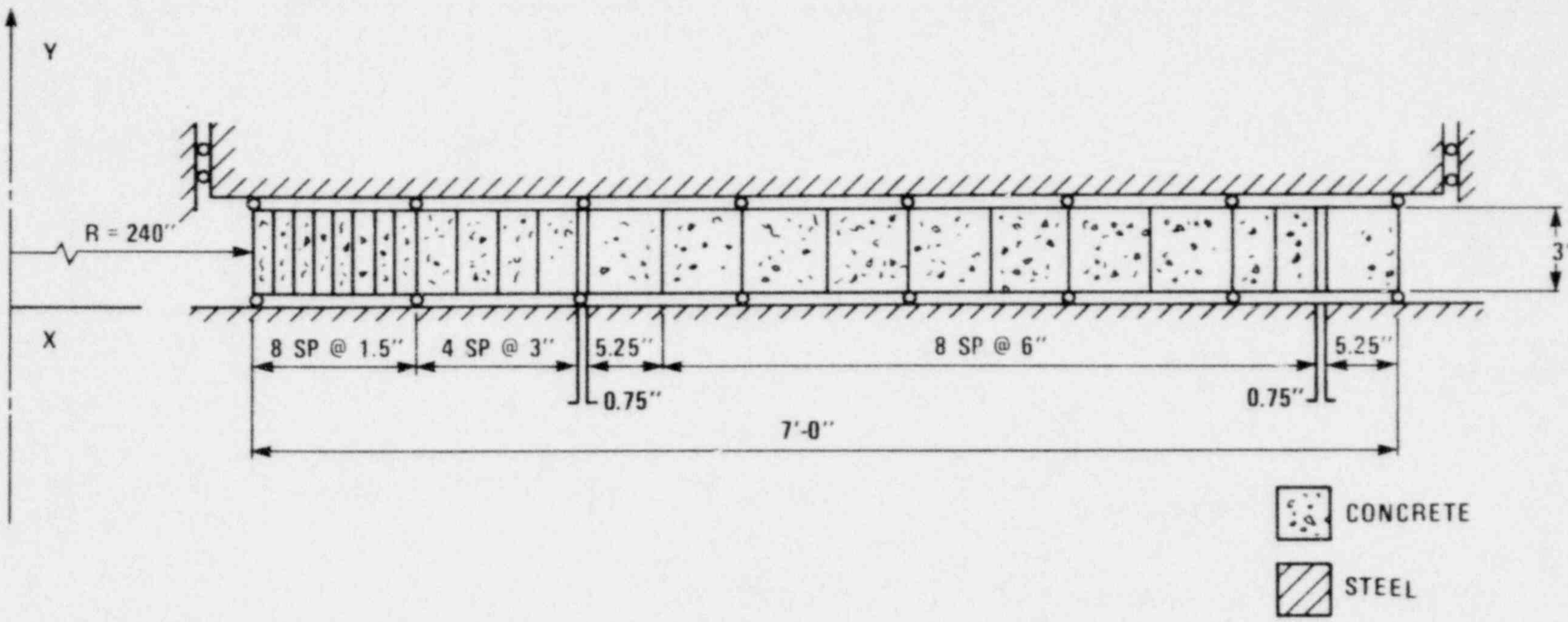

Figure 3-39. Reactor Cavity Wall – Finite Element Model for Long Cylinder Analysis

1966-72

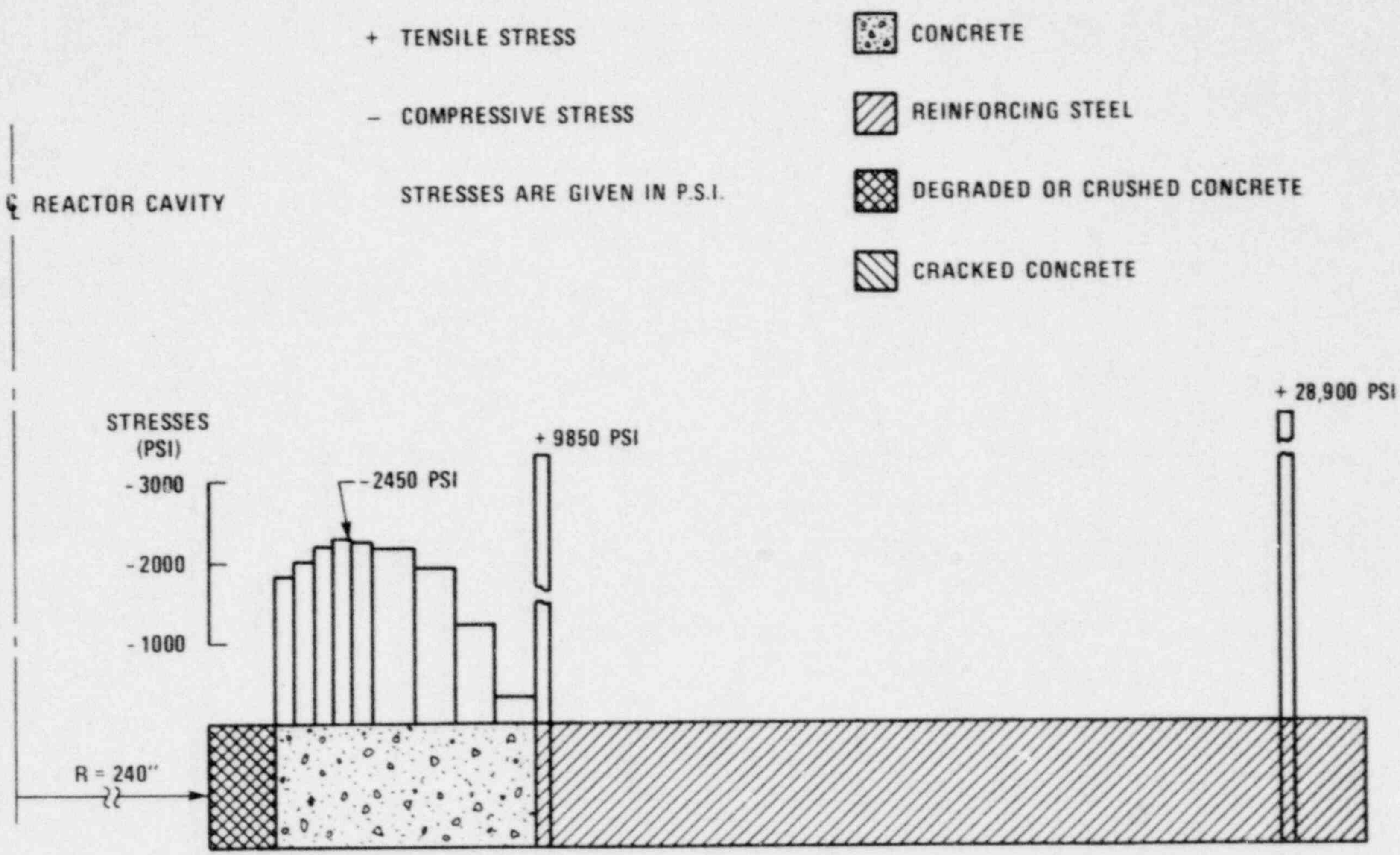

Figure 3-40. Results of Long Cylinder Analysis – Longitudinal Stresses at 132 Hours (Boildry)

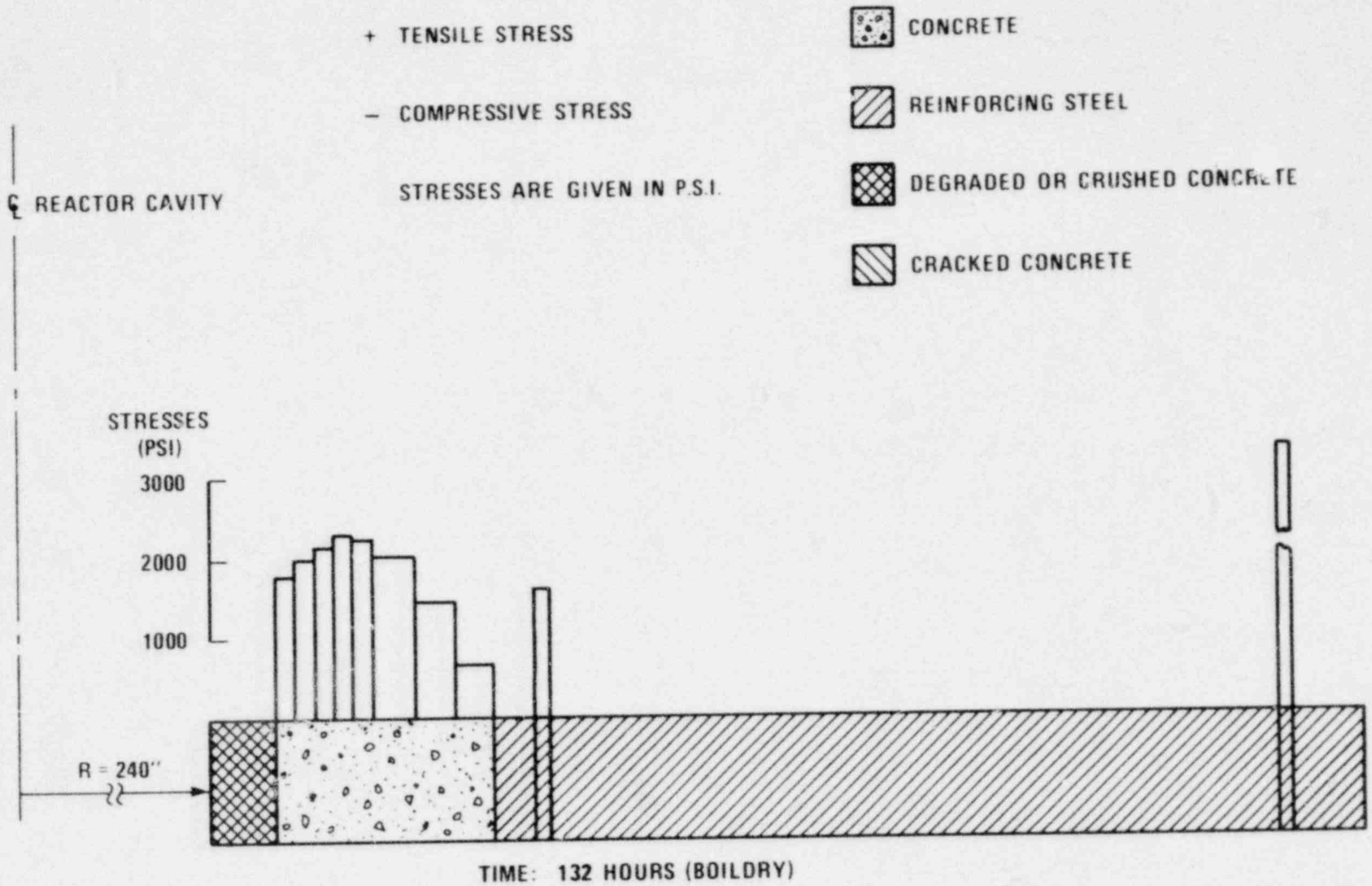

Figure 3-41. Results of Long Cylinder Analysis – Hoop Stresses at 132 Hours (Boildry)

1966-193

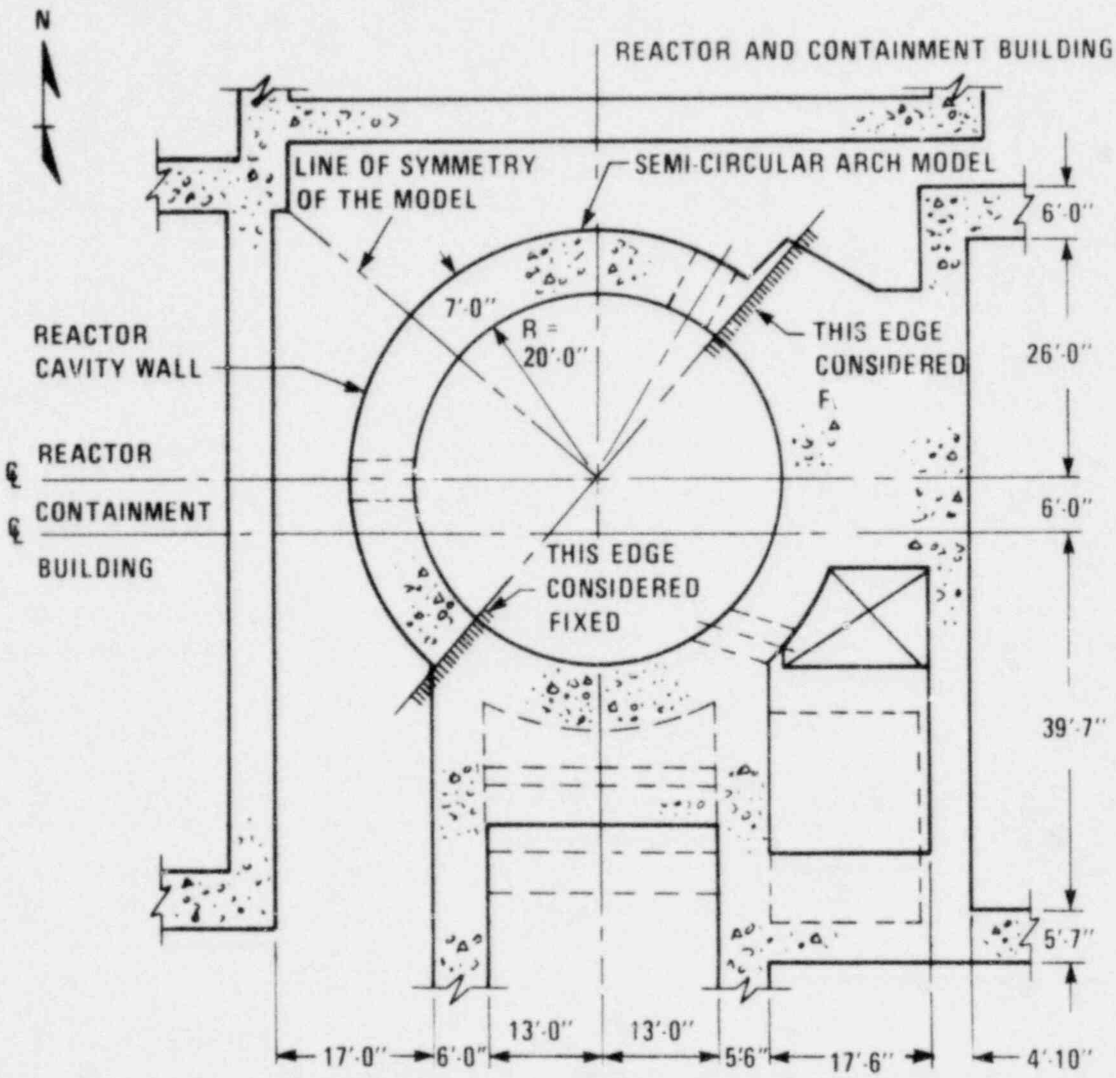

Figure 3-42. Arch Model for Lower Portion of the Reactor Cavity Wall

1966-74

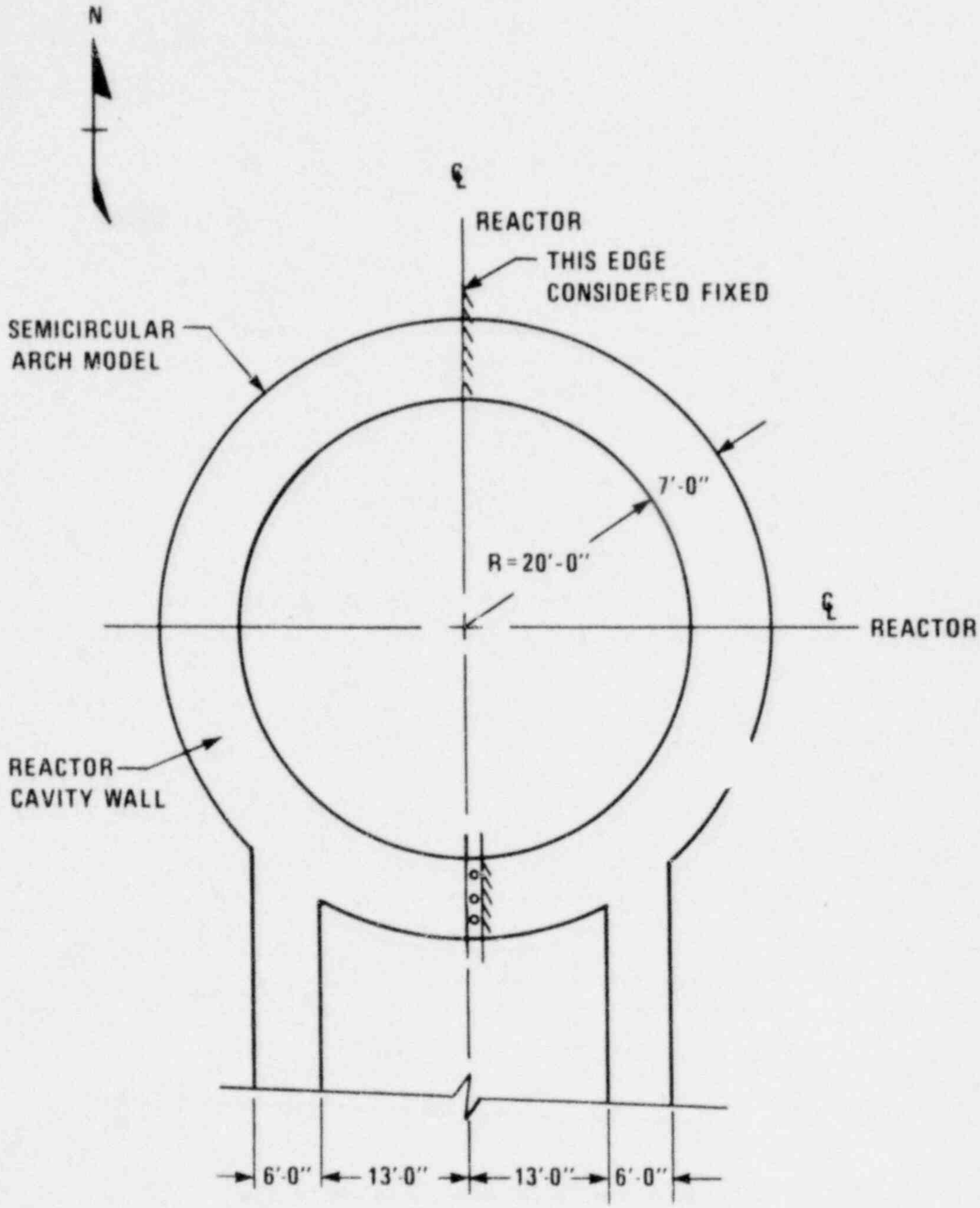

Figure 3-43. Arch Model for the Upper Portion of the Reactor Cavity Wall

1966-75

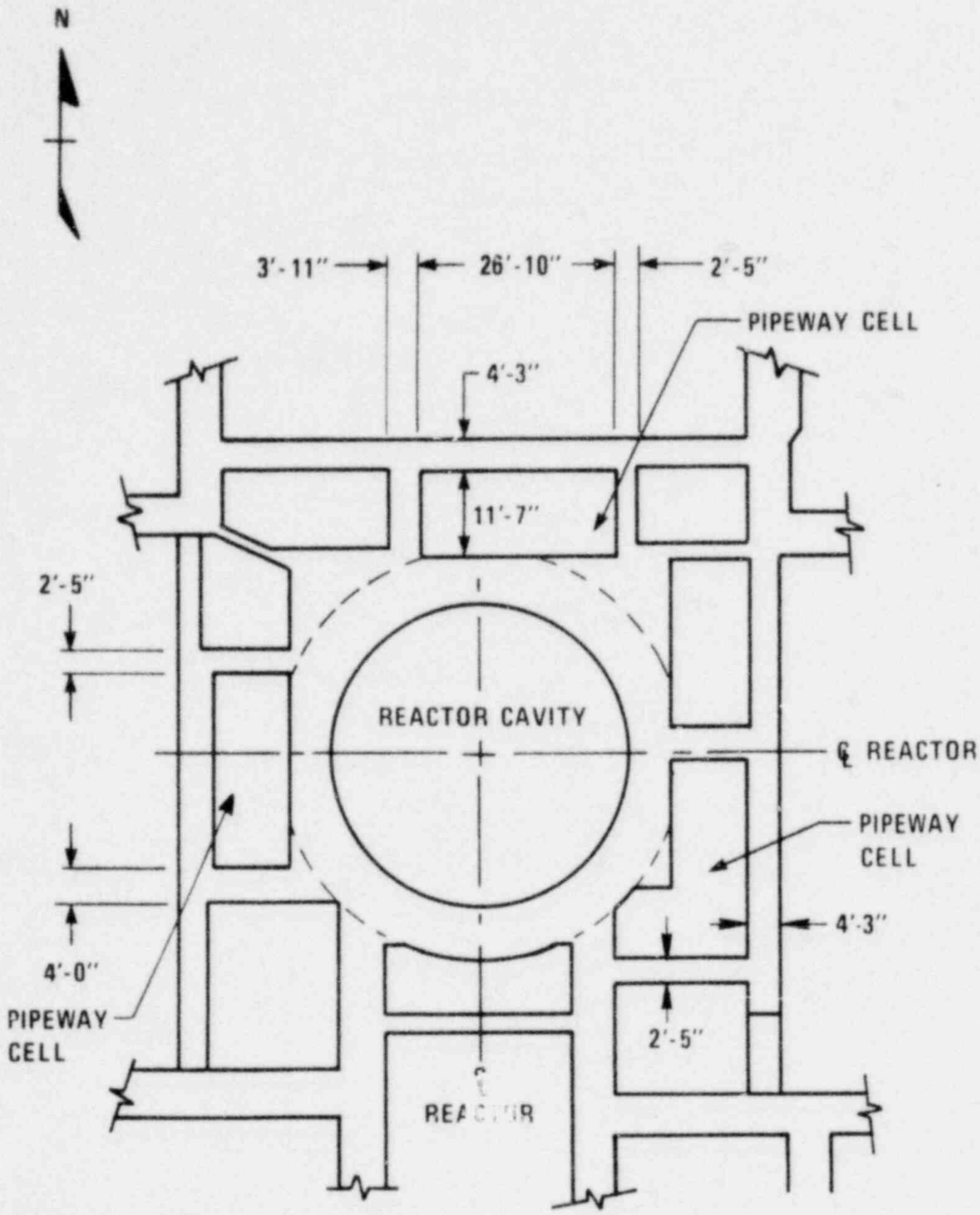

Figure 3-44. Pipeway Cells – Plan at El. 786.3

1966-76

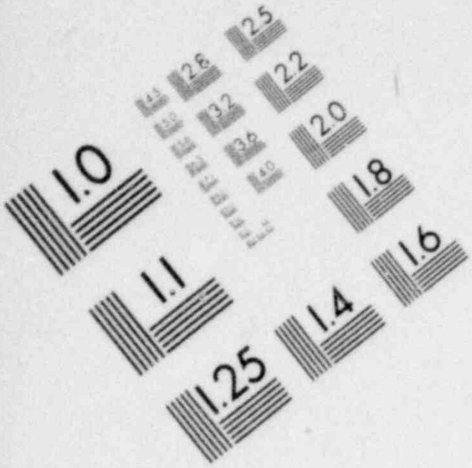

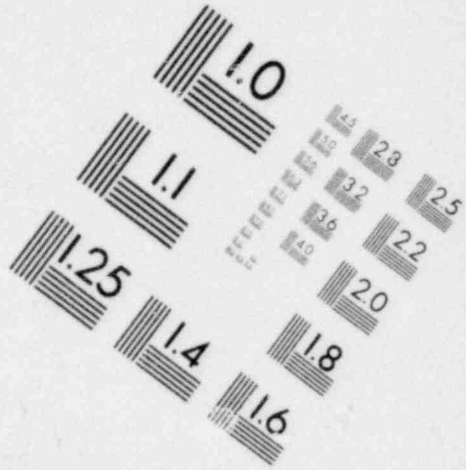

IMAGE EVALUATION
TEST TARGET (MT-3)

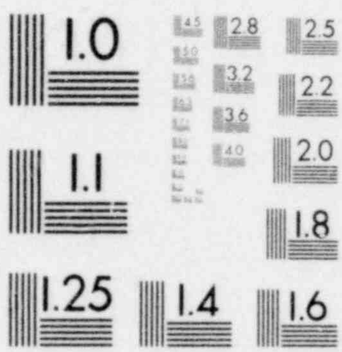

6″

MICROCOPY RESOLUTION TEST CHART

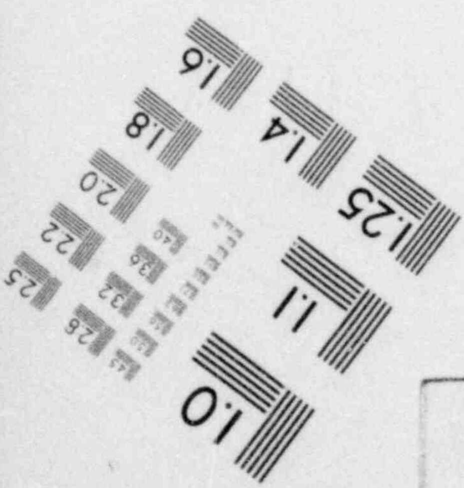

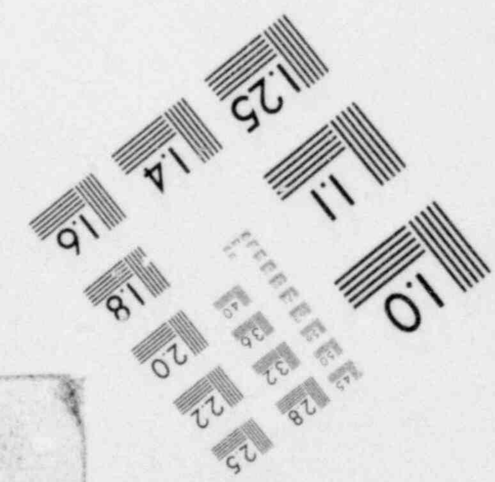

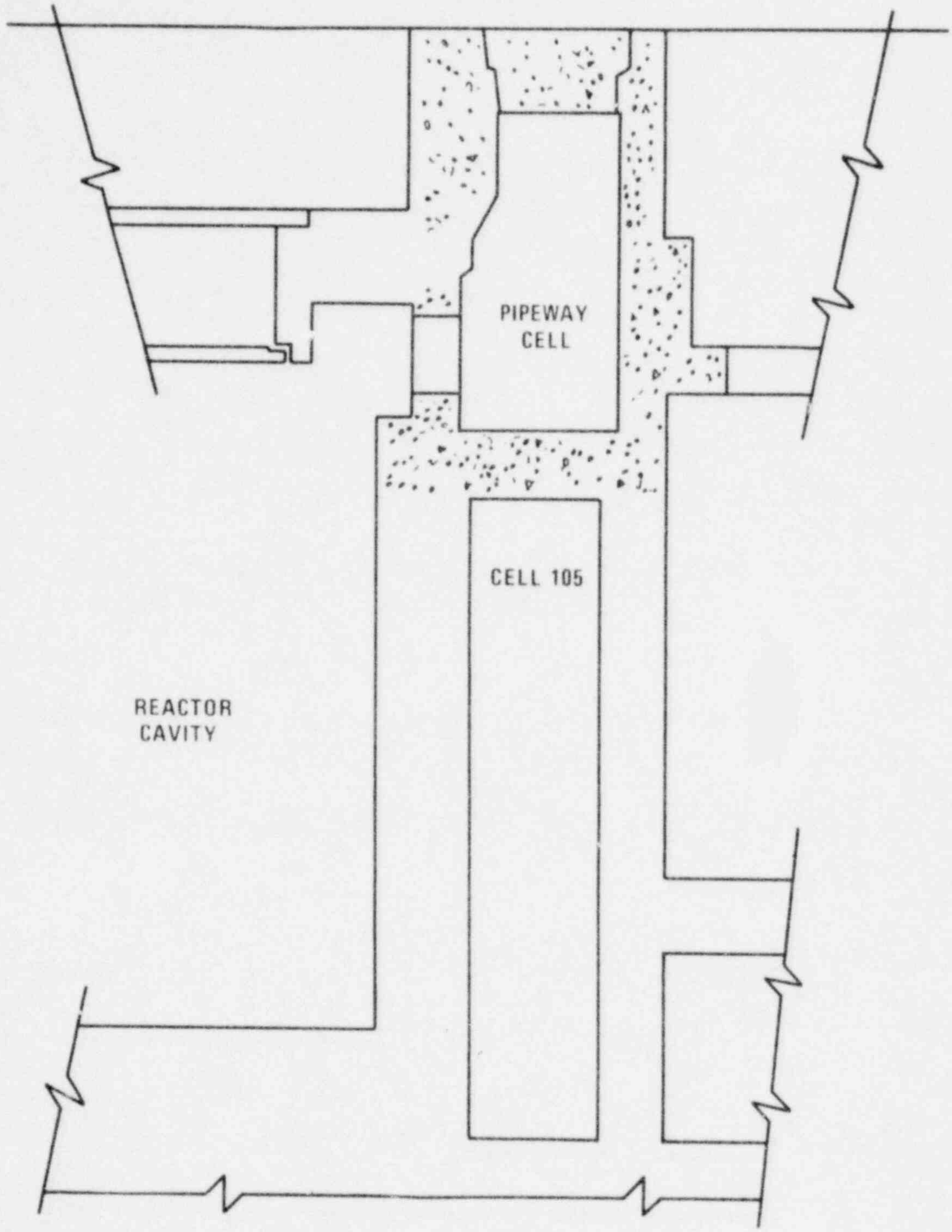

Figure 3-45. Pipeway Cell Cross Section

1966-77

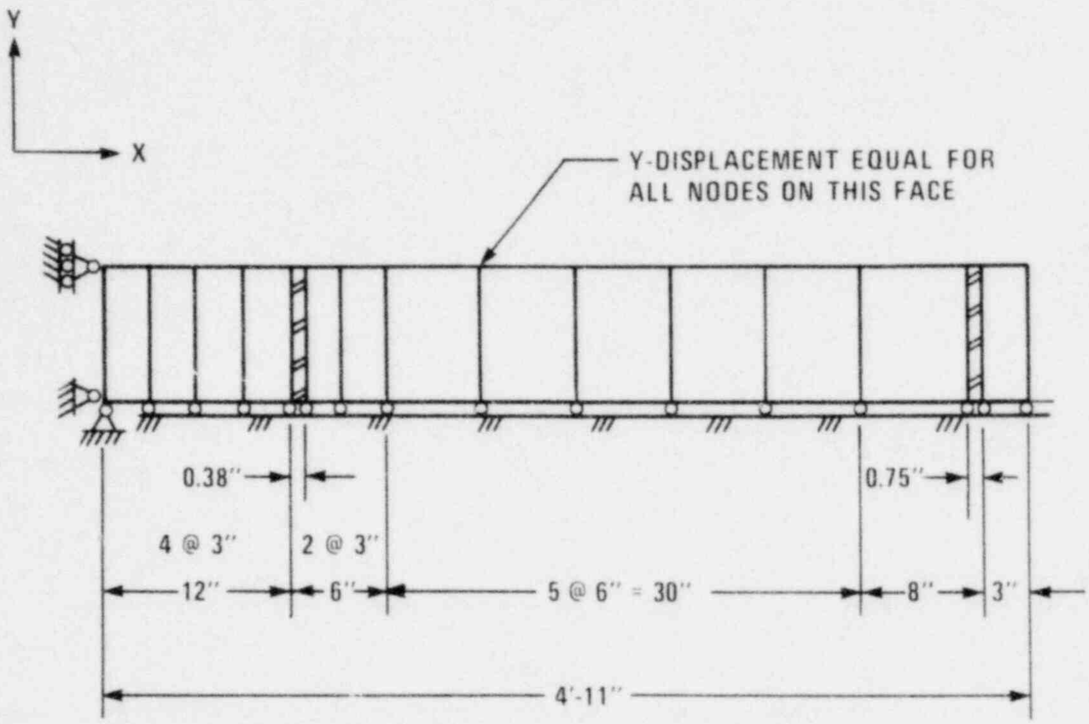

Figure 3-46. Finite Element Model for Strip of Pipeway Floor

1966-78

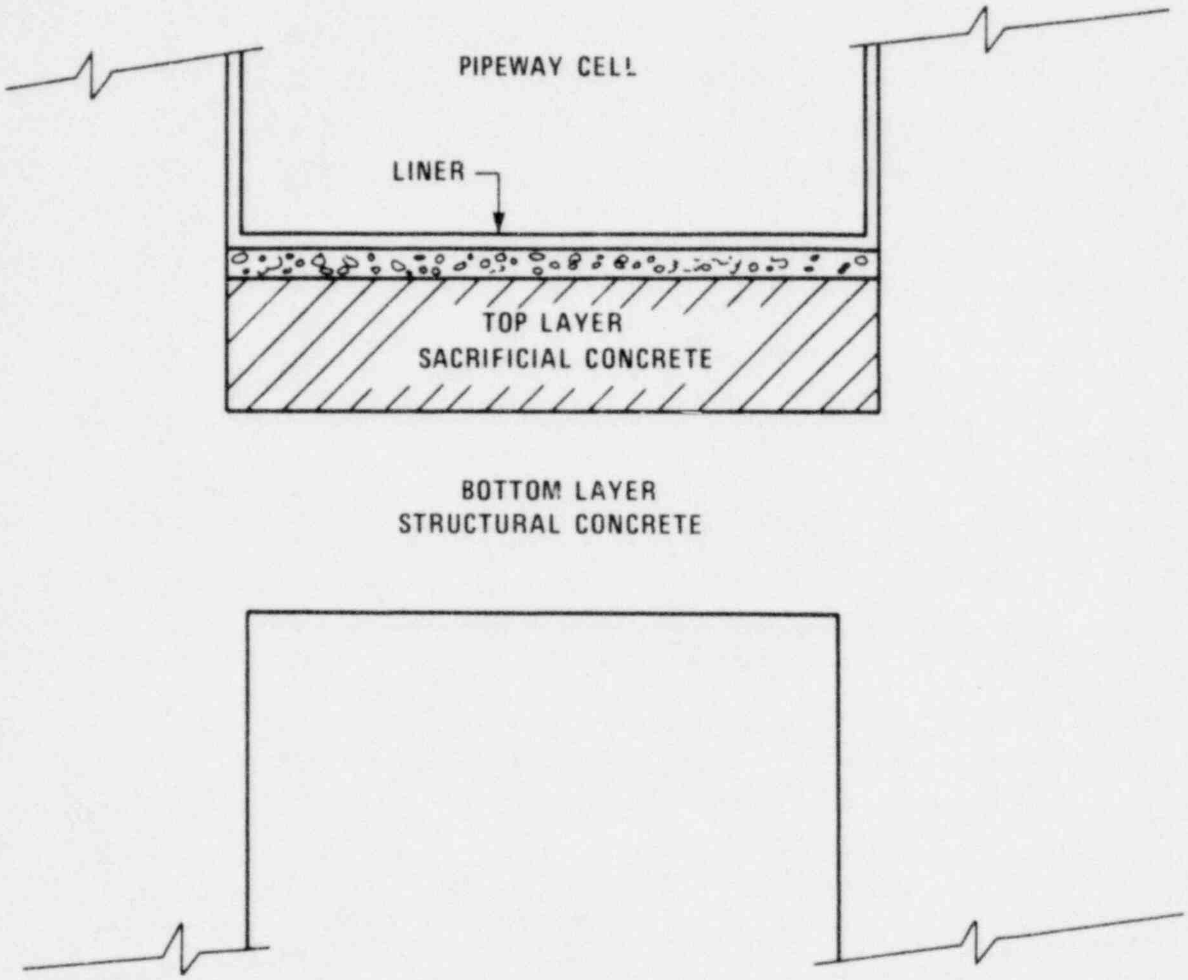

Figure 3-47. Pipeway Cell Floor – Two Layer System

1966-79

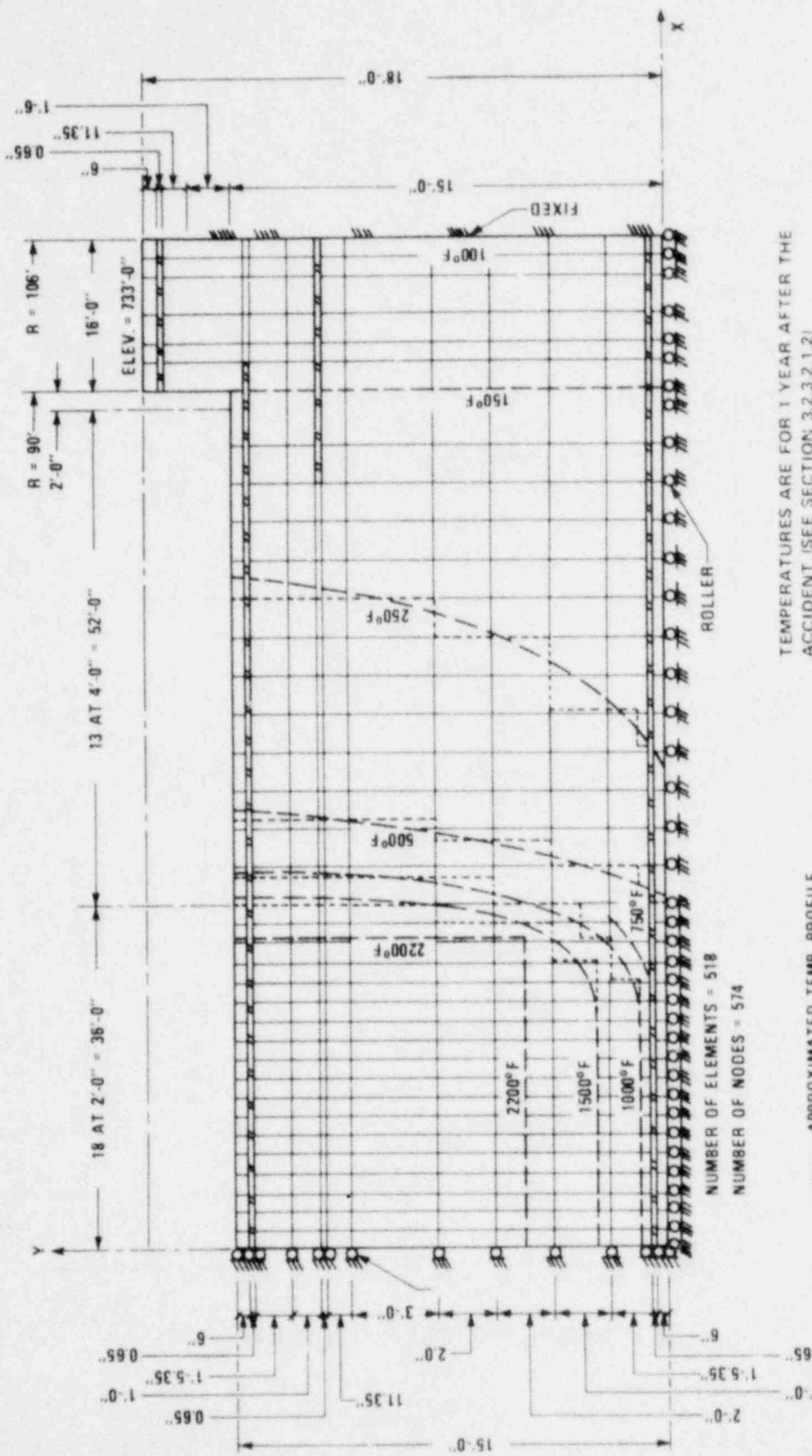

Figure 3-48 Basemat Model after Boil Dry

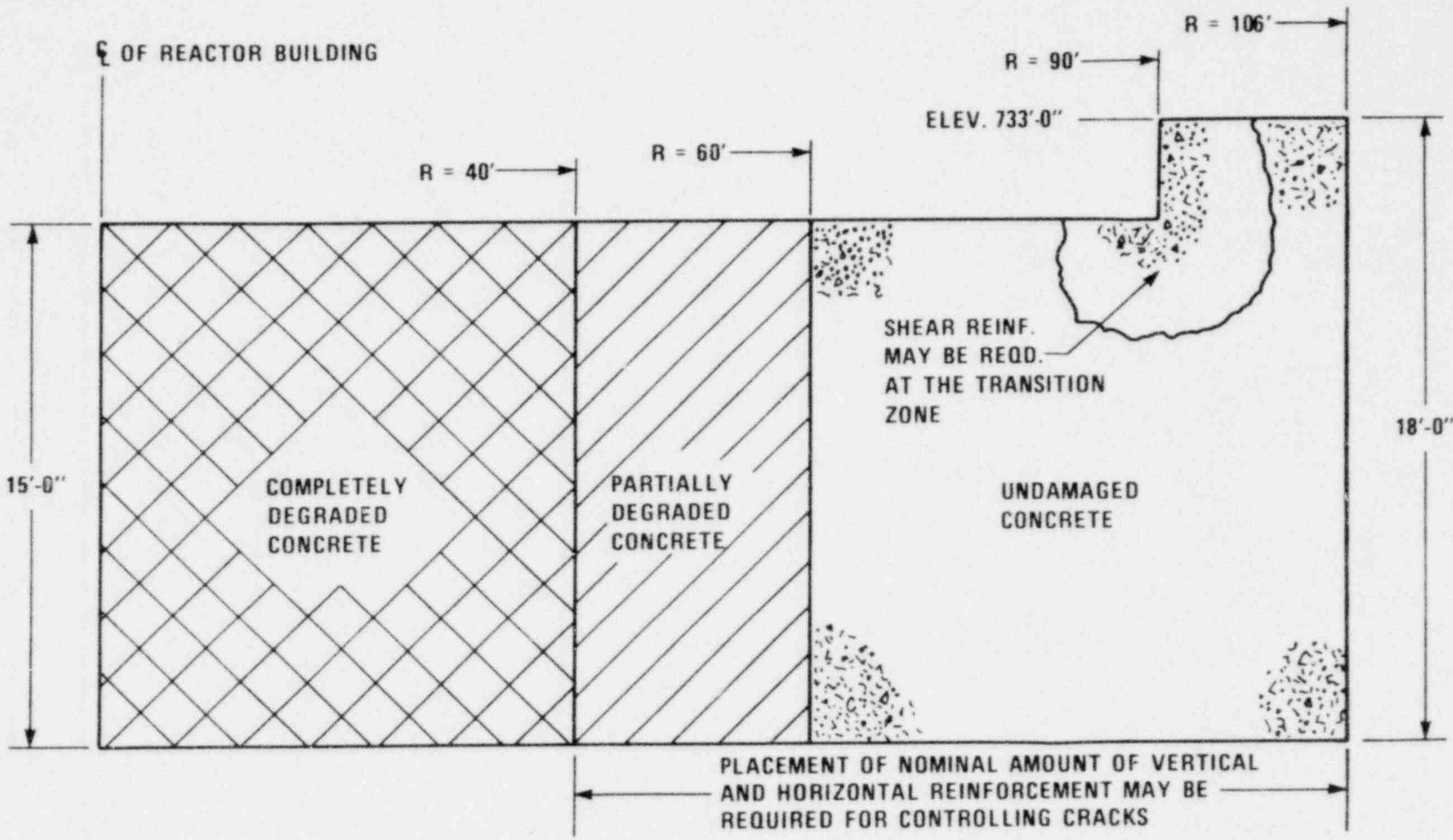

Figure 3-49. Basemat Structural Analysis Results

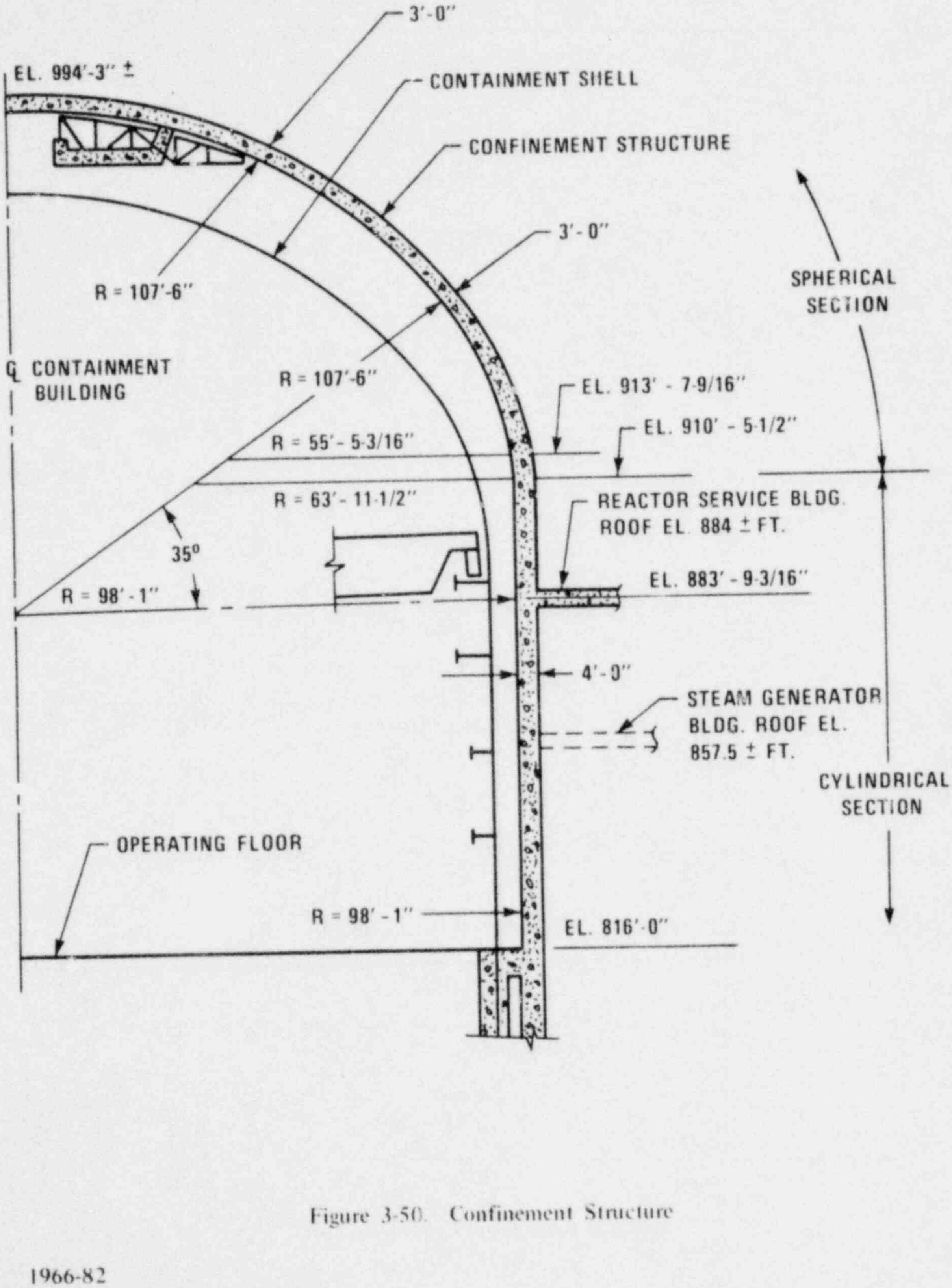

Figure 3-50. Confinement Structure

1966-82

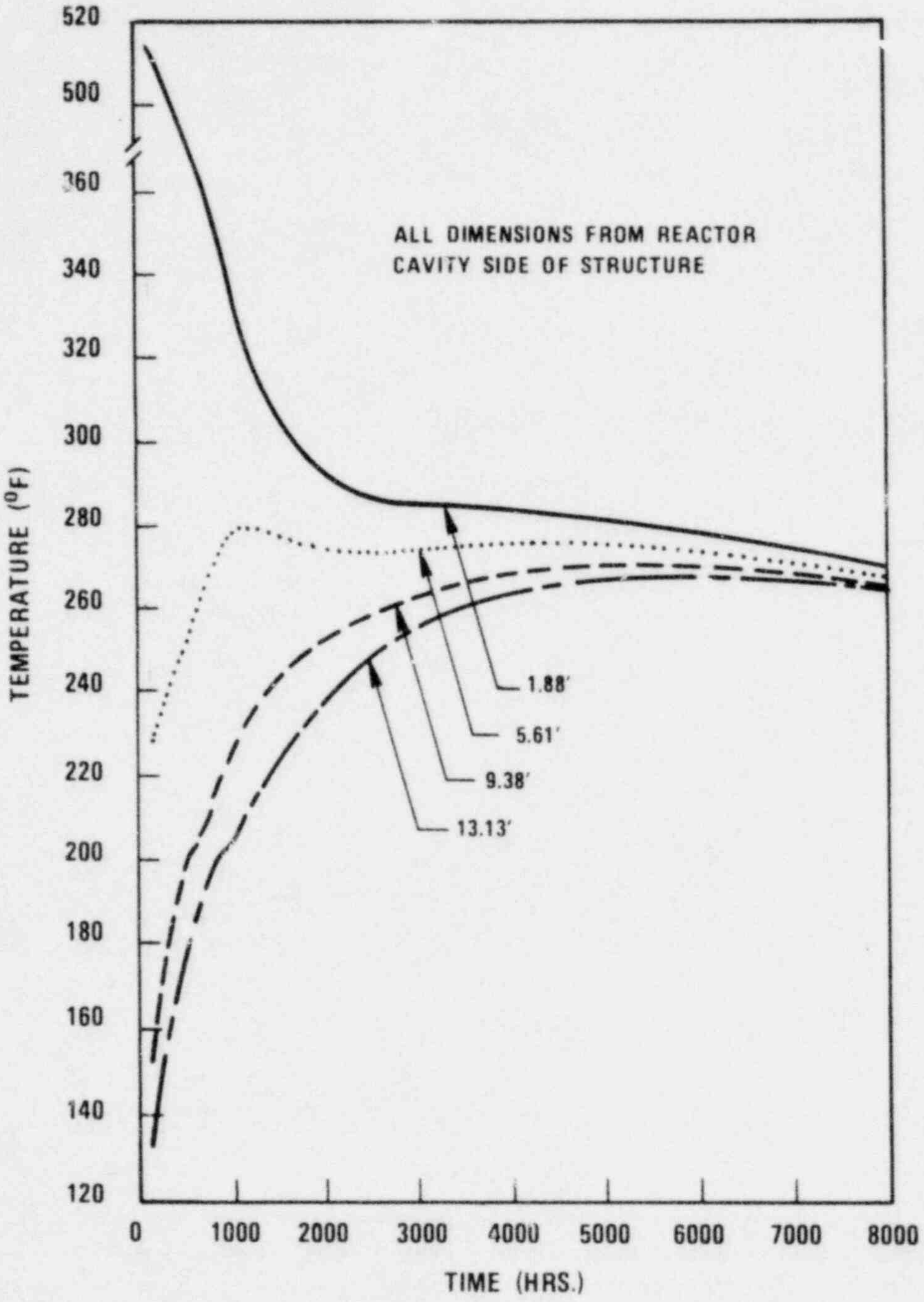

Figure 3-51 Reactor Cavity Ledge (Elevation 797.5) Temperatures
1.0 HR · FT^2 · °F/BTU Crust Resistance

1966-83

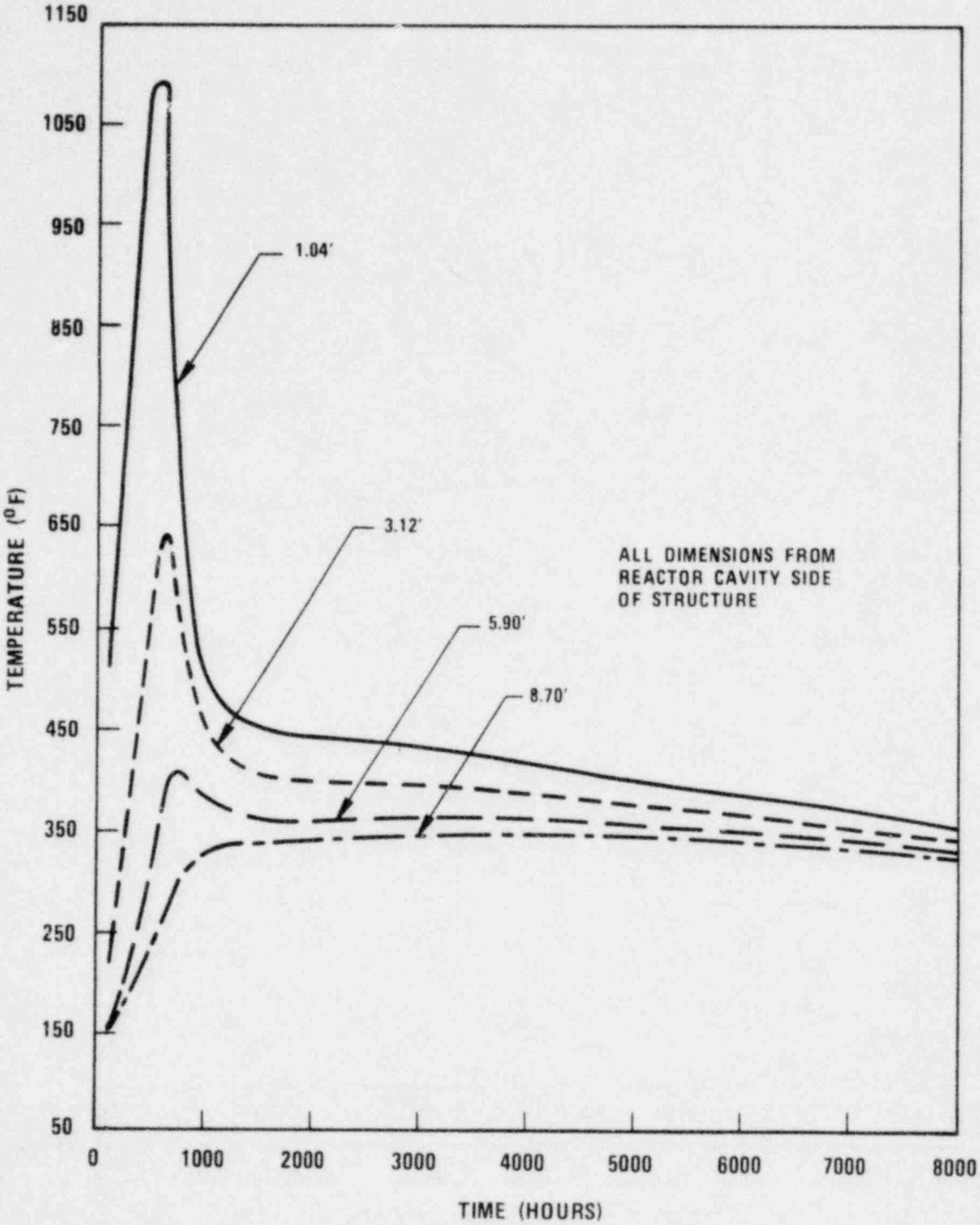

Figure 3-52 Reactor Cavity Ledge (Elevation 789.5) Temperatures
1.0 HR · FT^2 · ^{0}F/BTU Crust Resistance

1966-84

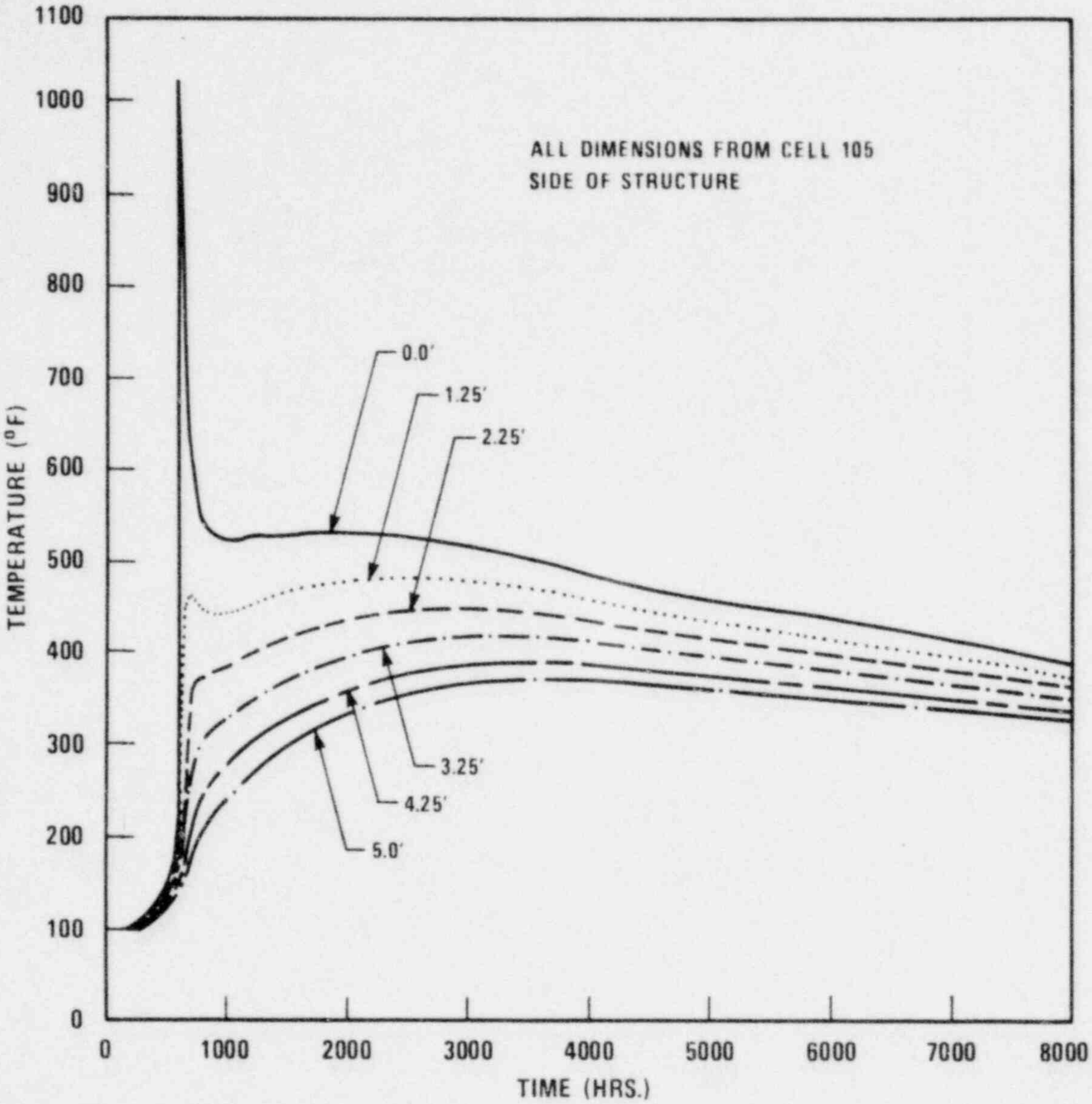

Figure 3-53. PHTS Wall (Facing RC Wall) Temperatures
1.0 HR • FT^2 • °F/BTU Crust Resistance

1966-85

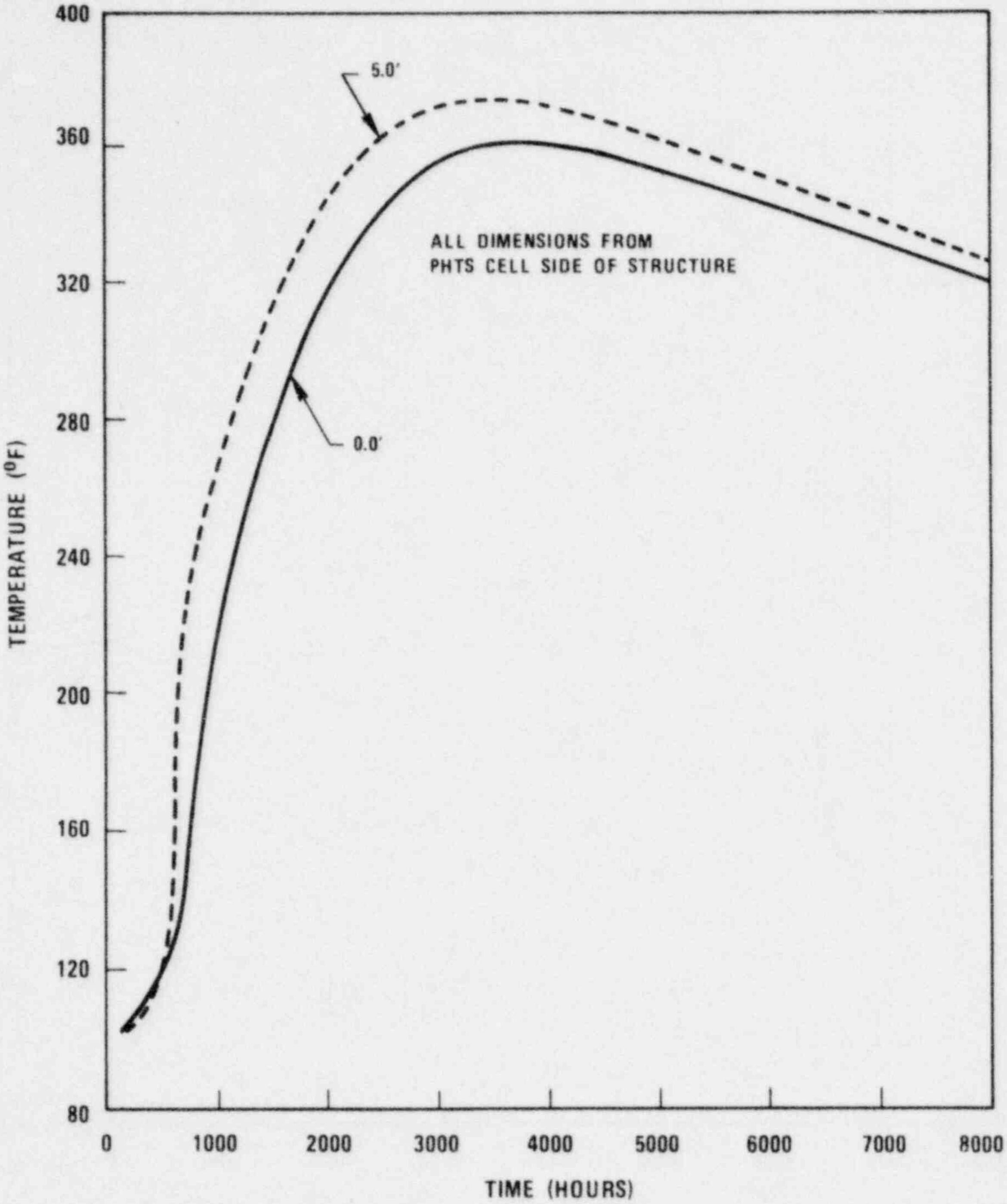

Figure 3-54 PHTS Wall (Not Facing RC Wall) Temperatures
1.0 HR · FT^2 · °F/BTU Crust Resistance

1966-86

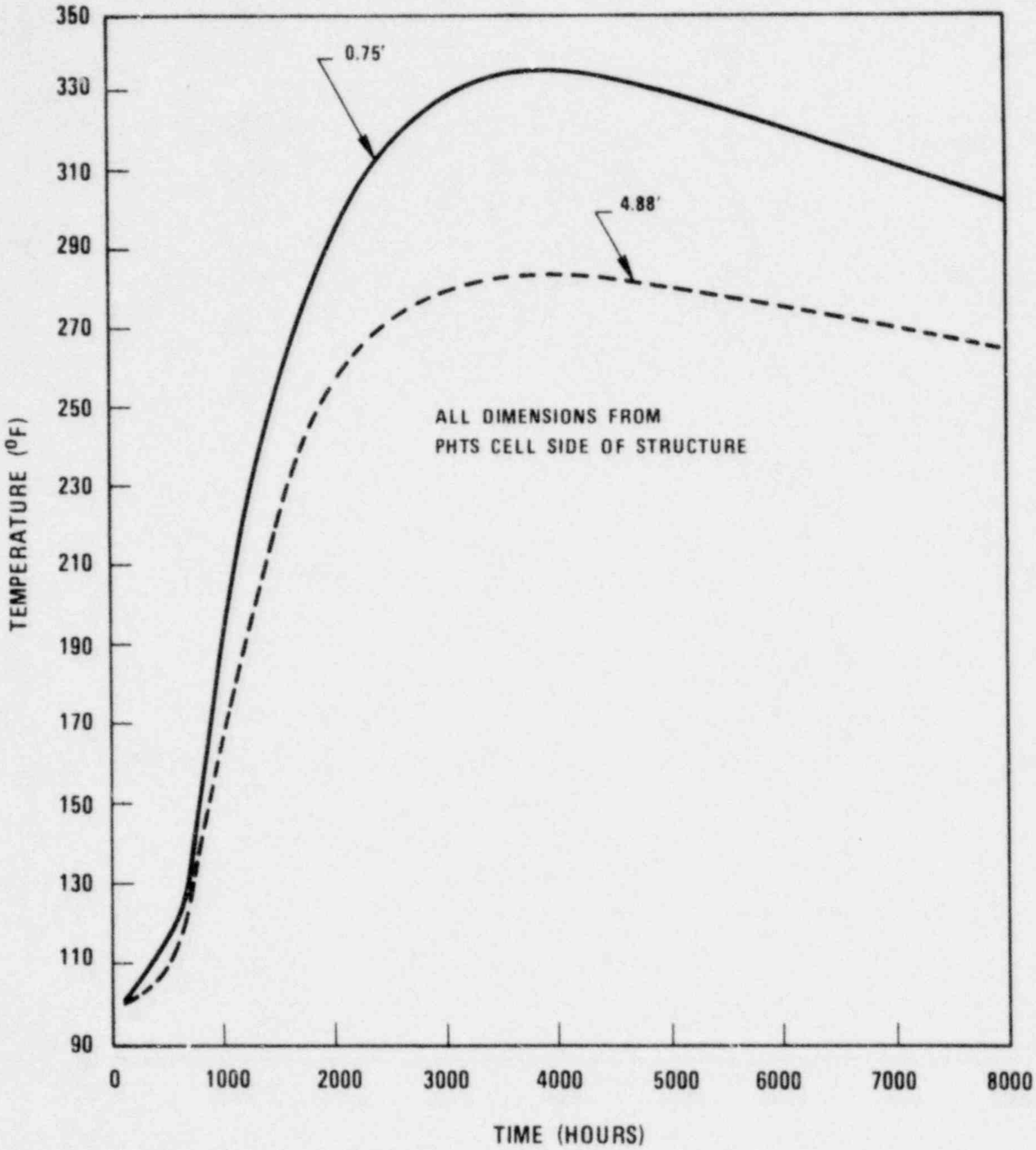

Figure 3-55 Containment Wall (Adjacent to PHTS Cell Walls) Temperatures
1.0 HR · FT^2 · ^oF/BTU Crust Resistance

1966-87

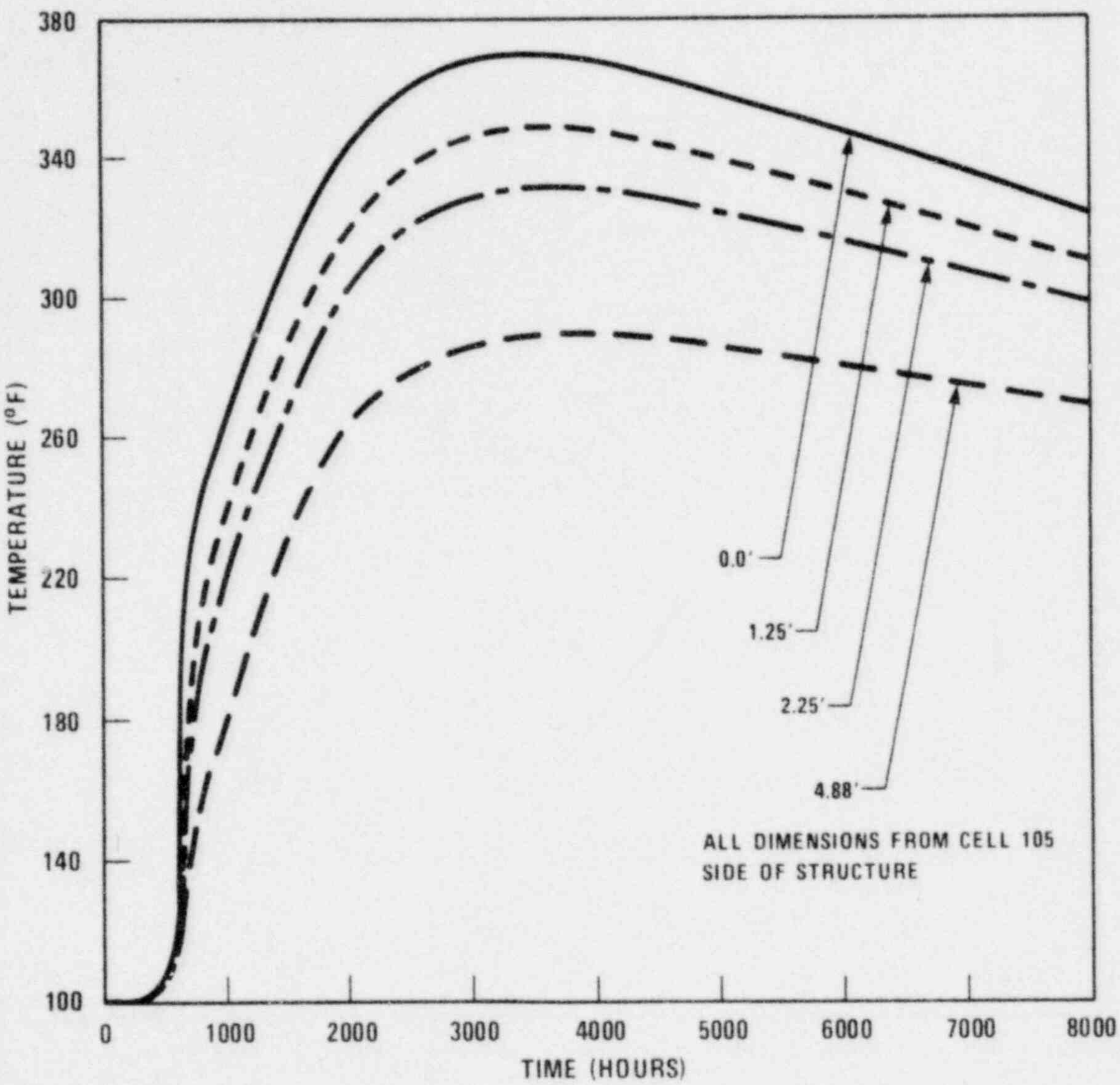

Figure 3-56. Containment Wall (Adjacent to Cell 105) Temperatures
1.0 HR • FT^2 • °F/BTU Crust Resistance

1966-88

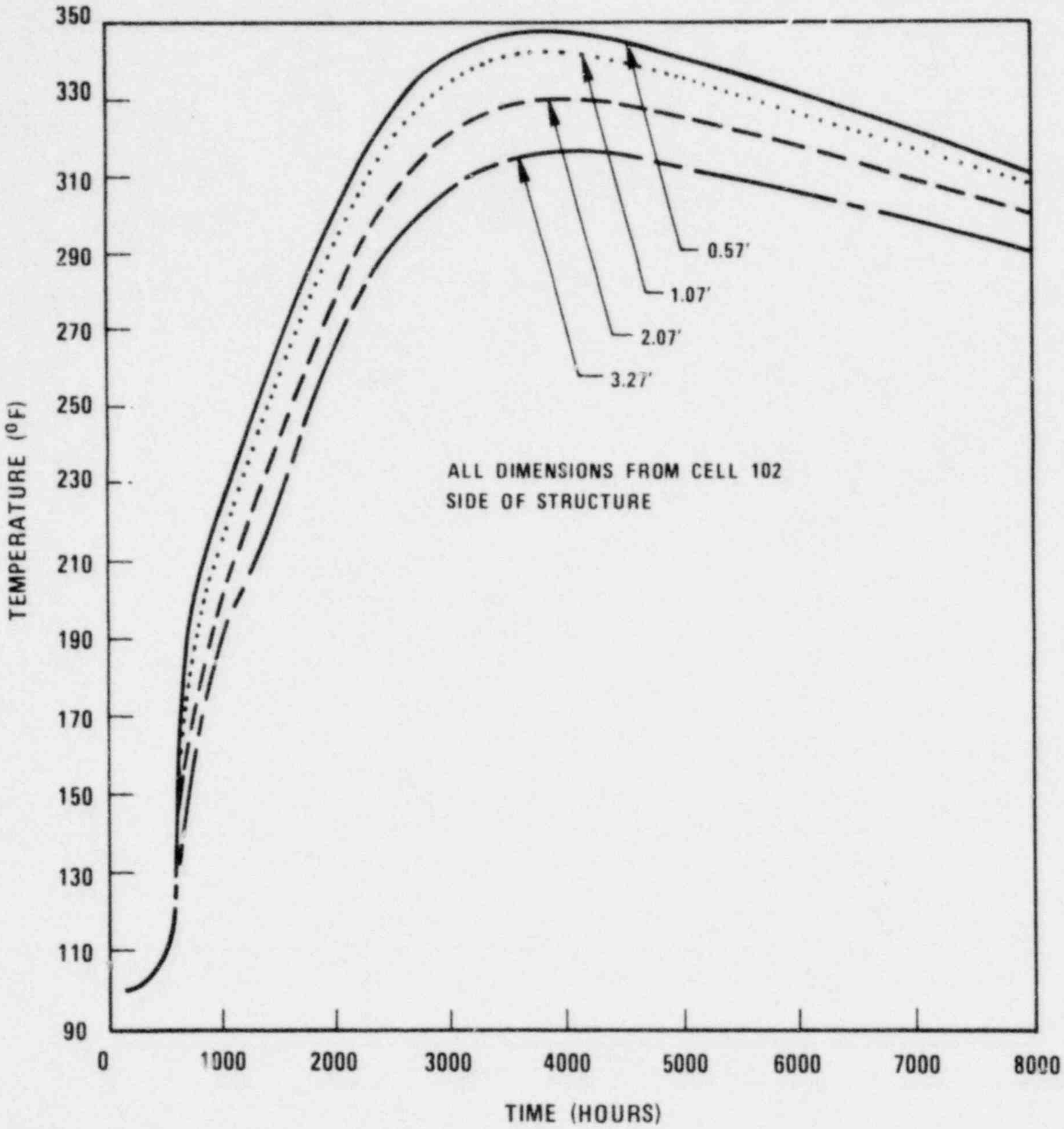

Figure 3-57 Containment Wall (Adjacent to Cell 102A) Temperatures
1.0 HR · FT^2 · °F/BTU Crust Resistance

1966-89

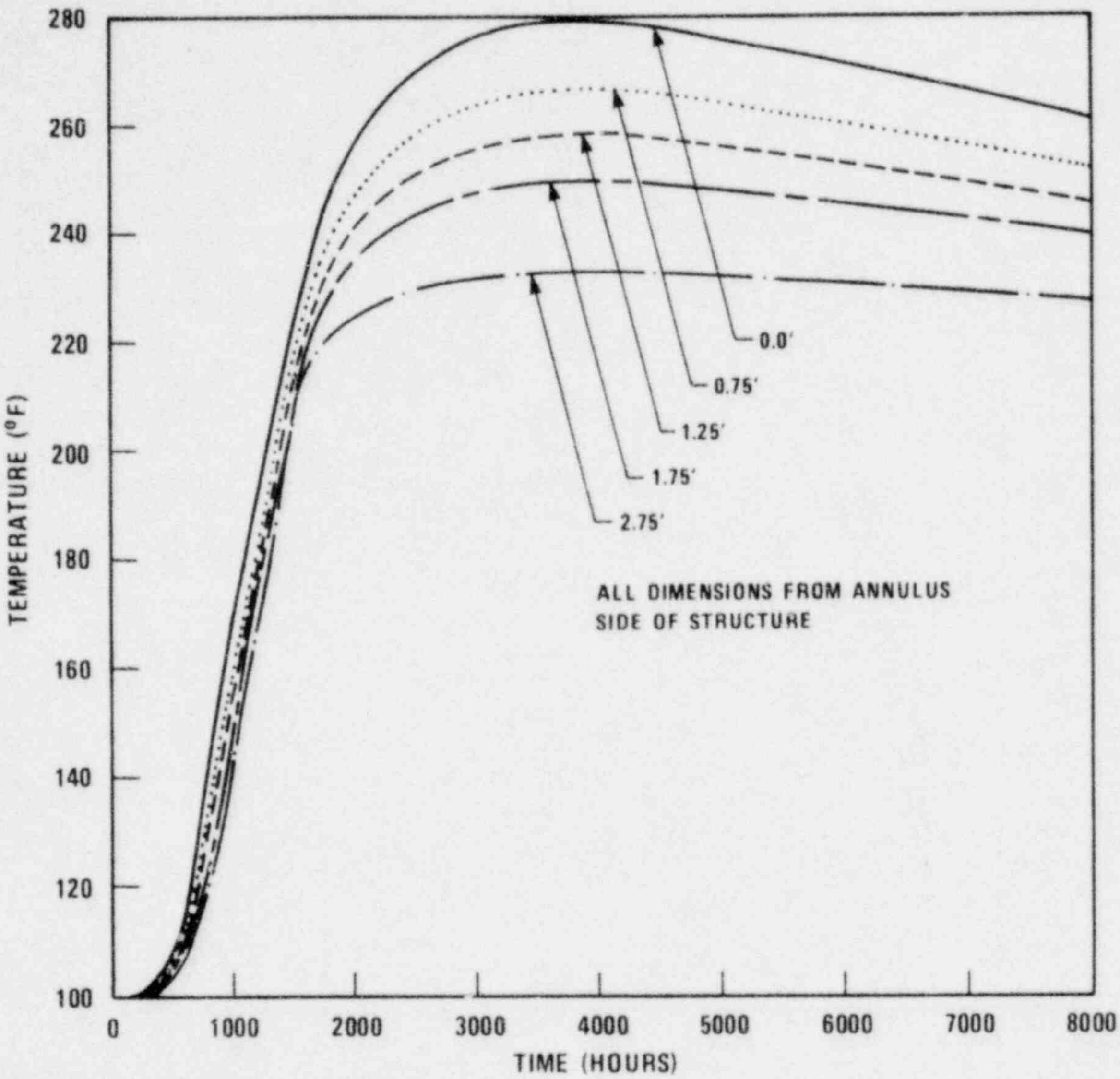

Figure 3-58. Confinement Wall Temperatures 1.0 HR • FT^2 • °F/BTU Crust Resistance

1966-90

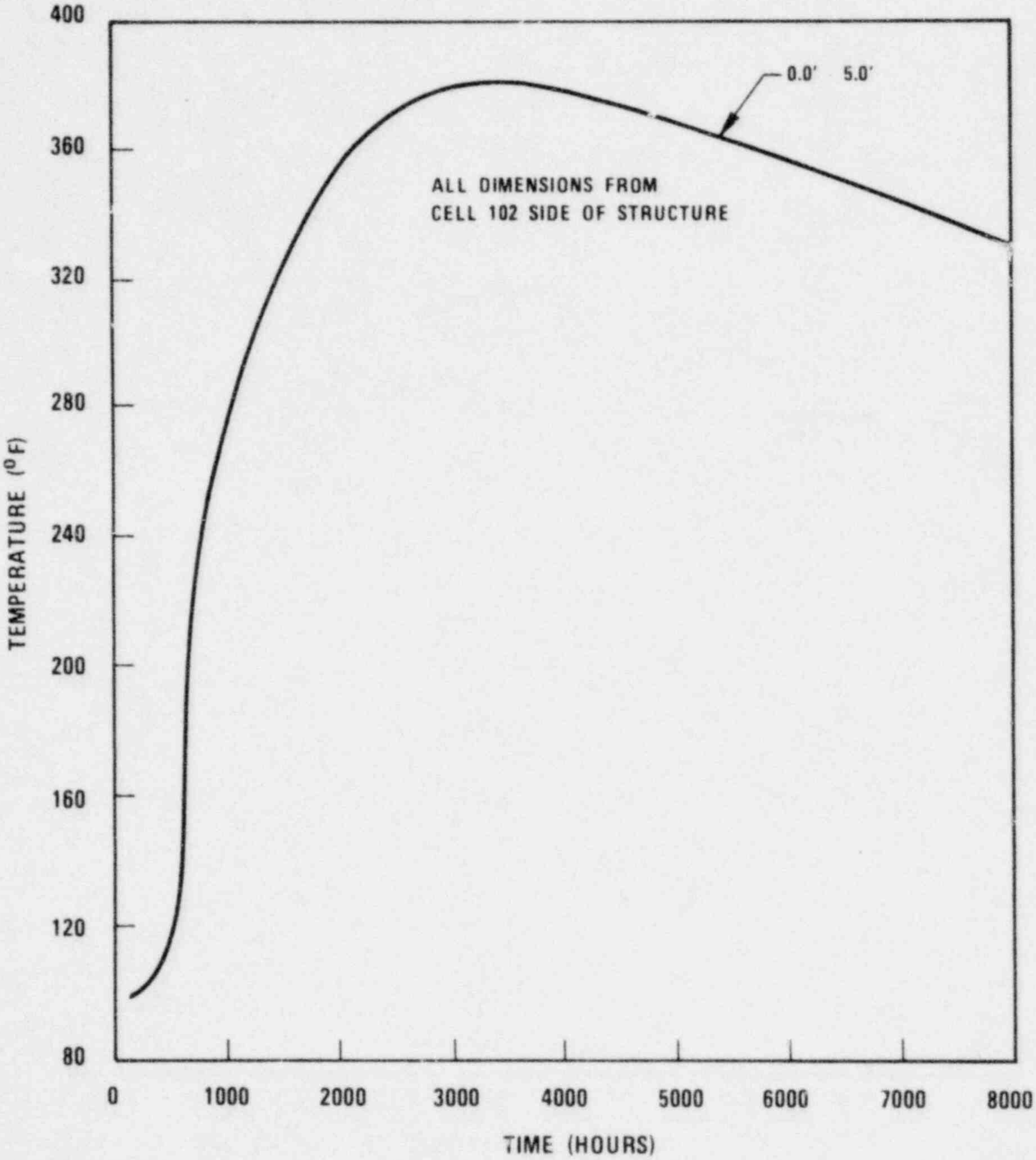

Figure 3-59 Wall Between Cells 102 and 105 Temperatures
1.0 HR · FT^2 · ^{o}F/BTU Crust Resistance

1966-91

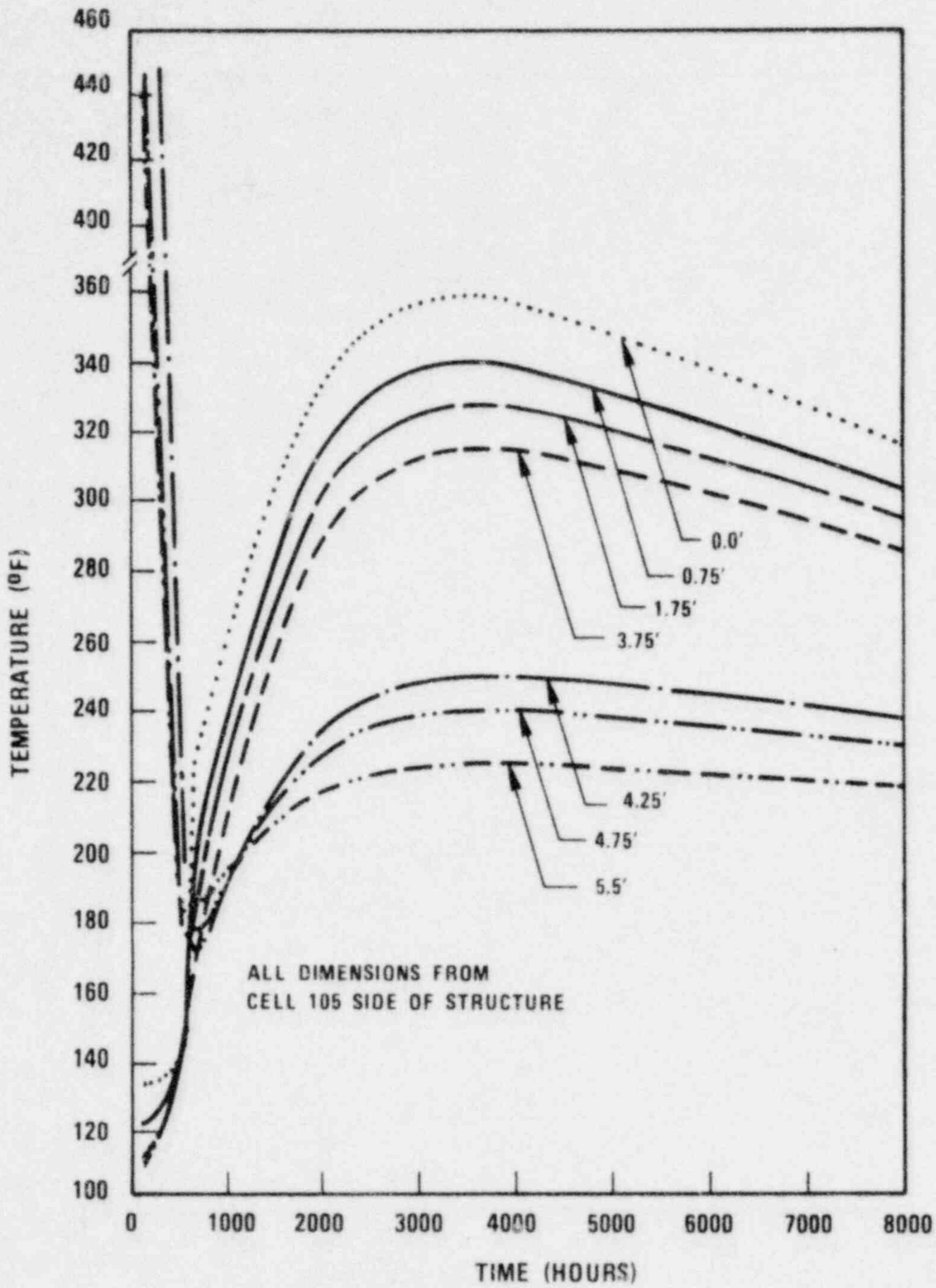

Figure 3-60 Operating Floor (Above Cell 105) Temperatures
1.0 HR · FT^2 · °F/BTU Crust Resistance

1966-92

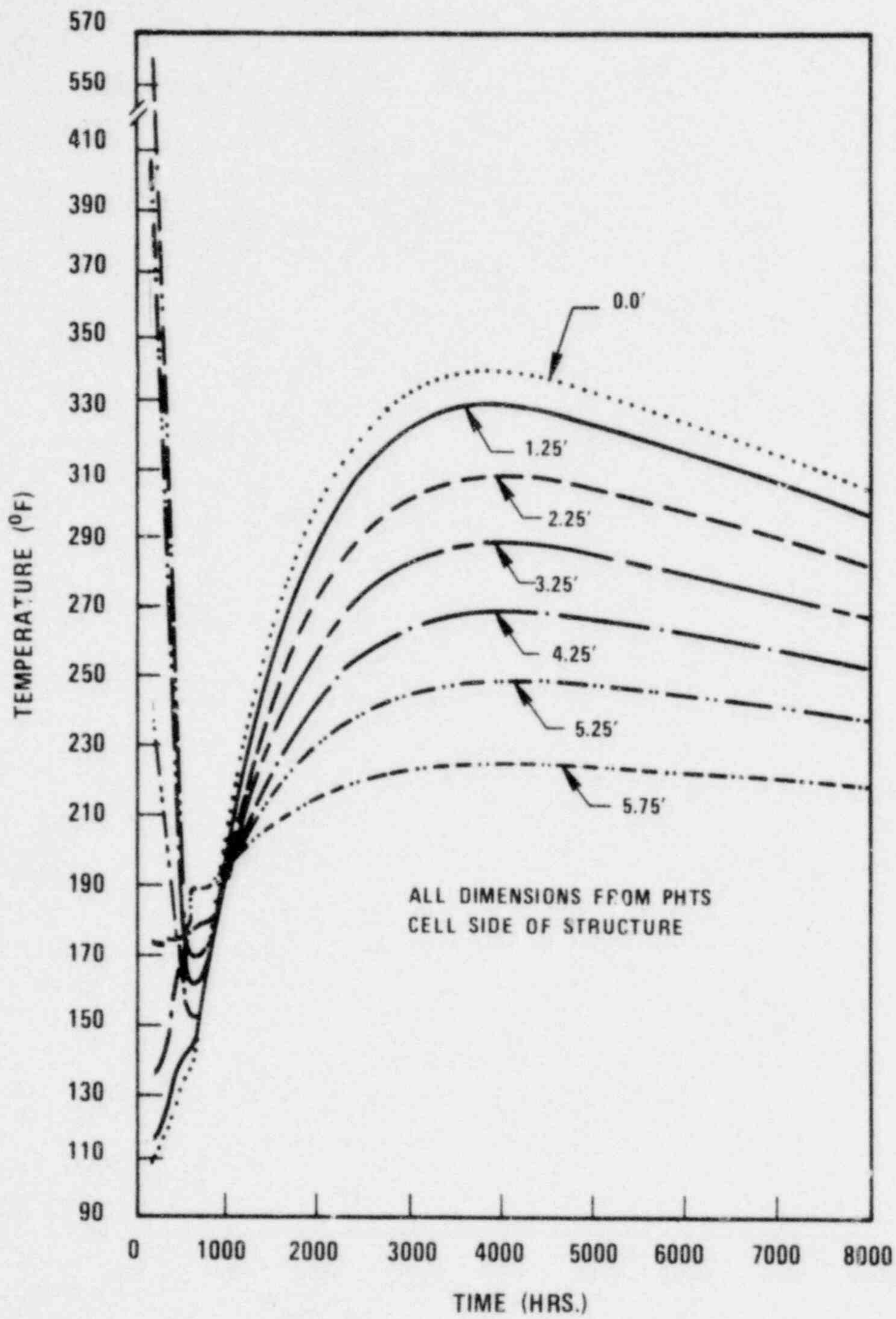

Figure 3-61 Operating Floor (Above PHTS Cells) Temperatures
1.0 HR · FT^2 · °F/BTU Crust Resistance

1966-93

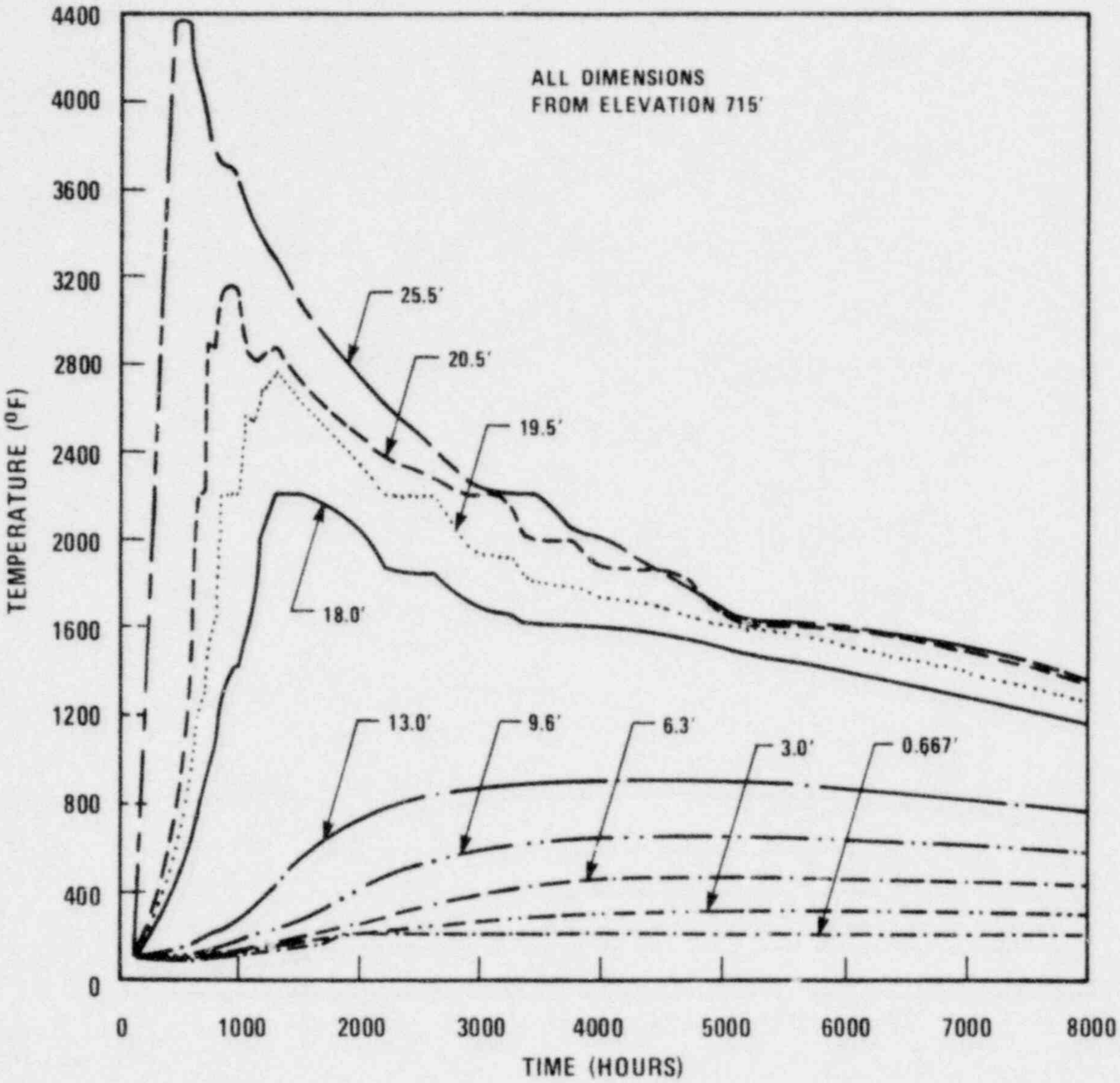

Figure 3-62. Reactor Cavity Floor and Basemat (Axial Centerline) Temperatures
1.0 HR • FT^2 • °F/BTU Crust Resistance

1966-94

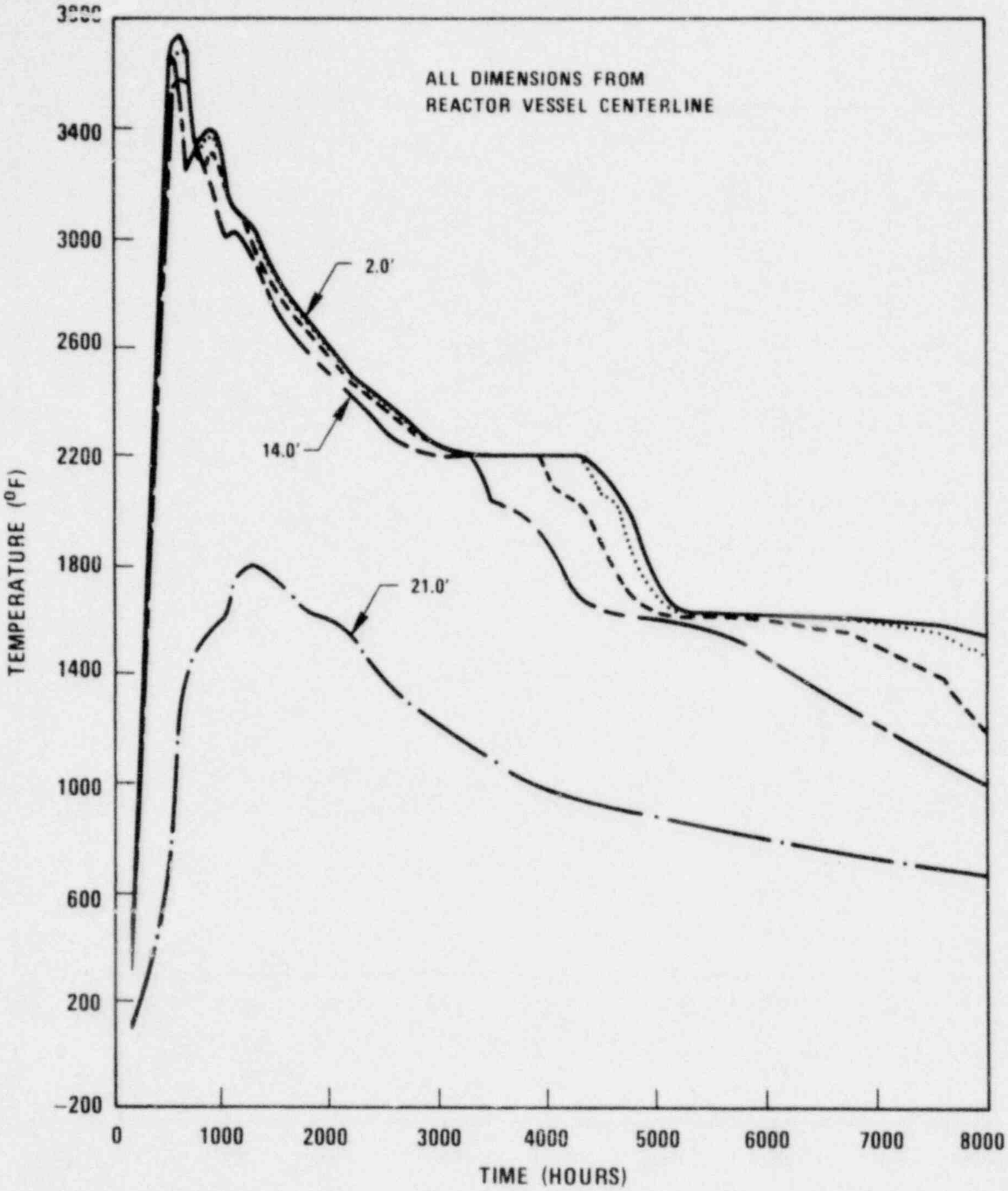

Figure 3-63 Reactor Cavity Floor (Elevation 737.5) Temperatures
1.0 HR · FT^2 · °F/BTU Crust Resistance

1966-95

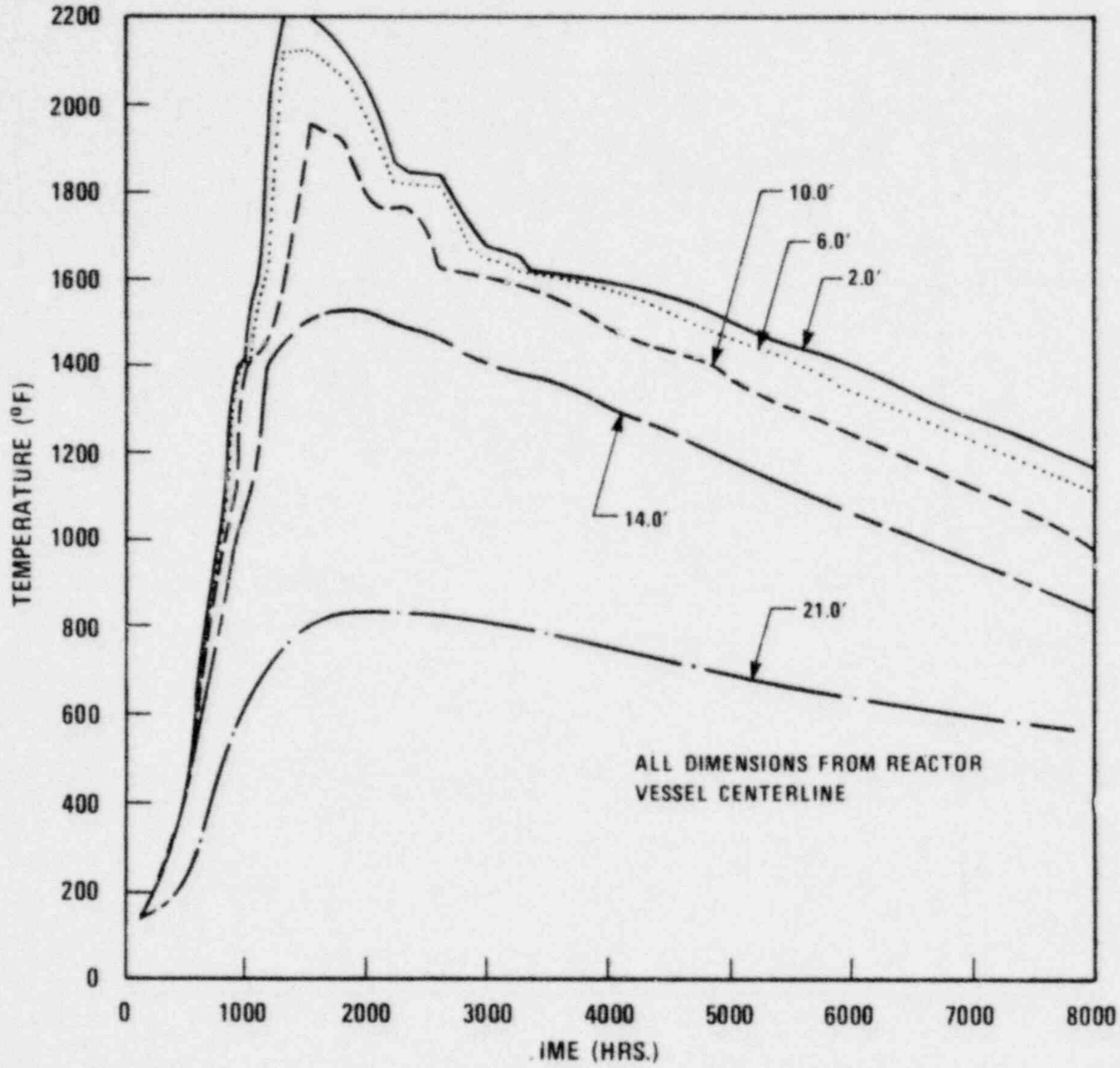

Figure 3-64. Reactor Cavity Floor (Elevation 733.5) Temperatures
1.0 HR • FT^2 • °F/BTU Crust Resistance

1966-96

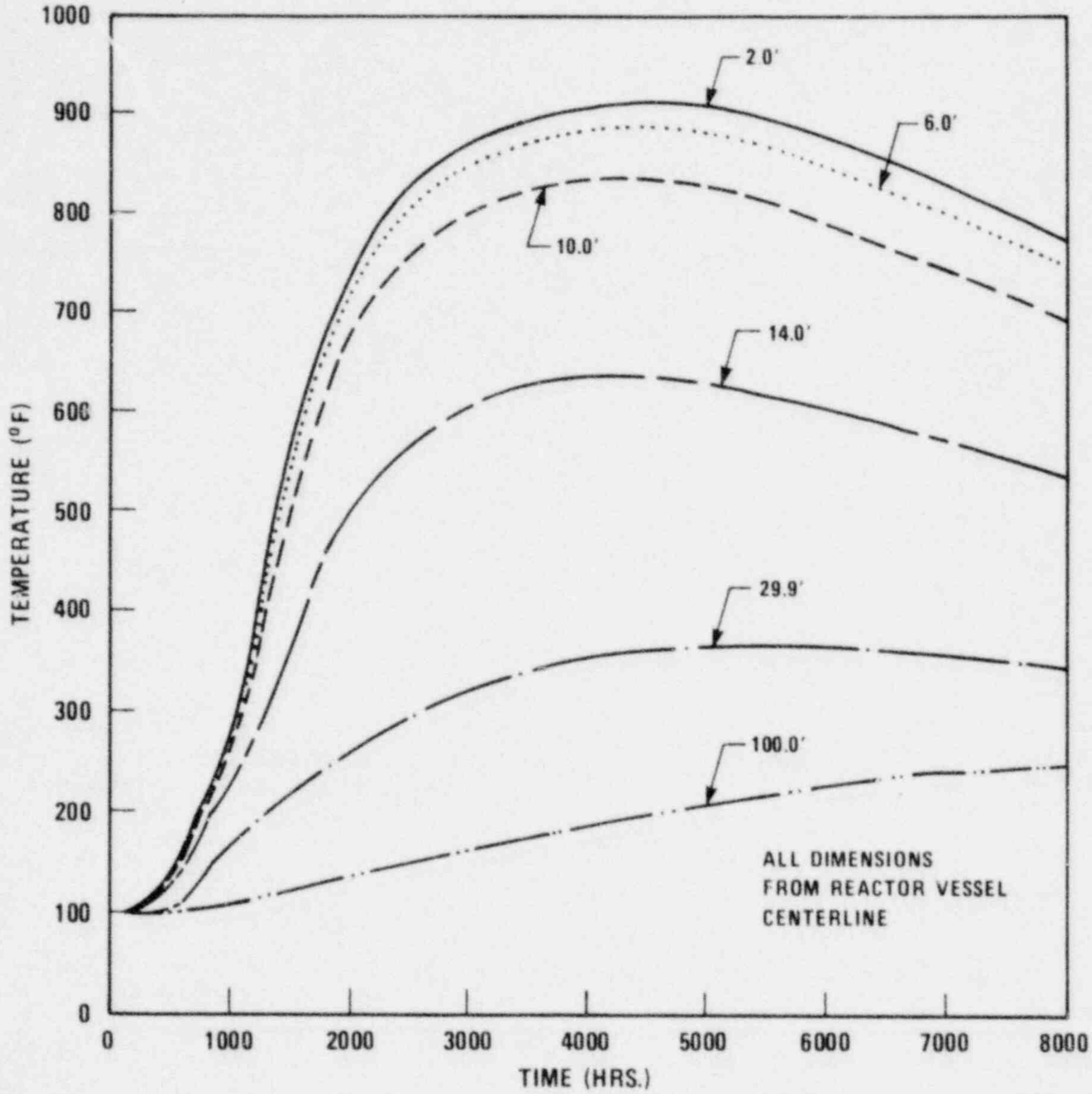

Figure 3-65. Basemat (Elevation 728.0) Temperatures 1.0 HR • FT^2 • °F/BTU Crust Resistance

1966-97

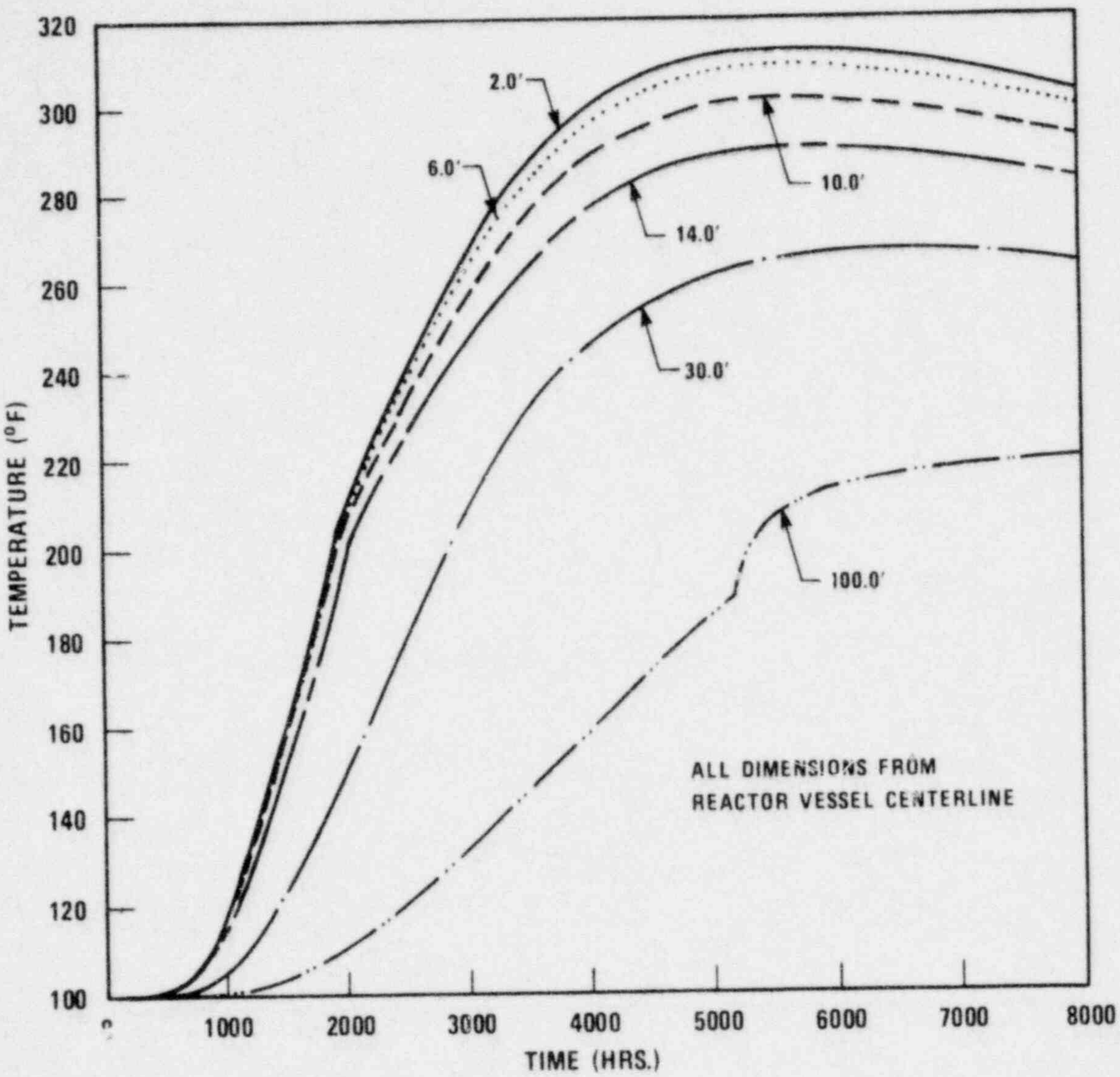

Figure 3-66. Basemat (Elevation 718.0) Temperatures 1.0 HR• FT^2 • °F/BTU Crust Resistance

1966-98

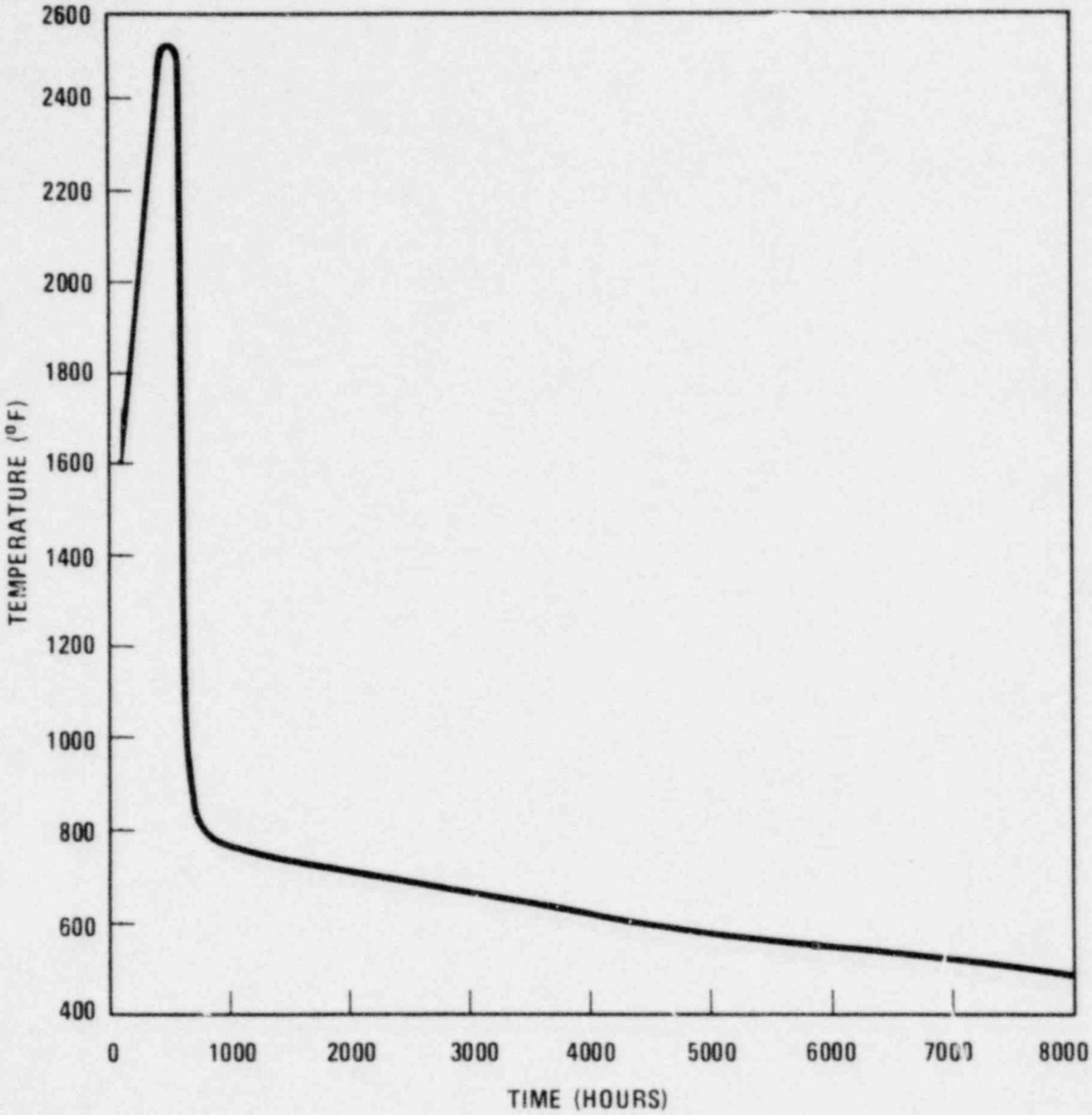

Figure 3-67. Reactor Cavity Steel Equipment Temperatures
1.0 HR • FT^2 • °F/BTU Crust Resistance

1966-99

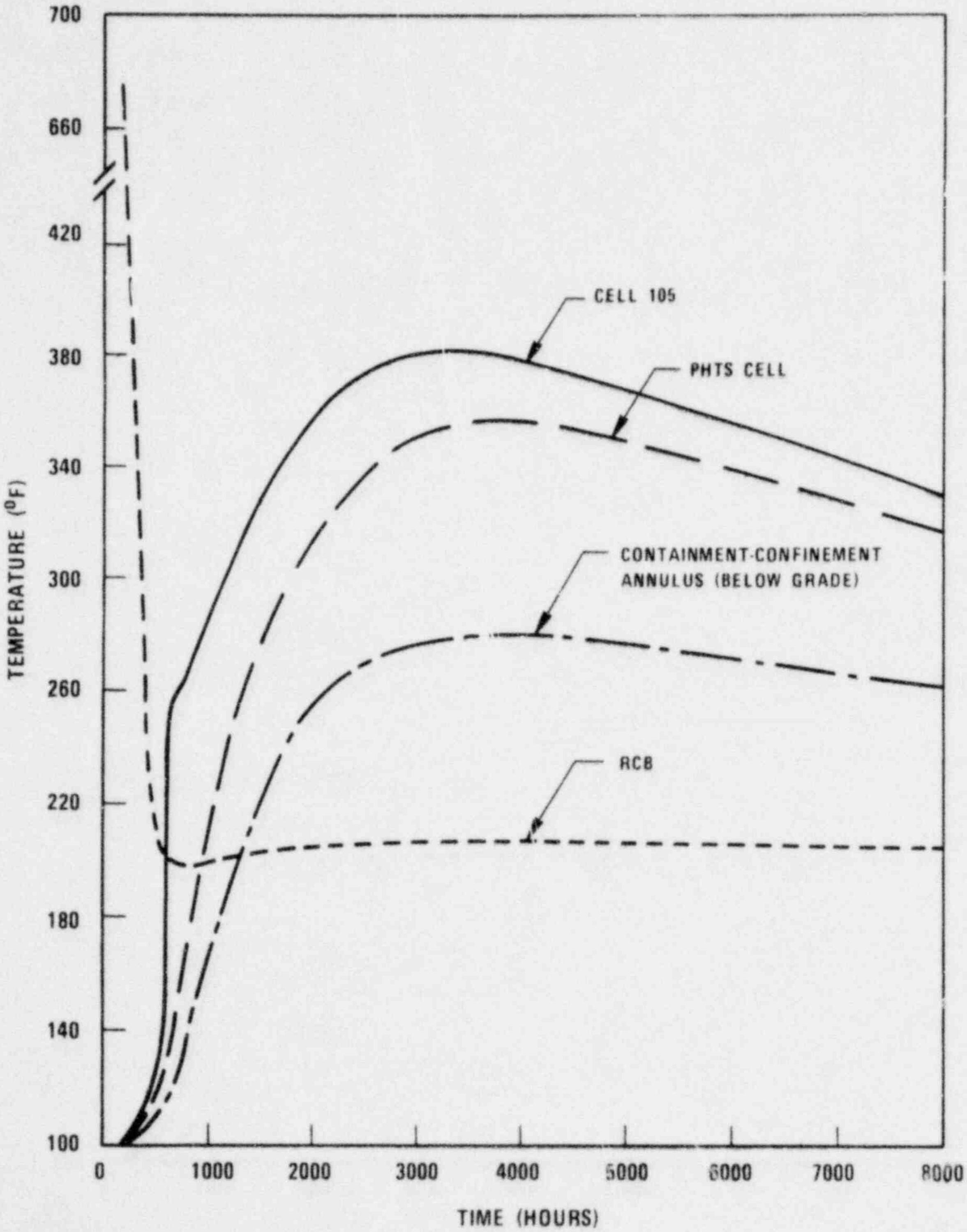

Figure 3-68 Gas Temperatures 1.0 HR · FT^2 · °F BTU Crust Resistance

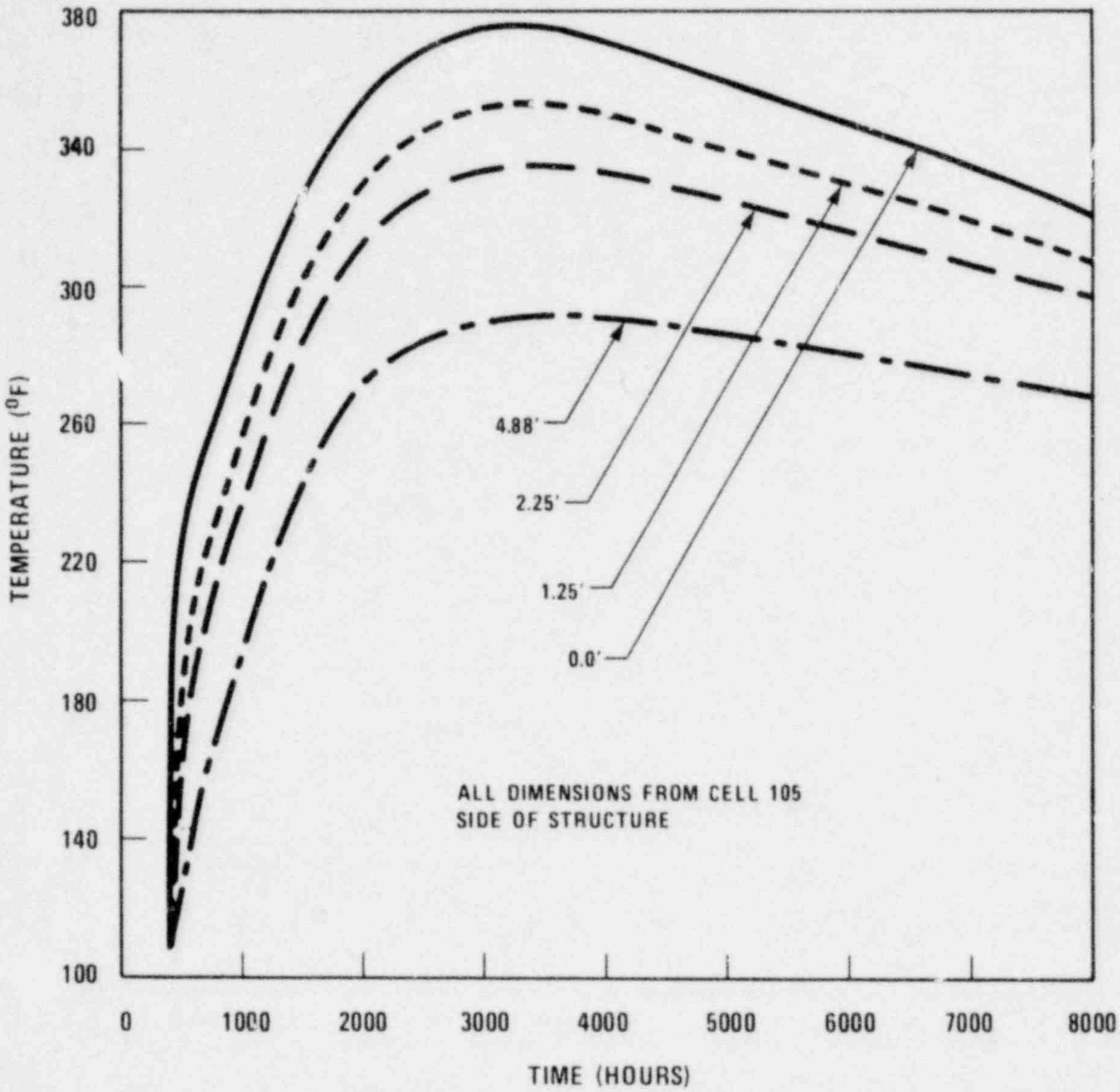

Figure 3-69. Containment Wall (Adjacent to Cell 105) Temperatures
0.10 HR • FT^2 • °F/BTU Crust Resistance

1966-101

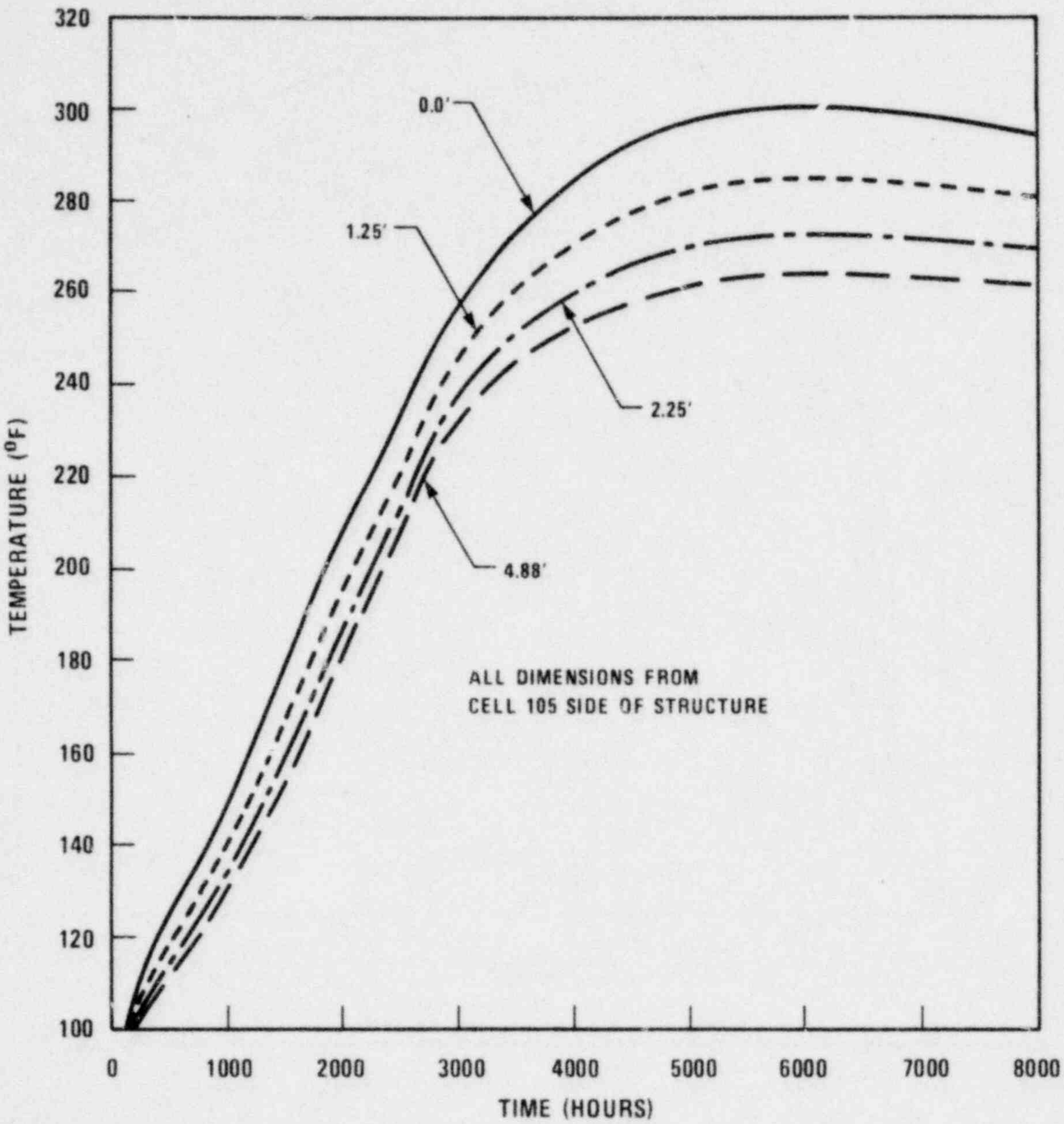

Figure 3-70. Containment Wall (Adjacent to Cell 105) Temperatures
10.0 HR • FT^2 • °F/BTU Crust Resistance

1966-102

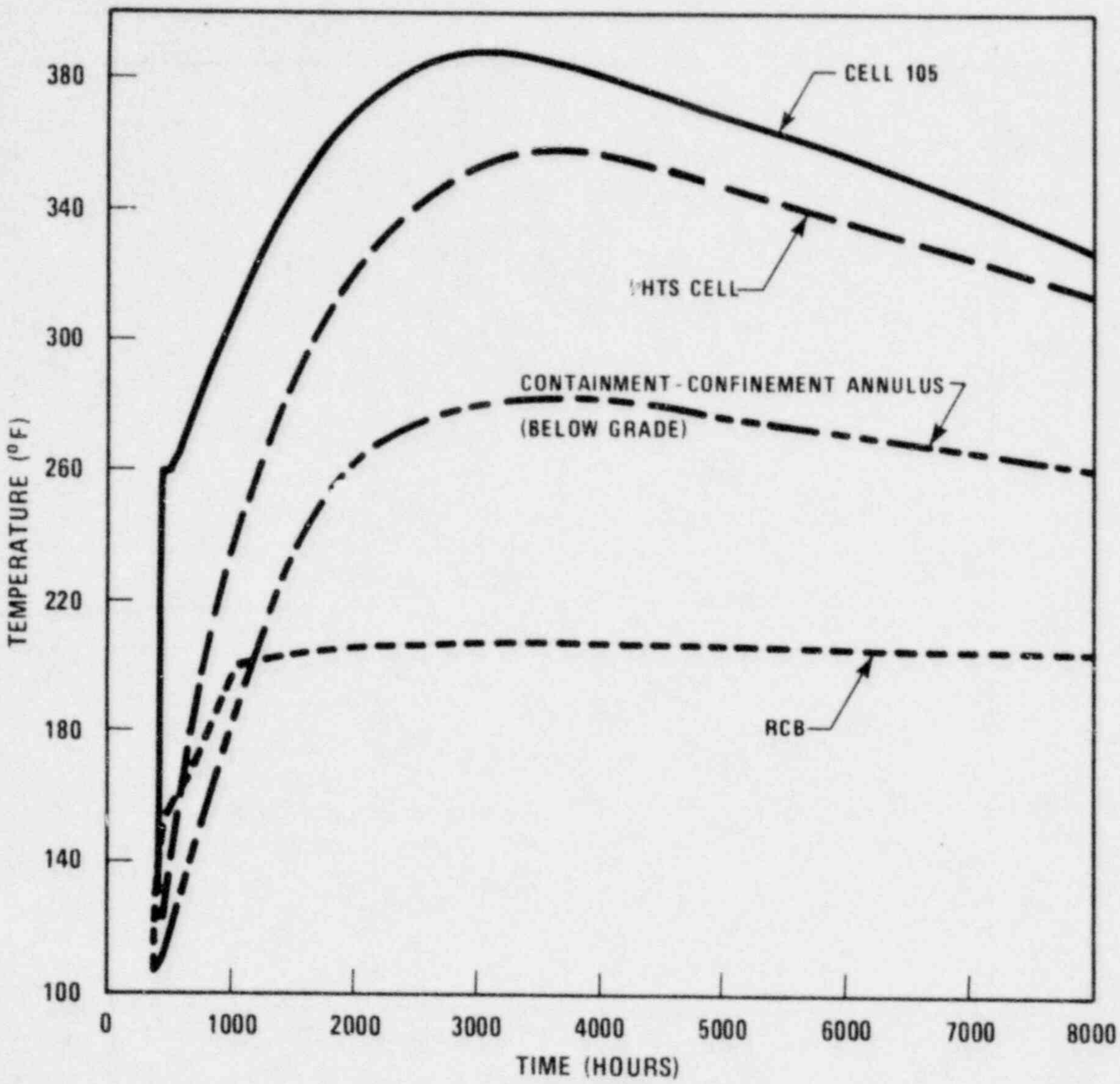

Figure 3-71. Gas Temperatures 0.10 HR • FT^2 • °F/BTU Crust Resistance

1966-103

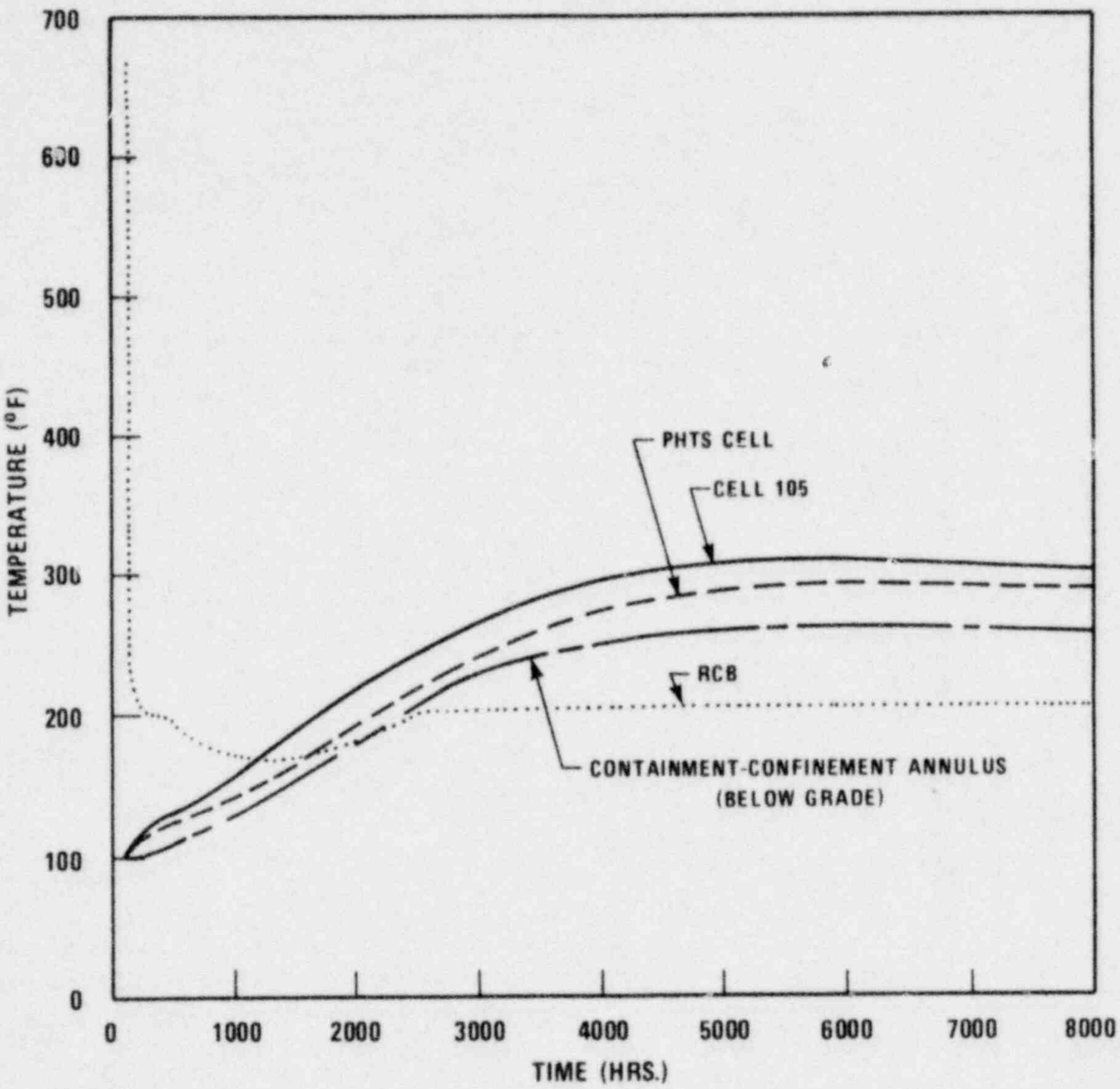

Figure 3-72. Gas Temperatures 10.0 HR • FT^2 • ^{o}F/BTU Crust Resistance

1966-104

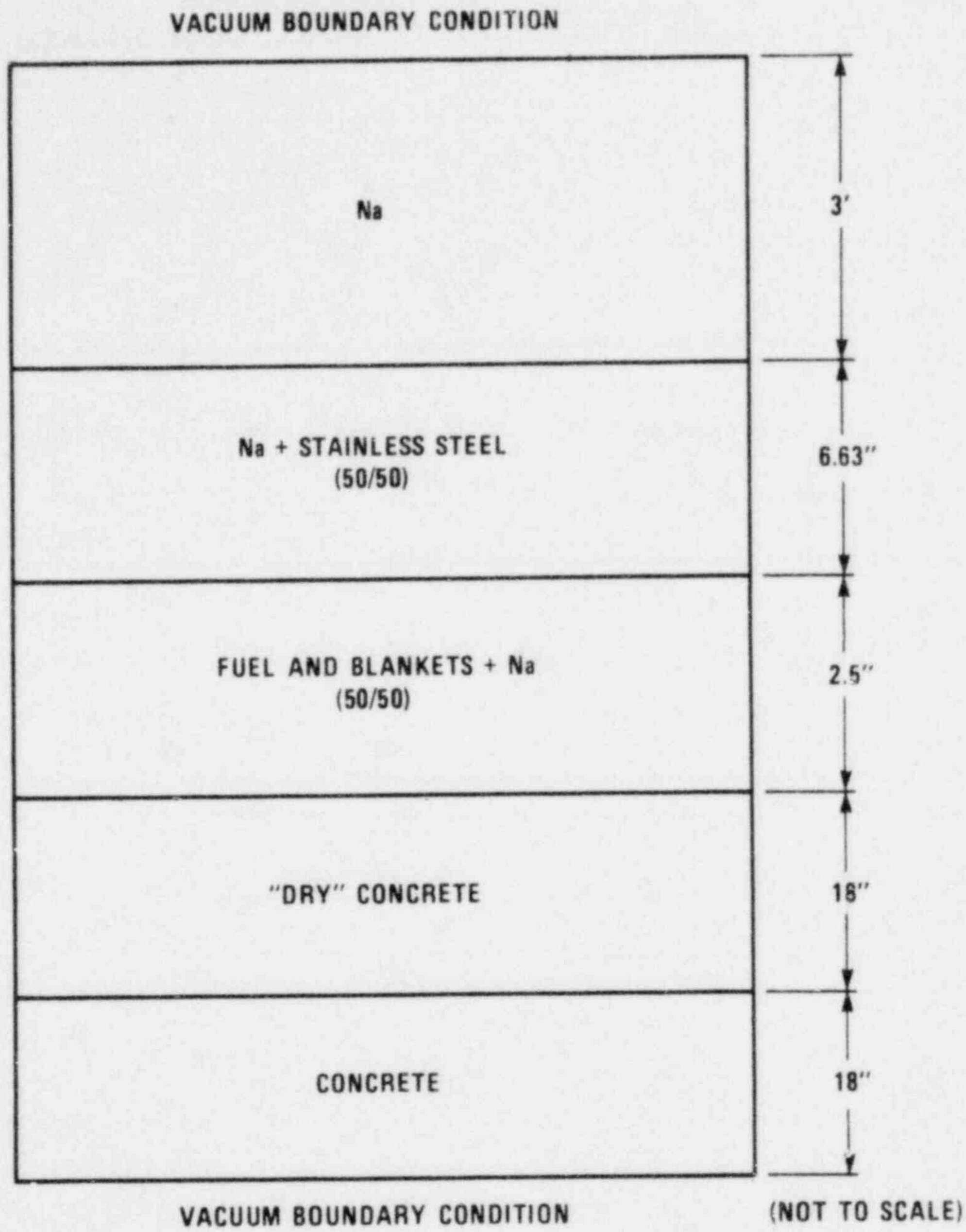

Figure 3-73. Reactor Cavity Criticality Model "Boiling" Case. One Dimensional (Slab) ANISN Geometry. No Transverse Leakage

1966-105

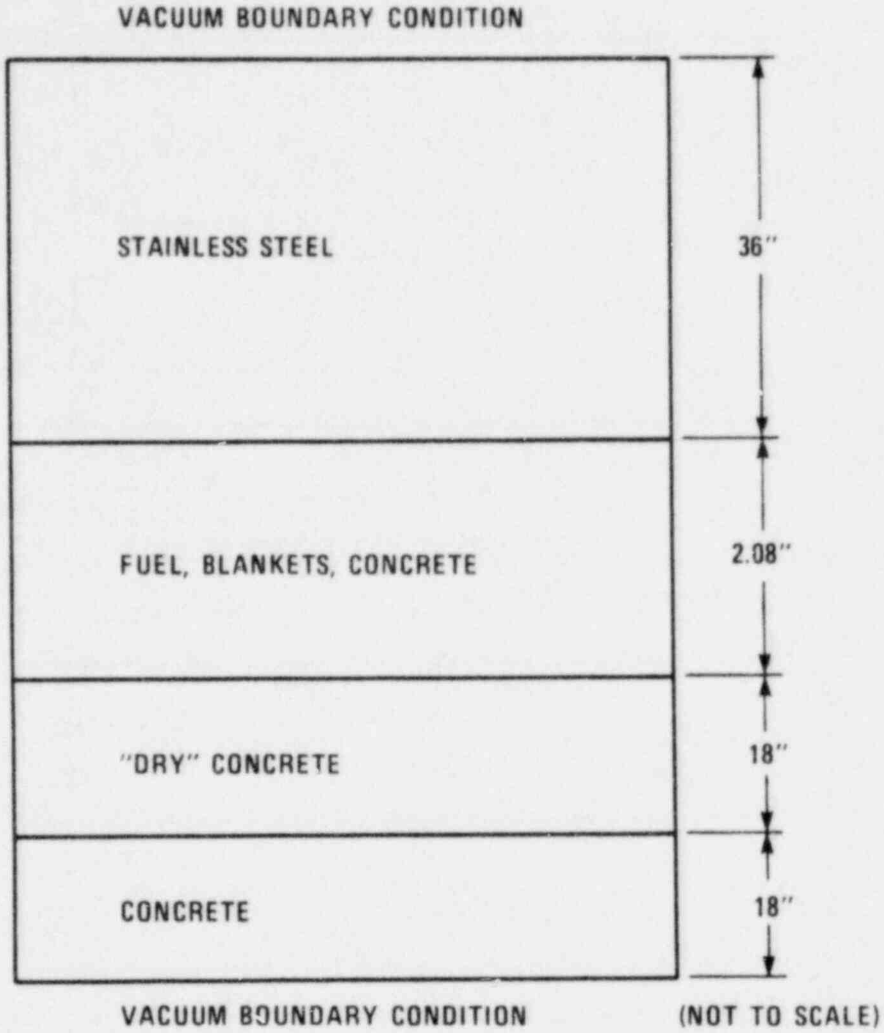

Figure 3-74 Reactor Cavity Criticality Model "Dry" Case. One Dimensional (Slab) ANISN Geometry. No Transverse Leakage

1966-106

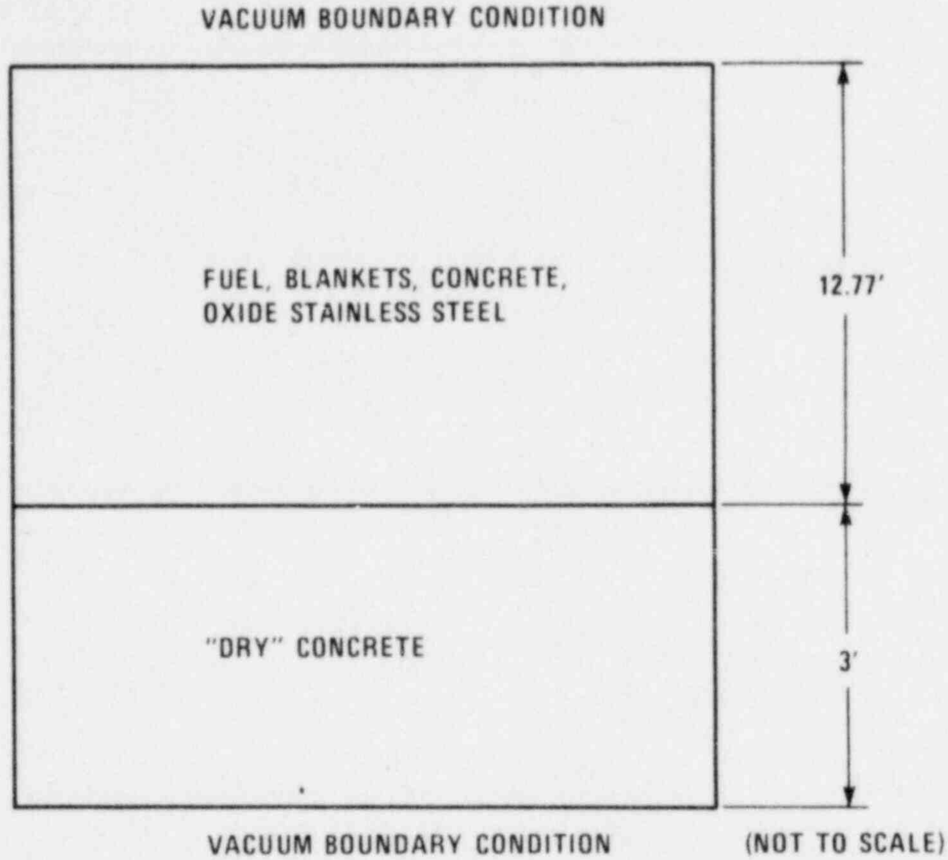

Figure 3-75 Reactor Cavity Criticality Model "Steady State" Case. One Dimensional (Slab) ANISN Geometry. No Transverse Leakage

1966-107

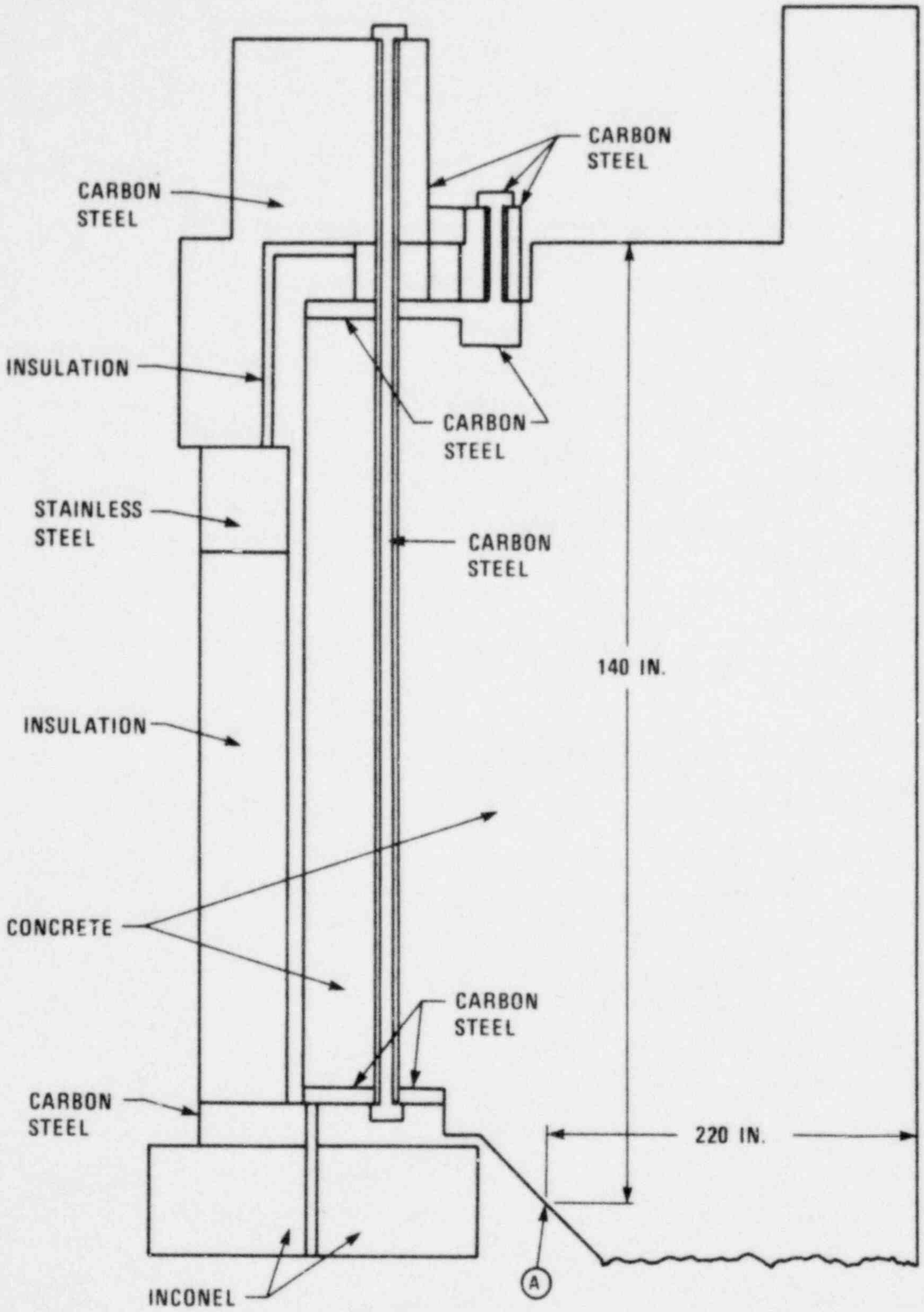

Figure 3-76. Reactor Cavity Ledge Schematic

1966-108

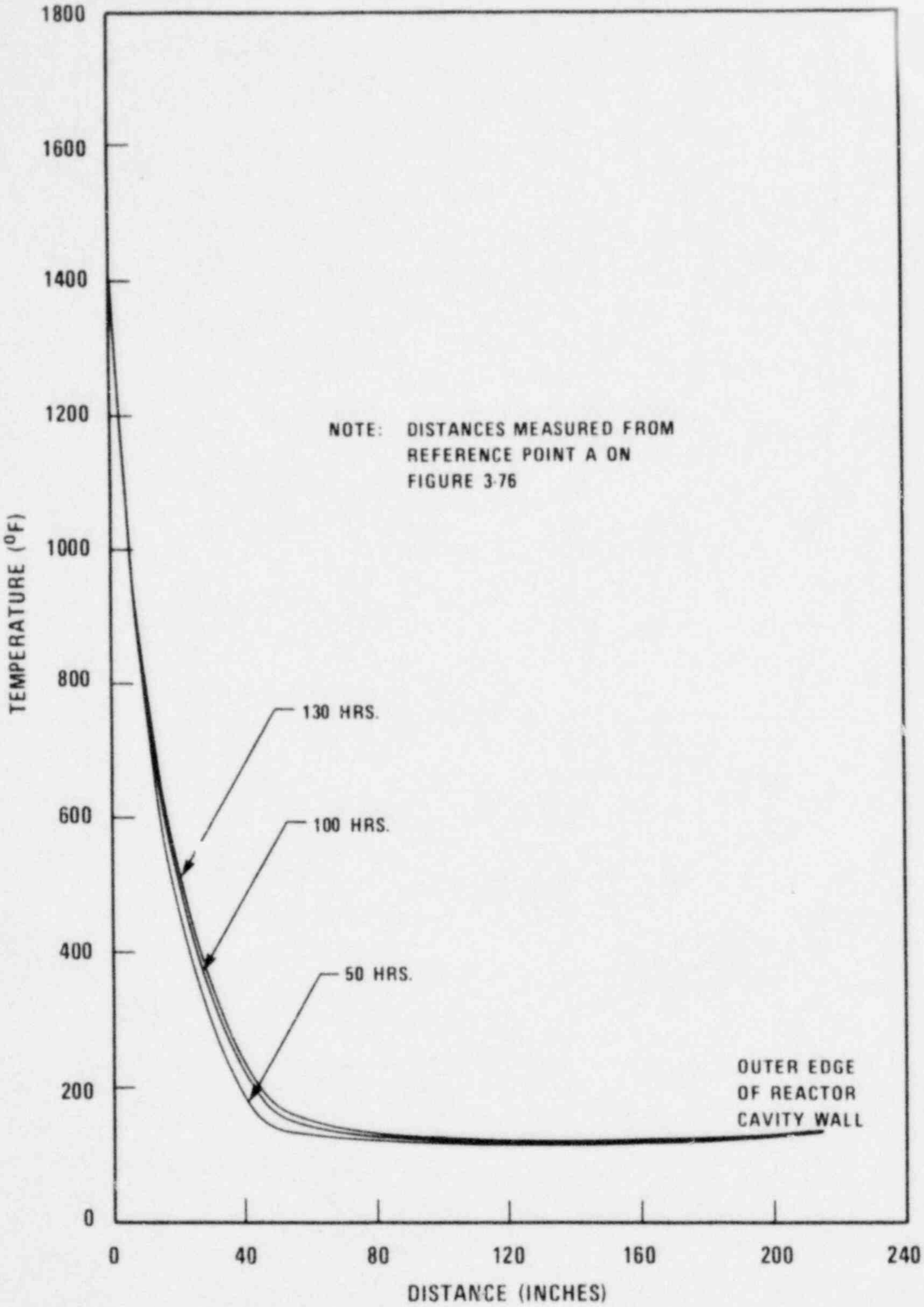

Figure 3-77. Reactor Cavity Ledge Radial Temperature Profile

1966-109

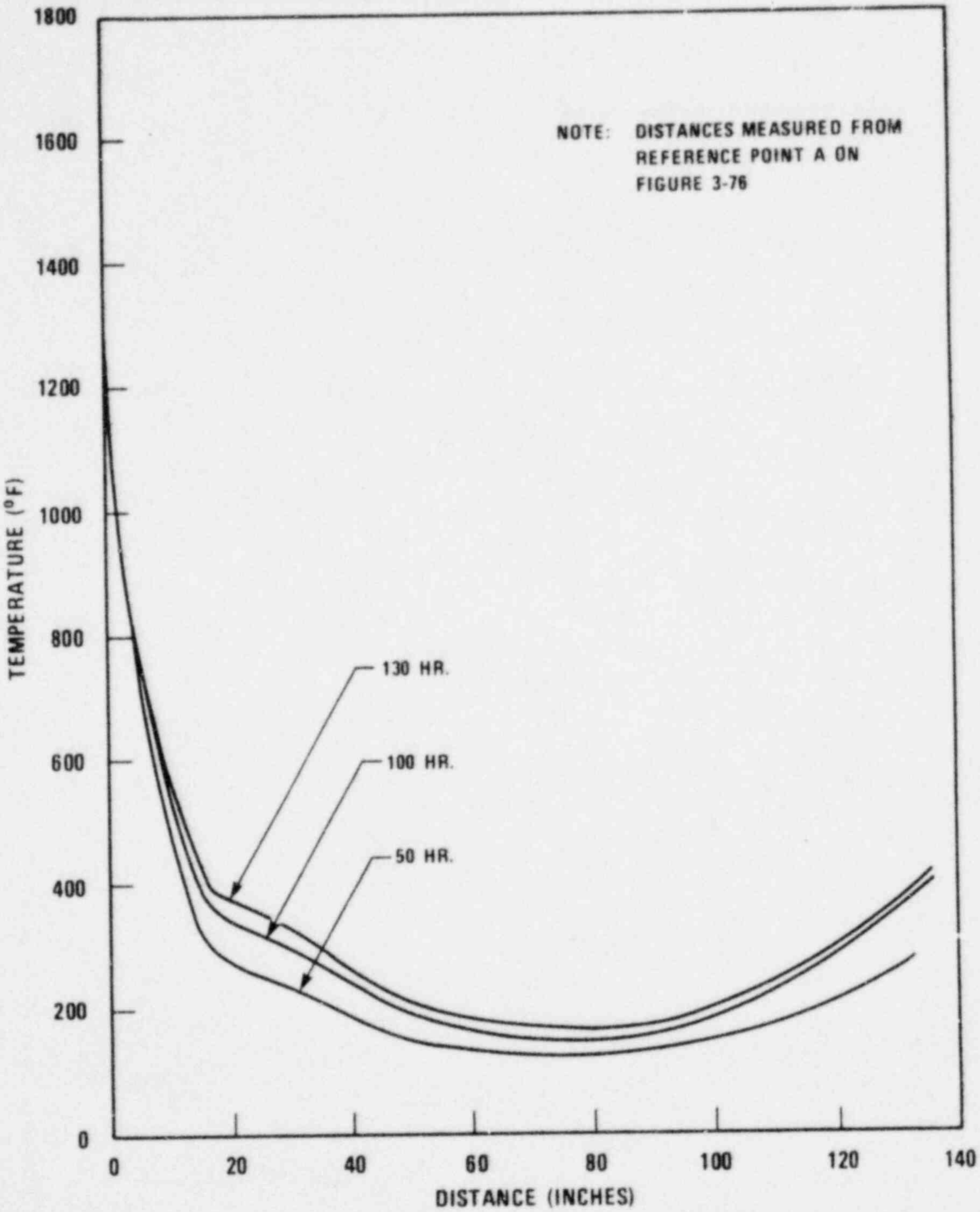

Figure 3-78. Reactor Cavity Ledge Axial Temperature Profile

1966-110

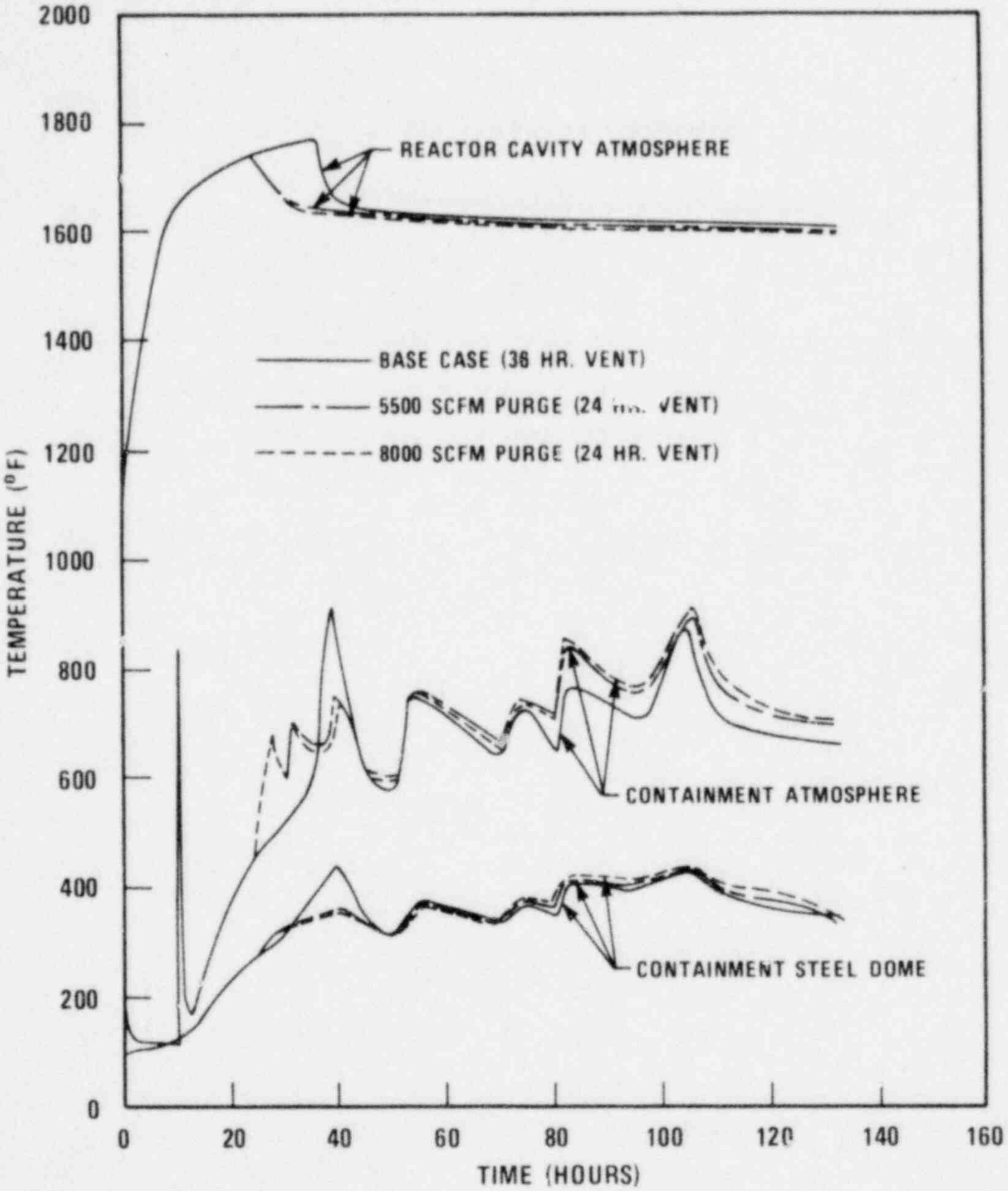

Figure 3-79. Reactor Cavity and Containment Atmosphere and Containment Steel Dome Temperatures

1966-111

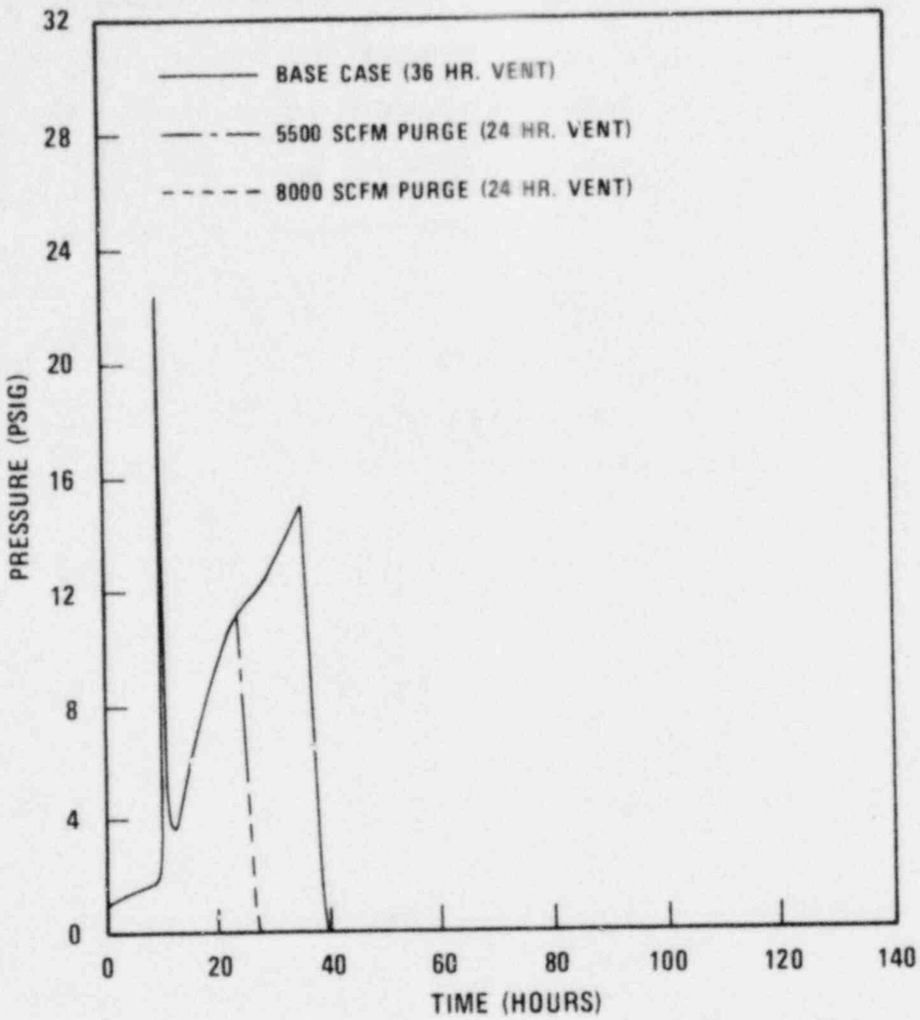

Figure 3-80. Containment Building Pressure

1966-112

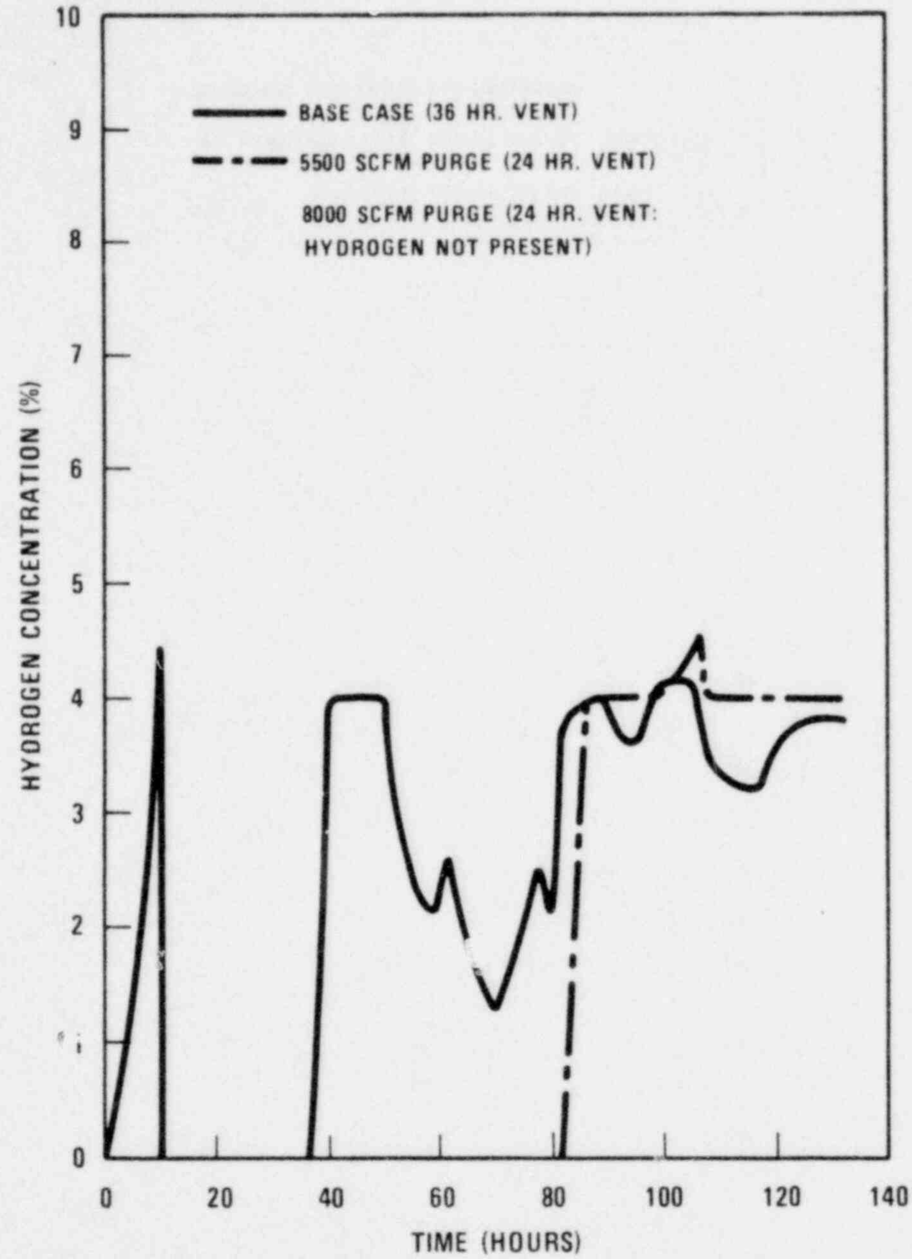

Figure 3-81. Containment Building Hydrogen Concentration

1966-113

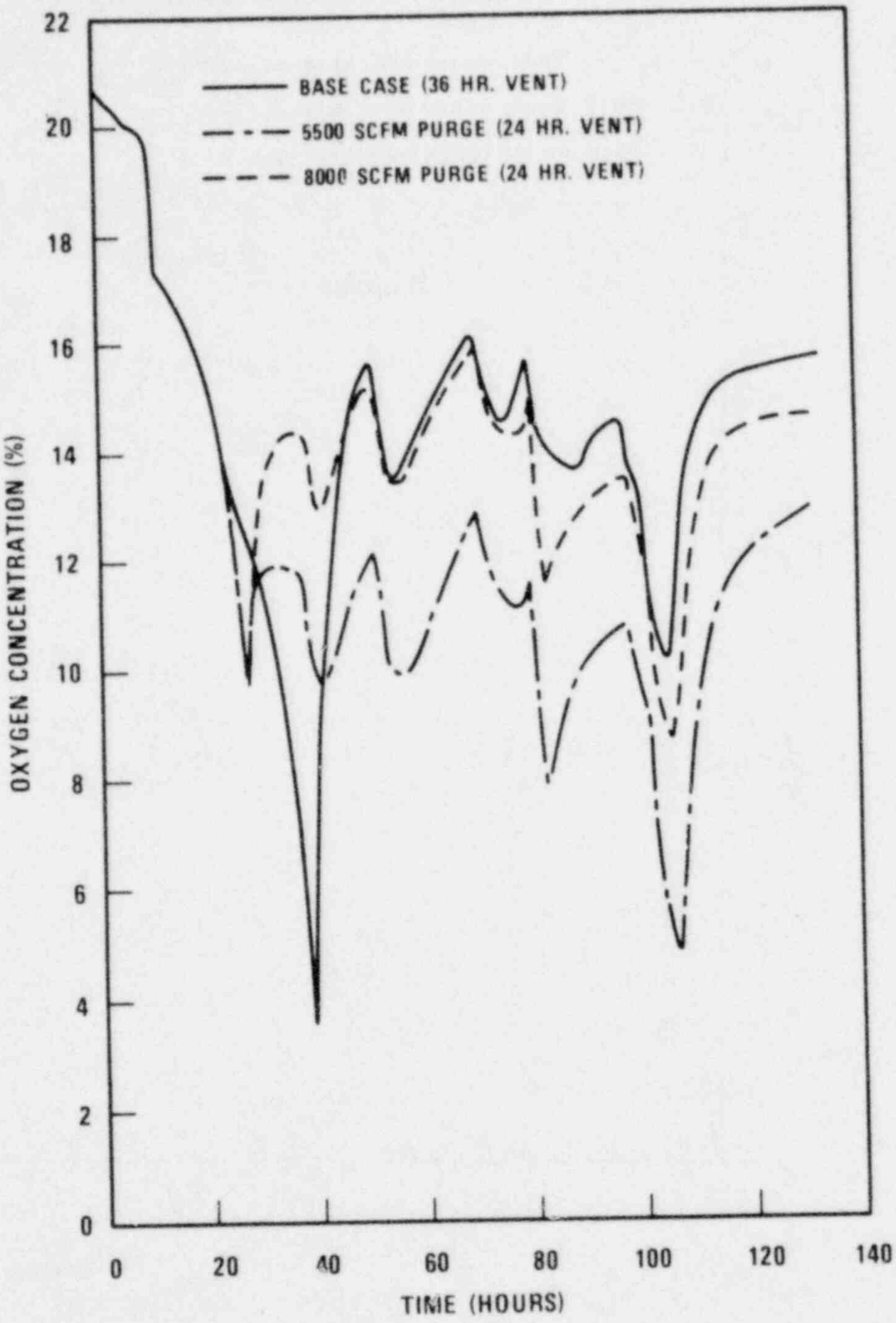

Figure 3-82. Containment Building Oxygen Concentration

1966-114

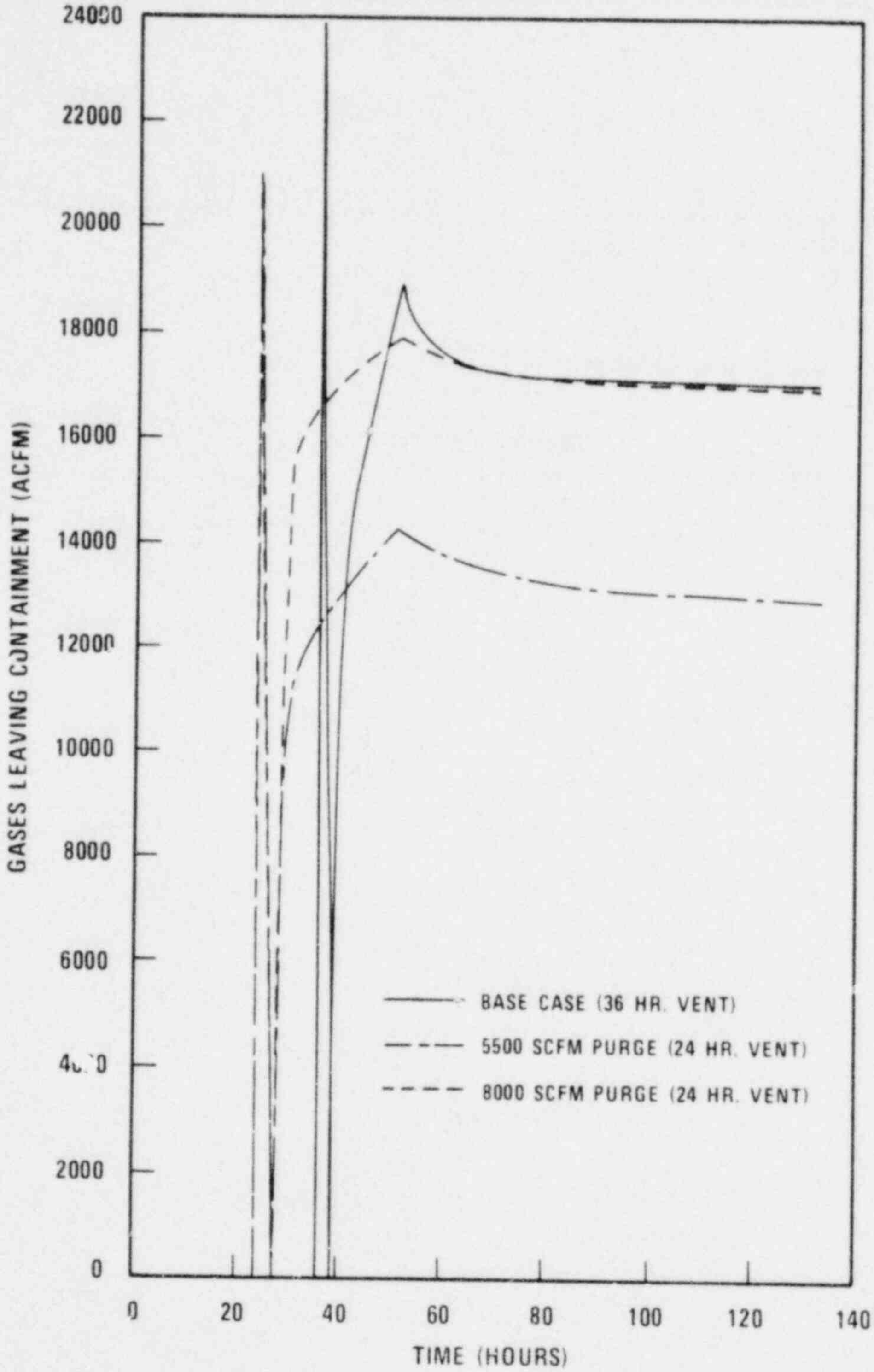

Figure 3-83. Gases Leaving Containment

1966-115

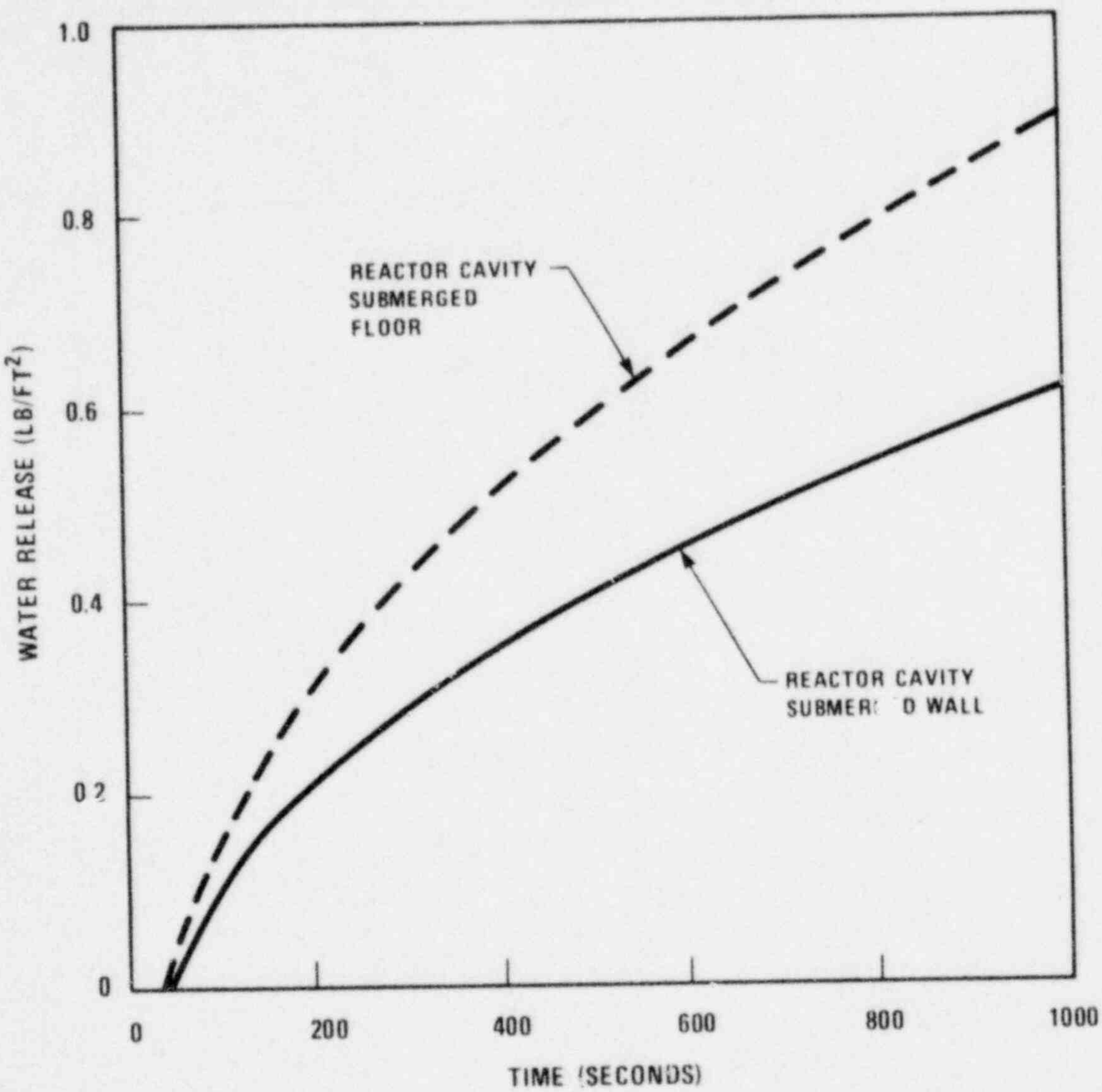

Figure 3-84. Integrated Water Release from Concrete Structures

1966-116

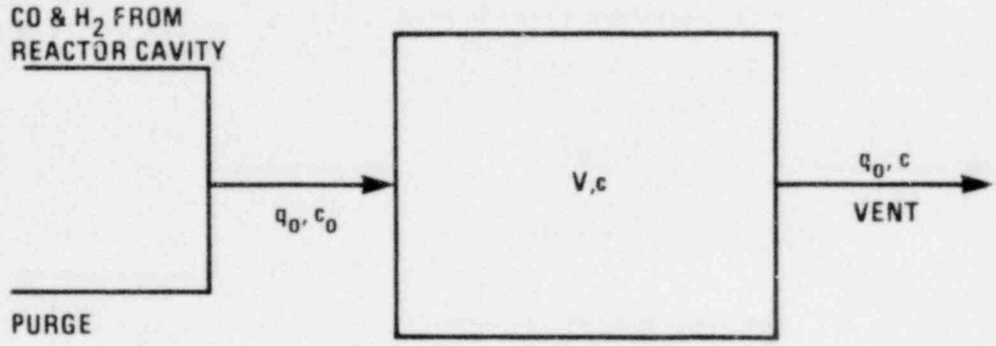

Figure 3-85. Schematic of Mixed Tank Model

1966

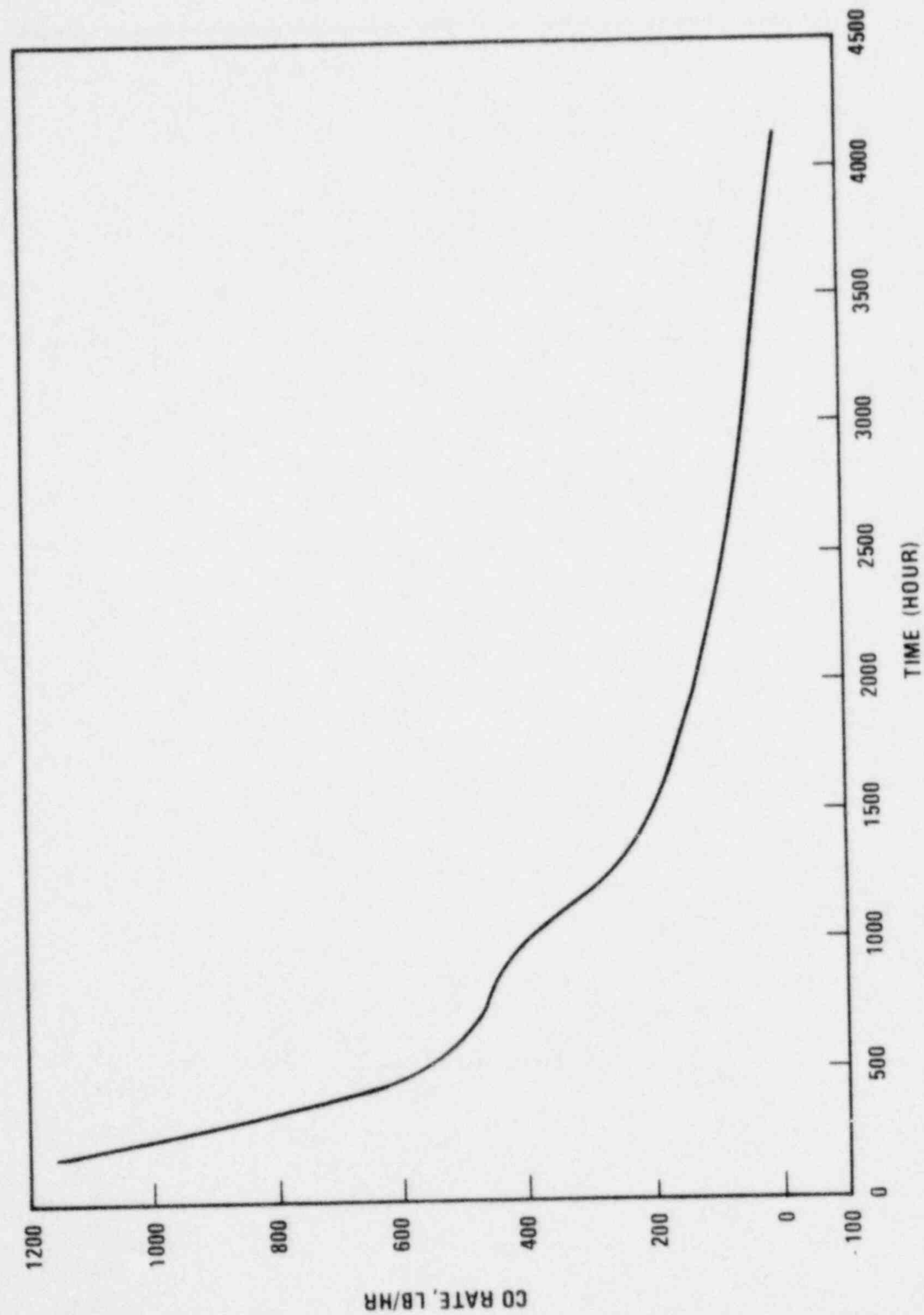

Figure 3-86. CO Ge tion Rate

1966

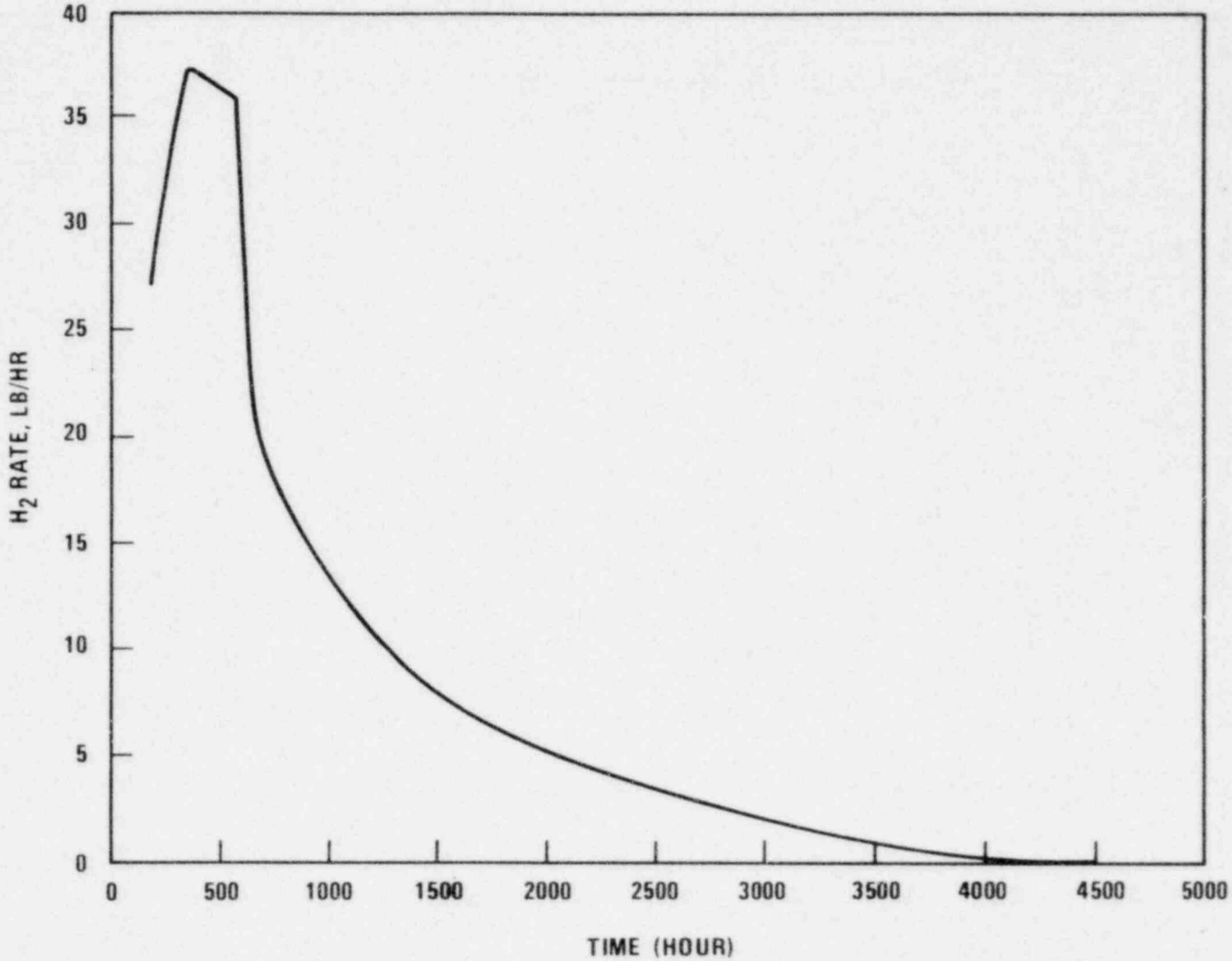

Figure 3-87. H_2 Post Boildry Generation Rate

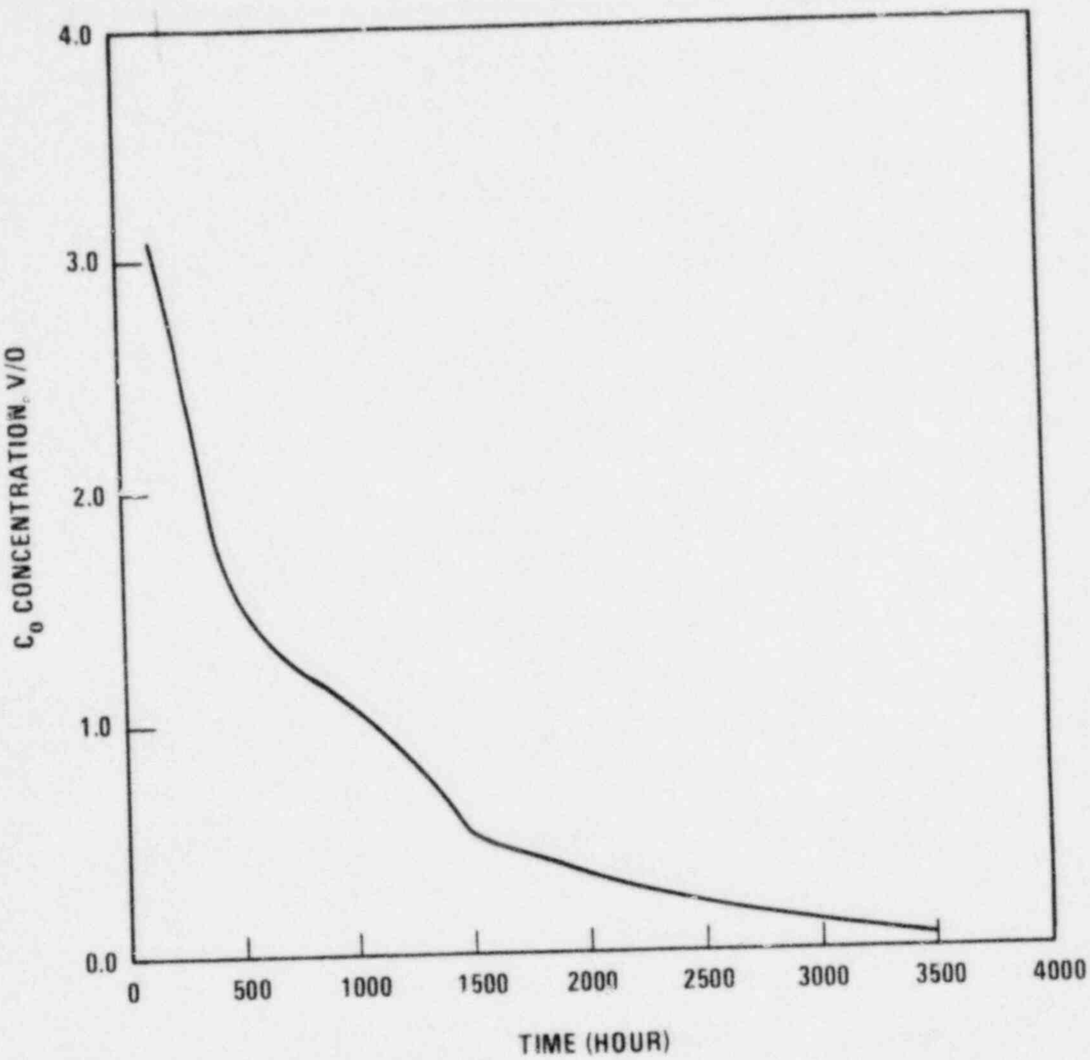

Figure 3-88. CO Concentration with Continuous Purge

1966

1966

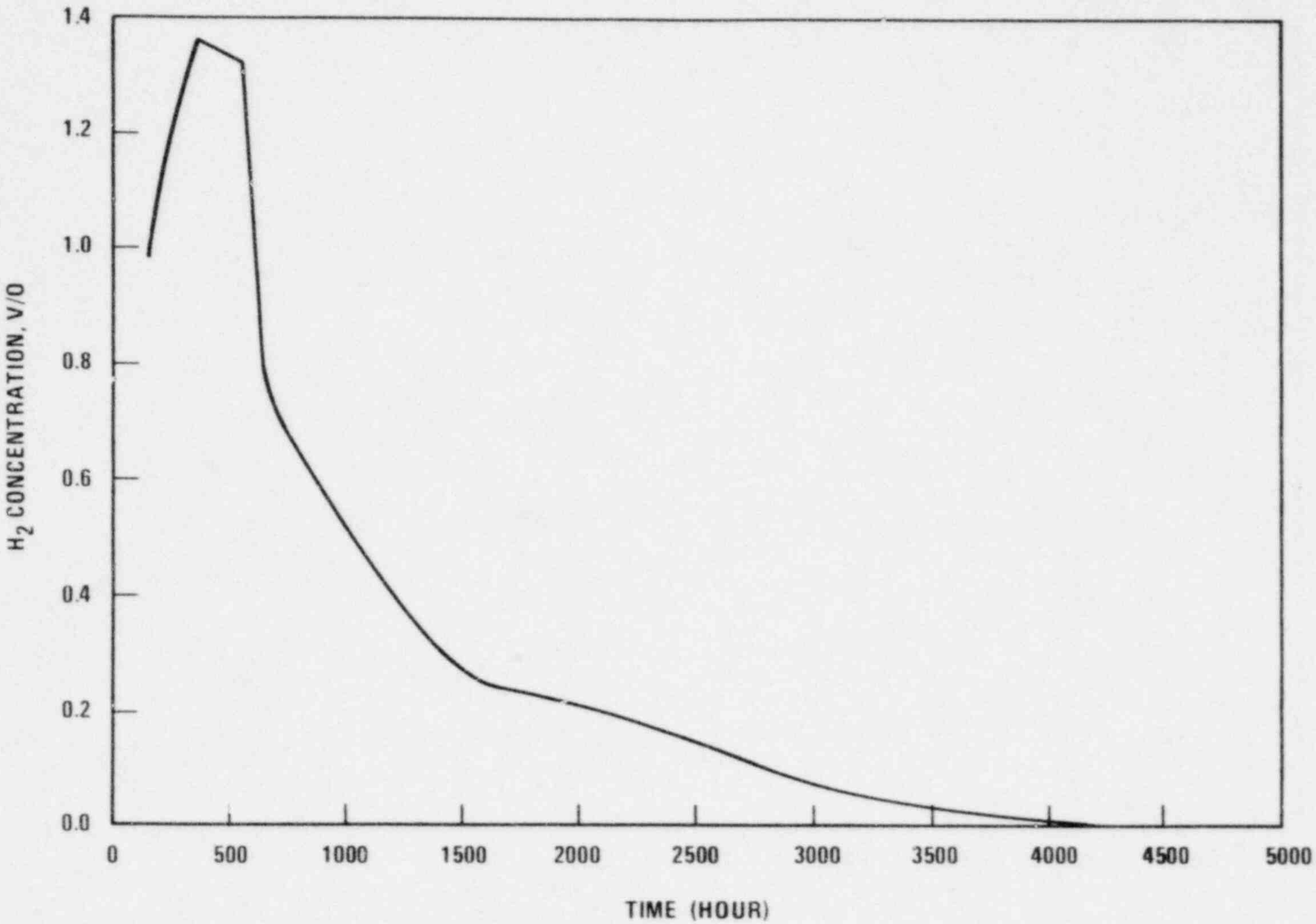

Figure 3-89. H_2 Concentration with Continuous Purge

4.0 ASSESSMENT OF RADIOLOGICAL CONSEQUENCES

This section addresses the radiological consequences associated with an HCDA. These radiological analyses are based on the design described in Section 2 and the thermal and structural analyses presented in Section 3. Section 4.1 discusses the development of the radiological source terms considered in the cases analyzed. A wide range of assumptions on materials initially released to the RCB is used. Section 4.2 provides the results of radiological calculations for atmospheric releases. Section 4.3 considers potential releases to the groundwater.

The radiological calculations are based on the homogeneous core design. Section 4.4 discusses the impact of the heterogeneous core design and concludes that the radiological consequences for the heterogeneous core are bounded by the homogeneous core results. The overall conclusions on radiological consequences are provided in Section 4.5.

4.1 HCDA RADIOLOGICAL SOURCE TERM

The radiological consequences associated with the TMBDB scenario are based on a complete core meltdown. The release of radioactive material from the reactor cavity to the RCB is considered in two parts: an initial release phase, and a sodium boil-up phase. The types and amounts of radioactivity released from the RC depend on how much damage occurs to the head as a result of the HCDA, which in turn, depends on how much energy is assumed to be released as a result of the HCDA. Four cases, representing varying degrees of immediate leakage through the head, were evaluated. The first case represents the best estimate consequence of a hypothetical core disruptive accident. Subsequent cases assume greater initial releases through the reactor vessel head.

4.1.1 Non-Energetic Core Meltdown

Initial Release Phase

The initial release phase includes materials that, because of their physical state or high volatility, are not expected to be retained to an appreciable extent in the liquid sodium. For a non-energetic meltdown, 100% of the noble gases (Kr, Xe) and 100% of the more volatile elements (Cs, Rb) are assumed to be released immediately from the molten fuel. Although no appreciable release of these nuclides to the RCB would be expected until after the penetration of the reactor vessel and guard vessel and subsequent release through the RC to RCB vent (beyond 1000 seconds), the radiological analyses conservatively are based on the release at time zero.

Boil-Up Phase

During the sodium boil-up phase the non-gaseous radioactivity trapped in the sodium pool enters the RCB atmosphere as the sodium pool boils.

One hundred percent of the halogens (principally I) and the remaining volatile elements (Se, Sb, Te) are assumed to have been released from the molten fuel, uniformly distributed in the sodium pool, and then released to the RCB atmosphere in proportion to the sodium vaporization (i.e., no credit for partitioning).

The term volatile, as used here, refers to the elements Cesium (Cs), Rubidium (Rb), Tellurium (Te), Selenium (Se), and Antimony (Sb). In addition to these five, Reference 4-1 includes Xenon (Xe), Krypton (Kr), Iodine (I), and Bromine (Br) in the category of volatile fission products. This report refers to these four additional elements as noble gases (Xe and Kr) and halogens (I and Br), but it does recognize the volatility of these four additional elements as they are also considered to be 100% released from the molten fuel. References 4-2 and 4-3 present the results of a study of existing experimental and theoretical data on the volatility of elements in molten fuel. This study generated a list of volatility factors for fission products. These factors represent conservative estimates of the percent release of elements from molten fuel. The volatility of Xe, Kr, I, and Br are given as 100%. The volatility of Cs, Rb, Te, Se, and Sb are given as 90%. The next largest volatility factor given is 4% which is significantly lower than the 90 to 100% values. Elements with factors of 4% and lower are considered in the class of non-volatiles.

It was assumed that after release from the sodium pool 100% of the volatiles will co-agglomerate with sodium based particulates. That assumption is based on two premises. First, the volatiles are in a non-gaseous state (i.e., they are either a liquid or solid aerosol) and as such are capable of agglomerating. Second, an aerosol composed of different chemical species will coagulate into single aggregates and settle as one material.

An evaluation of the first premise, based on the physical conditions associated with the release of volatile fission products from the sodium pool, residence in the RCB and release from the RCB has been made. The volatiles are assumed to be released from the sodium pool as a gas at a temperature corresponding to the temperature of burning sodium. The time required for these volatile fission products to reach thermal equilibrium with the RCB atmosphere (minutes) is short compared to the average residence time in the RCB (hours). The RCB atmosphere temperature (peak $\sim$900°F, average <750°F over the release period) is well below the boiling points of the volatile fission products and their oxides so they would condense to liquids or solids very quickly and have ample time to agglomerate before being vented. Experimental evidence supporting the second premise is reported in Reference 4-11.

The non-volatile fission products would be quenched in the sodium and form particulates. Based on measurements of particle size distributions in the ANL M-series tests, approximately 15% of the fuel could exist in particles small enough to remain suspended in the sodium pool (Reference 4-4). These suspended fuel particles would contain a proportionate amount of solid fission products.

Based on a recent survey (Reference 4-5) of experimental data on liquid carry-over from commercial evaporators and entrainment of solid particles in the vapor stream from an evaporating liquid pool, it was concluded that the decontamination factor (partitioning factor) for plutonium particles would be at least a factor of 1000.

Partitioning of solid fission products in the sodium as it vaporizes is based on the method summarized in Reference 4-6. The combined partitioning of the fuel and sodium results in a release of 1% of the total non-volatile solid fission product inventory. A more detailed evaluation of the overall solid fission product release is presented in Appendix E.

The fuel release during the sodium boilup phase is estimated by considering the two attenuating mechanisms discussed above, i.e., 15% of the fuel particulate remaining in suspension following meltdown and reparticulation, and a partition factor of 1000. This would result in approximately 300 grams of plutonium being carried into the RCB atmosphere with the boiling sodium. See Appendix E for a more detailed discussion of plutonium release from the boiling sodium.

Additional mechanisms for transporting plutonium from the reactor cavity to the RCB have been investigated and found to be negligible in comparison to the 300 grams considered above. These additional mechanisms are also discussed in Appendix E.

The initial release phase and boilup phase source terms described above for a non-energetic core meltdown are used in Case 1 in Table 4-1.

Post Boil-Dry Phase

After the sodium pool in the reactor cavity has evaporated a bare fuel/steel debris bed is left. Most of the fission product release is expected to occur prior to boil-off (Reference 4-1). Potential mechanisms for further release of fission products and plutonium from the dry debris bed are: (1) surface vaporization; (2) particle levitation; and (3) gas sparging. The first two mechanisms are considered for plutonium in Appendix E and are shown to result in a negligible contribution to the release associated with the boiling sodium pool. The volatile fission products are assumed to have been completely released. The non-volatile fission products have vapor pressures similar to or lower than the vapor pressure of fuel (Reference 4-4). Thus, like the fuel, no significant fraction of the remaining fission products would be released from the molten surface due to the first two mechanisms.

The release of fission products and plutonium due to gas sparging has also been evaluated (see Appendix E). The results of this evaluation show that those products whose releases are enhanced the most by sparging are the more volatile products which the analysis already considers to be totally released. The release of the other less volatile products by sparging is accounted for by the 1% release fraction assigned to the non-volatile fission products in the boil-up phase source term. Plutonium release from the molten pool by sparging could be on the order of 13 Kg over a several month period and this has been assumed to be released to the RCB. The evaluation of this additional plutonium source is discussed in Appendix E. Assuming a 99% filter efficiency and taking credit for aerosol fallout and plate-out, about 45 grams of plutonium could be released to the atmosphere over a several month period beginning at sodium boildry ($\sim$ 5 days) after the start of the accident.

4.1.2 Energetic HCDA

Initial Release Phase

The case described in Section 4.1.1 is based on the expected consequence of a hypothetical core disruptive accident; namely a non-energetic condition and consequently, no significant immediate release of sodium or non-volatile fission products through the reactor vessel head. Several variations of the expected case were analyzed using successively more pessimistic assumptions on the initial releases through the reactor vessel head.

The second case analyzed (Case 2 in Table 4-1) is similar to the expected case (Case 1) except that an energetic hypothetical core disruptive accident is assumed. The available work energy, if the fuel vapor were expanded to one atmosphere, is 661 MJ. The fraction of the core inventory of fuel which is vaporized and transported to the cover gas region as a vapor is conservatively based on a single hemispherical bubble model which takes no credit for heat losses from the bubble while rising through the sodium pool and core structure (Reference 4-3). The results of this analysis indicate that 7.3% of the core fuel inventory could reach the cover gas space in the form of vapor. Since the reactor vessel, head and primary system are designed to retain their structural integrity for the dynamic loadings corresponding to the 661 MJ condition, the immediate releases would still be limited. To represent this condition, an immediate release of 1000 pounds of sodium and gas leak rate of 1000 standard cubic centimeters per second for the first 1000 seconds are used.

The combination of the 1000 scc/sec leak rate and aerosol depletion in the cover gas region would limit the amount of fuel and fission products in the initial release phase to 0.026% of the core inventory. This fraction was assumed to be released at time zero in Case 2 described in Table 4-1.

The two additional cases evaluated (Cases 3 and 4) arbitrarily employed progressively larger initial releases of fuel, sodium, and the less volatile fission products. These cases were useful to examine the sensitivity of the consequences to releases that are much larger than expected.

Boil-Up Phase

The release associated with the sodium vapor phase for Case 2 is similar to that of Case 1. As Cases 3 and 4 were considered more severe and released more fuel and fission products in the initial phase, correspondingly lesser amounts of these products would be present in the sodium boil-up phase. The source terms for these four hypothetical accident scenarios are summarized in Table 4-1.

Fission product and activation product activity levels are based on the end-of-equilibrium-cycle core inventory identified in Table 12.1-32 of the PSAR. The beginning-of-equilibrium-cycle plutonium inventory was used because it results in a slightly higher dose value than for end-of-equilibrium-cycle plutonium.

Post Boil-Dry Phase

The same considerations apply here as discussed in Section 4.1.1.

4.2 RADIOLOGICAL DOSES FROM ATMOSPHERIC RELEASES

4.2.1 Methods and Data Base

Aerosol Depletion

The radiological release from the RCB to the environment depends on the concentration of suspended radioactivity in the RCB and the RCB vent rate. The RCB vent rate (which includes the effect of purging) is varied as required to maintain the hydrogen concentration at an acceptable level (<6%) (see Section 3.2.2). The suspended concentration of radioactivity in the RCB is a function of the source generation rate, RCB vent rate, and aerosol deposition rate. The HAA-3 computer code calculates the time dependent suspended aerosol concentration taking these interacting effects into account. For a more detailed discussion of the HAA-3 code and its basis see Appendix D. The rate of aerosol depletion calculated by HAA-3 is input to the COMRADEX code.

COMRADEX Radiological Analysis

COMRADEX computes the time-rate of release of radioactivity from the RCB. The COMRADEX calculations include the effects of radioactivity decay and aerosol depletion within containment. COMRADEX also determines, as a function of time and downwind location, doses resulting from direct gamma shine, inhalation of radioactive material, and cloud submersion taking into account atmospheric dispersion.

Meteorology

The atmospheric dispersion parameters (X/Q's) used for the TMBDB evaluation are provided in Table 4-2. These dispersion factors are based on the "50% cumulative frequency" (atmospheric dispersion more favorable 50% of the time) X/Q values (Reference 4-7).

Dose Factors

Dose conversion factors (rem/ci) used in the COMRADEX code to calculate specific organ doses were taken from References 4-8 and 4-9 where possible. Factors for isotopes not given in these References are from Reference 4-10.

Containment Modeling

The time dependent radiological source term is released directly to the RCB. The release rate from the RCB is that calculated by the CACECO code. For the first 36 hours of the scenario the RCB atmosphere leaks at a low rate (based on 0.1%/day at 10 psig) to the annulus filter system (described in Section 6.2.5 of the PSAR). During this 36 hour period unfiltered bypass leakage at the rate of 1% of the filtered leakage is considered. After 36 hours the RCB is vented and subsequently purged (Figures 3-13 and 3-14) to maintain the hydrogen concentration at an acceptable level. During this phase filtering is by the TMBDB filter system which is designed for the higher vent rates. The efficiency of the TMBDB filter system is 99% for solid fission products and fuel and 97% for condensible fission products (halogens, Se, and Sb). Noble gases are assumed to pass through the filter system unattenuated. (There is some question of the effectiveness of the filter system to remove Na_2CO_3 and the fission products which may be tied up with this aerosol component. This subject is addressed in Appendix E.) Because the bypass leakage rate is expected to be so small relative t the high vent rate after 36 hours, the bypass leakage is not expected to make a significant contribution to the released radioactivity and is therefore not considered beyond 36 hours.

The direct gamma contribution to the whole body dose considers the shielding provided by the steel RCB and the concrete confinement building.

Figure 4-1 shows the dose rate inside the reactor containment building for Case 2.

4.2.2 Radiological Doses

Using the methods described in Section 4.2.1 the radiological doses at the Exclusion Boundary (0.42 miles) and the Low Population Zone (2.5 miles) were calculated for the four different source terms described in Section 4.1. These doses are summarized in Table 4-3. The 30 day LPZ doses include the plutonium released after boil-dry to 30 days. Plutonium release beyond 30 days could result in an additional 10 rem to the LPZ bone dose. Control room doses were provided in Section 2.2.15.

The dose consequences of the four cases that assumed varying degrees of severity of the hypothetical accident are all quite low for accidents beyond the design base. For example, the maximum whole body dose is predicted to be about 3 rem and the maximum thyroid dose would be about 100 rem. Bone doses are about 30 rem.

The results also show that the consequences are not strongly sensitive to the degree of severity of the initial release source term. As the initial release to the RCB increases, the rate of aerosol depletion increases which acts as an inverse feedback to limit the release from the RCB. Consequently, so long as the initial release does not result in failure of the containment barrier, the radiological consequences are relatively insensitive to the magnitude of the release. For the full range of releases considered in Cases 1 through 4, the RCB pressure and temperatures would not result in failure of the containment barrier.

Table 4-4 compares the consequences, in terms of curies released, of a comparable scenario (core meltdown with enough containment leakage to prevent containment failure by overpressure) for CRBRP and light water reactors (LWR). The CRBRP values are for the worst of the above four cases. The LWR releases are for the accident scenarios PWR-6 and BWR-4 described in Section 2 of Appendix VI of WASH-1400. This comparison shows the atmospheric releases for CRBRP to be comparable to those for LWRs. Figure 4-2 shows the integrated radioactivity released to the environment for Case 2.

4.3 GROUNDWATER CONSIDERATIONS

The radiological consequences associated with the release of radioactive material to the groundwater following a hypothetical core disruptive accident (HCDA) have also been evaluated and the consequences are compared to those determined for typical light water reactors.

As noted in Section 3.2.1 of this report, following an HCDA that results in penetration of the reactor vessel and guard vessel, the fuel, fission products and sodium would spread on the reactor cavity floor. The sodium would heat to its boiling temperature as a result of the decay heat in the fuel and fission products and subsequently boil. Following boiloff of the sodium (between 100 and 150 hours), the residual decay heat could cause fuel to melt and penetrate into the concrete in the floor of the reactor cavity. Under these conditions it is not certain whether the reactor containment steel liner (located beneath 11 feet of concrete) would be penetrated. If it is penetrated, the meltfront could proceed some distance into the 15 feet of concrete located beneath the reactor containment building steel liner. Although calculations indicate that complete penetration of this concrete is unlikely (Section 3.2.3), for purposes of the following analysis, complete penetration is assumed to occur. This assumption provides a mechanism to assess the radiological impact on the groundwater in a very conservative manner. The following analyses are similar to those performed for the Reactor Safety Study and reported in Appendix VII of WASH-1400. The primary exceptions are that:

1. at melt-through, no water is available from the reactor containment vessel to add to the groundwater, and

2. site specific data on the flow system were taken from the Hydrology and Geology Sections of the CRBRP Preliminary Safety Analysis Report (Sections 2.4 and 2.5).

The groundwater at the CRBRP site has been measured to flow toward the Clinch River at about 57 ft/year with a gradient of about 0.007 feet/foot. At this rate the travel time from the CRBRP plant to the Clinch River, 1600 feet away, is 28 years. The flow system for the transport of radioactivity from the melt-through point to the Clinch River was defined as a rectangular-horizontal column 50 feet wide by 60 feet high by 1600 feet long. This flow system is conservative since it neglects dispersion or flow system spreading which would reduce the effluent concentrations at the end of the 1600 foot length.

Heat balance calculations presented in WASH-1400 indicate that for about one year after the melt-through, the heat flow from the molten mass is sufficient to dry out the surrounding ground which effectively insulates the groundwater from the debris. After the groundwater makes contact with the debris, radioactivity would begin to be leached out. Thus before the groundwater becomes contaminated the radioactivity in the debris would undergo one year of decay. During the 28 year transit to the Clinch River radioactive decay would further reduce the activity level. Additional reduction in the activity level of the groundwater would take place before it reaches the river due to sorption of the dissolved radionuclides in the soil material of the groundwater system.

The results of this analysis are presented in Table 4-5, which gives the peak effluent concentration of the most significant isotopes at the entry point to the Clinch River. It also gives the corresponding values for a typical LWR as presented in WASH-1400, and the maximum permissible concentrations (MPC) of those isotopes in effluent water during normal operation, as given in 10CFR20 Appendix B, Table II. The results show the peak effluent concentrations for CRBRP following an HCDA to be lower than the predicted concentrations following an assumed LWR meltdown and even lower than the 10CFR20 MPC values (applied to routine releases).

It is concluded that groundwater releases would not contribute significantly to the overall environmental consequences of accidents beyond the design base.

4.4 HETEROGENEOUS CORE CONSIDERATIONS

The TMBDB radiological analyses in the previous sections are based on a homogeneous reactor core configuration. The dose consequences of an HCDA involving the CRBRP core (heterogeneous) are estimated to be less than those currently predicted for the homogeneous core. Table 4-6 provides the plutonium inventory (in kg and curies) for the homogeneous and heterogeneous cores. Although the heterogeneous core contains more kilograms of plutonium, the change in isotopic content results in less kilograms of the nuclides Pu-238 and Pu-241, which are radiologically most important. The heterogeneous core inventory of Pu-238 is a factor of 5 less than the homogeneous core inventory; the Pu-241 inventory is about a factor of 4 less. When the curies of each plutonium isotope are weighted by the dose conversion factors of Reference 4-9, and the results are added, the heterogeneous core plutonium has less radiological impact than the homogeneous core plutonium. Since the fission product inventories are approximately the same in the two cores, differences in dose consequences depend on the contribution of plutonium to the particular organ dose being considered. In general, plutonium contributes most to the bone dose, has a minor role in lung and whole body doses, and has no effect on thyroid doses. In particular, the 2 hour bone doses for cases in which the initial fuel release is greater than or equal to 1% and the 30 day bone doses for all cases (because of the major contribution of sparged plutonium to the 30 day bone dose) will decrease by approximately 50% for the heterogeneous core configuration. This is due to the high degree of dependence of the bone dose on the Pu in the reactor fuel. In general, the lung and whole body doses will decrease by 5-10% due to a lesser dependence on fuel release; these doses are primarily dependent on solid fission product release and noble gas release, respectively. The thyroid dose is expected to remain essentially the same, since halogen release (mostly I) will be the same in both core configurations.

Therefore, the radiological consequences for the heterogeneous core are bounded by the consequences for the homogeneous core presented herein.

4.5 CONCLUSIONS ON RADIOLOGICAL CONSEQUENCES

Radiological releases associated with the TMBDB accident scenario have been assessed. The consequences of both atmospheric releases and groundwater releases were considered. To examine the sensitivity of the atmospheric consequences to larger releases than expected, several cases of varying degrees of severity were evaluated. The results of these analyses show the radiological dose consequences to be acceptably low and insensitive to the initial release phase over the range of releases considered.

Groundwater contamination levels resulting from reactor cavity melt-through were shown to be lower than the predicted concentrations following an assumed LWR meltdown and even lower than the 10CFR20 MPC values for routine releases.

The radiological consequences reported herein were based on the homogeneous core. It has been shown that these results bound the consequences for the heterogeneous core.

It is concluded that the radiological consequences of a hypothetical core disruptive accident would be acceptable considering the highly improbable nature of the conditions analyzed.

4.6 REFERENCES

4-1. "Reactor Safety Study - An Assessment of Accident Risks in U.S. Commercial Nuclear Power Plants, Appendix VII, Release of Radioactivity in Reactor Accidents," WASH-1400, Appendix VII, October 1975.

4-2. "Radiological Assessment Models, Fourth Quarterly Report, June-August 1975," GEAP-14034-4, October 1975. (Availability: U.S. DOE Technical Information Center).

4-3. "Radiological Assessment Models, Fifth Quarterly Report, September-November 1975," GEAP-14034-5, December 1975. (Availability: U.S. DOE Technical Information Center).

4-4. L. Baker, Jr., et al., "Post Accident Heat Removal Technology," ANL/RAS 74-12, July 1974. (Availability: U.S. DOE Technical Information Center).

4-5. "Radiological Assessment Models, Tenth Quarterly Report, December 1976-February 1977," GEFR-14034-10, March 1977. (Availability: U.S. DOE Technical Information Center).

4-6. "Radiological Assessment Models, Ninth Quarterly Report, September-November 1976" GEAP-14034-9, December 1976. (Availability: U.S. DOE Technical Information Center).

4-7. "Clinch River Breeder Reactor Plant Environmental Report, Amendment VIII, Section 2.6.6.1, Calculations," Docket 50-537, U.S. Nuclear Regulatory Commission, Washington, D.C., February 1977.

4-8. U.S. Nuclear Regulatory Commission, "Calculation of Annual Doses to Man from Routine Releases of Reactor Effluents for the Purpose of Evaluating Compliance with 10CFR Part 50, Appendix I," Regulatory Guide 1.109, Revision 1, October 1977.

4-9. G. R. Hoenes and J. K. Soldat, "Age-Specific Radiation Dose Commitment Factors for a One-Year Chronic Intake," NUREG-0172, November 1977.

4-10. E. R. Specht, "Internal Dose Factors for COMRADEX-II," TI-001-130-051, February 24, 1975.

4-11. BNWL-1350, "FFTF Site Safety Analysis, Appendix D - Aerosol Behavior Analysis," April 1, 1970.

TABLE 4-1

CORE SOURCE TERMS RELEASED TO THE REACTOR CONTAINMENT BUILDING FOR HYPOTHETICAL ACCIDENT SCENARIOS CONSIDERED

	Initial Release Phase	Sodium Boil-Up Phase
Case 1	100% Noble Gases	100% Halogens
	100% Cs and Rb	100% other Volatile F.P. 1% solid F.P. 0.015% Fuel 1.1 x 10^6 lb. of Na
Case 2	100% Noble Gases	100% Halogens
	100% Cs and Rb	100% other Volatile F.P.
	1000 lb. of Na with 100PPB Pu	1% solid F.P.
	0.026% Fuel*, Solid F.P.,	0.015% Fuel
	Halogens	1.1 x 10^6 lb. of Na
Case 3	100% Noble Gases	1% of remaining 99% of solid F.P.
	100% Halogens	0.015% Fuel
	100% all Volatiles	1.1 x 10^6 lb. of Na
	1% Fuel*	
	1% Solid F.P.	
	1000 lb. of Na	
Case 4	100% Noble Gases	1% of remaining 95% of solid F.P.
	100% Halogens	0.015% Fuel
	100% all Volatiles	1.1 x 10^6 lb. of Na
	5% Fuel*	
	5% Solid F.P.	
	3300 lb. of Na	

Note: After boil-dry the only significant contribution to the source term is plutonium release due to gas sparging. This additional source amounts to about 13 kg of plutonium released from the molten pool, which has been assumed to be freely transmitted to the RCB over a several month period and is considered the same for all four cases.

*Includes plutonium in blankets and core.

TABLE 4-2

ATMOSPHERIC DILUTION FACTORS

50% X/Q Values*

Exclusion Boundary (0.42 miles)	X/Q (sec/M^3)
0-2 hours	2.20×10^{-4}
Low Population Zone (2.5 miles)	
0-8 hours	5.90×10^{-5}
8-24 hours	5.35×10^{-6}
1-4 days	3.45×10^{-6}
4-30 days	3.70×10^{-6}

*See Section 2.3 of the CRBRP PSAR.

TABLE 4-3

DOSE SUMMARY FOR HYPOTHETICAL ACCIDENT
SCENARIOS CONSIDERED

Doses in REM

	Organ	Case 1	Case 2	Case 3	Case 4
	Bone	0.0043	0.028	0.93	3.83
2 Hour	Lung	0.0035	0.0055	0.15	0.39
Exclusion	Thyroid	0.0067	0.0096	11.3	9.51
Boundary	W. Body	0.16	0.16	0.24	0.32
30 Day	Bone	32.1	32.1	32.7	33.2
Low	Lung	3.08	3.09	2.15	2.15
Population	Thyroid	99.2	99.2	5.31	1.72
Zone	W. Body	2.98	2.97	2.54	2.41

TABLE 4-4

COMPARISON OF RADIONUCLIDE RELEASES TO ATMOSPHERE FOR CRBRP WITH LWR'S FOR A COMPARABLE MELTDOWN SCENARIO

	Radioactivity Released (curies)		
Element	CRBRP	PWR(3)	BWR(3)
Xe-Kr	2.4×10^7	1.0×10^8	2.1×10^8
I	1.6×10^5	2.0×10^6	1.1×10^6
Cs, Rb	5.4×10^0	1.2×10^4	7.6×10^4
Te, Sb	3.5×10^4	2.2×10^5	8.6×10^5
Ba, Sr	6.5×10^2	3.3×10^4	2.2×10^5
Ru(1)	1.5×10^3	3.9×10^4	3.3×10^5
La(2)	3.7×10^3	2.9×10^4	2.9×10^5

(1) Includes: Ru, Rh, Co, Mo, Te

(2) Includes: Y, La, Zr, Nb, Ce, Pr, Nd, Np, Pu, Am, Cm

(3) From WASH-1400 Appendix VI, Calculation of Reactor Accident Consequences, October 1975. The LWR scenarios used for comparison here are PWR-6 and BWR-4 described in Section 2 of WASH-1400 Appendix VI.

TABLE 4-5

COMPARISON OF CALCULATED GROUNDWATER EFFLUENT CONCENTRATIONS FOR CRBRP AND TYPICAL LWR

Nuclide	Concentration (μCi/cc) CRBRP	LWR	MPC (10CFR20)*
Sr 90	3.6×10^{-9}	7.1×10^{-4}	3×10^{-7}
Tc 99	6.8×10^{-8}	3.6×10^{-6}	2×10^{-4}
Pu 239	7.1×10^{-7}	8.0×10^{-7}	5×10^{-6}

*The 10CFR20 MPC values are for routine releases and are not required to be met for accidental releases. They are presented here simply to illustrate the very low levels of radioactivity predicted in the groundwater following an assumed penetration of the basemat.

TABLE 4-6

PLUTONIUM INVENTORY IN CORE AND BLANKETS

Isotope	Homogeneous Core Beginning of Equilibrium Cycle (Used in TMBDB Radiological Analyses)		Heterogeneous Core End of Equilibrium Cycle	
	Kg	Ci	Kg	Ci
Pu-238	16	2.70×10^5	3	5.07×10^4
Pu-239	1464	8.97×10^4	2261	1.39×10^5
Pu-240	374	8.23×10^4	220	4.84×10^4
Pu-241	131	1.33×10^7	32	3.25×10^6
Pu-242	45	1.76×10^2	3	1.17×10^1

Notes:

1. The homogeneous core analyses assumed the isotopic content of the feed plutonium is 0.8% Pu-238, 72.1% Pu-239, 18.4% Pu-240, 6.5% Pu-241 and 2.2% Pu-242. The isotopic content of the feed plutonium for the heterogeneous core is 0.1% Pu-238, 86.0% Pu-239, 11.7% Pu-240, 2.0% Pu-241 and 0.2% Pu-242.

2. For the homogeneous core, the limiting doses are associated with the beginning of equilibrium cycle plutonium inventory. For the heterogeneous core, the limiting doses are associated with the end of equilibrium cycle plutonium inventory.

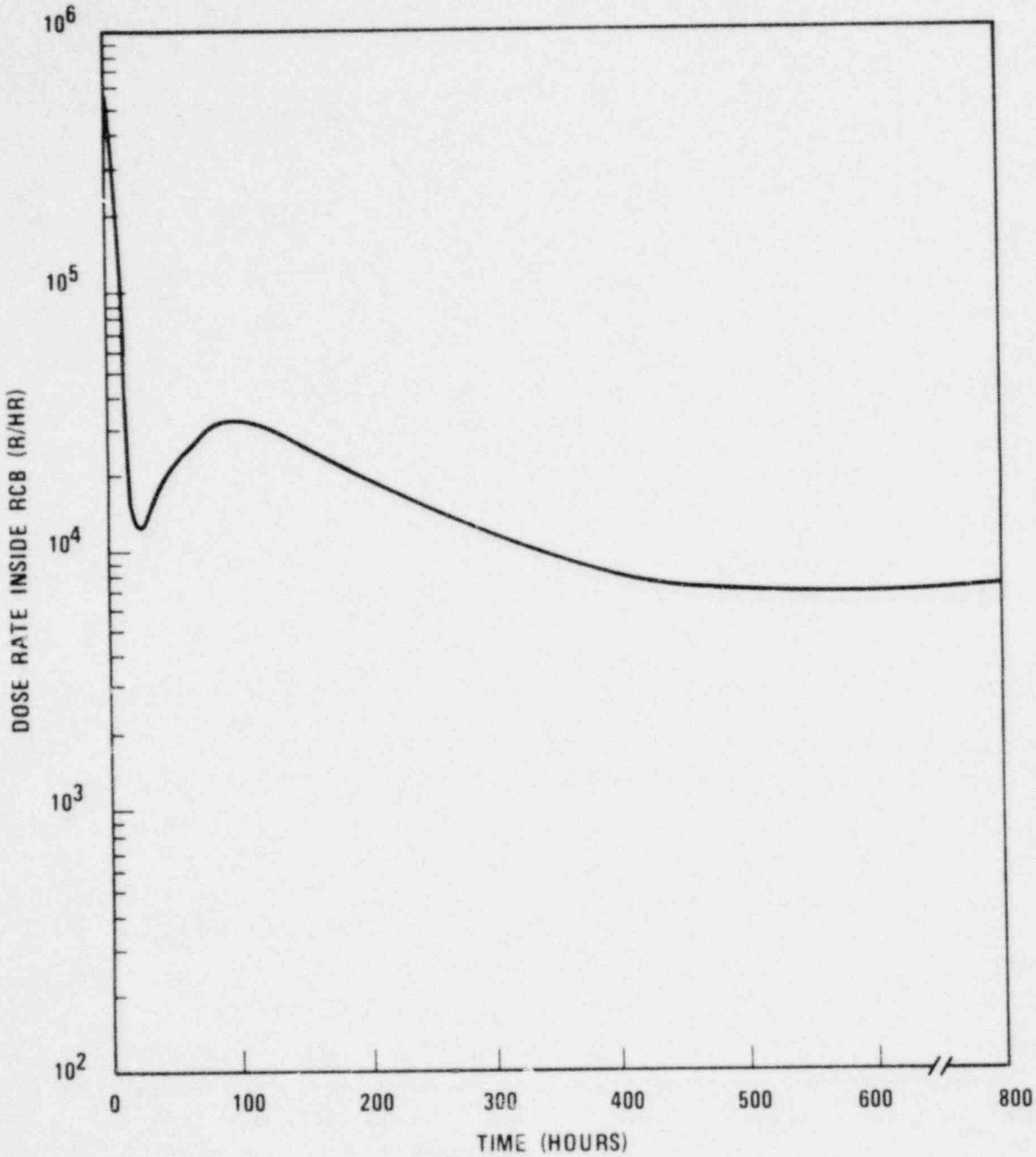

Figure 4-1 Dose Rate Inside the Reactor Containment Building for Case 2

3379-2

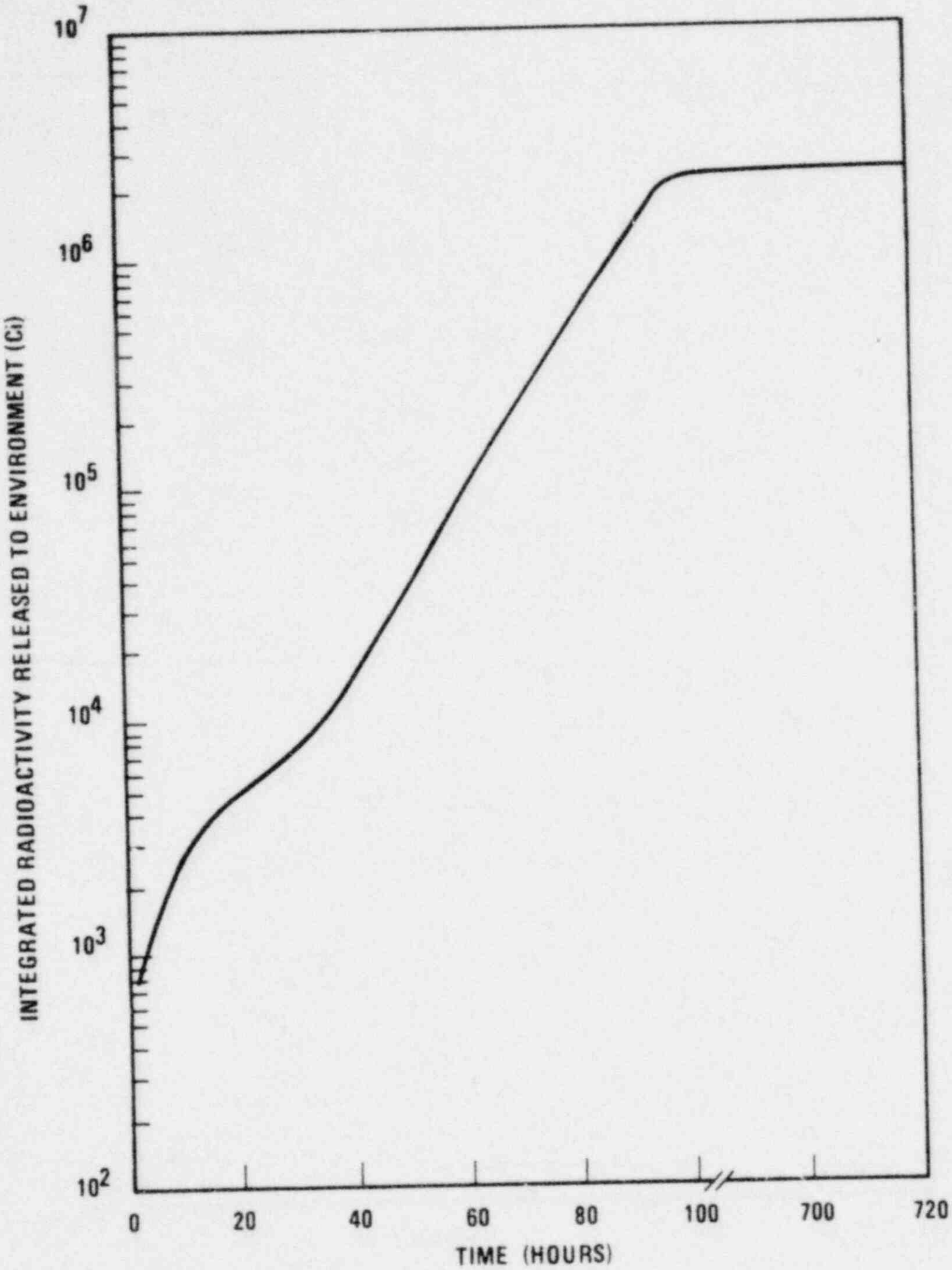

Figure 4-2 Integrated Radioactivity Released to Environment for Case 2.

3379-1

5.0 SUMMARY AND CONCLUSIONS

Volume 1 of this report assesses the potential for energetics arising from an HCDA and concludes that the best estimate of the progression is a non-energetic termination with partial to whole core involvement. Nevertheless, the reactor coolant boundary is being designed with adequate structural margins to accommodate energetic hypothetical core disruptive accident dynamic loads without loss of structural integrity. The requirements placed on the reactor coolant boundary to provide structural margins were identified.

Volume 2 addresses the thermal loads that could result from an HCDA with whole core involvement. The evaluation of in-vessel margins shows that a potential for penetration of the reactor vessel and guard vessel exists. Consequently, emphasis has been placed on providing margins external to the reactor vessel and guard vessel to assure that the radiological consequences of an HCDA are acceptable.

To evaluate the adequacy of the plant thermal and radiological margins, the release of the entire core, blankets and primary sodium into the reactor cavity was considered. Requirements have been placed on plant components and structures to assure that containment integrity would be maintained without venting until evacuation procedures could be implemented. For this report this period is taken to be 24 hours, consistent with the NRC requirement (analyses show a capability for about 36 hours). Features are also included to provide long term mitigation of HCDA consequences. The principal features that provide the thermal margin beyond the design base are:

- o Steel lined cells that house the primary system components.
- o Reactor cavity liner vent system to remove gases released behind the liner.
- o Reactor cavity-to-containment vent system to relieve pressure in the reactor cavity.

- o Reactor Containment Building vent and purge systems to provide capabilities to maintain long term containment integrity.

- o Reactor Containment Building annulus cooling system to maintain long term containment integrity.

- o A containment cleanup system to reduce the radiological consequences of vented materials.

Based on the evaluations considering these features it is concluded that the radiological consequences of a hypothetical core disruptive accident would be acceptable, considering the extremely low probability of such a condition. The consequences would be comparable to those for light water reactors for events beyond the design base.

The specific conclusions on Thermal Margin Beyond the Design Base are:

1. Thermal loads resulting from an HCDA could cause failure of the reactor vessel and guard vessel.

2. Containment integrity (without venting) would be maintained for more than 24 hours. This provides time to implement evacuation procedures and meets the requirement imposed by NRC.

3. Long term containment capability above the basemat would be maintained indefinitely by controlled venting and purging.

4. The atmospheric releases would result in radiological dose consequences that are acceptably low and insensitive to the initial release through the reactor head and compare favorably to WASH-1400 for Class 9 events.

5. Even if fuel penetration of the basemat would occur, ground water contamination levels would be lower than the predicted concentration following an assumed LWR meltdown.

APPENDICES

The follo ing Appendices contain detailed supplemental information which supports the TMBDB assessments. Included are sensitivity analysis in several areas. The following index notes the locations of the various sensitivity studies contained in the Appendices.

INDEX TO SENSITIVITY STUDIES IN APPENDICES

Appendix	Description of Sensitivity Assessments
A	None.
B	Reactor vessel and guard vessel penetration mechanisms and penetration times.
C	None.
D	Aerosol behavior characterization.
E	Plutonium and fission products release mechanisms.
F	Sensitivity of containment conditions to less severe initial conditions: decay heat, pool chemistry, thermophysical property data, sodium inventory variations, reactor and guard vessel penetration times coupled with decay heat removal, reactor head leakage prior to 24 hours, variation in liner failure times and concrete surface interaction area.
G	Sensitivity of containment conditions to: energetic sodium-concrete reactions, mal-operation of the reactor cavity-to-containment vent system, initial release of fission products and sodium through the head, variation in aerosol depletion parameters and variations in debris bed formation and leveling in the reactor cavity.
H	Containment response to the hydrogen burning criterion and flame characteristics.
I	Fuel in the PHTS piping.
J	None.

APPENDIX A

DEVELOPMENT PROGRAMS SUPPORTING THERMAL MARGIN ASSESSMENTS

The majority of the development work needed to support the evaluations in this report has either been completed or is at an advanced stage. In some instances all the data required have been obtained, but the final report has not been issued. Such testing is not included in this Appendix since the data have already been incorporated.

This Appendix focuses on the relatively small program of future experimental testing required. It should be noted that the dates cited for such items as program completion, final report release, etc., were updated as of November 1979.

A.1 SODIUM-CONCRETE INTERACTIONS DEVELOPMENT PROGRAM

A.1.1 Purpose

The large number of sodium-concrete interaction experiments performed at HEDL and Sandia (Appendix C.1, and References A-1 through A-3) resulted in the model of this phenomenon used in the analysis in Section 3.2.2. These tests included both bare concrete and simulated faulted liners. The remaining work is aimed at larger scale tests to confirm the results of the earlier tests.

A.1.2 Program

Two additional sodium-concrete reaction tests have been performed.

A Large Sodium-Concrete Test (designated LSC-2) has been performed with bare concrete. The test specimen had an interaction surface of 3 feet by 3 feet and used limestone concrete prototypic of CRBRP. The specimen was approximately 2 feet thick. Approximately 1000 pounds of hot (~1100°F) sodium was poured onto the test specimen and heated to approximately 1600°F and maintained near this temperature for about 100 hours.

A Large-Scale Faulted Liner Feature Test (designated LFT-6) has also been performed with a steel liner and a layer of MgO gravel above the concrete specimen. The liner contained a 6 inch diameter centered hole. The concrete specimen was similar to that described above for the LSC-2 test. Approximately 1000 pounds of hot (~1100°F) sodium was poured onto the test specimen and heated to approximately 1600°F and maintained near this temperature for about 100 hours.

Monitoring during the tests and post-test examinations provided information on temperature histories, gas release rate and composition, depth of sodium penetration into the concrete and sodium-concrete reaction product composition.

A.1.3 Schedule

The tests were performed in accordance with the following schedule:

Legend:

1 Complete LSC-2 test (complete)
2 Complete LFT-6 test (complete)
3 Issue report on test results

A.1.4 Criteria of Success

In order to confirm the scenario for the Thermal Margin Beyond the Design Base evaluation, this program is required to evaluate the penetration and interaction of sodium with the reactor cavity concrete floor including the effects of a potential floor liner failure. The criteria of success are that the test program confirms that the sodium-concrete reactions are approximately as modeled and are self-terminating because of the buildup of reaction products, and that spalling and mechanical breakup of the concrete will not enable the reaction front to proceed through the concrete structure.

A.1.5 Fallback Position

In the event that the tests do not substantiate the current models that show that the sodium-concrete reactions are self terminating, the experimental results will be factored into the analyses along with other updated information and thermal margins will be provided.

A.2 HYDROGEN AUTO-CATALYTIC RECOMBINATION

A.2.1 Purpose

Hydrogen auto-catalytic recombination is important in assessing the Thermal Margin Beyond the Design Base as indicated in Section 3.2.2. The burning criteria are based on extensive experimentation (Reference A-4) including the following ignition tests:

- o Ignition of Hydrogen-Nitrogen Jets
- o Ignition of Hydrogen-Nitrogen-Sodium Jets
- o Ignition of Hydrogen-Nitrogen-Sodium-Water Jets
- o Effects of Oxygen Depletion on Hydrogen Burning
- o Hydrogen Formation in Sodium-Water-Air Atmospheres
- o Effects of Jet Velocity

and the following extinguishment tests:

- o Effects of Oxygen Depletion on Hydrogen Jet Burning Efficiency
- o Effects of Jet Sodium Concentration
- o Effects of Jet Velocity
- o Effects of Jet Temperature
- o Effects of Atmosphere Water Vapor Concentration

These tests were performed in a simulated containment vessel having a volume of 3.5 ft^3. The remaining tests are aimed at confirming the validity of the burning criteria in a larger simulated test vessel. These tests employed a vessel having a volume of 3800 ft^3, which provided a scaleup of a factor of more than 10^3.

A.2.2 Program

To provide more prototypic conditions to assess hydrogen auto-catalytic recombination, three large scale tests involving sodium-concrete interactions were performed and hydrogen ignition characteristics were determined. A simulated containment vessel having a volume of 3800 ft^3 was attached to the sodium-concrete reaction test components. The oxygen concentration in the containment vessel can be controlled. The three tests run were:

- LSC-2 (See Section A.1.2 for description)
- LFT-6 (See Section A.1.2 for description)
- LFT-5. This is similar to LFT-6 except that faulted liner conditions for FFTF were being simulated; below the faulted liner are firebrick, insulating brick, and refractory mortar above the basalt concrete test specimen.

For the naturally generated hydrogen from these tests, ignition conditions were determined in terms of the jet gas temperature, jet sodium concentration and the oxygen concentration of the simulated containment vessel.

A.2.3 Schedule

The schedule for developing the hydrogen burning information from these tests is as follows:

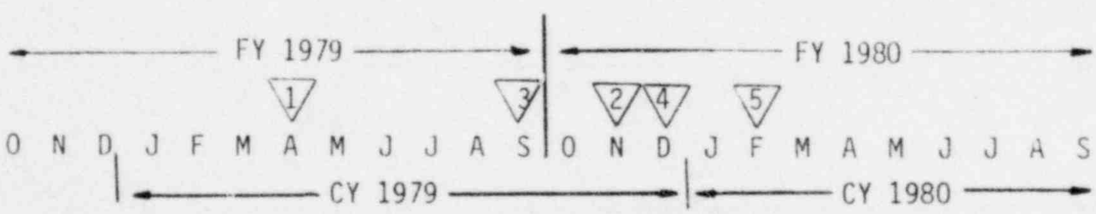

Legend:

1 Complete analysis of hydrogen burning data from LFT-5 (complete)
2 Complete analysis of hydrogen burning data from LSC-2
3 Complete analysis of hydrogen burning data from LFT-6 (complete)
4 Issue summary report on LFT-5
5 Issue summary report on LSC-2 and LFT-6

A.2.4 Criteria of Success

The test results will be considered to be successful if the hydrogen auto-catalytic burning conditions from these tests are consistent with the data from the smaller scale tests reported in Reference A-4.

A.2.5 Fallback Position

In the event the tests do not substantiate the hydrogen burning models currently being used, appropriate modifications will be made to the models to be consistent with the data from the larger scale tests. Those revised models will then be used in assessing the Thermal Margin Beyond the Design Base.

A.3 FURTHER VALIDATION OF THE CACECO COMPUTER CODE

A.3.1 Purpose

The objectives of this activity are to further validate the CACECO computer code used in many of the analyses in this report. Initial validation is reported in References A-5 and A-6. In these references, the code and input data were validated using experimental results available through 1976 and some results from 1977. With the additional experimental data that subsequently became available or will be available in the near future, further confirmatory validation is appropriate and is planned.

A.3.2 Program

The further validation of the CACECO code will include the following items:

1. A report which has been issued describes the analytical validation of the code. This included a comparison of the code with analytical solutions, other validated codes and hand calculations.

2. A revised users guide has been issued to provide updated user information.

3. A report will be issued summarizing the experimental information used in the code and/or code input. The code and input data will be compared with data from appropriate sodium-concrete and heated concrete tests, the HEDL hydrogen auto-ignition experiments, and appropriate concrete water release experiments.

A.3.3 Schedule

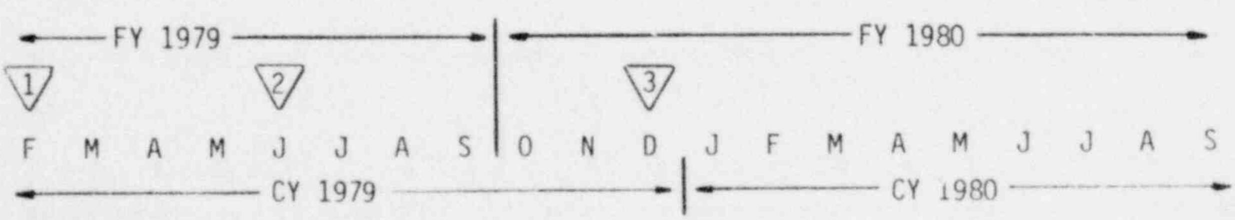

Legend:

1 Complete analytical validations and issue report (complete)

2 Issue revised users guide (complete)

3 Issue report on experimental validations

A.3.4 Criteria of Success

The purpose of this program is to further validate a code that predicts the conditions in containment following an HCDA. The criteria of success will be to show by comparisons with analytical and experimental data that the code simulates the consequences in containment following an HCDA.

A.3.5 Fallback Position

If the current version of the CACECO code does not satisfy the criteria of success, the code will be modified until a satisfactory duplication of the analytical and experimental data can be obtained and the TMBDB consequences will be assessed based on this revised model.

A.4 COMPREHENSIVE TESTING PROGRAM FOR CONCRETE AT ELEVATED TEMPERATURES

A.4.1 Purpose

The purpose of this testing program was to establish a data base of the analysis and design of concrete exposed to elevated temperatures under conditions commensurate with nuclear power plant applications.

The specific objectives of this testing program were:

a. To define the variations in the physical (thermal) properties of limestone aggregate concrete and lightweight insulating concrete exposed to elevated temperatures resulting from a postulated large sodium spill.

b. To develop thermal relationships for use in the analysis and design of reinforced concrete components under high temperature conditions resulting from postulated large sodium spills in equipment cells.

c. To define the variations in the mechanical (strength) properties of limestone aggregate concrete and lightweight insulating concrete exposed to elevated temperatures resulting from a postulated large sodium spill.

d. To develop strength relationships for use in the analysis and design of reinforced concrete components under high temperature conditions resulting from postulated large sodium spills in equipment cells.

A.4.2 Program

The program of research specified in the Comprehensive Testing Program for Concrete at Elevated Temperatures defined the variations in the physical (thermal) and mechanical (strength) properties of prototypic CRBRP limestone aggregate concrete and lightweight insulating concrete exposed to elevated temperatures.

The Comprehensive Testing Program for Concrete at Elevated Temperatures consisted of two major phases. The scope of the testing program phases consisted of the following:

Phase I: Confirmation of Mechanical Properties

This phase consisted of testing to determine the effect of elevated temperature exposure on the strength properties of structural concrete and lightweight insulating concrete. A limited number of tests were performed on the lightweight concrete to determine its load response characteristics at penetration locations where localized crushing due to thermal expansion is likely to impact the penetration design. All testing were performed in an open moisture migration state while the concrete is at test temperature (open-hot condition). Each test sample was heated to test temperature at a rate of 30°F/hr and was heat soaked for 336 hours, unless otherwise noted, prior to mechanical testing. All samples were a minimum of 60 days old at the time of initial heat-up. The tests conducted are shown in Table A-1.

Part 1

Concrete cylinders 6" x 12" were tested for each temperature in the designated quantities in Table A-1 for the following parameters:

a. Compressive Strength (f'_c)
b. Modulus of Elasticity (E_c)
c. Stress-Strain Relationship (σ versus ϵ)
d. Moisture and Weight Loss
e. Poissons Ratio (μ) (Standard Weight Concrete Only)

TABLE A-1

OPEN-HOT MOISTURE MIGRATION STATE

Test Temperature (°F)	Standard Weight Concrete (No. of Cylinders)	Lightweight Concrete (No. of Cylinders)
72°F (Control Cylinders)	3 (min) per each concrete batch	
*150°F	6*	3
*225°F	6*	3
*350°F	6*	3
500°F	3	3
700°F	3	3
900°F	3	3
1150°F	3	0
Total	30	18

* Three cylinders - (standard weight concrete only) for each of the above designated temperatures were heat soaked for approximately 672 hours prior to mechanical testing, to evaluate the long term heating effect on the mechanical properties of standard weight concrete.

Part 2

A sufficient number of tests (estimated below) were performed to determine with a high degree of accuracy the following properties for the temperature range 72°F to 1150°F for standard weight limestone aggregate concrete in the open-hot moisture migration system:

a. The variation of concrete shear strength (v_c) with temperature (Approximately 24 specimens).

b. The variation of concrete/rebar bond strength (u) with temperature (Approximately 24 specimens).

c. The variation of sustained load (creep) characteristics with temperature (Approximately 15 specimens).

Phase II: Confirmation of Physical Properties

This phase consisted of testing to determine the effect of elevated temperature exposure on thermal properties of structural concrete and lightweight insulating concrete. The concrete properties investigated included: the instantaneous and average coefficients of thermal expansion, conductivity, specific heat, density, moisture migration rate and weight loss.

A sufficient number of tests (estimated below) were performed to determine with a high degree of accuracy the coefficients listed below over the temperature range of $72^{\circ}F$ to $1150^{\circ}F$ for standard weight and lightweight insulating concrete. The concrete was tested in an open moisture migration environment while at test temperature (open-hot condition). All samples were a minimum of 60 days old at the time of initial heat-up.

a. Instantaneous and Average Coefficient of Thermal Expansion $(\bar{\alpha}_i)$ and $(\bar{\alpha})$ of concrete at elevated temperatures.[+]
b. Thermal Conductivity (k)[++]
c. Specific Heat (C_p)[+++]
d. Density at Elevated Temperatures (ρ)[*]
e. Moisture and Weight Loss[**]

A.4.3 Schedule

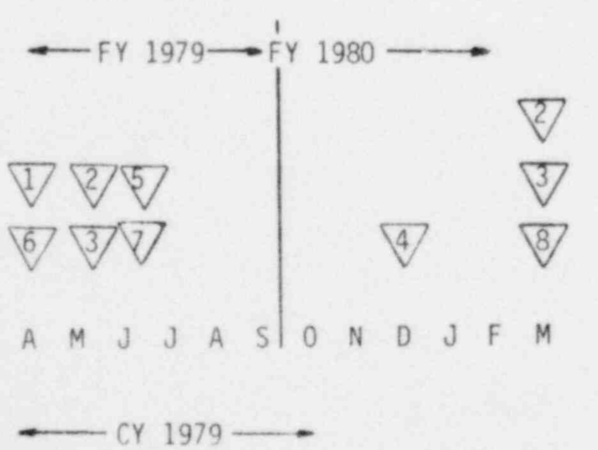

+ Approximately 3 specimens for each property
++ 2 specimans for each material
+++ 6 specimans for each material
* Natural outfall of Phase I
** Natural outfall of Phase I and Phase II, item d.

Legend:

1 Complete mechanical property test (336 hour soak) (complete)

2 Complete conf rmation of thermal properties (thermal conductivity and specific heat)

3 Complete confirmation of thermal properties (instantaneous and average coefficients of thermal expansion)

4 Complete concrete bond test

5 Complete concrete shear test (complete)

6 Complete mechanical property test (672 hours soak) (complete)

7 Complete sustained load (creep) test (complete)

8 Complete Data Assessments and Final Report

A.4.4 Criteria of Success

Since the purpose of the tests is to establish materials properties, it is not possible to state a specific, quantitative success criterion. The tests will be successful when materials properties have been defined, with reasonable accuracy, over the ranges of interest. It is expected that the result will substantiate the data used in the present analysis.

A.4.5 Fallback Position

In the event that the test results do not confirm the validity of the data used in the present analysis, the results of this program will be factored into the analysis.

A.5 BASE MATERIALS TEST FOR LINER STEEL

A.5.1 Purpose

To obtain physical material data, under strictly controlled conditions, for the cell liner steel and weldment material.

A.5.2 Program

The experimental program was designed to produce tensile, creep and thermal expansion data on materials for the cell liners. The materials of interest are the cell liner steel, and the weldment material.

The base material and weldment materials underwent mechanical properties testing in the as-received condition. All tests were performed in an air atmosphere.

A.5.2.1 Uniaxial Tensile Tests

Uniaxial tensile tests were performed on the base material and the weldment materials to determine their temperature and strain rate dependency. All tests were performed in an air atmosphere. The number of tests for each material tested and the test condition are presented in the test matrix on the following page.

Number of Uniaxial Tension Tests
Per Material Type and Condition

Test Temp. (^oF)	Type 1 (Fig. A-1, A-2) Base Material & Weldment (See Note 1) A	B	C	Type 2 (Fig. A-2) Weldment (See Note 2)	Type 3 (Fig. A-2) Weldment (See Note 2)
Room Temp.	2	1	1	1	1
600	2	1	1	1	-
800	2	1	1	1	-
1000	2	2	2	1	-
1200	2	2	2	1	-
1400	2	2	2	1	-
1500	2	-	-	-	-
1600	2	2	2	-	-
1700	2	-	-	-	-
Totals: Weldment	18	11	11	6	1
Base Material	18	11	11	0	0

Note 1 - Column A at 10^{-4} in/in/sec strain rate

Column B at 5 x 10^{-3} in/in/sec strain rate

Column C at 10^{-1} in/in/sec strain rate

Note 2 - All type 2 and type 3 uniaxial tension tests shall be performed at the 10^{-4} in/in/sec strain rate.

A.5.2.2 Creep and Stress-Rupture Tests in Air

Uniaxial creep tests in air are required over the temperature range 800^oF to 1600^oF, at 200^oF intervals. Four stress levels are required at each temperature, in order to obtain meaningful creep and rupture relationships. The stress levels at each temperature were selected so that the rupture times would not exceed 500 hours.

A.5.2.3 Thermal Expansion Tests

In addition to the mechanical property tests described above, mean and instantaneous coefficients of thermal expansion are required to supplement existing data, limited to temperatures below 800°F. These supplementary tests were performed over the temperature range 700°F to 1700°F, at 100°F intervals. Two tests were run at each temperature for the ASME SA-516, Grade 55 material only.

A.5.3 Schedule

Tensile Tests

Base Material Phase - Complete

Weldment Material Phase - Complete

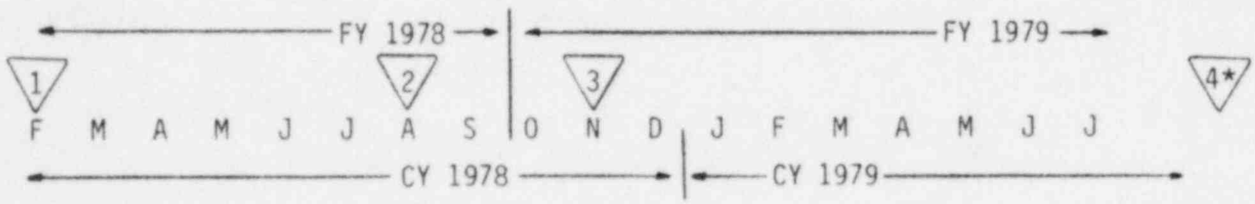

Creep Stress Rupture Tests (Air)

Base Material Phase - Complete

Weldment Material Phase - Complete

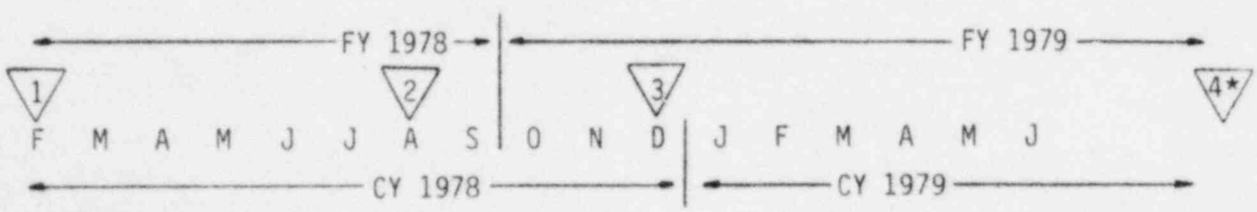

*Release date February 1980

Legend:

1 Initiate Material Procurement and Specimen Fabrication (complete)

2 Initiate Testing (complete)

3 Complete Testing (complete)

4 Issue Final Report

A.5.4 Criteria of Success

Since the purpose of the test is to establish materials properties, it is not possible to state a specific, quantitative success criterion. The tests will be successful when materials properties have been defined, with reasonable accuracy, over the range of interest. It is expected that the result will substantiate the data used in the present analysis.

A.5.5 Fallback Position

In the event that the test results do not confirm the adequacy of the data used in the present analysis, the results of this program will be factored in the analysis along with other updated TMBDB data.

A.6 SODIUM SPILL DESIGN QUALIFICATION TEST (LT-1)

Note that this program is now essentially complete. Information gained from the test has been factored into the scenario presented, and so details of testing are not appropriate for this Appendix. Reference is made to this Program only because the Final Report (scheduled for January 1980) has yet to be issued.

A.7 TMBDB AIR CLEANING SYSTEM PERFORMANCE TESTS

A.7.1 Purpose

Although the components which make up the TMBDB air cleaning system (quench spray chamber jet venturi fume scrubber and high efficiency fibrous bed scrubber) are commercially available and have been used in a variety of industrial applications, the performance of these components to the requirements of Section 2 in removing sodium and other reaction products generated during the CRBRP TMBDB scenario has not been demonstrated. This testing program will confirm the adequacy of the TMBDB air cleaning system.

The specific objectives of this program are:

a. Confirm the performance of the TMBDB air cleaning system for conditions characteristic of the CRBRP TMBDB scenario.

b. Provide data in support of the environmental qualification of the TMBDB air cleaning system equipment (quencher, venturi scrubber, high efficiency fiber bed scrubber and associated valves).

A.7.2 Program

A sodium aerosol will be generated and aged in a test facility to simulate the in-containment conditions predicted from the CRBRP TMBDB scenario. These products will be vented through the air cleaning system. The TMBDB in-containment conditions and air cleaning system flow rate will be simulated. The parameters to be measured both upstream and downstream of each component are listed on the following page.

A state-of-the art report has been prepared to demonstrate the capability of the air cleaning system to remove fission products in the form of NaI, SeO_2, and Sb_2O_3 (Reference A-7).

Data Requirements

The following in-containment data will be obtained as a function of time during the conduct of the test:

- o atmosphere temperature
- o NaO concentration
- o NaOH concentration
- o Na_2CO_3 concentration
- o Metallic Sodium concentration
- o Particle electrical charge
- o containment absolute pressure
- o Na_2O concentration
- o particle size
- o total mass concentration
- o atmosphere concentration (% N_2, O_2, CO_2, H_2)
- o relative humidity
- o determination of fallout % from appropriate data above

The following data will be obtained outside of the containment atmosphere at these locations:

(a) Between the quench unit and venturi scrubber (b) between the venturi scrubber and high efficiency fibrous bed scrubber (c) between the high efficiency fibrous bed and the HEPA filter, and (d) downstream of the HEPA filter.

- o temperature (both liquid & gas)
- o Na_2O concentration
- o NaOH concentration
- o Na_2CO_3 concentration
- o flow rate ((a) and (c) only) (liquid and gas)
- o water solution concentration of NaOH, Na_2CO_3
- o particle size distribution
- o pressure differential across each component
- o removal efficiency of each component for particle size distribution

Additionally, the following specific information will be obtained.

- o Quench unit humidity
- o Determination of % of sodium reaction products generated in the test facility which are vented through the air cleaning system.
- o Determination of % of duct and air cleaning equipment which becomes plugged by sodium reaction products.
- o Visual inspection of air cleaning system components at intervals of 24 hours of operation for any indication of degradation of performance or conditions which might be expected to preclude long term operation.
- o Evaluation of effect of increasing sodium reaction product (NaOH and Na_2CO_3) concentration in the water used for air cleaning equipment (separate water supplies should be provided for each unit (quencher, venturi scrubber, and high efficiency fibrous bed scrubber) in order that each component can be evaluated separately, and also so that an additional means for determining component removal efficiency can be provided).

A.7.3 Schedule

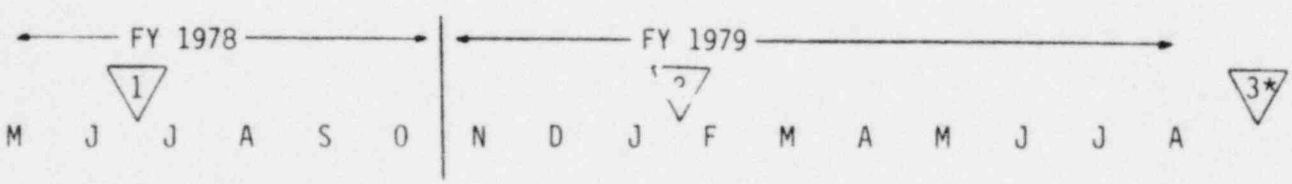

*Release date January 1980

Legend:

1 Complete test article design

2 Start test

3 Complete test and report results

A.7.4 Criteria of Success

These test results must substantiate the air cleaning data used in tł analytical model.

A.7.ᴗ Fallback Position

The results of the tests will be factored into the overall analysis together with other updated results. If cleanup system performance is inadequate, investigations of the cause will result in a modified design which provides adequate thermal margin beyond the design base.

A.8 REFERENCES

A-1. J. A. Hassberger, "Intermediate Scale Sodium-Concrete Reaction Tests," HEDL-TME-77-99, August 1977. (Availability: U.S. DOE Technical Information Center).

A-2. R. K. Hilliard and W. D. Boehmer, "Concrete Protection from Sodium Spills by Intentionally Defected Liners, Small Scale Tests S9 and S10," HEDL-TME 75-75, July 1975.

A-3 J. A. Hassberger, R. K. Hilliard and L. D. Muhlestein, "Sodium-Concrete Reaction Tests," HEDL-TME-74-36, June 1974.

A-4. R. W. Wierman, "Experimental Study of Hydrogen Jet Ignition and Jet Extinguishment," HEDL-TME 78-80, April 1979.

A-5. R. D. Peak, "Users Guide to CACECO Containment Analysis Code," HEDL-TME 79-22, June 1979.

A-6 R. D. Peak, "CACECO Code Verification," in Fast Reactor Safety Technical Progress Report, April-June 1977, HEDL-TME-77-67.

A-7 A. K. Postma and R. K. Hilliard, "Nucleation and Capture of Condensible Airborne Contaminants in an Aqueous Scrubbing System," HEDL-TME 78-82, September 1978.

1966-118

TYPE PECIMENS

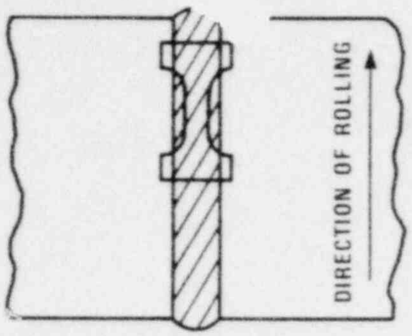

APPROX. SIZE

GAGE LENGTH	1"
WIDTH	1/4"
SPECIMEN LENGTH	4-3/8"
THICKNESS	1/4" (TENSION) 15" (CREEP RUPTURE)

CONFIGURATION
ASTM E-8

NUMBER OF TESTS

TENSION – 40
CREEP RUPTURE – 20

DESIGN AS FOR PLATE MATERIAL

TYPE 2 SPECIMENS

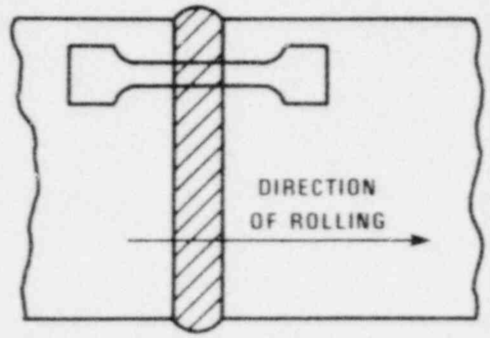

APPROX. SIZE

GAGE LENGTH	2"
WIDTH	1/2"
SPECIMEN LENGTH	8" MIN.
THICKNESS	~ 3/8"

CONFIGURATION ASTM E-8

NUMBER OF TESTS

TENSION – 6

SPECIMENS SHALL BE TESTED IN THE AS-WELDED CONDITION WITHOUT GRINDING OR FINISHING (IE: BACKING BAR SHALL BE LEFT IN PLACE).

TYPE 3 SPECIMENS

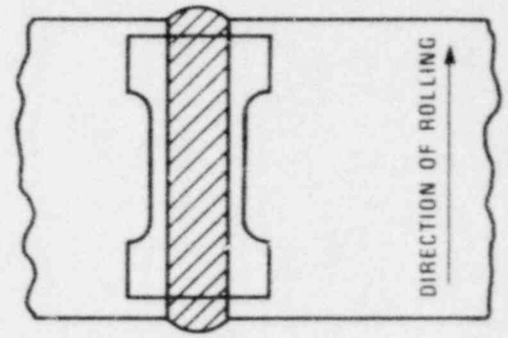

APPROX. SIZE

GAGE LENGTH	8"
WIDTH	1-1/2"
SPECIMEN LENGTH	18" MIN.
THICKNESS	~ 3/8"

CONFIGURATION ASTM E-8

NUMBER OF TESTS

TENSION – 1

GRIP ENDS SHALL BE OVERSIZED (l&w) TO ASSURE SUFFICIENT GRIP AREA DURING TESTING. THE GRIP END AREA ONLY SHALL BE GROUND SMOOTH. THE REMAINING AREA SHALL BE LEFT IN THE AS-WELDED CONDITION (IE: BACKING BAR SHALL BE LEFT IN PLACE).

Figure A-2. Tension and Creep Rupture Tests – Weldment Material

APPENDIX B
REACTOR AND GUARD VESSEL PENETRATION ANALYSIS

B.1 INTRODUCTION

To estimate the initial conditions for the thermal margin evaluation, an analytical model was developed to compute reactor vessel and guard vessel penetration times. Estimates of the penetration times were made for several cases. In each case, the amount of steel and blanket material that is assumed to form in the debris bed with the core fuel was varied parametrically. The following cases were considered:

1. All of the core fuel melts forming an evenly distributed, level debris bed on the vessel. No hold up time above the core support structure is assumed.

2. All of the core fuel melts forming a uniformly distributed, level debris bed on the vessel. Hold up times of 1000 and 5000 seconds are assumed between the time of the accident and the time the fuel reaches the sodium beneath the core support structure.

3. All of the core fuel melts and forms an uneven layer of debris on the vessel. No hold up time is assumed.

4. Fractions of the core fuel form an evenly distributed debris bed on the vessel. No hold up time is assumed.

For all cases the penetration scenario is assumed to be the same. After an HCDA, the fuel is displaced from the core region. The molten fuel and steel are assumed to pass through the core support and lower internals and come into contact with a large volume of relatively cold sodium and form a particulate. The particulate falls through the sodium and forms a debris bed on the bottom head of the reactor vessel. If the heat generation rate in the debris bed exceeds the maximum coolable load, the debris bed may dry out and result in higher bed temperatures. Following dryout, the heat transferred to the overlying sodium is reduced substantially; therefore, the possibility of a reactor vessel penetration is increased. The heat transfer processes that take place and the sequence of events are given in Table B-1.

B.2 ASSUMPTIONS

To compute penetration time, several assumptions of the heat transfer processes and of the penetration sequence of events must be made. The following assumptions were made for this analysis:

1. Molten fuel leaving the core region encounters sodium coolant. The molten fuel-sodium interaction results in the quenching of molten core materials into particulate debris. Particulate debris falls at an average velocity of 10 cm/sec (Reference B-1) through the sodium due to density differences. The particles settle on the bottom surface of the reactor vessel forming a debris bed.

2. Sodium temperature above the debris bed are determined by the shutdown to 3-loop natural circulation transient.

3. The fuel remains subcritical following the core meltdown. Heat generation is considered only in the fuel debris and conservatively includes the entire fission product decay heat including uncertainties and the heat generation from sodium soluble products and noble gases.

4. Prior to dryout, heat is transported upward from the debris bed to the overlaying sodium. The bottom of the debris bed is insulated. Temperature of the sodium pool is constant while the debris bed is being heated.

5. Debris bed porosity (volume fraction of sodium) is 0.40 (Reference B-2). This assumption is in variance with the one in Section 3.1 (porosity of 0.50); however, the basic conclusions of Section 3.1 and this appendix are not sensitive to this assumption.

6. Dryout heat flux is computed by considering the total bed loading (fuel plus steel).

7. Steel particulate is assumed to be above the fuel particulate in the debris bed because this arrangement will yield the lowest dryout flux (Reference B-2).

8. The vessels fail when the steel in the debris bed becomes molten. The average calculated temperature of the vessel when this failure is assumed to occur is approximately 1600^{o}F. This assumption is quite conservative; however, the temperature of the vessel would begin to rapidly increase after steel melting since the molten steel would greatly increase the thermal conductivity of the bed.

9. The "wetted" portion of the reactor vessel fails and is included in the debris bed on the guard vessel.

10. The debris bed on the guard vessel forms immediately after the reactor vessel fails.

B.3 DESCRIPTION OF PENETRATION ANALYTICAL MODEL

Each phenomenon that occurs during the reactor vessel and guard vessel penetration sequence is considered separately by calculating the time for the event to occur and the temperature of the debris bed at the end of the event.

A description of each phenomenon and the method of solution are included in Table B-1.

B.4 DESCRIPTION OF CASES

Level Core Debris Distribution on the Reactor Vessel Bottom Surface

In the first case it is assumed that all the molten material particulates and forms an evenly distributed debris bed of depth ℓ on the vessel surface. Experimental results reported in Reference B-2 indicate that bed self levelling would occur.

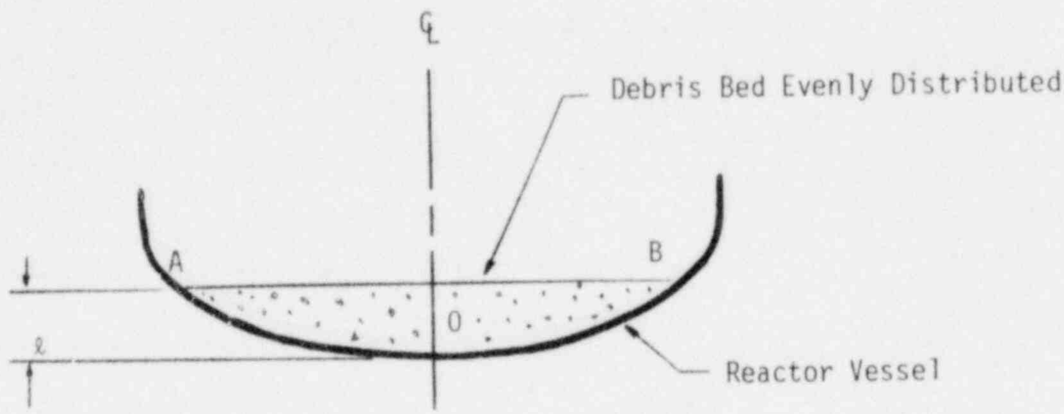

The bed is self-heated to the boiling point of sodium. If the heat flux exceeds that required for dryout, the sodium in the bed is boiled dry. The debris bed is then heated to the melting point of steel. After the steel in the debris bed becomes molten, the vessel is assumed to fail. A new debris bed, initially at the surrounding sodium temperature, is then formed on the guard vessel. The wetted portion of the reactor vessel (Arc AOB) is assumed to melt and is included in the evenly distributed debris bed on the guard vessel.

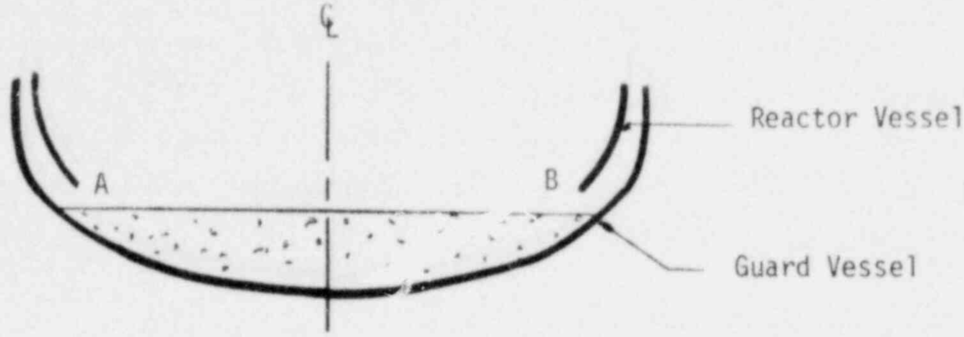

The same sequence of events which occurred on the reactor vessel now occurs on the guard vessel.

Uneven Distribution of Debris Bed

The heat flux required to cause a sodium dry out is inversely proportional to total loading (fuel plus steel). Since a level distribution of debris cannot be assured, a non-uniform debris layer was simulated. Uneven distribution would result from the particles 'piling up' at the axial centerline.

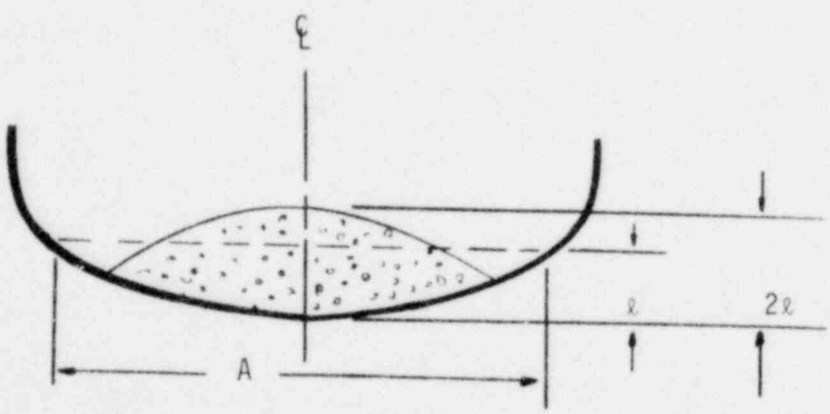

Fuel Delay Inside Core

In the previous cases, the core fuel was assumed to arrive below the core support structure with no hold up time. In this analysis, the fuel was assumed to be delayed in the core by 1000 and 5000 seconds. The mechanism for cooling the sodium prior to penetration is three-loop natural circulation. A level debris bed and all of the core fuel in the debris bed was assumed.

Partial Core Meltdown

Cases were considered where less than the entire inventory of core fuel forms in the debris bed. For these cases the amounts of reactor steel and blanket were varied parametrically. A level debris bed is assumed and the fuel was assumed to arrive below the core support structure at the time of the accident. The sequence of events is the same as described in Table B-1.

B.5 RESULTS

Results of this analysis indicate penetration times are strongly dependent on the amount of reactor steel and blanket that forms in the debris bed. As the amounts of steel and/or blanket forming in the debris bed are increased, the time required for penetration is increased. The addition of this material increases the heat capacity of the bed. Eventually the capacity of the bed is such that it can be cooled without a sodium dryout occurring.

Penetration times were calculated for a variety of cases; even and uneven core debris distribution on the vessel bottom; with and without hold up times inside the core; and with part or all of the core fuel forming in the debris bed. In each case, the amount of reactor steel and blanket in the debris bed was varied parametrically. Tables B-2 through B-6 illustrate the results obtained for the aforementioned cases.

Level Core Debris Distribution on Reactor Vessel

Penetration times ranging from 400 seconds to infinity were obtained for the case where all of the core fuel forms in the debris bed. For a total core meltdown, it would appear that the 10,000 pounds of steel in the active core region would be the minimum amount of steel that would melt. If in addition to this amount of steel, the lower axial blanket also melts, a penetration time of 1200 seconds is computed. This time should be quite conservative since it assumes no delay time inside the core and it assumes that all of the core fuel forms in the debris bed. Table B-2 illustrates the parametric results for the level debris bed.

Uneven Distribution of Debris Bed

An uneven distribution of the debris bed on the vessel surface could result from the particles 'piling up' at the axial centerline. This was found to have a minimum effect on the time required to penetrate the guard vessel. Due to the high heat generation rate, heat is not rapidly conducted out of the debris bed. Hence there is little temperature gradient through the bed and the debris bed depth is not an important parameter.

In this analysis, penetration times are reduced slightly for uneven distribution on the vessel surface. Less of the debris is assumed to be in contact with the vessel if it 'piles up' at the center and consequently a smaller portion of the reactor vessel is assumed to fail. As a result, the debris bed that forms on the guard vessel contains less steel and slightly shorter penetration times result. The results for this case are shown on Table B-3.

Fuel Delayed Inside Core

Several cases were examined where the fuel was delayed inside the core. In this analysis, the in-vessel sodium was assumed to be cooled prior to guard vessel penetration. Tables B-4 and B-5 illustrate the parametric results for 1000 and 5000 second delays. The obvious conclusion that can be drawn from this is that as the core hold up time is increased the possibility of a guard vessel penetration is decreased and the penetration time is greatly increased.

Partial Core Meltdown

Cases where less than the entire inventory of core debris settles on the bottom of the vessel were examined. This analysis only considers the fuel which goes downward and does not consider any of the material which remains in the vessel or is ejected upward.

There is approximately 10,000 pounds of stainless steel in the active fuel region (flow ducts, cladding, wire wrap, etc.). Assuming the amount of steel that forms in the debris bed corresponds to the fraction of the fuel (i.e., 50 percent of the core with 5000 pounds of steel) the following results were obtained:

Percentage of Core Which Forms in Debris Bed	Mass of Steel in Debris Bed (pounds)	Guard Vessel Penetration Time (seconds)
100	10000	900
50	5000	1000
20	2000	1200
10	1000	1500
1	100	----

These results assume that no blanket material has formed in the debris bed. Additional parametric results which include the effect of the blanket material are shown in Table B-6.

B.6 CONCLUSIONS

Due to the uncertainty of the nature of the core meltdown accident, the amount of reactor steel and blanket material that would form in the debris bed is uncertain. As a result of this uncertainty, a time of 1000 seconds for penetrating the reactor and guard vessels is used for determining initial conditions in the TMBDB scenario. For a total core meltdown, it would appear that at least the lower axial blanket and the steel in the active core region would also melt. For this amount of steel and blanket, penetrations times greater the 1000 seconds were obtained. Consequently, 1000 seconds is a conservative penetration time.

B.7 REFERENCES

B-1. J. C. Hesson, R. H. Sevy and T. J. Marciniak, "Postaccident Heat Removal in LMFBRs: In-Vessel Considerations," ANL-7859, September 1971.

B-2. L. Baker, Jr., et al., "Postaccident Heat Removal Technology," ANL/RAS-74-12, July 1974. (Availability: U.S. DOE Technical Information Center).

B-3. H. S. Carslaw and J. C. Jaeger, Conduction of Heat in Solids, Clarendon Press, Oxford, 1959.

B-4. L. A. Bromley, "Heat Transfer in Stable Film Boiling," Chem. Eng. Progr., 46, pp. 221-227 (1950).

TABLE B-1

PENETRATION PHENOMENA

Phenomenon	Method of Solution
Core meltdown assumed to occur; fuel arrives below core support structure in debris form.	This is the initial condition assuming no hold up time within the core or core support structure.
Debris falls through sodium from below core support structure to reactor vessel head.	The debris falls through the sodium at a velocity of 10 cm/sec. The distance between the core support structure and the reactor vessel head is 218 cm. The temperature of the debris when it arrives at the surface is that of the sodium, which is determined by the shutdown transient to 3 loop natural circulation.
Debris bed is heated internally to the boiling point of sodium.	The temperature response of the debris bed is determined by solving the heat conduction equation for a slab generating heat at the rate of Ao EXP $(-\lambda t)$

$$V = \frac{\alpha A_o}{\lambda K}\left\{\frac{\cos x\,(\lambda/\alpha)^{1/2}}{\cos \ell\,(\lambda/\alpha)^{1/2}} - 1\right\} \mathrm{EXP}\,(-\lambda t)$$

$$+ \frac{4\alpha A_o}{\pi\lambda K}\sum_{n=o}^{\infty}\frac{(-1)^n \mathrm{EXP}\left[-\alpha(2n+1)^2\pi^2 t/4\ell^2\right]\cos\left[(2n+1)\pi x/2\ell\right]}{(2n+1)\left\{1-\left[(2n+1)^2\pi^2\alpha/4\lambda\ell^2\right]\right\}}$$

(See last page of Appendix B for nomenclature.)

TABLE B-1 (Continued)

Phenomenon	Method of Solution
	V represents the temperature difference between the bed and the overlying sodium. The temperature of the overlying sodium is held constant. Time is incremented until the temperature at the bottom of the bed (x=o) reaches the boiling point of sodium.
Sodium in debris bed is boiled off if the dryout heat flux is exceeded.	The dryout heat flux is calculated as a function of the total bed loading (Reference B-2). $$Q_v = \left(\frac{L}{L + L_{ss}}\right) \left[988-20.85\ (L+L_{ss}) + 0.1148\ (L + L_{ss})^2\right]$$ The heat flux from the bed is calculated from the decay heat generation rate and the surface area of the bed. All the heat being generated is assumed to be transferred from the top of the bed. If the dryout flux is exceeded, the time to boil off the sodium in the debris bed is computed. If there is no bed dryout, boiling will not take place and eventually the bed will begin to cool without penetrating the vessel.

TABLE B-1 (Continued)

Phenomenon	Method of Solution
Debris bed is heated to the melting point of steel.	After a sodium dryout occurs, the temperature of the debris bed would increase rapidly due to the poor thermal conductivity of the dried out bed. The time for the debris bed to reach the melting point of steel is computed by considering the following energies: heat content of debris bed (fuel, blanket and steel), heat generated by fuel and blanket, and the heat transferred from the bed due to film boiling (Reference B-4). It is assumed that no heat is conducted out of the bottom of the debris bed to the vessel.
Steel in debris bed melts and the reactor vessel fails.	The time required to melt the steel in the debris bed is calculated from the heat of fusion of the steel. The reactor vessel is assumed to fail after the steel in the debris bed is at the melting point of steel.
Particles settle to bottom of guard vessel and form a debris bed.	The debris is assumed to arrive at the bottom of the guard vessel at the same time it penetrates the reactor vessel. The debris is quenched to the sodium temperature as it falls through the sodium.
Debris bed is heated to the boiling point of sodium.	Method is same as in reactor vessel. The portion of the reactor vessel head which failed is also part of the debris bed on the guard vessel.
Sodium in debris bed is boiled off if the dryout heat flux is exceeded.	Same as in reactor vessel.

TABLE B-1 (Continued)

Phenomenon	Method of Solution
Debris bed on the guard vessel bottom is heated to melting point of steel.	Same as in reactor vessel.
Steel in debris bed melts and the guard vessel fails.	Same as in reactor vessel. Problem is terminated.
Debris falls through guard vessel and onto reactor cavity floor.	

TABLE B-2

PENETRATION TIMES FOR REACTOR VESSEL AND GUARD VESSEL*

Amount of Steel (lbs)**	Amount of Blanket: 0%	Lower Axial (11.3%)	Lower Axial+ Upper Axial (22.6%)	Lower Axial+ Upper Axial+ 50% of Radial (61.3%)	100%
0	400(2)	700	900	2400	4400
1,000	500	800	1000	2500	4500
5,000	700	900	1200	2800	(1)
10,000	900	1200	1500	3300	----
20,000	1400	1700	2100	4400	----
30,000	2000	2400	2900	(1)	----
40,000	2800	3200	3800	----	----
50,000	3600	(1)	(1)	----	----
60,000	(1)	----	----	----	----

*Time in seconds based on 100% core fuel, even distribution of core debris and no delay time to debris accumulation on the reactor vessel bottom.

**Stainless steel in various regions.

Active fuel region	9400 lbs.
Upper axial blanket region	3660 lbs.
Lower axial blanket region	5270 lbs.
Radial blanket region	9320 lbs.

(1) Sodium dryout on guard vessel does not occur.

(2) Debris bed depth is 11 inches for this case.

TABLE B-3

PENETRATION TIMES FOR REACTOR VESSEL AND GUARD VESSEL

100% Core
Uneven debris distribution (depth = 2ℓ)
No delay time

	Blanket (percent)				
Steel (lb)	0	11.3	22.6	61.3	100
0	400	600	800	1800	3500
1000	400	600	900	1900	3600
5000	600	800	1000	2100	4000
10000	800	1000	1300	2600	4700
20000	1300	1600	1900	3500	(1)
30000	1900	2200	2600	4600	----
40000	2500	3000	3500	(1)	----
50000	3300	3900	(1)	----	----
60000	(1)	(1)	----	----	----

(1) Sodium dryout on reactor vessel does not occur.

TABLE B-4

PENETRATION TIMES FOR REACTOR VESSEL AND GUARD VESSEL

100% Core
Uneven debris distribution
1000 Second delay

	Blanket (percent)				
Steel (lb)	0	11.3	22.6	61.3	100
0	1800	2200	2600	4400	(1)
5000	2100	2500	3000	4900	----
10000	2500	2900	3400	(1)	----
20000	3200	3600	4200	----	----
30000	3900	4400	(1)	----	----
40000	(1)	(1)	----	----	----

(1) Sodium dryout on guard vessel does not occur.

TABLE B-5

PENETRATION TIMES FOR REACTOR VESSEL AND GUARD VESSEL

100% Core
Even debris distribution
5000 Second delay

	Blanket (percent)				
Steel (lb)	0	11.3	22.6	61.3	100
0	6200	7000	7800	(2)	(1)
5000	6600	7400	8300	----	----
10000	7100	7900	(2)	----	----
20000	(2)	(2)	----	----	----

(1) Sodium dryout on reactor vessel does not occur.

(2) Sodium dryout on guard vessel does not occur.

Nomenclature

A_o volumetric heat source at time zero, $Btu/hr\text{-}ft^3$

K thermal conductivity of debris, $Btu/hr\text{-}ft\text{-}^oF$

ℓ debris bed depth, ft

x location in debris bed, ft

t time, hr

V temperature difference in debris bed, ^oF

Q_v heat flux required for sodium dryout in 10^3 $Btu/hr\text{-}ft^2$

L Fuel loading in gm/cm^2

L_{ss} steel loading in gm/cm^2

α thermal diffusivity, ft^2/hr

λ time constant of tne decay heat curve, hr

ℓ bed depth, ft

APPENDIX C ANALYTIC THERMAL MODELS AND DATA BASE

This Appendix provides additional information on the analytic models and data base used in the thermal and structural evaluations in Section 3. Specifically, C.1 discusses the models and the data base for the pre-sodium boildry thermal analyses; C.2 discusses the models and data base for the post-sodium boildry thermal analyses; C.3 discusses the material properties used in the structural analyses.

APPENDIX C.1
PRE-SODIUM BOILDRY MODEL AND DATA BASE

C.1.1 Physical Description

C.1.1.1 Cell Description and Initial Conditions

The CACECO code (Reference C.1-1) performs energy and mass balances (including chemical reactions) in four cells - the reactor cavity, the pipeway cells (reactor cavity side of the bellows), the containment volume above the operating floor including the head access area, and the volume below the operating floor (Cell 105). The cells are shown schematically in Figure C.1-1. Volumes, initial atmosphere compositions, initial temperatures, and initial pressures of each of the cells are shown in Table C.1-1.

C.1.1.2 Heat Structures

The energy balances of the cells consider the energy sources, (Section C.1.2) the energy carried by mass movements into and out of the cells, (Section C.1.3.2) and the heat sinks of the containment structures. The heat structures used to simulate the structure heat absorbing capability are a series of one dimensional structures thermally connected to each other and the cell atmospheres described in Section C.1.3.1. The description of each heat structure is given in Table C.1-2 and the location of each structure is shown schematically in Figure C.1-1.

The concrete heat structure representing the reactor cavity walls and roof and the pipeway cells walls, roof, and floor (structures numbered 8, 9, 11, 12, 13, 18, 19 and 20) are composed of the steel liner (0.375 inches thick), 4 inches of insulating concrete followed by the structural limestone aggregate concrete. The 1/4 inch space behind the liner was not considered because radiative heat transfer across the gap results in minimal thermal resistance as compared to the thermal resistance of a small thickness of concrete. The MgO gravel between the liner and RC floor (concrete structure 10) was neglected in the analysis.

Energy transfer within the structures was determined by solving the one-dimensional transient heat conduction equation by finite difference techniques.

C.1.1.3 Materials Released at Penetration of Reactor Vessel and Guard Vessel

An initial spray of 1000 pounds of sodium and all of the noble gases were considered to be injected into the containment building prior to penetration. However, in the CACECO model these releases were considered to occur at the time of penetration, which is the starting time of the CACECO transient analysis.

At penetration, assumed to be 1000 seconds after the HCDA, most of the primary system sodium would flow into the reactor cavity. A fluid mechanical analysis indicates that 1.1 x 10^6 lbs of sodium would syphon from the system when the outlet nozzles are uncovered. This amount of sodium was used in the analysis. Any additional sodium that could be pumped into the vessel from the makeup system was ignored. This is conservative with respect to reactor cavity and containment building integrity.*

The temperature of the sodium mass at penetration would be 990^oF based on adiabatic heating of the sodium prior to penetration.

The initial average temperature of the reactor vessel and internals would be 1035^oF. This value was obtained from the mass average of the steel and the sodium in the reactor vessel only.

The total fuel and blanket inventory was assumed to be within the reactor cavity after penetration, providing decay heat.

---

* Since it would not be conservative for the estimate of materials reaching the containment cleanup system, margin has been provided in the cleanup system requirements (Section 2.1.2.9) to accommodate the possibility of additional sodium entering the reactor cavity from the makeup system.

C.1.2 Heat Sources

C.1.2.1 Decay Heat

The decay heat is based on steady state operation at 975 MW without uncertainties - the nominal heat. The nominal decay heat is based on the homogeneous core design. The heterogeneous core design will have little or no impact on the scenario since the integrated decay heat over the first 24 hours is less than 5% of the previous homogeneous design. Table C.1-3 gives the decay power for the various classes of fission products. The code uses a log-log interpolation technique to determine the power levels at intermediate times.

The decay heat associated with the noble gases is input to the containment atmosphere at penetration of the reactor vessel and guard vessel. The heat associated with the halogens and volatiles is assumed to be contained in and carried with the sodium. The remainder of the decay heat is released at the bottom of the reactor cavity. This is a conservative approach, since some of the volatiles may boil away from the sodium pool before sodium boiling begins. Less decay heat in the reactor cavity would reduce the sodium boiloff rate and therefore would result in less severe containment conditions.

C.1.2.2 Sodium Activity

The energy associated with the decay of Na-24 was added to the sodium in both the reactor cavity sodium pool and the reactor cavity and containment atmospheres. The initial activity would be 25 milli-curies per cubic centimeter. The energy would decay with a 15 hour half-life.

C.1.2.3 Sodium-Concrete Interactions

The sodium-concrete reaction parameters used in this study are based on small and intermediate scale tests. These values are:

1. A penetration attack rate of 1/2 inch/hour
   (References C.1-2, C.1-3 and C.1-4).

2. A total penetration of 2 inches. The accumulation of reaction products limits the penetration depth. (Reference C.1-4).

3. A chemical heat release of 331 Btu/lb of concrete. (Reference C.1-2) This sodium-concrete reaction energy (Na-H_2O and Na-CO_2 reactions are considered in the next section) is only 5% of the decay power during the 4 hour reaction period, therefore, it is not a significant energy source and the conclusions of the analyses would not be impacted by considering the range of experimental uncertainty.

These reaction parameters are represented in the code as an energy input. The analysis assumed that the liner failure permitted sodium to attack the concrete across the full extent of the floor, or 1257 square feet, in the cavity.

C.1.2.4 Chemical Reactions

At the outset of the analysis, sodium vapor reacts with all of the oxygen in the cavity to form sodium oxide.

Sodium pool reactions occur next. When both water and carbon dioxide (from exposed heated concrete) are directed into the sodium pool, sodium reacts according to the molar ratio until either sodium or the carbon dioxide-water is consumed, producing sodium hydroxide or sodium oxide, sodium carbonate, carbon and hydrogen. The production of sodium hydroxide or sodium oxide is dependent on the hydrogen partial pressure and system temperature as presented in Figure C.1-2 (Reference C.1-18).

Upon reaching containment, the sodium vapor would react with the oxygen, carbon dioxide and water vapor according to their molar concentrations. The reaction with water vapor would take place if the water vapor concentration is greater than the oxygen concentration. If the water vapor concentration is less than the oxygen concentration the sodium vapor would react with oxygen and carbon dioxide according to their molar ratios.

Hydrogen reacting with oxygen is considered in the analysis, in the reactor containment building. The criteria for auto-ignition, are if either conditions (a) or (b) and condition (c) are met (see Appendix H.1).

a. The N_2-H_2 mixture entering the RCB is above $1450^{\circ}F$.

b. The Na-H_2-N_2 mixture entering the RCB contains at least 6 g/m^3 of Na at $500^{\circ}F$ or above.

c. The containment oxygen concentration is above 8%. With the oxygen concentration above 5% and the hydrogen concentration above 4%, the hydrogen in excess of 4% would burn.

For the first 10 hours following penetration of the reactor vessel and guard vessel neither criterion (a) nor (b) is satisfied. During this time, hydrogen would accumulate in containment reaching a concentration of 4.5%. At 10 hours criterion (b) would be met and hydrogen burning would continue until 36 hours, when criterion (c) is no longer satisfied. At this time the oxygen concentration drops below the 8% level. Although the oxygen concentration remains above 5% until 38 hours (satisfying criterion (c)) reignition does not occur because the accumulation of hydrogen is less than 4%. During this time span (10 to 36 hours) the hydrogen accumulated during the first 10 hours would burn as natural convective processes move it through the flame zone. As this hydrogen burns, the containment concentration would be reduced to a negligible value at the time of flame extinguishment (36 hours).

The specific chemical reactions covered by the code analysis and the heats of reaction are listed in Table C.1-4.

The code does not consider reaction dynamics, it considers all reactions to occur instantaneously.

C.1.3 Heat and Mass Transfer

C.1.3.1 Cell Heat Transfer Model

The energy transfer model employed in the reactor cavity was:

Convective transfer was considered between the cavity atmosphere and the cavity walls; the pipeway walls and ceiling; the inside surface of the guard vessel and reactor vessel; the outside surface of the reactor vessel and reactor internals.

The heat transfer coefficients are based on free convective heat transfer coefficients (Reference C.1-7) during the early part of the scenario when non-condensible vapors (H_2, N_2, Ar) are present in the reactor cavity and pipeway cells (the presence of argon is neglected in the analysis). After depletion of the non-condensible gases, the analysis considers condensing sodium heat transfer coefficients (Reference C.1-20). The heat transfer coefficients are listed in Table C.1-5.

Radiative transfer was considered between the sodium pool and the reactor cavity walls; between the sodium pool and reactor internals; between the guard and reactor vessels; between the reactor head and internals; between the head and reactor vessel; and between the reactor vessel and internals. All emissivities were taken as 0.1 (based on experimental evidence in Reference C.1-7 and theoretical computations) to be representative of the sodium pool surface and condensed sodium on the other surfaces.

The lower internals (core support plate), lower reactor vessel, lower guard vessel, and guard vessel skirt were taken to be in intimate contact with the sodium pool. These masses are initially submerged in the sodium pool. After these masses become exposed, because of the sodium pool level decreasing when sodium boils away, they will remain in thermal equilibrium with the cavity atmosphere and sodium pool. This is because the small heat losses from these masses are balanced by heat absorbed from radiation from the pool and by convection from the atmosphere.

The reactor cavity atmosphere and sodium pool are assumed to be in thermal equilibrium for computational convenience. This is a reasonable assumption because the sodium pool is at or near the boiling point for most of the scenario.

The sodium pool is assumed to be at a uniform temperature because of the high thermal conductivity of molten sodium and the low viscosity with resulting convection currents. Temperature variations, local boiling, and subsequent pressurization would be insignificant. Calculations have shown that the maximum temperature difference across the sodium pool would be about 30^{o}F, which would result in a local vapor pressure increase of only 7%. This small potential increase in vapor pressure would not be significant because most of the additional vaporized sodium would be condensed in the reactor cavity.

The energy transfer in containment and Cell 105 is by convection from the heat structures to the cell atmospheres (Reference C.1-5 and 6). Table C.1-5 contains the heat transfer coefficients.

C.1.3.2 Inter-Cell Venting and Leakage Models

The vents between the reactor cavity and the pipeway cells, the pipeway cells and containment, and between Cell 105 and containment are modeled by an orifice equation:

$$L = 283,000 \times A \times \sqrt{\rho \Delta p}$$

where L is the vent rate, A is the effective area, ρ the cell atmosphere density, and Δp is the pressure differential. The effective area was 0.15 ft^2 for the reactor cavity - pipeway cells - containment vent and 0.1 ft^2 for the Cell 105 to containment vent. After RCB venting was initiated the reactor cavity - pipeway cells - containment vent was increased to 0.25 ft^2.

The leakage from containment to the atmosphere before venting would be initiated was determined from:

$$L = 17.0 \times \sqrt{\rho \Delta p}$$

where L is the leak rate, ρ is the containment density and Δp is the pressure differential between containment and the outside atmosphere. The constant (17.0) was determined so the equation would yield the design leak rate (0.1 volume percent per day) at the design pressure (10.0 psig).

C.1.4 Material Properties

C.1.4.1 Structural Concrete

The thermal properties used for limestone aggregate structural concrete are shown in Table C.1-6. Two categories are listed, one representing properties appropriate for a high surface heating rate and the second representing properties for a low surface heating rate.

The heat capacity for a low surface heating rate is taken from Reference C.1-8 (employs classical techniques analyzing ordinary conduction). These properties were measured after the specimen reached steady state at each temperature, thereby precluding any transient heat transfer processes.

The thermal conductivity data used are for a similar type of concrete and are a composite from the experimental values in References C.1-2, 8, 9, 10, 11, and 12.

The high heating rate properties were derived from the LT-1 experiment conducted at HEDL (Reference C.1-19). These data are a measure of effective concrete property data. At higher heating rates thermal effects other than ordinary conduction become important. Examples of additional thermal processes are the heat capacity effects of diffusing pore water and internal heat sinks due to heat absorption upon dehydration and decomposition of concrete. Those properties derived from the transient heating in LT-1 are considered prototypic of the short term TMBDB scenario where high heating rates exist. These data were applied to all heat structures adjacent to the reactor cavity (i.e., the floor and walls of the reactor cavity and the pipeway cells).

Experiments conducted at HEDL (Reference C.1-13) and subsequent analysis using the WATRE code indicated significant resistance to water vapor flow in concrete when it is heated to low temperatures ($\sim$300^{o}F). When concrete is heated to temperatures approaching the boiling point of sodium, significant resistance to water vapor flow was not observed. Therefore, in the CACECO code simulation of the water released from concrete structures, two water releases were employed. These are given in Table C.1-6. The data in the section labeled high temperature-high heating rate concrete were obtained from experiments using small samples of concrete (Reference C.1-14). With the small samples, significant flow resistance would not occur;* therefore, these data are appropriate for concrete heated to high temperatures. The data in the section labeled low temperature - low heating rate concrete were obtained from analyses based on the WATRE code using the concrete surface temperature transient appropriate for containment, confinement, and Cell 105 structures. Since comparisons between experiments and WATRE code predictions (Reference C.1-13) indicated the code underpredicts water release by 20-25%, the WATRE code predictions were increased by 30% and used for low temperature concrete structures.

The high temperature-high heating rate concrete water release data were used in the reactor cavity and pipeway structures in the CACECO model. The containment building floor used the low temperature-low heating rate concrete water release data.

Both of the water release curves conservatively neglect concrete drying which could occur between construction and the time of the hypothetical accident.

The carbon dioxide released from heated concrete is based on data from experiments reported in Reference C.1-2. Measured amounts of carbon dioxide were collected over different temperature increments as shown in Table C.1-7. These quantities represent the maximum possible amount of gas that could be released, as the temperature of the specimen was rapidly increased from one level to the next and held at that level until gas evolution ceased. Since the specimen was small (3.9 g) any resistance to gas flow was minimal and therefore the values in Table C.1-7 should be higher than expected for large structures.

*Small samples of concrete offer little mass transfer resistance; therefore the water release rate would be maximized, thus resulting in a more severe hydrogen transient.

C.1.4.2 Insulating Concrete

The thermal conductivity of the insulating concrete in the reactor cavity and the pipeway cell double-heated wall is 0.12 Btu/hr-ft-^{o}F. The insulating concrete conductivity in the remaining pipeway cell structures is 0.24 Btu/hr-ft-^{o}F. The heat capacity is given in Table C.1-8. Water release was assumed to be identical to that of the structural concrete. This assumption is not significant because the water released from the insulating concrete is a small fraction of that of the structural concrete. The density of the insulating concrete is 72 lb/ft^3. Carbon dioxide release was assumed to be identical to that of structural concrete because of code limitations. The insulating concrete would not release carbon dioxide because it contains pearlite as the aggregate. This assumption is not significant because of the small mass of the insulating concrete compared to the structural concrete.

C.1.4.3 Steel

The properties of all the steel in the containment building were taken as (Reference C.1-15):

Thermal Conductivity	26 Btu/hr-ft-^{o}F
Heat Capacity	0.11 Btu/lb-^{o}F
Density	490 lb/ft^3

C.1.4.4 Sodium

The properties of sodium used in the CACECO code analyses are taken from Reference C.1-16. The code considers the sodium boiling point as a function of pressure as given in the reference.

C.1.5 References

C.1-1 R. D. Peak, "Users Guide to CACECO Containment Analysis Code," HEDL-TME 79-22, June 1979.

C.1-2 S. A. Meacham, "The Interaction of Tennessee Limestone Aggregate Concrete with Liquid Sodium," WARD-D-0141, December 1976.

C.1-3 J. A. Hassberger, R. K. Hilliard and L. D. Muhlestein, "Sodium - Concrete Reaction Tests," HEDL-TME-74-36, June 1974.

C.1-4 J. A. Hassberger, "Intermediate Scale Sodium-Concrete Reaction Tests," HEDL-TME-77-99, March 1978. (Availability: U.S. DOE Technical Information Center.)

C.1-5 A. J. Ede, "Advances in Free Convection," in Advances in Heat Transfer, Vol. 4, pp. 1-64, Academic Press, New York, 1967.

C.1-6 A. P. Colburn and O. A. Hougen, "Studies in Heat Transmission," Ind. Eng. Chem. 22, No. 5 pp. 522-539 (1930).

C.1-7 J. G. Yevick and A. Amcrosi, Fast Reactor Technology Plant Design, p. 413, MIT Press, Cambridge, MA, 1966.

C.1-8 T. Z. Harmathy and L. W. Allen, "Thermal Properties of Selected Masonry Unit Concretes," J. Amer. Concrete Inst. 70, No. 2, pp. 132-142 (1973).

C.1-9 E. Crispino, "Studies on the Technology of Concretes Under Thermal Conditions," Paper SP 34-25, Concrete for Nuclear Reactors, Vol. I, ACI SP-34, pp. 443-479, American Concrete Institute, Detroit, Michigan, 1972.

C.1-10 T. Harada, J. Takeda, S. Yamane and F. Furumura, "Strength, Elasticity and Thermal Properties of Concrete Subjected to Elevated Temperatures," Paper SP 34-21, Concrete for Nuclear Reactors, Vol. I, ACI SP-34, pp. 377-406, American Concrete Institute, Detroit, Michigan, 1972.

C.1-11 L. Baker, Jr., et al, "Postaccident Heat Removal Technology," ANL/RAS-77-2, Section VII, January 1977. (Availability: U.S. DOE Technical Information Center).

C.1-12 N. G. Zoldners, "Effect of High Temperatures on Concretes Incorporating Different Aggregates," Amer. Soc. Test. Mater., Proc. 60, pp. 1087-1108 (1960).

C.1-13 A. K. Postma, J. D. McCormack and J. A. Schur, "A Study of Water and Gas Release from Heated Concrete," HEDL-TC-996, December 1977.

C.1-14 J. D. McCormack and A. K. Postma, "Water and Gas Release from Heated Concrete," HEDL-SA-1117, 1976. (Availability: U.S. DOE Technical Information Center).

C.1-15 F. Kreith, Principles of Heat Transfer, Third Edition, Intex Educational Publishers, New York, 1973.

C.1-16 G. H. Golden and J. V. Tokar, "Thermophysical Properties of Sodium," ANL-7323, August 1967.

C.1-17 "Advanced Safety Analysis Fourth Quarterly Report June - August 1975," GEAP-14038-4, September 1975. (Availability: U.S. DOE Technical Information Center).

C.1-18 E. M. Mitkevich and B. A. Shikhov, "The Metallic Sodium-Sodium Hydroxide System," Russ J Inorg Chem, II, No. 3, pg. 343 (March 1966).

C.1-19 R. W. Wierman, L. D. Muhlestein and L. D. Simmons, "Experimental Evaluation of Cell Liners," in R. H. Mallett and B. R. Nair, ed., Coolant Boundary Integrity Considerations in Breeder Reactor Design, PVP-PB-027, pp. 113-131, American Society of Mechanical Engineers, New York, 1978.

C.1-20 D. G. Kroger and W. M. Rohsenow, "Condensation Heat Transfer in the Presence of a Non-condensable Gas," Int J Heat Mass Trans, II, pp. 15-26, 1968.

TABLE C.1-1

CONTAINMENT CELL VOLUMES, INITIAL ATMOSPHERE COMPOSITIONS, INITIAL TEMPERATURES, AND INITIAL PRESSURES

Cell	Volume (ft^3)	Initial Atmosphere Composition O_2 (Volume %)	Initial Atmosphere Composition N_2 (Volume %)	Initial Temperature (^oF)	Initial Pressure (psia)
Reactor Cavity	5.24×10^4	2	98	120	14.7
Pipeway Cells	1.62×10^4	2	98	120	14.7
Reactor Containment Building	3.5×10^6	21	79	95	14.7
Cell 105	4.8×10^5	21	79	95	14.7

TABLE C.1-2

HEAT STRUCTURE DESCRIPTION

Structure Number	Surface Area (ft^2)	Description
1	1.2×10^4	1.5×10^6 lbs of steel containment equipment.
2	9.1×10^4	1.5 inch thick steel containment dome.
3	2.4×10^4	6.3 foot thick concrete floor of containment building not over reactor cavity.
4	1.2×10^5	4.0 foot thick concrete confinement building.
5	2.0×10^3	5.5 foot thick concrete walls of head access area.
6	3.3×10^2	1.0×10^6 lbs of steel and shielding of reactor vessel head.
7	6.2×10^2	7.0×10^5 lbs of reactor vessel internals.
8	5.2×10^3	7.0 foot thick concrete walls of reactor cavity above sodium pool.
9	1.1×10^3	7.0 foot thick concrete walls of reactor cavity submerged by sodium pool (9 foot upper submerged wall).
10	1.3×10^3	14.0 foot concrete floor of reactor cavity submerged by sodium pool.
11	4.6×10^2	4.0 foot thick pipewall cell double heated wall.
12	1.0×10^3	5.3 foot thick pipeway cell floor.
13	1.6×10^3	6.3 foot thick pipeway cell roof and HAA walls.
14	1.3×10^5	6.0 foot thick floor and wall of cell 105.
15	2.7×10^3	7.9×10^5 lbs of reactor vessel.

TABLE C.1-2 (Continued)

HEAT STRUCTURE DESCRIPTION

Structure Number	Surface Area (ft^2)	Description
16	2.0×10^3	9.4×10^4 lbs of guard vessel and outlet pipes
*17	1.9×10^3	3.7×10^5 lbs of submerged internals in the sodium pool.
18	3.4×10^3	4.0 foot thick pipeway cell outside wall.
19	8.1×10^2	2.5 foot thick pipeway cell outside wall.
20	1.0×10^3	7.0 foot thick concrete walls of reactor cavity submerged by sodium pool (8 foot lower submerged wall).

*At 30 hours structure 17 was redefined as 6.3 foot thick pipewall cell HAA walls.

TABLE C.1-3

DECAY HEAT FOR 975 MW POWER LEVEL WITHOUT UNCERTAINTIES

Time	Decay Power Input To The Reactor Cavity (Fission Products and Solid Fuel Particulate)	Decay Power Carried By Sodium Vapor (Volatiles and Halogens)	Decay Power Input To RCB (Noble Gases)
1000 Secs.	14.28 MW	5.98 MW	.78 MW
30 Min.	12.12	5.24	.65
60 Min.	10.09	4.29	.55
2 Hr.	8.61	3.17	.48
12	5.77	1.49	.23
24	4.91	1.13	.14
96	2.97	.55	.05
240	2.00	.24	.02
720	1.31	.06	.002
1440	0.92	-	-
2160	0.74	-	-
4320	0.49	-	-
8640	0.31	-	-
17,280	0.18	-	-
25,920	0.13	-	-

TABLE C.1-4

CHEMICAL REACTIONS

Reaction Equation	Heat of Reaction	Type of Reaction
* $2Na + H_2O = Na_2O + H_2$	1,600 Btu/lb Na	Pool
* $2Na + 2\ H_2O = 2\ NaOH + H_2$	4,514 Btu/lb Na	Pool
$4\ Na + 3\ CO_2 = 2\ Na_2CO_3 + C$	4,326 Btu/lb Na	Pool
Na + Concrete	331 Btu/lb Concrete	Pool
$4\ Na + CO_2 = 2\ Na_2O + C$	3,800 Btu/lb Na	Atmosphere
$2\ Na + H_2O = Na_2O + H_2$	3,400 Btu/lb Na	Atmosphere
$4\ Na + O_2 = 2\ Na_2O$	5,700 Btu/lb Na	Atmosphere
$2\ H_2 + O_2 = 2\ H_2O$	54,425 Btu/lb H_2	Atmosphere
$2\ Na + H_2 = 2\ NaH$	1,050 Btu/lb Na	Atmosphere
$H_2O + Na_2O = 2\ NaOH$	1,500 Btu/lb Na	Atmosphere

*The production of sodium hydroxide or sodium oxide is dependent on the hydrogen partial pressure and system temperature as indicated in Figure C.1-2.

TABLE C.1-5

CONVECTIVE HEAT TRANSFER COEFFICIENTS

Typical Values ($Btu/hr\text{-}ft^2\text{-}^oF$)	Description
1.21 at 700°F ΔT	Atmosphere of nitrogen (49%), hydrogen (49%) and sodium vapor (2%) inside the reactor cavity.
6.11 at 100°F ΔT	Atmosphere of hydrogen (21%) and sodium vapor (79%) inside the reactor cavity.
200.0	Natural convection film coefficients for sodium submerged surfaces.
1.13 at 75°F ΔT	Containment building and cell 1^nr atmospheres.
1.74 at 500°F ΔT	

TABLE C.1-6

STRUCTURAL CONCRETE PROPERTY DATA

Low Heating Rate - Low Temperature Concrete
(Concrete not adjacent to the reactor cavity)

Temperature (°F)	Volumetric Heat Capacity (Btu/ft^3-°F)	Thermal Conductivity (Btu/hr-ft-°F)	Water Release (lb/ft^3)	Carbon Dioxide Release (lb/ft^3)
0.	28.7	1.0	0.	0.
190.			0.	
200.		0.98		
212.	28.7			
275.			0.31	
285.			0.47	
392.	32.45			
420.			0.56	
572.	36.82			
700.			0.61	
752.	41.81			
800.			0.67	
932.	43.07			
1000.		0.65		
1100.				0.
1112.	44.94			
1200.				1.
1292.	38.38			
1300.				2.5
1400.				5.5
1422.	31.52			
1500.			0.78	17.5
1550.				28.
1600.		0.55		42.
1630.				52.5
1652.	28.7			
5000.	28.7	0.55	0.78	52.5

Heat of Fusion = 220 BTU/lb (Reference C.1-17)

TABLE C.1-6 (Continued)

STRUCTURAL CONCRETE PROPERTY DATA

High Heating Rate - High Temperature Concrete
(Concrete adjacent to the reactor cavity)

Temperature (°F)	Volumetric Heat Capacity (Btu/ft^3-°F)	Thermal Conductivity (Btu/hr-ft-°F)	Water Release (lb/ft^3)	Carbon Dioxide Release (lb/ft^3)
0.	29.7	1.5	0.	0.
190.			0.	
192.(-)	29.7			
192.(+)	45.2			
200		1.4		
214.(-)	45.2			
214.(+)	94.7			
275.			3.85	
285.			5.78	
300.(-)	94.7			
300.(+)	48.0			
400.(-)	48.0	1.28		
400.(+)	41.2			
420.			6.84	
500.				
600.		1.15		
700.			7.51	
750.(-)	41.2			
750.(+)	47.8			
800.		1.02	8.28	
830.(-)	47.8			
830.(+)	44.7			
1000.		.88		
1100.				0.
1200.				1.
1300.				2.5
1400.(-)	44.7	.6		5.5
1400.(+)	206.			

TABLE C.1-6 (Continued)

STRUCTURAL CONCRETE PROPERTY DATA

High Heating Rate - High Temperature Concrete
(Concrete adjacent to the reactor cavity)

Temperature (^{o}F)	Volumetric Heat Capacity (Btu/ft^3-^{o}F)	Thermal Conductivity (Btu/hr-ft-^{o}F)	Water Release (lb/ft^3)	Carbon Dioxide Release (lb/ft^3)
1500.(-)	206.			
1500.(+)	378.		9.63	17.5
1550.(-)	378.			28.
1550.(+)	492.			
1600.(-)	492.	.46		42.
1600.(+)	608.			
1630.(-)	608.			
1630.(+)	19.2	.35		52.5
1800.				
2000.	19.2	.35	9.63	52.5

Heat of Fusion = 220 Btu/lb (Reference C.1-17)

TABLE C.1-7

CONCRETE CARBON DIOXIDE RELEASE DATA
(RAW DATA FROM EXPERIMENTS REPORTED IN REFERENCE C.1-2)

Temperature Level	Total Gas Released	CO_2 Mole	Incremental CO_2 Released	Total CO_2 Released	Total CO_2 Released	Incremental Release (1)	Accumulated Release (1)
°F	cm^3 (STP)	Percent	cm^3 (STP)	cm^3 (STP)	Percent	lb/ft^3	lb/ft^3
302	1.432	0.48	0.007	0.007	0.002	0.001	0.001
572	0.904	0.90	0.008	0.015	0.003	0.002	0.003
842	0.954	20.33	0.194	0.209	0.062	0.032	0.035
1112	2.644	64.62	1.708	1.917	0.544	0.286	0.321
1382	27.881	98.10	27.351	29.268	8.702	4.568	4.889
1652	287.700	99.07	285.024	314.292	90.687	47.610	52.500

(1) Normalized to a total theoretical release of 52.5 lbs/ft^3 to compensate for losses in the collection system. The theoretical release is based on the following equation:

Maximum CO_2 release = density of concrete X weight fraction of carbonates in concrete (.79) X weight fraction of carbonates which converts to CO_2 (.44).

TABLE C.1-8

THERMOPHYSICAL PROPERTIES OF INSULATING CONCRETE

Thermal Conductivity

0.12 Btu/hr-ft-°F (Reactor Cavity and Pipeway Cell Double Heated Wall Structures - a Constant Value)

0.24 Btu/hr-ft-°F (Remaining Pipeway Cell Structures - a Constant Value)

Heat Capacity

Temperature °F	Heat Capacity* Btu/ft^3-°F
32	14.4
212	14.4
392	18.15
572	22.52
752	27.51
932	28.77
1112	30.64
1292	24.08
1472	17.22
1652	14.4
2000	14.4

*The volumetric heat capacity was assumed to be equivalent to that of the low heating rate - low temperature structural concrete adjusted for the differences in density of the two concretes.

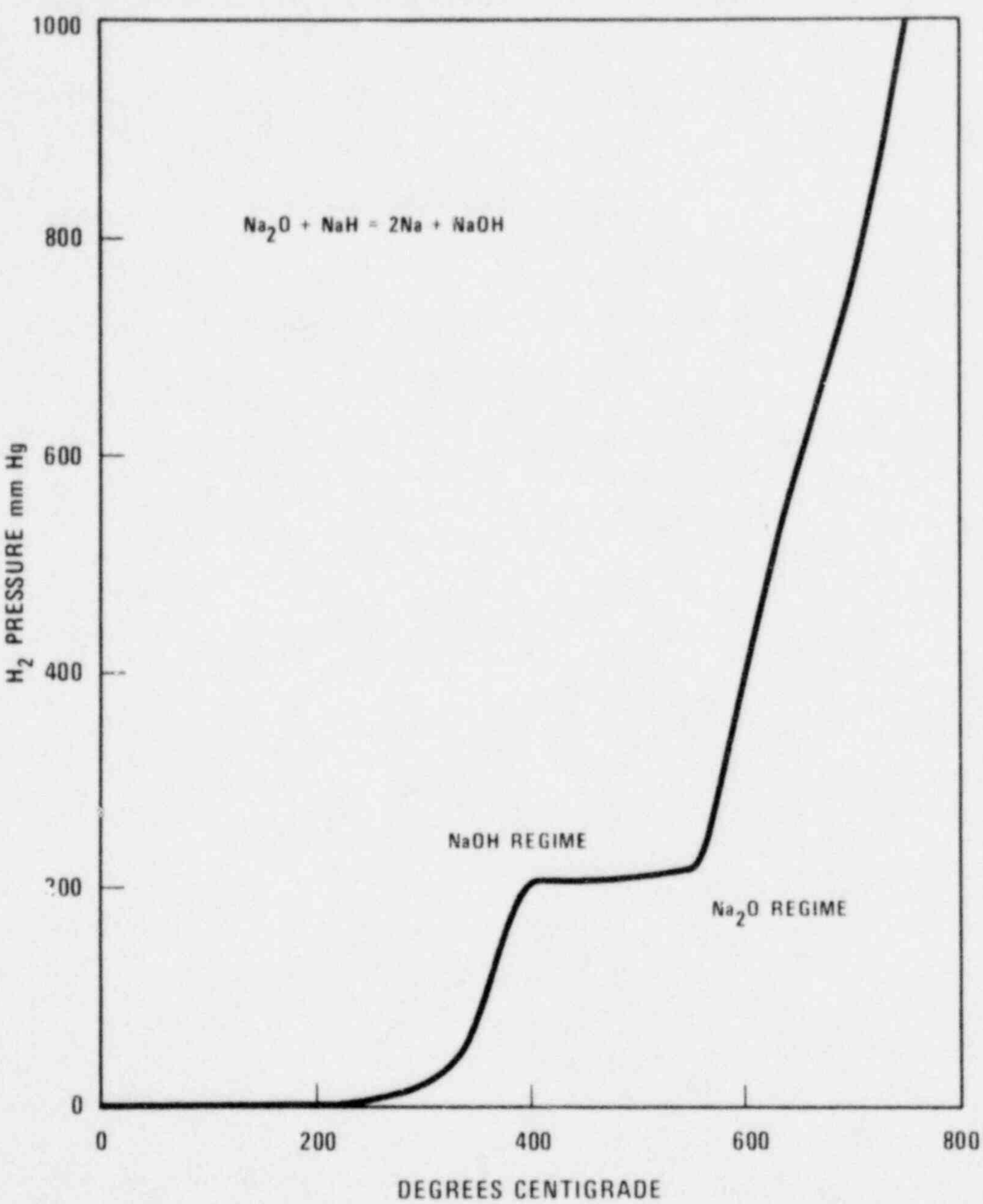

Figure C.1-2. Na — NaOH System

1966-120

APPENDIX C.2
POST SODIUM BOILDRY MODEL AND DATA BASE

C.2.1 Analytical Model

The major structures in containment were included in the thermal model of the post sodium boildry conditions. These structures include the reactor cavity, basemat, Cell 105 walls, Cell 102 walls, PHTS cell walls, operating deck, head access area (HAA) walls, containment wall, confinement wall, and the steel equipment inside the reactor cavity. The TRUMP computer code (Reference C.2-1) was used for this analysis.

The structures considered in the model are described in Table C.2-1 and illustrated in Figures C.2-1, 2, 3 and 4. Structures inside the reactor cavity (upper and lower cavity wall, support ledge and HAA wall) and the basemat are modeled in cylindrical geometry while the structures outside the cavity are modeled as one-dimensional slabs. The heat transfer mechanisms considered are thermal radiation from structure to structure, convection from the structure to the surrounding atmosphere, and conduction through the structure. An emissivity of 0.90 (Reference C.2-2) was used for surfaces inside the reactor cavity while a value of 0.60 (Reference C.2-3) is used for structures outside the cavity. A convective heat transfer coefficient of 1.0 Btu/hr-ft^2-^oF was used between all structures and cell atmospheres (a typical value for free convective heat transfer). To account for uncertainties in molten pool heat transfer, the fraction of decay heat conducted into the basemat was varied from 10 to 90%. This range of downward heat split is considered to bracket the uncertainty in fuel penetration, including the effects of cracking and spalling.

Initial temperature distributions were obtained from the results from the base case CACECO output. An isothermal boundary of 212^oF was assumed at the basemat-ground interface because a constant heat sink would be provided by the ground water. The same boundary is assumed adjacent to the confinement wall at elevations below the operating deck. Above the operating deck, either an annulus cooling system or an ambient (outside confinement) temperature served as the boundary condition.

Structural failures were assumed in the model when specified criteria were met. The criteria used in this evaluation were: 1) when the concrete wall mid-plane reached 700°F, failure was assumed to occur (Section 3.2.3.2) and 2) the reactor closure head has assumed to fail at the approximate melting point of steel (2500°F). After a structural failure, the atmosphere temperatures of the two cells would equalize. Radiative transfer between structures in the two cells is taken into account. The mass of the failed wall remains in the simulation; however, the area of the failed wall was reduced to 10% of its non-failed value.

The oxides from the concrete, steel, and fuel were assumed to mix completely as observed from the phase diagram (Reference C.2-4) of the major constituents of concrete with UO_2 (Figures C.2-5, 6, 7 and 8). Experiments recently conducted at ANL, in which electrically heated UO_2 was melted into limestone concrete, confirmed the equal distribution of the oxides (Reference C.2-5). Fuel oxides would not react with the concrete oxides as discussed in Section 3.2.2. Molten steel would not chemically react with the oxides of concrete; however, the gases released from heated concrete (CO_2 and H_2O) would oxidize the molten steel (Reference C.2-5). Iron oxide would then lower the melting (eutectic) point of the oxide mixture and penetration (ordinary melting) would occur (Reference C.2-5). The reaction energy from the molten steel-gas reactions would be less than 10% of the decay power.

Considering the magnitude of this energy compared to decay power, and the fact that the downward heat transfer was bracketed from 10 to 90% in Section 3.2.3, the effect of this chemical reaction would be insignificant.

Any additional chemical energy generated after sodium boildry would increase the rate at which the molten debris attacks the concrete basemat. Although calculations (Section 3.2.3) indicate complete basemat penetration is unlikely, penetration of the basemat and subsequent groundwater contamination would not contribute significantly to the overall consequences of accidents beyond the design base (see Section 4.3).

The concrete was assumed to melt at the lowest eutectic point (~2200°F) for CaO-Fe_2O_3 in air (Figure C.2-8). No particular shape of the pool is presumed. Sufficient amounts of steel are assumed to be reduced to Fe_2O_3

to allow continual melting of the concrete at the eutectic temperature. The phase diagrams in Figures C.2-5, 6 and 7 indicate eutectic temperatures of SiO_2, CaO, and MgO with UO_2 to be 3000°F, 3780°F, and 4200°F; thus, the assumption of a 2200°F melting point is conservative.

Fuel penetration was assumed to be ordinary melting as previously discussed and because recent experiments (Reference C.2-6) indicate concrete spalling and cracking would not be significant to the penetration process. The upward heat transfer from the molten pool to the atmosphere is governed by the thermal resistance of the oxide crust on top of the pool (the higher the resistance the lower the heat flux in the upward direction). Convective processes in the pool, which are in series with the oxide crust resistance, are considered to be a second order effect and are not specifically considered.

In the model, the volumetric heat generation is simulated by using a heating plane on the reactor cavity floor. As the underlying concrete is melted, the thermal conductivity is increased several orders of magnitude. This effectively simulates a uniformly distributed heat source in the molten pool and an approximate uniform temperature in the molten pool. Gas evolution from the concrete was observed to stir the melt in tests conducted at Sandia (Reference C.2-6) giving an approximate uniform temperature.

Molten steel was not considered in the model except for providing a source for iron oxide. The thermal conductivity of molten steel is so much higher than that of the oxides present that its thermal resistance is insignificant. The heat capacity of the steel is considered as part of the reactor cavity equipment.

C.2.2 Data Base

Decay Power

The decay power is based on nominal decay values for an operating power level of 975 MW. The noble gases, halogens and sodium soluble volatiles are assumed to be released to the containment or carried along with the sodium vapor to the containment building. Following sodium boildry, only the fuel, solid fission products and sodium reaction products (containing halogens and sodium soluble volatiles) would remain on the reactor cavity floor. The decay power associated with this heat source is given in Table C.1-3.

Thermal Properties

The thermal properties of the high heating rate-high temperature structural concrete used in the analysis are given in Table C.1-6. Energy absorption effects of the gases being released (water vapor and carbon dioxide) from the heated concrete are included in the volumetric heat capacity.

C.2.3 References

C.2-1 A. L. Edwards, "TRUMP: A Computer Program for Transient and Steady-State Temperature Distributions in Multidimensional Systems," UCRL-14754, Rev. 2, July 1969.

C.2-2 E. M. Levin, et al., Phase Diagrams for Ceramics, American Ceramic Society, Columbus, Ohio, 1964.

C.2-3 "Light Water Reactor Safety Research Program Quarterly Report, January-March 1976," SAND 76-0369, August 1976.

C.2-4 "Advanced Safety Analysis Fourth Quarterly Report June - August 1975," GEAP-14038-4, September 1975. (Availability: U.S. DOE Technical Information Center).

C.2-5 L. Baker, Jr., et al., "Postaccident Heat Removal Technology," ANL/RAS-77-2, Section VII, January 1977. (Availability: U.S. DOE Technical Information Center).

C.2-6 D. A. Dahlgren, "Light Water Reactor Safety Research Program Quarterly Report," SAND 76-0369, NUREG 766506, August 1976.

TABLE C.2-1

LOWER CONTAINMENT STRUCTURE DESCRIPTION

Structure Number	Structure Name	Structure Description	Figure Number
1	Reactor Cavity Upper Wall	Reactor Cavity wall between elevations 750' and 785'. Complete wall (360° arc) Cylindrical geometry.	C.2-3 and 4
2	Reactor Cavity Lower Wall	Reactor cavity wall between elevations 741'-1" and 750'. Complete wall (360° arc) Cylindrical geometry.	C.2-4
3	Support Ledge	Reactor support ledge. Diagonally between top of reactor cavity wall and closure head.	C.2-4
4	PHTS Wall (Facing the Reactor Cavity)	PHTS cell walls between elevations 752'-11" and 781'. Irradiated by thermal radiation from reactor cavity.	C.2-3 and 4
5	PHTS Wall (Not Facing the Reactor Cavity)	PHTS cell walls that separate Cell 105 and the PHTS cells.	C.2-2, 3 and 4

TABLE C.2-1 (Continued)

LOWER CONTAINMENT STRUCTURE DESCRIPTION

Structure Number	Structure Name	Structure Description	Figure Number
6	Containment Wall (Adjacent to the PHTS cell walls)	Containment wall between elevations 784' and 810' exposed to the PHTS cells atmospheres.	C.2-2 and 4
7	Containment Wall (Adjacent to Cell 105)	Containment wall between elevations 733' and 811' exposed to the atmosphere of Cell 105.	C.2-3 and 4
8	Containment Wall (Adjacent to Cell 102A)	Containment wall between elevations 733' and 765' exposed to the Cell 102A atmosphere.	C.2-3 and 4
9	Confinement Wall	Structure between elevations 733' and 811'. Continuous around containment.	C.2-3 and 4
10	Wall Between Cells 102 and 105	Structure between elevations 733' and 802' that extends from the reactor cavity wall to containment.	C.2-2 and 3
11	Operating Floor (Above Cell 105)	The operating floor above Cell 105.	C.2-1
12	Operating Floor (Above the PHTS cells)	The operating floor above the PHTS cells.	C.2-1
13	Reactor Cavity Floor	Concrete below the reactor cavity and reactor cavity walls between elevations 730' and 741'.	C.2-4

TABLE C.2-1 (Continued)

LOWER CONTAINMENT STRUCTURE DESCRIPTION

Structure Number	Structure Name	Structure Description	Figure Number
14	Basemat	Structure between elevations 715' and 730' below the reactor cavity and reactor cavity walls and the rest of the containment basemat between elevations 715' and 733'.	C.2-4
15	Reactor Cavity Steel	Steel in the reactor cavity which includes the reactor vessel, internals, head and guard vessel.	C.2-4

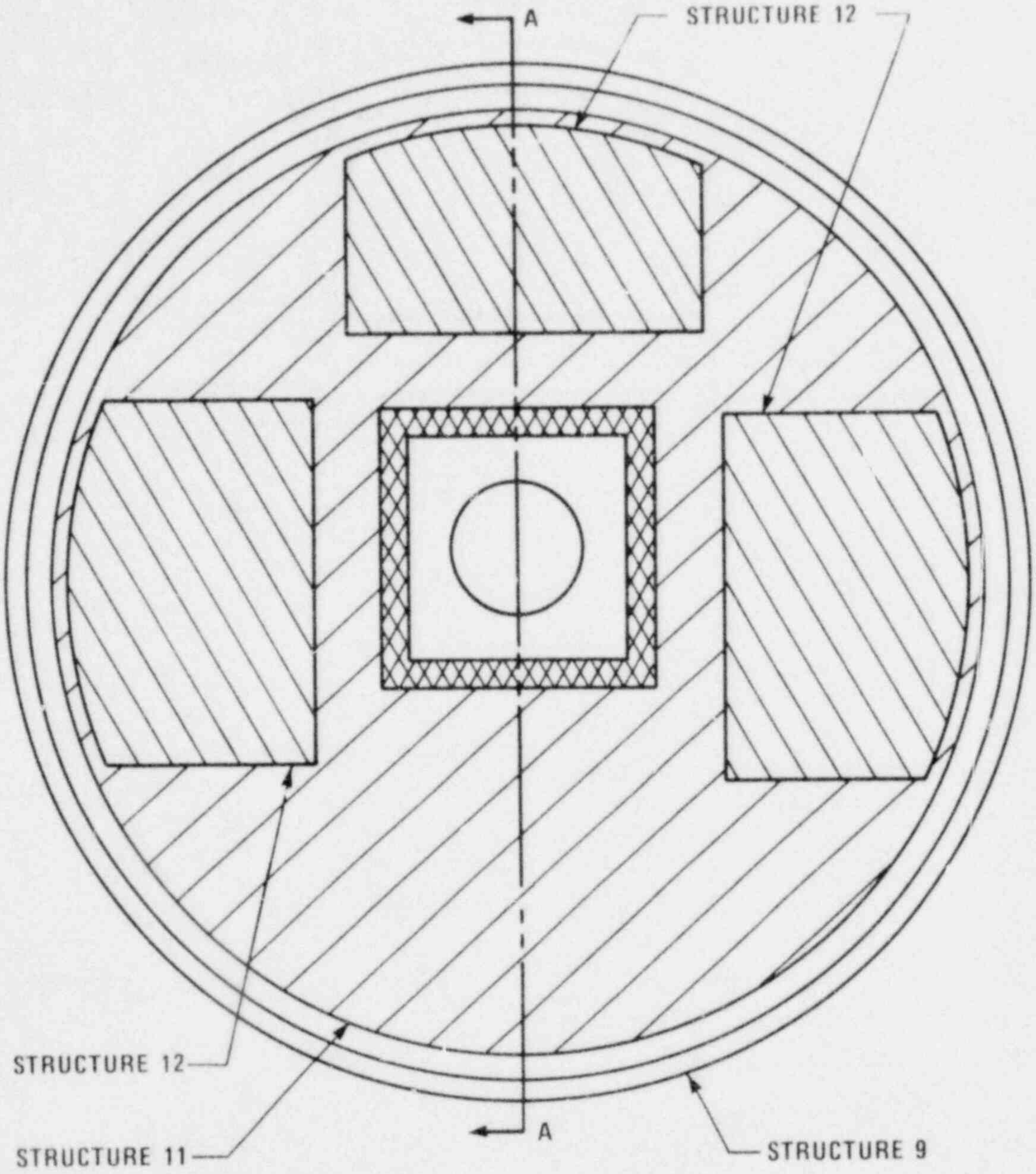

Figure C.2-1. Plan View at Elevation 816.0

1966-121

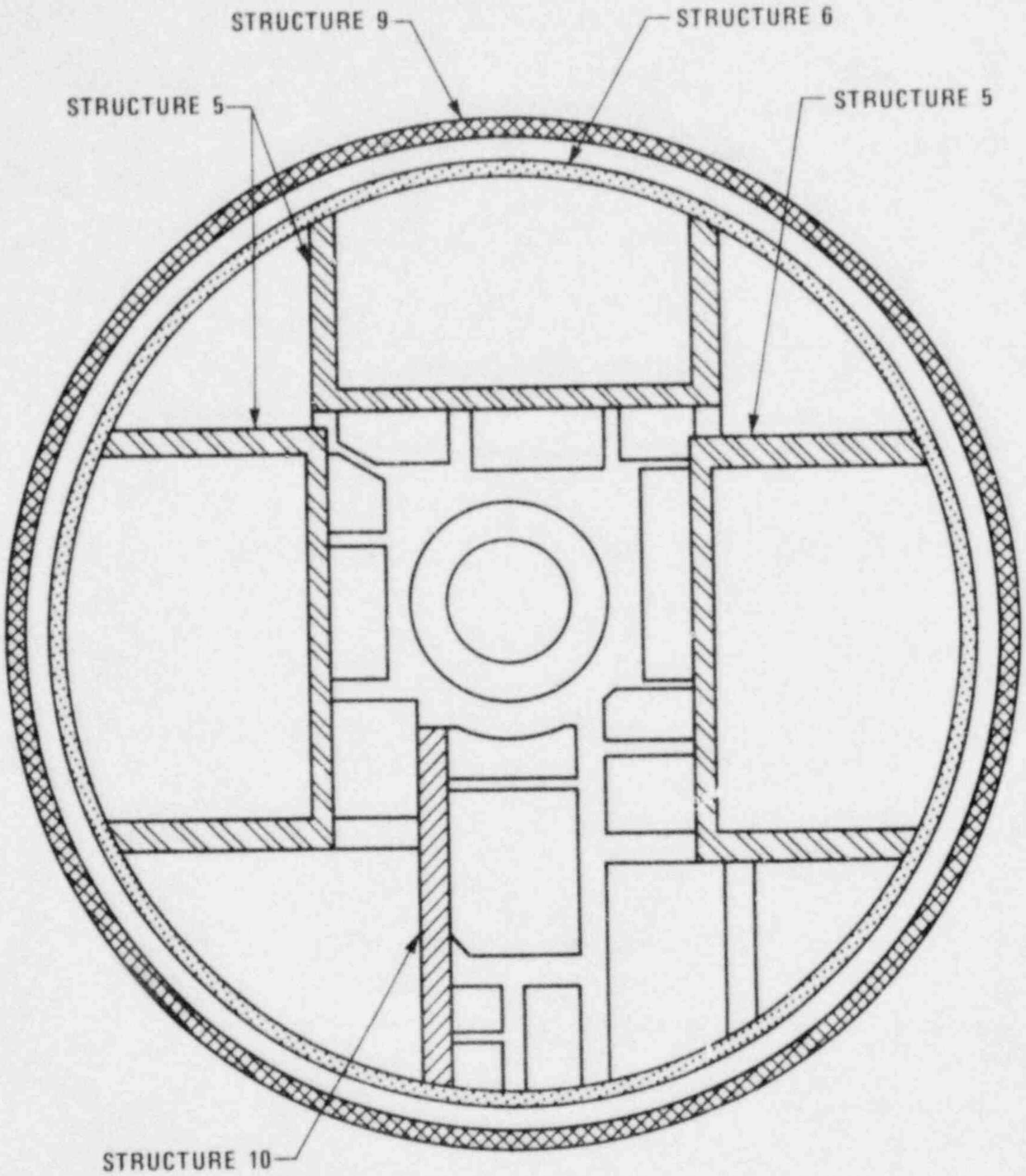

Figure C.2-2. Plan View at Elevation 785.0

1966-122

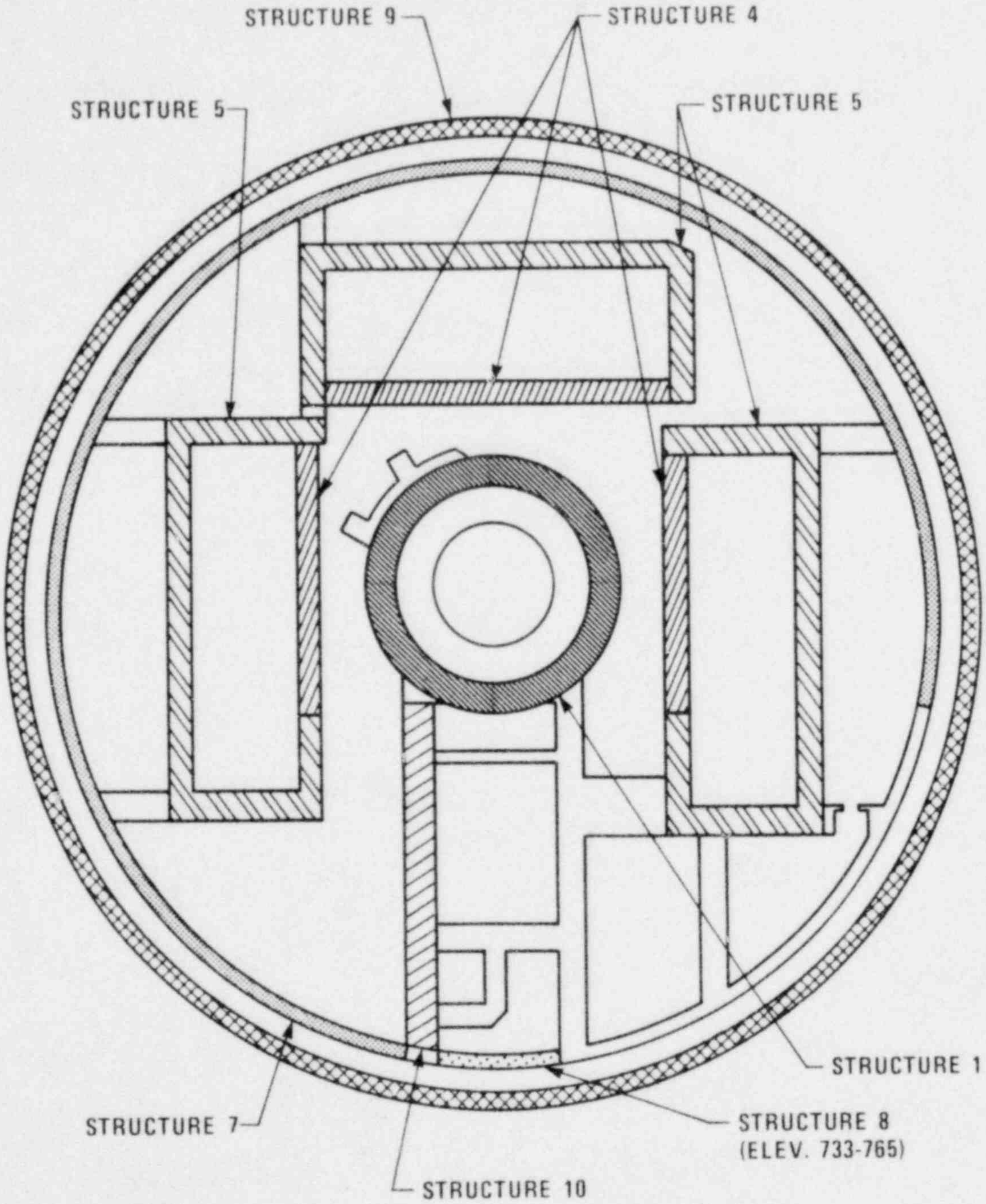

Figure C.2-3. Plan View at Elevation 766.0

1966-123

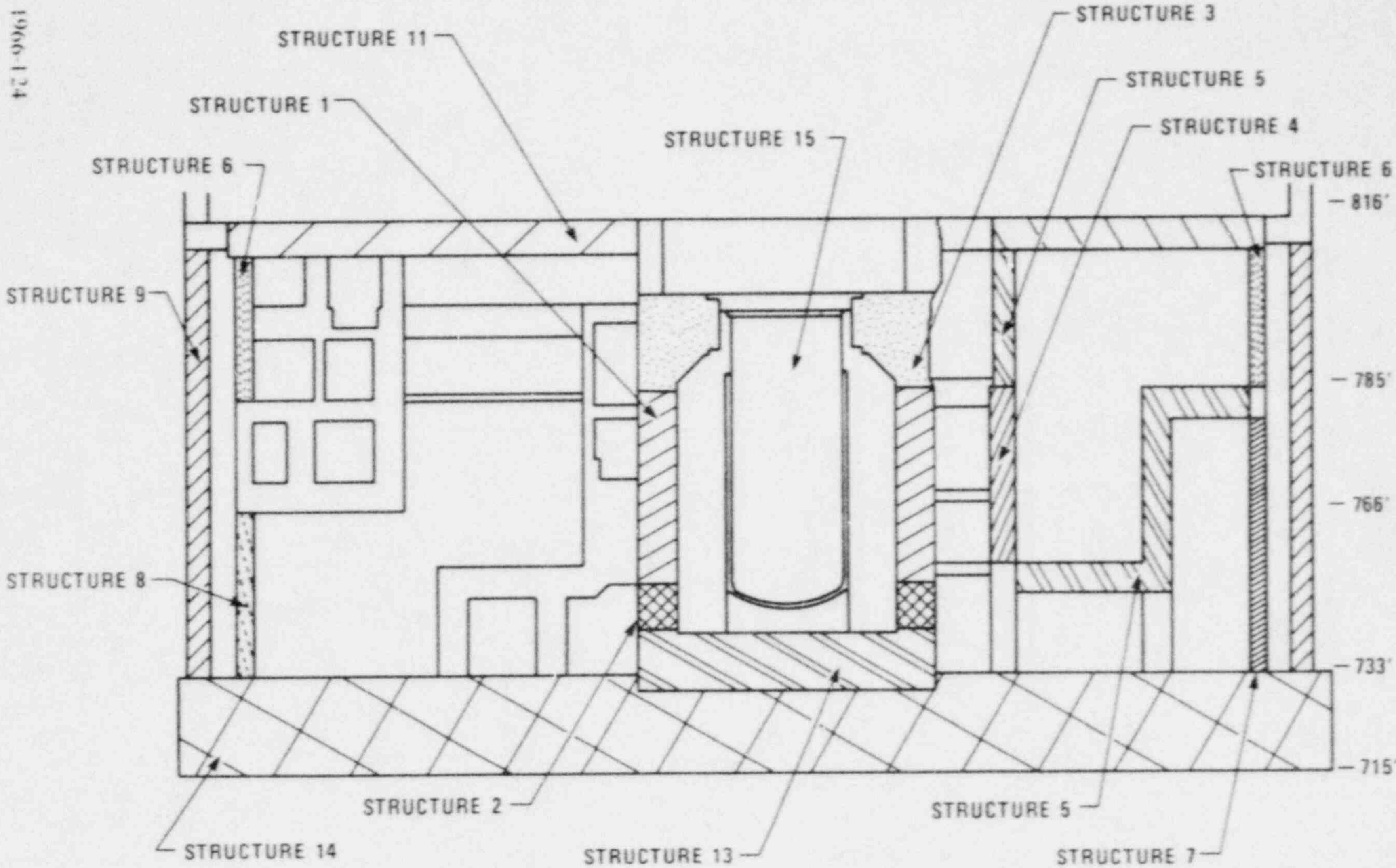

Figure C.2-4. Elevation of Lower Containment (Section A-A)

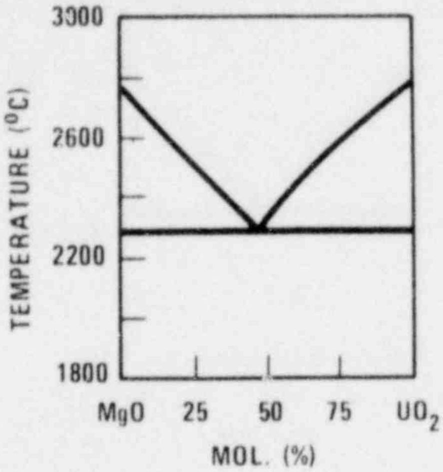

Figure C.2-5. Phase Diagram $MgO-UO_2$ System

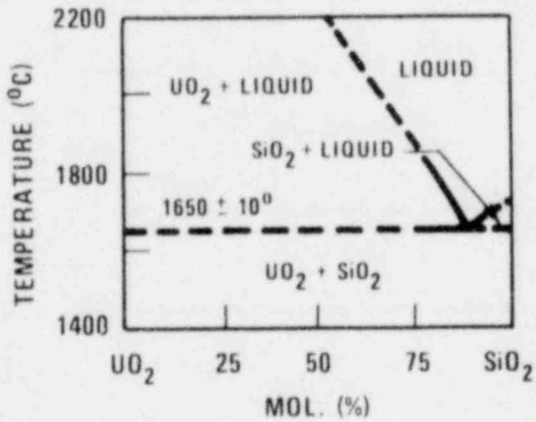

Figure C.2-6. Phase Diagram SiO_2-UO_2 System

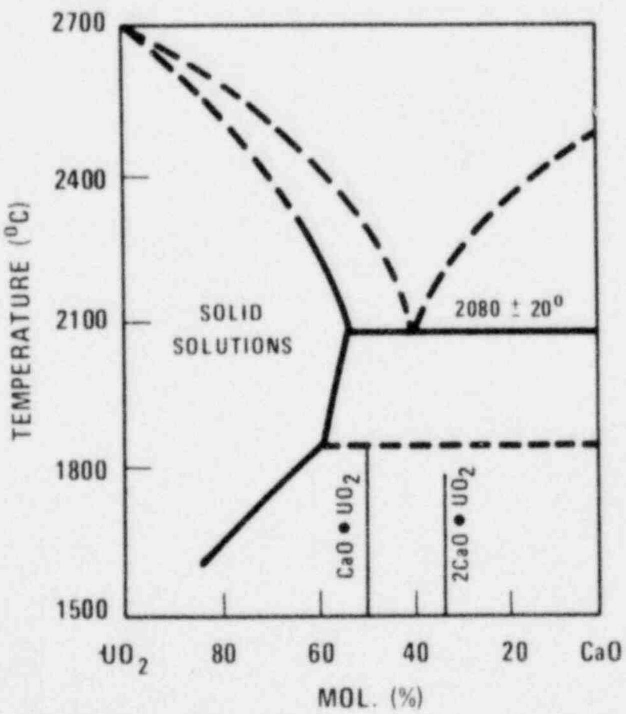

Figure C.2-7. Phase Diagram $CaO-UO_2$ System

1966-125

1966-126

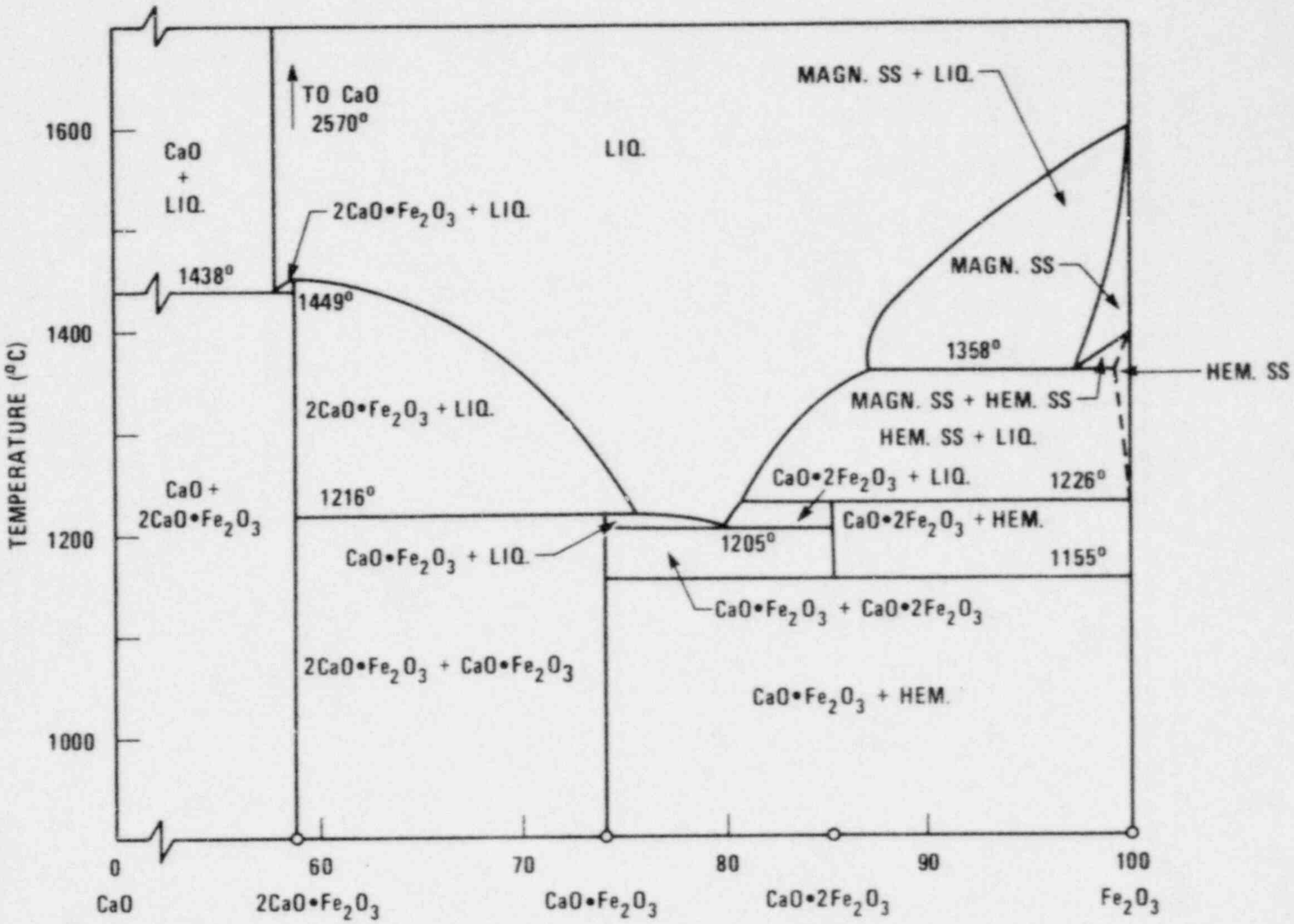

Figure C.2-8. Phase Diagram $CaO-Fe_2O_3$ in Air

APPENDIX C.3

STRUCTURAL MATERIAL PROPERTIES AT ELEVATED TEMPERATURES

C.3.1 Introduction

The evaluation of the structures in the containment requires knowledge of material properties at high temperatures and involves criteria which are not covered explicitly in any of the present codes. For this reason, it is necessary to define stress deformation relationships and other important properties at normal and elevated temperatures and to establish criteria appropriate for TMBDB conditions.

The relationships for concrete and liner steel at elevated temperatures have been based on published experimental studies and the results of testing carried out as part of the CRBRP development programs. The relationships for reinforcing steel have been based on generally accepted data.

C.3.2 Concrete Properties

C.3.2.1 Compressive Strength and Elasticity

C.3.2.1.1 Behavior at Elevated Temeperatures and Design Relationships

The compressive strength and the modulus of elasticity of structural concrete decrease with exposure to elevated temperatures. The magnitude and variation of the reduction in these properties with temperature is influenced by a multitude of factors resulting in a wide scatter of experimental results. For this reason an extensive literature study was carried out to determine the factors governing the elevated temperature strength and elasticity properties, to determine bounding exposure conditions for use in the development of a testing program, and to establish reliable and representative relationships. The published test results considered cover the range of temperatures from normal to 1600^{o}F and demonstrate that the effect of elevated temperature exposure is highly dependent upon the concrete mix and the testing methods and exposure conditions.

Elevated temperature testing for compressive strength and modulus of elasticity is generally separated into two categories representing "cold" and "hot" testing. In cold testing the test specimens are heated gradually to a specified temperature, are allowed to remain at that temperature for a period of time, then are allowed to cool to normal temperatures and are tested. In hot testing the specimens are heated to a specified temperature and are tested while at that temperature. In both cases the test specimens are maintained in either an "open" environment where water vapor can escape or in a "closed" moisture migration system where moisture is contained. Specimens are either "loaded" or "unloaded" during the heating and cooling phases. The following general observations are based on the literature study.

a. Specimens heated and then allowed to cool before testing lose more strength than those tested when hot (Figures C.3-1, C.3-2).

b. Specimens lose more strength if water (moisture) is not allowed to escape while heating than do specimens where the moisture is allowed to escape.

c. Concrete specimens loaded during heating lose less strength than unloaded specimens.

d. The longer the duration of heating before testing, the larger the loss in strength. This loss of strength, however, stabilizes after a period of long isothermal exposure.

e. The decrease in the modulus of elasticity, due to elevated temperature exposure, is more pronounced than the decrease in compressive strength (Figures C.3-1 to C.3-3).

f. Mix proportions and type of aggregate influence the strength of heated concrete as follows:

    lean mixes (low cements/aggregate ratio) lose less strength due to heating than richer mixes.

concrete made with limestone aggregate degrades less due to heating than concrete made with siliceous aggregate.

g. The strength of concrete before heating has little effect on the percentage of strength retained at elevated temperatures. (Reference C.3-1)

Published results on the residual compressive strength of concrete exposed to elevated temperatures are shown in Figure C.3-1 for hot testing and in Figure C.3-2 for cold testing. The effect of high temperature on the modulus of elasticity is shown in Figure C.3-3. A summary of the test conditions and mix properties cor.esponding to these data is given in Reference C.3-19.

The literature results provided a basis for establishing design relationships that represent the upper and lower bound response of concrete elevated temperature exposure. These relationships for compressive strength are shown in Figures C.3-1 and C.3-2 for hot and cold test conditions respectively. The design relationships for the modulus of elasticity are shown in Figure C.3-3. Due to the lack of sufficient data on this property, however, different relationships for hot versus cold testing were not revealed by the literature.

In the evaluation of concrete structures at elevated temperatures, a lower bound curve for compressive strength is conservative for capacity while an upper bound curve for E, a measure of stiffness, is conservative with respect to thermal forces. Design relationships, however, based on a lower bound curve of one parameter and an upper bound curve for the other will lead to undue conservatism since the test results indicate correspondence between the upper and lower bound curves. More rationally the response to thermal gradients may be bracketed by one pair of lower bound and one pair of upper bound curves. In the investigation for TMBDB, however, due to the generally high temperatures involved, the elastic part of the σ-ϵ curve is not expected to be a significant factor and thus properties based on lower bound curves are expected to result in the most critical response.

C.3.2.1.2 Verification Testing Programs

The information obtained from the study of the published results was used as a basis for implementing a confirmatory verification testing program which was carried out at Oak Ridge National Laboratory (ORNL) and published in Reference C.3-4. The objective of the program was to test mature concrete under prototypic exposure conditions to verify the bounding relationships established via the literature study. To obtain a lower bound relationship of concrete strength, the cylinders were tested in a semi-closed moisture migration environment after gradual cool down ("closed-cold"). To establish a relationship for hot testing the cylinders were tested in an open moisture migration environment while at the elevated temperature ("open-hot"). In both cases the test cylinders were exposed to high temperatures while unloaded.

The testing was performed on 8 to 19 month old concrete cylinders (6" diameter X 12") of a limestone aggregate mix similar to that proposed for use in the CRBRP structures. All of the concrete cylinders tested were heated to their test temperature for 14 days. Details of the testing equipment, procedures and the specimens are given in References C.3-4, and C.3-31.

The relationships for residual compressive strength obtained from this testing program are shown in Figures C.3-4 and C.3-5 for open-hot and closed-cold test conditions respectively. On the same figures are shown the relationships established from the literature which are confirmed by the verification test results. Relationships for the residual modulus of elasticity under open-hot and closed-cold conditions are shown in Figures C.3-6 and C.3-7. These results fall within the established bounds and are closer to the lower bound design relationship.

The residual compressive strength was established by comparing the actual compressive test results with the strength of the cylinders immediately before heat up. The strength of companion cylinders was used in the determination of the test cylinder strength before heating. This procedure eliminated the variable of strength gain with age from the design relationship.

The strength gain with age, for the particular concrete mix used in this testing is shown in Figures C.3-4 and C.3-5. The upper curves show the ratio of values for approximately one year old cylinders heated to the test temperature over companion unheated specimens tested at 28 days. These curves indicate that cylinders which have gained strength with age degrade to values below the 28 day strength only after significant heating. Although similar gains occur in the modulus of elasticity (Figure C.3-7), the age effect often results in conservatism which may be an important factor to consider in a realistic evaluation of structures.

C.3.2.2 Stress-Strain Relationship at Normal Temperature

The generally accepted stress-strain diagram for concrete starts out with a nearly linear portion that extends to about 30 percent of the maximum stress, then as cracking takes place it deviates from linearity at an increasing rate until it reaches the maximum stress. Beyond this point, at which significant cracking takes place, the curve descends until failure occurs.

A number of mathematical equations have been proposed by various authors to express the relationship between stress and strain in concrete. In general, these expressions are in good agreement in the ascending part of the curve but differ significantly beyond the point of maximum stress. The stress-strain relationship by Kent and Park (Reference C.3-10) which exhibits a sharply descending branch was selected in this study to describe the behavior of concrete at normal temperatures and to serve as a basis in establishing relationships for concrete at elevated temperatures. This relationship is given by the following expressions:

$$f_c = f'_c \left[2 \frac{\varepsilon_c}{\varepsilon_o} - \left(\frac{\varepsilon_c}{\varepsilon_o} \right)^2 \right] \qquad 0 < \varepsilon < \varepsilon_o \qquad (1a)$$

$$f_c = f'_c \left[1 - Z \ (\varepsilon_c - \varepsilon_o) \right] \qquad \varepsilon > \varepsilon_o, \ f_c \geq 0.2 \ f'_c \qquad (1b)$$

$$f_c = 0.2 \ f'_c \qquad \varepsilon > \varepsilon_o, \ f_c < 0.2 \ f'_c \qquad (1c)$$

where:

f'_c is the maximum stress,

ε_o is the strain corresponding to maximum stress and is equal to 0.002 in/in, (at normal temperature),

$Z = 0.5/(\varepsilon_{50h} + \varepsilon_{50\mu} - \varepsilon_o)$ is the slope of the descending branch of the curve,

$\varepsilon_{50\mu} = (3 + 0.002\ f'_c)/(f'_c - 1000)$ is the strain corresponding to $0.5\ f'_c$ on the descending branch of the σ-ε curve for unconfined concrete

ε_{50h} is the difference in strain between confined and unconfined concrete; at $0.5\ f'_c$ on the descending branch of the σ-ε curve. For unconfined concrete considered here ε_{50h} equals zero.

The expression for the ascending part of the curve is essentially the same as that proposed by Hognestad (Reference C.3-9). Beyond the maximum stress the curve, for unconfined concrete, descends at a faster rate than the curves proposed by other authors and has been found to agree well with experimental results.

The stress-strain relationship for concrete at elevated temperatures is similar to that at normal temperature except that the maximum stress is attained at much higher strains in the case of elevated temperatures. In Reference C.3-2, it is shown that the relationship at elevated temperatures may be derived from that at normal temperatures if the variation of maximum stress and the corresponding strain with temperature is known.

The variation of ε_o, the strain corresponding to maximum stress, with temperature has been derived using the results obtained by Furamura and reported in Reference C.3-2 together with results from the testing program at ORNL. The proposed relationship is shown in Figure C.3-8 where the ratio of ε_o at elevated temperatures to ε_o at normal temperature is plotted against temperature. Using these data, together with the design relationships for compressive strength and elasticity, stress-strain curves have been established (Reference C.3-19) for 4000 psi concrete tested under hot or cold conditions (Figures C.3-9 to C.3-11). Of these, the curves derived from the lower bound design relationships for cold testing are significant for post accident evaluations of structures. The curves corresponding to hot conditions are more realistic for structures under thermal gradients and provide sufficient conservatism since they are based on bounding relationships.

C.3.2.3 Limiting Values of Strains

In the previous section it was pointed out that beyond the point of maximum stress the σ-ϵ curve descends and finally failure occurs at some lower stress level. This fact indicates that the material failure should be related to strains rather than stresses and any criteria for failure must be expressed in terms of strains in order to be meaningful and to avoid undue conservatism. According to the ACI 318-77 Code Section 10.2.3 (Reference C.3-3) the maximum usable strain is 0.003 in/in or approximately 50 percent higher than the strain corresponding to maximum stress. The values of ultimate strains reported in literature vary widely depending on the type of concrete mix, the testing methods, the degree of confinement and other factors. Reference C.3-20 reports maximum compressive strains between 0.003 and 0.004 in/in for unconfined concrete while other investigations, (Reference C.3-21) have shown that considerably higher strains, even beyond 0.010 in/in can be developed in uniaxial compression. For concrete at elevated temperatures the strains corresponding to maximum stress are substantially higher than those at normal temperatures (Figure C.3-8) and it is expected that failure strains are also higher. Based on these facts the following recommendations are made for uniaxial compression:

(a) For concrete at temperatures of 500°F and higher the failure strain in compression shall be equal to 0.004 in/in.

(b) For concrete at temperatures below $500^{\circ}F$ the failure strain in compression shall be equal to 0.003 in/in.

Thus, for temperatures up to $500^{\circ}F$ the strains are conservatively limited to the same value specified in the 1977 ACI Code (Reference C.3-3). For higher temperatures a modest increase to 0.004 in/in is deemed both realistic and safe in view of the above considerations. It should be emphasized that exceeding the limiting value does not mean collapse of a particular structure or component but rather local failure of the material. Due to redundancies and the self relieving nature of thermal stresses, structural integrity as required for TMBDB may be retained beyond local material failure and structures will be evaluated on that basis.

C.3.2.4 Tensile Strength

The tensile strength, f_{tu}, at normal temperature is given by the following equation in accordance with Section 9.5.2.3 of Reference C.3-3:

$$f_{tu} = f_r = 7.5\sqrt{f'_c}$$

where f_{tu} or f_r represent the cracking strength and f'_c is equal to the maximum compressive strength. In the case of elevated temperature the same equation is used in TMBDB evaluation with f'_c at elevated temperatures being the maximum strength at the temperature in question.

As indicated by the above equation, concrete is weak in tension and due to the likely presence of shrinkage cracking its tensile strength is neglected in capacity calculations. In thermal calculations neglecting the tensile strength is nonconservative since thermal stresses are affected by the stiffness of a given member and the degree of restraint against deformations. For this reason the tensile strength will be considered in detailed thermal stress analysis calculations. In simplified thermal analyses, where a single element represents the thickness of a member, the tensile strength will also be considered and the stiffness of the elements will be based on gross or cracked properties depending on whether the extreme fiber tensile stress is lower or higher than the tensile strength.

C.3.2.5 Shear Strength

The testing program for the CRBRP includes the study of shear at elevated temperatures. Until such data become available the shear strength will be based on the ACI Code (Reference C.3-3) relationships but using values for f'_c that include the effect of high temperature exposure on the compressive strength as discussed earlier.

C.3.2.6 Bond Strength

The effect of high temperature exposure on the bond strength of concrete has not been studied effectively. The results reported by Harada et. al., in Reference C.3-8 for normal portland cement and silica aggregate show a very substantial reduction in bond strength with temperature (Figure C.3-12) much greater than the corresponding decrease in compressive strength. These results will be used in the TMBDB evaluation until data are obtained from the testing program.

C.3.2.7 Thermal Expansion

At normal temperatures the thermal expansion of concrete depends on a number of factors including mix proportions, moisture content, age, and the rate of heating. The most important factor, however, is the mineral composition and structure of the aggregate. Concrete mixtures with high quartz content in the aggregate have the highest coefficients of thermal expansion while those containing little or no quartz, such as limestone have the lowest coefficients.

The coefficient of thermal expansion varies with temperature and generally increases with increasing temperature. Test results on the variation of the coefficient of expansion with temperature for limestone concrete, under consideration here, are reported in References C.3-8, C.3-22 and C.3-23. The average coefficient, α_{ave}, deduced from these references is shown in Figure C.3-13 together with a proposed relationship for use in the TMBDB study. In this relationship α_{ave} starts out with a value equal to that specified in the code for normal temperature then follows the trend of the experimental results remaining practically constant up to 300^{o}F beyond which it increases linearly with temperature.

In addition to the average coefficient of thermal expansion, the instantaneous coefficient of thermal expansion, α_i, referring to the rate of change of thermal strain with temperature, is of interest particularly in incremental analysis procedures. A proposed relationship for α, corresponding to α_{ave}, is also given in Figure C.3-13.

The determination of the coefficient of thermal expansion and its variation with temperature for the particular limestone aggregate portland cement concrete mix used in the CRBRP is one of the objectives of the testing program referred to previously. The results of this program will serve as a check on the proposed relationship.

C.3.2.8 Poisson's Ratio

At normal temperatures the value of Poisson's ratio, ν, for concrete is generally between 0.15 and 0.25. Exposure to high temperatures usually results in lower values for ν and Reference C.3-24 indicates a reduction of about 50 percent at 300^{o}C (572^{o}F). Due to the lack of sufficient data, however, a constant value of about 0.17 will be assigned to ν over the entire temperature range.

C.3.2.9 Biaxial and Triaxial Stress-Strain Distributions

In biaxial and triaxial compression, test results at normal temperatures (References C.3-29 and C.3-30) indicate a marked increase in the compressive strength of concrete and the strains at which the maximum strength is attained. The initial portion of the curve, and hence the modulus of elasticity, is not appreciably affected.

In the TMBDB investigation for the CRBRP, only cases of uniaxial and biaxial stress states are considered. The stress-strain relationship derived for uniaxial compression will be used in the case of biaxial compression. In special cases where biaxial stress-strain distributions will be used, the relationships will be derived using the biaxial stress-strain characteristics reported in Reference C.3-29 and the strength-temperature and modulus of elasticity-temperature design relationships described earlier.

C.3.3 Properties of Reinforcing Steel

C.3.3.1 Strength and Elasticity

Stress-strain curves for reinforcing steel at normal temperatures exhibit an initial elastic portion up to the yield point, a plastic range where strain increases at a constant or nearly constant stress, and a strain-hardening range where strain increases with stress again. A relationship at normal temperatures was developed for Grade 60 bars using the results reported in Reference C.3-25 together with the ASTM Specification (A615) for yield stress and tensile strength.

The behavior at elevated temperatures for reinforcing bars is assumed similar to the behavior of structural steels described in Reference C.3-26. The σ-ϵ curves at higher temperatures are similar to the normal temperature curve but become more rounded as the temperature increases. The tensile and the yield strength generally decrease and the modulus of elasticity also drops with increasing temperature. These effects are shown in Figure C.3-14 for a high strength low alloy steel which approximates best the Grade 60 reinforcing bars and for which the behavior curves are lower bounds.

For the purpose of the TMBDB investigation the σ-ϵ curves for reinforcing steel at elevated temperatures shown in Figure C.3-15 were obtained from the normal temperature curve shown on the same figure by adjusting the yield value, modulus of elasticity and tensile strength, according to the reductions indicated in Figure C.3-14. The limiting strain value over the entire range of temperature exposure is assumed equal to [illegible]5 percent of the minimum elongation value (7% for No. 11 bars) specified in ASTM.

C.3.3.2 Thermal Expansion

The coefficient of thermal expansion for reinforcing bars may be assumed the same as that recommended in the AISC Specification (Reference C.3-27) for structural steels. Thus, for temperatures up to $100^{o}F$ the average coefficient is equal to 6.5×10^{-6} ($in/in/^{o}F$) and for the range between $100^{o}F$ to $1200^{o}F$ it may be calculated from the equation

$$\alpha_{ave} = (6.1 + 0.0019T) \times 10^{-6} \quad (in/in/^{o}F)$$

in which T is the temperature in degrees Fahrenheit. The corresponding instantaneous coefficient, α_i, shown in Figure C.3-16 together with α_{ave}, may be approximated by the following expression:

$$\alpha_i = (6.0 + 0.0038T) \times 10^{-6} \quad (in/in/^{o}F)$$

C.3.4 Properties of Liner Steel

C.3.4.1 Tensile Properties

The cell liner material in the CRBRP Reactor Containment Building is ASME SA 516 (Grade 55), a low carbon steel. A comprehensive test program was carried out at Westinghouse as part of the development programs for the CRBRP to determine properties of this material at elevated temperatures. The relationships used in the TMBDB evaluations are based on the results of this testing.

The test results on the tensile properties of SA 516 steel are reported in Reference C.3-28 for strain rates of 10^{-1}, 10^{-3}, and 10^{-4} in/in/sec. and cover the range of temperatures to $1700^{o}F$. The properties corresponding to the rate of 10^{-4} in/in/sec. show the highest deterioration of strength with temperature and were used throughout this investigation except where the effect of using higher strain rates during the initial temperature rise was studied.

Additional tensile tests were made at temperatures of 1350°F and 1800°F using strain rates of 10^{-4}. The results of these tests, which are not included* in Reference C.3-28, follow the general trends of the test results at other temperatures (Figures C.3-17 to C.3-19.)

The idealized stress strain curves used in this investigation are shown in Figures C.3-17 and C.3-18. A very sharp rate of decrease of strength with temperature is noted in the range between 800°F and 1350°F; beyond 1350°F the strength continues to drop but at a much slower rate. The uniform elongation, ϵ_u, an important property since it relates directly to the failure criteria, also drops sharply with temperature in the range 600°F to 1200°F (Figure C.3-19), levels off between 1200°F and 1500°F, increases at 1600°F and drops again at higher temperatures. The sharp changes beyond 1200° are probably due to the flat plateau of the stress strain curve in this temperature range and also the fact that the points at 1350°F and 1800°F are based on one test. For these reasons the point of 1350°F was disregarded in arriving at the strain allowables.

C.3.4.2 Coefficient of Thermal Expansion

Test results on the variation of the coefficient of thermal expansion for SA 516 steel with temperature, in the range of 100°F to 1700°F are reported in Reference C.3-28. The average coefficient of thermal expansion (Figure C.3-20) increases with temperature up to 1350°F, decreases sharply between 1350°F and 1550°F as the transformation of the body centered cubic iron to a face centered cubic structure takes place, and then increases again beyond 1550°F.

---

* The tests at these temperatures were performed after Reference C.3-28 was issued and will be incorporated into future reports.

C.3.4.3 Creep Behavior

Test results on the creep behavior of SA 516 steel at elevated temperatures are reported in Reference C.3-28 and show that at high temperature and stress levels considerable creep can occur in just a few hours of sustained temperature (Figures C.3-21). It should be pointed out, however, that in the case of structural elements which are mainly subjected to thermal strains, such as the cell liners, the effect of creep will generally be to relieve or relax compressive strains by exchanging mechanical strains with creep strains.

C.3.4.4 Failure Criteria

The criteria for failure of the material are expressed in terms of strains, and are as follows for the stress states considered here:

1. Tension or compression in stud anchors

   a. Axial Strains

   $$\varepsilon_e = 0.90\ \varepsilon_u$$

   b. Axial plus bending strains

   $$\varepsilon_e = 0.95\ \varepsilon_u$$

2. Membrane strains-biaxial tension

   $$\varepsilon_e = 0.50\ \varepsilon_u$$

3. Membrane plus bending strains, tension in both directions

   $$\varepsilon_e = 0.67\ \varepsilon_u$$

4. Membrane strains or membrane plus bending strains, compression in at least one direction

$$\varepsilon_e = 0.90\ \varepsilon_u$$

Where ε_e is the generalized von Mises strain and ε_u is the strain corresponding to the ultimate tensile strength in the uniaxial test.

Criteria (2) and (3) are the same as those used for extremely unlikely faulted conditions in the cell liner design. These limits are conservative and are based on failure under biaxial tension. Under uniaxial tension or under compression the generalized von Mises strain may reach ε_u but for conservatism, the criteria adopted lower limits, allowing reasonable margins, for TMBDB conditions.

C.3.5 References

C.3-1 M. S. Abrams, "Compressive Strength of Concrete at Temperatures to 1600°F," in Temperature and Concrete, ACI-SP-25, pp. 33-58, American Concrete Institute, Detroit, MI, 1971.

C.3-2 R. Baldwin and M. A. North, "A Stress Strain Relationship for Concrete at High Temperatures," Mag Concr Res 25, No. 85, pp. 208-212 (December 1973).

C.3-3 "Building Code Requirements for Reinforced Concrete (ACI 318-77)," American Concrete Institute, Detroit, Michigan, 1977.

C.3-4 J. P. Callahan, G. C. Robinson and R. C. Burrow "Uniaxial Compressive Strengths of Concrete for Temperatures Reaching 1003K," Nuc Eng Design, 45, No. 2, pp. 439-448 (1978).

C.3-5 D. Campbell-Allen, E.W.E. A. Lower and H. Roper, "An Investigation on the Effect of Elevated Temperatures on Concrete for Reactor Vessels," Nucl Struct Eng, 2, pp. 382-388 (1965).

C.3-6 "Effect of Long Exposure of Concrete to High Temperatures," Concrete Information, Portland Cement Association, ST 32-3-53.

C.3-7 D. J. Hannant, "The Effects of Heat on Concrete Strength," Engineering 197, No. 5105, p. 302 (1964).

C.3-8 T. Harada, J. Tokeda, S. Yamane and F. Furumura, "Strength, Elasticity and Thermal Properties of Concrete Subjected to Elevated Temperatures," in Concrete for Nuclear Reactors, ACI-SP-34, Vol. 1, pp. 377-406, American Concrete Institute, Detroit, MI, 1972.

C.3-9 E. Hognestad, "A Study of Combined Bending and Axial Load in Reinforced Concrete Members," Univ Ill Eng Exp Sta, Bull. Ser., No. 399, (November 1951).

C.3-10 D. C. Kent and R. Park, "Flexural Members with Confined Concrete," Proc ASCE, 97, No. ST7, pp. 1969-1990 (1971).

C.3-11 D. R. Lankard, et al., "Effects of Moisture Content on the Structural Properties of Portland Cement Concrete Exposed to Temperatures of Up to 500°F," in Temperature and Concrete, ACI-SP-25, pp. 59-102, American Concrete Institute, Detroit, MI, 1971.

C.3-12 H. L. Malhotra, "The Effect of Temperature on the Compressive Strength of Concrete," Mag Concr Res, 8, No. 2, pp. 85-94 (1956).

C.3-13 J. C. Marechal, "Variations in the Modulus of Elasticity and Poisson's Ratio with Temperature," in Concrete for Nuclear Reactors, ACI-SP-34, Vol. 1, pp. 495-503, American Concrete Institute, Detroit, MI, 1972.

C.3-14 K. W. Nasser and R. P. Lohtia, "Mass Concrete Properties at High Temperatures," J. Amer. Concr. Inst., 68, pp. 180-1[illegible] (1971).

C.3-15 S. Ohgishi, S. Miyasaka and J. Chida, "On Properties of Magnetite and Serpentine Concrete of Elevated Temperatures for Nuclear Reactor Shielding," in Concrete for Nuclear Reactors, ACI-SP-34, Vol. 3, pp. 1243-1253, American Concrete Institute, Detroit, MI, 1972.

C.3-16 S. C. Pihlajavaara, "An Analysis of the Factors Exerting Effect on Strength and Other Properties of Concrete at Elevated Temperatures," in Concrete for Nuclear Reactors, ACI-SP-34, Vol. 1, pp. 347-354, American Concrete Institute, Detroit, MI, 1972.

C.3-17 F. J. Roux, "Concrete at Elevated Temperatures," Ph.D. Thesis, University of Capetown, South Africa, August 1974.

C.3-18 N. G. Zoldners, "Effect of High Temperatures on Concrete Incorporating Different Aggregates," Proc ASTM, 60, pp. 1087-1108 (1960).

C.3-19 G. H. Freskakis, R. C. Burrow and E. B. Debbus, "Strength Properties of Concrete at Elevated Temperatures," Proc. ASCE Conference on Civil Engineering and Nuclear Power, Volume 1, April 1979.

C.3-20 E. Hognestad, N. W. Hanson and D. McHenry, "Concrete Stress Distribution in Ultimate Strength Design," J. Amer. Concr. Inst., 27, pp. 455-479 (1955).

C.3-21 R. F. Blanks and D. McHenry, "Plastic Flow of Concrete Relieves High Load Stress Concentrations," Civil Eng. 19, No. 5, pp. 40-43 (1949).

C.3-22 V. V. Bertero and M. Polivka, "Influence of Thermal Exposure on Mechanical Characteristics of Concrete," in Concrete for Nuclear Reactors, ACI-SP-34, Vol. 1, pp. 505-531, American Concrete Institute, Detroit, MI, 1972.

C.3-23 E. Crispino, "Studies on the Technology of Concretes Under Thermal Conditions," in Concrete for Nuclear Reactors, ACI-SP-34, Vol. 1, pp. 443-479, American Concrete Institute, Detroit, MI, 1972.

C.3-24 J. C. Marechal, "Variations in the Modulus of Elasticity and Poisson's Ratio with Temperature," in Concrete for Nuclear Reactors, ACI-SP-34, Vol. 1, pp. 495-503, American Concrete Institute, Detroit, MI, 1972.

C.3-25 A. S. Abbasi and C. P. Siess, "Effect of Stress-Strain Characteristics of High-Strength Reinforcement on the Behavior of Reinforced Concrete Beam-Columns," Structural Research Series No. 354, University of Illinois, Urbana, Illinois, September 1969.

C.3-26 R. L. Brockenbrough and B. G. Johnson, Steel Design Manual, U.S. Steel Corp., Pittsburgh, PA. 1968.

C.3-27 Manual of Steel Construction, American Institute of Steel Construction, Inc., 7th Edition, New York, 1970.

C.3-28 M. G. Cowgill, B. C. Gowda and K. C. Thomas, "Final Report on Base Materials Tests for Cell Liner Steels," WARD-D-0252, January 1980.

C.3-29 H. Kupfer, H. Hilsdorf and H. Rusch, "Behavior of Concrete Under Biaxial Stresses," J. Amer. Concr. Inst. 66, No. 8, pp. 656-666 (1969).

C.3-30 S. Freedman, "Properties of Materials for Reinforced Concrete," in M. Fintel, ed., Handbook of Concrete Engineering, pp. 141-211, Van Nostrand Reinhold Co., 1974.

C.3-31 Letter from P. S. VanNort to R. S. Boyd, Transmittal of "Third Level Thermal Margins Report," Docket 50-537, S:L:977, April 22, 1976. (Availability: Nuclear Regulatory Commission, Public Document Room.)

* The material concerning weldments in Reference C.3-28 became available after this Appendix was prepared and the structural evaluations described in Section 3.2 of this report were completed. The weldment properties will be taken into account in the final evaluation.

1966-127

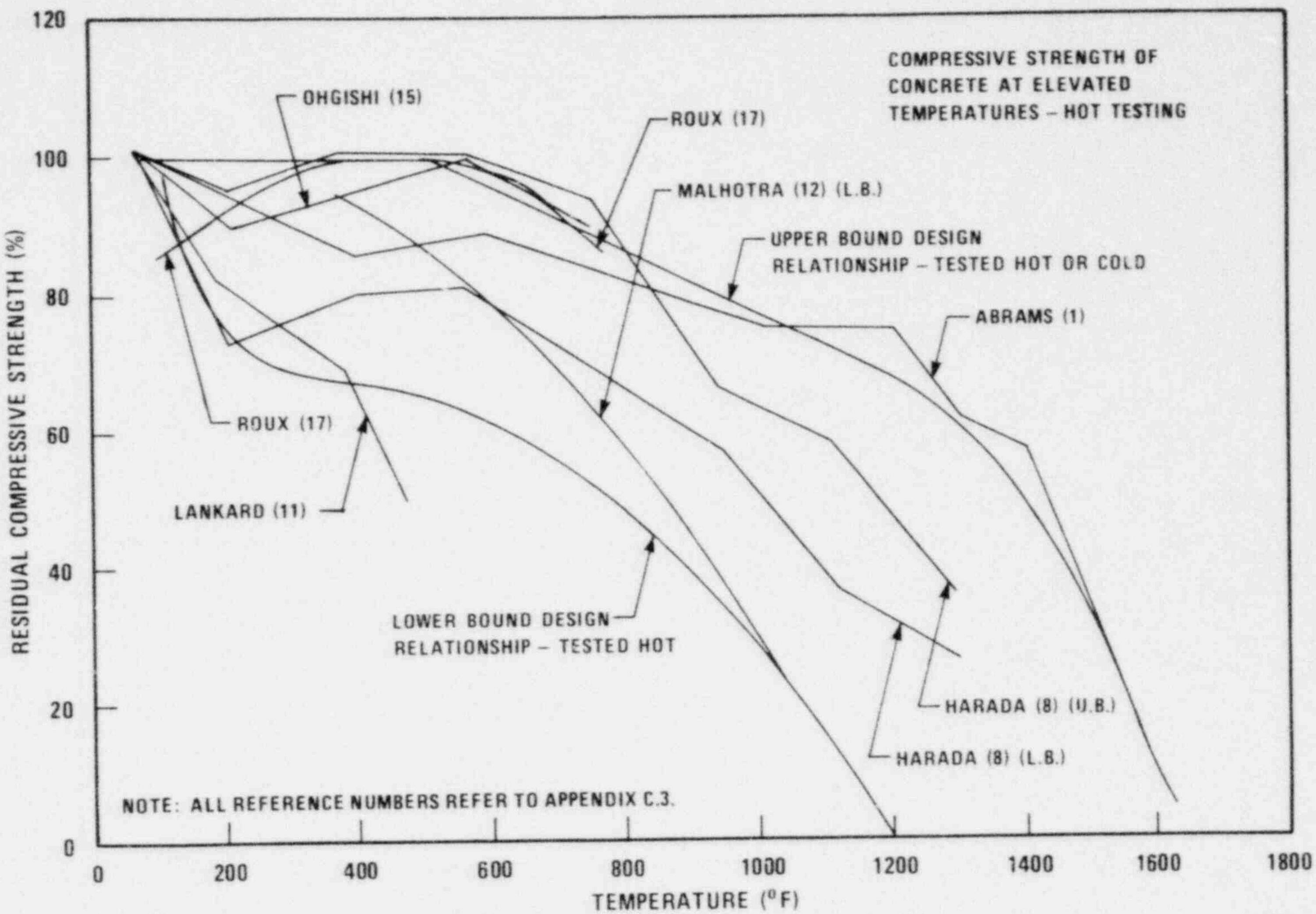

Figure C.3-1. Effect of Temperature Exposure on the Compressive Strength of Concrete – Hot Testing

1966-128

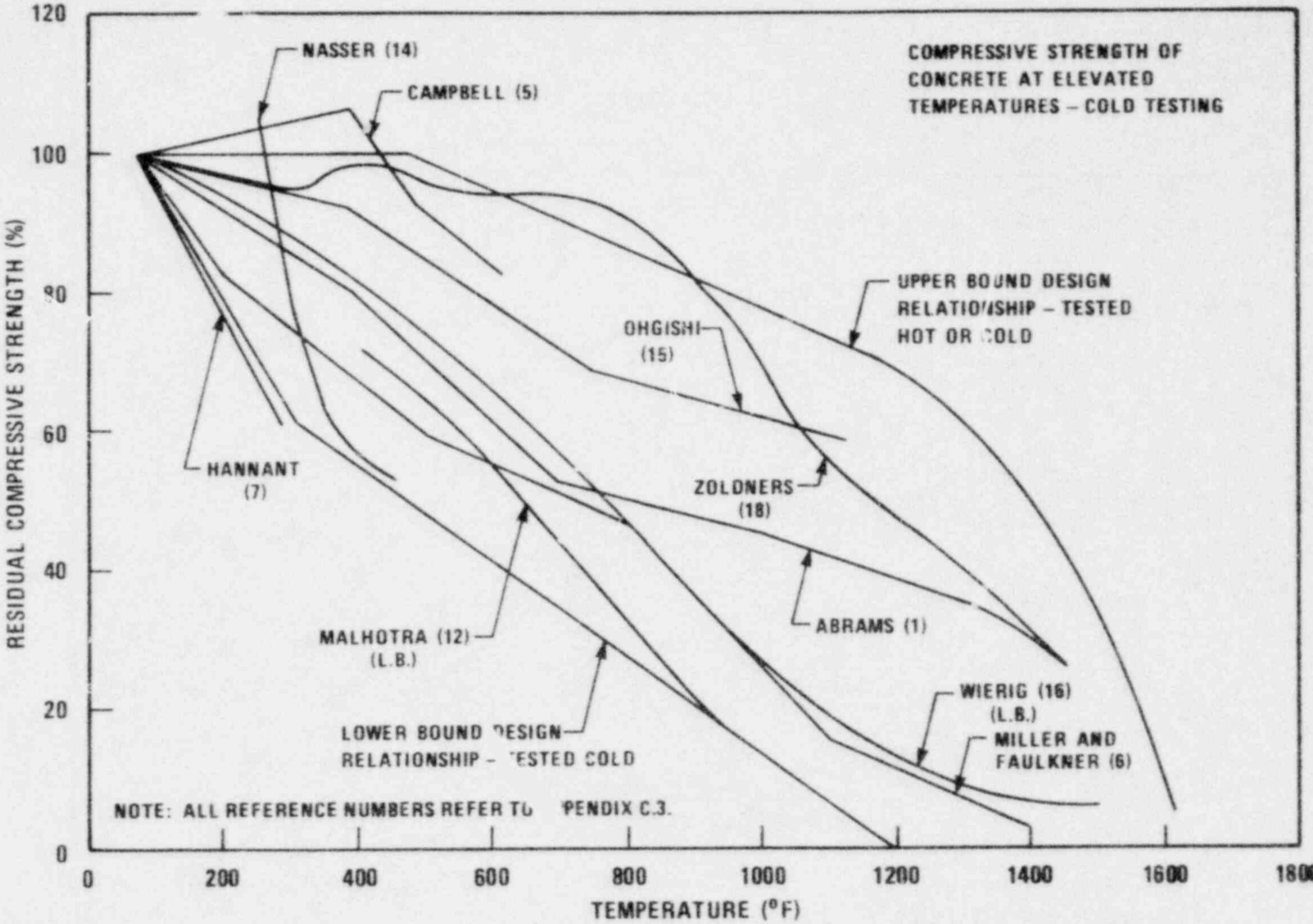

Figure C.3-2. Effect of Temperature Exposure on the Compressive Strength of Concrete – Cold Testing

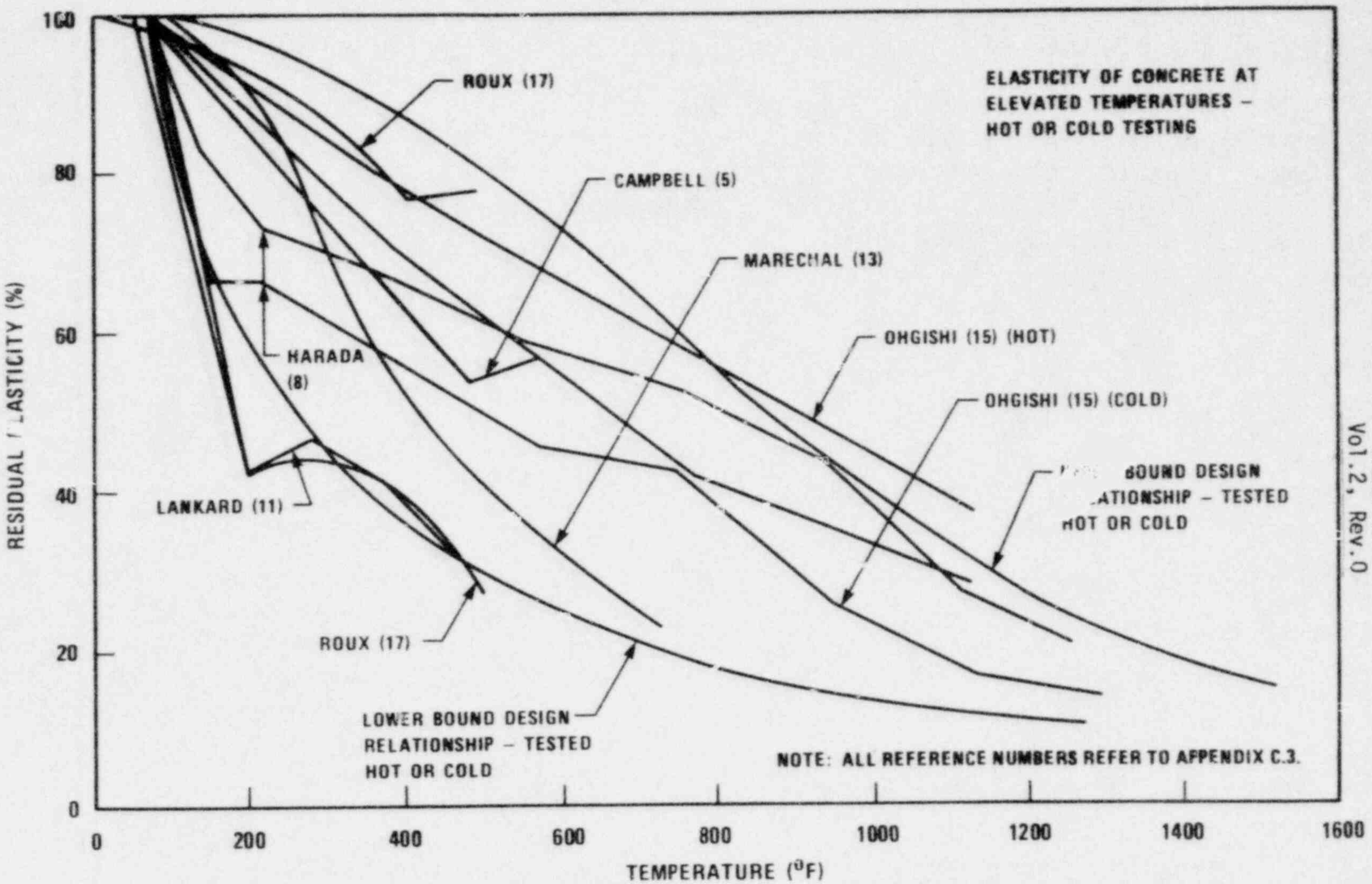

Figure C.3-3. Effect of Temperature Exposure on the Modulus of Elasticity of Concrete – Hot or Cold Testing

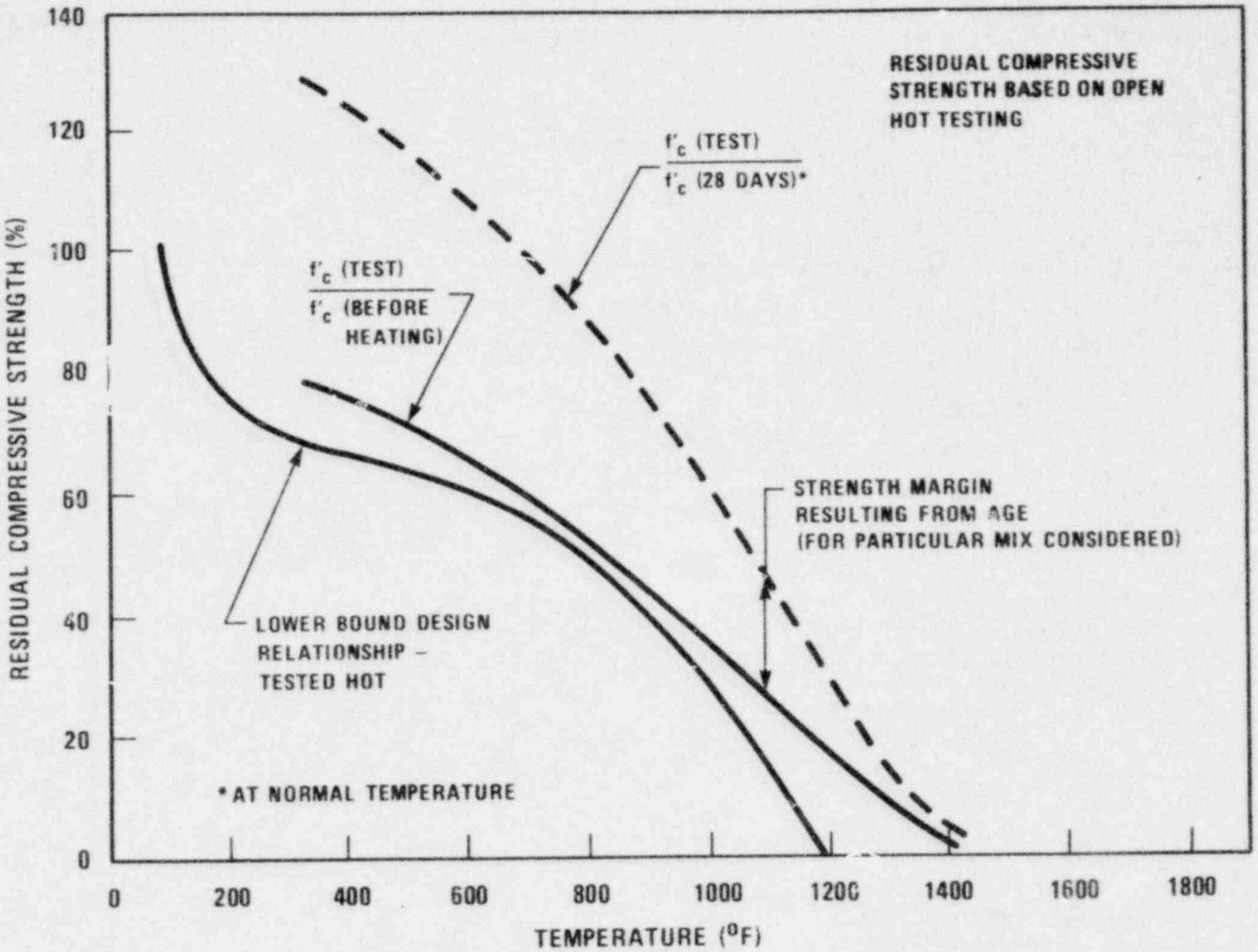

Figure C.3-4. Residual Compressive Strength of Concrete Based on Open-H[illegible] [illegible]esting

1966-130

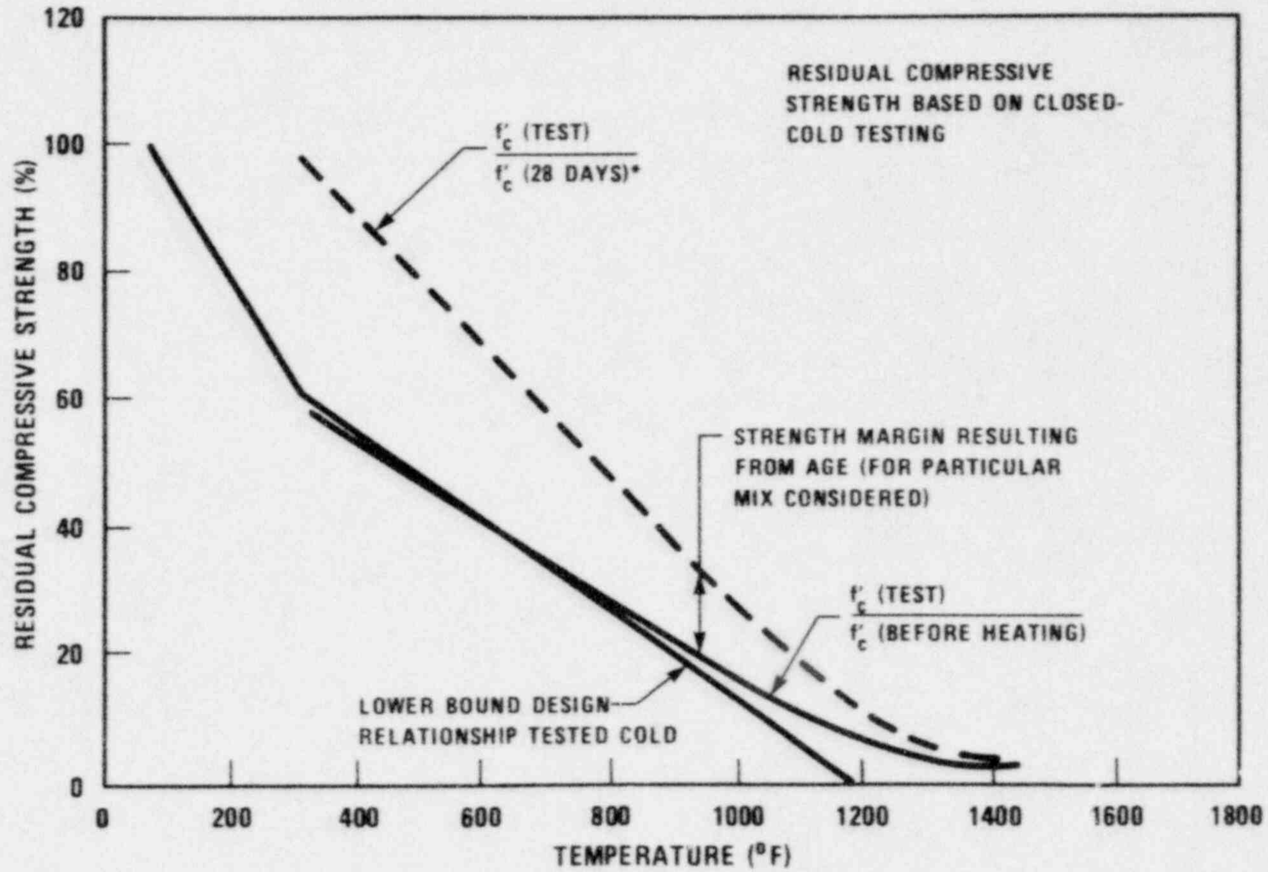

*AT NORMAL TEMPERATURE

Figure C.3-5. Residual Compressive Strength of Concrete Based on Closed-Cold Testing

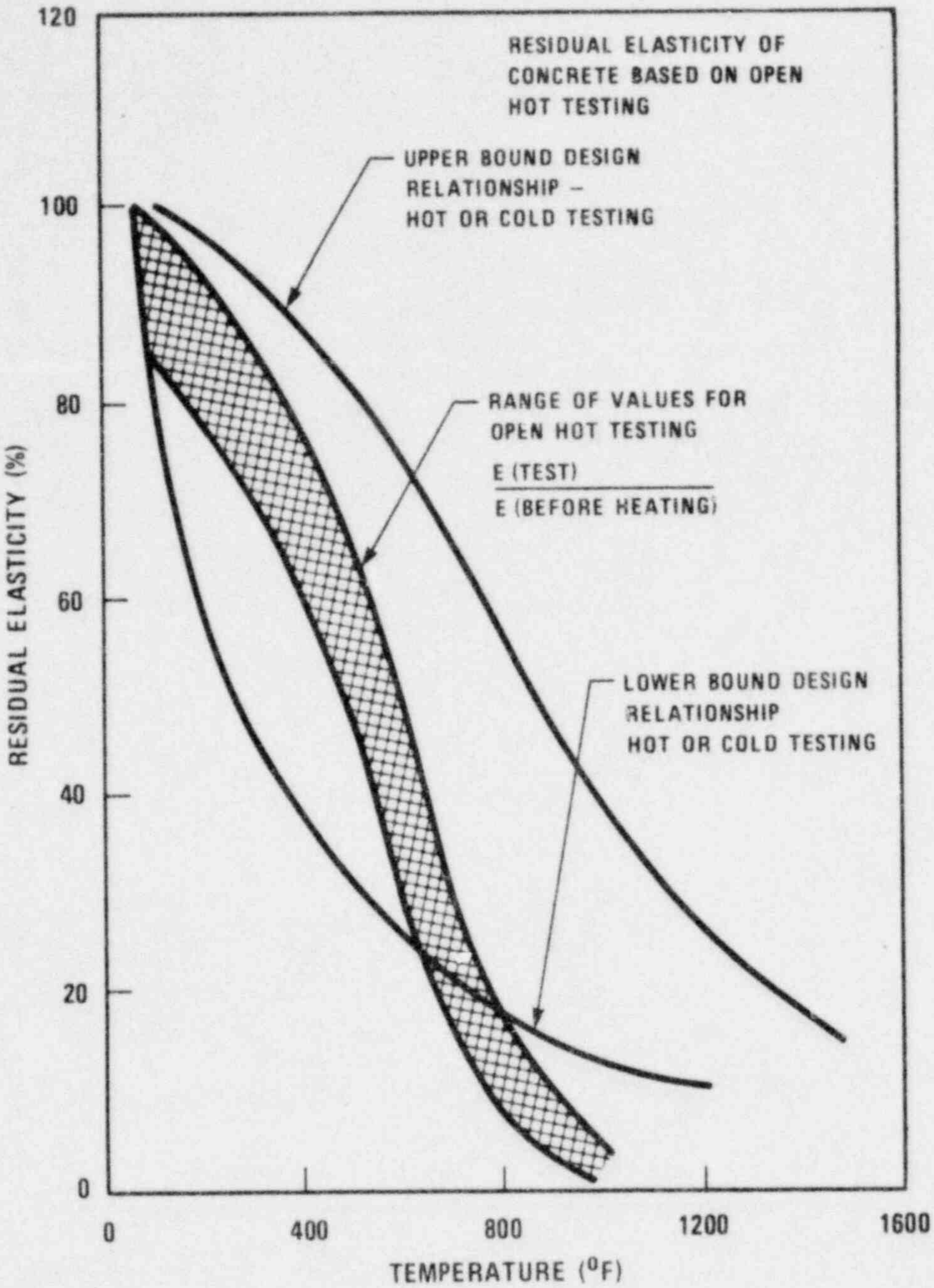

Figure C.3-6. Residual Modulus of Elasticity of Concrete Based on Open-Hot Testing

1966-132

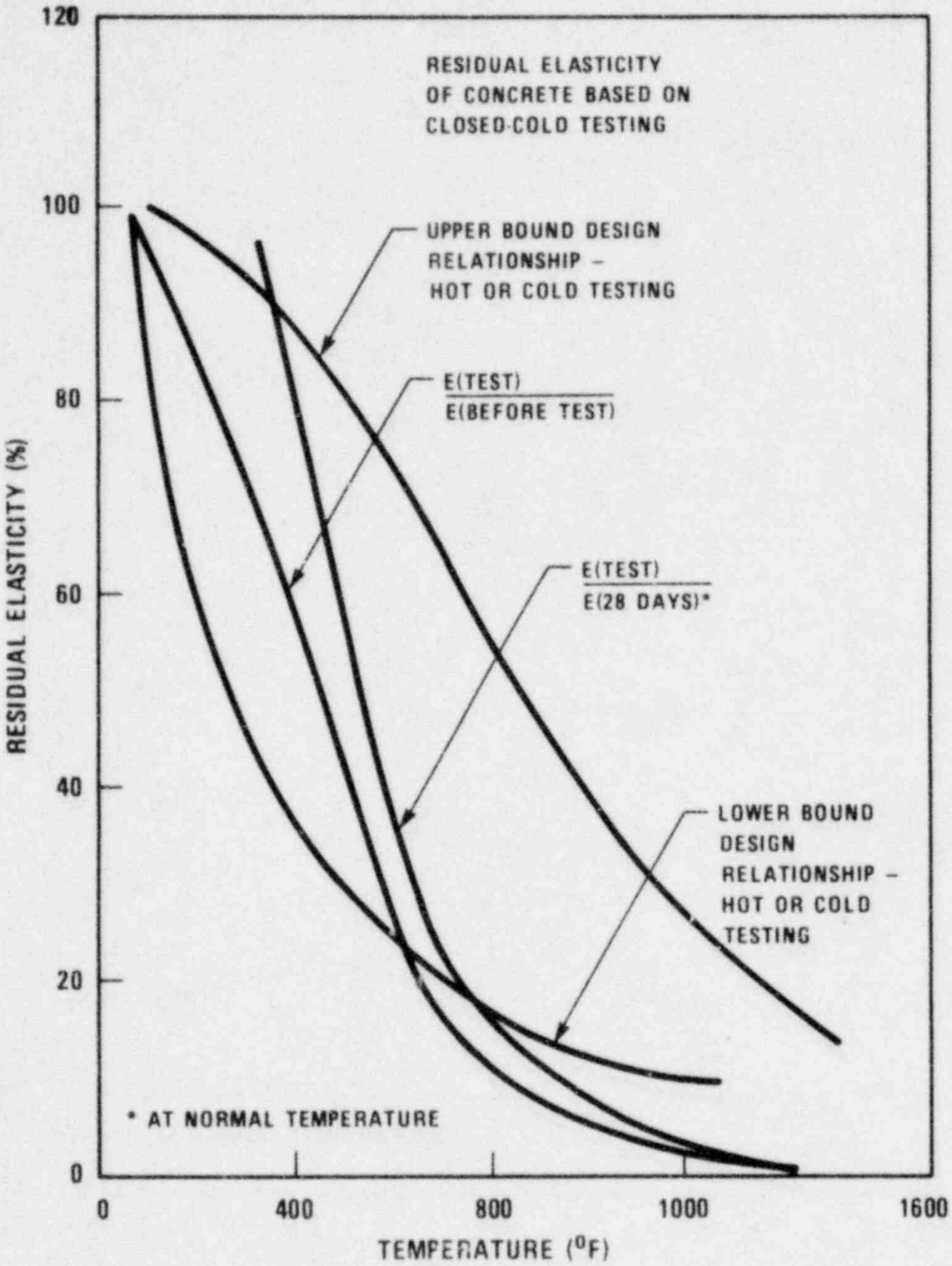

Figure C.3-7. Residual Modulus of Elasticity of Concrete Based on Closed-Cold Testing

1966-133

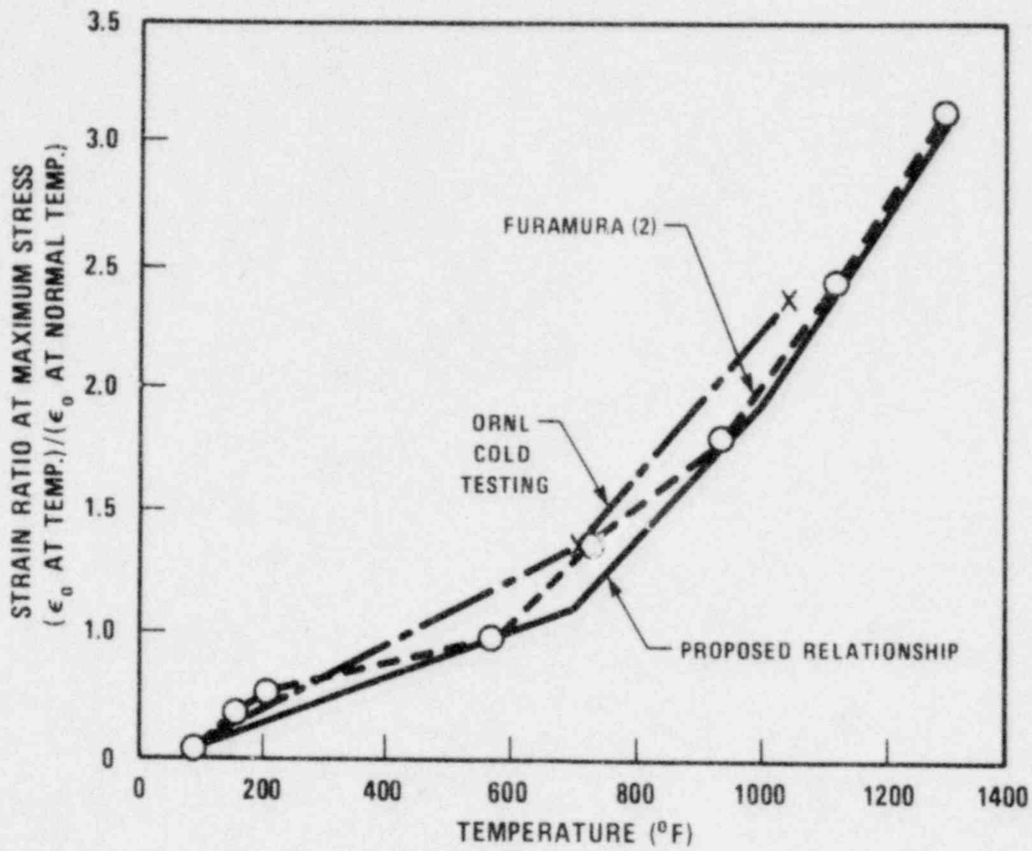

NOTE: REFERENCE NUMBER REFER TO APPENDIX C.3.

Figure C.3-8. Effect of Temperature on the Strain at Maximum Stress

1966-134

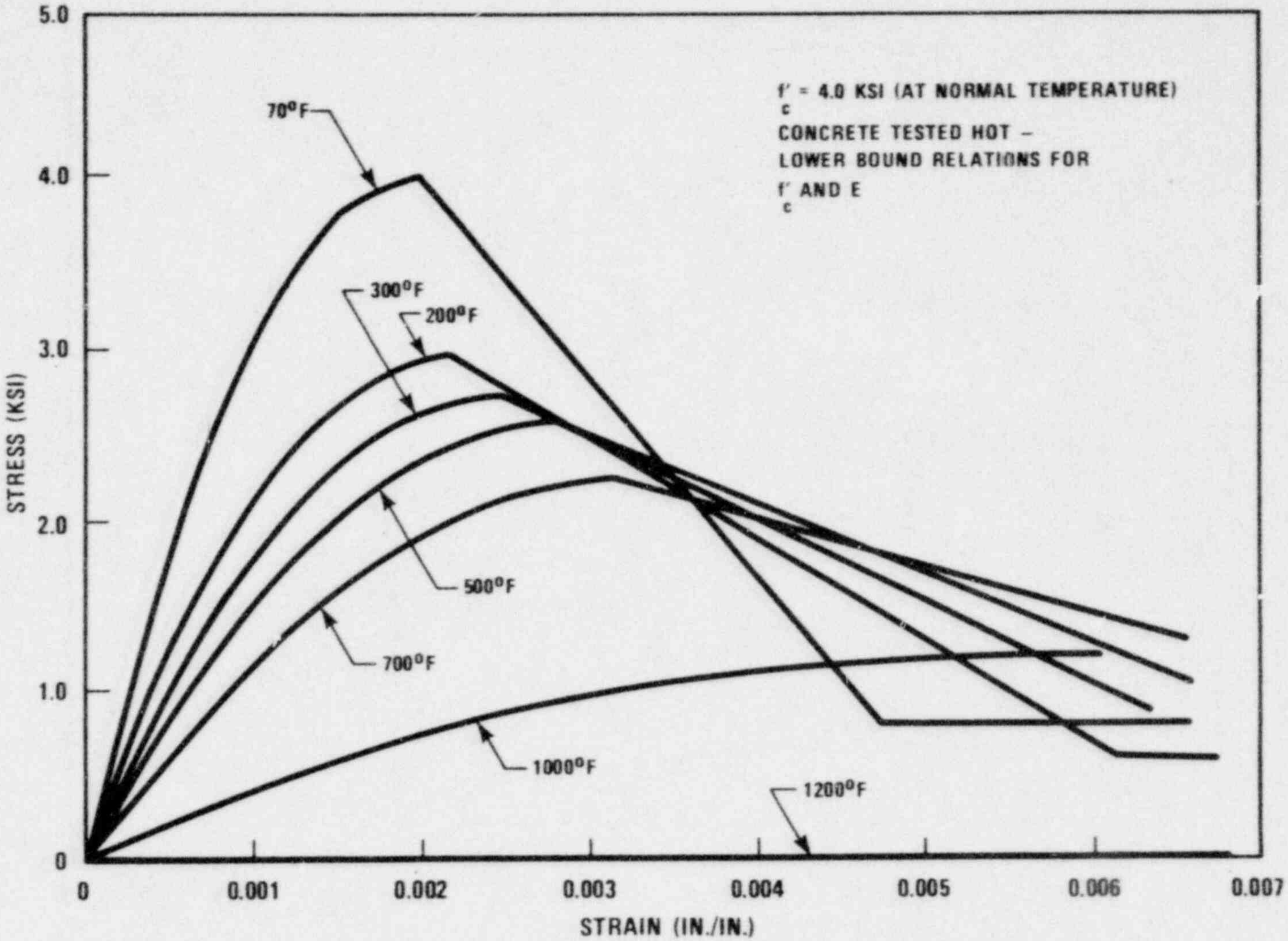

Figure C.3-9. Stress-Strain Relationship – Concrete Tested Hot

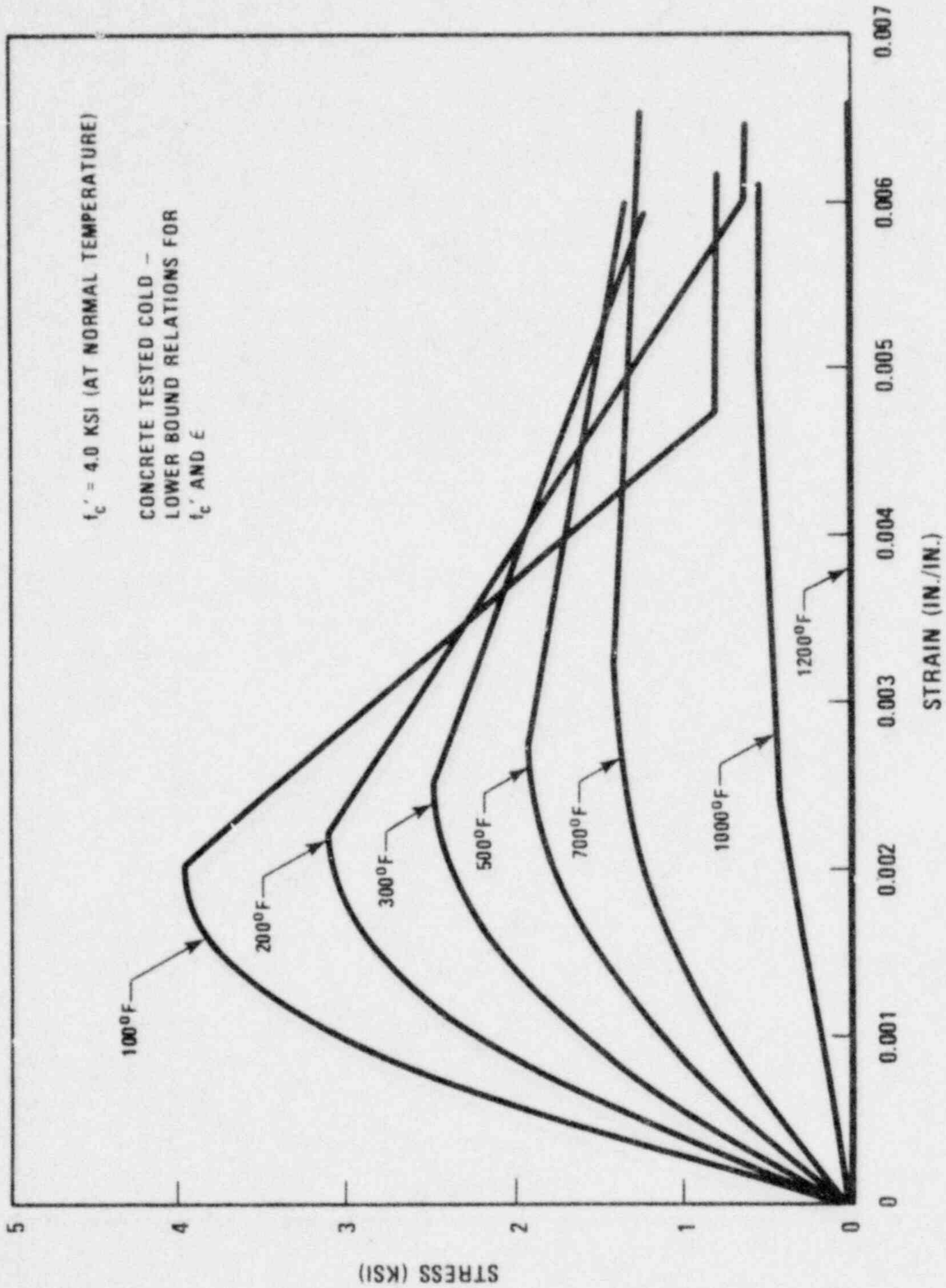

Figure C.3-10. Stress Strain Relationship – Concrete Tested after Cooling Down

1966-136

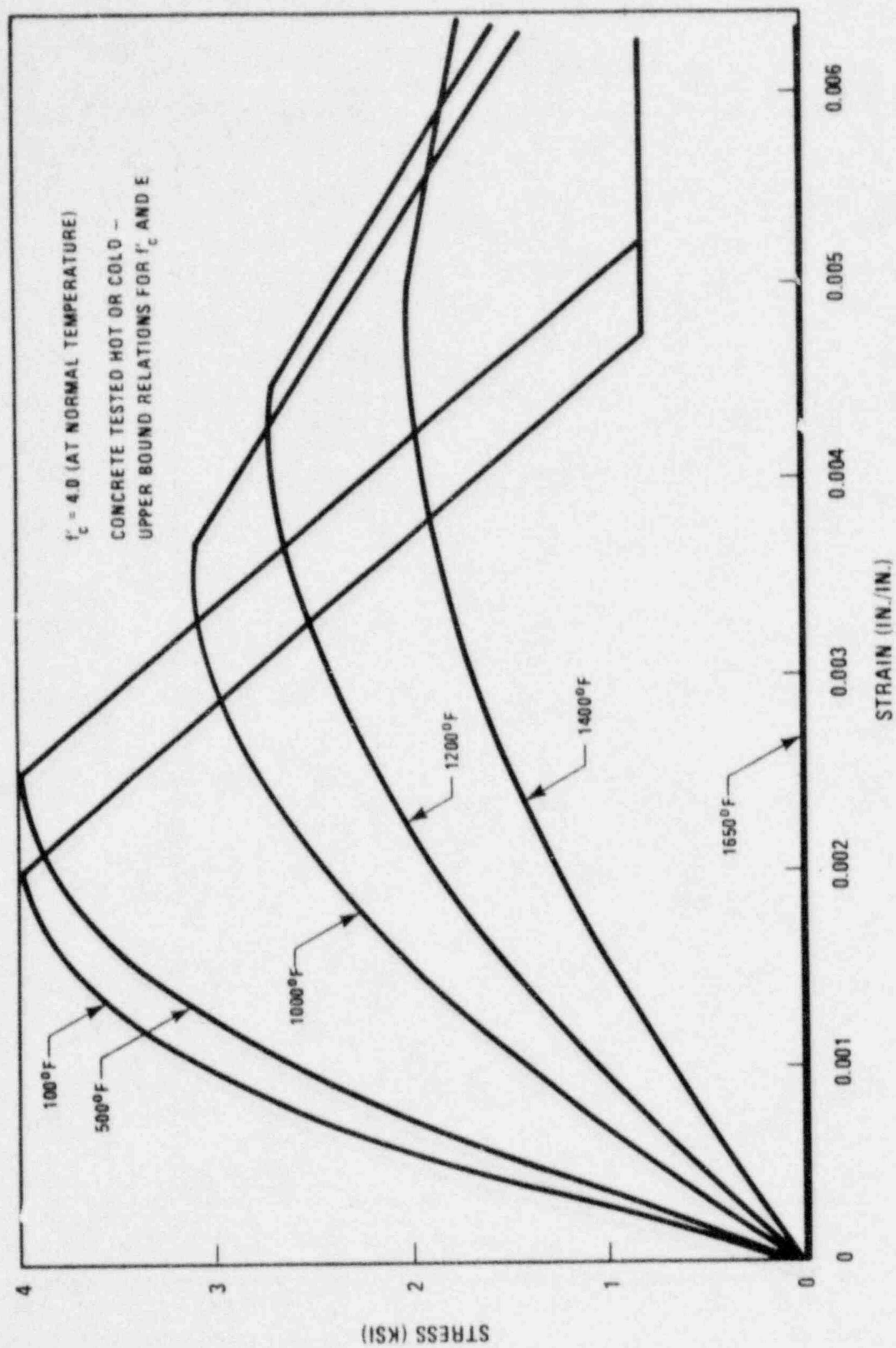

Figure C.3-11. Stress Strain Relationship – Concrete Tested Hot or Cold

1966-137

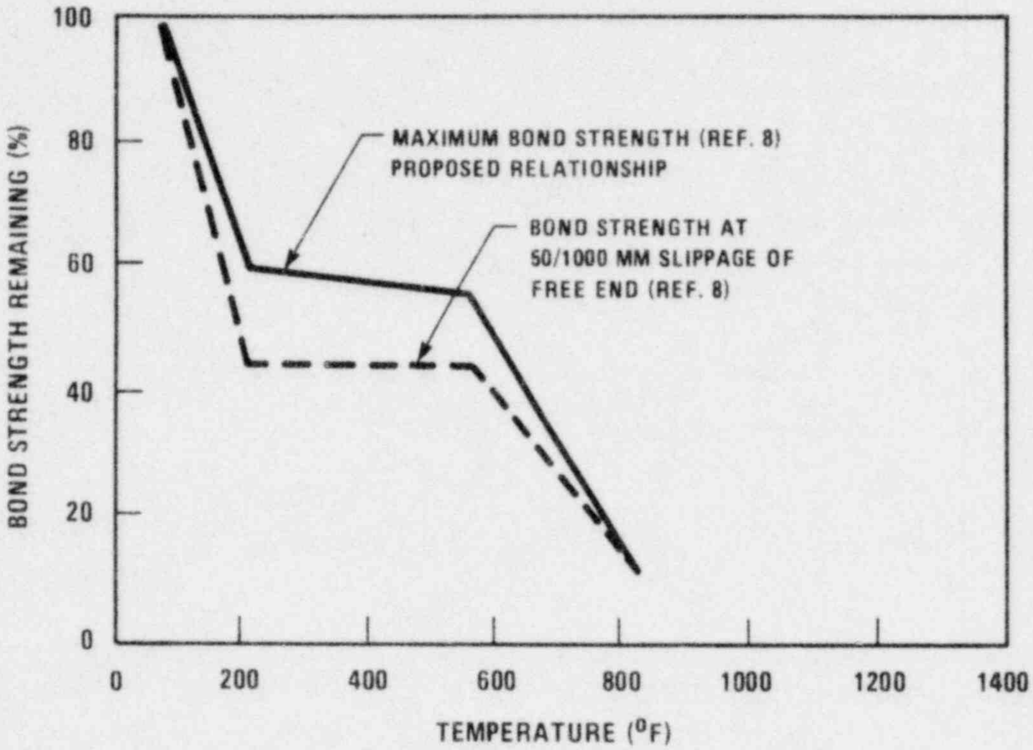

NOTE: ALL REFERENCE NUMBERS REFER TO APPENDIX C.3.

Figure C.3-12. Effect of Temperature Exposure on Bond Strength

1966-138

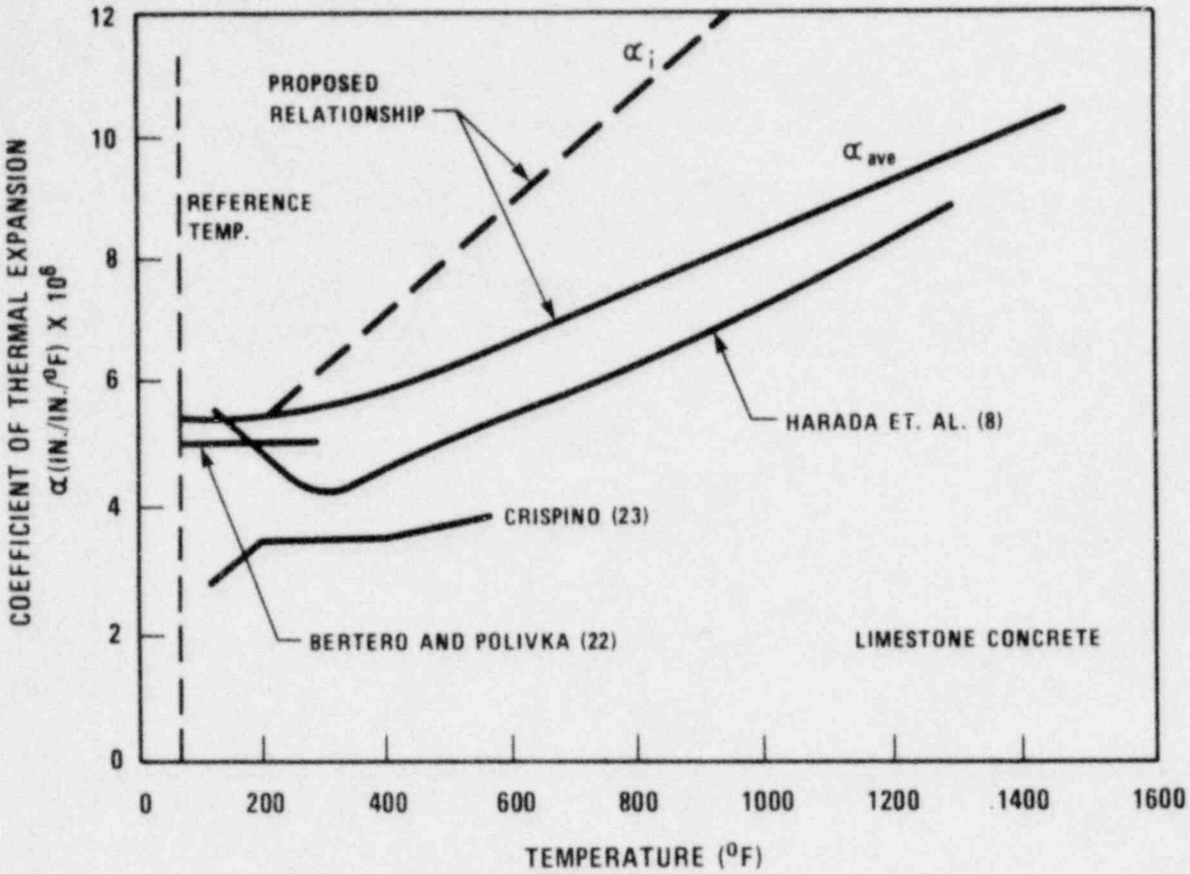

NOTE: ALL REFERENCE NUMBERS REFER TO APPENDIX C.3.

Figure C.3-13. Variation of the Coefficient of Thermal Expansion for Concrete with Temperature

1966-139

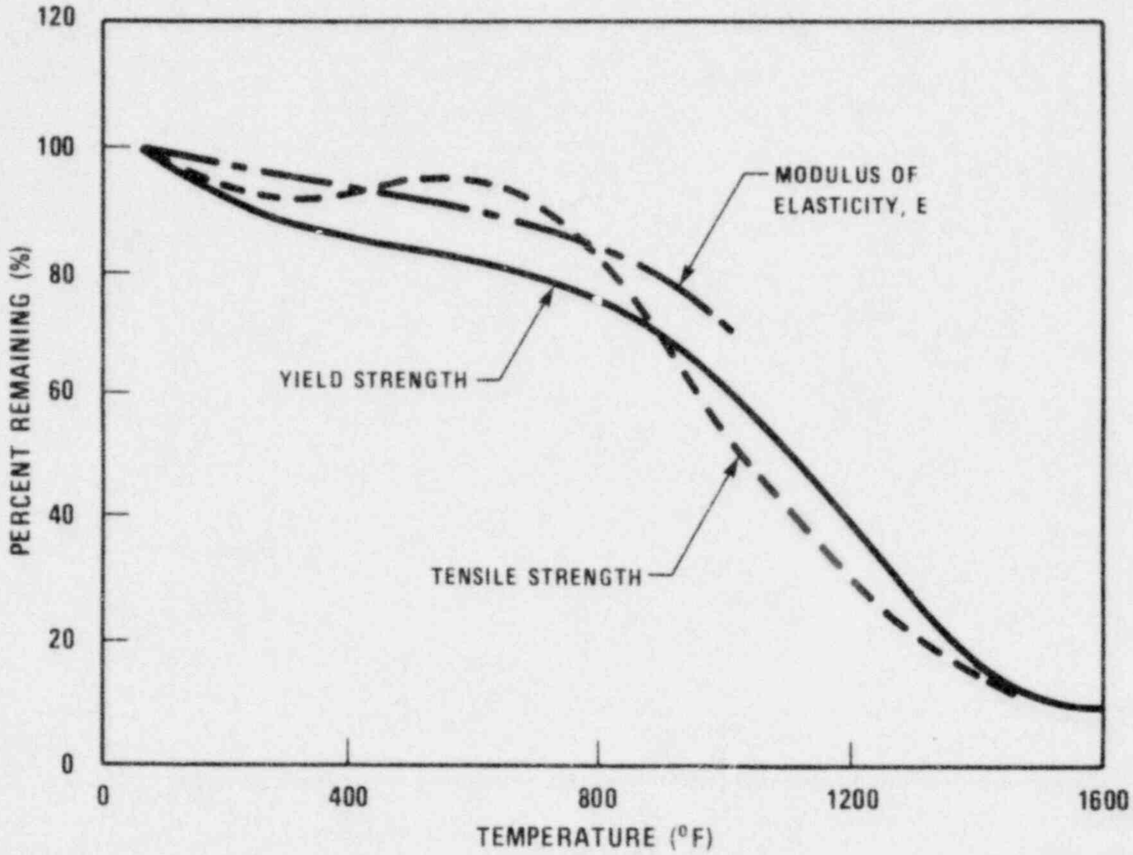

Figure C.3-14. Effect of Temperature on the Structural Properties of Reinforcing Steel Bars

1966-140

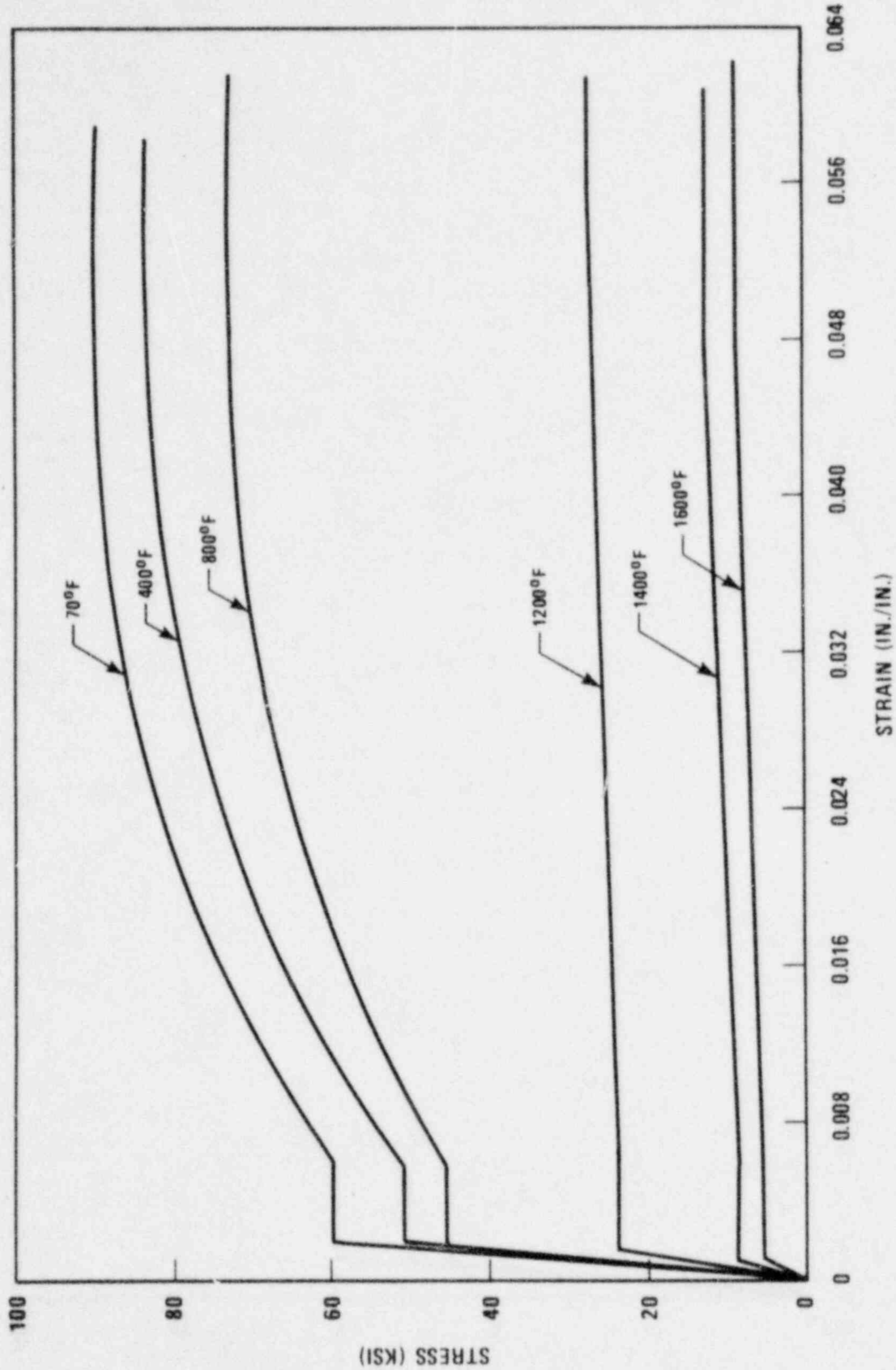

Figure C.3-15. Stress-Strain Relationships — Reinforcing Steel Bars

1966-141

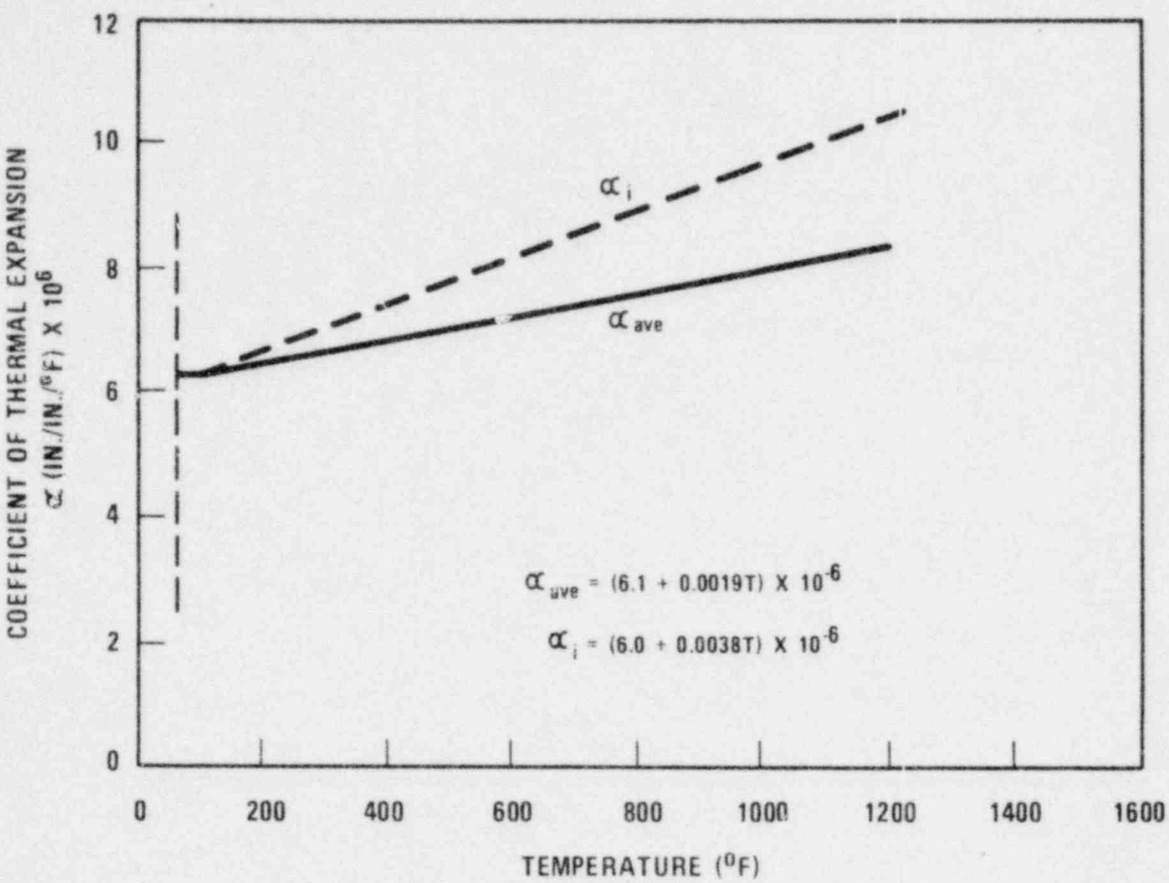

Figure C.3-16. Coefficient of Thermal Expansion – Reinforcing Steel

1966-142

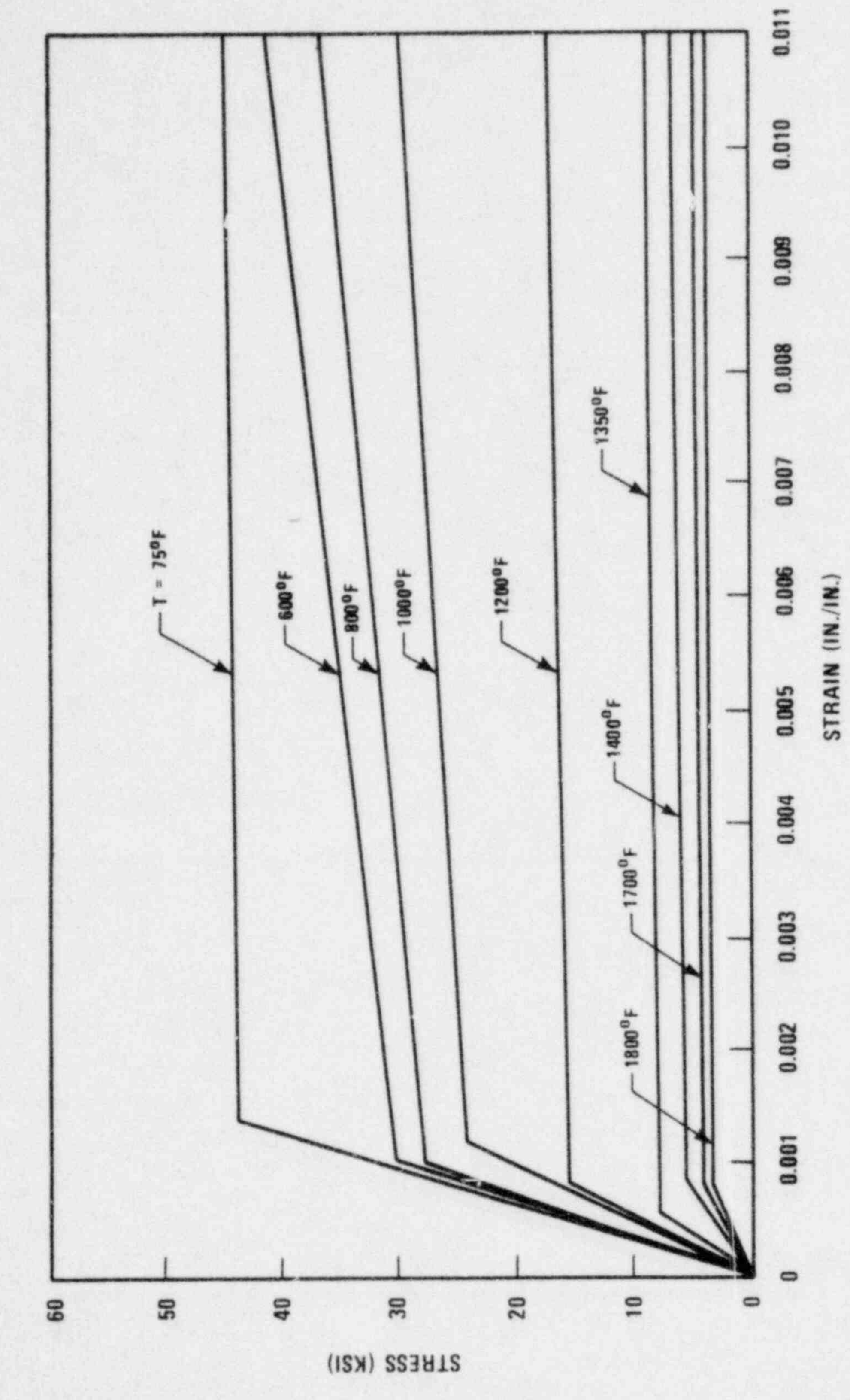

Figure C.3-17. Variation of the Stress-Strain Relationship for SA-516 (Grade 55) Steel with Temperature (Strain Rate 10^{-4} sec^{-1})

1966-143

1966-144

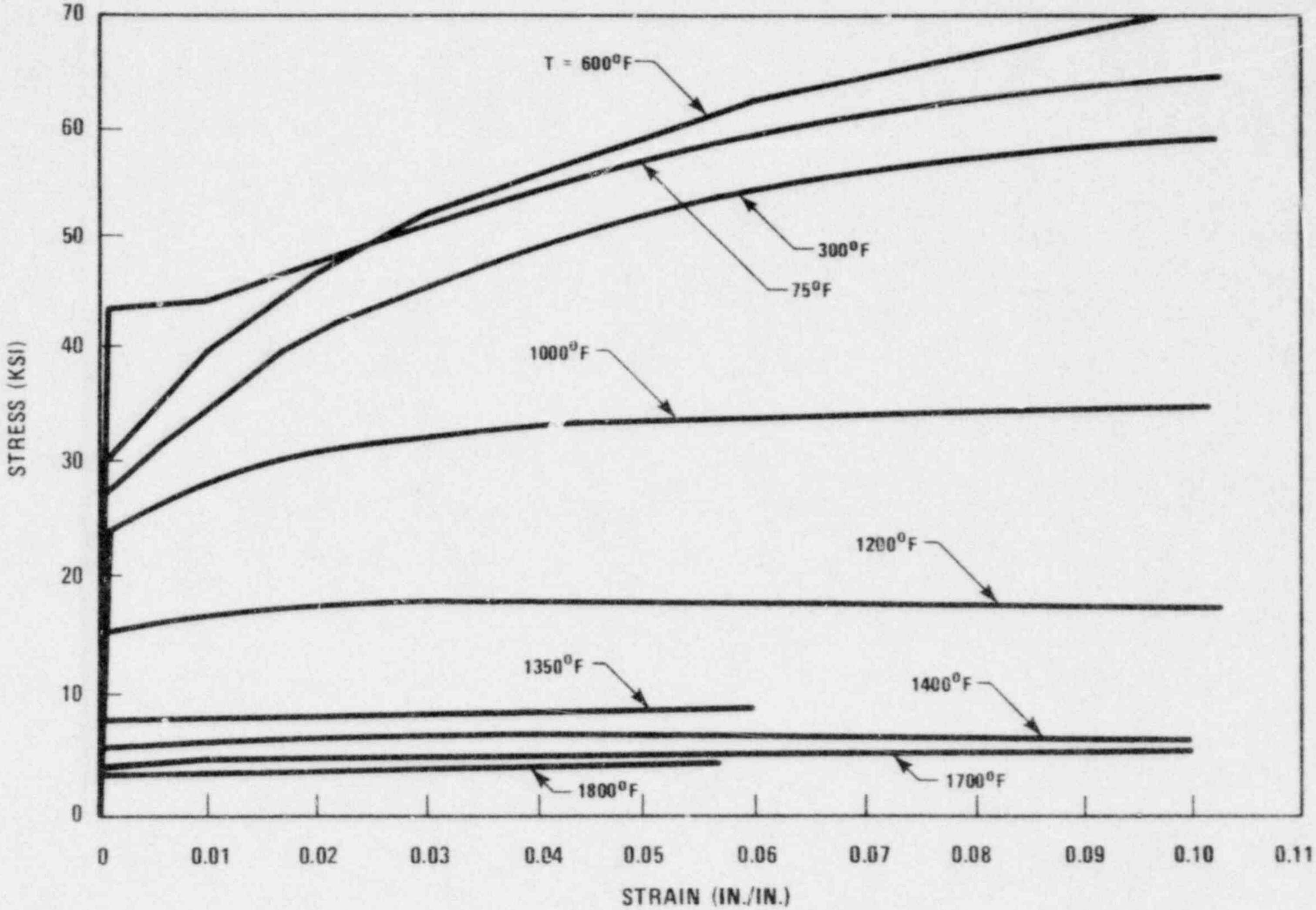

Figure C.3-18. Variation of the Stress-Strain Relationship for SA-516 (Grade 55) Steel with Temperature (Strain Rate 10^{-4} sec^{-1})

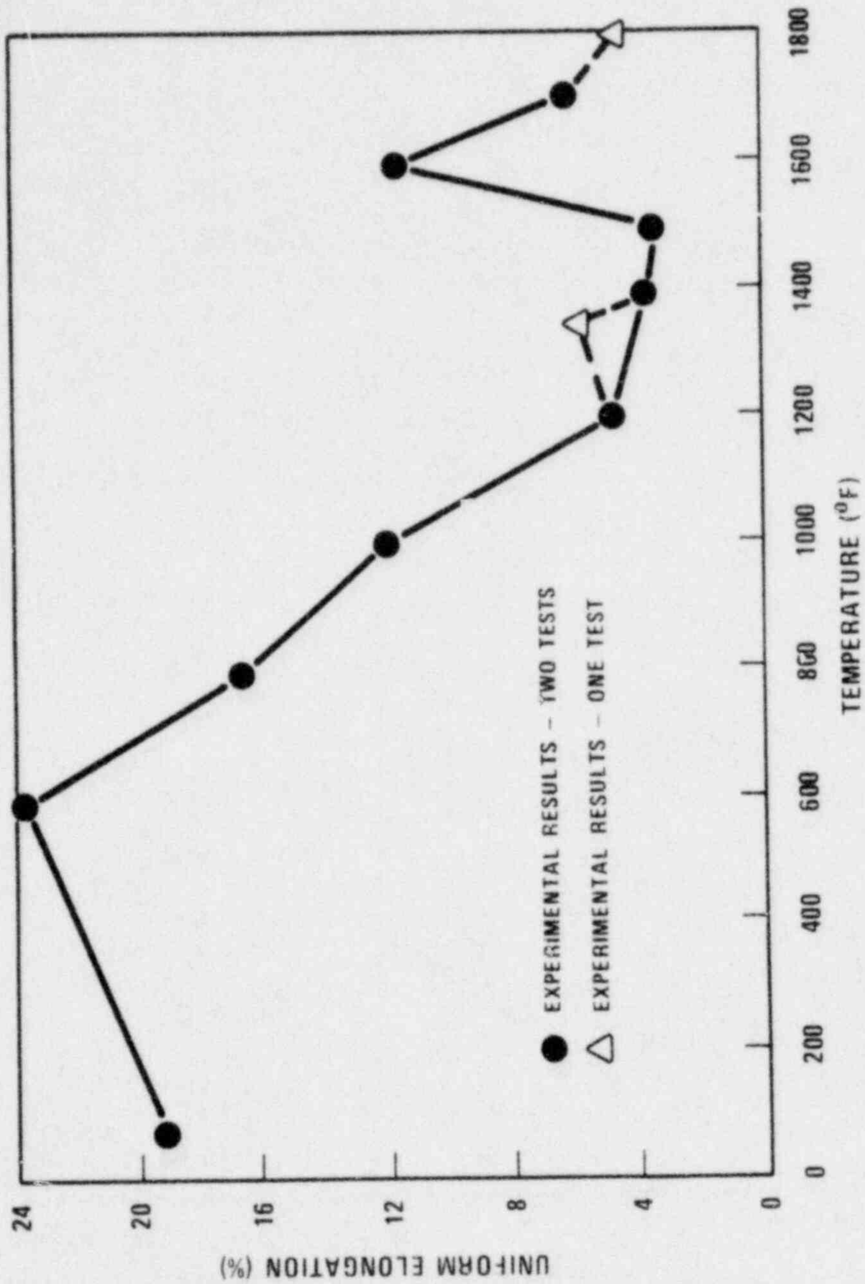

Figure C.3-19. Variation of the Uniform Elongation for SA-516 (Grade 55) Steel with Temperature (Strain Rate 10^{-4} sec^{-1})

1966-145

1966-146

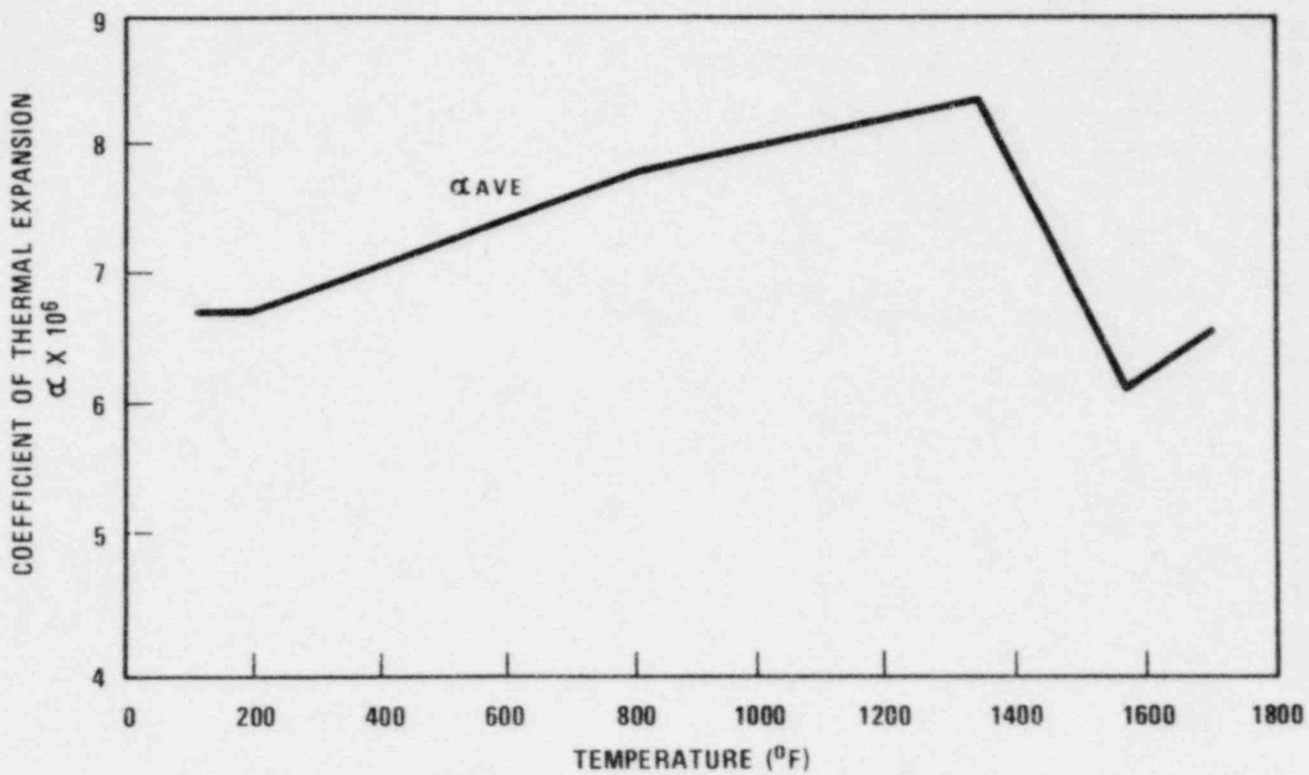

Figure C.3-20. Variation of the Average Coefficient of Thermal Expansion for SA-516 (Grade 55) Steel

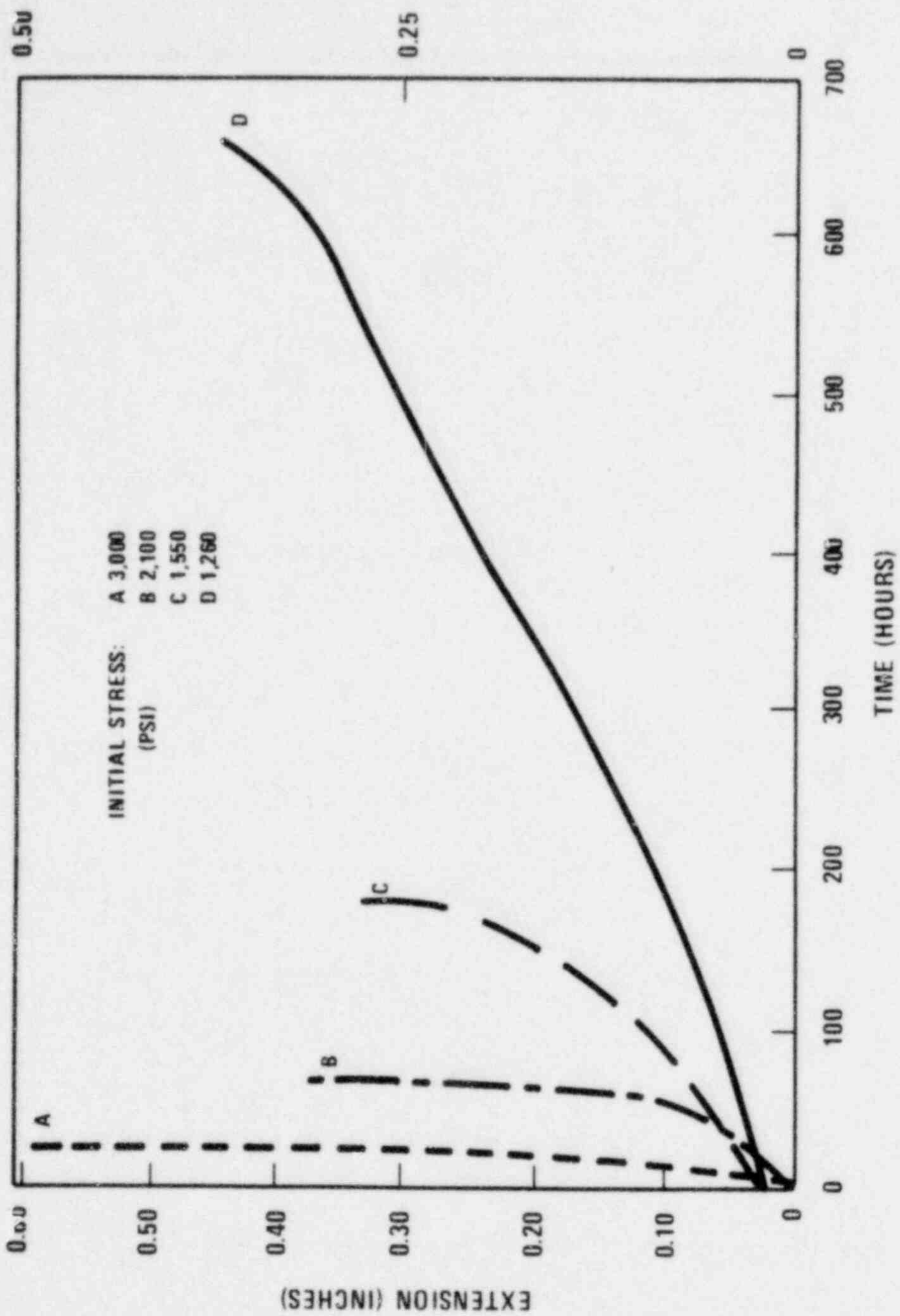

Figure C.3-21. Creep Extension versus Time for SA-516 (Grade 55) at 1400°F (Reference C.3-28)

1966-147

APPENDIX D
AEROSOL BEHAVIOR MODEL

D.1 INTRODUCTION

As indicated in this report the CACECO code was utilized to determine the mass rate of sodium and water vapor released to the RCB. The vapor was assumed to react instantly with oxygen to form Na_2O and then with available water vapor to produce NaOH. The reaction products and associated fission products were assumed to remain airborne as aerosol material. The rate of depletion of the aerosol, via natural deposition processes during retention within the RCB, was determined by the HAA-3B code and used to obtain the input to the COMRADEX code for the radiological dose calculation. In the HAA-3B analysis, the temporal aerosol source rate (RCB vent rate) was based on the CACECO results. Experimental calibration of the HAA-3B code indicated that good agreement between test data and code results could be obtained for the test conditions if code input parameters were suitably selected (Reference D-1). However, it should be noted that extrapolations from the test conditions are required for aerosol environments encountered in the TMBDB evaluation (these extrapolations are discussed in subsequent sections).

D.2 AEROSOL MODELLING AND BASES

The HAA-3B code was developed to predict aerosol behavior and transport following various hypothetical reactor accidents. The analytical model accounts for particle production (source term); Brownian and gravitational agglomeration; and settling, plating and leakage removal mechanisms. Two basic assumptions involved in the HAA-3B code are: (1) the source-term particles are evenly and instantaneously distributed throughout the entire chamber, and (2) the particle size distribution is log-normal at all times.

For the TMBDB evaluation, the assumption that the particles are well mixed is expected to be conservative because of the flow pattern which is likely to have a central plume and recirculating flow. The agglomeration rate should be much larger in the plume than in a uniformly distributed aerosol because of the higher concentration in the plume; this would result in larger fall-out rates. Hence, the well-mixed assumption used in the HAA-3B code should be conservative and as such, would provide an upper bound estimate for suspended mass in the TMBDB evaluation. Experimental measurements (Reference D-2) showed the suspended particle concentration resulting from a sodium pool fire was fairly uniform throughout the containment vessel. These data were obtained in a vessel smaller than the reactor containment vessel. However, since the mechanism (recirculating flow induced by buoyant and viscous forc causing uniform or well mixed aerosols should exist for small and large volumes, the uniform concentration approximation should be applicable to the reactor containment vessel.

The experimental characterization of sodium oxide aerosol produced by sodium fires indicated that the aerosol particles initially had a log-normal size distribution (References D-1, 3, 4). However, it was found that the distribution did not remain log-normal if the aerosol concentration was large as in the TMBDB evaluation case (Reference D-5). However, a comparison (Reference D-6) between the results obtained with a mathematical model which does not use the log-normal distribution and the HAA-3B code showed similar results. The HAA-3B code did predict a slightly more conservative result. The independent model used for the comparison solves the same equations as HAA-3B, but approximates continuous particle size spectra with a number of discrete size intervals within which the particle size is constant. Although the comparison was not performed to test the validity of the assumption of log-normal particle size distribution it does provide reasonable assurance that the assumption of log-normal particle size distributions is adequate. In general, the HAA-3B code is based on analytically sound models, and when used with conservatively selected input parameters, can be used to obtain conservative results.

The required input data for the HAA-3B code includes the mass mean radius and the geometric standard deviation of the aerosol particle size distribution; these were chosen to be 0.3μm and 2, respectively. Although the final sodium reaction product is expected to be NaOH, the selection of the mean particle radius was based on the size of sodium oxide particles since experimental data for NaOH were not available. The value (0.3μm) used for the mass mean radius is at the lower end of the particle size ranges, and the standard deviation of 2 is about the average value reported by different experimentalists (Reference D-7). It is realized that the particle size will increase as sodium oxide particles absorb water and convert to sodium hydroxide (Reference D-8). For conservatism, the growth of particles by this conversion mechanism was neglected; that is, the calculated suspended mass will be larger than realistically expected.

For high concentrations in large containments, as in the TMBDB analysis, the effect of initial particle size on the over-all mass deposition is small. The particle size assumed is only important in situations where particle growth is not appreciable, e.g., low concentrations in large vessels (Reference D-9). Because the aerosol source term (production rate) in the TMBDB case was very large, the suspended particle concentration remained very high, and as expected the particle size increased dramatically due to the huge agglomeration rate. The HAA-3B results showed that the mass mean radius and suspended mass were essentially constant during the period when the source term was large. This indicates the particle size history is more dependent on the magnitude of the source term than on the assumed particle size of the source. That is, the time-averaged particle size was rather insensitive to the initial particle size since the source was very large.

In some of the TMBDB cases evaluated the initial release of products to the RCB is dominated by fuel. There is some uncertainty in the size of fuel aerosol particles following an energetic core disruptive accident.

Reference D-7 summarizes a number of experimental results of fuel aerosols produced by vaporization of core materials. These results give values of the mass mean radius from 0.05 to 0.5 μm. To determine how sensitive the leaked aerosol mass is to R_{50}, a parameter study was made. The results of this study are shown in Table D-1. These results indicate that the HAA-3 analysis is not sensitive to the initial R_{50} value. A value of 0.1μm was used for fuel aerosol source terms in this report.

The Stokes correction factor (α) and the gravitational collision efficiency (ε) are included in the HAA-3B code to account for nonspherical particles and nonuniform density of particle aggregates, and to include hydrodynamic effects on gravitational agglomeration, respectively. The values of α and ε used in the analysis were based on experimental calibrations performed at AI (Reference D-1). It was found that in a 6 ft high chamber a value of $\alpha\varepsilon$ near unity gave good agreement between the code results and the experimental data. It was also found that a value of $\alpha\varepsilon = 0.33$ was required to achieve good agreement with the data obtained with a 30-ft high chamber. This inverse variation is expected since as the height of the chamber is increased the time for coagulation increases and therefore, airborne particles should become more irregular in shape and density. An extrapolation was used to determine the value of $\alpha\varepsilon$ for the RCB which has a height of 180 feet. As the height increased in the experiments from 6 to 30 feet, the value of $\alpha\varepsilon$ decreased from 1.0 to 0.33. Thus, since the height of the RCB is 180 feet, the value of $\alpha\varepsilon$ was estimated by extrapolation to be 0.1.

Since the aerosol in the form of NaOH is liquid, the droplet shape should be spherical and the density should equal that of the composite (compact) material. Hence, the Stokes correction factor in this case should be equal or very close to unity. Also, since two liquid drops should coalesce when they collide, the gravitational collision efficiency should be about unity. This means that the values of both α and σ should be unity and independent of the geometry in which the liquid aerosol is suspended. However, for conservatism, the value of 0.1 for $\alpha\varepsilon$ was used in the analysis.

D.3 SENSITIVITY TO RCB TEMPERATURE

The rate of aerosol depletion is also affected by the RCB atmosphere temperature. The temperature of the RCB atmosphere varies from ambient to about $900^{o}F$ with an average of about $750^{o}F$ during the sodium vapor phase of the TMBDB scenario (base case values). Since the HAA-3 code cannot consider variable temperatures, a single value must be chosen. To be conservative the highest RCB atmosphere temperature encountered during the TMBDB scenario is used. An evaluation was made to see what effect the RCB temperature has on the aerosol depletion analysis. The results of this evaluation, shown in Table D-2, verify that use of the peak temperature is conservative and shows that the mass of aerosol leaked is not strongly sensitive to the RCB atmosphere temperature.

D.4 REFERENCES

D-1. "LMFBR Safety Programs Annual Technical Progress Report, GFY 1971," AI-AEC-13006, September 1971.

D-2 M. A. Greenfield, R. L. Koontz and D. H. Hauscknecht, "Characteristics of Aerosols Produced by Sodium Fires, Volume II. Comparisons of Experiment with a General Equation for the Coagulation of Heterogeneous Aerosols," AI-AEC-12878, October 1969.

D-3 H. J. Ettinger, et al., "Characteristics of the Aerosol Produced from Burning Sodium and Plutonium," Nucl. Sci., Eng., 30, pp. 1-13 (1967).

D-4 S. Kitani, et al., "Behavior of Sodium Oxide Aerosol in a Closed Chamber," J. Nucl. Sci. Tech. 10, pp. 566-573 (1973).

D-5 G. C. Lindauer and A. W. Castleman, Jr., "The Importance of Gravitational Coagulation on the Settling of High-Mass Density Aerosols," Nucl. Sci. Eng. 42, pp. 58-63 (1970).

D-6 L. D. Reed and J. A. Gieseke, "Aerosol Behavior Modeling for Fast Reactor Safety. Quarterly Progress Report for July-September 1975," BMI-X-666, October 1975.

D-7 T. C. Huang and R. K. Stitt, "Review and Evaluation of Current Aerosol Models for LMFBR Safety Analysis," GEAP-14054, June 1975. (Availability - U.S. DOE Technical Information Center).

D-8 W. S. Clough and J. A. Garland, "Behaviour in the Atmosphere of the Aerosol from a Sodium Fire," AERE-R-6460, 1970.

D-9 J. A. Gieseke and L. D. Reed, "Sensitivity Analyses for Postulated LMFBR Accident Conditions," BMI-X-664, October 1975.

TABLE D-1

SENSITIVITY OF TMBDB HAA-3 ANALYSIS TO R_{50}

R_{50} (μm)	Aerosol Leaked Mass* (Grams)	
	1 Day	30 Days
0.20	2.41 + 2**	7.6 + 3
0.10	2.44 + 2	7.6 + 3
0.05	2.45 + 2	7.6 + 3

TABLE D-2

SENSITIVITY OF TMBDB HAA-3 ANALYSIS TO RCB ATMOSPHERE TEMPERATURE

Temperature (^{o}F)	Normalized Na Aerosol Leaked Mass***
917	1.00
750	0.98

*Leaked mass from initial head release of 10% fuel and solid fission products, 100% volatiles and halogens, and no sodium.

**2.41 + 2 = 2.41×10^2

***Based on release occurring during the sodium vapor phase of the TMBDB base case scenario.

APPENDIX E

RELEASE OF PLUTONIUM AND FISSION PRODUCTS

E.1 INTRODUCTION

This section considers the potential release of plutonium to the RCB subsequent to that assumed released as part of the initial release phase. Possible mechanisms for transporting plutonium from the reactor cavity to the RCB have been investigated. These mechanisms include potential plutonium release from burning the oxygen originally available in the reactor cavity, plutonium release from the boiling pool of sodium, plutonium release from the dry debris bed, and release due to gas sparging.

E.2 PLUTONIUM RELEASE FROM SODIUM-OXYGEN REACTIONS IN THE INERTED CELLS

Because primary sodium could be released to the RC and PHTS cells, sodium burning can be postulated. The amount of sodium burned would be limited however because of the 2% oxygen level present. This Section addresses the potential plutonium source associated with postulated sodium reactions.

When a sodium pool containing plutonium burns, a small amount of plutonium is released along with the sodium reaction products. This release has been quantified experimentally.

In Reference E-1, Chatfield determined that a plutonium release fraction of 2.9×10^{-5} resulted from the burning of sodium containing PuO_2.

Recent experiments at Atomics International (Reference E-2) have further assessed the airborne concentration of plutonium resulting from the combustion of plutonium contaminated sodium. In these tests, sodium was doped with from 13 to 250 ppm PuO_2 or Na_4PuO_5 and then ignited in air at temperatures of 500 to 550°C. The aerosol released from this burning pool of sodium was collected and analyzed for plutonium content. For the sodium containing PuO_2, nine experiments resulted in plutonium release fractions ranging from 1×10^{-6} to 8.7×10^{-5}. The average release fraction was 2.0×10^{-5}. For sodium-plutonate, the preliminary results indicate the release fractions are several orders of magnitude less than for PuO_2. The fractional release of plutonium from burning sodium used in these analyses is 3×10^{-5}. This is consistent with the data in References E-4 and E-5 and may be highly conservative if a substantial amount of the plutonium is in the form of sodium plutonate.

If the total amount of oxygen present in the RC and three PHTS cells completely reacts with sodium, the amount of sodium burned would be 1785 pounds.

Based on the particle distributions from the M-Series tests at ANL, about 15% of the fuel would be in small enough particulates to be suspended in the sodium. If it is assumed that 15% of the total plutonium inventory (2030 Kg) is uniformly distributed throughout the total primary sodium inventory (1.1×10^6 lbs) then the amount of plutonium contained in the burning sodium is (0.15) (2030 Kg) ($1785/1.1 \times 10^6$) = 494 grams. Applying the 3×10^{-5} release fraction gives a plutonium release of 0.015 grams to the RCB. This is an insignificant amount compared to that assumed in the initial release phase source term.

E.3 PLUTONIUM RELEASE FROM A BOILING POOL OF SODIUM

The primary sodium which drains out of the reactor vessel and primary piping forms a pool in the reactor cavity. The pool contains the fuel debris from the core. The interaction of molten fuel with sodium results in a fuel particle distribution. Based on measurements of particle size distributions in the ANL M-series tests (Reference E-3), approximately 15% of the fuel could exist in particles small enough to remain in suspension in the sodium pool. The remaining fuel would form a settled bed on the bottom of the sodium pool.

The fuel debris heats the sodium to boiling due to decay heat. As the sodium pool boils, plutonium is released from the pool by vaporization of the plutonium and plutonium particle entrainment in sodium droplets carried from the pool by the sodium vapor. Based on a recent survey (Reference E-4) of experimental data on liquid carry-over from commercial evaporators and entrainment of solid particles in the vapor stream from an evaporating liquid pool, it was concluded that the experimental data of Jordan and Ozawa (Reference E-5) is most directly applicable for estimating the potential plutonium release from a boiling pool of sodium. Their results show a minimum decontamination factor of about 1000. Thus if 15% of fuel is suspended in the sodium and if 1/1000 of this is released, then the net fuel release is 0.015% of the total inventory. Since there are approximately 2000 kg of plutonium in the CRBRP core the plutonium release from the boiling sodium pool to the RCB atmosphere could be about 300 grams. However, because of aerosol depletion and filtering less than one gram would actually be released from the RCB cleanup system.

Once the fuel and core debris penetrates the RC liner, carbon dioxide and steam would be released and bubble through the sodium pool. The effect of this gas sparging on additional plutonium and fission product release has been investigated by Parsly and Fontana (Reference E-6). Using the model and distribution coefficients of Reference E-6 the effect of gas sparging on additional releases from CRBRP has been evaluated. Most of the fission products fall into two categories: (1) those with predicted high fractional releases due to sparging, which are the more volatile products that have already been considered totally released either initially or during sodium boiling, (2) those with low release fractions which are conservatively covered by the assumed 1% solid fission product release during the sodium boiling phase. A few isotopes do have sparging release fractions larger than the 1% used in the TMBDB analysis; however, these represent a less significant contribution to the dose consequences than does the increased plutonium release (Reference E-7). Additional plutonium release during the boil-up phase due to sparging is not significant relative to that resulting from the boiling sodium pool. Sparging effects after boildry were found to be more significant as discussed below.

E.4 PLUTONIUM RELEASE AFTER SODIUM BOILDRY

After the sodium pool in the reactor cavity has evaporated, a bare fuel/steel debris melt is left. Communication is assumed between the reactor cavity and the reactor containment building. This results in a natural convection current through the cavity. The potential mass transport of plutonium via this convection depends on the debris temperature and the convection velocity. The debris surface temperature at the top of the crust was determined to be $\sim 2500^{o}F$. The methods and assumptions related to the calculation of bed surface temperature are discussed in Section 3.2.3.1 of this report. The convection velocity was calculated as follows: First, the natural circulation heat transfer rate was calculated (for a specified PuO_2 surface temperature) using the correlation in Reference E-8 for heat transfer from a hot disk to a large volume of gas. Next, an expression for the temperature rise of the circulating gas was derived as a function of gas flow rate. Finally, expressions for the form pressure loss were derived and set equal to an expression for the buoyancy pressure driving forces (acceleration and frictional losses were conservatively ignored). This last expression, which contained only flow rate as unknown, was solved and the maximum velocity was calculated as that through the opening between the reactor cavity and the RCB.

The analysis of the convection velocity used the following assumptions:

1. The temperature of the debris surface was $5500^{o}F$. This is highly conservative for the calculation of the convection velocity since the predicted surface temperature is $\sim 2500^{o}F$.*

2. The temperature of the gas in the reactor containment building (RCB) was $500^{o}F$.

*Because mass transfer from the debris surface is a function of the convective velocities within the reactor cavity, a $3000^{o}F$ margin was added to the debris temperature to enable the calculation of a higher than expected mass transfer coefficient. This coefficient, when applied at the predicted condition, will result in higher mass transfer rates, providing margin in the calculation.

3. The temperature of the air outside the RCB was $70^{o}F$.

4. The PuO_2 bed was uniformly distributed over the bottom of the reactor cavity.

5. The natural circulation velocity was based on the open reactor cavity (no reactor head) with the vessel in place.

The resulting peak natural convection velocity is 12 ft/sec. Two transport modes were considered for plutonium removal from the debris bed, plutonium vapor removal from the particles and particle levitation.

The plutonium vapor transport mode is due to the plutonium trying to establish a vapor pressure corresponding to the surface particle temperature and the convection current removing the vapor thus establishing a concentration gradient down which the vapor molecules move. This subject of mass transfer is treated in Reference E-9. Based on a maximum convection velocity of 12 ft/sec and maximum bed surface temperature of $2500^{o}F$ the vapor removal rate was calculated to be only 5×10^{-5} grams/hour. At this rate the amount of plutonium released to the RCB in a period of one month is only 0.04 grams.

Plutonium removal by particles being physically swept up from the surface of the bed by the convection current (levitation) was also considered.

The surface of the debris would be solid, i.e., covered with a layer of steel, or in the form of molten iron oxide. In either case, plutonium particles are not present to be picked up by the convection current. Even if the debris were composed of plutonium particles in a molten steel pool, a velocity of only 12 ft/sec would not be sufficient to detach particles from the liquid steel.

The effect of gas sparging after boildry has also been evaluated. After boildry the melt volume relative to the gas volume is smaller because of the loss of the sodium pool and the longer time period involved leads to more released gases. These factors enhance gas sparging and could result in a plutonium release greater than that by all mechanisms before boildry. The results of the sparging analysis indicate that as much as 10 kg of plutonium could be released to the RCB in 30 days and an additional 3 kg over the next several months. An HAA-3 analysis shows that about 70% of the sparged plutonium will remain inside the RCB due to aerosol plate-out and fallout. Filtering (99% efficiency) further reduces the amount of plutonium released by a factor of 100.

E.5 CONCLUSIONS ON PLUTONIUM RELEASE

An evaluation of potential plutonium release from the reactor cavity to the RCB during sodium boiling and following boildry has been made. This evaluation indicates that, in addition to that considered in the initial release phase, about 300 grams of plutonium could be released from the boiling sodium, and about 13 kg (0.64% of core inventory) could be released to the RCB over a several month period following boildry due to gas sparging.

E.6 FISSION PRODUCT RELEASE TO THE RCB

The overall release fraction of fission products from the fuel to the RCB atmosphere is the product of the release fraction from the molten fuel and the release fraction from the sodium pool. References E-10 and E-11 present the results of an evaluation of existing experimental and theoretical data on the volatility of elements in molten fuel. This study developed a list of volatility factors for fission products. These factors represent conservative estimates of the percent release of elements from molten fuel. The volatility of those elements in the categories of noble gases and halogens is 100%. Those elements in the category of volatile fission products have volatility factors of 90%. The remaining fission products, in the category of solid fission products, have volatility factors of 4% or less. Of those in the 4% group only a few are present in the CRBRP EOEC fission product inventory in sufficient quantities to be significant. Strontium and barium have factors of 2%. All other fission products have factors of 1%. These release fractions from molten fuel are summarized in Table E-1.

Once released from the fuel to the liquid sodium, additional partitioning of the fission products can occur during vaporization of the sodium. A method for calculating the extent of fission product release from a sodium pool as a function of sodium vaporized using the Rayleigh equation is reported in References E-12 and E-13.

$$F_i = 1\ (1 - F_{Na})^{A_i}$$

where:

F_i = fraction of a given element released
F_{Na} = fraction of sodium vaporized
A_i = parameter for given element (from Ref. E-12)

Reference E-12 shows that measured values of cesium release from vaporized sodium agree with values predicted by this method.

The TMBDB base case CACECO analysis indicates that 76% of the sodium pool is vaporized. Using 0.76 for F_{Na} and the A_i values from Reference E-12, the fraction of fission products released can be calculated for a number of products of interest. The fractions of these products released from sodium are given in Table E-2.

For the TMBDB analysis the overall release of fission products from the molten fuel to the RCB atmosphere is determined by considering the product of the factors in Tables E-1 and E-2. A complete set of release factors for all elements is not available; however, values for some elements from each group are available and were applied to the other elements within the group. The noble gases are assumed to be released directly from the fuel to the RCB with no attenuation or delay by the sodium pool. The volatile elements cesium and rubidium are also assumed to be released with no attenuation or delay by the sodium. The early release of Cs and Rb is suggested by Reference E-13 which shows almost 100% release of these elements before less than 10% of the sodium has vaporized. Table E-2 indicates that on the order of one third of the iodine, in the form of NaI, would be released from the sodium. It is conservatively assumed that 100% of the iodine is released as the sodium vaporizes.

Of the remaining fission products, the next largest release fraction from the sodium is 0.074. Applying this factor to the fuel release fractions for the solid fission product group gives overall release fractions of 0.003 for those few elements in the 4% group, 0.0015 for Sr and Ba, and 0.0007 for the remaining majority of the solid fission products. Thus the largest overall release of any single solid fission product is about 0.3%.

The TMBDB radiological analysis conservatively assumes the overall release of all the solid fission products to be 1% during the sodium boiling phase.

The majority of the fission products reaching the RCB would be in the form of liquid or solid oxides. Some chemically uncombined fission products may also be released from the sodium as vapor but would condense in the RCB atmosphere (Section 4.1.1 discusses the behavior of the volatile fission products). These fission products would physically co-agglomerate and settle with the predominately Na_2O aerosol. Co-agglomeration of a mixture of aerosol products is addressed in Section 4.1.1. A kinetic analysis of the conversion of iodine to sodium-iodide shows that on the order of 0.2% of the available iodine could remain in the elemental form and, as such, would be less subject to aerosol depletion and filtration. If the entire 0.2% of elemental iodine were released unattenuated by the containment cleanup system, it would result in an additional 30 day LPZ dose to the thyroid of about 40 rem.

E.7 EFFECT OF CO_2 REACTION WITH NaOH ON FISSION PRODUCT RELEASE FROM THE RCB

This section addresses the effect of CO_2 reactions with airborne NaOH, as it may affect the behavior and release of airborne radioactivity.

Because of the slow reaction rate of CO_2 with NaOH, relative to the high RCB vent rate during the TMBDB scenario, it is not likely that a significant amount of CO_2 would react with NaOH before being vented. Any CO_2 that does react would most likely react directly with Na to form Na_2CO_3. Even if an infinite heat transfer coefficient between the reactor cavity atmosphere and the cell liner is assumed to estimate the CO_2 release and all of this

CO_2 reacted completely with either Na or NaOH, the resulting Na_2CO_3 would be no more than 8% of the total aerosol products. This amount of sodium carbonate would not have a significant effect on the overall aerosol behavior and amount of radioactivity reaching the filter system.

Because of the limited solubility of sodium carbonate in water, the filter removal efficiency for Na_2CO_3 for a wet filter/scrubber system could be somewhat lower than for the NaOH. If the maximum amount of Na_2CO_3 possible is formed and if the removal efficiency of the filter is substantially lower (factor of 10) for Na_2CO_3, then the amount of sodium getting through the filters and released to the atmosphere could exceed that predicted in the current analysis by about 70%. If it is assumed that the other radioactive species (except noble gases) are transported with sodium (independent of the chemical form of the sodium), the released radioactivity of these products could then also increase by about 70%. This shows that the radiological results are not highly sensitive to the effect of CO_2 reactions with airborne NaOH.

The effectiveness of the TMBDB filter in removing Na_2CO_3 will be determined as part of the TMBDB Air Cleaning System Performance Test to be performed at the Containment System Test Facility of the Hanford Engineering Development Laboratory. Appendix A.7 provides a description of these tests. Should these tests show the removal efficiency for Na_2CO_3 to be comparable to that expected for other aerosol products (99%) then it can be concluded that the formation of Na_2CO_3 presents no increased radiological consequence. If however the tests show a significantly lower removal efficiency for Na_2CO_3, then a more detailed evaluation of the extent of Na_2CO_3 formation would be required to assess the radiological impacts.

E.8 REFERENCES

E-1 E. J. Chatfield, "Some Studies of the Aerosols Produced by the Combustion or Vaporization of Plutonium Alkali Metal Mixtures, I," J. Nucl. Mat. 32, pp. 228-246 (1969).

E-2 "Nuclear Safety Characterization of Sodium Fires and Fast Reactor Fission Products, Quarterly Technical Progress Report October-December 1975," AI-ERDA-13166, February 1976.

E-3 L. Baker, Jr., et al., "Postaccident Heat Removal Technology," ANL/RAS 74-12, July 1974. (Availability: U.S. DOE Technical Information Center).

E-4 "Radiological Assessment Models, Tenth Quarterly Report, December 1976-February 1977," GEFR-14034-10, March 1977. (Availability: U.S. DOE Technical Information Center).

E-5 S. Jordan and Y. Ozawa, "Fuel Particle and Fission Product Release from LMFBR Core Catcher," in "Fast Reactor Safety and Related Physics, Chicago, October 5-8, 1976," CONF-761001, 1976, pp. 1924-1929.

E-6 "Reactor Safety Study- An Assessment of Accident Risks in U.S. Commercial Nuclear Power Plants, Appendix VII, Release of Radioactivity in Reactor Accidents," WASH-1400 Appendix VII, October 1975.

E-7 S. F. Bankert, et al., "Containment Margins in FFTF for Postulated Failure of In-Vessel Post-Accident Heat Removal," HEDL-TME-77-18, April 1977. (Availability: U.S. DOE Technical Information Center).

E-8 J. G. Yevick, Fast Reactor Technology: Plant Design, p. 61, The MIT Press, Cambridge, MA. 1966.

E-9 R. B. Bird, W. E. Stewart and E. N. Lightfoot, Transport Phenomena, John Wiley and Sons, New York, 1962.

E-10 "Radiological Assessment Models, Fourth Quarterly Report, June-August 1975," GEAP-14034-4, October 1975. (Availability: U.S. DOE Technical Information Center).

E-11 "Radiological Assessment Models Fifth Quarterly Report, September-November 1975," GEAP-14034-5, December 1975. (Availability: U.S. DOE Technical Information Center).

E-12 A. W. Castleman and I. N. Tang, "Fission Product Vaporization from Sodium Systems," BNL-13099, November 1968.

E-13 G. W. Keilholtz and G. C. Battle, Jr., "Fission Product Release and Transport in Liquid Metal Fast Breeder Reactors," ORNL-NSIC-37, March 1969.

TABLE E-2

RELEASE OF FISSION PRODUCTS FROM SODIUM

Group	Elements	Release Parameter, A_i (at 1600°F)	Fraction Released From Sodium
Halogens	I	0.324	0.37
Volatile F.P.	Rb	8.25	1.0
	Sb	1.00×10^{-5}	1.4×10^{-5}
	Te	3.90×10^{-4}	5.6×10^{-4}
	Cs	10.2	1.0
Solid F.P.	Sr	0.054	0.074
	Ba	3.79×10^{-3}	5.4×10^{-3}

APPENDIX F
EVALUATION OF ALTERNATE SCENARIOS

This Appendix provides an evaluation of the sensitivity of the scenario (specifically the containment pressure, temperature and hydrogen histories relative to the 24 hour criterion) analyzed in Section 3.2 to a wide range of parameters and assumptions. The sensitivity studies included a number of cases which nominally would appear to be less severe. However, some aspects could make the consequences more severe. For example, less heat addition to the pool could delay the initiation of auto-catalytic hydrogen burning and, perhaps, lead to a higher hydrogen concentration in the reactor containment building. Thus it was necessary to consider a wide variety of conditions. Specifically, this Appendix considers the sensitivity of the base scenario to the following effects: decay heat, pool chemistry, thermophysical property data, sodium inventory variations, variations in reactor and guard vessel penetration times coupled with decay heat removal, reactor head leakage prior to 24 hours, variation in liner failure times and concrete surface interaction area.

F.1 EFFECT OF DECAY HEAT ON THE BASE TMBDB SCENARIO

F.1.1 Introduction

Three variations of the decay heat were analyzed to assess the sensitivity of the TMBDB scenario to this parameter. The first case investigated the effects of the heterogeneous core nominal decay heat (the base case decay heat was based on the earlier homogeneous core design). The second case considered the heterogeneous core but considered a lower bound decay heat curve. The third case was a limiting lower bound case which assumed no decay heat, thus simulating an accident early in core life.

F.1.2 Model Modifications

The CACECO Code model described in Section 3.2 and Appendix C.1 was modified to evaluate the above cases. Except for decay heat, no other changes were made to the base case.

F.1.3 Results

Table F.1-1 lists the results for all three cases. The containment pressure and temperature at 24 hours are less severe than the Section 3.2 values for all three cases. The case 3 hydrogen concentration however, is higher than the Section 3.2 analysis. This is because with less energy the hydrogen burning criteria are not met (insufficient energy in the sodium pool to support the required sodium vapor concentration of 6 g/m^3). Containment conditions when the burning criteria are met are slightly higher for cases 1 and 2 compared to the Section 3.2 analysis. Again with less energy available in the sodium pool, the time to reach sodium vapor conditions resultin; in a concentration of 6 g/m^3 is longer. As a result the hydrogen accumulates to a higher value prior to burning, and when the appropriate burning criteria are met, the resulting atmosphere temperature and pressure spikes are greater (the analysis assumes the hydrogen burns instantly).

F.1.4 Conclusions

Although containment conditions are slightly more severe when the hydrogen burning criteria are met, the base scenario has sufficient margin to accommodate variations in decay heat. It should be noted that the case 3 conditions could require containment venting prior to 36 hours (base case nominal vent time); however the resulting vent and purge rates would be significantly lower than the present design values reported in Section 2.

TABLE F.1-1

SUMMARY OF CONTAINMENT CONDITIONS FOR "LESS SEVERE" DECAY HEAT SENSITIVITY ANALYSES

Case Number	Case Description	At 24 Hours Pressure (psig)	At 24 Hours Temperature (°F)	At 24 Hours H_2 Concentration (%)	Near Time of H_2 Ignition Pressure (psig)	Near Time of H_2 Ignition Temperature (°F)	Near Time of H_2 Ignition H_2 Concentration (%)
Base Case	Section 3.2 Analysis	11.1	450	0.0	22.4 (10 Hours)	845	4.5
1	Heterogenous Core Nominal	9.3	384	0.0	25.6 (13 Hours)	934	5.1
2	Heterogenous Core With Lower Bound Uncertainty	8.3	337	0.0	26.1 (14.9 Hours)	954	5.4
3	No Decay Heat	1.0	99	2.5	Not Applicable*		

*H_2 burning criterion never met during the first 30 hours of the analysis.

F.2 SENSITIVITY TO SODIUM POOL REACTIONS

F.2.1 Introduction

The sensitivity of the base scenario (Section 3.2) to sodium pool reactions was evaluated. This analysis investigated the effect of considering the sodium-water reactions in the pool to be independent of the hydrogen partial pressure and pool temperature (see Appendix C.1 for description of the pool reaction sequence). As a result the analysis considered two cases. The first case considered the sodium-water reaction to produce sodium oxide and hydrogen. The second case assumed the sodium-water reaction to produce sodium hydroxide and hydrogen.

F.2.2 Model Modifications

The CACECO Code model described in Section 3.2 and Appendix C.1 was modified to evaluate the base case sensitivity to the sodium pool-water reactions. The specific changes resulted in only sodium oxide and hydrogen being produced in case 1 (the heat of reaction is approximately 3 times less than the sodium-water reaction which produces sodium hydroxide and free hydrogen). All other pool and atmosphere reactions were treated exactly as described in Appendix C.1.

F.2.3 Results

Table F.2-1 provides the results for both analyses. The first case results at 24 hours are very similar to the Section 3.2 analysis. The peak hydrogen concentration prior to meeting the burning criteria was approximately 1% greater than the Section 3.2 results (5.5 versus 4.5%). The increase in hydrogen is the consequence of neglecting sodium hydroxide formation (the reaction products remove 1 mole of free hydrogen). As a result of the increase in hydrogen before the burning criteria are met, the containment pressure and temperature peaks are slightly higher (the peaks are from the assumption that the hydrogen burns instantly). As in case 1, the case 2 results exhibited similar conditions in containment at 24 hours to the

Section 3.2 analysis. The containment conditions prior to and after the hydrogen burning criteria were met were less severe than the Section 3.2 results. In this case the reaction producing sodium hydroxide was assumed throughout the analysis, thus removing free hydrogen and effectively reducing the containment peak pressure and temperature once the burning criteria were met.

F.2.4 Conclusion

Although containment conditions at the time when the hydrogen burning criteria are met are slightly more severe (case [illegible]) the base scenario exhibits sufficient margin to accommodate variations in the pool chemistry.

TABLE F.2-1

SUMMARY OF CONTAINMENT CONDITIONS FOR "LESS SEVERE" POOL CHEMISTRY SENSITIVITY ANALYSES

Case Number	Case Description	At 24 Hours: Pressure (psig)	At 24 Hours: Temperature (°F)	At 24 Hours: H_2 Concentration (%)	Near Time of H_2 Ignition: Pressure (psig)	Near Time of H_2 Ignition: Temperature (°F)	Near Time of H_2 Ignition: H_2 Concentration (%)
Base Case	Section 3.2 Analysis	11.1	450	0.0	22.4 (10 Hours)	845	4.5
1	$2\ Na + H_2O = Na_2O + H_2$	11.1	450	0.0	26.6 (10.2 Hours)	990	5.5
2	$2\ Na + 2H_2O = 2\ NaOH + H_2$	11.7	436	0.0	14.6 (10.4 Hours)	570	2.7

F.3 SENSITIVITY TO CONCRETE THERMOPHYSICAL PROPERTY DATA

F.3.1 Introduction

An evaluation of the sensitivity of the base TMBDB scenario to concrete thermophysical properties has been made. This effect was simulated by increasing the thermal conductivity of the insulating concrete in the reactor cavity and pipeway cells by 20%. This simulates a more effective concrete heat sink.

F.3.2 Model Modifications

The CACECO Code model described in Section 3.2 and Appendix C.1 was modified to evaluate the base case sensitivity to concrete thermophysical property data. This was simply accomplished by increasing the insulating concrete thermal conductivity values by 20%. Thus the insulting concrete in the reactor cavity and the pipeway cell double-heated wall was increased from 0.12 to 0.144 Btu/hr-ft-^{o}F. The insulating concrete in the remaining pipeway cell structures was increased from 0.24 to 0.288 Btu/hr-ft-^{o}F.

F.3.3 Results

Table F.1-3 provides the results for this analysis. Containment conditions at 24 hours are less severe than the base scenario results. With an increase in the insulating concrete thermal conductivity, the effective heat sink capability of the reactor cavity and pipeway cells is increased. This results in a reduced sodium boiloff rate which reduces the severity of the containment transients. Conditions prior to and after the burning criteria are met are slightly more severe than the base scenario. This is because with more available heat sink in the reactor cavity and pipeway cells the time for the sodium pool to reach the necessary burning criteria is longer.

F.3.4 Conclusions

The base scenario has sufficient margin to accommodate variations in concrete thermophysical properties.

TABLE F.3-1

SUMMARY OF CONTAINMENT CONDITIONS FOR "LESS SEVERE"
THERMOPHYSICAL PROPERTY SENSITIVITY ANALYSIS

Case Number	Case Description	At 24 Hours: Pressure (psig)	At 24 Hours: Temperature (^oF)	At 24 Hours: H_2 Concentration (%)	Near Time of H_2 Ignition: Pressure (psig)	Near Time of H_2 Ignition: Temperature (^oF)	Near Time of H_2 Ignition: H_2 Concentration (%)
Base Case	Section 3.2 Analysis	11.1	450	0.0	22.4 (10 Hours)	845	4.5
1	20% Increase In Insulating Concrete Thermal Conductivity	10.0	413	0.0	23.1 (10.3 Hours)	864	4.6

F.4 SENSITIVITY TO SODIUM INVENTORY VARIATIONS

F.4.1 Introduction

An evaluation of the sensitivity of the base TMBDB scenario to variations in the amount of sodium that would drain or syphon to the reactor cavity has been made. Four cases were analyzed. The first two considered reductions in the amount of sodium that would drain or syphon from the primary piping to the reactor cavity. Specifically the first case considered a 33% reduction in the amount of sodium that would drain or syphon from 3 loops to the cavity. The second case considered a 66% reduction in the sodium mass that would drain or syphon to the cavity.

The remaining two cases evaluated the effect of additional sodium on the scenario. Case 3 considered the PSOV (Primary Storage Overflow Vessel) to drain to the reactor cavity. The entire gross volume of approximately 37,100 gallons at an average temperature of 1130°F was assumed to drain at a rate of 560 gpm to the reactor cavity. The fourth case assumed the same gross volume as mentioned above, however, the initial temperature was considered to be 800°F and the drain rate to the cavity was assumed to be 160 gpm. Cases 3 and 4 bracket the operating temperatures and drain rates of the PSOV.

F.4.2 Model Modifications

The CACECO Code model described in Section 3.2 and Appendix C.1 was modified to study the effect of varying sodium mass on the TMBDB scenario. For all four cases the sodium input data were modified accordingly.

F.4.3 Results

Table F.4-1 provides the results for all four cases. The results for the first 2 cases at 24 hours were found to be slightly more severe than the Section 3.2 analysis. For example the case 2 (66% reduction of sodium syphon mass) containment pressure and temperature were 11.3 psig and 468°F versus

TABLE F.4-1

SUMMARY OF CONTAINMENT CONDITIONS FOR "LESS SEVERE" SODIUM INVENTORY SENSITIVITY ANALYSES

Case Number	Case Description	At 24 Hours: Pressure (psig)	At 24 Hours: Temperature (°F)	At 24 Hours: H_2 Concentration (%)	Near Time of H_2 Ignition: Pressure (psig)	Near Time of H_2 Ignition: Temperature (°F)	Near Time of H_2 Ignition: H_2 Concentration (%)
Base Case	Section 3.2 Analysis	11.1	450	0.0	22.4 (10 Hours)	845	4.5
1	33% Reduction In 3 Loop Mass	11.2	461	0.0	20.4 (8.7 Hours)	780	4.1
2	66% Reduction In 3 Loop Mass	11.3	468	0.0	18.7 (7.4 Hours)	718	3.6
3	PSOV Drain To RC; 1130°F Initial Sodium Temperature; 560 gpm Drain Rate	11.1	455	0.0	24.0 (11.1 Hours)	895	4.9
4	PSOV Drain To RC; 800°F Initial Sodium Temperature; 160 gpm Drain Rate	10.5	428	0.0	25.5 (13.3 Hours)	929	5

F.5 SENSITIVITY TO REACTOR AND GUARD VESSEL PENETRATION TIMES AND SODIUM TEMPERATURE

F.5.1 Introduction

An evaluation of the sensitivity of the TMBDB scenario to reactor and guard vessel penetration times and considering different decay heat removal assumptions has been made. Four cases were considered. The first three analyzed penetration times of 100, 1000 and 10,000 seconds coupled with decay heat removal prior to penetration. The fourth case assumed penetration of the reactor and guard vessels did not occur. No decay heat removal was considered in this case.

F.5.2 Model Modifications

The CACECO Code model described in Section 3.2 and Appendix C.1 was modified to evaluate the above cases. For all three cases the decay heat was adjusted according to the assumed penetration time. Decay heat removal was accounted for by evaluating the initial sodium temperature at the time of vessel penetration from a normal plant transient corresponding to the same point in time (U-1A; trip from full power with normal decay heat was the transient assumed for all 3 cases). After penetration, the decay heat removal system was assumed to be inoperable.

The fourth case simulated a scenario with no guard vessel and reactor vessel penetration. Decay heat was input at time zero with a leakage path defined from the reactor vessel through the head to containment. The reactor head risers were modelled and treated as described in Section F.6. Only the reactor vessel sodium was considered in the analysis.

F.5.3 Results

Case 1 results (Table F.5-1) at 24 hours are slightly more severe than the Section 3.2 analysis. Since penetration occurs at 100 seconds versus 1000 seconds in the base scenario more decay heat is available to boil the sodium and subsequently results in a slightly more severe scenario.

Conditions prior to and after the meeting of the hydrogen burning criteria are slightly less severe than the base scenario results. This is due to the increase in decay heat which drives the sodium pool to sufficient temperature to produce the necessary sodium vapor to satisfy the burning criteria.

The case 2 results (Table F.5-1) exhibited less severe results at 24 hours than the base scenario results (Section 3.2). In this analysis the effect of decay heat removal can be seen since the assumed penetration time is identical to that used in Section 3.2. For example containment atmosphere temperature and pressure were found to be 386°F and 9.8 psig respectively versus 450°F and 11.1 psig reported in Section 3.2. The containment conditions near the time of hydrogen ignition, however, were found to be slightly worse. Again with a slightly cooler sodium pool, a longer time is required before the hydrogen burning criteria are met.

Case 3 showed the best results at 24 hours and the worst consequences prior to and after hydrogen ignition. Containment temperature and pressure were found to be 4.3 psig and 191°F at 24 hours compared to base scenario results of 11.1 psig and 450°F. The peak hydrogen concentration prior to hydrogen burning was 5.5% versus 4.5% in the Section 3.2 analysis. Similarly the pressure and temperature spikes once burning started were found to be 27.2 psig and 987°F.

The case 4 consequences at 24 hours were found to be more severe than the base scenario. Containment pressure, temperature and hydrogen concentration resulted in values of 12.2 psig, 815°F and 0.2% respectively. These compare to 11.1 psig, 450°F and 0% hydrogen found in the base case. The principal reason for the more severe consequences is the nature of the assumed scenario. Since penetration of the reactor and guard vessels is considered not to occur, the only available heat sinks are the vessels, internals, reactor vessel sodium inventory and the head. With the reduced heat sink availability the sodium reaches a boiling state sooner (6 hours versus 9 hours in the base scenario) and subsequently leaks to containment at a higher rate. Because of the more severe results the analyses were extended to sodium boildry. The venting, purging and cooling functions were initiated earlier in the analysis than in the base case to control the containment and confinement temperatures. The containment was vented at 24 hours resulting in a peak vent rate of 25,600 cfm (the maximum design value is 26,400 cfm). The operation of the annulus cooling system was initiated at 24 hours. The purge system was initiated at 26 hours. A value of 5000 scfm was used. This is less than the nominal value of 8000 scfm employed in the Section 3.2 analysis. With this purge rate, the peak hydrogen concentration was 3.1%. Figures F.5-1 through F.5-4 present containment atmosphere and steel temperatures, pressure, hydrogen concentration and vent rates up to boildry.

Preliminary analysis employing the two dimensional Trump thermal model (described in Section 3.2.2.2) indicated that the containment and confinement structural temperatures to boildry (∽106 hours) would be acceptable.

F.5.4 Conclusions

Cases 1 through 3 exhibit slight variations with respect to the base scenario results and sufficient margin exists to accommodate the variations. Case 4 results were significantly more severe at 24 hours, specifically containment temperature. Preliminary analyses indicate that structural integrity would be maintained throughout the scenario. Thus the conclusion that containment integrity can be maintained in excess of 24 hours without venting, purging or annulus cooling remains valid for this scenario.

TABLE F.5-1

SUMMARY OF CONTAINMENT CONDITIONS FOR "LESS SEVERE" PENETRATION TIME AND SODIUM INITIAL TEMPERATURE SENSITIVITY ANALYSES

Case Number	Case Description	At 24 Hours			Near Time of H_2 Ignition		
		Pressure (psig)	Temperature (°F)	H_2 Concentration (%)	Pressure (psig)	Temperature (°F)	H_2 Concentration (%)
Base Case	Section 3.2 Analysis	11.1	450	0.0	22.4 (10 Hours)	845	4.5
1	100 Sec. Penetration With Decay Heat Removal	11.8	482	0.0	19.8 (9 Hours)	759	4.1
2	1000 Sec. Penetration With Decay Heat Removal	9.8	386	0.0	26.1 (17.3 Hours)	955	5.2
3	10000 Sec. Penetration With Decay Heat Removal	4.3	191	0.0	27.2 (22 Hours)	987	5.5
4	No Reactor and Guard Vessel Penetration	12.2	815	0.2	Not Applicable*		

*H_2 burning criterion met early in the analysis thereby precluding H_2 buildup.

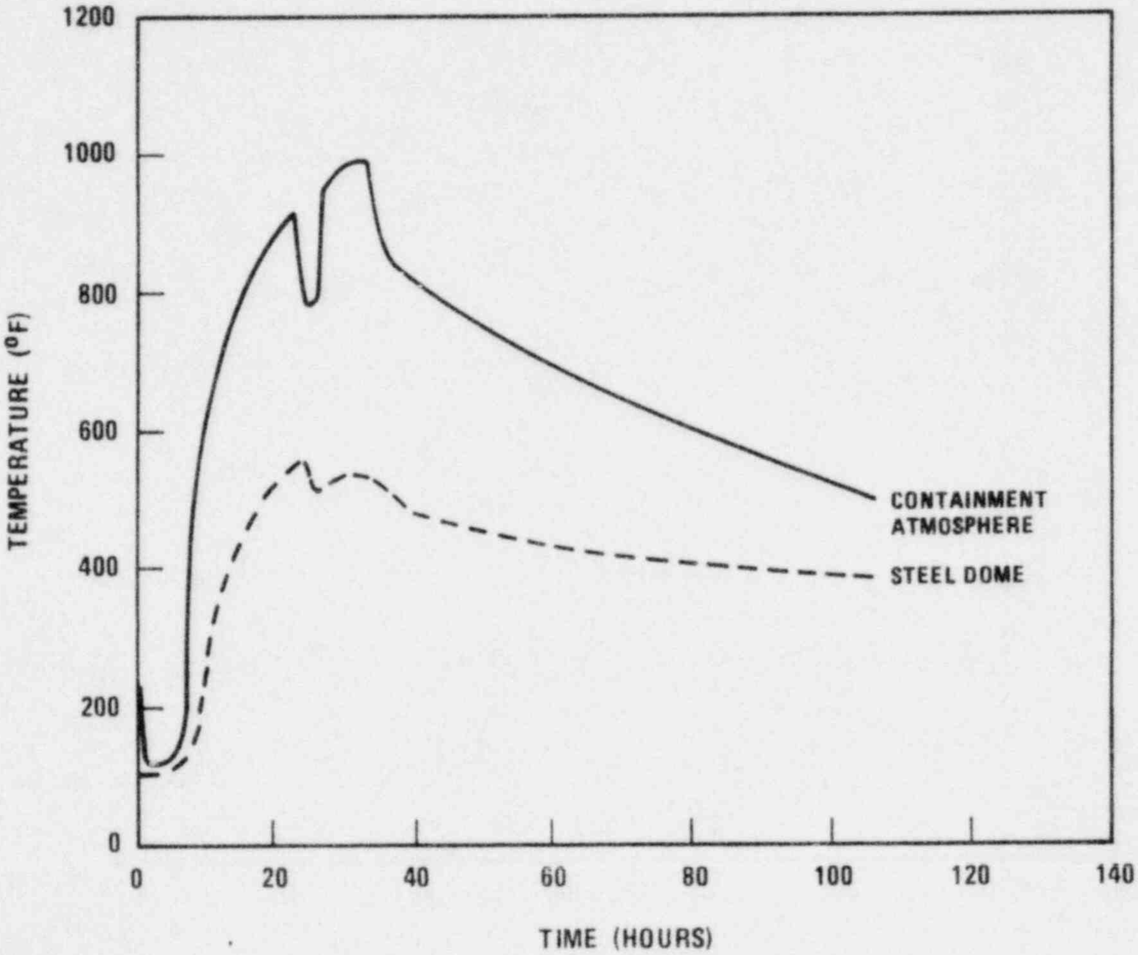

Figure F.5-1 Containment Atmosphere and Containment Steel Dome Temperatures (No Reactor and Guard Vessel Penetration)

1966-300

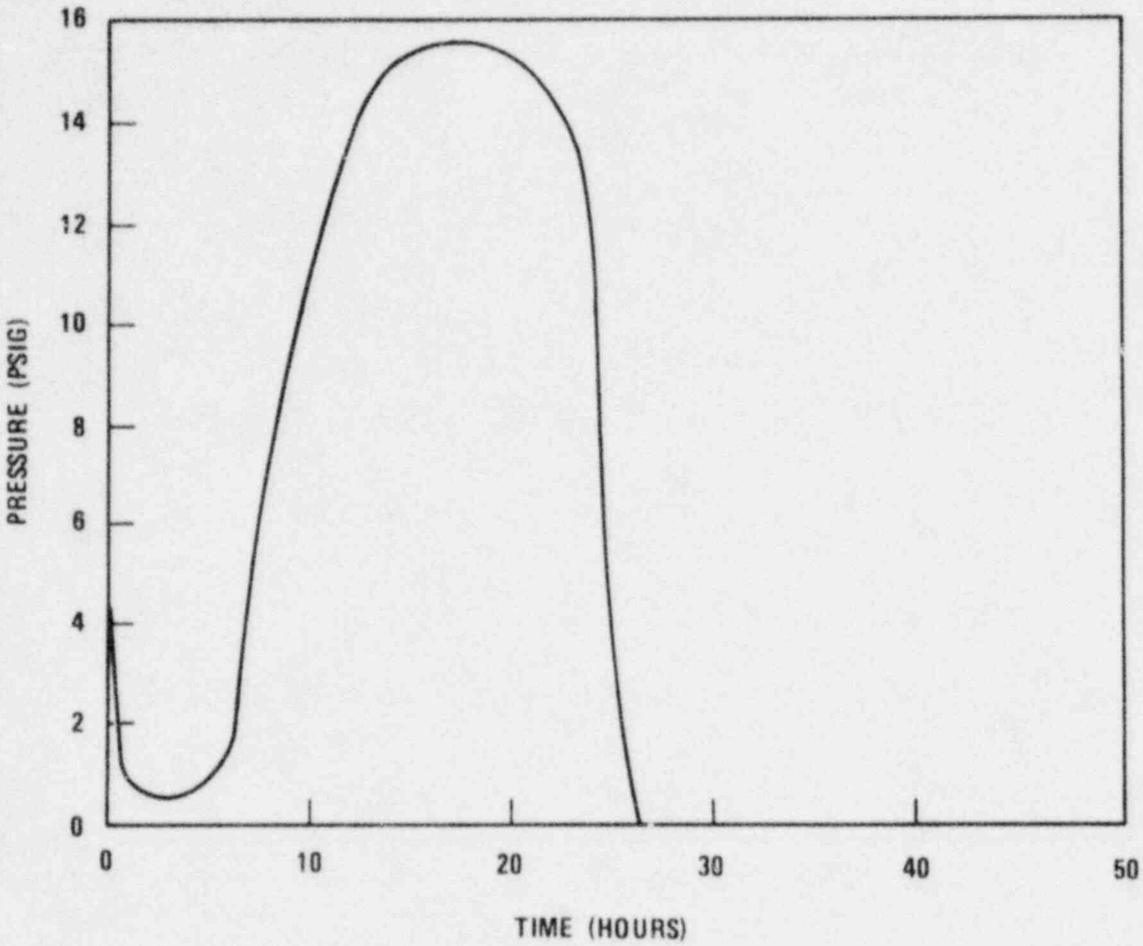

Figure F.5-2 Reactor Containment Building Pressure
(No Reactor and Guard Vessel Penetration)

1966-301

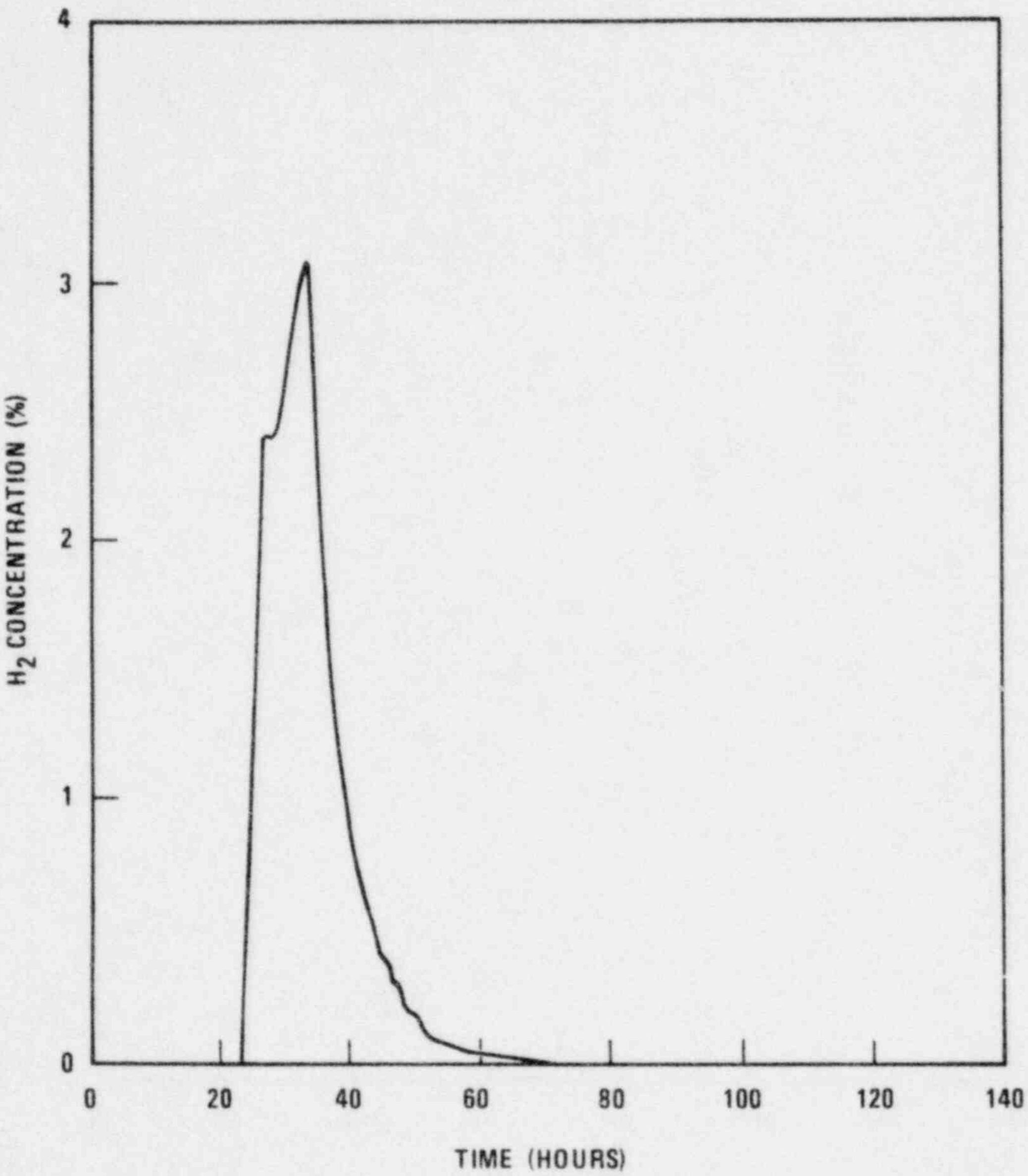

Figure F.5-3 Reactor Containment Building H_2 Concentration
(No Reactor and Guard Vessel Penetration)

1966-302

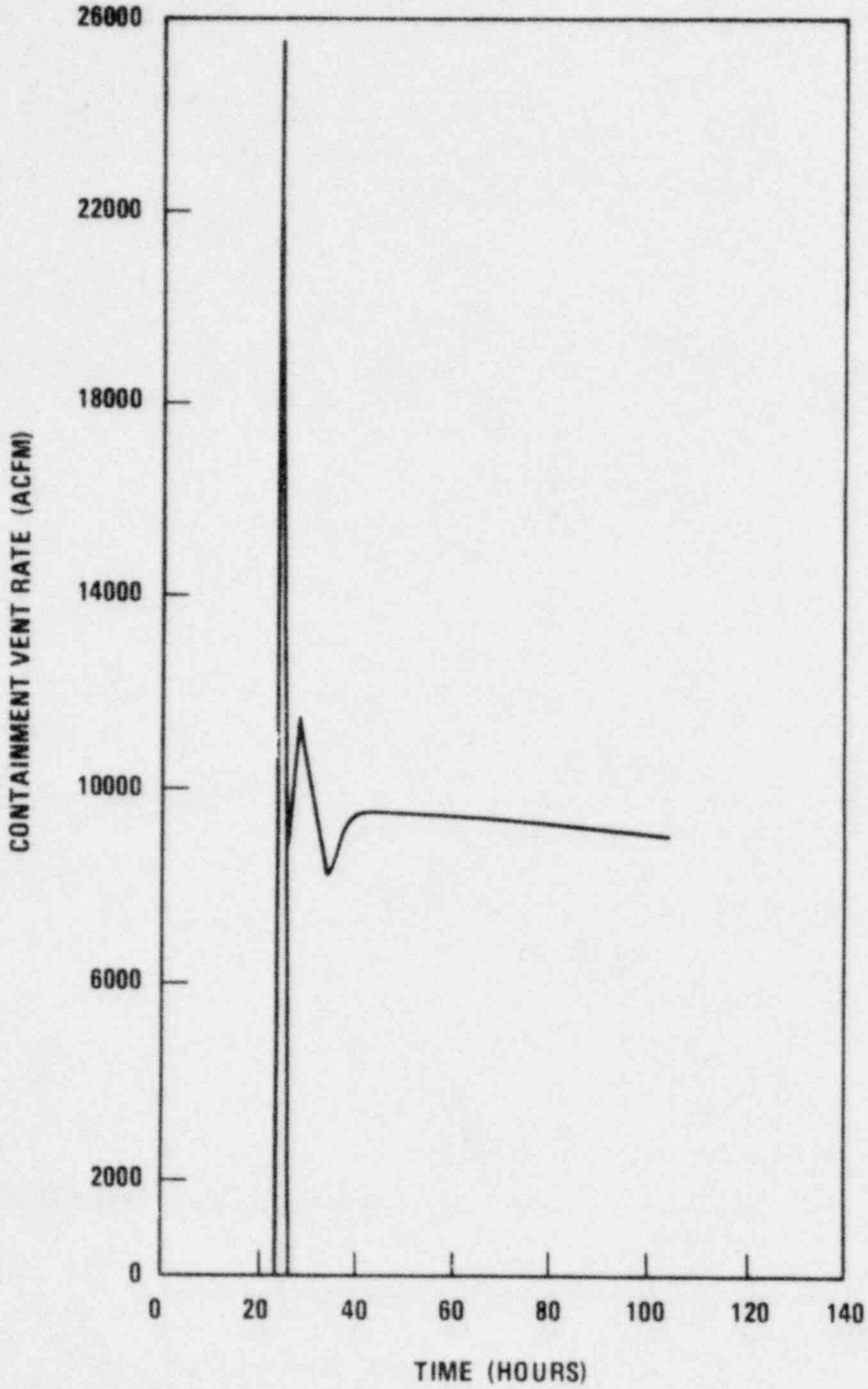

Figure F.5-4 Reactor Containment Building Vent Rate
(No Reactor and Guard Vessel Penetration)

1966-303

F.6 EARLY REACTOR HEAD LEAKAGE SCENARIO

F.6.1 Introduction

The thermal margin analyses described in Section 3.2 assumed the reactor head initially leaked all of the noble gases and 1000 pounds of sodium. Beyond this initial release, it was assumed that further leakage to the RCB would be through the RC to RCB vent up to 50 hours. Beyond 50 hours, the head was assumed to leak at a very high rate. As long as the elastomer seals at the top of the head risers remain below 500-600°F, significant head leakage would not occur. However, these seals may reach 500-600°F before 50 hours and begin to degrade and lose their sealing capability.

In the following, a modified scenario will be developed, based on the assumption that some fuel remains in the reactor vessel after penetration of the reactor and guard vessels; increased head leakage after 1000 seconds will be considered, taking into account the heat sink capability of the head risers.

F.6.2 Revised Scenario

The scenario described in Section 3.2.1 was modified to include increased reactor head leakage after 1000 seconds as follows:

A. After penetration of the reactor vessel and guard vessel at 1000 seconds, the fuel that can be sustained in a stable, coolable debris bed is assumed to be retained in the reactor vessel. All fuel above the sodium level and fuel in excess of the debris bed dryout thickness below the sodium level would penetrate the supporting surfaces and redistribute uniformly on the reactor cavity floor. In this case, the conservative approach is to consider as much fuel as possible in or directly under the reactor vessel.

B. All of the sodium vapor generated in the reactor vessel and in the region directly below the reactor vessel would be available for leakage through the head. The reactor vessel separates the sodium vapor generated in the reactor cavity from that generated in the remainder of the reactor vessel.

C. All of the sodium vapor generated in the remainder of the cavity would pass into the containment building through the pipeway cells and the reactor cavity venting system.

D. The reactor vessel head and plugs would remain intact for 50 hours; thus, the head risers would be effective as heat sinks. The principal leakage path through the head would be through the risers.

E. Since the analyses described below indicate the pressure, temperature, and hydrogen concentration conditions in containment at 24 hours would not challenge the containment integrity, the initiation of venting, purging and annulus cooling would not be required until after 24 hours.

F.6.3 Revised Analytical Models and Analysis Results

F.6.3.1 Fuel Distribution

The fuel distribution between the reactor vessel and the reactor cavity determines the relative amounts of sodium vapor leaking through the reactor head and through the pipeway cells. Because the largest amount of fuel within or directly below the reactor vessel is the most conservative condition for the analyses considered here, the following procedure for evaluating fuel distribution was employed.

The distribution of fuel between the reactor cavity and the reactor vessel internals was evaluated by considering that fuel would settle and form a stable boiling debris bed on all intact horizontal surfaces inside the reactor vessel covered by sodium after penetration of the reactor and guard vessel and draining of sodium into the reactor cavity. The remainder of the fuel is then assumed to penetrate its supporting structures and enter the reactor cavity. The horizontal surfaces which would retain fuel following penetration of the reactor and guard vessels are the core support plate and the flow inlet modules. As these are the only surfaces which would be covered by the sodium pool, other surfaces would be dry, and any debris bed formed would melt through the surface and deposit on a lower level surface which was covered by sodium or pass through the vessels onto the reactor cavity floor.

The surface area of the core support plate available for fuel retention includes the total area of the plate less the area occupied by the 61 inlet modules (60 ft^2). Additionally, a pocket exists outside of the core barrel at the juncture of the core support structure and the barrel (Figure F.6-1). Each of these regions is capable of retaining a debris bed whose maximum depth is limited only by the heat removal capability of the overlaying sodium.

The remaining in-vessel location for debris accumulation is the flow inlet module. Because the inlet modules contain openings to allow sodium flow, the depth of the bed retained in the module would not exceed the distance from the bottom of the module to the opening (3.77 inches - Figure F.6-1).

The depth of the stable bed was calculated at 1000 seconds assuming that all core and blanket material would form a uniform mixture. Steel was not considered to exist in the mixture as it would reduce the dryout heat flux, thereby reducing the amount of fuel in the bed. A greater amount of fuel in the reactor vessel is conservative in this analysis. The stable bed depth at 1000 seconds would be 6.5 inches* using the data in Reference F.6-1. Based on the 6.5 inch debris depth along with the area of the core support plate (60 ft^2), the dimensions from Figure F.6-1 of the pocket between the core support structure, and the dimensions of the inlet modules, the quantities of core debris remaining in the vessel are noted in Table F.6-1. This indicates that up to 16% of the core and blankets could remain in the vessel following penetration.

Of the core material reaching the reactor cavity, 25% would serve as a sodium vapor source for the reactor vessel because of the relative diameters of the reactor vessel and reactor cavity. This assumes that all vapor formed beneath the reactor vessel could be released to the vessel. This implies that the

* Note that this bed depth is greater than that quoted in Section 3.2.1 because of the intentional bias here toward greater bed depths to be conservative for this particular calculation.

hole in the reactor vessel is equal to the full diameter of the vessel. Combining this with the 16% retained in the vessel results in 37%* of the total sodium vapor passing through the reactor vessel.

In subsequent calculations 50% of the core debris was conservatively assumed to be in the vessel or directly beneath it.

F.6.3.2 Structural Considerations

For the consequences of this scenario to be similar to those in Section 3.2, the reactor vessel and reactor head must not fail for 50 hours. A creep rupture analysis of these two structures was performed.

Reactor Head

The maximum stress level in the reactor head (large rotating plug) under TMBDB loading conditions (dead weight only), is 1800 psi. Based on the results of the elevated temperature creep rupture tests for the SA-508 Class 2 material of the head and the reactor head temperatures shown in Figure F.6-2, the closure head would remain intact for well beyond 50 hours.

Stress (psi)	Temperature (^{o}F)	Time to Rupture Hours
1750	1750	138.5
2000	1750	86.3

Reactor Vessel

The weakest section of the reactor vessel at high temperature is the flange attaching it to the head. From the creep rupture material tests where the stress level was 2000 psi, the Larsen-Miller parameter ($P = T (20 + \log t_r)$) would be 48.4×10^3.

*0.25 (1.00 - 0.16) + 0.16 = 0.37

Using this value of the Larsen-Miller parameter to extrapolate to the maximum flange temperature of 1770°F (the flange temperatures are equal to the reactor cavity atmosphere temperature in Figures F.6-2 and 3-6), the time to rupture is calculated to be approximately 51 hours. At 1700°F, the time to rupture would be approximately 260 hours.

The flange temperature would not reach 1700°F until 18 hours into the event and thereafter would rise slowly to a peak value of 1770°F at about 36 hours into the event. Thus flange failure would not occur until well beyond the 24 hours specified by NRC for maintaining containment integrity and also beyond the 50 hour time assumed in the base case before gross leakage to the RCB (from the reactor cavity) bypasses the pipeway cells.

F.6.3.3 Revisions to the Containment CACECO Code Model

The CACECO model was modified to simulate the scenario developed in Section F.6.1. The modification accounted for heat transfer from sodium vapor, nitrogen and hydrogen flowing through the risers mounted on the head. Also, a cell was added to the CACECO model to allow simulation of the reactor vessel and therefore in-vessel and ex-vessel fuel debris distribution. Because of CACECO limitations, it was necessary to delete Cell 105, which is included in the base case. The four cells represented the reactor vessel (RV) and volume directly below the RV, the remainder of the reactor cavity (RC), the pipeway cells and the containment volume above the operating floor and reactor head (RCB).

At reactor and guard vessel penetration (1000 seconds), a direct inter-connection (orifice with an area of 0.25 ft^2) was inserted between the reactor cavity, pipeway cells and RCB to simulate the burst disk rupture and the reactor cavity to containment vent system. Also included was a direct inter-connection between the reactor vessel cell and containment representing leakage paths through the reactor head.

Heat Structures

The one-dimensional heat structures discussed in Appendix C.1 were again used in the head leakage analysis. The only variation was the inclusion of a structure representing the risers which would condense sodium vapor leaving the reactor cavity and transfer heat to containment. This structure was composed of a steel plate 0.1 inches thick with an area of 710 ft^2. The therm l boundary conditions of this structure are discussed later in this Appendix.

Decay Heat

As discussed in Appendix C, the decay heat associated with the noble gases is input to the containment atmosphere immediately. The heat associated with the halogens and volatiles is assumed to be contained in and carried with the sodium. The remainder of the decay heat is divided evenly betwen the reactor vessel and the reactor cavity cells because of the assumed equal division of the fuel debris between the two cells.

Energy Transport

The energy transfer model previously employed in the reactor cavity was modified as follows:

a. Those structures modelling the reactor vessel, internals, guard vessel and head employed the reactor vessel cell pool and atmosphere boundary conditions.

b. Those structures modelling the reactor cavit alls employed the boundary conditions associated with the cell representing the remainder of the reactor cavity.

Riser Heat Transfer Coefficients

During the flow of sodium vapor, nitrogen and hydrogen through leakage paths in the reactor vessel head, heat would be transferred from the vapor and gases to the surrounding structure. This would result in sodium vapor condensation in the passages, thereby reducing the quantity of sodium reaching the reactor containment building atmosphere. The amount of sodium that would condense is determined by the thermal resistances characteristic of the flow path through the small, intermediate and large riser assemblies (Figures F.6-3 and 4). Heat would be transferred from the sodium vapor stream to the riser assembly by convection. The riser assembly would radiate and convect heat to the surroundings. Since the riser assemblies are thin, the heat transfer coefficients on the two surfaces control the amount of heat transfer from the sodium vapor stream.

The convective heat transfer coefficient is based on the quantity of sodium vapor, nitrogen and hydrogen which enters the reactor containment building, i.e., the flow exiting the riser assemblies. The coefficient was determined as a function of time using CACECO code output for this case and the forced convective correlation.

$$Nu = 0.026\ Re^{0.8}\ Pr^{1/3}$$ (Reference F.1-2) (See Table F.6-2)

This was an iterative process in which heat transfer coefficients were entered, flows were calculated by the CACECO code and the heat transfer coefficients were recalculated based on the CACECO output. Table F.6-3 presents the heat transfer coefficients as a function of time together with the data used in their calculation.

Also shown in Table F.6-3 are the heat transfer coefficients used as input to the CACECO code model. The coefficients used in the analysis are very similar to the resulting calculated coefficients.

Radiation and convective heat transfer coefficients for heat flow from the head structures to the environment were determined from Reference F.6-3, for the condition of sodium vapor at 1600°F and a heat sink of 400°F. The radiative heat transfer coefficient was modelled by an emissivity and the appropriate shape factor, and then combined with the convective heat transfer coefficient to provide a total heat transfer coefficient.

The parameters used to calculate the heat transfer coefficient are shown in Table F.6-4. The overall heat transfer coefficient was used as input to the CACECO model as the heat transfer coefficient between the risers and the reactor containment building atmosphere.

F.6.3.4 Analysis Results

The results of the CACECO analysis are shown in Table F.6-5 at 24 hours. From this table, it is apparent that the early head leakage scenario results in containment transients that would not challenge the containment integrity at 24 hours. The results illustrate that the risers are very efficient heat sinks during the first 24 hours.

F.6.4 Summary and Conclusions

A modification was made to the CACECO model to simulate a TMBDB scenario in which a fraction of the fuel debris would be retained on in-vessel horizontal surfaces. The modification was made by adding a cell to the base case model to represent the reactor vessel and the volume immediately below it, and deleting this volume from the reactor cavity cell used in the base case. The distribution of fuel between the two cells (reactor cavity and reactor vessel) was conservatively taken to be 50% in each cell, with both cells having leakage paths to the reactor containment building.

Leakage through the reactor cavity venting system (through the pipeways) was modeled the same as in the base case. However, a heat structure was added to simulate heat transfer as the vapor flows through the risers on the head. Heat transfer through the risers was based on the sodium vapor flow entering the reactor containment building and on forced convection heat transfer correlations.

These analyses indicate that head leakage prior to 24 hours would result in containment conditions that would not challenge the integrity of the RCB at 24 hours. Consequently, the conclusion that containment integrity can be maintained in excess of 24 hours without venting, purging or annulus cooling remains valid for this alternate scenario.

F.6.5 References

F.6-1 L. Baker, Jr., et al., "Postaccident Heat Removal Technology," ANL/RAS 77-2, January 1977. (Availability: U.S. DOE Technical Information Center).

F.6-2 R. B. Bird, W. E. Stewart and E. N. Lightfoot, Transport Phenomena, p. 399, John Wiley and Sons, New York, 1960.

F.6-3 J. A. Wiebelt, Engineering Radiation Heat Transfer, p. 223, Holt, Rinehart and Winston, New York, 1966.

F.6-4 "Nuclear System Materials Handbook Design Data," TID-26666, Vol. 1, Book 2, Part V, Coolants. (Availability: Hanford Engineering Development Laboratory).

TABLE F.6-1

MAXIMUM FUEL DISTRIBUTION IN THE REACTOR VESSEL AFTER PENETRATION

Location	Quantity of Fuel (in^3)
Core Support	27,000
Core Barrel-Reactor Vessel Annulus	6,000
Inlet Modules	4,600
Total Quantity In-Vessel	37,600
Total Quantity of Fuel and Blanket	237,000
% Retained In-Vessel	16.

TABLE F.6-2

PARAMETERS USED IN THE RISER INTERIOR SURFACE
HEAT TRANSFER COEFFICIENT CALCULATION

Prandtl Number	0.67
Thermal Conductivity	0.032 Btu/hr-ft-^{o}F*
Viscosity	0.036 lb/ft-hr*
Hydraulic Diameter	2.00 in
Flow Area	11.15 ft^2

*Reference F.6-4

TABLE F.6-3

RISER CONVECTIVE HEAT TRANSFER COEFFICIENTS FOR THE INTERIOR SURFACE

		Heat Transfer Coefficient (Btu/hr-ft^2-^{o}F)	
Time, (hr)	Flow, (lb/hr)	Calculated From Correlation	Used in CACECO Model
1.	142.	.11	.12
4.	259.	.18	.17
6.	300.	.21	.20
8.	618.	.37	.36
10.	1383.	.70	.83
13.	1911.	.91	.65
15.	1846.	.89	.87
18.	2533.	1.14	1.25
20.	2982.	1.3	1.34
24.	5162.	2.02	1.62

TABLE F.6-4

RISER EXTERIOR SURFACE TO CONTAINMENT EFFECTIVE HEAT TRANSFER COEFFICIENT

Surface Area of Riser	710 ft^2
View Factor	0.75
Radiant Heat Transfer Coefficient	20 Btu/hr-ft^2-^oF (Reference F.6-2)
Convective Heat Transfer Coefficient	2 Btu/hr-ft^2-^oF (Reference F.6-2)
Emissivity	0.75 (Reference F.6-3)
Overall Heat Transfer Coefficient	13.0 Btu/hr-ft^2-^oF

TABLE F.6-5

COMPARISON OF RCB PARAMETERS AT 24 HOURS
WITH AND WITHOUT EARLY REACTOR HEAD LEAKAGE

	Section 3.2 Analysis (Limited Head Leakage Before 50 Hours)	Increased Head Leakage (After 1000 Seconds)
Containment Atmosphere Pressure (psig)	11.1	12.4
Containment Atmosphere Temperature (°F)	450	550
Hydrogen Concentration (%)	0.0	0.0
Mass of Sodium Entering Containment (pounds)	25,500	40,000

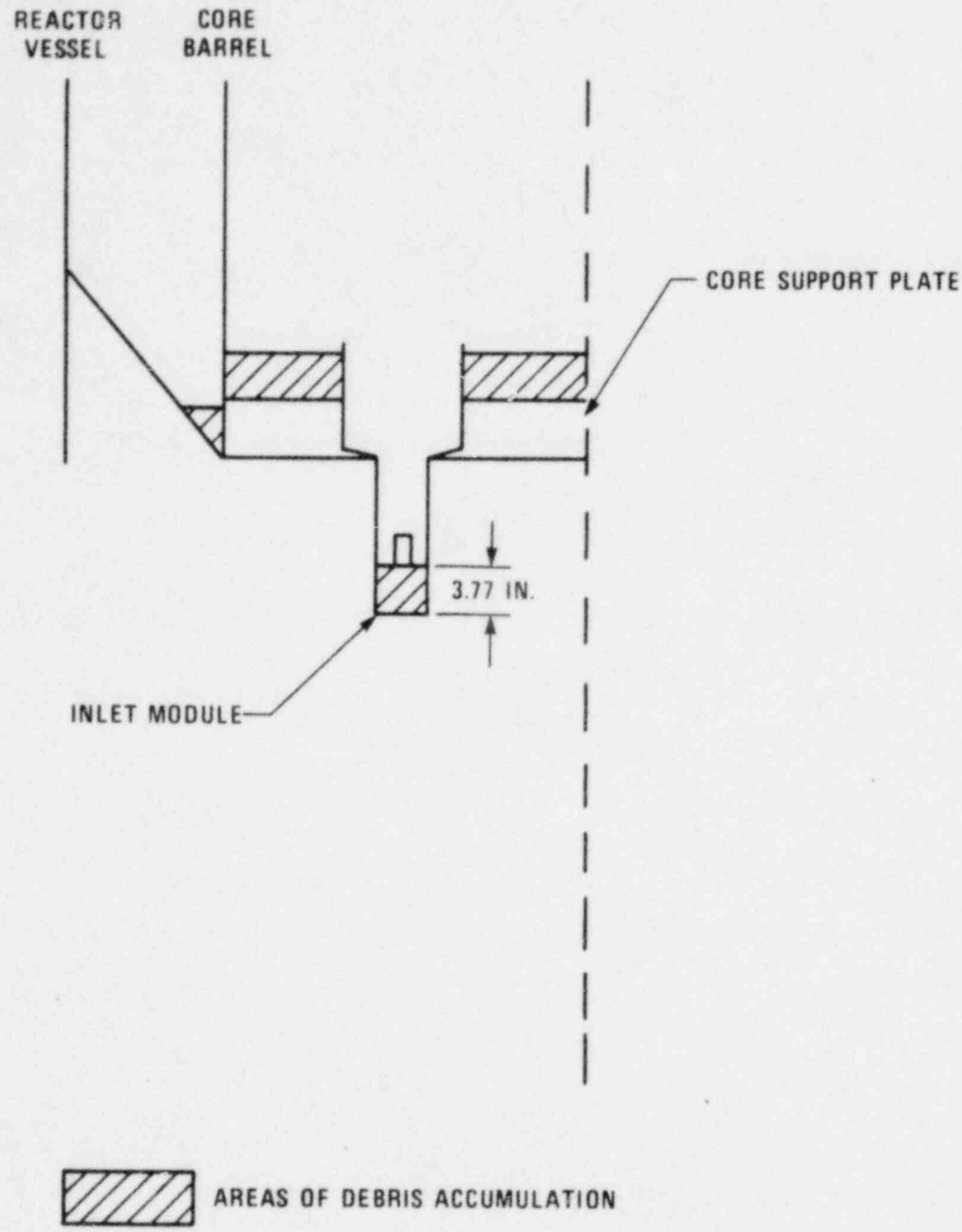

Figure F.6-1. Location of Debris Accumulation in Reactor Vessel after Penetration of Reactor Vessel and Guard Vessel

1966-148

1966-149

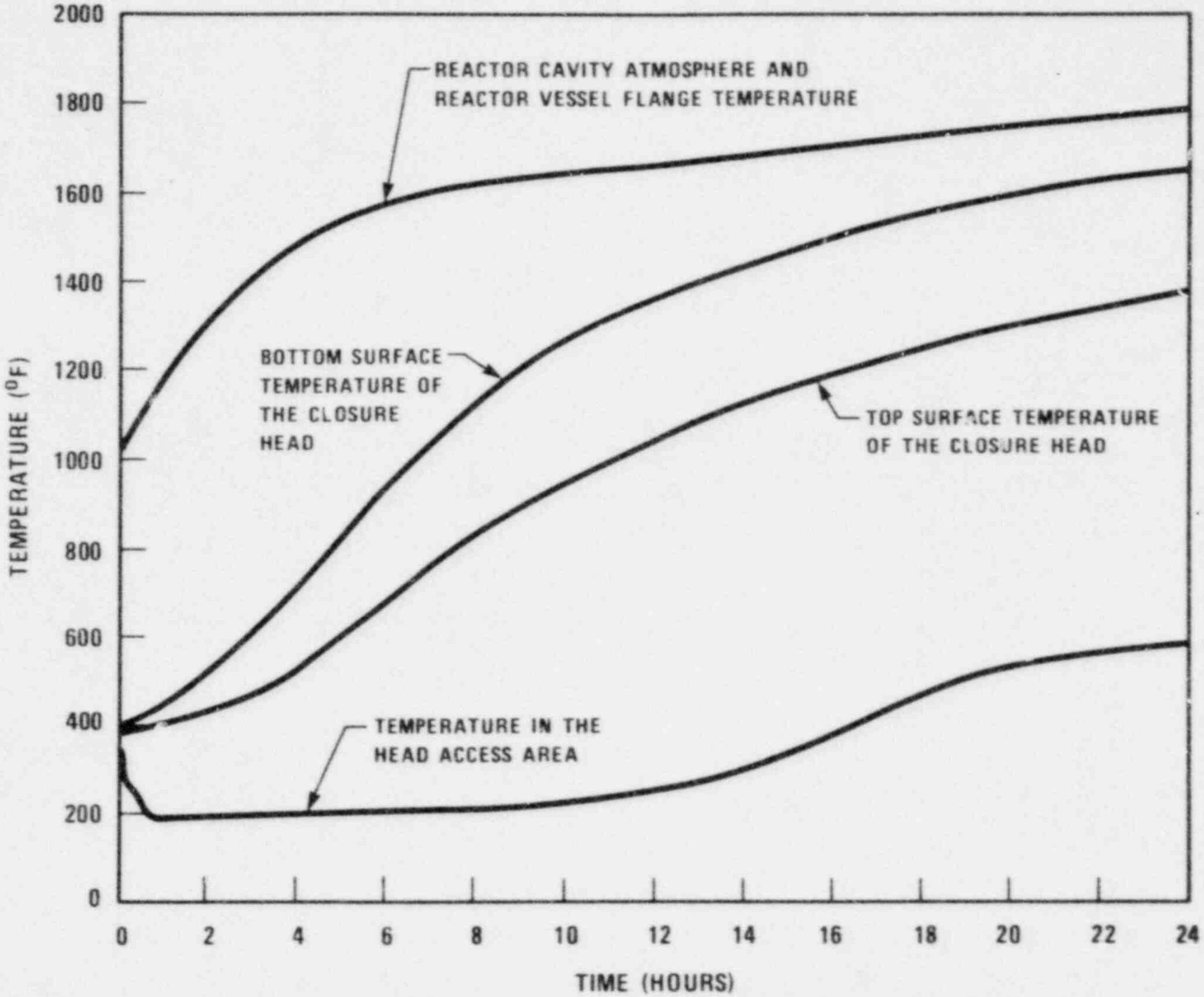

Figure F.6-2. Reactor Head Temperature Distribution

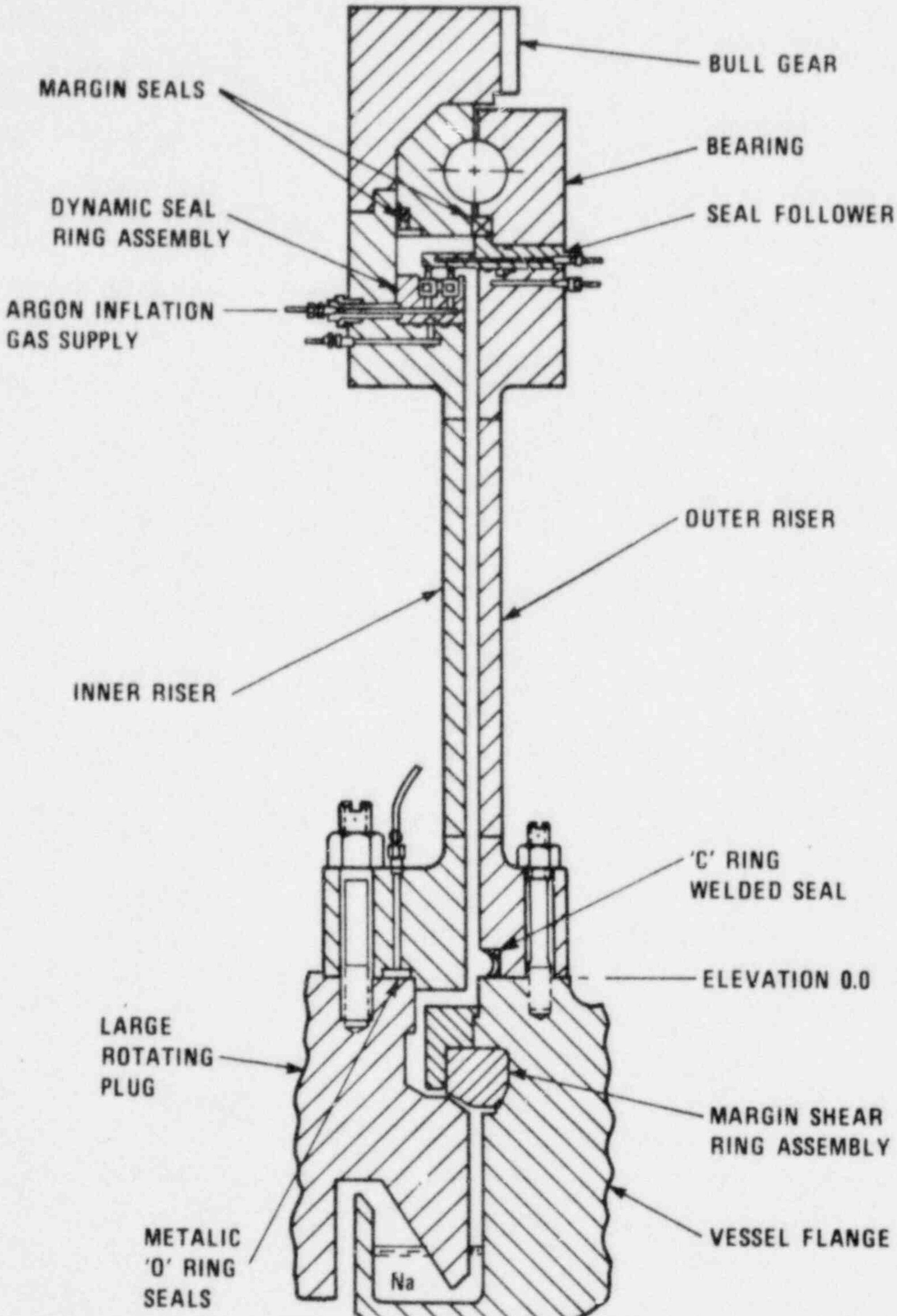

Figure F.6-3. Typical Riser Assembly

1966-150

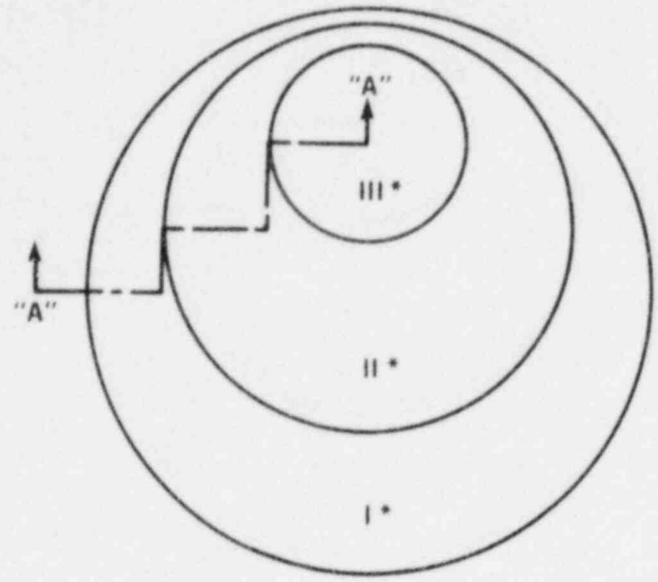

TOP VIEW OF RISERS

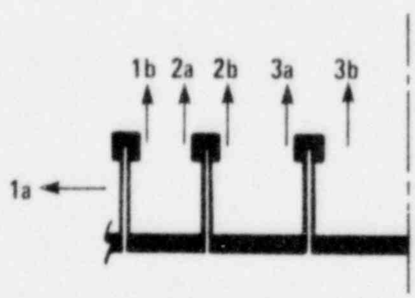

SECTION "A" – "A" SHOWING
FLOW DIRECTION

* RISER DIMENSIONS
DIAMETER

SMALL	71"
INTERMEDIATE	179"
LARGE	261"

APPROXIMATE HEIGHT 36"

Figure F.6-4. Outline Drawing of Risers

1966-151

F.7 SENSITIVITY TO LINER FAILURE TIMES

This section discusses the sensitivity of the base scenario to variations in the assumed times of liner failures in the reactor cavity and pipeway cells. Three specific areas were investigated: the reactor cavity floor, pipeway cell floor and pipeway cell double heated wall. The following provides a brief basis for the evaluations:

1. The floor of the pipeway cell was considered because it is the first liner predicted to fail (except for the reactor cavity floor liner which was assumed to fail at the time of penetration of the reactor vessel and guard vessel). Because of its relatively early failure time and large area, consequences were expected to be more sensitive to failure time than for most other liner sections.

2. The double-heated wall in the pipeway cell was considered because the structural analyses in Section 3.2.2.5.1.3 indicate that the failure time used in the base case may be slightly non-conservative.

The reactor cavity floor liner was assumed to fail at times othr than zero hours (vessel penetration time). Later failure times may result in less severe results relative to the Section 3.2 consequences, however some aspects may be more limiting. Also considered in the evaluation was the parameterization of the concrete floor surface area that would react with sodium.

F.7.1 Pipeway Cell Floor Liner Failure

F.7.1.1 Model

The CACECO analyses described in Section 3.2.2 assume that the pipeway cell floor liner fails at 30 hours and that sodium-concrete interactions occur over the entire floor area. To assess the consequences resulting from either earlier failures or sodium-concrete interactions occurring over just part of the floor area, a parametric study considered liner failures occurring at 0, 10 and 20 hours after penetration of the reactor and guard vessels and assumed either 50 or 100 percent of the floor area experienced sodium-concrete interactions. After liner failure, gases from the concrete from the portion of the floor area that experienced the sodium-concrete interactions was assumed to enter the pipeway cell. This was based on the expectation that the formation of reaction products beneath the liner would greatly restrict the communication of gases between the failure location and remote areas of the floor. If it had been assumed that gases released from the entire floor could enter the cell through the failure, the results for 50% interaction area would approach those for 100% interaction area. The base case in Section 3.2 and all of the cases in this Appendix that assume 100% interaction areas conservatively assume that gases from the entire section of failed liner communicate with the cell. The sodium-concrete, sodium-water, and sodium-carbon dioxide reactions were considered as heat additions to the cell.

All of these sensitivity studies assume containment venting at 36 hours, containment purging starting at 39 hours at a constant rate of 8000 cfm, and additional reactor cavity and pipeway cell liner failures as presented in Table 3-12.

F.7.1.2 Results

With the liner failing at 0 hours, no sodium pool exists in the pipeway cell. The water and carbon dioxide released from the heating pipeway cell floor concrete are directed into the pipeway cell atmosphere. As in all of the cases, a sodium pool does not start to form in the cell until approximately 7 hours following penetration, after which a maximum 2-inch deep pool covering the entire floor is maintained. When a sodium pool is formed at 7 hours due to condensing sodium, the water and carbon dioxide released from the concrete floor are redirected into the sodium pool and the sodium-concrete reactions start and continue until two inches of concrete have reacted. In the 10 and 20 hours liner failure cases, the water and carbon dioxide released from the pipeway cell floor were directed to Cell 105; after liner failure, both were redirected into the sodium pool on the pipeway floor. The reaction products formed by the sodium-water-carbon dioxide reactions and the corresponding energy associated with each reaction are described in Table C.1-4.

Prior to 30 hours, the Section 3.2.2 base case analysis has the floor liner intact; therefore all the water vapor and carbon dioxide released from the concrete are vented to Cell 105 with no sodium-water-carbon dioxide reaction occurring during that time. With the liner failing earlier than 30 hours, the water and carbon dioxide react with the sodium sooner, causing the pipeway cell to heat faster.

Tables F.7-1 to F.7-5 show the containment conditions at 24, 30, 36, and 50 hours and at boildry for both the 50 and 100 percent interaction areas. Prior to venting, the RCB temperatures and pressures are generally somewhat more severe than the base case due to the additional reaction energy following liner failure. No hydrogen was present at 24 hours in any of the cases. Subsequent to venting (and operation of the annulus cooling system) only small differences exist in containment conditions for the various liner failure assumptions. This is evident from Tables F.7-4 and F.7-5. Hydrogen concentration is maintained below 6% in all cases.

Table F.7-6 shows the limiting conditions for each case. The maximum hydrogen concentration generally occurs shortly after venting is initiated. The maximum hydrogen concentration predicted in any case was 5.9%. An additional sensitivity study indicated that this maximum concentration could be reduced to 5% by initiating the venting and purging one hour earlier than in the base case.

F.7.1.3 Conclusions

These sensitivity studies show that containment conditions would be slightly more severe prior to venting if the pipeway floor liner failed before 30 hours. At times greater than the vent time, the containment conditions are insensitive to the pipeway floor liner failure assumptions. The analyses also show that containment conditions would be slightly less severe if sodium-concrete reactions occur over only a fraction of the floor area rather than over the entire floor area. Overall, the studies show that margin exists to accommodate a range of pipeway floor liner failure assumptions without substantially impacting the TMBDB scenario presented in Section 3.2.

TABLE F.7-1

EFFECTS OF PIPEWAY FLOOR LINER FAILURE ON CONTAINMENT CONDITIONS AT 24 HOURS

	Reference Case Section 3.2.2 30 Hour Failure	0 Hour Failure		10 Hour Failure		20 Hour Failure	
Interaction Area	100%	50%	100%	50%	100%	50%	100%
RCB Conditions							
Atmospheric Temperature (^oF)	450	520	570	520	575	510	560
Pressure (psig)	11.1	12.0	12.7	12.0	12.5	12.3	13.4
H_2 Concentration (%)	0.0	0.0	0.0	0.0	0.0	0.0	0.0
O_2 Concentration (%)	13.7	11.8	10.3	12.1	10.5	13.3	12.9
Steel Temperature (^oF)	270	315	340	315	345	300	315

TABLE F.7-2

EFFECTS OF PIPEWAY FLOOR LINER FAILURE ON CONTAINMENT CONDITIONS AT 30 HOURS

	Reference Case Section 3.2.2 30 Hour Failure	0 Hour Failure		10 Hour Failure		20 Hour Failure	
Interaction Area	100%	50%	100%	50%	100%	50%	100%
RCB Conditions							
Atmospheric Temperature (^oF)	520	585	620	570	620	565	590
Pressure (psig)	12.5	13.1	13.3	12.8	13.3	13.2	13.5
H_2 Concentration (%)	0.0	0.0	0.6	0.0	0.6	0.0	0.0
O_2 Concentration (%)	11.7	9.2	7.4	9.5	7.5	10.8	9.9
Steel Temperature (^oF)	315	360	380	355	380	340	355

TABLE F.7-3

EFFECTS OF PIPEWAY FLOOR LINER FAILURE ON CONTAINMENT CONDITIONS AT 36 HOURS

	Reference Case Section 3.2.2 30 Hour Failure	0 Hour Failure		10 Hour Failure		20 Hour Failure	
Interaction Area	100%	50%	100%	50%	100%	50%	100%
RCB Conditions							
Atmospheric Temperature (°F)	620	635	675	635	665	630	630
Pressure (psig)	13.1	13.1	13.9	13.1	13.5	13.3	13.0
H_2 Concentration (%)	0.0	1.0	2.5	0.8	2.6	0.1	1.0
O_2 Concentration (%)	8.4	6.5	4.9	7.0	4.7	7.9	6.8
Steel Temperature (°F)	400	400	420	400	420	395	410

TABLE F.7-4

EFFECTS OF PIPEWAY FLOOR LINER FAILURE ON CONTAINMENT CONDITIONS AT 50 HOURS

	Reference Case Section 3.2.2 30 Hour Failure	0 Hour Failure		10 Hour Failure		20 Hour Failure	
Interaction Area	100%	50%	100%	50%	100%	50%	100%
RCB Conditions							
Atmospheric Temperature (^{o}F)	575	595	595	585	585	580	575
Pressure (psig)	*	*	*	*	*	*	*
H_2 Concentration (%)	4.0	4.0	4.0	4.0	4.0	4.0	4.0
O_2 Concentration (%)	15.4	15.2	15.2	15.4	15.3	15.4	15.5
Steel Temperature (^{o}F)	315	325	325	320	320	315	315

*Near atmospheric during purging.

TABLE F.7-5

EFFECTS OF PIPEWAY FLOOR LINER FAILURE ON CONTAINMENT CONDITIONS AT BOILDRY

	Reference Case Section 3.2.2 30 Hour Failure	0 Hour Failure	10 Hour Failure	20 Hour Failure
Interaction Area	100%	100%	100%	100%
RCB Conditions				
Atmospheric Temperature (^{o}F)	670	660	660	665
Pressure (psig)	*	*	*	*
H_2 Concentration (%)	3.7	3.6	3.8	3.8
O_2 Concentration (%)	15.2	15.5	15.5	15.5
Steel Temperature (^{o}F)	360	360	360	360

*Near atmospheric during purging.

TABLE F.7-6

DEPENDENCE OF PEAK CONTAINMENT CONDITIONS TO SODIUM BOILDRY ON PIPEWAY FLOOR LINER FAILURE ASSUMPTIONS*

	Reference Case Section 3.2.2 30 Hour Failure	0 Hour Failure		10 Hour Failure		20 Hour Failure	
Interaction Area	100%	50%	100%	50%	100%	50%	100%
RCB Conditions							
Atmospheric Temperature (^{o}F)	920 (39)	890 (39)	890 (39)	890 (39)	890 (39)	900 (39)	900 (39)
Pressure (psig)	22.5 (10)	20.0 (8)	15.5 (6)	22.5 (10)	22.5 (10)	22.5 (10)	22.5 (10)
H_2 Concentration (%)	4.5 (10)	4.0 (40)	5.6 (39)	4.5 (10)	5.9 (39)	4.5 (10)	4.6 (39)
Steel Temperature (^{o}F)	440 (39)	435 (39)	450 (39)	430 (39)	450 (39)	430 (39)	440 (39)

*Time (hours) at which the peak conditions is reached is shown in parentheses.

F.7.2 Double Heated Pipeway Wall Liner Failure

F.7.2.1 Model

The pipeway cell double heated wall liner could fail earlier than 90 hours, which was the failure time used in the base case analysis. To evaluate the consequences of this possibility the CACECO code model described in Section 3.2 and Appendix C.1 was modified to simulate the pipeway cell double heated wall liner failure at 45 hours (This value was chosen as a conservative bound to the expected 70 hour time as cited in Section 3.2.2.5.1.3). This modification directed water vapor and carbon dioxide from the double heated concrete wall into the reactor cavity starting at 45 hours. Otherwise, the conditions were identical to the base case in Section 3.2.

F.7.2.2 Results

Figure F.7-1 presents the containment atmosphere and metal temperatures and cavity atmosphere temperature. Figure F.7-2 presents the containment hydrogen concentration. Both figures show that the results are not sensitive to an earlier failure of the double heated pipeway cell liner.

F.7.2.3 Conclusion

The structural analysis in Section 3.2.2.5.1.3 indicates that the liner on the double heated pipeway wall may fail at about 70 hours. Although this is somewhat earlier than the failure time used in the base case (90 hours), this sensitivity study shows that the earlier failure time (70 hours, although 45 hours was used in this analysis) will not have a significant impact on the results.

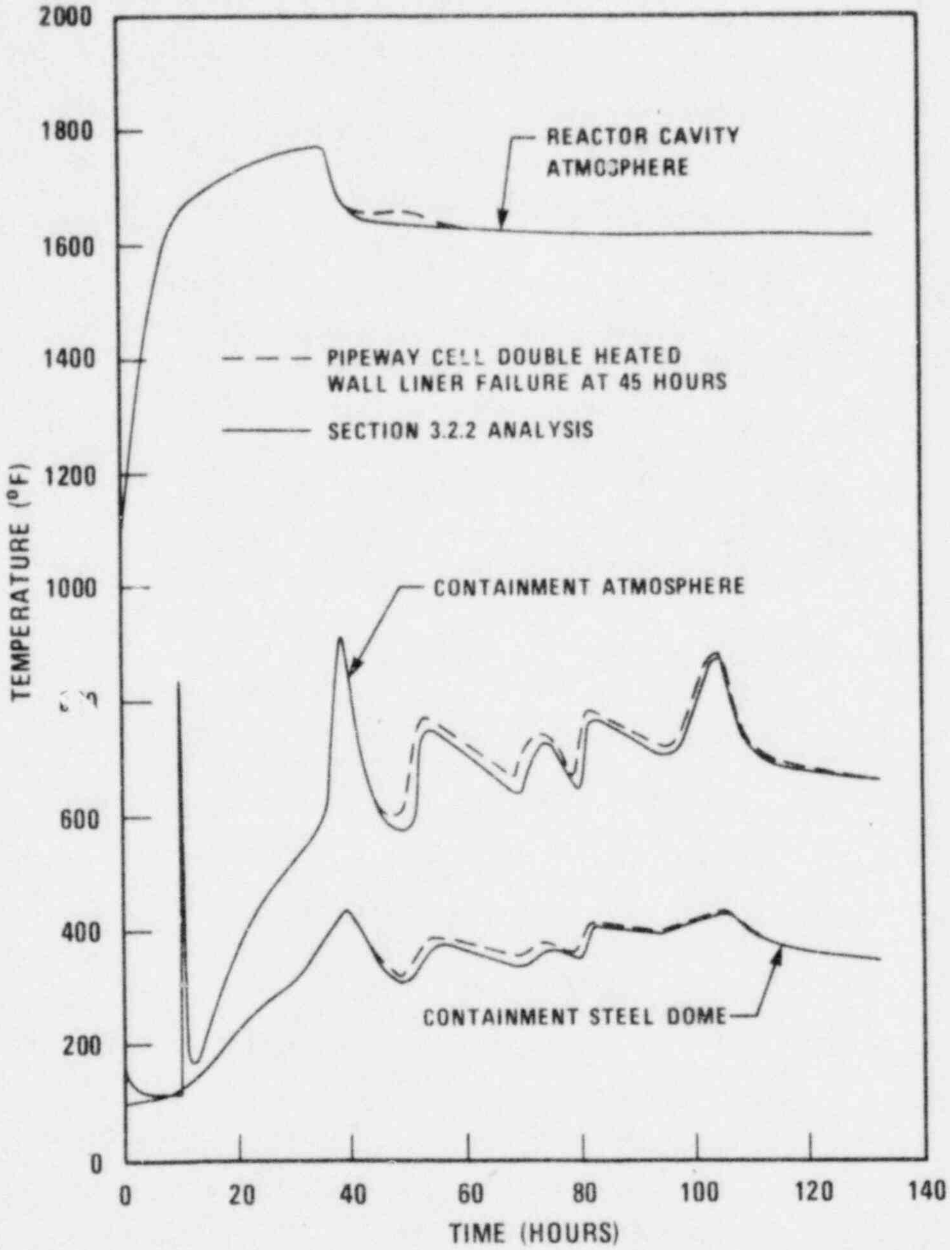

Figure F.7-1 Effect of Reactor Cavity Pipeway Cell Double Heated Wall Liner Failure on Reactor Cavity and Containment Atmosphere and Containment Steel Dome Temperatures

1966-152

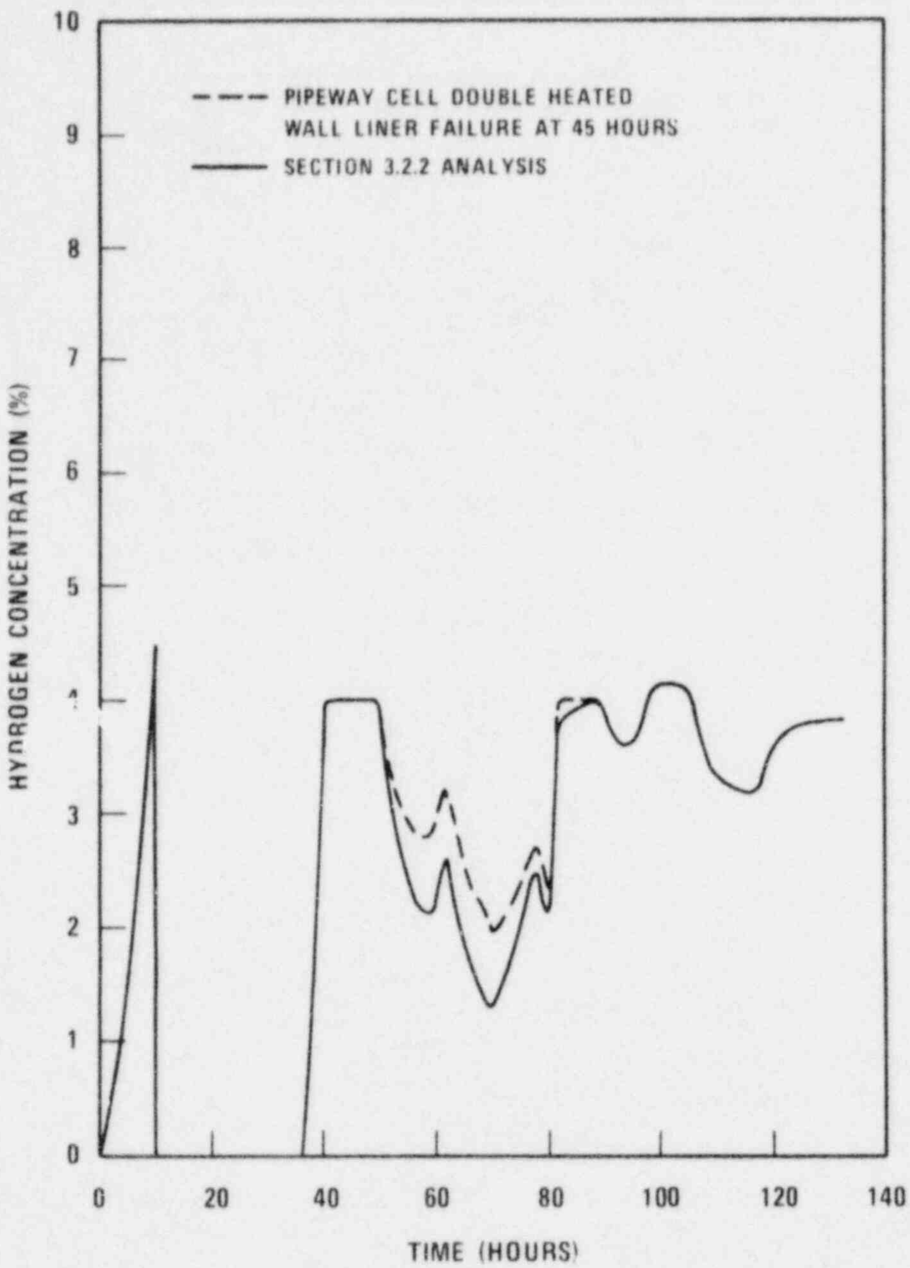

Figure F.7-2 Effect of Reactor Cavity Pipeway Cell Double Heated Wall Liner Failure on Containment Building Hydrogen Concentration

1966-153

F.7.3 Reactor Cavity Floor Liner Failure

F.7.3.1 Model

The CACECO analysis described in Section 3.2 and Appendix C.1 was modified to evaluate different liner failure conditions. Four cases were considered in the analysis. The first two parameterized the actual concrete surface that would react with sodium. A 20 and 30 foot diameter area were considered. The remaining two cases investigated the effect of varying the cavity floor liner failure time. An eight hour failure time and a no floor liner failure case were considered.

F.7.3.2 Results

Table F.7-7 presents containment conditions at 24 hours and at the time when the hydrogen burning conditions are met. The results for the 2 cases which parameterized the concrete surface reaction area were very similar to the Section 3.2 results. Containment conditions at 24 hours were less severe. This was expected since less concrete is assumed to react with the sodium. Containment consequences prior to and after the initiation of hydrogen burning were slightly more severe than the base scenario results. Because of the less energy produced by the sodium-concrete reactions, the time to reach the hydrogen burning criteria is increased and as a result the hydrogen accumulates to a greater value prior to ignition.

Table F.7-7 also presents the results for cases 3 and 4. Containment conditions at 24 hours were less severe than the Section 3.2 results. In the case 3 results the reactor cavity floor liner was assumed to fail at 8 hours. Prior to this period, the sodium-concrete, water and carbon dioxide reactions did not occur resulting in less severe consequences. Containment pressure and temperature were found to be 10.6 psig and 403^{O}F versus Section 3.2 values of 11.1 psig and 450^{O}F. Also consequences prior to and after hydrogen ignition were less severe since hydrogen formation did not occur until the cavity liner failed. As expected the case 4 results exhibited

TABLE F.7-7

SUMMARY OF CONTAINMENT CONDITIONS FOR "LESS SEVERE" LINER FAILURE SENSITIVITY ANALYSES

		At 24 Hours			Near Time of H_2 Ignition		
Case Number	Case Description	Pressure (psig)	Temperature (°F)	H_2 Concentration (%)	Pressure (psig)	Temperature (°F)	H_2 Concentration (%)
Base Case	Section 3.2 Analysis	11.1	450	0.0	22.4 (10 Hours)	845	4.5
1	20 Foot Diameter RC Floor Liner Failure	10.9	446	0.0	22.7 (10.3 Hours)	859	4.6
2	30 Foot Diameter RC Floor Liner Failure	11.0	448	0.0	22.7 (10.3 Hours)	850	4.5
3	RC Floor Liner Failure At 8 Hours	10.6	403	0.0	3.9 (13 Hours)	161	.2
4	No RC Floor Liner Failure	8.6	219	0.0	Not Applicable*		

*Hydrogen not generated in the analysis (assuming normal vent and purge operations).

APPENDIX G
SENSITIVITY STUDIES

Sensitivity studies have been performed to examine the consequences of more energetic sodium-concrete reactions, mal-operation of the reactor cavity-to-containment vent system, initial release of fission products and sodium through the head, variations in aerosol depletion parameters, and variations in debris bed formation and levelling in the reactor cavity. These sensitivity studies are reported in this Appendix.

G.1 SENSITIVITY TO BED LEVELLING CHARACTERISTICS IN THE REACTOR CAVITY

G.1.1 Introduction

In the TMBDB scenario (Section 3.2), it was assumed that after guard vessel penetration the fuel entering the reactor cavity fragmented and spread over the reactor cavity floor and did not melt into the concrete until the sodium boiled away. The fuel particulate formed a debris bed of thickness less than the dryout thickness and even though liner failure may have occurred (as was assumed) the fuel remained in debris form as long as sodium was present. The following sections describe the sensitivity to the bed levelling characteristics in the reactor cavity.

Appendix G.1.A summarizes the evidence that exists to substantiate the assumptions made on particulation and levelling. This evidence is in the following areas:

1. In-vessel particulation and the state of the fuel at time of penetration.

2. Particulation within the reactor cavity postulating molten fuel (even though the fuel should be in particulate form at the time of penetration).

3. Fuel spreading in the reactor cavity for the assumptions of (a) particulate fuel at the time of penetration of the reactor vessel and guard vessel or (b) fuel particulation in the reactor cavity.

4. Debris self-levelling due to boiling sodium agitation.

G.1.2 Summary

The evaluation o: the evidence in Appendix G.1.A relating to fuel fragmentation and debris bed self-levelling indicated the TMBDB assumptions are appropriate for a Class 9 "most probable" analysis. Nevertheless, studies were conducted to define the margins that exist to allow for the possibility of incomplete debris bed levelling. The conclusion from these studies is that a factor of 2 to 4 is available between the dryout depth and the depth corresponding to a uniform distribution over the reactor cavity floor. Recent experimental data using more prototypic experimental techniques indicate the dryout heat flux may be greater than predictions based on the original data and fuel melting does not necessarily occur when the dryout heat flux is reached. Thus, even larger margins than noted above are probable. These margins support the assumption in the TMBDB scenario that the debris bed would remain coolable until boildry of the sodium pool.

These assessments show that the assumption of complete fuel levelling is not necessary to predict acceptable containment conditions at 24 hours. Considerable margin exists to accommodate a range of more adverse assumptions.

G.1.3 Potential for Non-Uniform Debris Beds without Dryout

In this Section it will be demonstrated that the TMBDB scenario is not highly sensitive to the bed levelling assumption. Indeed, configurations that depart substantially from a bed of uniform thickness can be accommodated without difficulty.

Debris beds of fuel in sodium are self-cooling as long as the sodium boiling rate is not sufficient to result in vapor throughout the bed (or dryout). When dryout occurs the debris bed is no longer coolable and the fuel can re-coalesce and melt. The dryout condition is a function of debris bed height, composition, and heat generation rate.

Several experiments, both in-pile and out-of-pile, have been conducted to determine the bed loading at which debris bed dryout will occur. For this study, the correlation presented in Reference G.1-1 was used. This correlation was developed at ANL using data obtained from experiments in which UO_2 particles submerged in Na were volumetrically heated.

Recent experiments at ANL (Reference G.1-2) confirm the conserva ism of dryout depths as calculated on Table G.1-1. In the experiments, Teflon-coated steel particles immersed in water were subjected to three different means of heating, bottom, Joule, and induction, and the dryout heat flux was determined. It was found that for loadings of less than 600 Kg/m^2, induction heating, which better simulates decay heating, produces higher dryout heat fluxes than Joule heating. As the correlations used in the calculation are derived from Joule heating, it is probable that the correlations predict low values of dryout heat flux; hence, the calculated maximum bed depths, which are a function of the dryout heat flux, are low.

Further experimental verification of this correlation is based on three tests which were conducted in the Annular Core Pulsed Reactor (ACPR) at Sandia Laboratories (Reference G.1-3). These tests utilized debris beds composed of fully enriched UO_2 particles ranging in size from 100 to 1000 microns. These debris beds whose loadings ranged from 300 to 900 Kg/m^2 of UO_2 were submerged in subcooled sodium whose bulk temperature was varied from 673^oK to 873^oK.

Bed dryout was obtained in two of the three experiments (at bed loadings of 600 Kg/m^2 and 900 Kg/m^2). APCR power limitations precluded bed dryout during the experiment with a 300 Kg/m^2 bed loading. The data from these experiments together with the dryout correlations developed by personnel at UCLA and ANL are shown in Figure G.1-1. At 900 Kg/m^2, where the two correlations are in relatively good agreement, the dryout heat flux observed in the experiment is consistent with the correlations. However, at 600 Kg/m^2, the observed dryout power level occurs approximately midway between the correlations. As noted earlier, reactor power limitation precluded a dryout condition during the experiment with a bed loading of 300 Kg/m^2. Thus no data are available which would be applicable to the cases shown in Table G.1-1 where the debris is spread over a 40 foot diameter area or the cases where the core and some portion of the axial blankets are spread over a 20 foot diameter area. However, the reasonably good agreement at 600 and 900

Kg/m^2 loadings indicates that the ANL correlation is valid for this study if, as noted in Reference G.1-1, a maximum heat flux of 95 w/cm^2 is imposed in the calculations.

Furthermore, the SANDIA experiments have indicated that bed dryout may be a conservative criterion for the limiting bed depth. During the experiments, dryout was achieved; however, test instrumentation revealed that the temperature in the dryout region did not exceed 1265°K, a value well below the melting points of both fuel and steel. Thus it appears that bed dryout could occur without causing melting of either the fuel in the bed or the cell liner with which it is in contact. This suggests another level of conservatism when the dryout heat flux is used as the limiting heat flux.

Using the data in Reference G.1-1 together with the nominal decay heat at 1000 seconds the height of a debris bed that would cause dryout was computed for CRBRP and is shown in Table G.1-1. The table gives the dryout height as a function of core fuel and blanket material in the debris bed. Also shown in the table are the corresponding depths of the debris bed assuming uniform spreading over the entire reactor cavity (the expected case) or over only the restricted area within the guard vessel support (the 'worst' case). From the table, it is evident that, with uniform levelling over the entire reactor cavity, the dryout depth ranges from 2 to 4 times the actual depth of the debris bed. It is expected that the debris bed would only contain core fuel plus the lower blanket at early times when the decay heat is high.* Thus a large margin (3-4 inches) is available to allow for incomplete levelling over the entire 40' diameter of the reactor cavity. If no spreading beyond the guard vessel skirt is assumed, i.e., with uniform spreading over only the area within the 20' diameter guard vessel skirt, the dryout thickness is only

*For the heterogeneous core, additional blanket material is contained in the internal blankets. Although the power generation rate would be higher in these internal blanket assemblies than in other blankets, the power generation rate is low compared to the core fuel and meltdown of those assemblies would be expected to be on a longer timescale than the core fuel assemblies. Therefore, the information discussed herein is a reasonable approximation for the heterogeneous core.

marginally exceeded (6.1 inches vs. 5.3 inches) if the entire lower blanket is included in the debris bed. Again, it would be expected that very little of the upper and radial blankets would be in the reactor cavity debris (at early times when the decay heat is the highest).

Several debris bed configurations that would not cause dryout are shown on Figures G.1-2, 3 and 4. From these figures, it is evident that many configurations exist in which bed dryout would not occur. Further, even a modest degree of spreading beyond the guard vessel support skirt would be sufficient to prevent dryout. It is not necessary for spreading over the entire cavity floor to occur.

In conclusion, the debris bed on the reactor cavity floor should not dryout and cause fuel melting prior to sodium boildry because:

1. The debris bed would be distributed over the reactor cavity floor in a nearly uniform manner (Appendix G.1.A).

2. Self-levelling of the boiling debris bed would further level the bed (Appendix G.1.A).

3. A margin of a factor of 2 to 4 is available between the dryout depth and the depth corresponding to a uniform distribution over the entire reactor cavity. More recent experimental data using more prototypic experimental techniques indicate the dryout flux may be considerably greater than predicted by correlations based on the original data. Thus, the probable margins are even greater than indicated above.

4. Recent in-pile experiments demonstrate that the dryout heat flux condition does not necessarily lead to melting of the bed material.

G.1.4 References

G.1-1 L. Baker, Jr., et al., "Postaccident Heat Removal in Fast Reactors," ANL/F 3 75-44, November 1975. (Availability: U.S. DOE Technical Information Center)

G.1-2 L. Baker, Jr., et al., "Postaccident Heat Removal Technology," ANL/RAS 77-2, January 1977. (Availability: U.S. DOE Technical Information Center)

G.1-3 J. B. Rivard, "Postaccident Heat Removal: Debris-Bed Experiments D-2 and D-3," NUREG/CR-0421, November, 1978.

TABLE G.1-1

ASSESSMENT OF POTENTIAL FOR BED DRYOUT
IN THE REACTOR CAVITY

Fuel and Blanket*	Debris Bed** Height For Dryout (in.)	Debris Bed Height When Uniformly Spread Over The Reactor Cavity Floor (in.)	Debris Bed Height When Uniformly Spread Over The Area Within The Guard Vessel Support (in.)
Core	5.0	1.2	4.7
Core Plus Lower Blanket	5.3	1.5	6.1
Core Plus Upper and Lower Blankets	5.6	1.9	7.7
Core Plus All the Blankets	6.3	3.4	13.7

*Includes steel cladding, wire wrap, ducts, and part of the reactor vessel and guard vessel lower heads.

**Calculations were for homogeneous core design (has slightly higher decay heat than heterogeneous core).

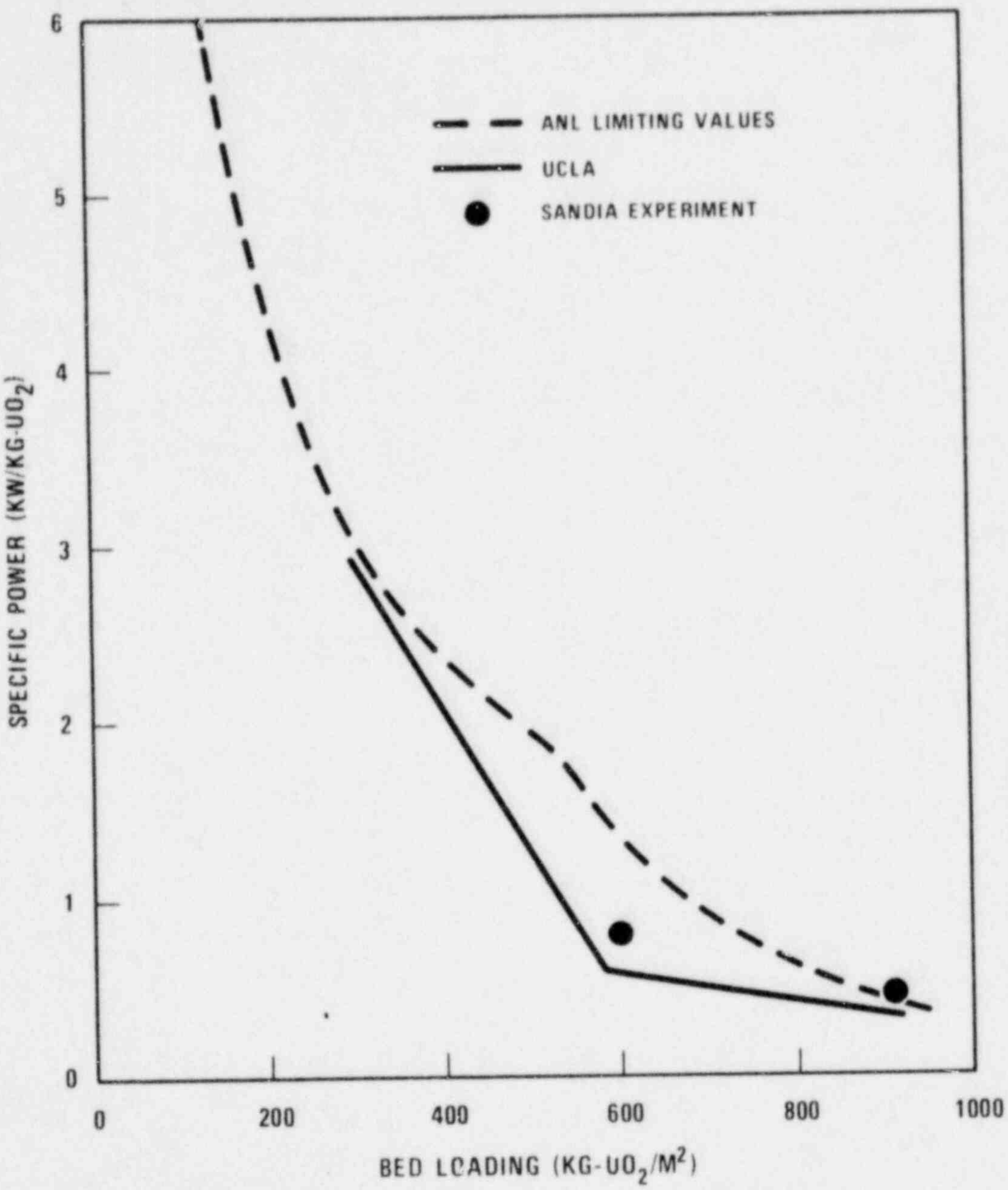

Figure G.1-1. Dryout Predictions and Results for the Initial D-Series Experiments at Sandia

1066-154

1966-155

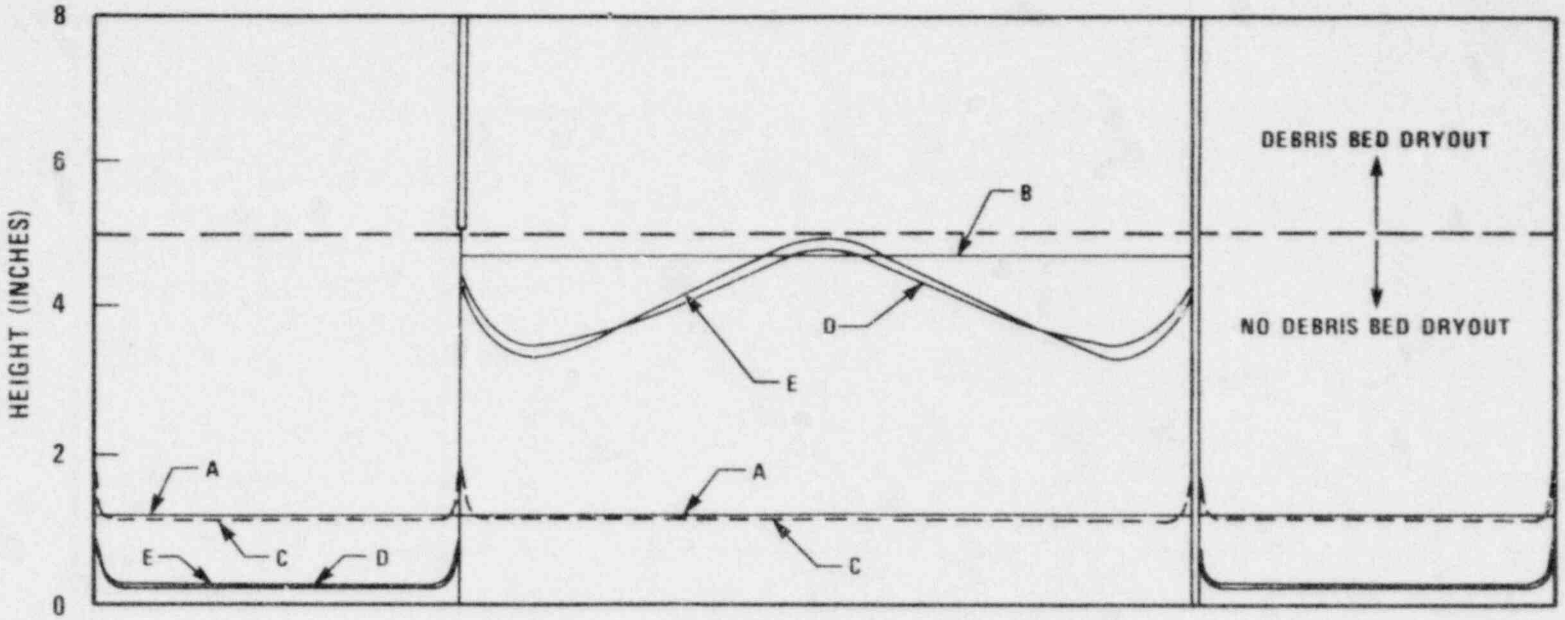

A UNIFORM SPREADING (40' DIA)
B UNIFORM SPREADING (20' DIA)
C UNIFORM SPREADING (40' DIA) EXCEPT AT VERTICAL SURFACES
D NON-UNIFORM SPREADING
E EXTREME NON-UNIFORM SPREADING

*INCLUDES STEEL CLADDING, WIRE WRAP, DUCTS AND PART OF THE REACTOR VESSEL AND GUARD VESSEL LOWER HEADS.

Figure G.1-2. Debris Bed Configurations That Would Not Result in Dryout Core Fuel*

1966-156

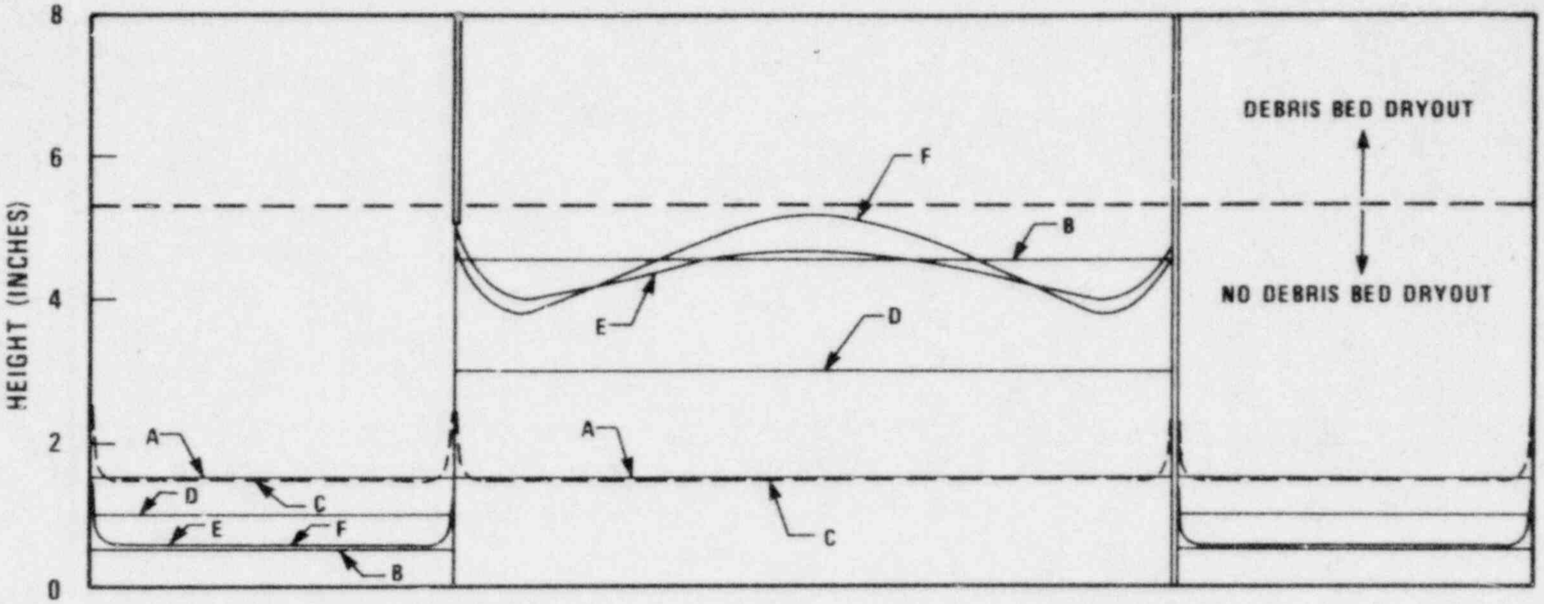

A UNIFORM SPREADING (40' DIA)
B UNIFORM SPREADING WITH 75% OF THE FUEL WITHIN THE GUARD VESSEL SUPPORT
C UNIFORM SPREADING (40' DIA) EXCEPT AT VERTICAL SURFACES
D UNIFORM SPREADING WITH 50% OF THE FUEL WITHIN THE GUARD VESSEL SUPPORT
E NON-UNIFORM SPREADING
F EXTREME NON-UNIFORM SPREADING

*INCLUDES STEEL CLADDING, WIRE WRAP, DUCTS AND PART OF THE REACTOR VESSEL AND GUARD VESSEL LOWER HEADS.

Figure G.1-3. Debris Bed Configurations That Would Not Result in Dryout Core Fuel Plus Lower Blanket*

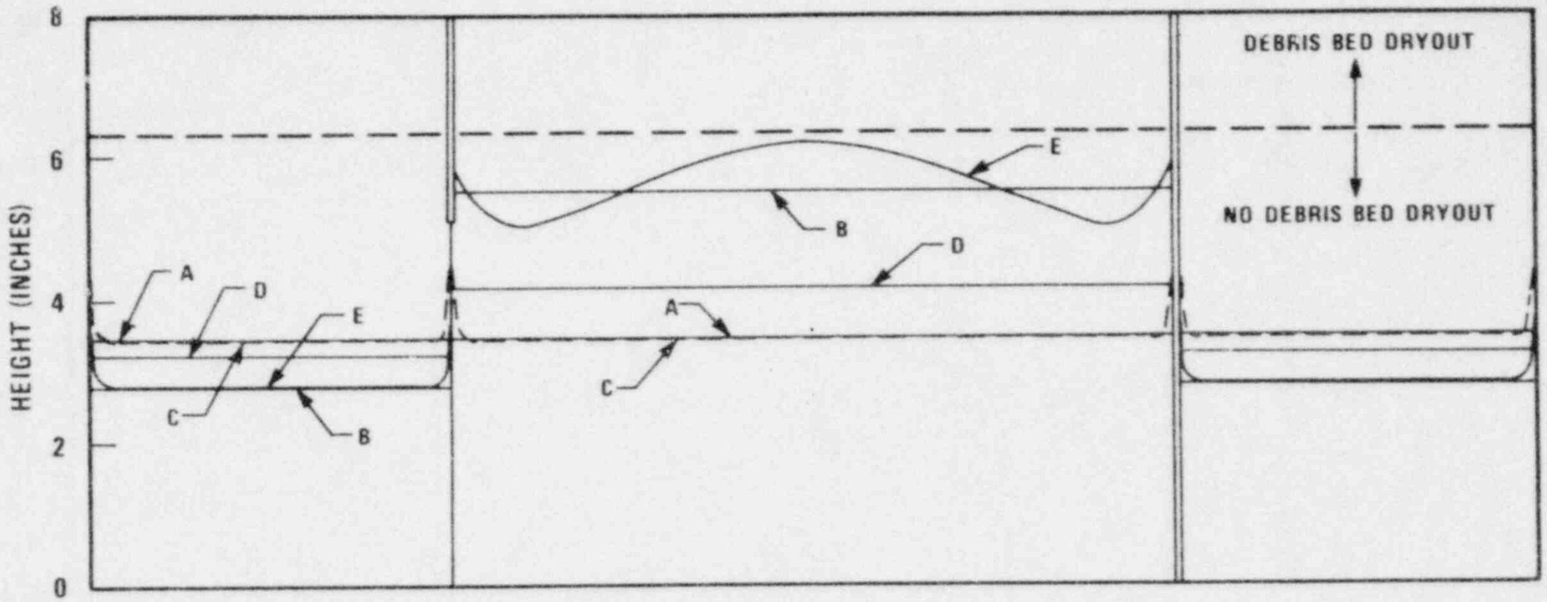

A UNIFORM SPREADING (40' DIA)
B UNIFORM SPREADING WITH 40% OF THE FUEL WITHIN THE GUARD VESSEL SUPPORT
C UNIFORM SPREADING (40' DIA) EXCEPT AT VERTICAL SURFACES
D UNIFORM SPREADING WITH 30% OF THE FUEL WITHIN THE GUARD VESSEL SUPPORT
E NON-UNIFORM SPREADING

* INCLUDES STEEL CLADDING, WIRE WRAP, DUCTS AND PART OF THE REACTOR VESSEL AND GUARD VESSEL LOWER HEADS.

Figure G.1-4. Debris Bed Configurations That Would Not Result in Dryout Core Fuel Plus All the Blankets*

G.1.A Support for TMBDB Assumptions on Debris Bed Particulation and Levelling

G.1.A.1 In-Vessel and Vessel Penetration Processes

G.1.A.1.1 In-Vessel Particulation

A considerable body of experimental data has accumulated that indicate fuel will particulate or fragment within the sodium in the reactor vessel immediately after an HCDA. These data are reported in Section 3.1 and are summarized below.

Two series of large scale out-of-reactor experiments provide data on above surface (M-series) and below surface (EDT-series) injection of molten fuel into liquid sodium. The M-series tests consisted of dropping kilogram quantities of 5500°F to 5800°F molten UO_2 into a pool of sodium. These tests indicated fine fragmentation of the fuel. In the EDT (Energy Dissipation Tests), molten UO_2 was injected below the surface of a sodium pool at temperatures of 900°F and 1335°F. These tests also indicated fine fragmentation of the fuel will occur. TREAT in-reactor experiments also indicated fuel fragmentation.

The above experiments were used by the FFTF project in Appendix A.5 of the FSAR to show fragmentation as part of their in-vessel fuel retention scenario. The conclusions with respect to fragmentation for CRBRP are identical. There is a preponderance of experimental data that demonstrates particulation or fragmentation will occur in the reactor vessel sodium immediately after an HCDA.

Fuel-Sodium Particulation Experiments

The major experiments supporting particulation in the UO_2 - sodium system (M-series, EDT-series, and TREAT series) will be described in detail followed by a literature review of other supporting fuel-sodium experiments.

ANL M-Series Experiments

Three large-scale, molten UO_2 contacting experiments were performed (Reference G.1.A-1). To simplify the problem of producing large quantities of molten UO_2, a method involving a "thermite-type" chemical reaction was developed. The reaction occurs between uranium metal powder and MoO_3 powder, yielding a mixture of molten UO_2 containing about 17 w/o molybdenum. Although molybdenum is not normally used as a structural material in sodium-cooled fast reactors, it is somewhat similar to stainless steel which is likely to be mixed with molten fuel immediately following an HCDA. Thus, the presence of a molten metallic constituent was not considered to be an undesirable feature of the experiment. It was found that the addition of a small amount of CrO_3 in the mixture helped accelerate the reaction.

The apparatus consisted of an 18-inch-diameter interaction vessel, Figure G.1.A-1, which held the 8-inch-diameter sodium-filled crucible. A reaction chamber bolted to the cover plate held the uranium-MoO_3-CrO_3 reactant mixture. The interaction vessel was designed to release gas through the spring-loaded vessel cover at pressures of approximately 100 psig, and through a 200-psi rupture disk. The apparatus was located in a decontaminated hot cell that was capable of containing any credible release from the interaction vessel.

The most important result to postaccident heat removal of the large-scale experiments was the demonstration of particulate debris formation. In two of the large-scale experiments, all of the UO_2 was converted to particulate. In one experiment, about 90% of the UO_2 was converted to particulate; the remaining 10% remained as large porous pieces after all of the residual UO_2-sodium mixture was treated with alcohol to remove the sodium. The tendency to form particulate is demonstrated by the fact that most of the UO_2 was converted to particulate even though the initial sodium depth was only about four inches. This is shown in the following tabulation:

Exp.	Quantity Fuel, lb	Na, lb	Na Temp. ^{o}F	UO_2 Loading $g\text{-}UO_2/cm^2$-crucible	Fraction Particulate
M1	1.4	6.6	550	2.0	1.0
M3	3.0	6.5	1160	4.2	1.0
M2	6.8	7.1	570	9.5	0.9

These results show that the particulation of all the fuel will occur for even large concentrations (up to equal weight with the sodium) of fuel in sodium, even for pools as shallow as four inches depth. Thus, in reactor situations where the molten fuel must move through many feet of sodium and the sodium mass is much greater than the fuel mass, the molten fuel will be completely converted to particulate.

The particle size distributions obtained from in-pile tests in TREAT and from previous small-scale tests are indicated on Figure G.1.A-2. The results indicate that distributions were obtained with mean particle sizes ranging from about 100 to 200 μm in diameter. The range of particle size distributions from the finest E2 to the coarsest S3 are indicated as dotted lines in Figure G.1.A-2 where the results from the three large-scale out-of-pile tests are plotted. The results show that the out-of-pile tests resulted in debris in the same general range as the in-pile tests, although some of the debris was slightly finer than obtained previously.

ANL EDT Experiments

Two out-of-pile tests, called Energy Dissipation Tests, were performed which involved the high pressure injection of thermite-generated molten UO_2 underneath the sodium surface contained in nominal 20" diameter tanks (Reference G.1.A-2). Test EDT-1 resulted in the finest particle size distribution of any fuel-sodium test to date. The distribution could be approximated in terms of the 100-1000 μm distribution plus 65 wt % of particulate less than 100 μm.

TREAT In-Pile Experiments

A number of experiments have been performed in TREAT using oxide fuel and sodium coolant (References G.1.A-3 and 4). These tests employed from one to seven fuel pins at various lengths and used both static and flowing sodium. The fuel that was displaced into the coolant particulated. The dashed lines in Figure G.1.A-2 indicate the distribution of the fragment sizes obtained.

Other Sodium-Fuel Experiments

Clerici, et al., (Reference G.1.A-5) present particle size data from their experiments at the ISPRA facility. The quantities of molten UO_2 ranged between 2 and 4 kg and the sodium temperature ranged between 350°C and 700°C.

Mizuta (Reference G.1.A-6) also noted fragmentation of small samples of UO_2 when dropped into sodium at temperatures between 200°C and 300°C.

Amblard (Reference G.1.A-7) gives data that shows particulation when a hundred liter column of sodium at 443°C was dropped onto 4.2 kg of UO_2, 80% of which was molten.

G.1.A.1.2 Fuel State During Vessel Penetration

The fuel would remain in particulate form while penetrating the reactor and guard vessels since the sequence of physical processes would be:

a. Immediately after an HCDA, fuel would be fragmented by the sodium and then settle on the reactor vessel lower head.

b. Due to the probable thickness of the debris bed and because of the heat generation rate debris bed dryout would occur within the reactor vessel.

c. Upon dryout, the bed would rapidly increase in temperature.

d. When the melting point of steel is reached in the bed, the steel within the bed would melt and provide an excellent medium for transporting heat to the vessel.

e. With molten steel at ~2500°F in contact with the vessel, it would fail before the debris bed temperature increased to the melting point of fuel (~5000°F).

The conclusion is that, at the time of vessel penetration, the fuel would be in particulate form and a combination of molten steel, fuel particulate, and sodium would enter the reactor cavity. The temperature in this mixture would be near the melting point of steel (~2500°F) and well below the melting point of fuel (~5000°F).

G.1.A.2 Fuel Particulation in the Reactor Cavity

As described in the previous section, fuel would be expected to be in particulate form when it enters the reactor cavity. However, the possibility of some molten fuel entering the reactor cavity followed by sodium will also be examined.

Pertinent experiments involving 3 to 5 kg of fuel have been performed at ANL, ISPRA, and CEA/Grenoble, see References G.1.A-3, 5, 7, 8 and 9. Some of these tests simulated the condition in which molten fuel is released first and is followed by sodium. Fragmentation of the fuel in sodium was observed in all pertinent tests.

The above experiments are on a small scale; however, fragmentation and particulation would be expected in larger scale as well since:

a. The experiments at ANL have indicated that with much larger amounts of sodium than fuel, which is the case for CRBRP, complete fragmentation would occur.

b. Fragmentation occurs at the interface of fuel and sodium because of the high temperature gradients, low thermal conductivity, and low tensile strength of the oxide fuel. After particulation at the fuel-sodium interface, the fluid turbulence would sweep the particles away, constantly exposing new fuel to the sodium. The low thermal conductivity of the fuel prevents reduction of the temperature gradients and thermal stresses until particulation is completed.

c. The very low thermal conductivity of the fuel oxide would limit the rate of reactor cavity liner heatup prior to particulation, even with larger quantities of fuel.

The conclusion is that fuel particulation or fragmentation should occur if some molten fuel is present in the reactor cavity, even though large scale experiments have not been performed to confirm this assessment.

G.1.A.3 Fuel Spreading Within the Reactor Cavity

The potential for fuel spreading within the reactor cavity will be described for the expected case in which fuel is in particulate form when entering the reactor cavity and for the postulated case of molten fuel entering the reactor cavity followed by early particulation. Fuel spreading due to debris bed self-levelling is described in Section G.1.A.4.

G.1.A.3.1 Fuel Spreading with Particulate Fuel at Time of Vessel Penetration

The fuel particulate entering the reactor cavity would be mixed with the sodium after impacting the reactor cavity floor due to the high turbulence that would result from the discharge of materials from the guard vessel.

Since much of the fuel debris would be very small, it would remain in suspension within the sodium for some period of time. Scoping calculations indicate the settling time for 75% of the fuel mass would be greater than 100 seconds. The time required for sodium to flow under the guard vessel support skirt and equalize heights in the reactor cavity was calculated to be less than 100 seconds, based on the area provided under the guard vessel skirt. The required velocity for particles to remain in suspension when contained in sodium flowing under the guard vessel support was calculated to be 4 ft/sec for an average size particle. This compares to an average velocity of sodium flowing under the support of 23 ft/sec.

Thus sufficient fluid energy is available to sweep the debris under the guard vessel support and into the entire reactor cavity; and the time required for the particles to settle onto the reactor cavity floor is larger than the time required for the sodium to flow under the support skirt. Therefore, the fuel would be expected to settle from the well-mixed sodium pool onto the reactor cavity floor in an approximately uniform distribution.

G.1.A.3.2 Fuel Spreading with Fuel Particulation in the Reactor Cavity

In the postulated case of molten fuel entering the reactor cavity and then particulating, the spreading of fuel would be similar to the more probable case of fuel entering the reactor cavity as particulate. This is because the impact of the fuel and sodium on the reactor cavity floor and the subsequent particulation would result in sufficient turbulence to suspend the fuel debris within the sodium pool. After suspension, the sodium would carry the fuel under the guard vessel skirt before the suspended fuel settles onto the floor, just as described in Section G.1.A.3.1.

G.1.A.4 Debris Bed Self-Levelling

Fuel debris beds in sodium self-level due to the agitation of the boiling liquid if the heat flux is sufficiently high to result in local boiling. Several experiments performed to verify this process are documented in the literature. The largest scale experiments were performed with 1-3 kg of fuel at ANL (Reference G.1.A-3). The degree of self-levelling was found to be dependent on the initial configuration of the debris bed. When the bed was initially peaked in the center, essentially complete levelling occurred. However, when the bed was initially peaked at the edge of the container, a residual difference in height of less than 1 inch was observed between the high and low locations for heat fluxes representative of CRBRP conditions. When related to CRBRP conditions, the non-levelling effect would occur principally near the vertical surfaces. In Section G.1.3 it was shown that a substantial margin exists to permit non-level beds without a significant impact on the TMBDB scenario.

The relatively small size of the experiments compared to the reactor cavity does not limit the usefulness of the results because the basic scaling consideration for self-levelling is that the bed area be large enough so that edge effects do not have a substantial impact on the results. This condition is satisfied when the number of vapor channels in the bed is much greater than one. A vapor channel is normally associated with each 4 to 5 cm^2 of bed surface area. The experimental configurations resulted in approximately 10 to 15 vapor channels. Thus, the requirement of being much greater than one is satisfied and the data can be applied to larger configurations including CRBRP.

G.1.A.5 References

G.1.A-1 T. R. Johnson, et al., "Post Accident Heat Removal: Large Scale Molten Fuel-Sodium Interaction Experiments," ANL/RAS 74-1, February 1974. (Availability: U.S. DOE Technical Information Center)

G.1.A-2 R. E. Henry, "Large Scale Vapor Explosions," In Proceedings of the Fast Reactor Safety Meeting," CONF-740401-P2, April 1974 pp. 922-934.

G.1.A-3 L. Baker, Jr., et al., "Postaccident Heat Removal Technology," ANL/RAS 74-12, July 1974. (Availability: U.S. DOE Technical Information Center)

G.1.A-4 J. J. Barghusen, et al., "Fuel-Coolant Interaction Effects During Transient Meltdown of LMFBR Oxide Fuel in a Sodium-Filled Piston Autoclave: TREAT Tests S2 to S8," ANL/RAS 74-13, June 1974. (Availability: U.S. DOE Technical Information Center)

G.1.A-5 G. Clerici, et al., "Interactions with Small and Large Sodium to UO_2 Mass Ratios," pp. 507-543, in Proceedings of the Third Specialist Meeting on Sodium/Fuel Interaction in Fast Reactors, March 1976, Tokyo, Japan, OECD Nuclear Energy Agency, Paris, France, 1976.

G.1.A-6 H. Mizuta, "Fragmentation of Uranium Dioxide after Molten Uranium Dioxide-Sodium Interaction," J. Nucl. Sci. Tech. 11, pp. 480-487 (1974).

G.1.A-7 M. Amblard, "Preliminary Results on a Contact Between 4 kg of Molten UO_2 and Liquid Sodium," pp. 545-560, in Proceedings of the Third Specialist Meeting on Sodium/Fuel Interactions in Fast Reactors, March 1976, Tokyo, Japan, OECD Nuclear Energy Agency, Paris, France, 1976.

G.1.A-8 M. Amblard, et al., "Out-of-Pile Studies in France on Sodium Fuel Interaction," "Proceedings of the Fast Reactor Safety Meeting," CONF-740401-P2, April 1974, pp. 910-921.

G.1.A-9 E. S. Sowa, et al., "Post-Accident Heat Removal: M-Series Molten Core Debri-Sodium Interaction Experiment," ANL/RAS 78-54, December 1978. (Availability: U.S. DOE Technical Information Center)

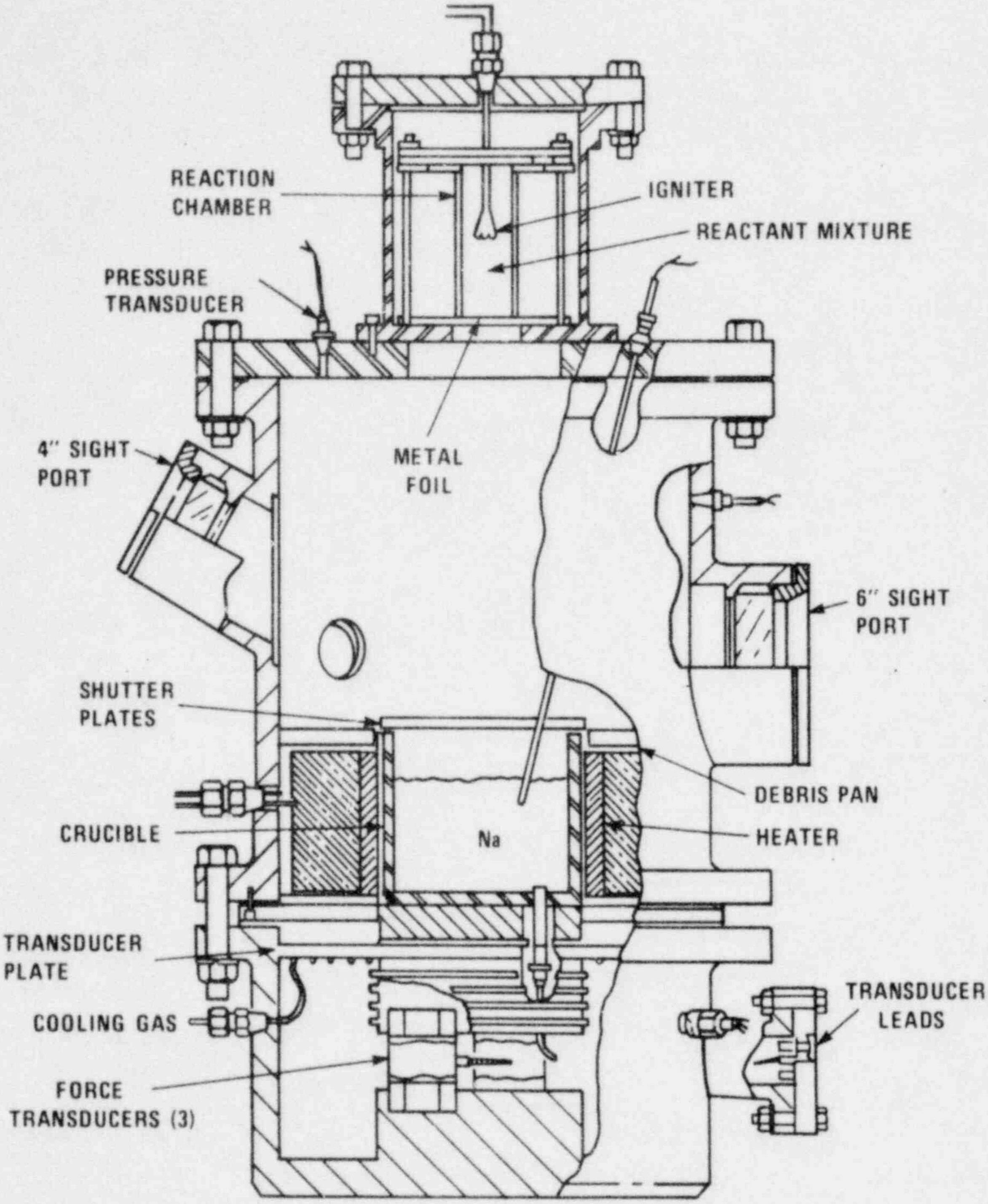

Figure G.1.A-1. Sodium Interaction Vessel Assembly

1966-158

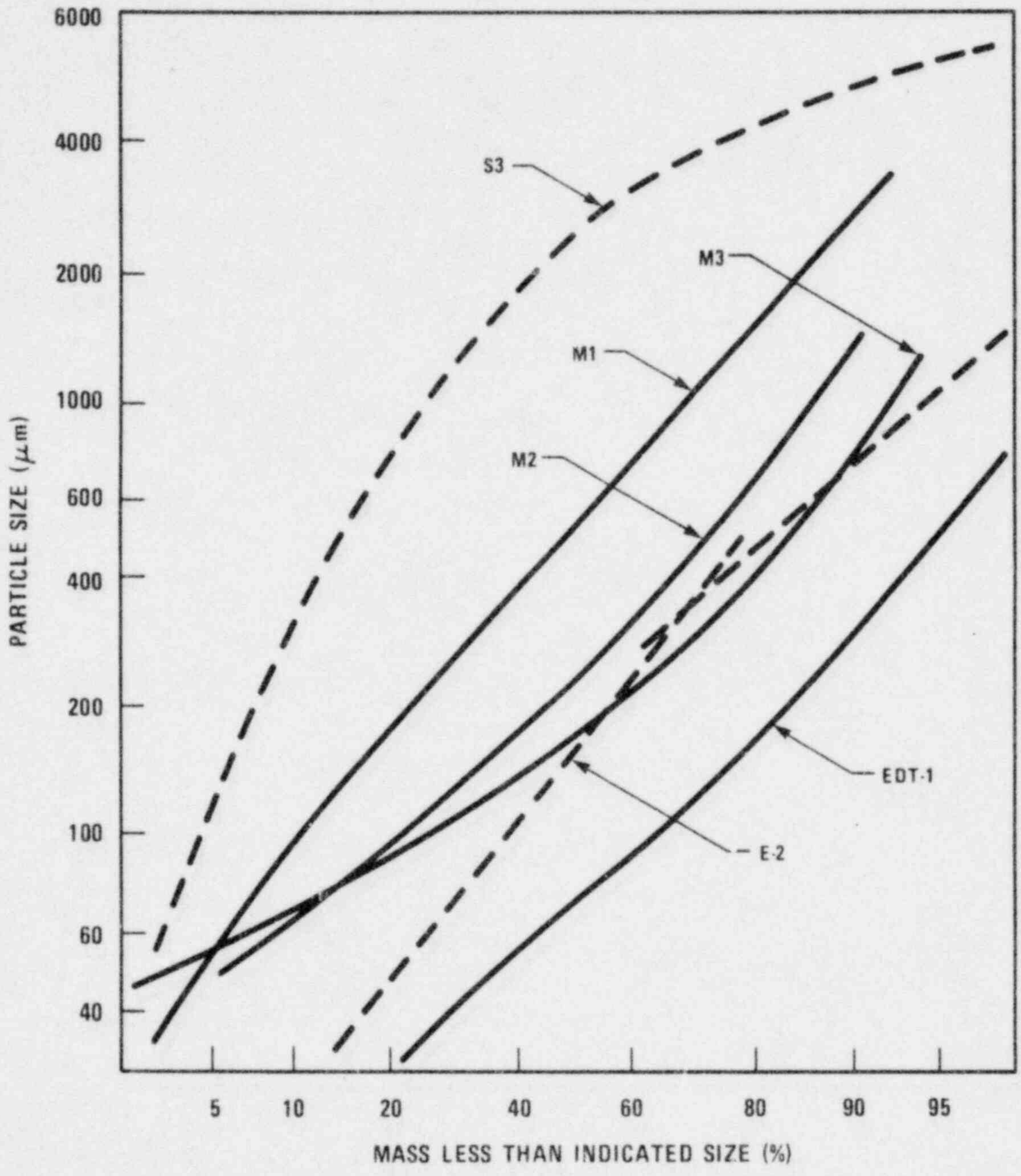

Figure G.1.A-2. Particle Size Distributions from Large-Scale Out-of-Pile Tests

1966-159

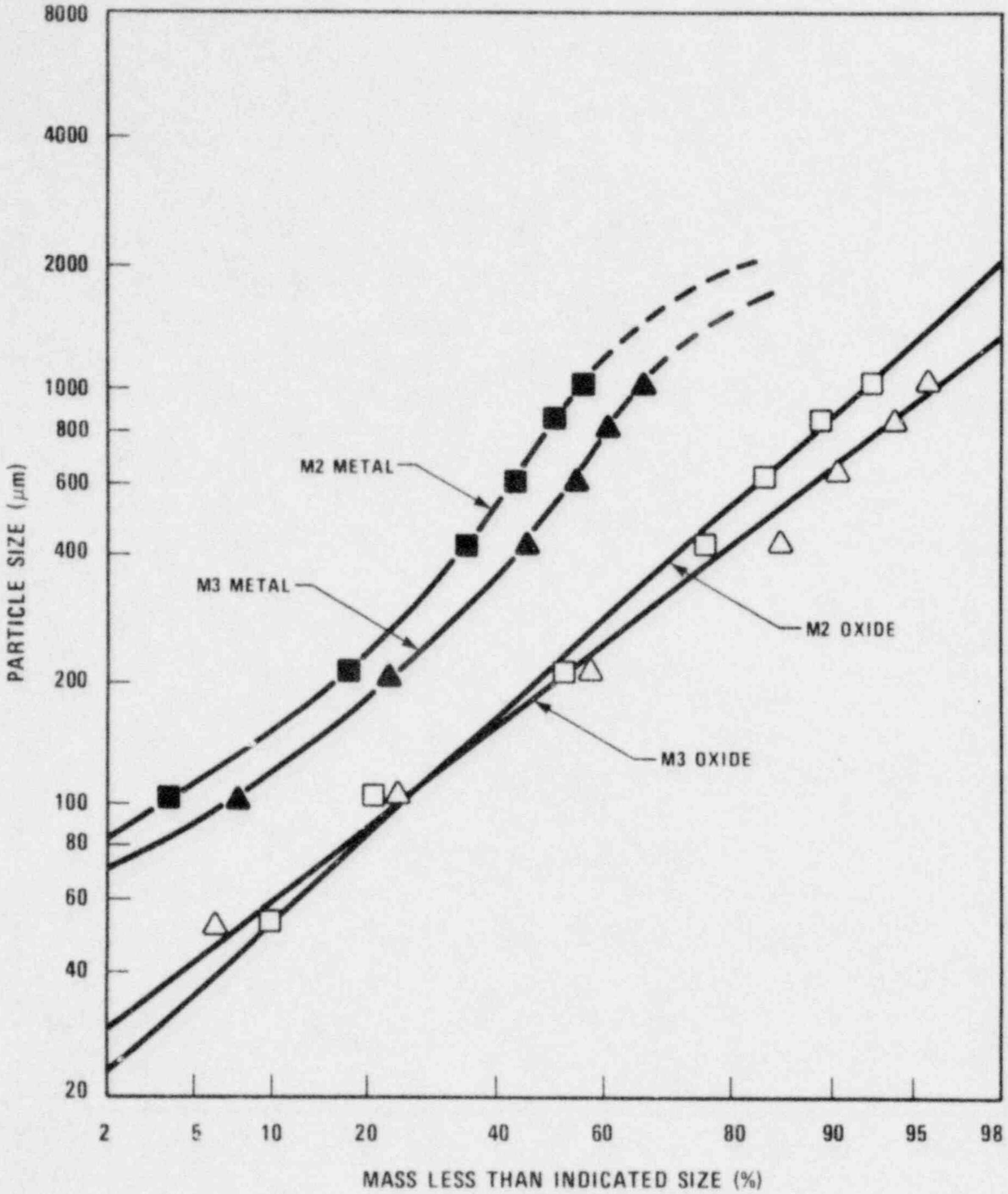

Figure G.1.A-3. Size Distributions of Metal and Oxide Particulate Debris Tests M2 and M3

1966-160

G.2 CONSEQUENCES OF INCREASED SODIUM-CONCRETE ACTIONS

G.2.1 Introduction

Experiments (References G.2-1 and G.2-2) have indicated that sodium-concrete reactions are self-limiting for conditions occurring during the TMBDB scenario. These reactions have been represented in the reference case CACECO analysis as a penetration attack of 0.5 inch per hour for a period of 4 hours. This reaction rate is used in Section 3.2.2 as described in Appendix C.1. The sensitivity of the consequences to increased sodium-concrete interactions is examined here.

G.2.2 Model

The CACECO code model defined in Appendix C.1 was modified to perform these sensitivity studies. The model used in the reference case analysis in Section 3.2.2 includes a sodium-concrete reaction rate of 0.5 inch per hour for 4 hours, starting at the time of reactor cavity liner failure (assumed to be at the time of penetration of the reactor vessel and guard vessel). To assess the potential impact of more severe sodium-concrete reactions, the CACECO model was modified to consider reaction rates of 0.5 inch per hour for 12 hours and 1.0 inch per hour for 12 hours. The reaction energy was maintained constant at 331 Btu/lb of concrete. The sensitivity analyses were run for 30 hours without venting and the results were compared to the reference case.

G.2.3 Results

The two cases in which more severe sodium-concrete reactions were assumed are compared to the reference case described in Section 3.2.2. The additional energy from the more severe sodium-concrete reactions causes the sodium pool to heat up faster. Sodium boiling begins at about 9 hours in the reference case; this is reduced to about 8 hours with a sodium-concrete reaction rate of 0.5 inch/hr for 12 hours, and to about 7 hours with a sodium-concrete reaction rate of 1.0 inch/hr for 12 hours. This additional energy source is reflected in slightly higher atmosphere temperatures in the reactor cavity and containment building and a higher containment steel temperature. However, as indicated in Figure G.2-1, these differences are minor and would not impact conclusions on the integrity of the containment.

Because of the additional energy source, the pressure in containment would be slightly higher (except for an early spike due to the treatment of hydrogen burning, discussed below). Again, the differences are minor as indicated in Figure G.2-2, and conclusions on containment integrity would not be impacted.

The hydrogen concentration in containment for the three cases is shown in Figure G.2-3. In all cases, the predicted hydrogen concentration at 24 hours and at 30 hours is zero. However, the short term (up to ∼10 hours) concentrations vary slightly with the sodium-concrete reaction assumptions. With more severe reactions, the sodium pool heatup would be more rapid and the sodium vapor from the pool would be increased. This would result in the hydrogen burning criteria (described in Section 3.2.1) being met earlier (∼8 or 9 hours compared to ∼10 hours in the reference case). The maximum hydrogen concentration prior to the hydrogen burning would be decreased slightly (from 4.5% to ∼4%). The analytic assumption of instantaneous burning when the criteria are met results in a predicted pressure spike as indicated in Figure G.2-2. The predicted spike is slightly less severe with increased sodium-concrete reactions but the variations are small enough to be of no consequence.

G.2.4 Conclusions

Table G.2-1 summarizes the results of these sensitivity studies on sodium-concrete reactions. The reference case considers a total depth of reaction of two inches of concrete. The sensitivity studies considered total depths of 6 inches and 12 inches. This provides factors of 3 and 6 on total energy from sodium-concrete reactions. The results show that the predicted containment conditions are not very sensitive to the sodium-concrete reaction assumptions. This is due to the fact that the reaction energy from sodium-concrete reactions is a small part of the total energy involved in the scenario from decay heat, chemical reactions in containment and other chemical reactions in the sodium pool.

Since the containment conditions are similar for the range of sodium-concrete reactions considered, it is concluded that sufficient margin exists to cover the uncertainties in sodium-concrete reactions.

G.2.5 References

G.2-1 J. A. Hassberger, R. K. Hilliard and L. D. Muhlestein, "Sodium Concrete Reaction Tests," HEDL-TME-74-36, June 1974.

G.2-2 J. A. Hassberger, "Intermediate Scale Sodium-Concrete Reaction Tests," HEDL-TME-77-99, March 1978. (Availability: U.S. DOE Technical Information Center)

TABLE G.2-1

SUMMARY OF SENSITIVITY STUDIES ON SODIUM-CONCRETE REACTIONS

Sodium-Concrete Reactions	Reference Case 0.5 in/hr for 4 hrs	0.5 in/hr for 12 hrs	1.0 in/hr for 12 hrs
PRE-24 HOUR RCB CONDITIONS			
Peak Hydrogen Concentration (%)	4.5	4.2	3.8
Time for Peak Concentration (hrs)	10.0	9.2	8.3
24 HOURS RCB CONDITIONS			
Atmosphere Temperature (^{o}F)	450.0	480.0	520.0
Pressure (psig)	11.1	11.8	12.6
Steel Temperature (^{o}F)	270.0	295.0	320.0
Hydrogen Concentration (%)	0.0	0.0	0.0
Oxygen Concentration (%)	13.7	13.3	12.7
30 HOURS RCB CONDITIONS			
Atmosphere Temperature (^{o}F)	520.0	550.0	580.0
Pressure (psig)	12.5	12.7	13.4
Steel Temperature (^{o}F)	315.0	335.0	360.0
Hydrogen Concentration (%)	0.0	0.0	0.0
Oxygen Concentration (%)	11.7	11.2	10.4

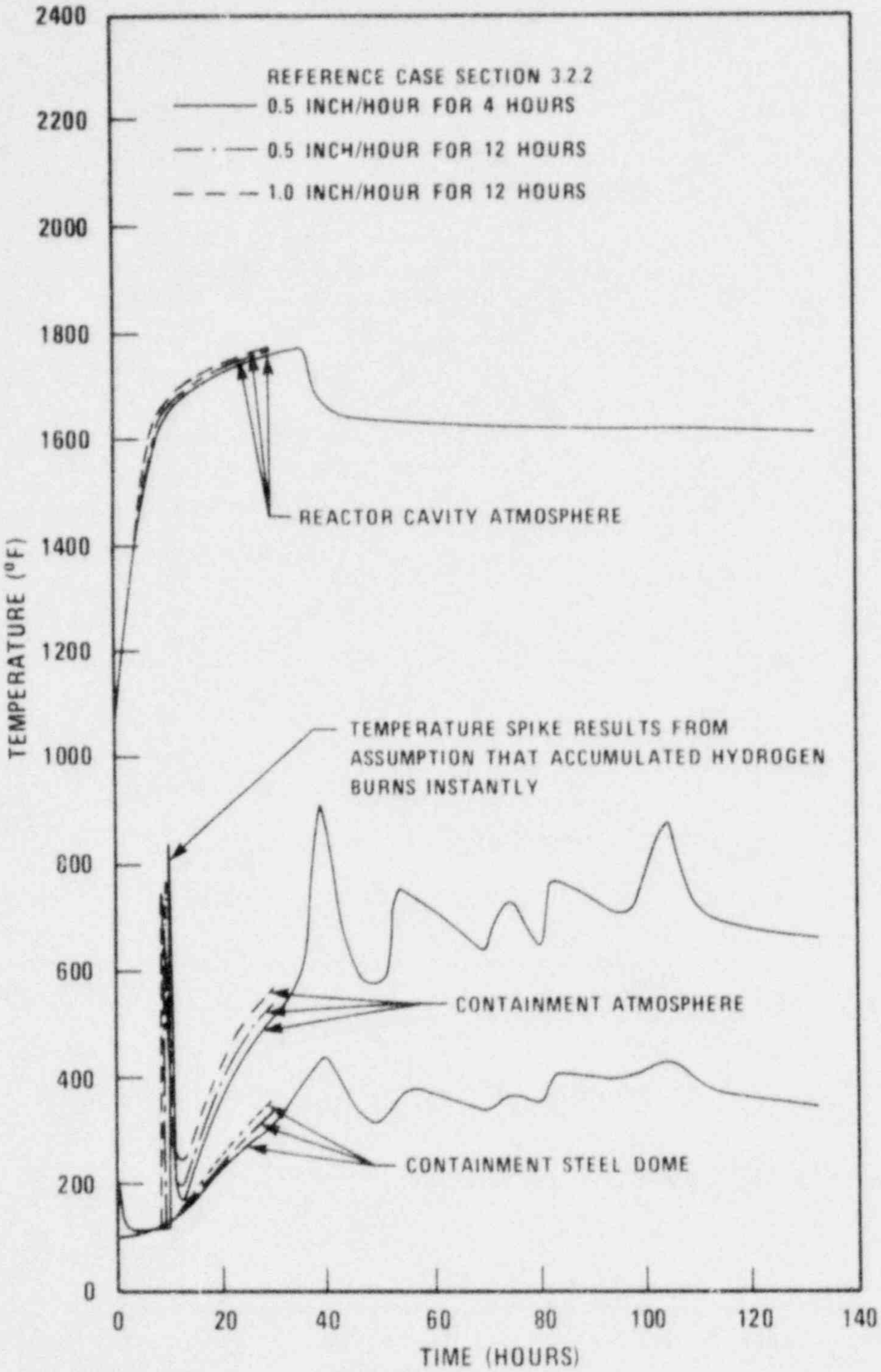

Figure G.2-1. Sensitivity of Reactor Cavity and Containment Atmosphere and Containment Steel Dome Temperatures to Sodium-Concrete Reactions

1966-161

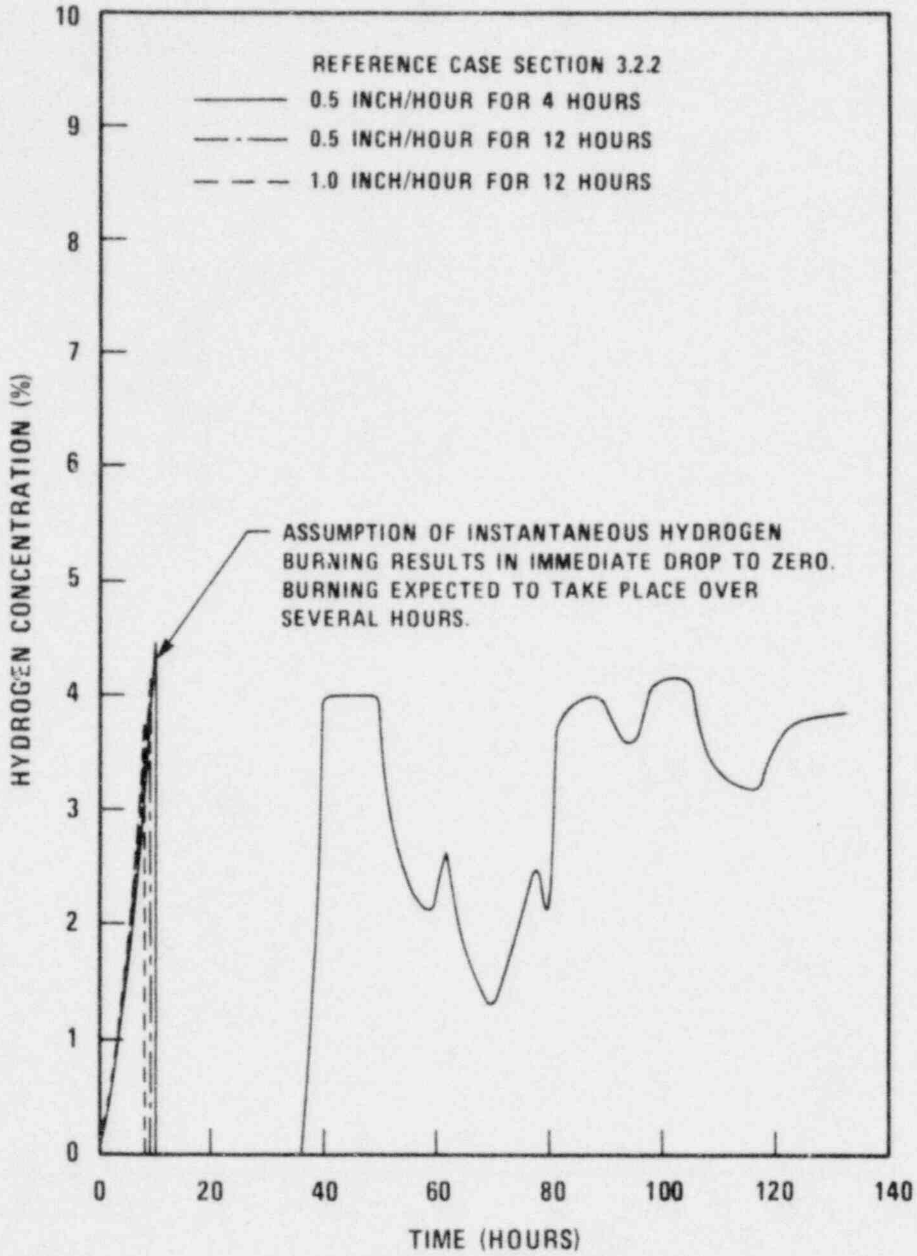

Figure G.2-3. Sensitivity of Hydrogen Concentration in the Containment Building to Sodium-Concrete Reactions

1966-163

G.3 EFFECT OF MAL-OPERATION OF RC-RCB VENT ON THE TMBDB SCENARIO

G.3.1 Introduction

The reactor cavity venting system function is to prevent overpressurization of the reactor cavity and to promote heat transfer between the vented gases and pipeway cell structures before the gases are released to containment. The effect of mal-operation of this system on the TMBDB scenario has been investigated. Three different modes of malfunction were identified and simulated by modifying the base case described in Section 3.2.2 and Appendix C.1. The first case analyzed partial RC-RCB vent line plugging. The second case simulated a plugging of one of the vent lines that interconnect the pipeway cells. The third case investigated the effects of sodium vapor flashing from the cavity sodium pool when the pressure is rapidly reduced.

G.3.2 CACECO Code Modeling

The CACECO Code model used to produce the Section 3.2.2 analysis was modified for the three postulated malfunction modes. To represent partial cavity-to-containment vent line plugging, blockages of 50, 80 and 98 percent were simulated by varying the nozzle area.

The second malfunction mode (plugging of one of the pipeway cells interconnecting vent lines) was simulated by removing the heat sink capacity of one pipeway cell, since line plugging would preclude vented gases from exchanging heat with one of the pipeway cell structures.

The third case simulated sodium vapor flashing. This was accomplished by allowing the sodium pool to reach boiling (approximately 10 hours) and then allowing cavity pressurization to a high value (35 psig cell design pressure) with the cavity assumed to be sealed. This was followed by cavity venting to containment (17 hours).

G.3.3 Results

The case 1 results showed a less severe containment hydrogen, temperature and pressure challenge at 24 hours for the three blockage conditions than the base case. Table G.3-1 lists the respective values of containment pressure, temperature and hydrogen concentration and reactor cavity temperature and pressure for the three blockages. The containment consequences for these calculations are less severe at 24 hours because less gases are vented. However, pressurization and temperature increases are found to occur in the cavity. For the 98 percent blockage, the peak cavity pressure was found to be 32 psig. The cavity design pressure is 35 psig; however, internal pressure is not the limiting parameter used for sizing the reactor cavity walls; therefore it is capable of withstanding internal pressures significantly greater than the design pressure. Thus structural failure would not be expected for a 98% blockage. However, this degree of blockage would appear to be near the upper bound of acceptable blockages, considering the combination of higher than normal temperatures and pressures.

Case 2 results indicate a more severe containment condition at 24 hours (Table G.3-1). For this particular malfunction, the pipeway cell interconnecting vent line would be plugged and the associated heat sink capability of the pipeway cell would be lost. Therefore the sodium boiloff rate to containment would be higher than the Section 3.2.2 analysis resulting in higher containment atmosphere temperature and pressure (590^{o}F and 12.8 psig versus 450^{o}F and 11.1 psig).

Figures G.3-1, 2 and 3 compare the containment pressure, temperature and hydrogen concentration plots for the case 2 and Section 3.2.2 analysis. In both cases, venting was assumed to be initiated at 36 hours. With the higher containment pressure the RCB peak vent rate increases slightly. The calculated value was found to be 26,200 CFM which is within the maximum design requirement of 26,400 CFM. The same purge rate that was used in the base case analysis was initiated approximately 45 minutes earlier to maintain an acceptable hydrogen condition.

Case 3 results at 24 hours are provided in Table G.3-1. The calculated containment pressure, temperature and hydrogen concentration values at 24 hours (12.9 psig, 545^{o}F and 0.0%) were similar to those calculated for case 2. The initial containment pressure spike after cavity depressurization was found to be 30 psig. This should not affect the structural integrity of containment since the steel temperature at the time of the pressure spike is approximately 110^{o}F. The associated atmosphere temperature spike has no effect on the containment metal temperature because of its large heat capacity. Figures G.3-4 and 5 present the containment pressure and atmosphere temperature plots with burst disk rupture at 17 hours (containment conditions are less severe than the base case between 10 and 17 hours because no venting from the reactor cavity occurs during that time). It should be noted that for case 3, the containment conditions after 24 hours would be very similar to the case 2 results.

G.3.4 Conclusion

It is concluded that the design has sufficient margin to accommodate postulated malfunctions of the RC-RCB vent system. Containment conditions at 24 hours for partial RC-RCB vent line plugging, for pipeway cell interconnecting vent line plugging and for sodium vapor flashing from the cavity sodium pool are similar to the calculated consequences from the Section 3.2.2 analysis. Acceptable containment conditions beyond 24 hours can be maintained (specifically case 2 and case 3) by initiating the purge system slightly earlier than assumed in the base case.

TABLE G.3-1

SENSITIVITY OF RCB AND RC CONDITIONS AT 24 HOURS TO RC VENT FAILURE MODES

	Section 3.2.2 Analysis	Case 1 (Partial RC-RCB Vent Line Plugging)			Case 2 (Plugging of 1 Pipeway Cell Interconnecting Vent Line)	Case 3 (Na Vapor Flashing Following Cavity Depressurization)
		50% Blockage	80% Blockage	98% Blockage		
RCB Pressure (psig)	11.1	11.1	10.4	6.1	12.8	12.9
RCB Atmosphere Temperature (^{o}F)	450	450	420	220	590	545
RCB Hydrogen Concentration (%)	0.0	0.0	0.0	0.0	0.0	0.0
RCB Oxygen Concentration (%)	13.7	13.7	14.0	15.4	12.3	11.5
RC Pressure (psig)	12.7	13.1	15.4	32.	14.4	14.4
RC Atmosphere Temperature (^{o}F)	1740.	1740.	1760.	1840.	1750.	1755.

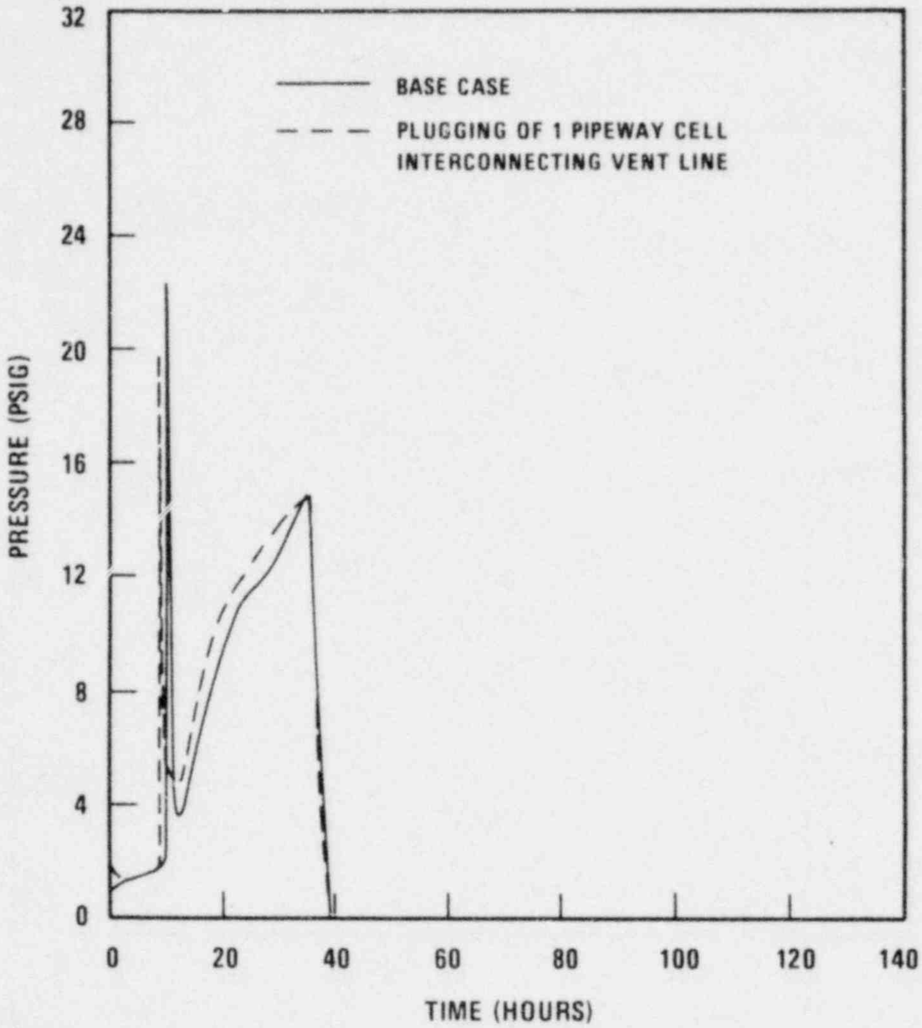

Figure G.3-1. Effect of Plugging One Pipeway Cell Interconnecting Vent Line on Containment Atmosphere Pressure

1966-164

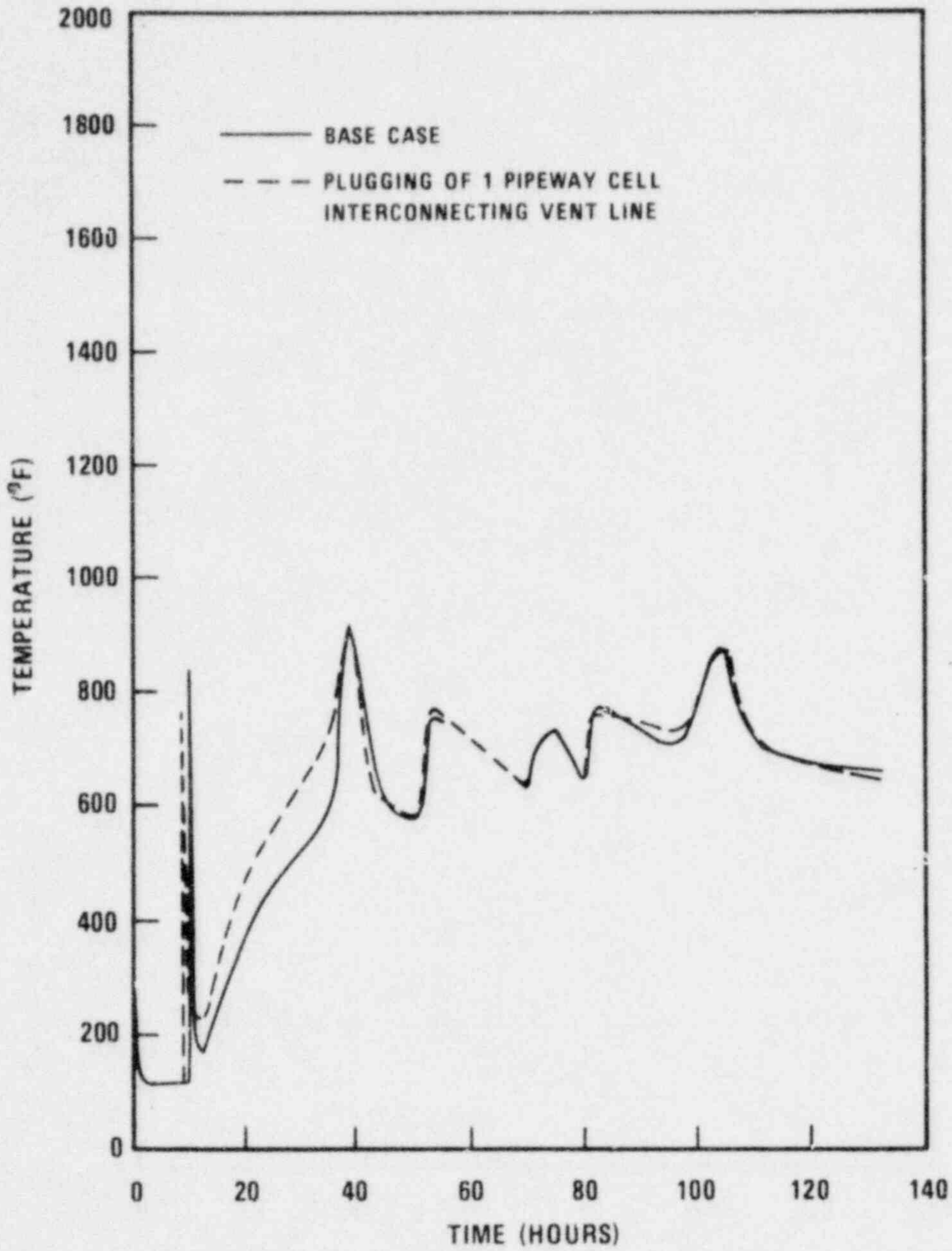

Figure G.3-2. Effect of Plugging One Pipeway Cell Interconnecting Vent Line on Containment Atmosphere Temperature

1966-165

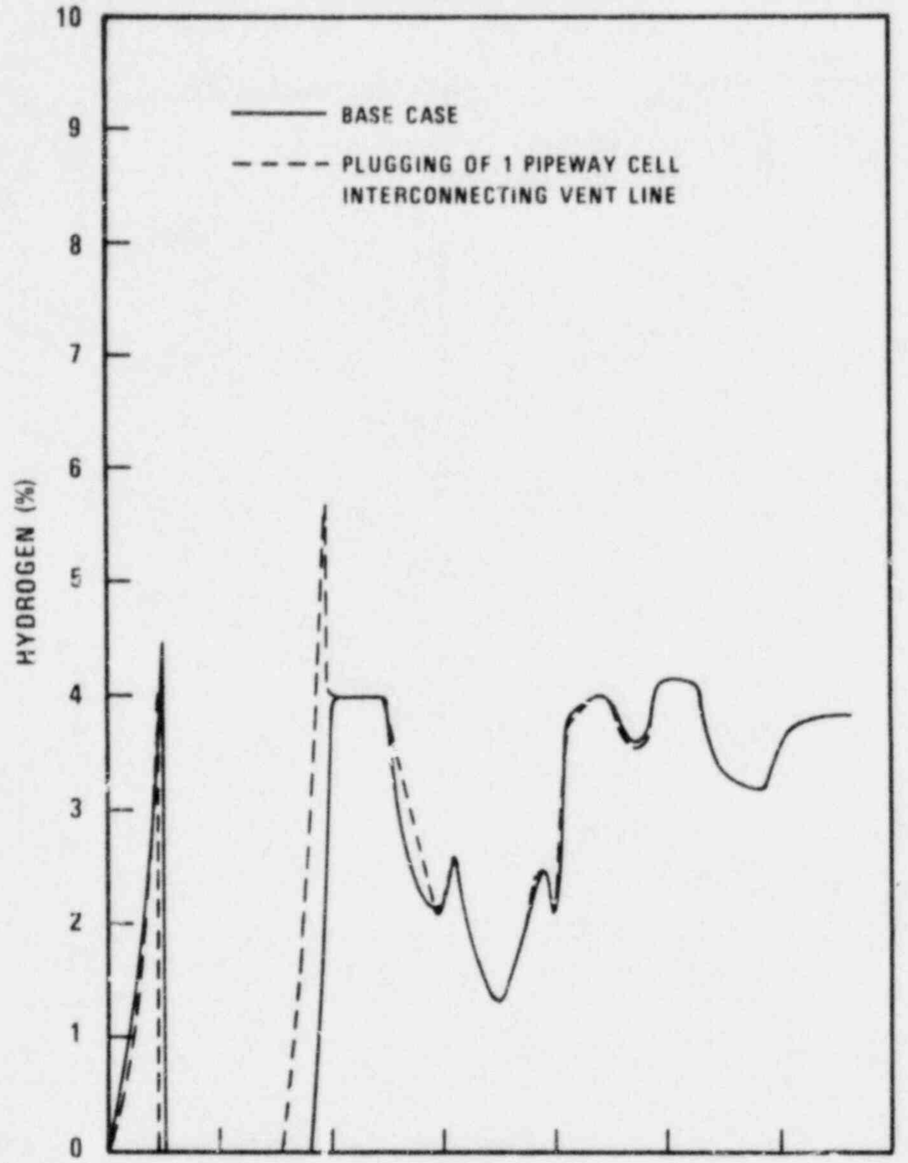

Figure G.3-3. Effect of Plugging One Pipeway Cell Interconnecting Vent Line on Containment Hydrogen Concentration

1966-166

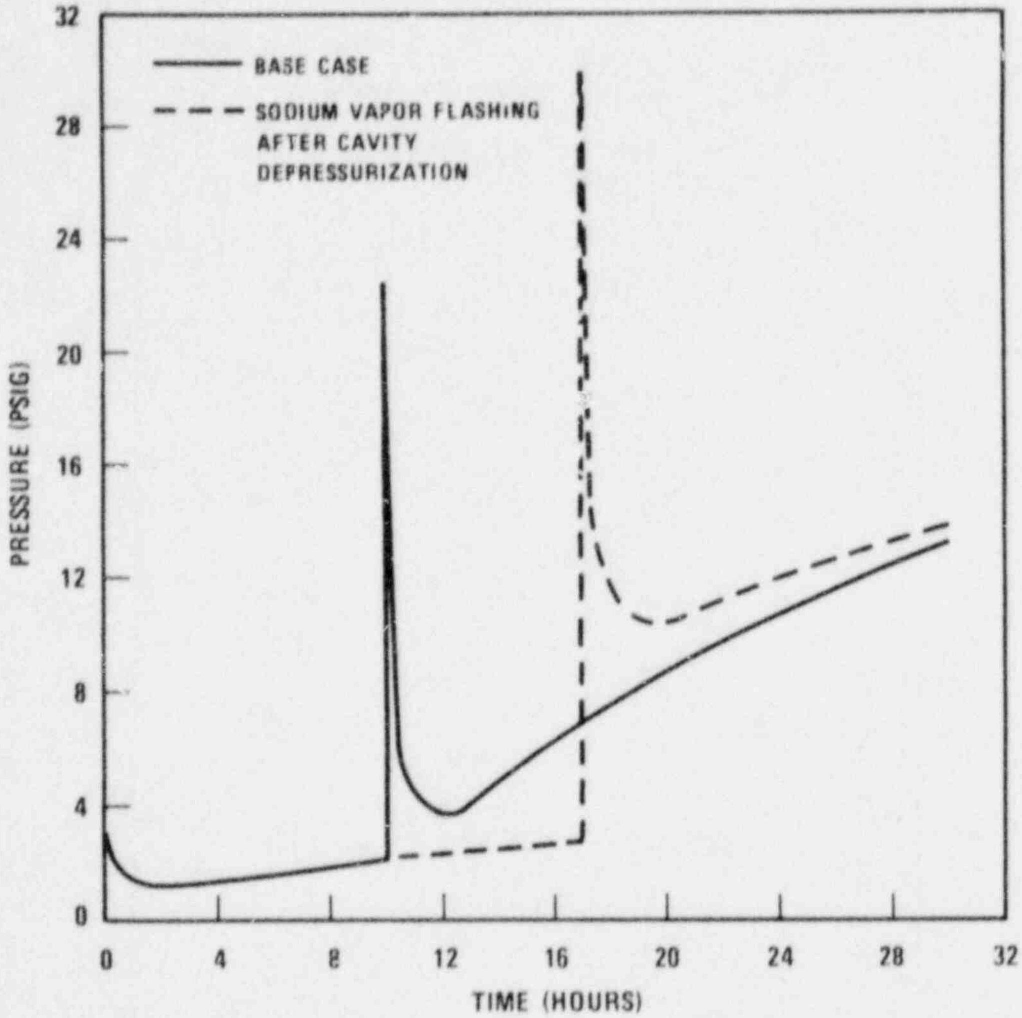

Figure G.3-4. Effect of Sodium Flashing on Containment Pressure

1966-167

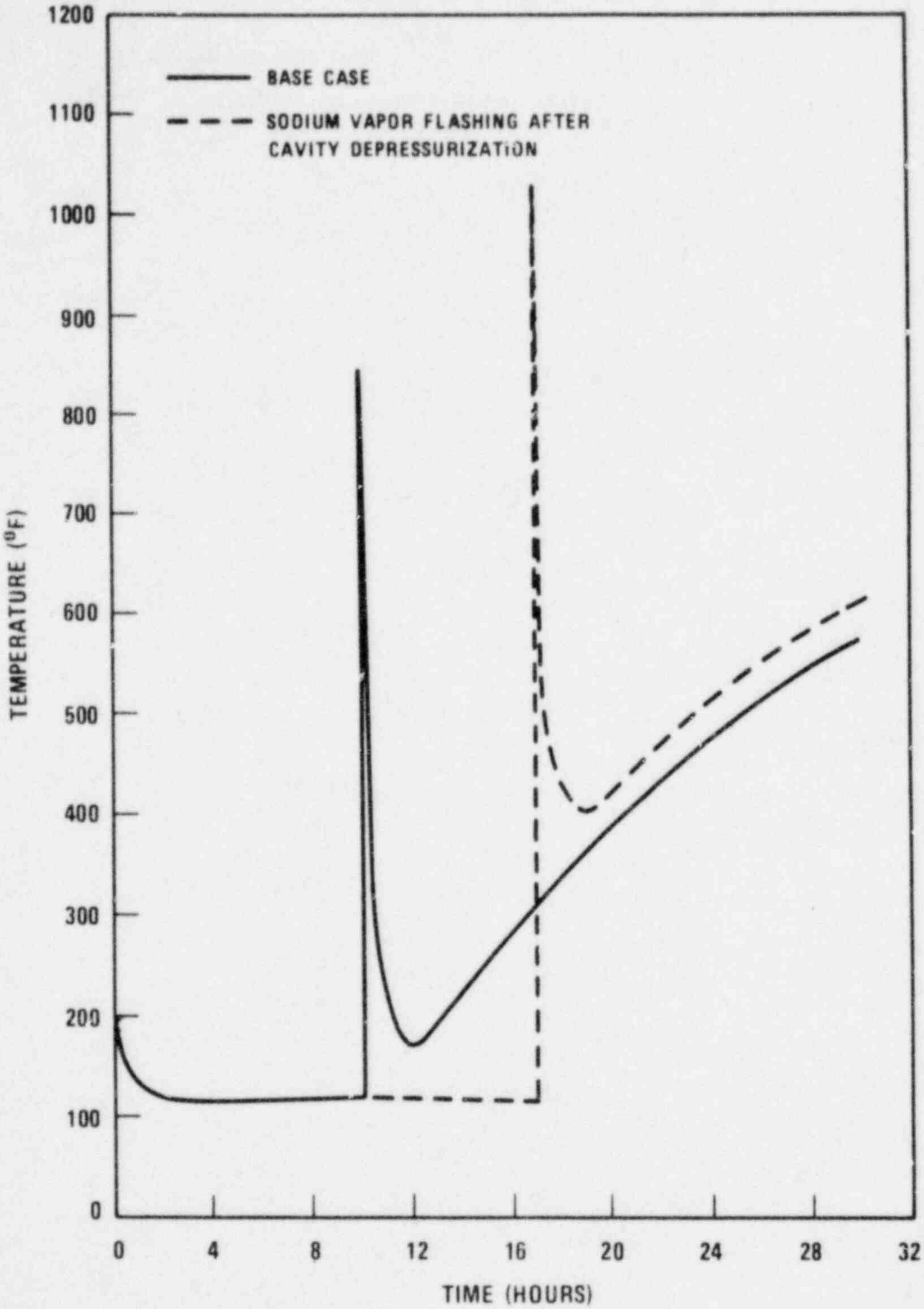

Figure G.3-5. Effect of Sodium Flashing on Containment Atmosphere Temperature

1966-168

G.4 EFFECT OF INITIAL HEAD RELEASE ON TMBDB DOSE CONSEQUENCES AND RCB ATMOSPHERE CONDITIONS

G.4.1 Introduction

Section 4 discussed the dose consequences of four cases, representing varying degrees of immediate leakage through the head. These cases covered initial fuel and fission products released from 0 to 5% along with the sodium release expected to accompany such fuel releases. The analysis presented here extends the range of these four cases and evaluates the sensitivity of the dose consequences to (1) changes in fuel release without an accompanying change in sodium release and (2) changes in sodium release for a fixed fuel release. Additional analyses were performed to evaluate the RCB atmosphere response, and therefore containment integrity, to these various releases.

G.4.2 Radiological Consequences

Table G.4-1 gives the dose consequences of three cases of initial release of fuel, fission products, and associated sodium assuming containment integrity (containment integrity is addressed in Section G.4.3). The results indicate that, for releases beyond 5%, the mitigating effect of aerosol depletion is stronger than the effect a larger initial source term might have on increasing the dose. The overall effect of various initial releases is best seen by looking at the 2 hour bone doses. From 1% to 5% fuel release, the bone dose increases about in proportion to the increase in the fuel release. However, at higher releases, the attenuating effect of the larger sodium releases exceeds the effect of the larger quantity of fuel and the overall 2 hour bone dose decreases as noted in the table.

The aerosol depletion effect alone of these releases can be seen by comparison of the thyroid doses. The thyroid dose is the result of the halogen release which is 100% for each of these cases. As the initial source term of fuel and sodium increases, the aerosol depletion rate increases which causes more of the halogen source to fall out leaving less available to leak out.

Table G.4-2 shows the dose consequences of from 1 to 50% fuel and fission products released initially without the accompaniment of the sodium which would be expected to be associated with such initial releases. Here the 2 hour bone doses are seen to be in direct proportion to the percent fuel released. The 2 hour thyroid doses show no benefit from aerosol depletion during the first two hours. The results in Table G.4-2 show that even for a 50% initial release, with minimal credit for aerosol depletion from sodium, the dose consequences are relatively low.

Finally, Table G.4-3 shows the effect of reducing the sodium in the initial release for the case of a 10% fuel and fission product release through the head assuming an integral containment. The bounding case of no sodium is compared to the case with 1,000 pounds of sodium. There is no difference in the 2 hour doses between the 0 and 1,000 pounds of sodium cases because there is little aerosol depletion during the first two hours. The 30 day doses are slightly higher with no sodium but are not highly sensitive to the aerosol effects of the initial release. This is due to the 30 day doses being more dependent on the boilup phase and gas sparging phase of the scenario.

The overall conclusion to be drawn from the results of this analysis is that the TMBDB scenario is not sensitive to a wide range of initial releases through the head with an integral containment barrier.

G.4.3 RCB Atmosphere Response To Initial Head Release

CACECO Code Model

The CACECO Code model, described in Section 3.2 and Appendix C.1, was modified to simulate the initial release of sodium and fuel through the head. To simulate the initial release of fuel and fission products, the latent heats of the fuel and various fission products were calculated up to the fuel vapor point. The energy calculated was then superimposed on top of the decay curve for a ten second interval. The appropriate partitioning factors were then calculated (i.e., code input that distributes decay heat to a designated cell). Similarly the sodium at 1000^{o}F was assumed to be injected to containment and burn completely within a ten second interval.

Results

Using the revised CACECO model, the containment conditions computed are listed in Tables G.4-1, 2 and 3 for the various cases. Tables G.4-2 and 3 indicate containment atmosphere temperature and pressure are more sensitive to the initial sodium release assumed than to the initial fuel release. The most severe results were found when 7,000 pounds of sodium and 7.5% of the fuel and solid fission products were assumed initially released to containment. The containment atmosphere temperature and pressure were found to be 1030°F and 24.4 psig. The containment metal temperature is not significantly affected by the sharp transient in atmosphere temperature because of its large heat capacity (at 1000 seconds the metal temperature is only 140°F). The containment could withstand all of the short term transients resulting from the initial head releases considered.

Conclusions

The calculations indicate that containment integrity after the initial release of fuel and fission products and sodium is not challenged for a wide range of assumptions. Considering the worst assumption (7,000 pounds of sodium and 7.5% fuel and fission products) containment integrity would be maintained following the initial head release.The general conclusion is that the TMBDB scenario has sufficient margin with respect to the amount of sodium and fuel assumed to be initially released.

TABLE G.4-1

EFFECT OF INITIAL FUEL, FISSION PRODUCT, AND SODIUM RELEASE*

		Dose (rem)		
		1% Fuel & F.P. 1000 lb. Na	5% Fuel & F.P. 3300 lb. Na	7.5% Fuel & F.P. 7000 lb. Na
	Bone	0.93	3.83	3.12
2 Hour	Lung	0.15	0.39	0.30
EB	Thyroid	11.3	9.51	5.19
	Whole Body	0.24	0.32	0.28
	Bone	32.7	33.2	32.8
30 Day	Lung	2.15	2.15	2.04
LPZ	Thyroid	5.31	1.72	0.83
	Whole Body	2.54	2.41	2.37

RCB Atmosphere Conditions**

Temperature (^{o}F)	270	580	1030
Pressure (psig)	4.6	12.7	24.4

*Initial release of noble gases, halogens, and volatile fission products to RCB = 100%.

**Peak values for 1 hour.

TABLE G.4-2

EFFECT OF INITIAL FUEL AND FISSION PRODUCT RELEASE
WITH SODIUM RELEASE FIXED AT 1000 LB.

		Dose (rem) Initial Release of Fuel and Fission Products*			
		1%	5%	10%	50%
2 Hour EB	Bone	0.93	4.56	9.10	45.4
	Lung	0.15	0.46	0.85	3.96
	Thyroid	11.3	11.3	11.3	11.3
	Whole Body	0.24	0.35	0.48	1.53
30 Day LPZ	Bone	32.7	35.5	37.6	60.7
	Lung	2.15	2.38	2.48	4.50
	Thyroid	5.31	4.43	3.53	3.53
	Whole Body	2.54	2.57	2.58	3.15
		RCB Atmosphere Conditions**			
Temperature (^oF)		270	290	310	450
Pressure (psig)		4.6	5.0	5.7	9.5

*Initial release of noble gases, halogens, and volatile fission products to RCB = 100%.

**Peak values for 1 hour.

TABLE G.4-3

EFFECT OF SODIUM RELEASE FOR A GIVEN 10% FUEL-FISSION PRODUCT RELEASE*

		Dose (rem) Pounds of Sodium in Initial Release	
		0	1000
	Bone	9.10	9.10
2 Hour	Lung	0.84	0.85
EB	Thyroid	11.2	11.3
	Whole Body	0.48	0.48
	Bone	40.5	37.6
30 Day	Lung	2.76	2.48
LPZ	Thyroid	5.28	3.53
	Whole Body	2.73	2.58
	RCB Atmosphere Conditions**		
Temperature (^{o}F)		260	310
Pressure (psig)		4.6	5.7

*Initial release of noble gases, halogens, and volatile fission products to RCB = 100%.

**Peak value for 1 hour.

APPENDIX H

HYDROGEN BURNING CHARACTERISTICS

This Appendix provides the hydrogen burning characteristics used in the various analyses. Specifically, the hydrogen burning criteria are addressed in Appendix H.1 and flame length considerations are addressed in Appendix H.2.

H.1 HYDROGEN BURNING IN THE TMBDB SCENARIO AND RESULTANT CONTAINMENT CONDITIONS

H.1.1 Introduction

Hydrogen burning in the reactor containment building and the resultant containment conditions will be described for the Thermal Margin Beyond the Design Base (TMBDB) scenario. It will be shown that burning will 'ways occur well before conditions that would support a detonation could exist. The hydrogen burning scenario will be presented along with a scenario that bounds the containment temperature and pressure. Containment conditions will be presented for these hydrogen burning scenarios. Conditions at 24 hours will be presented along with an evaluation of the margins beyond 24 hours before venting and purging would be required.

H.1.2 Review of Hydrogen Burning Literature

H.1.2.1 Flammability Limits for Hydrogen in Air

In this section, the flammability limits for hydrogen in air will be given for ambient conditions, followed by a discussion of the effects of TMBDB containment conditions on the flammability limits.

H.1.2.1.1 Flammability Limits at Ambient Conditions

The burning of hydrogen in air has been extensively studied at the U.S. Bureau of Mines and elsewhere. References H.1-1, 2 and 3 summarize much of this work.

The flammability limits of hydrogen in air at ambient conditions are indicated on Figures H.1-1 and 2 (Reference H.1-2). These two figures are different representations of the same information. As the figures indicate, hydrogen concentr.:ions in excess of 4% will burn if the oxygen content is above 5% and an ignition source is present. In the TMBDB scenario, the very large sodium flame presents a continuous ignition source. Regulatory Guide 1.7, which is applicable to water reactors, also indicates the lower limit of hydrogen flammability in air is 4% as long as the oxygen concentration is above 5%.

H.1.2.1.2 Effects of TMBDB Containment Conditions on Flammability Limits

In the TMBDB scenario, containment conditions at times of interest are an atmosphere temperature of $\sim$500^{o}F, a pressure of $\sim$11 psig, and a low concentration of water vapor in the atmosphere. The effects of these conditions on the flammability limits in the previous section will be discussed.

As described in Reference H.1-2, when the atmosphere temperature increases, the lowest hydrogen concentration at which hydrogen would burn decreases. A decrease of $\sim$35% in the lower flammability limit was noted between room temperature and 750^{o}F.

The lowest concentration of hydrogen that would be flammable in air increases with pressure up to $\sim$20 atmospheres (Reference H.1-2). The 4% limit increased to $\sim$6% with the 20 atmospheres pressure. For an increase of one atmosphere (approximate TMBDB condition) the increase would be negligible (to <4.1%).

At ambient temperatures the lowest concentration of hydrogen that would be flammable for saturated and dry air are 4.1% and 4% respectively (Reference H.1-2); therefore, the effect of water vapor in air is not significant at ambient conditions. At higher temperatures the lowest flammable hydrogen concentration rises slowly.

The net effect of the TMBDB conditions on the lowest concentration of hydrogen that would be flammable cannot be numerically determined; however, considering the small magnitudes of the individual effects and the opposing direction of these effects, a lower limit of 4% hydrogen concentration is considered appropriate. It is noted that Regulatory Guide 1.7 applies the 4% limit to water reactor containments where the temperature, pressure, and water content are considerably above normal.

H.1.2.2 Detonation Limit for Hydrogen in Air

Reference H.1-1 gives the lower hydrogen concentration detonation limit in air at 18.3% at ambient conditions. Other experimenters (Reference H.1-4) observed the lower hydrogen concentration detonation limit to be as low as 14%. Shapiro and Moffette (Reference H.1-5), in their evaluation of the safety aspects for LWRs, use 19% as the lower hydrogen concentration limit for detonation.

The effect of TMBDB conditions on the lower hydrogen concentration detonation limit is not known; however, the magnitude of the effects would not be expected to be significant compared to the margin between the flammability and detonation limits. This is supported by the hydrogen burning experiments at HEDL that have indicated detonations occur under conditions similar to those in TMBDB only at hydrogen concentrations above 10%. The exact concentration was not determined from those experiments.

As Figure H.1-3 indicates, it would not be possible in the TMBDB scenario to reach a hydrogen concentration in which a detonation and resulting high pressures (7-15 atmospheres) would occur. This is because the large ignition source would cause the hydrogen to burn at the flammability limit ($\sim$4% hydrogen) which is considerably below the detonation limit ($\sim$14 to 19% hydrogen). It is noted that the large quantity of sodium entering containment would provide a continuous ignition source (satisfying criterion (b)), even if for some unknown reason the sodium would not burn, because sodium at $\sim$1700^{o}F would be red hot.

Regulatory Guide 1.7 states that in water reactors with the oxygen content above 5%, the hydrogen concentration must not exceed 6% to insure that explosive concentrations are avoided.

H.1.2.3 Experiments Under Simulated TMBDB Conditions

Experiments have been performed at HEDL to study hydrogen burning under simulated TMBDB conditions (Reference H.1-6). A conservative interpretation of the experiments indicated that hydrogen would burn when entering the containment if either criterion (a) or (b) is satisfied in combination with criterion (c).

a. The hydrogen-nitrogen mixture entering containment is above 1450°F.

b. The hydrogen-sodium-nitrogen mixture entering containment contains at least 6 g/m^3 of sodium at temperatures above 500°F.

c. The oxygen concentration is above 8%.

Criterion, (c) above, was found to be highly conservative. Figure H.1-4 reproduces the experimental results under the conditions that approach those of the TMBDB event. The two symbols indicate the oxygen content of the inlet and outlet gases in the simulated containment vessel. The average vessel oxygen content is between the inlet and outlet values - probably closer to the outlet value. As the figure indicates, hydrogen burning continues until oxygen levels decrease to ~4%.

H.1.3 Hydrogen Burning Scenario for TMBDB

The predicted hydrogen burning scenario will be presented in this section followed by a scenario that bounds the containment pressure and temperature conditions.

H.1.3.1 Predicted Hydrogen Burning Scenario

With respect to ignition of hydrogen entering the reactor containment building through the reactor cavity vent in the TMBDB scenario, the criteria used in the Section 3.2.2 analysis are appropriate and supported by the HEDL data (Reference H.1-6).

With respect to hydrogen burning after ignition, when the oxygen content is reduced, applicable data are more numerous. Figure H.1-5 illustrates the burning limits from the HEDL experiments, the lower flammability limits derived by the U.S. Bureau of Mines and the flammability limit in Regulatory Guide 1.7. Considering that the HEDL data define when hydrogen burns as it passes through the sodium flame at the reactor cavity vent (establishing the 8% oxygen limit for complete hydrogen burning), and the Bureau of Mines data define the burning region in a hydrogen-air atmosphere with an ignition source (establishing the 5% oxygen limit for hydrogen burning above 4%), the predicted hydrogen burning scenario for TMBDB conditions is that shown on Figure H.1-6.

The complete hydrogen burning criteria are that hydrogen will burn when entering containment or within the containment when either criterion (a) or (b) is satisfied in combination with criterion (c).

a. The hydrogen-nitrogen mixture entering containment is above 1450^{o}F.

b. The hydrogen-nitrogen-sodium mixture entering containment contains at least 6 g/m^3 of sodium at temperatures above 500^{o}F.

c. The containment oxygen concentration is above 8%. With the oxygen concentration above 5% and the hydrogen concentration above 4%, the hydrogen in excess of 4% would burn.

H.1.3.2 Hydrogen Burning Scenario to Bound Containment Temperature and Pressure

Because of the possibility that hydrogen might burn at lower hydrogen concentrations than 4% in the presence of the large sodium ignition source, a bounding hydrogen burning scenario was developed to maximize the containment temperature and pressure effects. For this bounding case, it was assumed that all hydrogen burns if any oxygen is present in containment. This bound is indicated on Figure H.1-6.

H.1.4 Containment Conditions

H.1.4.1 Conditions Prior to Venting and Purging

Containment conditions were determined for the predicted and bounding hydrogen burning scenarios using the CACECO code model described in Section 3.2.2 and Appendix C.1. Figures H.1-7, 8 and 9 show the containment atmosphere temperatures, pressures, and hydrogen concentration for these cases as a function of time. Table H.1-1 provides the containment conditions at 24 hours for these cases. Figure H.1-10 indicates the containment conditions with respect to the flammability limits.

At 24 hours, the predicted scenario is identical to the bounding case that assumes complete hydrogen burning since the 8% oxygen cutoff value has not been reached. Consequently, no hydrogen accumulation is predicted in containment at 24 hours. Both cases indicate the containment does not require venting and purging until times beyond 24 hours.

Beyond 24 hours the pressure, temperature and hydrogen concentration of the predicted hydrogen burning case and the bounding case continue to climb. The pressure differential between the predicted burning case and the bounding case is an insignificant 1 psi. The atmosphere temperature differential is also small. The hydrogen concentration for both cases decreases between 45 and 48 hours. This is a temporary condition due to the formation of sodium hydride in the containment building. The reaction combines free hydrogen and sodium and as a result reduces the hydrogen concentration. In the predicted burning case, the hydrogen concentration is higher than in the bounding scenario; however, this is unimportant because burning (or detonation) cannot occur at the low oxygen concentrations. The time when venting and purging would be required is determined by pressure considerations and by possible local conditions when purging is initiated. Since the containment has a pressure capability of 30-40 psig, and a 6% hydrogen concentration limit is used to avoid any possibility of local concentration problems when purging is started, the time before venting is required would be approximately 1.5 days for the predicted burning scenario. For the bounding case, the time to vent would not be significantly decreased.

For the predicted hydrogen burning scenario, Figure H.1-10 shows the oxygen concentration decreases to 8% before hydrogen accumulates. The bounding case, with respect to containment pressure and temperature is illustrated on the figure as a decreasing oxygen content until the oxygen is depleted. The hydrogen concentration then increases.

H.1.4.2 Venting and Purging Considerations

When venting is initiated (exhausted through a filter system), the containment pressure would decrease. This would result in a decrease in the reactor cavity pressure which would cause the sodium boiling rate to increase, because of the reduced boiling point, as the pressure decreases. The higher sodium boiling rate would increase the sodium vapor venting to the containment and the resultant burning in containment. This would deplete the oxygen to the point where hydrogen accumulation would occur. The increase in hydrogen can be controlled by bringing fresh air into containment (purging). This process would, obviously, dilute the hydrogen and increase the oxygen toward a level that would support combustion.

In the predicted hydrogen burning case, venting at ~1.5 days to control pressure would increase the hydrogen concentration initially as the accumulated hydrogen in the reactor cavity vents to the containment building along with the sodium vapor. Hydrogen burning would not occur because the oxygen content in the containment building would be below 5%. Purging would be initiated to control the long term hydrogen concentration so that potentially explosive concentrations would not be attainable. When purging is initiated, the oxygen concentration would increase until it reached the 5% level and then hydrogen burning would begin and the hydrogen in excess of 4% would burn (the sodium vapor ignition source exists until sodium boil dry at $\sim$130 hours).

The analyses in Section 3.2.2 show that venting and purging can be used to suitably control the hydrogen during the longer term.

H.1.5 Summary and Conclusions

The review of the hydrogen burning literature (Section H.1.2) has indicated the lower limit of hydrogen flammability is 4% hydrogen with the oxygen content above 5%.

The review (Section H.1.2) also indicated hydrogen would burn well before conditions that would support a detonation could be reached because of the sodium flame which acts as a continuous ignition source whenever oxygen is present.

Based on the literature review and experimental data (Section H.1.2.3), a hydrogen burning scenario was determined along with a scenario that bounds the containment temperature and pressure conditions. In the predicted hydrogen burning scenario, hydrogen would burn completely when entering containment if the oxygen content is above 8%; any hydrogen accumulation in containment in excess of 4% would burn if the oxygen content is above 5%.

Containment conditions were determined for these hydrogen burning scenarios. The conditions at 24 hours were found to be acceptable for both scenarios. The pressures and temperatures were essentially identical for these cases, and both cases predicted no hydrogen accumulation at 24 hours.

H.1.6 References

H.1-1 B. Lewis and G. von Elbe, Combustion, Flames and Explosions of Gases, Second Edition, Academic Press, Inc., New York, 1961.

H.1-2 H. F. Coward and G. W. Jones, Limits of Flammability of Gases and Vapors, Bureau of Mines Bulletin 503, U.S. Bureau of Mines, Washington, D.C., 1952.

H.1-3 G. W. Keilholtz, "Hydrogen Considerations in Light-Water Power Reactors," ORNL-NSIC-120, February 1976.

H.1-4 W. E. Gordon, A. J. Mooradian and S. A. Harper, "Limit and Spin Effects in Hydrogen Oxygen Detonations," Seventh Symposium (International) on Combustion, Oxford, Aug. 28 - Sept. 3, 1958, pp. 752-759, Academic Press, New York, NY. 1959.

H.1-5 Z. M. Shapiro and T. R. Moffette, "Hydrogen Flammability Data and Application to PWR Loss-of-Coolant Accident," WAPD-SC-545, September 1957.

H.1-6 R. W. Wierman, "Experimental Study of Hydrogen Jet Ignition and Jet Extinguishment," HEDL-TME 78-80, April 1979.

TABLE H.1-1

CONTAINMENT ATMOSPHERE CONDITIONS AT 24 HOURS

	Predicted Hydrogen Burning Scenario	Bounding Hydrogen Burning Scenario
Atmosphere Temperature (^{o}F)	450	450
Atmosphere Pressure (psig)	11.1	11.1
Hydrogen Concentration (%)	0.0	0.0

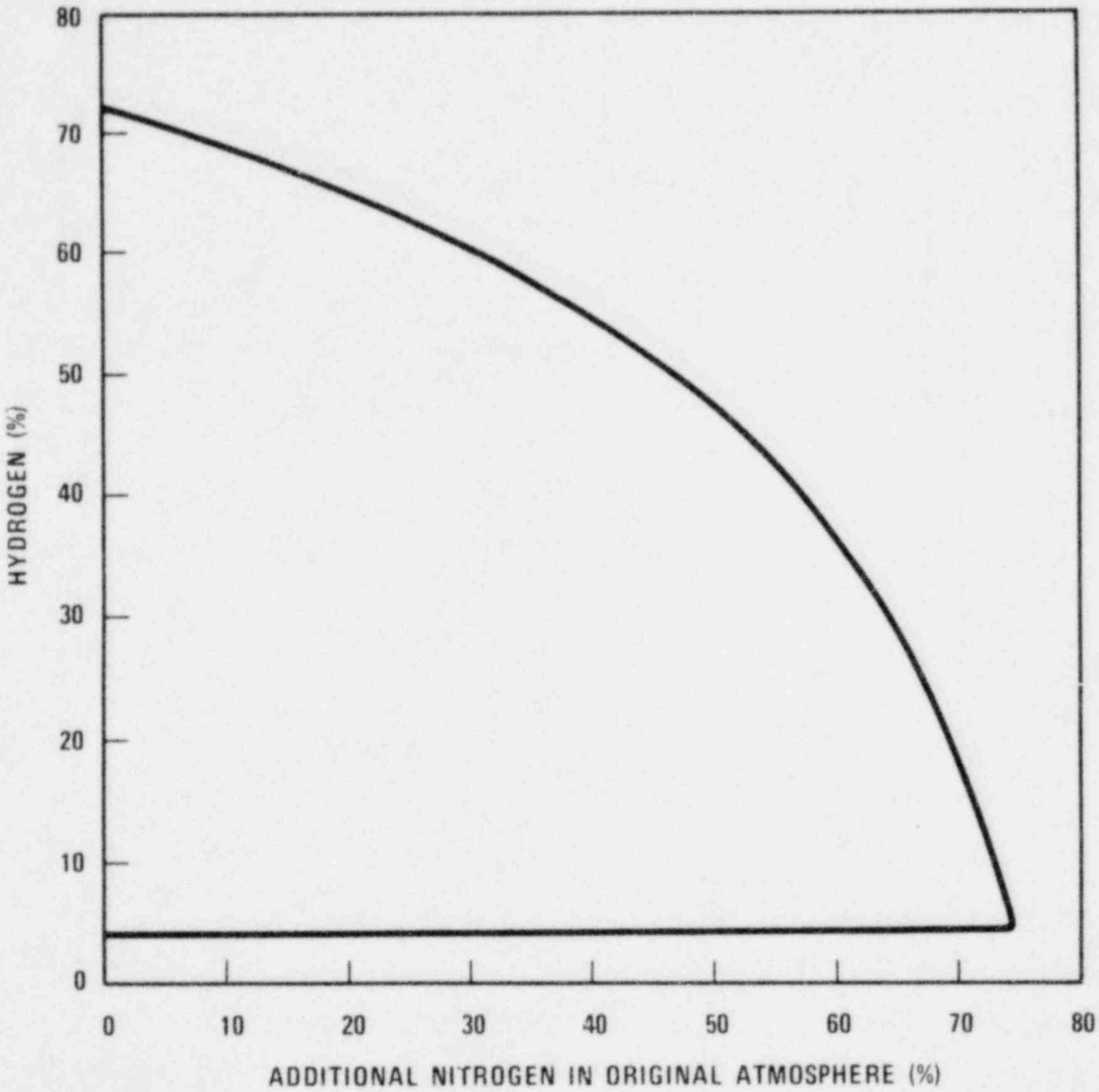

Figure H.1-1. Limits of Flammability of Hydrogen in Air and Nitrogen

1966-169

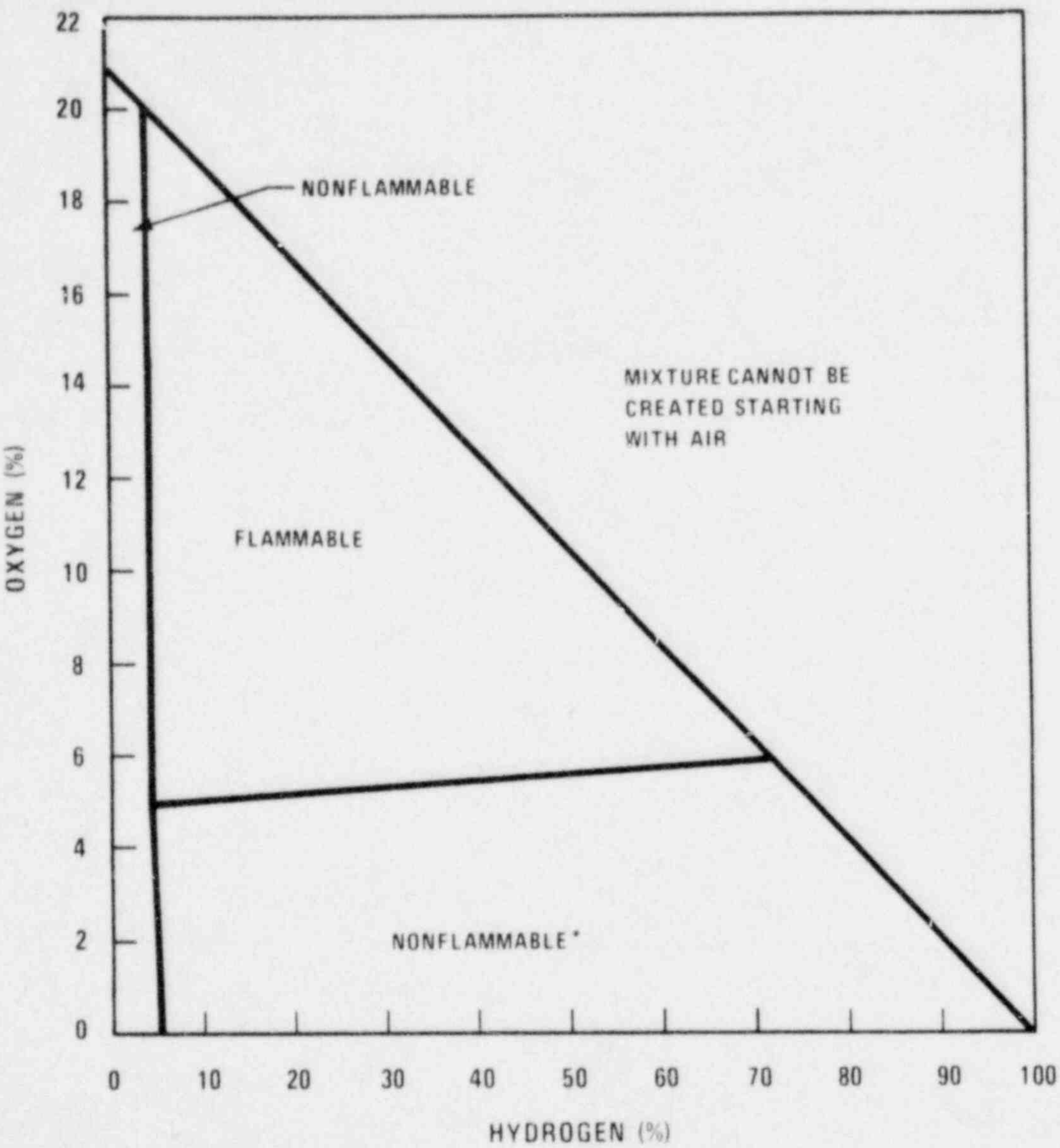

*FORMS FLAMMABLE MIXTURES WHEN MIXED WITH ADDITIONAL AIR.

Figure H.1-2. Hydrogen Flammability Limits in Air

1966-170

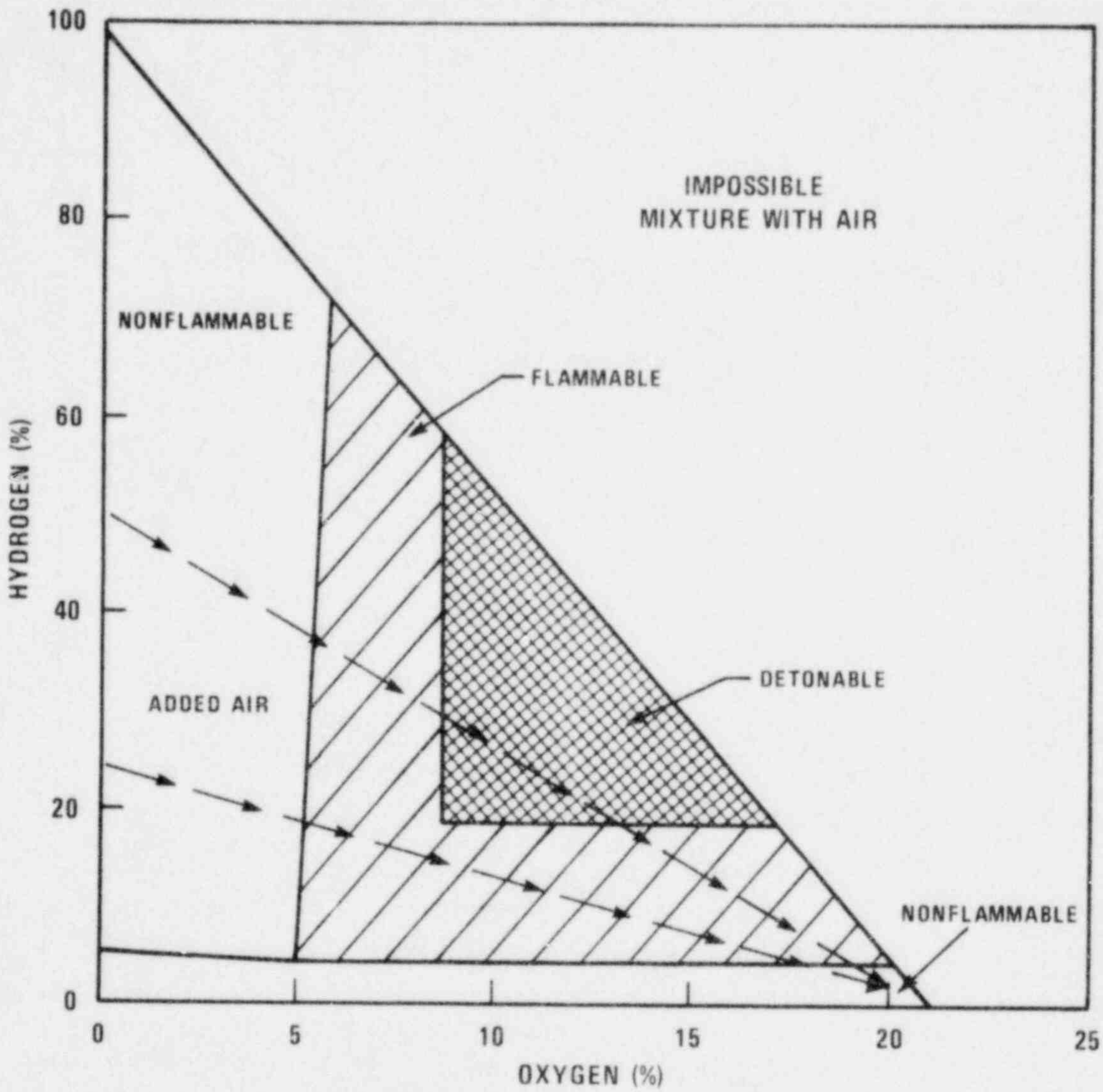

Fig re H.1-3. Detonation and Flammability Limits

1966-171

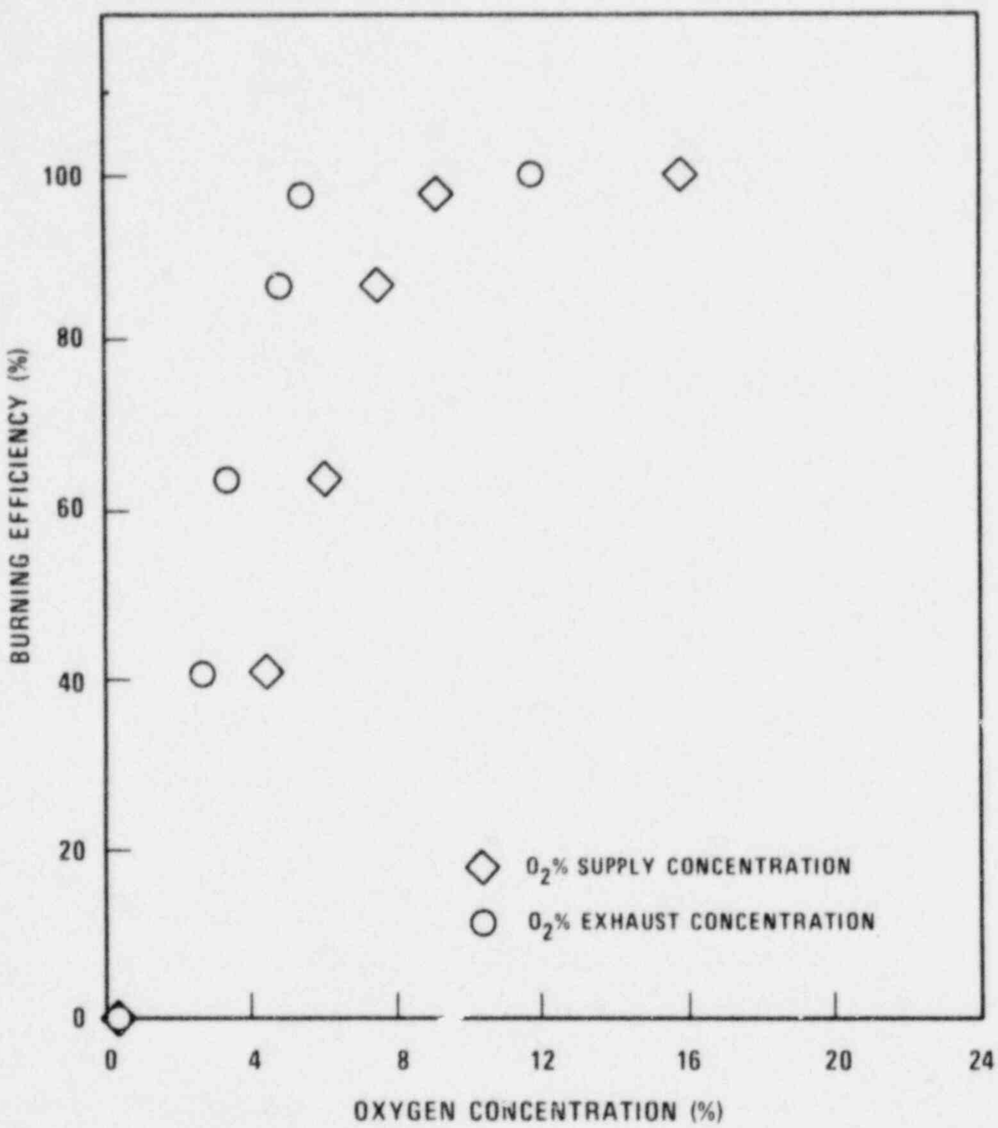

Figure H.1-4 Hydrogen Burning Efficiency for TMBDB Conditions

1966-173

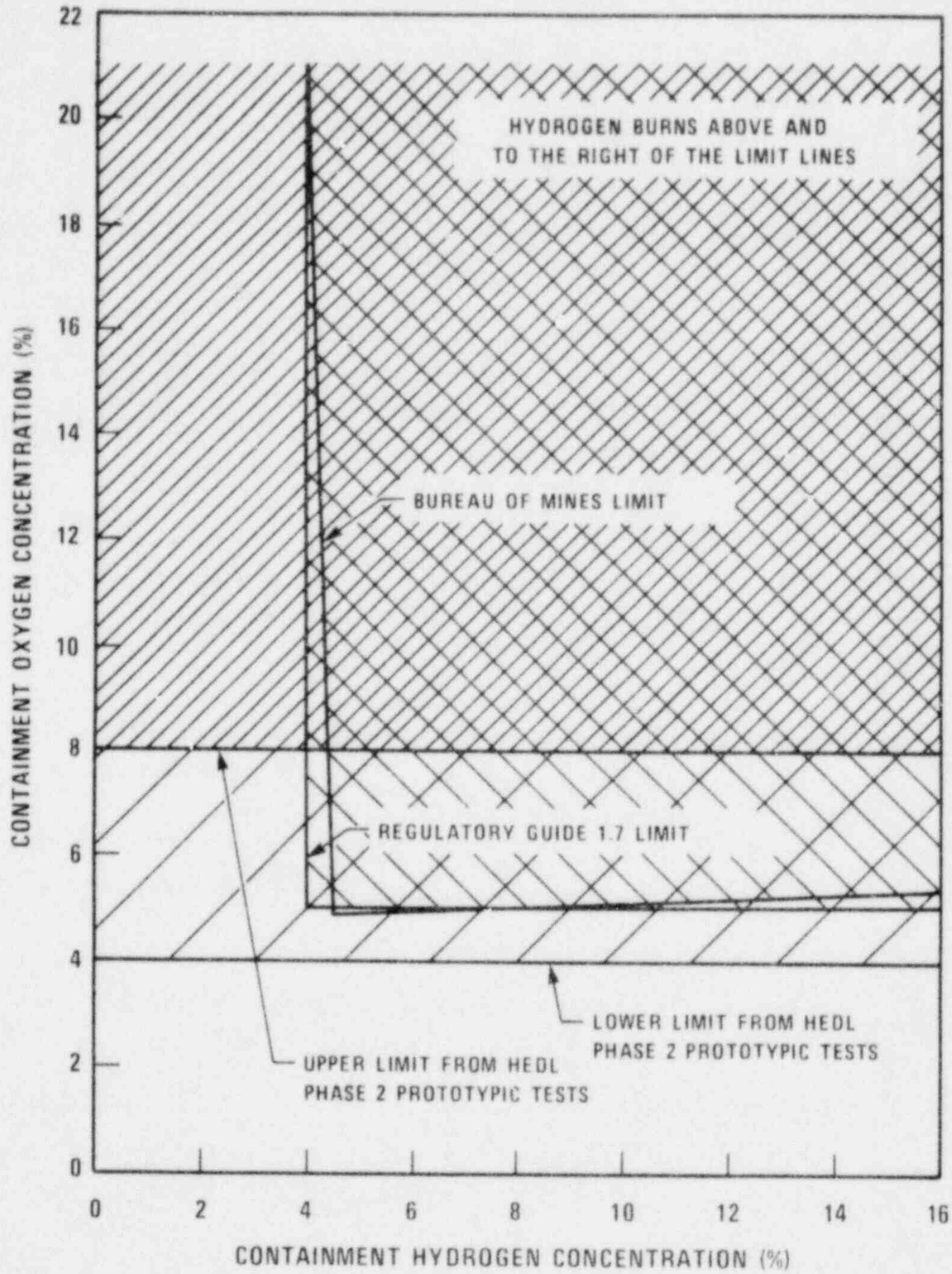

Figure H.1-5 Containment Hydrogen Flammability Limits

1966-174

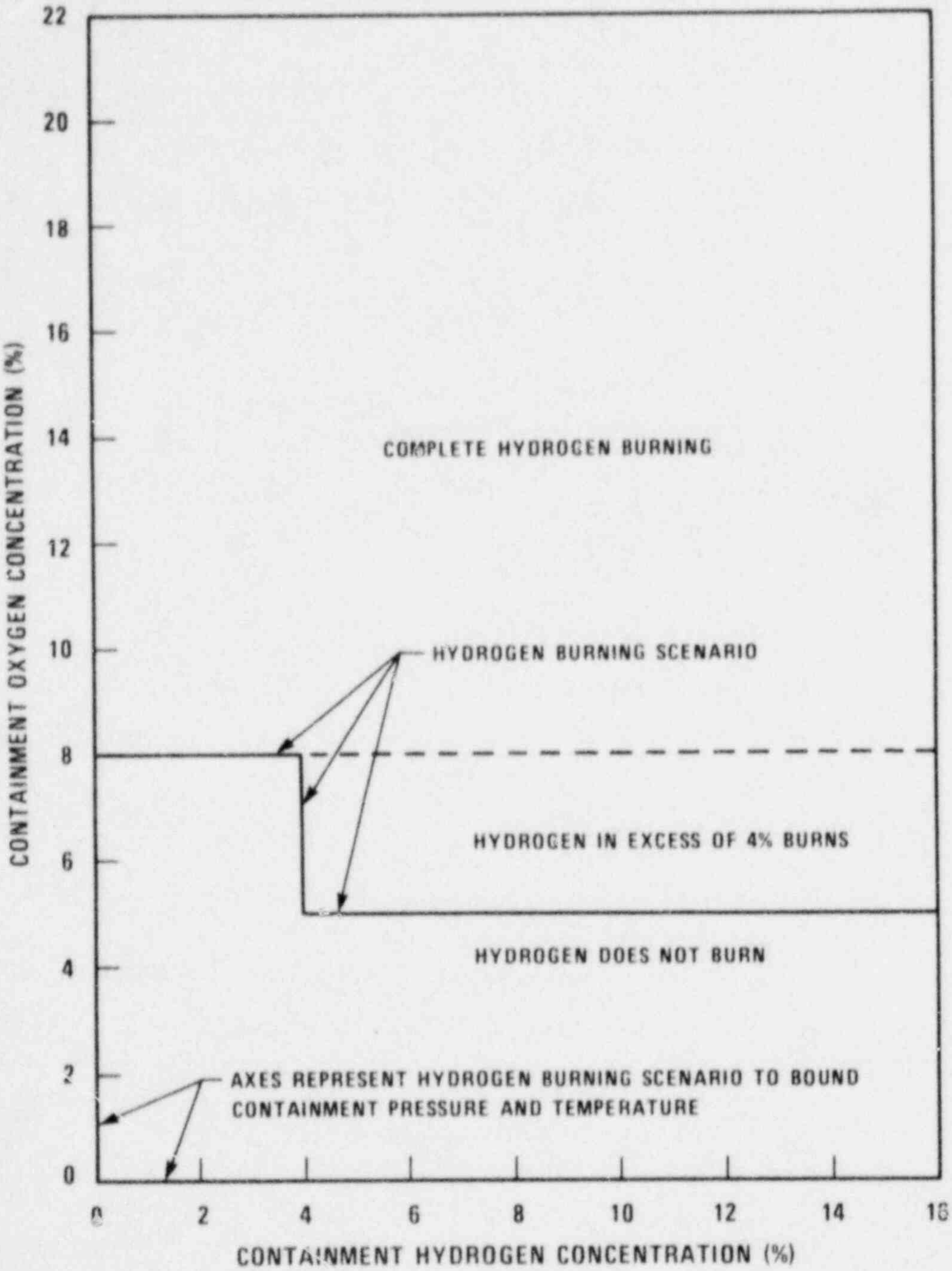

Figure H.1-6 Flammability Limits for Predicted Scenario and Hydrogen Burning Scenario that Bounds Containment Pressure and Temperature

1966-175

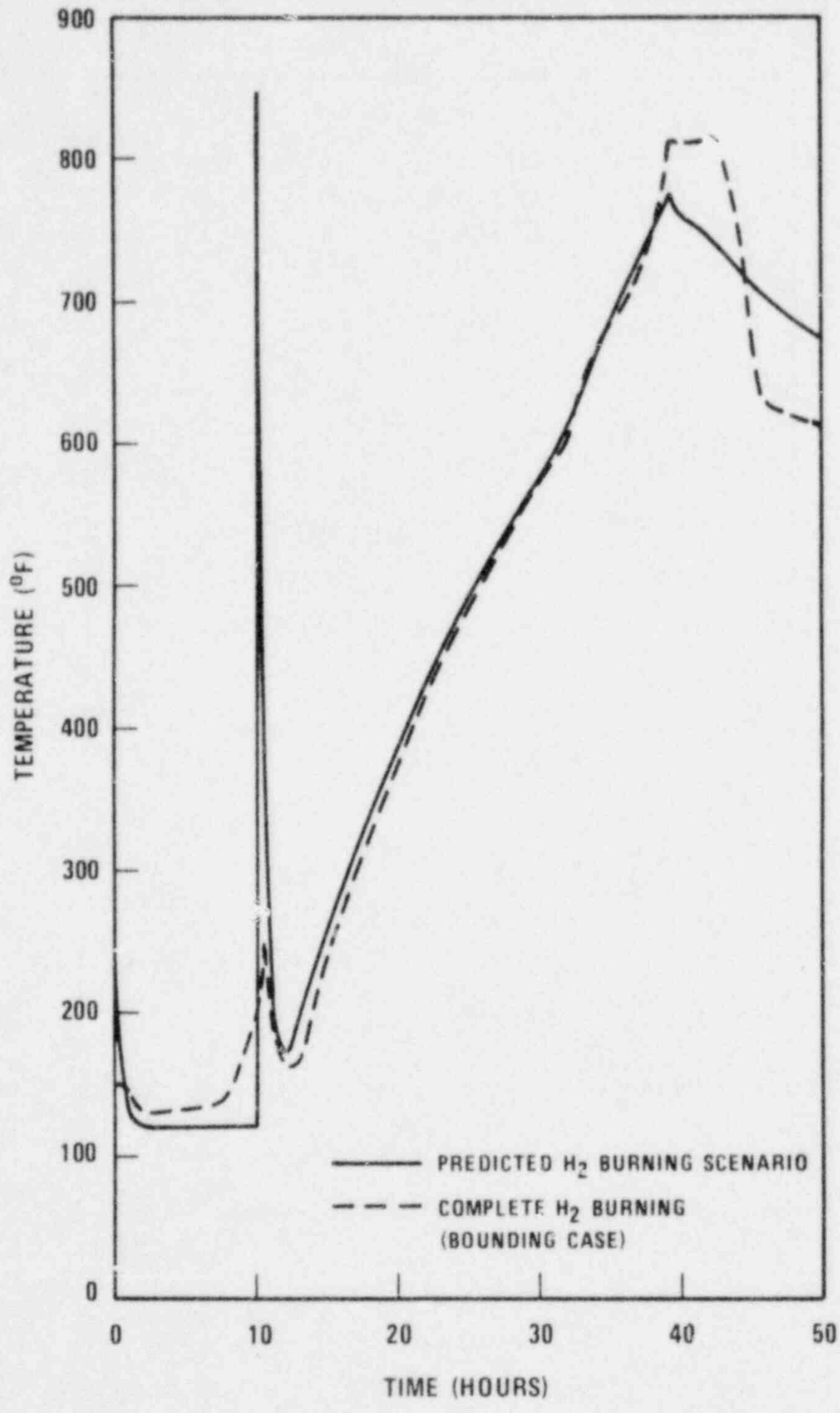

Figure H.1-7 Effect of Hydrogen Burning Assumptions on Containment Atmosphere Temperatures (Without Containment Venting and Purging)

1966-176

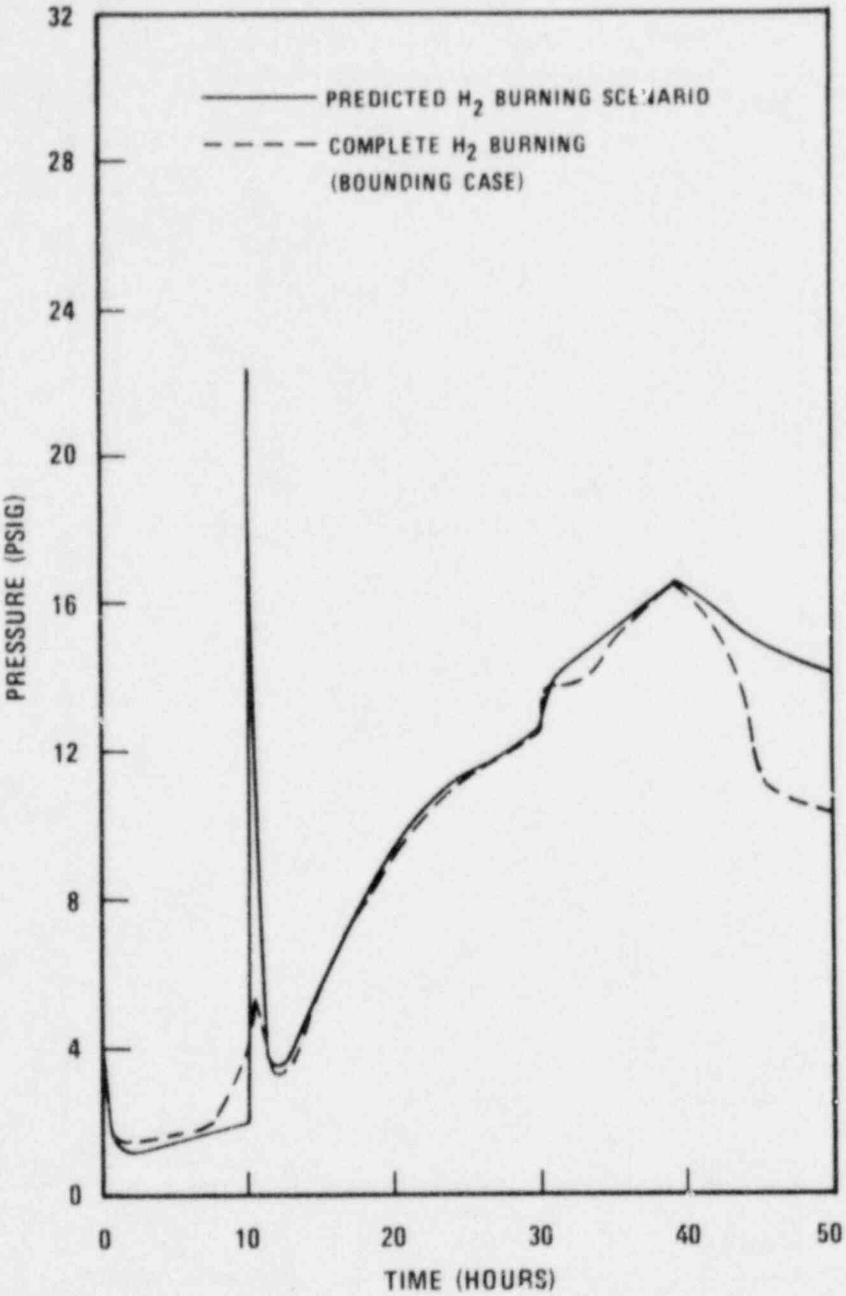

Figure H.1-8 Effect of Hydrogen Burning Assumptions on Containment Atmosphere Pressure (Without Containment Venting and Purging)

1966-177

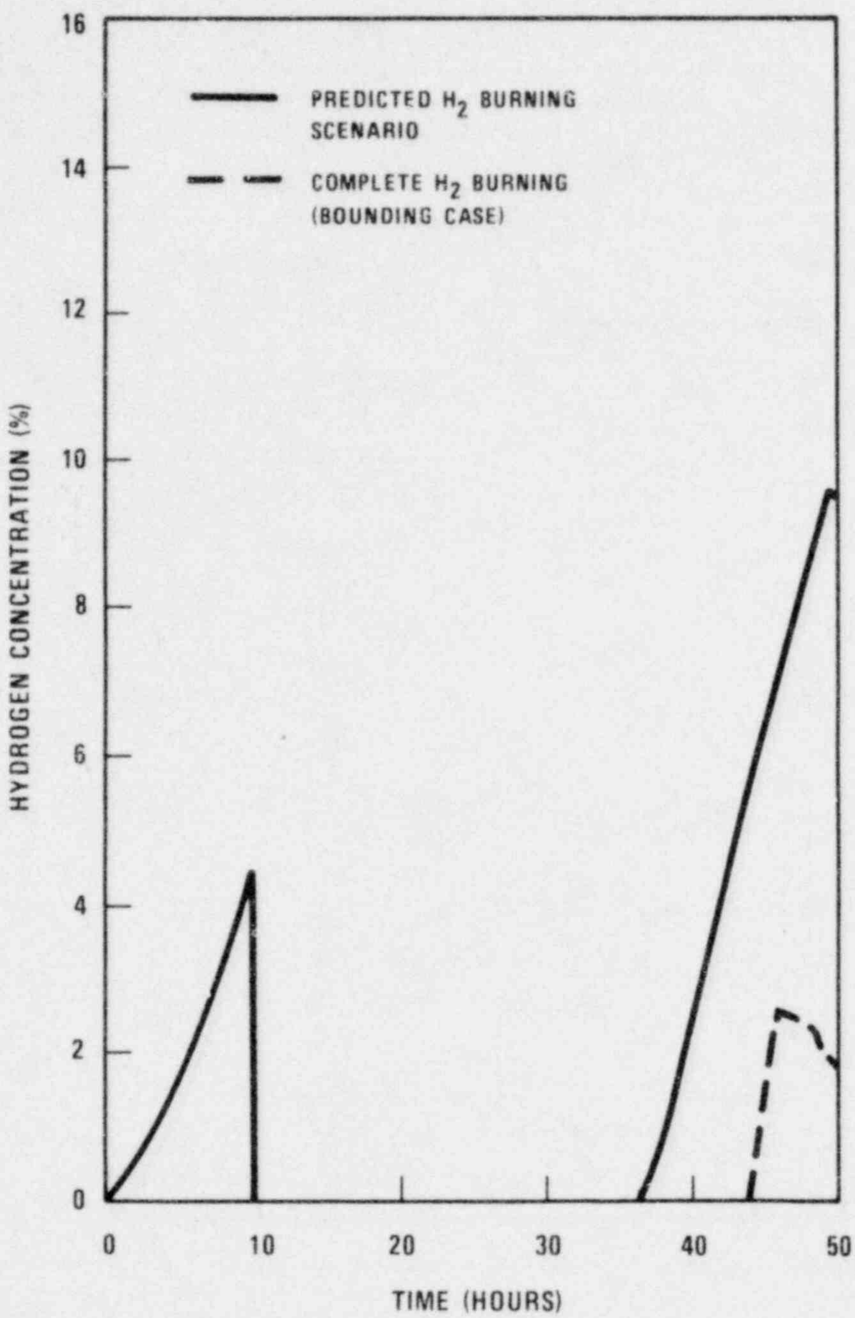

Figure H.1-9 Effect of Hydrogen Burning Assumptions on Containment Atmosphere Hydrogen Concentration (Without Containment Venting and Purging).

1966-178

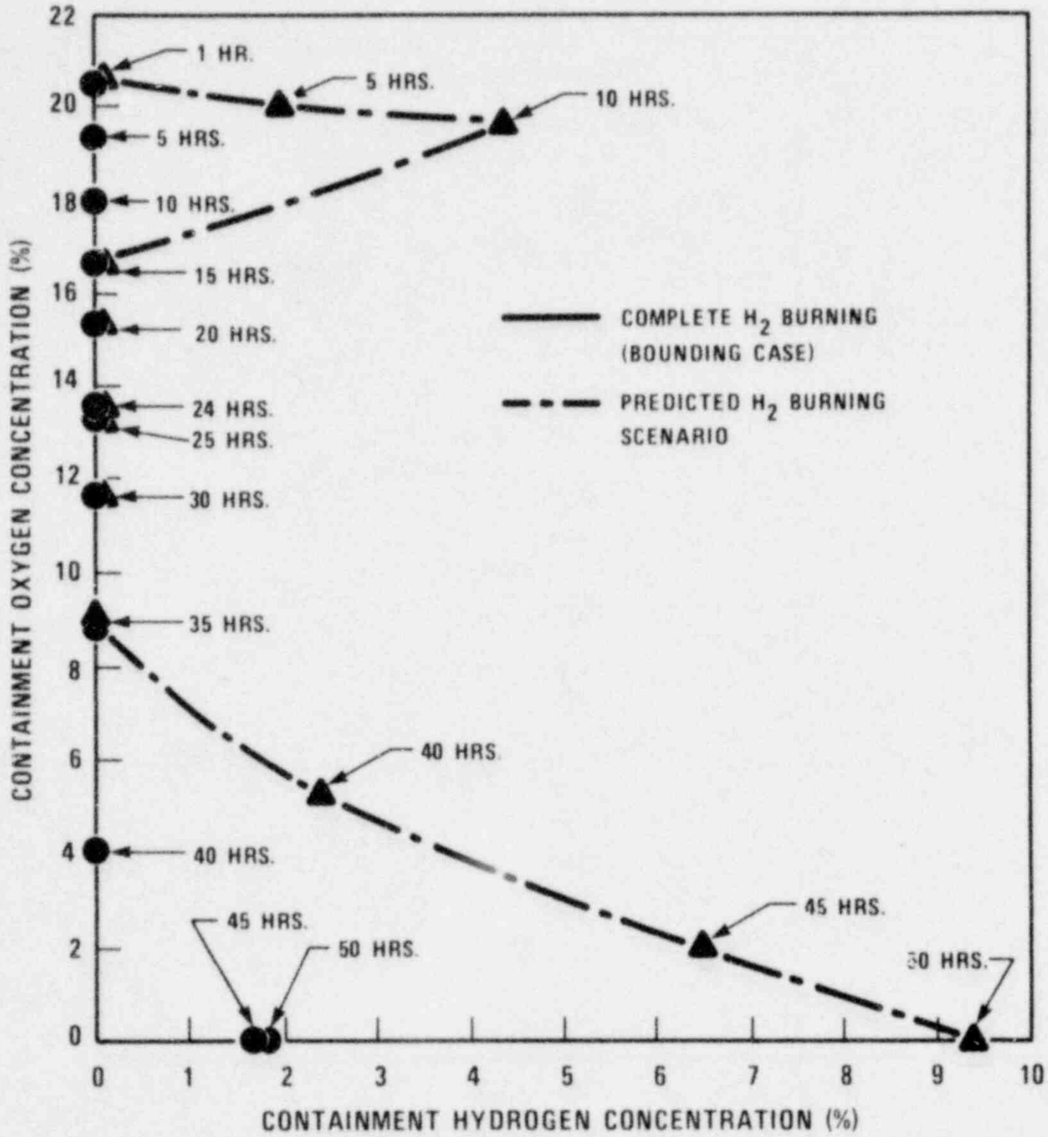

Figure H.1-10 Effect of Hydrogen Burning Assumptions on Containment Conditions With Respect to Flammability Limits (Without Containment Venting and Purging)

1966-179

H.2 FLAME LENGTHS FOR TMBDB SCENARIO

H.2.1 Introduction

The burning of a fuel, and the length of the ensuing flame, is a complex fluid flow-chemical kinetics problem. The length of a flame during fuel combustion is determined by the time required for the fuel to burn, and the distance that the reactants travel prior to complete combustion.

Combustion of gases such as sodium vapor and hydrogen occurs very readily when oxygen is present; thus, the time for complete combustion of either of these components is a function of the time required for sufficient oxygen to come in contact with either of the components. This in turn is determined by the flow characteristics of the gases, turbulent or laminar.

In the laminar flame depicted in Figure H.2-1(a), oxygen must diffuse from the surrounding atmosphere into the fuel jet, and a longer time is required for oxygen to reach the center of the jet than to reach the outer edges. Thus, the length of the flame is diffusion controlled. In a diffusion controlled flame, the distance the fluid travels before complete combustion occurs is determined by the volumetric flow rate.

If the flow is turbulent, the situation depicted in Figure H.2-1(b) exists. The oxygen is carried into the center of the fuel jet quite rapidly forming a homogeneous fuel-air mixture. For a given nozzle size, the turbulence intensity (and hence, the mixing) increases as the velocity of the fluid flowing through the nozzle increases. The time for complete mixing, which determines the flame length, has been found to be independent of the quantity of fluid flowing through the nozzle (so long as the flow is sufficient to be in the turbulent regime). Rather, it is a function of the diameter of the nozzle.

In the TMBDB scenario, flow through the reactor cavity vent pipe can, depending on the pipe size chosen, range from laminar to turbulent. Laminar flow is most likely to occur earlier in time when nitrogen has been totally expelled from the reactor cavity and sodium boiling has not yet commenced (see Figure H.2-2). At this time, the principal constituent of the fluid flowing from the reactor cavity is hydrogen which may be in the laminar flow regime. Approximately 19 hours after the initiation of the TMBDB event, sodium flow becomes dominant and the flow would be in the turbulent range for pipes having a diameter of approximately one foot.

Several variations on the reactor cavity to reactor containment building vent design are analyzed in the next section to show that sufficient flexibility exists so that an acceptable design can be provided.

H.2.2 Flame Length Calculation

H.2.2.1 Single Nozzle Configurations

Flame length calculations have been performed using the correlation presented in Chapter VII of Reference H.2-1. When flow through the vent pipe is in the laminar regime, equation 33 of Reference H.2-1 was used (see Appendix H.2.A). Laminar flow occurs when the principal constituent is hydrogen which, because of its low molecular weight, has a high volumetric flow rate per unit mass. From the correlation, it can be seen that the flame height is a function of the volumetric flow rate. Thus, the flame height will vary with time while the flow is in the laminar regime.

The length of a turbulent flame can be found from Equation 37 and Figure 255 of Reference H.2-1 (see Appendix H.2.A). From the correlation and the figure, it is apparent that in the turbulent regime, the height of the flame is a function of the nozzle (pipe) diameter, and the flame height is independent of the flow velocity. This results because the length of the flame is controlled by the rate at which oxygen can be mixed with the fuel while the fuel is flowing through the containment atmosphere. The longer the mixing time, the longer the flame length.

Higher velocities in the turbulent regime have two offsetting effects. The distance traveled by the gases in a given time is longer, and this, of itself, would tend to increase the flame length. However, in the turbulent flow regime, mixing occurs quite rapidly and mixing is enhanced by higher velocities which, of itself, decreases the flame length. Thus, for a given size nozzle, flame length is independent of flow velocity. As the nozzle becomes larger, the amount of material to be mixed increases; hence, the time for complete mixing and combustion increases with an increase in the flame length.

The length of the flame from the reactor cavity vent pipe in the TMBDB scenario would be a function of the composition of the fluid flowing from the pipe. The length of the turbulent flame is proportional to the square root of the ratio of the molecular weight of air to the average molecular weight of the fuel. Thus, a jet with a high hydrogen content would be expected to have a longer flame than a jet having a high sodium vapor content. Because of this, turbulent flame lengths were calculated for the extremes, pure hydrogen and pure sodium vapor.

These extremes are representative of the extremes predicted for the TMBDB scenario. Initially, there would be a high hydrogen and nitrogen content in the stream (mole basis) with the nitrogen being essentially depleted by the time that the hydrogen burning criteria are met at 10 hours. At 19 hours, sodium flow begins to be significant, and following the initiation of purging at 36 hours, sodium is the main constituent of the fluid flowing from the reactor cavity.

The calculated turbulent flame lengths range from 10-15 pipe diameters for the sodium flame up to 80 pipe diameters for the hydrogen flame. It should be noted that the value for hydrogen is consistent with the flame length measured in the HEDL autoignition tests; a 14-16 inch flame was observed for a 0.18 inch diameter nozzle (Reference H.2-2).

The height of the reactor containment building above the vent location is approximately 160 feet. Thus for pipe diameters up to one foot, a turbulent flame would always be well below the steel shell.

Figure H.2-3 shows flame heights as a function of time for pipe diameters of 1, 0.75, and 0.5 feet. As expected, the flame length at any point in time decreases with decreasing pipe diameter, caused primarily by the fact that flame length in the turbulent flow regime is a function of the pipe diameter.

A second factor influencing the flame length is that the smaller diameter piping produces a higher Reynolds number for a given flow:

$$Re = \frac{4Q}{\mu D \pi}$$

where

Q = mass flow rate, lb/hr

μ = viscosity, lb/ft-hr

D = pipe diameter, ft

Thus, transition from laminar to turbulent flow occurs at a lower mass (or volumetric) flowrate for the smaller diameter pipe. As the length of the laminar flame is proportional to the volumetric flowrate, the smaller diameter piping produces a shorter laminar flame.

At 19 hours, flow in the system consists essentially of sodium which has a much higher molecular weight than hydrogen, and the flow is in the turbulent regime. As the turbulent flame length is an inverse function of the molecular weight, the length of the sodium flame is only 10-15 pipe diameters, and there is a significant decrease in the flame length.

H.2.2.2 Multiple Nozzle Configurations

The flame heights shown in Figure H.2-3 were based on the assumption that the reactor cavity gases would flow into the containment building through a single pipe. If multiple pipes rather than a single outlet pipe were used (see

Figure H.2-4), the length of both the laminar flame and the turbulent flame could be reduced if the combined flow area of the multiple pipes were equal to the single pipe flow area.

The length of the laminar flame increases with the volumetric flow rate through a given nozzle. The use of multiple nozzles, rather than a single nozzle, reduces the volumetric flow rate through a given nozzle, thereby reducing the length of the flame.

The effect of the multiple nozzle arrangement on the length of the turbulent flame is a function of the nozzle diameter only. Thus, the smaller diameter outlet piping used in the multiple nozzle arrangement results in a reduced flame length.

Figure H.2-5 shows the effect of the multiple nozzles for a total flow area equivalent to a 1 foot diameter pipe (0.7853 ft^2). For turbulent flames, this arrangement is identical to reducing the pipe diameter. The individual nozzles have a smaller diameter than a single large nozzle, hence the turbulent flame is shorter.

Laminar flow using this arrangement exhibits a slightly different behavior. Because the flow is distributed among the three nozzles, the volumetric flow rate through each nozzle is lower, producing a shorter flame than the equivalent total flow through a single nozzle.

The reduction in individual nozzle diameter, however, decreases the Reynolds number*, thereby increasing the flowrate at which the transition from laminar to turbulent flow occurs. Thus at 15 hours flow through one or two nozzles

---

*$Re_n/Re_1 = \sqrt{1/n}$

where Re_n = Reynolds number for n pipes

Re_1 = Reynolds number for a single pipe would be turbulent while flow through three nozzles would be laminar, and at 19 hours the two and three nozzle arrangements both would have laminar flames which are longer than flame from a single nozzle which would have turbulent flow. These flames, however, wou.d be shorter than the maximum flame length calculated for the single nozzle because sodium, which has a shorter flame length would have become the dominant component at this time.

H.2.3 Effects on Containment

The effect of the flame on the containment shell will depend on the temperature of the combustion product gases when they come into contact with containment.

If there were no cooling of the product gases, and only a stoichiometric volume of air with the sodium or hydrogen, the temperature of the gases would be 3500-4000^{o}F. However, such high temperatures will not occur near the containment shell since mixing of the combustion gases and the cooler surrounding atmosphere will occur above the flame, causing the temperature of the resulting mixture to be much lower than the temperature within the flame.

A plot of average flame temperature as a function of flame length is given in Reference H.2-3 (see Figure H.2-6). It can be seen that the average flame temperature peaks near the middle of the flame and then drops off rapidly as the flame tip is approached. If it is assumed that the ambient temperature for the situation shown in Reference H.2-3 is approximately 100^{o}F, and that the composition of the product gases and the surrounding atmosphere is similar (i.e., they have similar thermal properties), an estimate of the amount of mixing that has occurred can be made.

The temperature of the mixture can be determined by taking a weighted average of the temperatures of the mixing streams:

$$T_{mix} = \frac{W_1T_1 + W_2T_2}{W_1 + W_2}$$

where

T_{mix} = temperature of mixture, ^{O}F
W_1 = weight of stream 1, lb
W_2 = weight of stream 2, lb
T_1 = temperature of stream 1, ^{O}F
T_2 = temperature of stream 2, ^{O}F

Using this principle, it is found that for the observed decrease of 1500^{O}F over a distance of one half the flame length 1.5 parts air are mixed with 1 part combustion gases. On this basis, the temperature of the gases contacting the containment shell, which is 3 flame lengths above the top of a forty foot hydrogen flame, would be 620^{O}F (ambient containment atmosphere temperature is $\sim$400^{O}F at 19 hours). For sodium burning, the containment shell is 20 flame lengths above the 7.5 foot flame, and the temperature of the gases contacting the containment shell would be 927^{O}F (900^{O}F ambient containment atmosphere temperature at 36 hours). These values are not significantly higher than the reactor containment building atmosphere temperatures calculated in the CACECO analysis. Thus, no detrimental effects on the containment shell would be expected to occur.

A similar calculation for the crane elevation, which is 1.5 flame lengths above the hydrogen flame and 12.3 flame lengths above the sodium flame, results in temperature estimates of 800^{O}F and 970^{O}F at 23 hours and 36 hours respectively. These values are not significantly different from the peak atmosphere temperature calculated in the CACECO analysis and no detrimental effects would be expected.

H.2.4 Conclusions

The maximum flame length that would be predicted to exist during the TMBDB scenario is 80 feet based on a one foot diameter single vent nozzle. This flame would come within 80 feet of the reactor containment dome, if unimpeded by anything in its path. There are at least two methods which can be used to reduce the length of the flame: 1) multiple outlet pipes, or 2) a smaller pipe diameter, with a six inch pipe being very effective.

The gases rising from the flame would be mixed with the surrounding atmosphere and would, at the time of contact with the containment shell, have a temperature near that of the containment atmosphere. Consequently, no adverse effects on the containment shell would be expected.

Based on these assessments, it appears that any detrimental effects that could be postulated from the flame contacting either the containment dome or other structures can be avoided by an appropriate design of the vent piping outlet.

H.2.5 References

H.2-1 B. Lewis and G. von Elbe, Combustion, Flames and Explosion of Gases, Academic Press, New York, 1961.

H.2-2 R. W. Wierman, "Experimental Study of Hydrogen Jet Ignition and Jet Extinguishment," HEDL-TME 78-80, April 1979.

H.2-3 J. Grummer, et al., Hydrogen Flare Stack Diffusion Flames: Low and High Flow Instabilities, Burning Rates, Dilution LImits, Temperatures, and Wind Effects, U.S. Bureau of Mines, Washington, D.C., 1970.

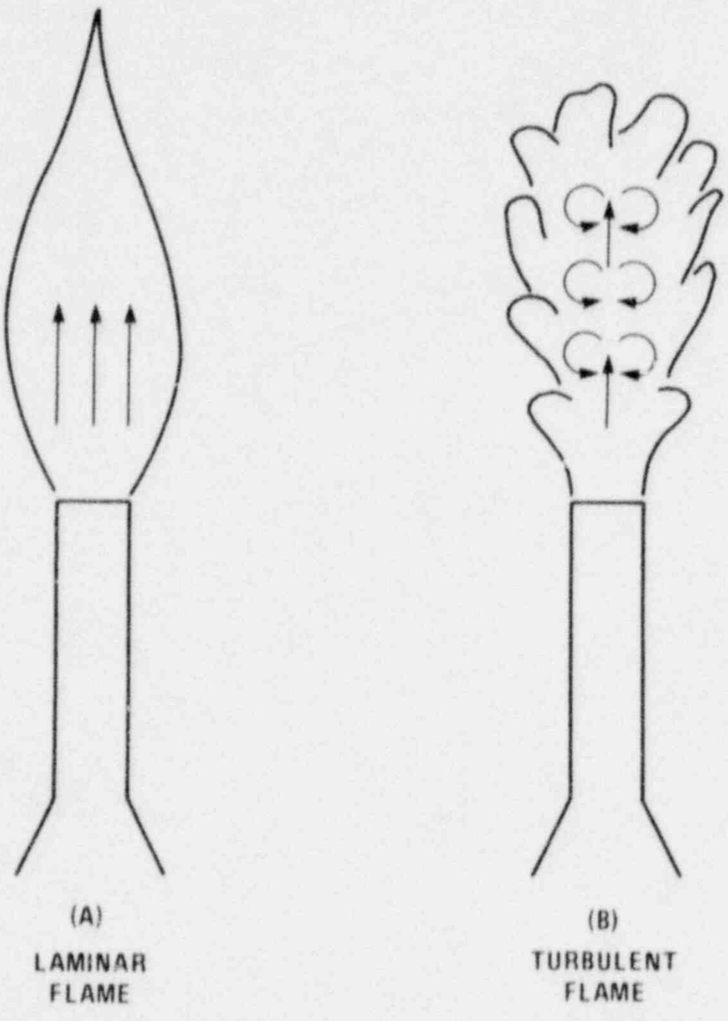

Figure H.2-1. Flow Patterns in Laminar and Turbulent Flames

1966-180

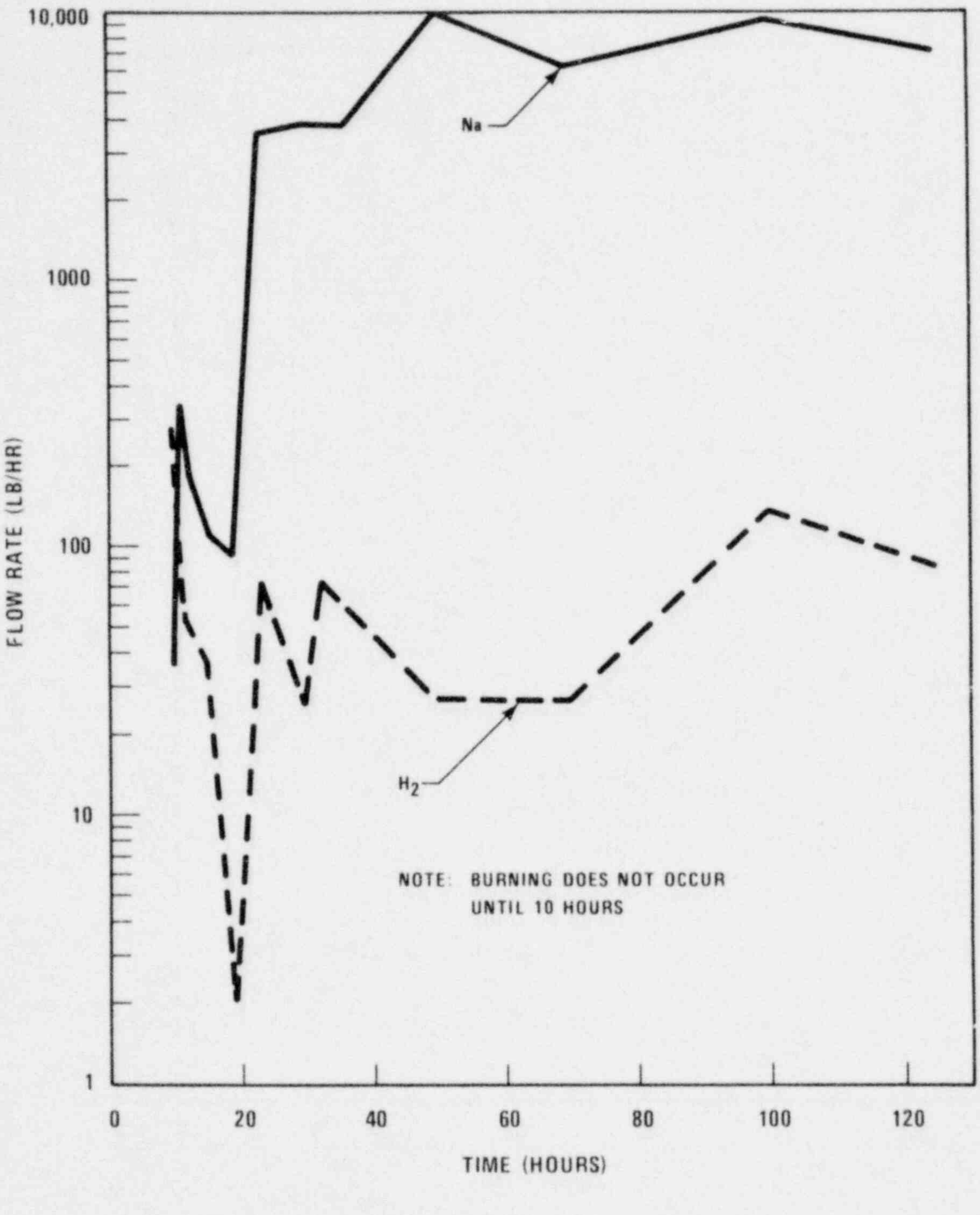

Figure H.2-2. TMBDB Mass Flow Rate Through the Reactor Cavity to RCB Vent

1966-181

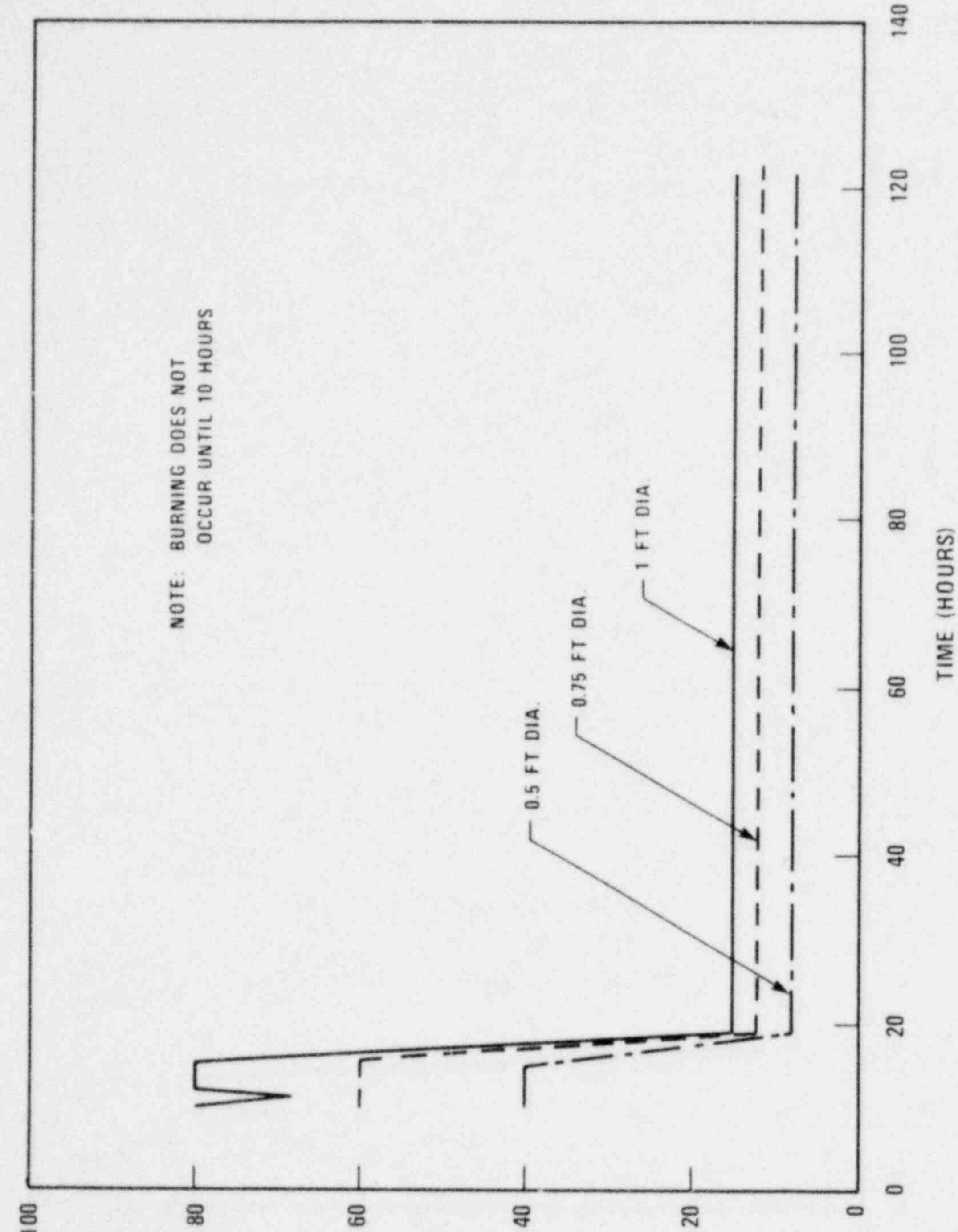

Figure H.2-3. Dependence of Flame Length on Nozzle Diameter

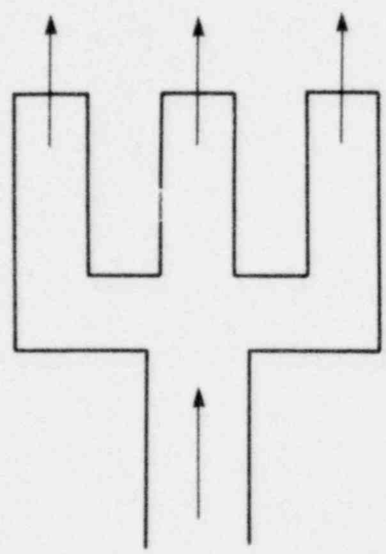

Figure H.2-4. Multiple Nozzle Arrangement

1966-183

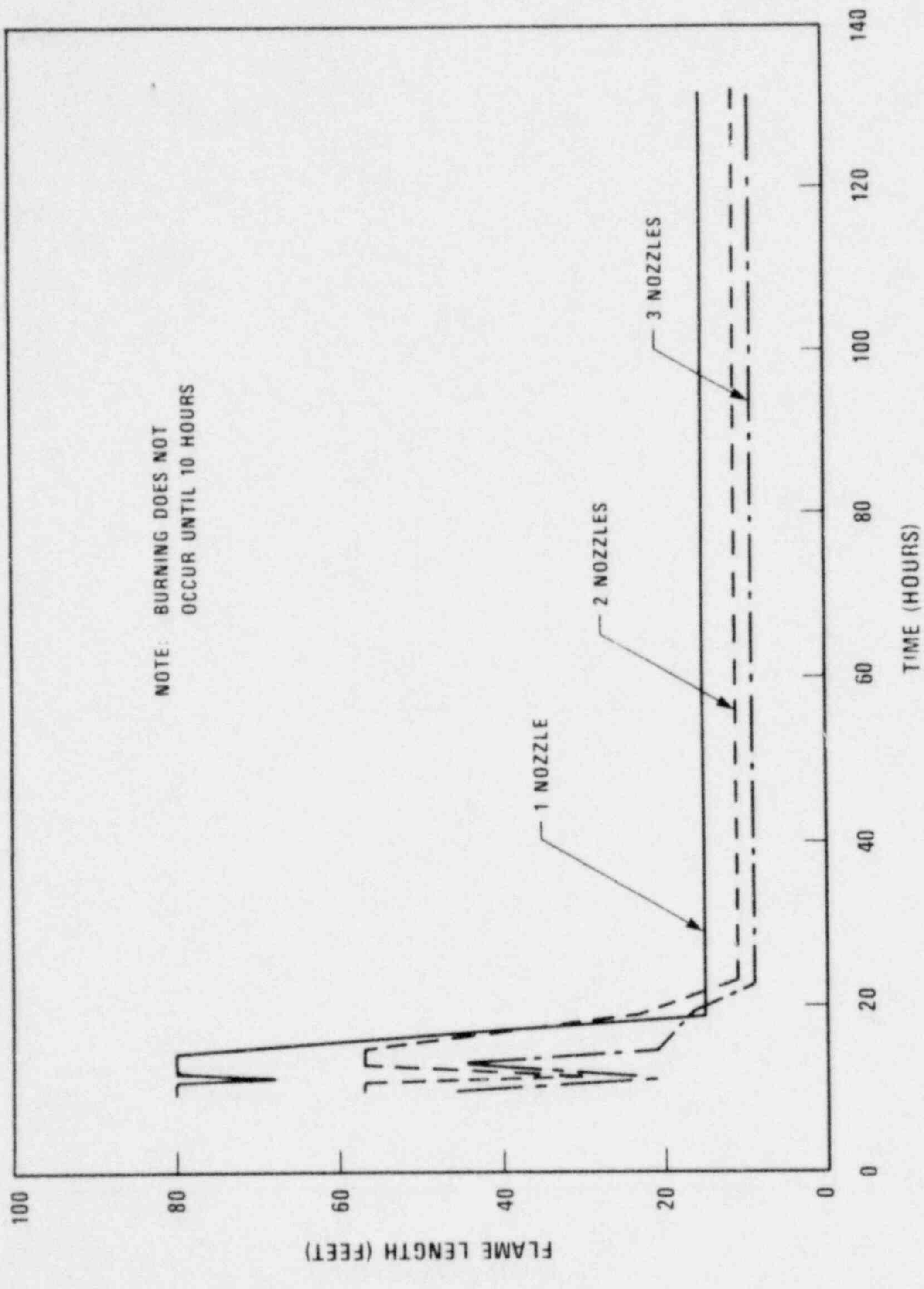

Figure H.2-5 Dependence of Flame Length of Number of Nozzles
(0.7853 FT^2 Total Area)

1966-184

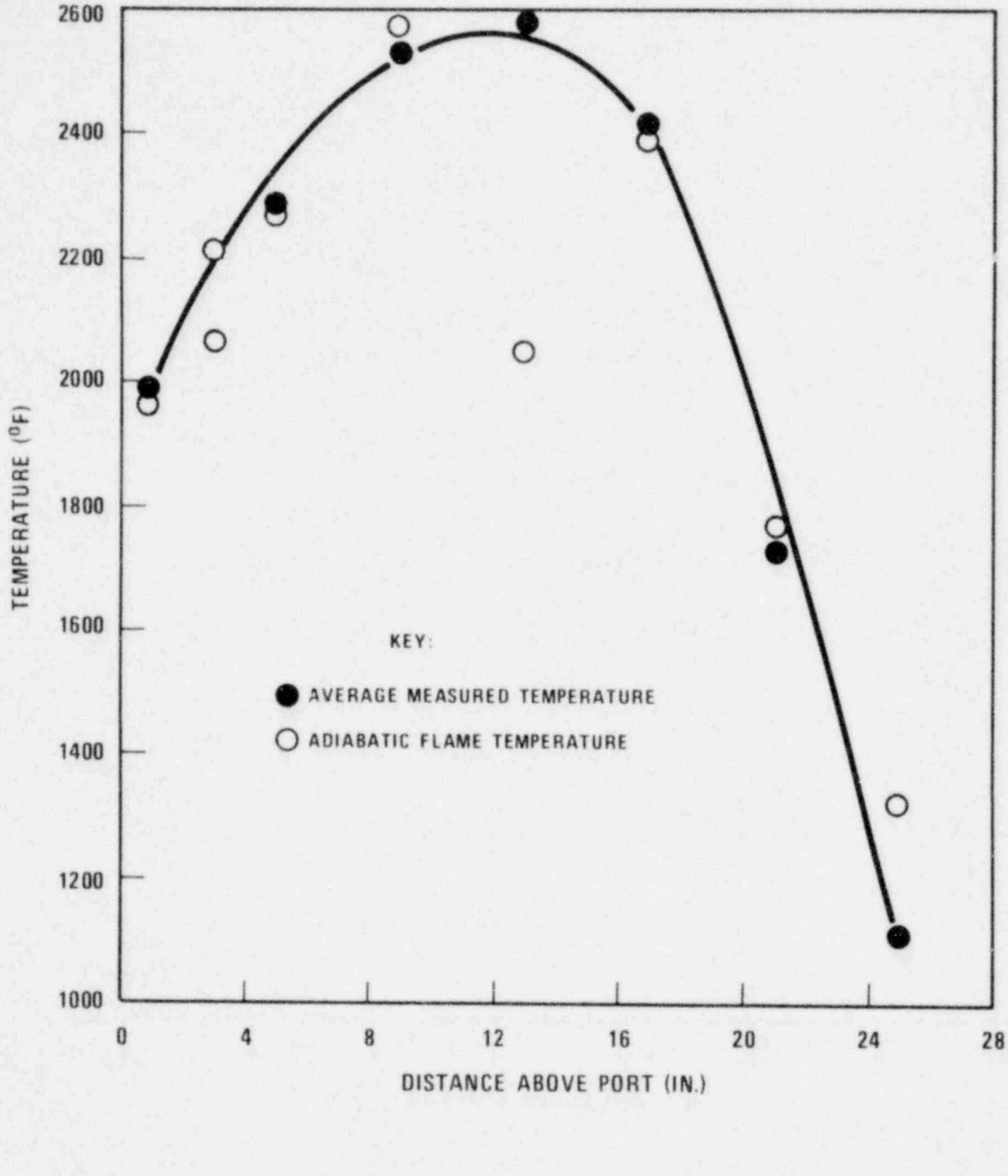

Figure H.2-6. Temperatures on Axis of a Hydrogen Diffusion Flame (Burner Diameter = 4 Inches, Flow Rate = 3.5 CFM)

1966-185

H.2.A Flame Length Correlation

H.2.A.1 Laminar Flame Length

Equation 33 of Reference H.2-1:

$$L = 1/(2(\pi k C_f/V(1-C_f/2))^{1/2} + 2\pi D_o C_f/V(1-C_f/2))$$

where

k = proportionality factor for diffusivity changes along the length of the flame*

C_f = molar concentration of nozzle fluid at the flame tip (same as C_t in Turbulent Correlation)

V = volumetric flow rate, ft^3/sec

D_o = diffusivity at fuel jet inlet temperature, ft^2/sec

H.2.A.2 Turbulent Flame Length

Equation 37 of Reference H.2-1:

$$2y_f/d = \frac{1}{C_t}\sqrt{\frac{T_f}{\alpha_t T_n}\left(C_t + (1-C_t)\frac{M_s}{M_n}\right)}$$

where

$2y_f/d$ = parameter plotted against L/d on Figure 255 of Reference H.2-1 (Figure H.2.A-1)

C_t = mole fraction of nozzle fluid in the designated plane

T_f = adiabatic flame temperature of the fuel, ^oR

α_t = stoichiometric ratio of reactants to products

M_s = average molecular weight of the fluid surrounding the fuel jet

*k was found by $(D_f-D_o)/L$ where D_f is the diffusivity at the adiabatic flame temperature.

M_n = average molecular weight of the nozzle fluid
T_n = temperature of the nozzle fluid, ^{o}R

H.2.A.3 Validity of Correlation

The correlations used in this study were based on experiments using nozzles of 0.4 inches or less. However, experimental information on flames from large nozzles are reported in Reference H.2-3. In this study, laminar flames of 3.2 and 6.2 feet (0.66 and 0.916 cfm respectively) were obtained using a 12 inch diameter stack, and a turbulent flame of 62-63 feet was obtained using a 31 inch diameter stack.* Comparison of these observed values with calculated values indicates that the correlation used in the evaluation may overpredict flame height.

The calculated flame height for a turbulent flame emanating from a 30 inch stack would be 80 pipe diameters, or 200 feet, while the measured value was 62-63 feet, an overprediction of a factor of three. Calculated laminar flame lengths are 9.4 feet (0.66 cfm) and 13.9 feet (0.916 cfm) versus measured lengths of 3.2 and 6.2 feet. Thus the laminar flame length correlation overpredicts the observed values by a factor of 2.2 and 2.9, values which are comparable to the factor of 3 overprediction for the turbulent correlation.

The foregoing analyses indicate that the Reference H.2-1 correlation can be used as a conservative estimate of flame lengths, since the experimentally observed flame lengths for large diameter nozzles are less than predicted by the correlations.

---

*An additional test involving supersonic flow resulted in a 275-330 foot flame for the 31 inch diameter stack. However, this test clearly is not prototypic of CRBR flow conditions.

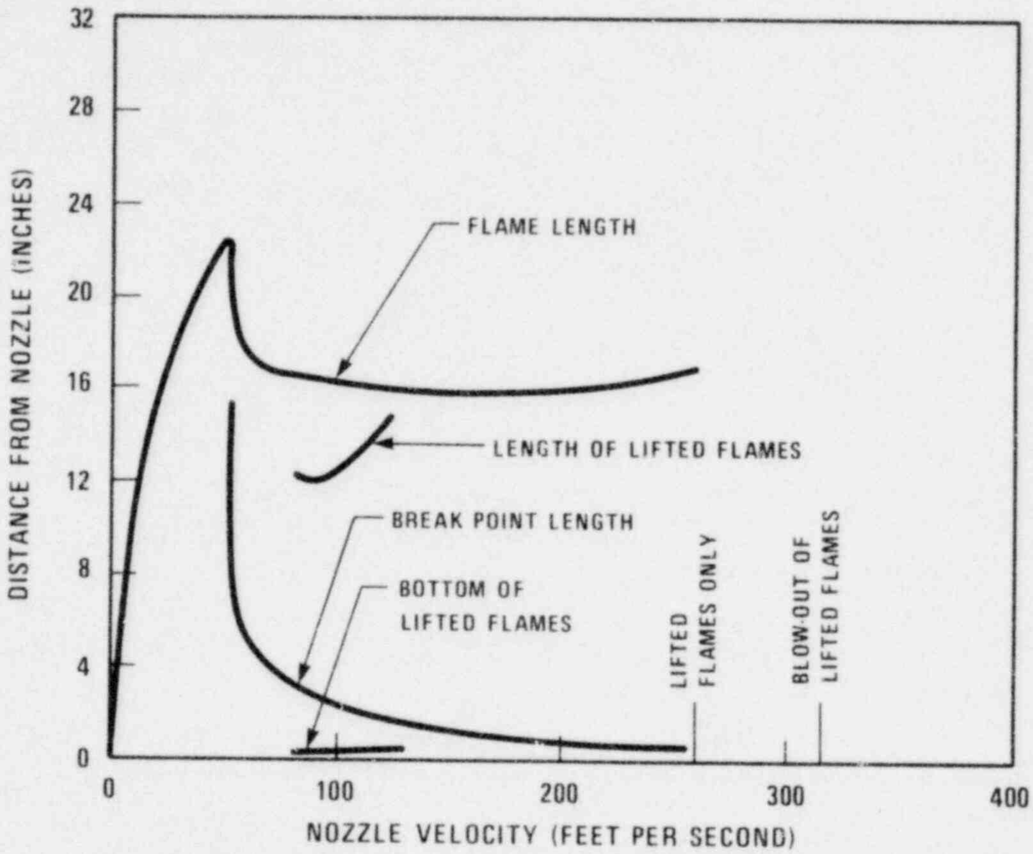

NOTE: CITY GAS, AVERAGE MOL. WEIGHT 19.7; STOICHIOMETRIC RATIO OF AIR TO FUEL, APPROXIMATELY 4.5; NOZZLE DIAMETER, 1/8 IN. (HOTTEL AND HAWTHORNE)

Figure H.2.A-2. Effect of Nozzle Velocity on Flame Length (Figure 246 of Reference H.2-1)

1966-187

APPENDIX I

ASSESSMENT OF CONSEQUENCES OF FUEL IN PHTS PIPING FOLLOWING REACTOR VESSEL DRAINING

I.1 INTRODUCTION

Section 3.1 describes the assessment of fuel debris transport following an HCDA. Based on an estimate that 70% of the fuel could be ejected upward from the core, and using the particle distribution measured in the M-3 test (which is considered to be representative of fuel-coolant interactions in the upper reactor vessel plenum), 18% of the core fuel was predicted to enter the reactor vessel outlet piping. This prediction is considered to be conservative since it assumes that the 70% fuel is all ejected from the core at the time the first fuel is predicted to be ejected. If fuel melting and ejection occurs over a longer timescale (as is more likely), the reduced flow (as a result of the flow coastdown) would sweep less fuel into the outlet piping.

Of the 18% fuel predicted to enter the outlet piping, most is predicted to settle in the piping between the reactor vessel outlet nozzles and the bellows that separates the pipeway cells from the PHTS cells, while less than 0.1% is predicted to settle in the section of piping between the bellows and the pump.

The fuel debris that remains in-vessel (82%) would settle on surfaces such as the reactor vessel lower head. Sufficient depth of fuel debris may exist to result in bed dryout and failure of the lower head of the reactor vessel and guard vessel. This would result in draining of sodium from the reactor vessel and primary heat transport system. Although draining of the piping may sweep some of the settled fuel within the PHTS piping into the reactor vessel, the quantity cannot be predicted accurately. Therefore, this assessment of the consequences of fuel in the PHTS piping following vessel draining is based on the quantity of fuel predicted to enter the PHTS piping.

As a sensitivity study, Section 3.1 also considered fuel transport based on the particle size distribution from the EDT-1 test, which resulted in the highest percentage of "fines". For that distribution, 25% of the fuel was predicted to enter the outlet piping, of which 12% settled in the piping before the PHTS bellows, 2% settled in the piping between the bellows and the pump and 6% was carried as far as the IHX. Although the EDT-1 distribution is not considered as representative of post-HCDA conditions as the M-3 distribution, some consideration is given to it as a sensitivity evaluation in Section I.4 of this Appendix.

The decay heat used is that associated with the entire core and all blanket assemblies less the amount attributable to the halogens and volatiles. The calculations assume an initial time of 1000 seconds.

I.2 EFFECT ON PHTS PIPING

When the fuel in the piping is uncovered as a result of sodium draining, the debris bed would still be a heat generating mass. If this heat is not removed, the piping temperature would increase and, eventually, melt the piping in which the debris is contained. The heat removal path from the debris bed after sodium drainage would be radially through both the pipe and the piping insulation to the atmosphere surrounding the pipe.

The locations at which the heat removal through the pipe wall and insulation is less than the heat production within the debris bed were calculated. Melt-through of the pipe would be expected at these locations. For this evaluation, the data from Tables I-1 and I-2 were used.

The evaluation was performed by calculating the temperature transient of a steel pipe initially at 1000°F which contains a varying quantity of fuel. The amount of fuel was varied until the minimum quantity that would result in a pipe melt-through was determined. This amount was then compared with the data of Table I-1, and the potential locations for a melt-through were determined.

Heat transfer from the pipe was calculated using the one-dimensional heat transfer equation in cylindrical coordinates.

$$\rho C \left(\frac{\partial T}{\partial t}\right) = k \ \frac{1}{r} \ \frac{\partial}{\partial r} \ \left(r \frac{\partial T}{\partial r}\right) \quad + Q_v$$

ρ = density of the material, lb/ft^3
C = heat capacity, Btu/lb
k = thermal conductivity, Btu/hr-ft-°F
r = radial distance, ft
T = temperature, °F
t = time, hr
Q_v = material volumetric heat generation, Btu/ft^3 hr

Because there are three materials to be considered, (see Figure I-1), three separate equations, one for each material, are necessary. However, because of the relatively thin, highly conductive pipe, some simplfication can be made.

By assuming that the pipe temperature is radially uniform (reasonable approximation because of the high conductivity) and calculating an overall heat transfer coefficient based on air gap conductivity, insulation conductivity, and the heat transfer coefficient to the cell atmosphere, the number of equations can be reduced to one, which is then solved numerically.*

As can be seen from Table I-3 and Figure I-2 a potential melt-through region exists in the reactor cavity pipeway cell, where a fuel volume of 0.3846 ft^3/ft exceeds the allowable value of 0.013 ft^3/ft. In the PHTS cells, the maximum concentration is predicted to be 0.004 ft^3/ft; therefore, no piping penetration in that area is predicted. Thus, following draining of the sodium from the reactor vessel and PHTS system, fuel debris could melt through the piping within the three pipeway cells but is not predicted to melt through the piping within the PHTS cells.

*It should be noted that the use of a single one-dimensional equation implies circumferential temperature uniformity, which is a reasonable approximation because of radiation heat transfer from the fuel to the pipe and the high conductivity of the pipe.

I.3 EFFECT ON CELL LINERS

Fuel which penetrates the piping would fall onto the piping insulation. The temperature of the fuel would continue to rise until the insulation is penetrated. This could occur when the fuel approaches the fusion temperature of the insulation ($\sim 3500^oF$). The debris material would then fall onto the cell liner and result in a thermal transient in the liner.

An analysis of the cell liner thermal transient has been conducted using the fuel debris distribution data given in Table I-1. The quantity of material at the peak location in the reactor cavity is first converted to an equivalent cell liner area coverage by calculating the chord length of the pipe segment in which the debris has deposited (see Figure I-3 and Table I-4). The fuel debris in the piping is then assu o fall onto the floor directly under the pipe segment with no further spreading cf the debris. (If the fuel debris is in the form of fine particles, considerably greater spreading would be anticipated.) After the fuel drops onto the floor immediately under the pipe, heat would be removed from the fuel by conduction into the cell liner with which it is in direct contact, and by radiation to the surrounding structures. Because the fuel concentration varies with location, a parametric study was performed to determine the liner temperature as a function of fuel density on the liner. The results of this study then permit an assessment of liner effects when the quantity of fuel in a piping section is known.

For this parametric study, two physical conditions of the debris on the floor have been assumed: (1) the fuel forms a dry 50% porous bed and (2) the fuel forms a 100% solid bed. These values represent a typical condition of the bed when it is covered by sodium ($\sim$50% porous) and the maximum fuel density that could exist in the bed (fully compacted fuel). The latter assumption is made to allow for physical and thermal effects which may cause a porosity reduction during the transition from a sodium covered bed to a dry bed and during the piping and insulation melt-through.

The calculations were performed using the TRUMP computer code, utilizing the model shown schematically in Figure I-4. In this model, the fuel, which is treated as a heat generating node, is in direct contact with the steel liner which is in contact with an underlayer of insulating gravel and structural concrete. There is also thermal communication between the fuel and the surrounding walls via radiation. For these calculations, the area of the surrounding walls has been set at 1000 ft^2, a value which approximates the wall area in the pipeway cell on the PHTS cell side of the wall separating the reactor cavity from the PHTS cell. The results of the parametric analyses are summarized in Figure I-5 which gives the peak steel temperature reached during the transient as a function of the fuel concentration on the liner.

Since fuel is not predicted to penetrate the piping within the PHTS cells, liner penetration analyses are not applicable in that area. In the reactor cavity pipeway cells, the concentration of fuel on the floor is predicted to exceed 0.15 ft^3/ft^2. As can be seen from Figure I-5, penetration of this section of the cell liner would be predicted. The penetration is estimated to extend the length of the pipeway cells The consequences of early pipeway cell floor liner failures on containment conditions are given in Appendix F.7.

I.4 SENSITIVITY ASSESSMENT OF FUEL IN PHTS PIPING

As can be seen from Table I-1, the quantity of fuel predicted to settle in the piping is dependent on the particle size distribution of the fuel debris in the upper plenum of the reactor vessel. To assess the sensitivity of the results to the particle size distribution, an evaluation identical to that delineated in Section I.2 and I.3 was performed using the finest debris distribution observed experimentally, the distribution obtained from the EDT-1 test. Because the concentration of fuel in the PHTS cell piping for this distribution is considerably higher than that estimated for the M-3 test (see Table I-1), it is estimated that a section of piping ~9 feet in length would melt.

From the data of Table I-4 and Figure I-5, the fuel concentration based on the EDT-1 distribution would result in liner temperatures in the range of approximately 2000°F, close to the melting point of steel, depending on the porosity of the fuel debris mass. At these higher fuel volumes, the heat generated in the center region of the fuel mass cannot be adequately conducted to the surfaces where it would be removed by either radiation to the surrounding structures or conduction into the steel liner. As a result, the temperature of the fuel rises with a concurrent rise in the steel temperature. This effect becomes even more pronounced with a porous bed which has reduced conductivity as a result of the voids within the bed. On the basis of the preceding, it is concluded that PHTS liner penetration would not occur for the M-3 and some range of smaller particle size distributions but becomes questionable as the EDT-1 distribution is approached.

The evaluation of the reactor cavity pipeway cell remains as before, with a penetration of the cell liner being predicted.

IMAGE EVALUATION
TEST TARGET (MT-3)

6"

MICROCOPY RESOLUTION TEST CHART

TABLE I-1

DISTRIBUTION OF UPWARD EJECTED DEBRIS FOR LOF HCDA

Material	Particle Size Distribution	Volume Ejected Upward (ft^3)	Volume Remaining In-Vessel (ft^3)	Post-Accident Distribution of Debris (ft^3 per loop): Piping Prior to PHTS Cell Wall	Between PHTS Cell Wall and Pump	Between Pump and IHX	IHX
Fuel and Blanket	M-3	74.0	54.5	6.5	<0.1	0.	0.
	EDT-1	74.0	46.9	6.0	0.8	0.	2.2
Steel*	M-3	40.6	37.6	0.78	0.06	C.	0.16
	EDT-1	40.6	37.6	0.84	0.14	0.	0.02

DEBRIS BED CHARACTERIZATION

	Particle Size Distribution	Piping Prior to PHTS Cell W-ll	Between PHTS Cell Wall and Pump	Between Pump and IHX
Maximum Bed Depth (Fuel and Steel) (ft)	M-3	0.497	Negligible	0.
	EDT-1	0.367	0.213	0.
Maximum Bed Loading (Kg UO_2/m^2)	M-3	757.	Negligible	0.
	EDT-1	559.	324.	0.

*Steel values are based on an earlier analysis which used a flow coastdown curve higher than that presently used for the fuel. Sensitivity studies show that this has negligible impact on the final fuel distribution as the amount of steel entering the piping would be reduced.

TABLE I-2

HEAT GENERATION AS A FUNCTION OF TIME FOR TOTAL CORE AND BLANKETS

Time (Hours)	Q, $(10)^7$ Btu/hr	Qv, $(10)^5$ Btu/hr-ft^3
0.	5.14	4.72
.2	4.36	4.00
.7	3.63	3.33
1.7	3.10	2.85
11.7	2.05	1.88
23.7	1.72	1.58
95.7	1.03	0.95
239.7	0.69	0.63

Note: t_o is 1000 seconds after event initiation.

TABLE I-3

PARAMETERS FOR PIPE MELTING ANALYSIS

Particle Size Distribution	Location Of Pipe Analyzed	Maximum Bed Depth, ft. (50% Porous)	Volume of Bed ft^3/ft (50% Porous)	Quantity of Fuel ft^3/ft
M-3	Reactor Cavity Pipeway Cell	0.497	0.7692	0.3846
EDT-1	PHTS Cell	0.213	0.2226	0.1113

TABLE I-4

FLOOR PENETRATION ANALYSIS PARAMETERS

Particle Size Distribution	Location Of Liner Analyzed	Fuel Volume ft^3/ft	Chord Length (50% Porous)*	Chord Length 0% Porous*	Density of Fuel on Floor ft^3/ft^2 50% Porous*	Density of Fuel on Floor ft^3/ft^2 0% Porous*
M-3	Reactor Cavity Pipeway Cell	0.3846	2.236	1.826	0.172	0.2106
EDT-1	PHTS Cell	0.1113	1.541	1.235	0.0722	0.0901

*Refers to condition while in the piping prior to melt-through.

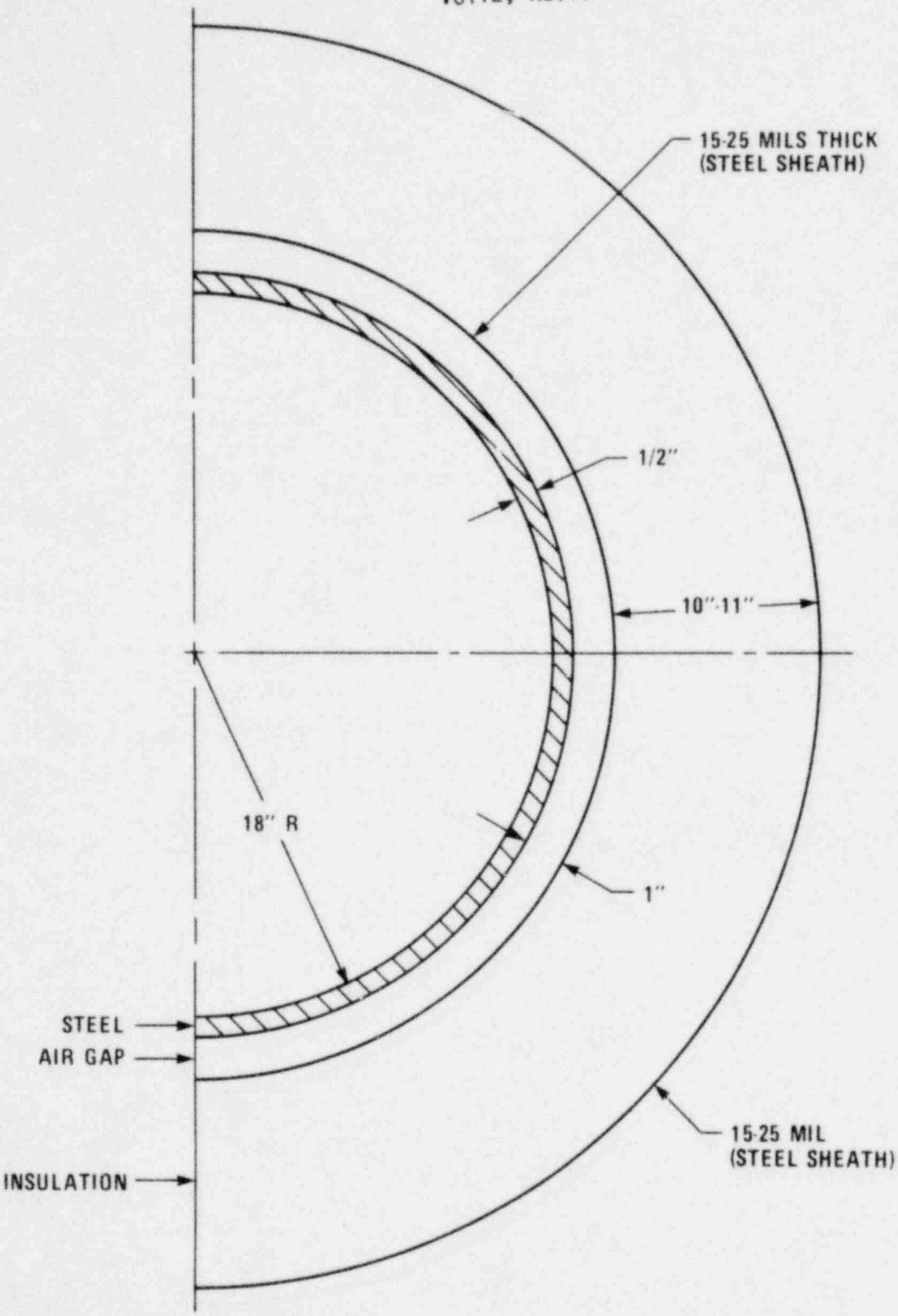

Figure I-1. PHTS Pipe and Insulation Configuration

1966-188

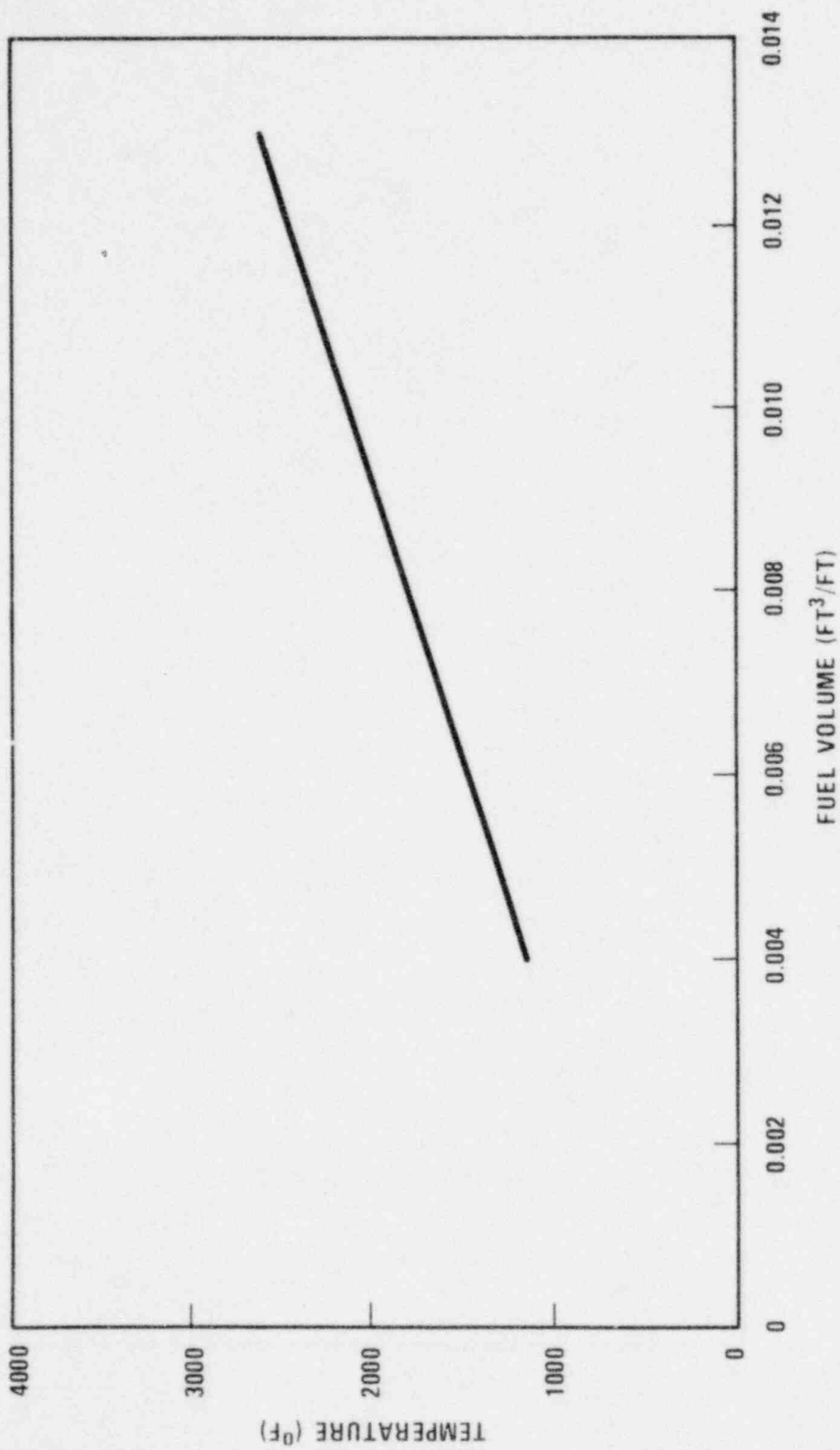

Figure I-2. Peak Pipe Temperature versus Fuel Content

1966-189

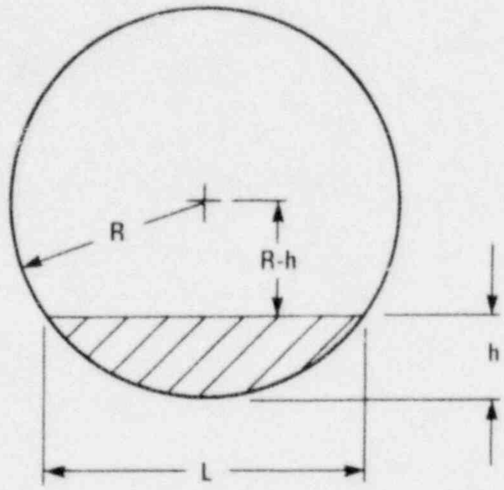

$$V/FT = R^2 \cos^{-1} \frac{R-h}{R} - (R-h)\ (2Rh - h^2)^{1/2}$$

$$L = 2\,R\,\cos(\sin^{-1} \frac{R-h}{R})$$

$R = 1.5$ FT.

$h = .213$ FT.

$V/FT. = .2226\ FT.^3/FT.$

$L = 1.541$

$$\rho = \frac{(.2226)\ (.5)}{1.541} = 0.0722$$

Figure I-3. Sketch of Fuel Debris in Pipe

1966-190

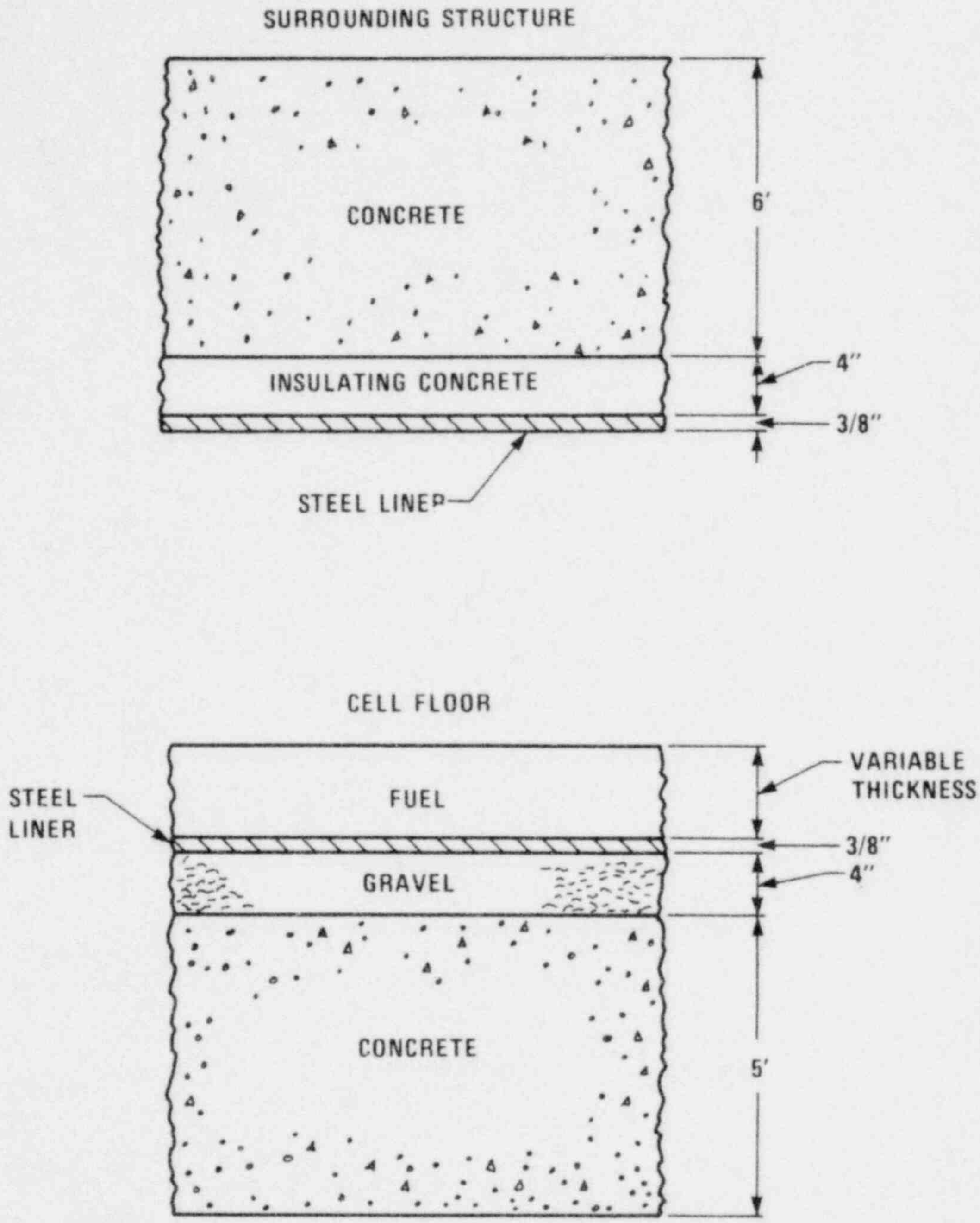

Figure I-4. Cell Liner Thermal Model Schematic

1966-191

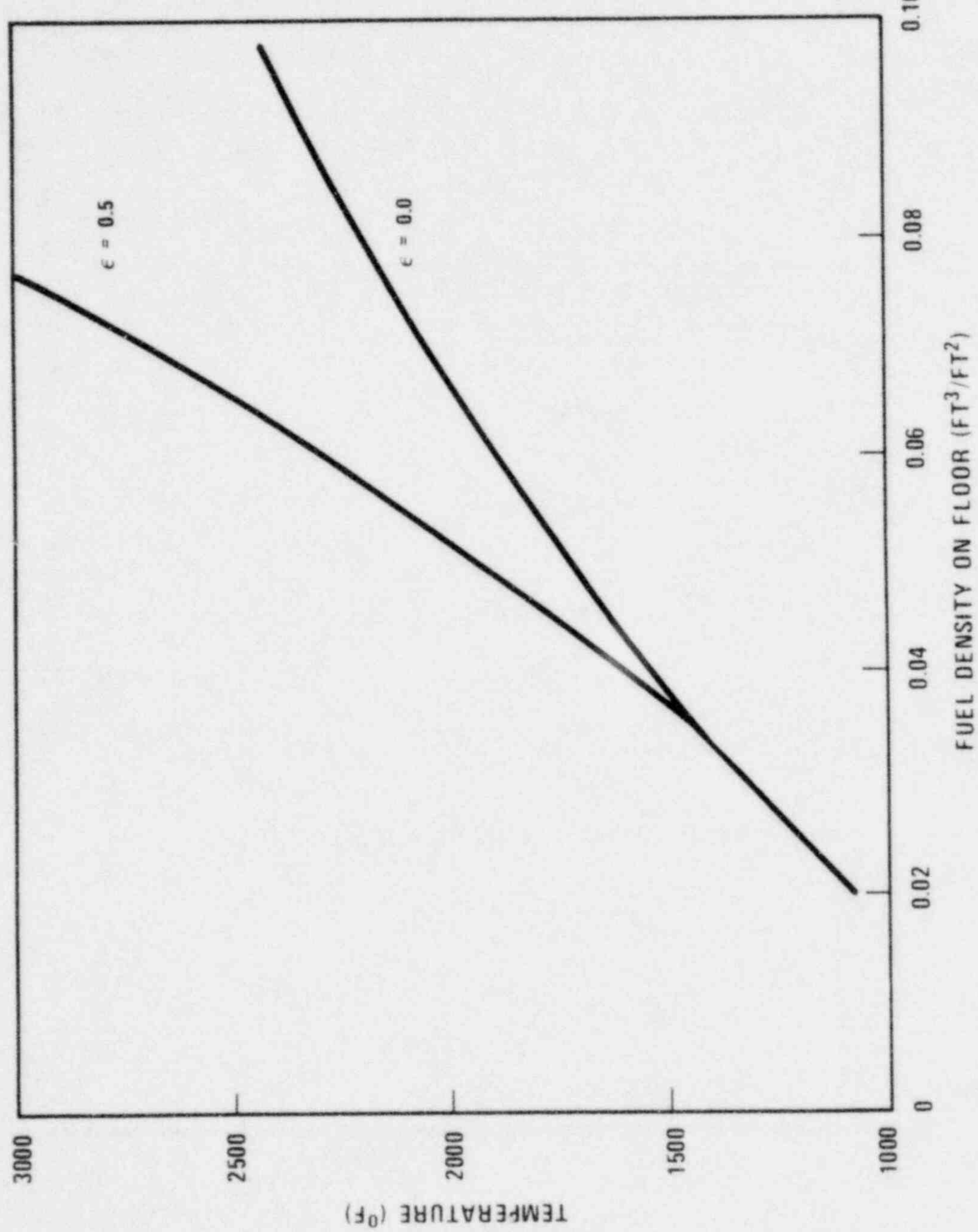

Figure I-5. Liner Mid-Plane Peak Temperature versus Fuel Density

APPENDIX J

NRC'S REQUESTS FOR ADDITIONAL INFORMATION (RAI'S) ON CORE MELTDOWN CONSIDERATIONS

Since the Project's initial submittal of the PSAR on April 10, 1975, the Project has received several RAI's from the NRC. During the same time period, revisions to the PSAR have been made and, in many cases, these revisions respond to the RAI's or alter their basis. Many of the RAI's concern the plant's capability to deal with the effects of hypothetical core disruptive accidents (HCDA's). This appendix is provided to lend clarification to the manner in which each of the RAI's on the subject of core melt has been responded to and the location of that response.

The initial submittal of the PSAR addressed the accommodation of HCDA's in Appendix F. This appendix was considered as a parallel design approach which implied that the accommodation of HCDA's was a design basis accident. In April 1976, the Project submitted the report, "Third Level Thermal Margins in the CRBRP." This report assessed the consequences of HCDA's when these events are evaluated on a realistic basis (Class 9, events beyond the design basis). It became obvious that two separate plant designs could not be properly reviewed and a merging of the reference and parallel designs was effected.

On May 6, 1976, the NRC and the Project reached agreement that the probability of HCDA's can and must be reduced to a sufficiently low level to justify their exclusion from the design basis accident spectrum and that the PSAR should reflect this as the single design approach.

The CRBRP-3 document (Vols. 1 and 2) is thus designed to revise and recast all information addressing HCDA's as DBA's and to compile the currently relevant information into this single document. This document addresses the issues relating to RAI's on HCDA's from energetics (CRBRP-3, Vol. 1) to longer term accommodation (CRBRP-3, Vol. 2), but does not necessarily point out the specific location of responses to RAI's. This appendix provides tabulations of the RAI's generally addressed by CRBRP-3, Vol. 2, as follows:

A. This list is a compilation of RAI's from the NRC concerning PSAR Appendix F, "Core Disruptive Accident Accommodation." Many of the questions concern features which are no longer part of the CRBRP TMBDB design, thus they are not applicable. They are, however, listed here for completeness.

001.433	222.90 thru 222.94
001.500 thru 001.536	222.96
001.558	222.97
001.566	310.33
020.40 thru 020.43	
110.57	
130.42	
130.46	
130.47	

B. This list is a compilation of RAI's from NRC on the TLTM Report which was submitted in April 1976.

001.615 thru 001.692
011.25
040.28
130.101 thru 130.114
222.99 thru 222.101
310.52 thru 310.67

Each of these RAI's is responded to and the specific responses are to be found in the PSAR question response section.